ISBN 978-82-326-3694-5 (printed version)
ISBN 978-82-326-3695-2 (electronic version)
ISSN 1503-8181

Doctoral theses at NTNU, 2019:45

Øyvind Storesund Hetland

Theoretical and Computational Studies of the Scattering of Light from Randomly Rough Dielectric Surfaces

NTNU
Norwegian University of
Science and Technology
Faculty of Natural Sciences
Department of Physics

NTNU
Norwegian University of
Science and Technology

Øyvind Storesund Hetland

Doctoral Thesis

Doctoral theses at NTNU, 2019:45

NTNU

NTNU
Norwegian University of
Science and Technology

Øyvind Storesund Hetland

Theoretical and Computational Studies of the Scattering of Light from Randomly Rough Dielectric Surfaces

Thesis for the degree of Philosophiae Doctor

Trondheim, February 2019

Norwegian University of Science and Technology
Faculty of Natural Sciences
Department of Physics

NTNU
Norwegian University of
Science and Technology

NTNU
Norwegian University of Science and Technology

Thesis for the degree of Philosophiae Doctor

Faculty of Natural Sciences
Department of Physics

ISBN 978-82-326-3694-5 (printed version)
ISBN 978-82-326-3695-2 (electronic version)
ISSN 1503-8181

Doctoral theses at NTNU, 2019:45

Printed by Skipnes Kommunikasjon as

Abstract

To understand and predict the diffuse scattering of electromagnetic waves through randomly rough surfaces is a relevant problem in many branches of science and engineering. We have investigated the scattering of polarized light from two-dimensional randomly rough dielectric interfaces, in order to look for scattering patterns of interest in the angular intensity distributions of the diffusely scattered light. The basis for our investigations has been the reduced Rayleigh equations and their numerical solutions. Our overall contribution is towards an increased understanding of diffuse scattering from randomly rough surfaces, especially for three-dimensional systems where we allow for cross-polarized scattering. This can be useful in a wide range of optical systems, since the non-invasive method of surface characterization through the analysis of scattering data is interesting for both industry and research.

When light is scattered diffusely in either reflection or transmission from or through a weakly rough interface, two phenomena of interest can be observed in the scattering intensity distributions. These are the *Yoneda phenomenon*, relatable to the idea of total internal reflection from a planar interface, and the *Brewster scattering phenomenon*, relatable to the polarizing angle observed for a planar interface. These scattering phenomena have only partially been investigated in the past, and their study has been the core of this thesis.

The Yoneda phenomenon is characterized as an enhancement of the intensity of the light scattered diffusely by a weakly and randomly rough interface between two dielectric media when the light is observed in the optically denser medium. The intensity enhancement occurs above a critical angle of

scattering which is independent of the angle of incidence of the excitation. This critical angle is always the polar angle, in the denser medium, for which the wavenumber of a plane wave turns non-propagating in the less dense medium.

The Brewster scattering phenomenon is characterized by directions for which we observe zero, or near-zero, scattered intensity in either the diffusely reflected or diffusely transmitted p-polarized light. These scattering angles depend on the angle of incidence. A consequence of the directionality of electromagnetic fields, the Brewster scattering phenomenon has been shown to represent the major difference in the scattering distributions of diffusely scattered s- and p-polarized light.

In this thesis we investigate these phenomena thoroughly through perturbative and non-perturbative numerical and theoretical work, also with the aid of new experimental results. We show, describe, explain and predict the behavior of both phenomena based on a lowest non-zero order perturbative approach, and as such we conclude that they are so-called single-scattering phenomena. We also investigate the physical mechanisms that underpin these phenomena, and attempt to describe them in terms of simple notions such as scalar waves, oscillating and rotating dipoles and geometrical arguments.

For a system of randomly rough dielectric film configurations on a substrate, we investigate the appearance of *Selényi interference rings* in the diffusely reflected and transmitted light. We show how the interference rings can be explained using simple sums of optical paths, and provide a more complete model than what is available in the literature. This work also ties in with the Yoneda and Brewster scattering phenomena, since they explain some of the observed results. Theory is developed and presented that can treat multiple rough interfaces in a stack. This theory is employed numerically to show how the interface roughness cross-correlation between two interfaces may selectively enhance and attenuate the Selényi rings.

Lastly, when medium interfaces are randomly rough, it is of value if we can infer the statistical properties of the roughness along with the properties of the scattering media based purely on the non-invasive scattering of light. Through the use of numerical phase perturbation theory based on the reduced Rayleigh equations, we investigate the reconstruction of such properties through a minimization method based on the reflected intensity distributions.

To the non-physicist

We are surrounded by light being scattered from surfaces all around us, both natural and man-made. Improving our understanding of exactly how light interacts with and scatters from or through surfaces, such as a solar cell, paint or a glass window, is of value and importance to both industry and society as a whole. It gives us a better understanding of the world around us and how we perceive it, and it can also enable us to develop new technologies and improve upon existing ones. This thesis is a collection of work where we have tried to better understand some of these interactions through the use of theory, experimental results and computer simulations.

In the following, I will tell you a short introductory story about light scattering, free from equations but with some interesting (in my opinion) visuals. Imagine a ray of light, the laser beam from a laser pointer for example, hitting a surface. If the surface were a mirror, it would be reflected at the same outgoing angle as the angle it had coming in, right? But what happens if the surface were a more "everyday" surface like a piece of wood, a painted wall or a piece of brushed steel? It turns out that such surfaces actually give rise to a marvelous show, where light appear to bounce and bend in a blur of scattered light — on a microscopic scale, that is. Imagine for a second that you could focus that laser beam to be just a couple of micrometers wide, and that you could observe this light show through a microscope[1]. What would you see?

Computer simulations allow us to see what this would have looked like as seen from the side, as if these were sun-rays piercing through the clouds on

[1] Or, equivalently, imagine that the laser beam is made up of radio waves, and that those waves hit a mountainous landscape. It would (kind of) be the same thing!

a rainy day. Or, in a more physics kind of wording: let's have a look at our scattering system seen in cross-section (from the side). We start out with our thin laser beam bouncing off a perfectly flat metallic silver surface:

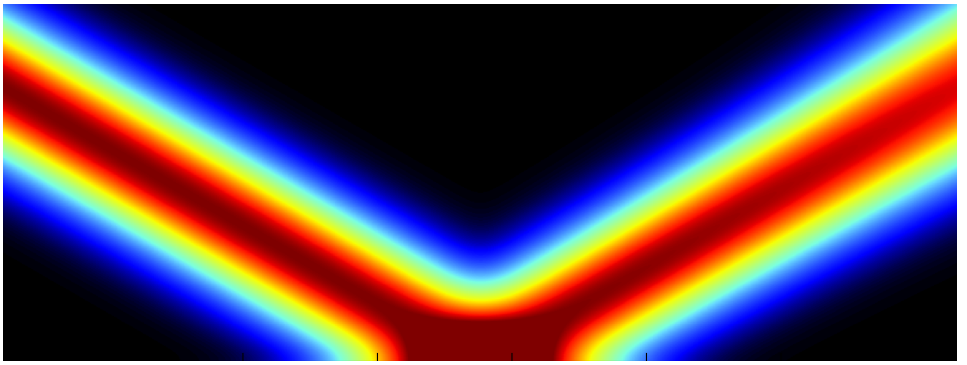

I assume the figure just above might not be entirely self-explanatory, so I'll explain. What we're looking at is a simulation of a laser beam coming in at an angle from the left. It propagates down to the metal surface and is then reflected at the same outgoing angle to the right. The color scale shows the brightness of the beam (the intensity of its electromagnetic field) with red at its most intense. But wait a minute — why is the beam not equally bright at all points across its cross-section, like a laser pointer? It turns out that this is what a thin laser beam really looks like at a microscopic scale. This is a *Gaussian* laser beam where the cross-section intensity of the beam adheres to a Gaussian distribution (also called a normal distribution, or a "bell curve"). By the way, all simulations have been performed on my laptop while writing this text using home-made software.

Let us now introduce some random nano-bumps to the silver surface and see what happens:

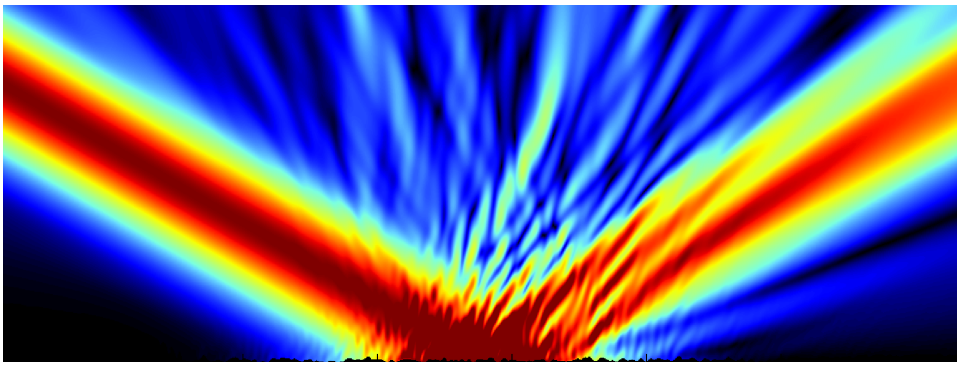

Now this is more interesting. Can you see the nano-curves on the surface at the bottom of the figure? They are only about a hundred nanometers high[2], but they really change the distribution of our reflected beam. This is light *scattering*. Most of the light is still reflected into an angle similar to the angle of the incoming light, but a good part of the beam is now spread in all directions producing a beautifully complicated pattern. The complex pattern is due to interference. The reflected light interacts with itself just like waves on water, giving us varying light intensity wherever the many electromagnetic waves that make up the light overlap.

The scattering of light into all kinds of directions from slightly rough surfaces is called *diffuse* scattering of light, and this diffuse scattering is actually the reason why you can read this text right now. All surfaces are rough at a microscopic scale, and this is what makes the light bounce in all directions when it interacts with such a surface in the real world. On a microscopic scale this interaction might look similar to what we have seen in the previous figure, but the overall macroscopic (large-scale) result of this diffuse light scattering is that most of the surfaces we observe in our everyday lives behave very differently from mirrors (luckily).

What happens if we replace the metallic surface with a slab of glass? We can assume that some light should be reflected and some should be transmitted? Let us have a look, with a slightly rougher surface as our glass-air interface:

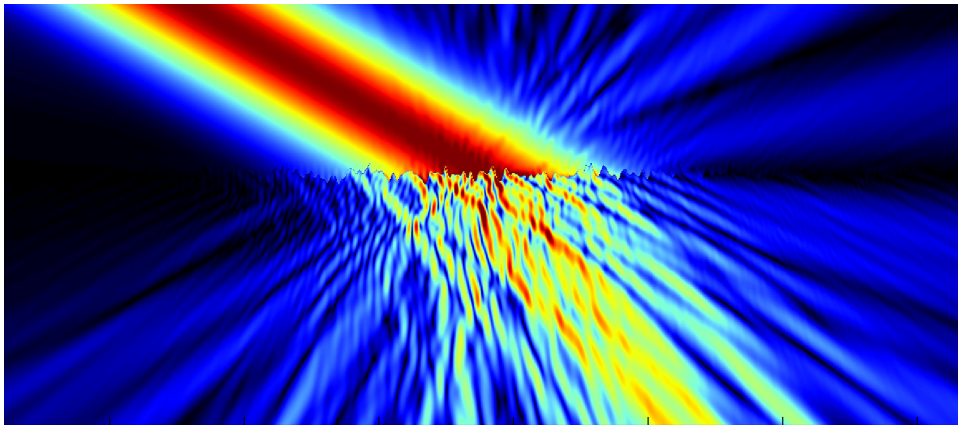

Look closely at the glass surface. Can you see that some of the nano-bumps on the surface act as magnifying glasses at a very small scale? We see

[2]If we assume that the laser is made up of visible light.

that most of the light actually penetrates the glass, but that the smooth incoming laser beam has become a very wide and random collection of light waves as they continue their journey deeper into the bulk of the glass[3].

The last two visuals actually do a reasonable job at showing what this thesis is all about[4]. We use well-known equations that describe how electromagnetic waves behave when they interact with a material interface, and through the use of computer simulations we attempt to understand and predict to which angles the incident light will scatter. We do depend on a number of approximations and assumptions, of course. Our computers are still not powerful enough to perfectly simulate reality, not even such a small part of it. Still, we are able to describe some fairly interesting details in how light behaves when it interacts with randomly rough surfaces, details that seem to match well with experimental results.

> “
> It fills me with joy to make discoveries, every day, of things that I've never seen before.
>
> — Carl Sagan

[3] According to the wave interpretation of light, a laser beam consists of a huge amount of light waves (electromagnetic waves) to begin with, it's just that they are very well orchestrated so that they together form the smooth laser beam. Each of these waves then interact with the glass interface, which forces many of them to “randomly” change direction. What emerges from the interface is then a more chaotic mix of waves, and we get the interference patterns that we observe.

[4] Well, the visuals are based on solutions of the extinction theorem, an exact method but too computationally demanding to be used (in three dimensions) for the main results presented in this thesis.

Preface

This thesis is submitted as part of the requirements for the degree of Philosophiae Doctor at the Norwegian University of Science and Technology (NTNU), in Trondheim, Norway. As is common, the body of this thesis is organized into two parts. The second part consists of the scientific papers [1–6] submitted as the main body of work to be considered for the degree. In the first part I present the most important concepts and motivations behind the succeeding papers. These introductory chapters do not include any new results, but attempts to present a more-or-less stepwise journey through the scientific basis for the second part of the thesis together with some discussions, details and considerations that did not naturally become part of the included scientific papers.

> “
> It feels good to be lost in the right direction.
>
> — Unknown

The last years have been quite the scientific journey, and while I'm just as fascinated by electromagnetism now as I was some years ago, I now have a much deeper respect for how the scientific method can find its way in the sometimes frustratingly entangled and messy landscape which is nature. What is light, really? Now I know that I really do not know. I do know, however, to fully appreciate www.phdcomics.com, hand-ground coffee, supercomputers, California, www.xkcd.com, wrist support, a cozy office, flexible working hours and vim. And, more importantly, I've learned that any journey is all about the people you meet along the way. Thank you, Ingve, for being the informal, friendly and knowledgeable supervisor you are.

Thank you for believing in me. I believe that your journey will continue to lead to great things both for science and for those around you. Thank you, Tor, for being exactly the anecdotal and supportive co-supervisor I needed. You have a great attitude towards science and also towards life, which I find truly inspiring. Alex, thank you for welcoming me in California and teaching me the joy of a good Zinfandel while also being a source of scientific inspiration. Thank you for your kindness, generosity and support as a coauthor. Dear Torstein and Jean-Philippe. Together we have climbed some mountains and have definitely fallen into a good amount of traps. Thank you for making the PhD journey an adventure, and thank you for making it a laugh. I couldn't have done it without you.

Thank you Morten S., for making everyday work more enjoyable and for joining me down the political rabbit hole. Thank you Jacob, Sindre, Stan, Isha, Magnus, Kristoffer, Eivind, Morten V., Thomas & Thomas, Nora, Marianne, Arne & Arne, Elisabeth, Justin, Leander and Paul Anton for being great colleagues in every sense of the word. Thank you Peder and Kristin, for giving me so many chances at improving my presentation skills and for your valuable trust and support. Thank you DION for giving me a shot at being a politician and teaching me a lot about the human aspect of academia, and NTNUI for letting me attempt to run a company on my "spare time". Thank you dear colleagues at Dept. of Physics and NTNU, for support and a great work environment. I also want to thank Jon Andreas and Patrick for entrusting me with the temporary title of assistant professor. I learned a lot, about electronics and teaching, and about myself.

I am sincerely grateful for the time and effort taken on by Dr. José A. Sánchez-Gil and Dr. Gabriel Soriano in agreeing to evaluate my work. I also want to thank Prof. Alex Hansen for organizing the assessment committee.

Thank you, dear family, for your endless support, both during the PhD but also during the twentysomething years leading up to it. Thank you for being who you are. And to my dear wife... Laura, we did it! We did it together. Thank you for inspiring me, thank you for your patience and for believing in me. You are the best.

Øyvind S. Hetland, Trondheim, October 2018

List of papers

In the following, the author's contributions to the papers included in the thesis are clarified in detail. All theoretical work included in this thesis is based on the reduced Rayleigh equations.

Paper 1

I. Simonsen, Ø. S. Hetland, J. B. Kryvi, and A. A. Maradudin, "Determination of the normalized-surface-height autocorrelation function of a two-dimensional randomly rough dielectric surface by the inversion of light-scattering data," *Phys. Rev. A*, vol. 93, no. 4, p. 043829, 2016

This paper presents a derivation of phase perturbation theory for the reflection of s-polarized light from a two-dimensional randomly rough dielectric surface, and utilizes this theory in a scattering inversion scheme in order to reconstruct various parameters of the scattering surface and dielectric. My main contribution to this work was in providing the numerical non-perturbative scattering intensity results, based on the reduced Rayleigh equations, that were used to assess the quality of the perturbative results and as input data to the inversion scheme.

Paper 2

Ø. S. Hetland, A. A. Maradudin, T. Nordam, and I. Simonsen, "Numerical studies of the scattering of light from a two-dimensional randomly rough interface between two dielectric media," *Phys. Rev. A*, vol. 93, no. 5, p. 053819, 2016

This paper is an exploration of scattering in reflection from two-dimensional randomly rough dielectric surfaces, where the dielectric constants of both media sharing the rough interface are allowed to vary. The diffusely scattered light is studied through both perturbative and non-perturbative approaches, both derived in the paper. I extended the simulation code, ran all simulations, made all figures and were the overall principal author. The first draft of the introduction and theory was prepared by AAM, and the results and discussion was co-authored with IS. All authors contributed to the editing and final preparation of the manuscript.

Paper 3

A. K. González-Alcalde, J.-P. Banon, Ø. S. Hetland, A. A. Maradudin, E. R. Méndez, T. Nordam, and I. Simonsen, "Experimental and numerical studies of the scattering of light from a two-dimensional randomly rough interface in the presence of total internal reflection: optical Yoneda peaks," *Opt. Express*, vol. 24, no. 23, pp. 25995–26005, 2016

This paper presents the first experimental results for scattering of light from a randomly rough dielectric surface where the medium of incidence is the denser medium, hence showing diffuse reflection relatable to total internal reflection. My contributions to the paper were to co-author the extension of the simulation software with JPB, run all simulations used for comparison with experiment, produce the contour-map-based figure and co-author the main paper body. I presented the paper and related work in a talk at the IOP conference "Photon16" in Leeds, UK, and in a talk at the PIERS 2017 conference in St. Petersburg, Russia.

Paper 4

Ø. S. Hetland, A. A. Maradudin, T. Nordam, P. A. Letnes, and I. Simonsen, "Numerical studies of the transmission of light through a two-dimensional randomly rough interface," *Phys. Rev. A*, vol. 95, no. 4, p. 043808, 2017

This paper is similar in structure and concept to Paper 2, but for an investigation into the light scattered in transmission. I extended the simulation code, ran all simulations, made all figures and wrote the majority of the content except the theory section in the paper main body and Appendix A. I presented the paper and related work in a poster presentation at the PIERS 2017 conference in St. Petersburg, Russia.

Paper 5

J.-P. Banon, Ø. S. Hetland, and I. Simonsen, "Selective enhancement of Selényi rings induced by the cross-correlation between the interfaces of a two-dimensional randomly rough dielectric film," *Ann. Phys. (N.Y.)*, vol. 389, pp. 352 – 382, 2018

This paper is a thorough investigation into Selényi rings, an interference phenomena observable in the diffusely reflected light from a randomly rough thin film. The paper includes a derivation of the reduced Rayleigh equation for general n-rough-interface systems, and the impact on interference from controlled cross-correlation between two rough film interfaces is studied. My contributions to the paper were to co-author an extension in non-perturbative simulation software with JPB, run simulations, make several of the figures and contribute to the discussion, development and main body of the paper.

Paper 6

J.-P. Banon, Ø. S. Hetland, and I. Simonsen, "On the physics of polarized light scattering from weakly rough dielectric surfaces: Yoneda and Brewster scattering phenomena," *arXiv:1804.07507 (Accepted for publication in Phys. Rev. A)*, 2018

This paper is an investigation into the Yoneda and Brewster diffuse scattering phenomena through a detailed analysis of small amplitude perturbation theory and dipole scattering theory based on the extinction theorem. The paper continues the analysis made in previous papers, and argues for physical explanations valid for weakly rough surfaces. My contributions to the paper was to be an overall supporting co-author to JPB, the main author.

Contents

Chapter 1

Introduction - the challenging wonder of electromagnetism

> “The dimmed outlines of phenomenal things all merge into one another unless we put on the focusing-glass of theory, and screw it up sometimes to one pitch of definition and sometimes to another, so as to see down into different depths through the great millstone of the world.
>
> — James Clerk Maxwell

Electromagnetic waves are everywhere around us, and their interaction with the world we live in is both a critical component of life on earth as well as a fundamental part of the universe as we know it. From a human perspective, light is of course all that we see, and through science we have learned to explore both the small and the big building blocks of the universe using the entire electromagnetic spectrum. Ranging from submarine communication systems operating at a few oscillations per second, all the way through visible light and to the ionizing radiation called gamma rays and further — electromagnetic waves are a part of absolutely every part of our everyday lives. The main reason for the ubiquity of electromagnetic waves is that they interact so strongly with matter, both when they are created and when their journey comes to a halt when their energy is transferred into something else.

Considering how relevant these electromagnetic waves are to us, it can be almost surprising how little we know about their true nature. They are

Figure 1.1: Rocks formations and the Dedo de Deus peak in the background, at the Serra dos Órgãos National Park, Brazil. By Carlos Perez Couto [CC BY-SA 3.0], via Wikimedia Commons.

elusive and counter-intuitive in much of their behavior, and even if electromagnetic theory is considered one of the greatest successes of the human mind, there still is a lot to learn. Creating a mental picture of the electromagnetic wave in its simplest form may not seem like a big challenge at first. However, this so-called wave reveals itself also to behave like a massless particle, the photon, for which time itself comes to a standstill. The particle-wave duality of electromagnetic radiation has become much clearer to us in the past century, but even with deep insights obtained through theories such as quantum field theory, the rabbit hole seems to become deeper still. The strangeness of the electromagnetic world, however, has not prevented the immense success of what we now call *classical* electromagnetism in general. In the rest of this thesis, we will rely on these classical advancements of electromagnetic theory. Even if many aspects of electromagnetism are scale-invariant, our main explorative probe will be visible light and our main concern will be the diffuse scattering of this light.

1.1 When the electromagnetic waves scatter

Subjectively one might argue that the interaction between light and matter range from the mundane to the outright beautiful. When we see a red sun

slowly disappearing behind a snowy mountain, its red rays illuminating a blanket of clouds above us, we are witnessing a complex interaction between electromagnetic waves in the form of light and the materials that scatter them. We have observed these interactions on a wide variety of length scales since the dawn of biological vision, and we are slowly learning how to describe them in the more general language of physics and mathematics. This insight is continuously providing us with tools applicable for both science and engineering, while also expanding into a wide range of other parts of our lives, such as philosophy[1] and entertainment[2]. The work presented in this thesis is an investigation into the scattering of electromagnetic waves in the form of visible light from weakly and randomly rough dielectric interfaces, with an emphasis on polarization effects and behavior. For the interested reader, Ref. 7 provides an excellent overview and introduction into the rough surface scattering topics that are most relevant for this thesis.

We will mainly focus on *diffusely* scattered light[3], light which for randomly rough interfaces is (mostly) scattered away from the specular direction (direction of reflection or transmission given a completely flat interface). A strongly simplified overview of this terminology is given in Fig. 1.2, where we see that interface roughness increases the diffuse component in both reflection and transmission at the expense of the specular component.

What do polarized sunglasses (those that help us see when driving on a wet road with a low sun), electronic displays of all kinds, projectors and fiberoptic cables, windows and lasers all have in common? Many of these technologies depend on or are affected by two well known optical phenomena; *total internal reflection* and the gradual polarization of reflected and transmitted light accentuated by *the Brewster angle*. We will, in this thesis, aim to shed light on the diffuse scattering analogs of the two aforementioned phenomena through theoretical, numerical and experimental results and discussions.

If you let sunlight reflect from the layer of water vapor hovering some micrometers above the reflective surface of your morning cup of tea, you might

[1] In the author's experience, even simple questions regarding the actual behavior of light quickly turn into fundamental discussions on quantum mechanics and time itself.

[2] Computer generated graphics are closing in on so-called photo realism, even when generated in real-time: A mix of physical insight and clever algorithms have allowed the construction of these mathematical worlds that now are starting to look real to us, largely based on our understanding of light scattering.

[3] Also called *incoherently* scattered light. The exact definitions of these terms are often a topic of discussion, but this is good enough for now.

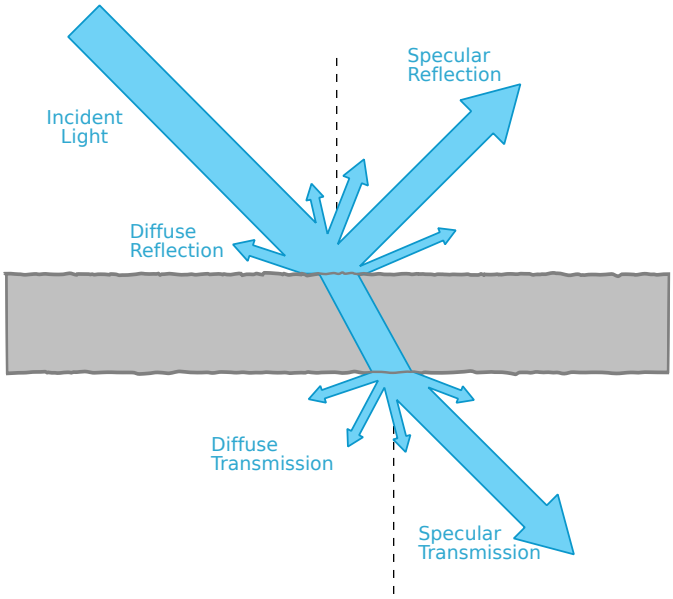

Figure 1.2: Simplified overview over the reflection and transmission of unidirectional light interacting with a thin transparent slab.

observe some colored rings of light when you look into the reflection. These rings are a variety of *Selényi rings*[4], an interesting interference effect that emerges when light is scattered diffusely by thin dielectric films. We investigate this effect thoroughly in this thesis, and describe the Selényi phenomenon theoretically and numerically.

1.2 Outline of this thesis

The following chapters will present the most important concepts and motivations behind the succeeding papers. These introductory chapters do not include any new results, but attempt to present a stepwise journey through the scientific basis for the second part of the thesis. These chapters introduce discussions, details and considerations that did not naturally become part of the included scientific papers. Chapter 2 introduces classical electromagnetic theory through Maxwells equations and also includes an introduction to plane waves and the polarization of light. It is followed by

[4]These colored rings specifically are usually called *Quételet rings*, but are still intimately connected to Selényi rings.

Chapter 3, an introduction to the realm of surface scattering. This chapter attempts to give an overview of the theoretical scattering framework without making any assumptions on the use of the Rayleigh hypothesis. In addition, the scattering surfaces assumed in the thesis work are introduced along with the most important observables. Chapter 4 finalizes the theoretical introduction through an introduction to the Rayleigh hypothesis and its use in this thesis. The main theoretical framework used in the thesis papers is derived in a brief manner. This includes the perturbative and non-perturbative methods along with a discussion of their strengths and weaknesses, some comments on the challenges in the numerical implementation of said methods and a discussion of the Rayleigh hypothesis. Chapter 5 introduces the physical phenomena at the core of this thesis: The Brewster scattering phenomenon, the Yoneda phenomenon and Selényi rings. As these phenomena are the subject of most of the thesis papers, this chapter is kept rather brief. The first part of the thesis is then concluded with a summary and some thoughts on future work in Chapter 6.

Chapter 2

Basic electromagnetic theory

> “From a long view of the history of mankind, seen from, say, ten thousand years from now—there can be little doubt that the most significant event of the 19th century will be judged as Maxwell's discovery of the laws of electrodynamics. The American Civil War will pale into provincial insignificance in comparison with this important scientific event of the same decade.
>
> — Richard P. Feynman (1964)

One might argue that Maxwell's equations are not merely a collection of equations that are useful in the scientific field of electromagnetism, but that to some extent, electromagnetism *is* Maxwell's equations. When they were first put together by Maxwell in 1861, they were the culmination of millennia of curious exploration. In their modern form, they still lie at the core of our understanding of the world around us.

This chapter aims to present the main electromagnetic background theory of the optical phenomena most relevant for this thesis. We will also start introducing the assumptions and simplifications that eventually lead to the equations solved in the thesis papers.

2.1 Maxwell's Equations

When James Clerk Maxwell published his seminal work "A Dynamical Theory of the Electromagnetic Field" [8] in 1865 much was already known about the then-novel topics of electricity and magnetism. A series of contributions to the understanding of these almost magical concepts had accumulated into a new branch of science, a branch with unprecedented explanatory power for the natural world and a wide range of practical applications. Using the concept of fields, as popularized by Michael Faraday, Maxwell was able to formally tie electricity and magnetism together. The result was a number of equations that became the foundation of what we know today as "electromagnetism". Oliver Heaviside later[1] used modern vector calculus to reformulate these equations into four equations that still serve as the starting point for any scientific journey into electromagnetism:

$$\nabla \cdot \mathbf{E} = \frac{1}{\varepsilon_0}\rho \tag{2.1a}$$

$$\nabla \cdot \mathbf{B} = 0 \tag{2.1b}$$

$$\nabla \times \mathbf{E} = -\partial_t \mathbf{B} \tag{2.1c}$$

$$\nabla \times \mathbf{B} = \mu_0 \mathbf{J} + \mu_0 \varepsilon_0 \partial_t \mathbf{E}, \tag{2.1d}$$

where $\mathbf{E}$ denotes the electric field and $\mathbf{B}$ the magnetic induction[2], ε_0 is the permittivity of vacuum, μ_0 the permeability of vacuum, ρ is the charge density and $\mathbf{J}$ is the current density. The notation $\partial_t \equiv \partial/\partial t$ denotes the partial derivative with respect to time t. Here and in the remainder of this thesis we will let bold symbols indicate vectors. Equations (2.1) are Maxwell's equations presented in their *differential* form, which for several reasons is the form most convenient as a starting point for investigations of electromagnetic scattering. The equivalent *integral* form is, however, often seen as a more physically intuitive form since it has an easier macroscopic interpretation.

> "
> Maxwell, like every other pioneer who does not live to explore the country he opened out, had not had time to investigate the most direct means of access to the country, or the most systematic way of exploring it. This has been reserved for Oliver

[1] In 1884. For a more complete story of the post-Maxwell journey see the book "The Maxwellians"[9].

[2] Also called the magnetic flux density.

> Heaviside to do. Maxwell's treatise is cumbered with the debris of his brilliant lines of assault, of his entrenched camps, of his battles. Oliver Heaviside has cleared those away, has opened up a direct route, has made a broad road, and has explored a considerable tract of country.
>
> — George Francis Fitzgerald (1893)

Equations (2.1) are in practice most useful for point charges in vacuum. In order to handle the behavior of electromagnetic fields in various materials it is therefore practical to introduce the *effective fields* $\mathbf{D}$ and $\mathbf{H}$, where $\mathbf{D}$ is known as the electric displacement and $\mathbf{H}$ is known simply as the magnetic field:

$$\mathbf{D} = \varepsilon_0 \mathbf{E} + \mathbf{P} \tag{2.2a}$$

$$\mathbf{B} = \mu_0(\mathbf{H} + \mathbf{M}). \tag{2.2b}$$

For linear electromagnetism $\mathbf{P}$, the polarization, is a function of the electrical field $\mathbf{E}$, and $\mathbf{M}$, the magnetization, is a function of the magnetic induction $\mathbf{B}$. Assuming that these effective fields can include the proper response of any material to an electromagnetic field, Eqs. (2.1) becomes

$$\nabla \cdot \mathbf{D} = \rho_f \tag{2.3a}$$

$$\nabla \cdot \mathbf{B} = 0 \tag{2.3b}$$

$$\nabla \times \mathbf{E} = -\partial_t \mathbf{B} \tag{2.3c}$$

$$\nabla \times \mathbf{H} = \mathbf{J}_f + \partial_t \mathbf{D}, \tag{2.3d}$$

where the terms ρ_f and $\mathbf{J}_f$ are referred to as the free source terms, representing the origin of the electric and magnetic fields.

Equations (2.3) are general, and in theory they allow for an almost unbounded range of exploration into electromagnetics. However, in this thesis we are interested in the scattering of monochromatic plane waves by interfaces separating linear, isotropic, source-free, non-magnetic and homogenous materials. This is a strong set of assumptions and simplifications, but as with any modeling of the physical world our goal is to make our model as simple as possible while still enabling the scientific insight we are aiming for. In the following, we will use our assumptions regarding the limits of our study to simplify the relevant theory to practically usable relations.

Our external fields, usually represented as electromagnetic waves of frequency ω incident on the scattering interface, do not require any sources to

be included in the system we investigate. We will simply assume that the waves are a part of the system, letting us assume $\rho_f = 0$ and $\mathbf{J}_f = \mathbf{0}$. For our purposes we will also assume a *stationary regime* where the time dependence of *all* fields is carried in the factor $e^{-\mathrm{i}\omega t}$, that is, the fields are time harmonic with an angular frequency ω. It will therefore be advantageous to work in the frequency domain from here on. As an example, the electric field evaluated at a point $\mathbf{x}$ at time t is then

$$\mathbf{E}(\mathbf{x}, t) = \mathbf{E}(\mathbf{x}|\omega)\, e^{-\mathrm{i}\omega t}. \tag{2.4}$$

Hence, and in summary, we can simplify Eqs. (2.3) by letting $\partial_t \to -\mathrm{i}\omega$, $\rho_f \to 0$ and $\mathbf{J}_f \to \mathbf{0}$, and from now on we will let a reference to a field as e.g. $\mathbf{E}$ implicitly mean $\mathbf{E}(\mathbf{x}|\omega)$:

$$\nabla \cdot \mathbf{D} = 0 \tag{2.5a}$$
$$\nabla \cdot \mathbf{B} = 0 \tag{2.5b}$$
$$\nabla \times \mathbf{E} = \mathrm{i}\omega \mathbf{B} \tag{2.5c}$$
$$\nabla \times \mathbf{H} = -\mathrm{i}\omega \mathbf{D}. \tag{2.5d}$$

We now want to relate the fields and the effective fields in a simpler manner than Eqs. (2.2), meaning that we will make some assumptions regarding the materials we study and their field response through $\mathbf{P}$ and $\mathbf{M}$.
Linearity: If the fields are sufficiently weak, we can assume the non-exotic materials we study to have a proportional response to the driving fields, i.e. $\mathbf{D} \propto \mathbf{E}$, $\mathbf{B} \propto \mathbf{H}$. *Homogenity:* For materials that appear homogenous relative to the wavelength, the field response of the material is independent of position as long as we are in the bulk of the material. *Isoptropy:* We assume the field response of the material to be independent of the field direction, meaning that all materials under study are isotropic. *Locality in space:* It is common to assume that the field response of a material is only dependent on the field at the same point in space as the point of observation. The permittivity and permeability do then not depend directly on the wavenumber $\mathbf{k}$ of the field in any way. Note, however, that we do *not* assume locality in time: we allow the field at past times (assuming causality) to affect the material response at a given point in space. This has the consequence that both the permittivity and permeability are functions of time, or, as we will assume *time invariance*, they will be functions of time differences and therefore of frequency ω. This is usually summarized by saying that the material is *dispersive*. The effects of dispersion are very visible in our everyday life, as dispersion is a part of the explanation for why things look the way they do, e.g. why some dielectric materials are

transparent. Given the recently mentioned assumptions and simplifications, the constitutive relations become

$$\mathbf{D}(\mathbf{x}|\omega) = \varepsilon_r(\omega)\varepsilon_0\mathbf{E}(\mathbf{x}|\omega) \tag{2.6a}$$
$$\mathbf{B}(\mathbf{x}|\omega) = \mu_r(\omega)\mu_0\mathbf{H}(\mathbf{x}|\omega). \tag{2.6b}$$

Here ε_r and μ_r are the relative permittivity and relative permeability, respectively, for $\varepsilon = \varepsilon_r(\omega)\varepsilon_0$ and $\mu = \mu_r(\omega)\mu_0$, while $\mathbf{x}$ represents a position vector in Euclidian space. We will in the following assume non-magnetic media, meaning that $\mu_r = 1$. From Eqs. (2.6) it is clear that $\varepsilon_r(\omega)$ then completely describes the field response of *any* material we may encounter, as long as we stay true to the assumptions already made. A typical value of the relative permittivity is the widely used value for "regular glass" and visible light, for which $\varepsilon_r(\omega) \approx 2.25$. Given our sign convention if a material's permittivity has an imaginary part greater than zero, $\operatorname{Im}\varepsilon_r > 0$, that material is a *lossy* material.

2.1.1 Electromagnetic waves

Taking the curl of Eq. (2.5c) while also utilizing the simple constitutive relations from Eqs. (2.6) provides us with

$$\nabla \times (\nabla \times \mathbf{E}) = \mathrm{i}\mu\omega(\nabla \times \mathbf{H}) \tag{2.7}$$

and corresponding for Eq. (2.5d), both valid for monochromatic fields. Now using the vector identity $\nabla\times(\nabla\times\mathbf{A}) = \nabla(\nabla\cdot\mathbf{A})-\nabla^2\mathbf{A}$ together with the the source-free divergence relations from Eqs. (2.5a) and (2.5b), we obtain the (homogenous) Helmholtz[3] equations for the electric field and the magnetic flux in the frequency domain:

$$(\nabla^2 + \varepsilon\mu\omega^2)\mathbf{E}(\mathbf{x}|\omega) = 0 \tag{2.8a}$$
$$(\nabla^2 + \varepsilon\mu\omega^2)\mathbf{B}(\mathbf{x}|\omega) = 0, \tag{2.8b}$$

where ∇^2 denotes the Laplace operator. These equations are valid for homogenous, source-free, isotropic, linear media. It is here important to note that we used Maxwell's equations for the divergence of $\mathbf{D}$ and $\mathbf{B}$, Eqs. (2.5a) and (2.5b), when we derived Eqs. (2.8). Since any solution of the Helmholtz equations must also satisfy the assumptions made in its

[3]Following the same procedure for the time dependent fields in Eq. (2.3) gives a variety of the time dependent wave equations.

derivation, Maxwell's equations for the divergence of **D** and **B** must also be satisfied at all times. The most common solution to Eq. (2.8) in Euclidian space is the *plane wave* solution

$$\mathbf{E}(\mathbf{x}|\omega) = \boldsymbol{\mathcal{E}}\, e^{\mathrm{i}\mathbf{k}\cdot\mathbf{x}}, \tag{2.9}$$

where the electric vector field amplitude $\boldsymbol{\mathcal{E}}$ is a constant vector and $\mathbf{k}$ is the wave vector pointing in the direction of propagation. From Eq. (2.8) it is clear that for the plane wave to be a solution of the homogenous Helmholtz equations the wavenumber $|\mathbf{k}| = k$ and the angular frequency ω must be related by

$$k = \sqrt{\varepsilon\mu}\,\omega, \tag{2.10}$$

called the *dispersion relation*. The phase velocity of the wave is then

$$v = \frac{\omega}{k} = \frac{1}{\sqrt{\varepsilon\mu}} = \frac{c}{n}, \tag{2.11}$$

where $n = \sqrt{\varepsilon_r\mu_r}$ is the index of refraction and $c = 1/\sqrt{\varepsilon_0\mu_0}$ is the speed of light in vacuum. Satisfying Maxwell's equations also implies that a propagating plane wave solution must be a wave for which both **E** and **B** are perpendicular to the direction of propagation, **k**. All such plane wave solutions are therefore *transverse waves*.

> “
> We can scarcely avoid the inference that light consists in the transverse undulations of the same medium which is the cause of electric and magnetic phenomena.
>
> — James Clerk Maxwell

Using only Maxwell's equations, a unification of the electromagnetic knowledge available in 1861, we have now seen what was by far the most novel part of the equations' introduction back then. The equations seem to suggest that not only are electricity and magnetism intimately linked, but their mutual interaction turns out to be the very fabric of which radio waves, x-rays, gamma rays and light are made of. The speed of this transfer of energy, these waves, is a constant c in vacuum — all assumptions aside. This speed has turned out to be the speed of any massless elementary particle, and it is a fundamental speed in our universe. As magnetic fields can be interpreted as a manifestation of special relativity applied to electric fields [10], it is maybe not so surprising to us today that electromagnetic waves travel at the speed of light. They are, after all, maybe a fundamental resonance in space-time itself.

2.1.2 The electromagnetic wave as an energy carrier

We previously mentioned that, clearly, any solution of the Helmholtz equations must also satisfy the assumptions made in its derivation, namely Maxwell's equations as in Eq. (2.5). From this it follows that a plane wave solution on the form given by Eq. (2.9), and its magnetic equivalent, must also satisfy

$$\boldsymbol{\mathcal{B}} = \sqrt{\mu\varepsilon}\,\hat{\mathbf{k}} \times \boldsymbol{\mathcal{E}}, \tag{2.12}$$

where a caret over a vector indicates that it is a unit vector. Interestingly, we see that the magnetic flux amplitude $\mathcal{B}$ is proportional to $\sqrt{\mu\varepsilon}\mathcal{E} = \mathcal{E}/v$. If we now assume $\hat{\mathbf{k}}$ to be real, we see that $\mathbf{E}$ and $\mathbf{B}$ must be in phase, and Eq. (2.12) shows that the vector field amplitudes $\boldsymbol{\mathcal{E}}$ and $\boldsymbol{\mathcal{B}}$ are perpendicular to each other in addition to being perpendicular to the direction of propagation. The time-averaged flux of energy carried by such a plane wave is then given by the real part of the complex Poynting vector [10]:

$$\langle \mathbf{S} \rangle_t = \mathrm{Re}\left(\frac{1}{2}\mathbf{E} \times \mathbf{H}^*\right). \tag{2.13}$$

where $\mathbf{S}$ is the Poynting's vector itself, indicating both the direction and magnitude of the flow of energy carried by the electromagnetic wave. $\langle\cdot\rangle_t$ represents the time average, and * denotes the complex conjugate.

If $\hat{\mathbf{k}}$ is complex, the plane wave solution given by Eq. (2.9) becomes an *inhomogeneous* plane wave [10]. Such waves possess exponential growth or decay in some directions, and are a critical part of the solution space for almost all interactions between electromagnetic waves and matter.

2.2 Polarization

Electromagnetic waves are not scalar waves like sound waves, where the pressure gradient typically is in the direction of wave propagation. According to the preceding section they are transverse waves. Like sound waves, electromagnetic waves have a direction of propagation, but unlike sound waves the directions of the oscillating fields that they are made up of stay at right angles to each other and with some nonzero angle with the direction of propagation, depending on the medium in which they are traveling.

If we are merely interested in the vector directions and not their amplitudes, it is quite common to specify only the direction of propagation, $\hat{\mathbf{k}}$ and the

direction of the electric field $\hat{\mathbf{E}}$ or the magnetic field $\hat{\mathbf{H}}$. The direction of one of these fields (by convention the electric field) for a given direction of propagation is called the *polarization* of the electromagnetic wave. This polarization might be linear, circular or elliptical, with the latter representing the more general case. Light that is traveling in a straight line and is linearly polarized will have its electric (and therefore also magnetic) field maintain a fixed direction of oscillation. This direction might always be decomposed into two directional components forming an Euclidean 2-coordinate system, for example the two well-known orthogonal basis vectors $\hat{\mathbf{x}}$ and $\hat{\mathbf{y}}$ for a wave traveling along the $\hat{\mathbf{z}}$-direction. When light interacts with a material interface it is common to name these directional components p and s, where p indicates the (in our case) well defined direction *parallel* with the plane of incidence or scattering: the plane defined by $\hat{\mathbf{k}}$ and the (average, or similar) interface normal $\hat{\mathbf{n}}$. The s-polarized light, where the s comes from the German word *senkrecht* (eng.: perpendicular) is oriented perpendicular to the same plane of incidence/scattering. The definitions we will use for these polarizations will be given in the next chapter.

Light might also be circularly polarized, meaning that the two linear components of the electromagnetic fields maintain a fixed phase difference of $\pm 90°$ ($\pm\pi/2$) relative to each other. This phase difference leads to a constant change in the direction of e.g. the electric field as it propagates through space, making the electric field vector trace out a spiral of either right-hand or left-hand sense relative to its direction of propagation. Elliptically polarized light is the generalization of circularly polarized light where we allow *any* phase difference between the two fields[4].

In the quantum particle representation of light, the polarization is an intrinsic quantum mechanical property of any photon quantified by its spin angular momentum, a component of its total angular momentum. There are two such spin states for a photon: it can either spin in the right-hand sense or the left-hand sense about its direction of travel.

[4]Interestingly both linear and circular polarizations might be considered to be the "fundamental" basis of polarization – any state of polarization can be equally well represented by either basis.

Chapter 3

The scattering problem

While electromagnetic fields are themselves interesting, understanding their interaction with physical objects has always been one of the main goals in studying them. One such class of interactions, and an entire branch of physics on the metaphorical tree of science, is the interaction between electromagnetic fields and surfaces/interfaces separating different media. However, for us to be able to study this interaction through a model we need to continue the process of introducing assumptions and simplifications started in the previous chapter, and in order to do so we need to know what systems and observables we are interested in. In the current work, our interest is in a specific part of what is called the *scattering problem*: Given monochromatic light incident on a stack of n stochastically rough semi-infinite layered media, how is the light scattered in reflection and transmission?

We will make the assumptions that we have deemed necessary to solve our variety of the scattering problem as we go along, but we will start with a quick summary of the assumptions that were made in the previous chapter. First, we will limit ourselves to the use of classical physics, neglecting any direct influence of physical quantum behavior in our model. Second, we will assume *stationarity*, letting us consider time only as an implicit variable. Third, we assume all materials of interest to be isotropic, homogeneous, local and completely described by their frequency-dependent permittivity ε, thereby also assuming the materials to be non-magnetic. The third assumption reduces our model to one where the scattering interaction between an electromagnetic field and our physical system is specified by the boundaries

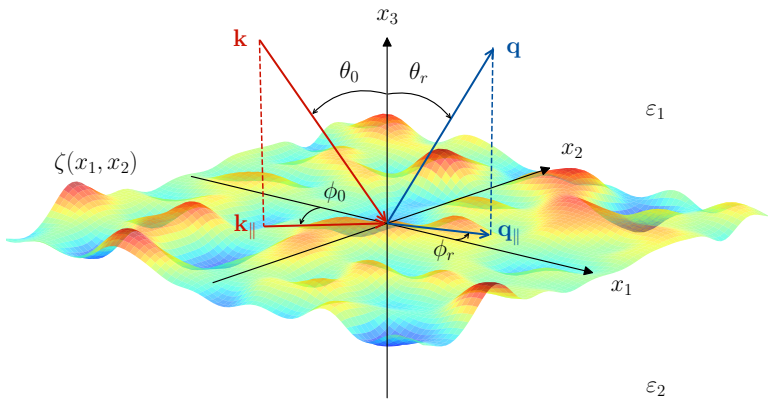

Figure 3.1: A sketch of the scattering geometry assumed in parts of this work. The figure also shows the coordinate system used, angles of incidence (θ_0, ϕ_0) and scattered reflection (θ_r, ϕ_r), and the corresponding lateral wavevectors $\mathbf{k}_\parallel$ and $\mathbf{q}_\parallel$, respectively.

between two different materials — the *interfaces*[1]. A fourth assumption is that we can represent *any* electromagnetic field as an expansion in propagating and evanescent plane waves. With these assumptions we have a model which is completely specified through the dielectric functions of its media, the media boundaries, and what we call the incident light[2].

In the following we will define the systems that we will investigate more formally, along with some concepts, relations and observables that will prepare us for the next chapter.

3.1 The scattering system

The presented work in this thesis on the scattering of light by rough interfaces is limited to *stochastically* rough interfaces where the interface profile function is assumed to be a single-valued function of the coordinates in the mean plane. The structure of such an interface is specified completely by its statistical properties. Most natural and man-made surfaces in our surround-

[1]Note, however, that physically the entire media participate in the scattering process. This fact might seem obvious, but it is still a source of some misconceptions and misinterpretations, some of which are discussed in Ref. [6].

[2]This light is really just an imposed constraint on our final equations.

ings have some degree of random roughness at some length scale, making the study of light scattering by such surfaces useful in many contexts.

In the current work the number of layers in the scattering models vary, and in the following we for readability leave out the subscript j from variables that are associated with the j-th interface in a multiple interface system whenever possible. The definition of the geometry is set in the three-dimensional space endowed with a Cartesian coordinate system $(O, \hat{\mathbf{e}}_1, \hat{\mathbf{e}}_2, \hat{\mathbf{e}}_3)$, with the vector plane $(\hat{\mathbf{e}}_1, \hat{\mathbf{e}}_2)$ parallel to the mean plane of the interfaces. In the following we will take a vector with subscript $\parallel$ to indicate that the vector has a zero third component, i.e. $\mathbf{x}_\parallel \cdot \hat{\mathbf{e}}_3 = 0$. The origin O can be arbitrarily chosen, only affecting the complex reflection and transmission amplitudes by an overall phase factor which plays no role in the intensity of the scattered light. Figure 3.1 presents a simple overview over the coordinate system, including a sample of an interface with a typical height distribution (but with exaggerated heights).

3.1.1 Statistical description of interface roughness

> “The true logic of this world is the calculus of probabilities.
>
> — James Clerk Maxwell

The interface profile function $x_3 = \zeta(\mathbf{x}_\parallel)$ we will use in our work is assumed to be a *single-valued* function of $\mathbf{x}_\parallel$ that is differentiable with respect to x_1 and x_2, and constitutes a stationary, zero-mean, isotropic, Gaussian random process. In addition to the specification of the Gaussian height distribution of the interface we also need to know how the heights are placed relative to each other in the $\mathbf{x}_\parallel$-plane. This property is given by

$$\langle \zeta(\mathbf{x}_\parallel)\zeta(\mathbf{x}_\parallel')\rangle = \delta^2 W(|\mathbf{x}_\parallel - \mathbf{x}_\parallel{}'|), \tag{3.1}$$

where $W(x_\parallel)$ is the *isotropic surface height autocorrelation function*, normalized so that $W(0) = 1$. The angle brackets here and in all that follows denote an average over an ensemble of realizations of the surface profile function $\zeta(\mathbf{x}_\parallel)$. The root-mean-square height of the surface is given by

$$\delta = \langle \zeta^2(\mathbf{x}_\parallel)\rangle^{\frac{1}{2}}. \tag{3.2}$$

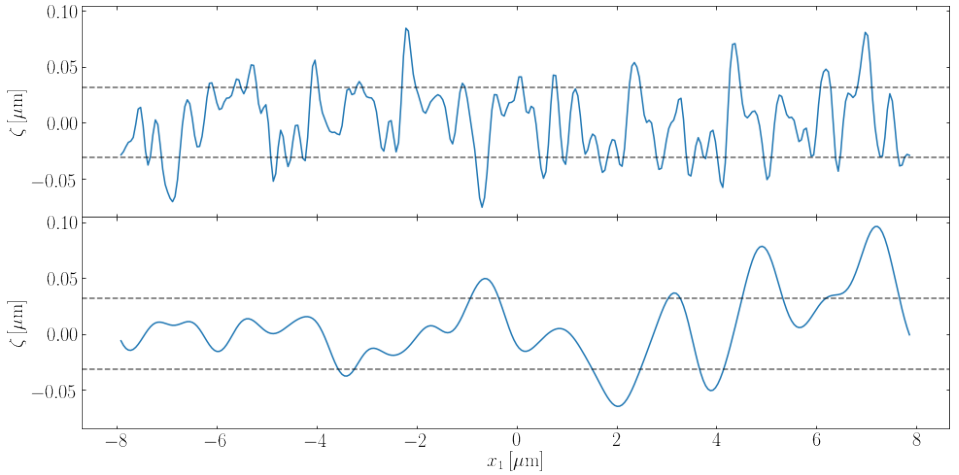

Figure 3.2: Examples of realizations of randomly rough interfaces, shown as $\zeta(x_1)$ for a randomly selected value of x_2. Both realizations have the same rms height $\delta = 32\,\mathrm{nm}$ and a Gaussian correlation function, but the transverse correlation length of the interface roughness is (a) $a = \lambda/4 = 158\,\mathrm{nm}$, (b) $a = \lambda = 632\,\mathrm{nm}$. The rms height $\pm\delta$ is illustrated as stipled black lines.

The surface profile function has a Fourier integral representation,

$$\zeta(\mathbf{x}_\parallel) = \int \frac{\mathrm{d}^2 Q_\parallel}{(2\pi)^2} \hat{\zeta}(\mathbf{Q}_\parallel) \exp(\mathrm{i}\mathbf{Q}_\parallel \cdot \mathbf{x}_\parallel), \tag{3.3}$$

where $\mathbf{Q}_\parallel = (Q_1, Q_2, 0)$ is a two-dimensional wave vector. By Fourier inversion we find that the coefficient $\hat{\zeta}(\mathbf{Q}_\parallel)$ is given by

$$\hat{\zeta}(\mathbf{Q}_\parallel) = \int \mathrm{d}^2 x_\parallel \zeta(\mathbf{x}_\parallel) \exp(-\mathrm{i}\mathbf{Q}_\parallel \cdot \mathbf{x}_\parallel), \tag{3.4}$$

and it also constitutes a zero-mean Gaussian random process defined by

$$\langle \hat{\zeta}(\mathbf{Q}_\parallel) \hat{\zeta}(\mathbf{Q'}_\parallel) \rangle = (2\pi)^2 \delta(\mathbf{Q}_\parallel + \mathbf{Q'}_\parallel) \delta^2 g(|\mathbf{Q}_\parallel|), \tag{3.5}$$

where the power spectrum of the surface roughness $g(|\mathbf{Q}_\parallel|)$ is defined by

$$g(|\mathbf{Q}_\parallel|) = \int \mathrm{d}^2 x_\parallel W(x_\parallel) \exp(-\mathrm{i}\mathbf{Q}_\parallel \cdot \mathbf{x}_\parallel). \tag{3.6}$$

For $W(|\mathbf{x}_\parallel|)$ and $g(|\mathbf{Q}_\parallel|)$ we assume either the Gaussian form

$$W(|\mathbf{x}_\parallel|) = \exp\left(-\frac{{x_\parallel}^2}{a^2}\right) \tag{3.7a}$$

$$g(|\mathbf{Q}_\parallel|) = \pi a^2 \exp\left(-\frac{a^2|\mathbf{Q}_\parallel|^2}{4}\right), \tag{3.7b}$$

or the exponential form

$$W(|\mathbf{x}_\parallel|) = \exp\left(-\frac{x_\parallel}{a}\right) \tag{3.8a}$$

$$g(|\mathbf{Q}_\parallel|) = \frac{2\pi a^2}{\left(1 + a^2|\mathbf{Q}_\parallel|^2\right)^{\frac{3}{2}}}. \tag{3.8b}$$

where the characteristic length a is the transverse correlation length of the surface roughness. Figure 3.2 shows two examples of realizations of a cross-section of such a two-dimensional interface profile $\zeta(x_1, x_2)$, for the Gaussian form of $W(|\mathbf{x}_\parallel|)$. The two realizations share rms height $\delta = 34\,\text{nm}$, but illustrate the differences in ζ for the transverse correlation lengths $a = \lambda/4 = 158\,\text{nm}$ [Fig. 3.2(a)] and $a = \lambda = 632\,\text{nm}$ [Fig. 3.2(b)]. These surface profiles were generated by the Fourier filtering method (see Refs. 11 and 12), the method that has been used in all papers included with this thesis.

Figure 3.3 presents the power spectra corresponding to the interfaces from Fig. 3.2, as defined by Eq. 3.6 and with the Gaussian form presented in Eq. (3.7). As is to be expected, a longer transverse correlation length a leads to a more narrow power spectrum, since the interface profile from a Fourier perspective is then represented by a superposition of (relatively speaking) smaller wavenumbers.

3.1.2 Single interface systems

The simplest system to study consists of a single interface: a dielectric medium (medium 1), whose dielectric constant is ε_1, in the region $x_3 > \zeta(\mathbf{x}_\parallel)$, and a dielectric medium (medium 2), whose dielectric constant is ε_2, in the region $x_3 < \zeta(\mathbf{x}_\parallel)$ [Fig. 3.1]. This system is the only system considered in the papers included as Refs. 1, 2, 4 and 6.

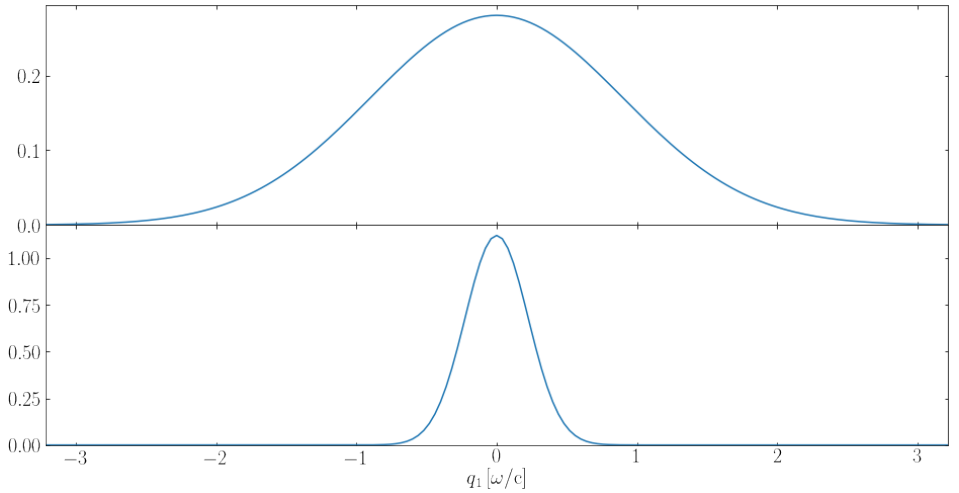

Figure 3.3: Power spectra, as defined in Eq. (3.6), for the corresponding profiles in Fig. 3.2. The spectra therefore have the Gaussian form presented in Eq. (3.7)(b), and are normalized to unity.

3.1.3 Film/multilayer systems

Multilayered systems, such as a thin film suspended on a substrate, can give rise to rich scattering phenomena. A natural extension of the single interface system is therefore that of a stack of dielectric media, with several randomly rough and/or planar interfaces. We let each medium interface j, separating media j and $j+1$, be represented by an offset interface profile function

$$h_j(\mathbf{x}_\parallel) = d_j + \zeta_j(\mathbf{x}_\parallel) \tag{3.9}$$

where $d_j = \langle h_j \rangle$ denotes the average of the jth profile and can be though of as an offset from the origin. A system with three media and two interfaces will then have a dielectric medium whose dielectric constant is ε_1 in the region $x_3 > h_1(\mathbf{x}_\parallel)$, a dielectric medium whose dielectric constant is ε_2 in the region $h_2(\mathbf{x}_\parallel) < x_3 < h_1(\mathbf{x}_\parallel)$ (the film), and a dielectric medium whose dielectric constant is ε_3 in the region $x_3 < h_2(\mathbf{x}_\parallel)$. An instance of the most general such system, one where both the interfaces are rough, is displayed in Fig. 3.4. This system geometry is the only system considered in the papers included as Refs. 3 and 5.

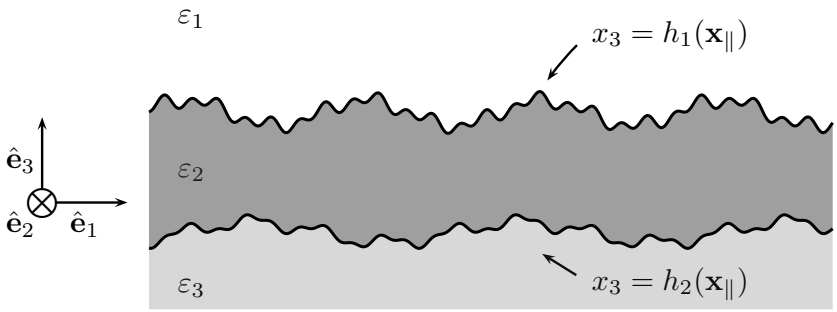

Figure 3.4: Simple schematic of a typical film system with three media and two rough interfaces.

3.2 Rough interface scattering

We have now defined the systems that are of core interest for the work presented in this thesis, namely the scattering of plane electromagnetic waves from interfaces separating semi-infinite media. The remainder of this chapter will attempt to describe and introduce some topics that will be useful in the next chapter, but that are relevant for several different methods of analysis.

3.2.1 Fields in semi-infinite media

We know that a solution to the Helmholtz equations, Eqs. (2.8), in general can be written as a linear combination of plane waves, each of them in the form of Eq. (2.9). If we now consider the total *far field* in each of our media (both semi-infinite and bounded, but far away from any material boundary), characterized by ε_j, we can express this linear combination of plane waves as

$$\mathbf{E}_j(\mathbf{x}) = \sum_{a=\pm} \int_{\mathbb{R}^2} \frac{\mathrm{d}^2 q_\parallel}{(2\pi)^2} \left[\mathcal{E}^a_{j,p}(\mathbf{q}_\parallel)\, \hat{\mathbf{e}}^a_{p,j}(\mathbf{q}_\parallel) + \mathcal{E}^a_{j,s}(\mathbf{q}_\parallel)\, \hat{\mathbf{e}}_s(\mathbf{q}_\parallel)\right] \times \exp\left(\mathrm{i}\mathbf{q}^a_j(\mathbf{q}_\parallel) \cdot \mathbf{x}\right) , \tag{3.10}$$

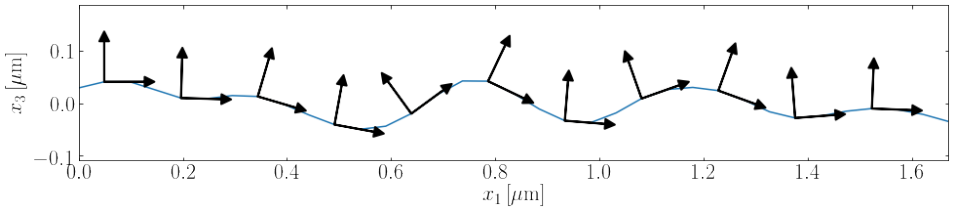

Figure 3.5: Illustration of some normal and tangential vectors at some points on a boundary profile ζ typical for the work presented in this thesis. The arrows indicating the vector directions are normalized, and of uniform but arbitrary length.

and similarly for $\mathbf{H}_j$, where we have defined

$$\alpha_j(q_\parallel) = \sqrt{\varepsilon_j \left(\frac{\omega}{c}\right)^2 - {q_\parallel}^2}, \quad \mathrm{Re}\,(\alpha_j), \mathrm{Im}\,(\alpha_j) \geq 0 \tag{3.11a}$$

$$\mathbf{q}_j^{\pm}(\mathbf{q}_\parallel) = \mathbf{q}_\parallel \pm \alpha_j(q_\parallel)\,\hat{\mathbf{e}}_3 \tag{3.11b}$$

$$\hat{\mathbf{e}}_s(\mathbf{q}_\parallel) = \hat{\mathbf{e}}_3 \times \hat{\mathbf{q}}_\parallel \tag{3.11c}$$

$$\hat{\mathbf{e}}_{p,j}^{\pm}(\mathbf{q}_\parallel) = \frac{c}{\sqrt{\varepsilon_j}\omega}\left(\pm\alpha_j(q_\parallel)\hat{\mathbf{q}}_\parallel - q_\parallel\,\hat{\mathbf{e}}_3\right)\,. \tag{3.11d}$$

Equations (3.11) show that the wave vector $\mathbf{q}_j^{\pm}(\mathbf{q}_\parallel)$ of an elementary plane wave is decomposed into its projection $\mathbf{q}_\parallel$ in the lateral vector plane [$(\hat{\mathbf{e}}_1, \hat{\mathbf{e}}_2)$, the plane of the mean interface profile indexed by j] and the component $\pm\alpha_j(q_\parallel)$ along $\hat{\mathbf{e}}_3$. The sum for $a = \pm$ takes into account both upwards $(+)$ and downwards $(-)$ propagating and evanescent waves. The field amplitude of argument $\mathbf{q}_\parallel$ is decomposed in the local polarization basis $(\hat{\mathbf{e}}_{p,j}^a(\mathbf{q}_\parallel), \hat{\mathbf{e}}_s(\mathbf{q}_\parallel))$. Hence, $\mathcal{E}_{j,\alpha}^a(\mathbf{q}_\parallel)$ denotes the component of the field amplitude in the polarization state α of the mode characterized by a and $\mathbf{q}_\parallel$. In this basis, the directions given by $\hat{\mathbf{e}}_{p,j}^{\pm}(\mathbf{q}_\parallel)$ and $\hat{\mathbf{e}}_s(\mathbf{q}_\parallel)$ are the directions of the p- and s-polarization of the electric field amplitude, respectively.

The field expansion in Eq. (3.10) is complete, as it does not introduce any assumptions or limitations on the fields other than those already mentioned in previous sections. Since we have stated that we so far stay far away from any material boundary, we have not yet invoked the Rayleigh hypothesis [Sec. 4.1], which under certain conditions allows us to use expansions like those in Eq. (3.10) also to satisfy boundary conditions.

3.2.2 Boundary conditions

General electromagnetic fields described by field vectors $\mathbf{E}$ and $\mathbf{H}$ have to satisfy the following boundary conditions at any interface j separating two media, identified by indices j and $j+1$, of different permittivity:

$$\mathbf{n}_j(\mathbf{x}_\parallel) \times \Big[\mathbf{E}_{j+1}(\mathbf{s}_j(\mathbf{x}_\parallel)) - \mathbf{E}_j(\mathbf{s}_j(\mathbf{x}_\parallel))\Big] = \mathbf{0} \tag{3.12a}$$

$$\mathbf{n}_j(\mathbf{x}_\parallel) \times \Big[\mathbf{H}_{j+1}(\mathbf{s}_j(\mathbf{x}_\parallel)) - \mathbf{H}_j(\mathbf{s}_j(\mathbf{x}_\parallel))\Big] = \mathbf{0}\,, \tag{3.12b}$$

where $\mathbf{n}_j(\mathbf{x}_\parallel)$ is a vector normal to the interface at the (single valued) surface point $\mathbf{s}_j(\mathbf{x}_\parallel) = \mathbf{x}_\parallel + \zeta_j(\mathbf{x}_\parallel)\hat{\mathbf{e}}_3$, given by

$$\mathbf{n}(\mathbf{x}_\parallel) = \hat{\mathbf{e}}_3 - \frac{\partial\zeta}{\partial x_1}(\mathbf{x}_\parallel)\,\hat{\mathbf{e}}_1 - \frac{\partial\zeta}{\partial x_2}(\mathbf{x}_\parallel)\,\hat{\mathbf{e}}_2\,. \tag{3.13}$$

Here, $\partial\cdot/\partial x_i$ denotes the partial derivative along the direction $\hat{\mathbf{e}}_i$. Figure 3.5 illustrates some normal and tangential vector directions for some points on a boundary profile typical in this thesis.

3.2.3 Scattering amplitudes

We will in the next chapter see that we may use field expansions like Eq. (3.10) and the recently mentioned boundary conditions, under certain assumptions and conditions, to relate plane waves incident upon our interface(s) to scattered plane waves leaving our interface(s). The Green's function is principally the most exhaustive characteristic of a given scattering problem, in the sense that it in principle can relate sources and resulting fields in all of space. However, in light scattering investigations using what is generally known as the *scattering amplitude* (SA)[13] often suffices. It is closely related to the relevant Green's function, but it is now assumed that both the source and the observer are at infinity. In practice we therefore investigate our scattering system using linear superpositions of plane waves where we exploit the symmetry of our scattering interface having an average boundary, and we limit our investigations to the far field.

Let now $\boldsymbol{\mathcal{E}}_j^{\pm}(\mathbf{q}_\parallel) = (\mathcal{E}_{j,p}^{\pm}(\mathbf{q}_\parallel), \mathcal{E}_{j,s}^{\pm}(\mathbf{q}_\parallel))^{\mathrm{T}}$ denote a column vector of the polarization components of the scattered plane wave field amplitudes in medium j, uniquely identifying the scattering direction through the lateral wave vector $\mathbf{q}_\parallel$. Let us also, for reasons to become apparent later, assume that the field amplitude vector $\boldsymbol{\mathcal{E}}_0$ describes the field amplitudes of the *only* plane

wave incident on the scattering system, with its direction determined by the incident lateral wave vector $\mathbf{k}_\parallel$. In the current context of light scattering we are not as interested in the scattered plane wave field amplitudes themselves as we are in the *ratios* of the scattered field amplitudes to the incident field amplitudes. To this end we assume that the scattered field amplitudes are linearly related to the incident field amplitude $\boldsymbol{\mathcal{E}}_0$ via the *reflection* $[\mathbf{R}(\mathbf{q}_\parallel|\mathbf{k}_\parallel)]$ and *transmission* $[\mathbf{T}(\mathbf{q}_\parallel|\mathbf{k}_\parallel)]$ amplitudes, defined as

$$\boldsymbol{\mathcal{E}}_1^+(\mathbf{q}_\parallel) = \mathbf{R}(\mathbf{q}_\parallel|\mathbf{k}_\parallel)\boldsymbol{\mathcal{E}}_0 \tag{3.14a}$$

$$\boldsymbol{\mathcal{E}}_t^-(\mathbf{q}_\parallel) = \mathbf{T}(\mathbf{q}_\parallel|\mathbf{k}_\parallel)\boldsymbol{\mathcal{E}}_0, \tag{3.14b}$$

where $\boldsymbol{\mathcal{E}}_1^+(\mathbf{q}_\parallel)$ and $\boldsymbol{\mathcal{E}}_t^-(\mathbf{q}_\parallel)$ represent the field amplitudes for plane waves propagating *away* from the scattering system in the semi-infinite medium of reflection or transmission, respectively. In writing $\boldsymbol{\mathcal{E}}_t^-$ the subscript t is therefore meant to indicate that the medium in question is the final medium in the stack.

The matrix valued amplitudes $\mathbf{R}$ and $\mathbf{T}$ essentially tell us how the scattered field originating from an incident plane wave with wavenumber $\mathbf{k}_\parallel$ is distributed by the scattering system. The reflection and transmission amplitudes are then necessarily described by 2×2 matrices, so that for $\mathbf{X} = \mathbf{R}$ or $\mathbf{T}$

$$\mathbf{X} = \begin{pmatrix} X_{pp} & X_{ps} \\ X_{sp} & X_{ss} \end{pmatrix}. \tag{3.15}$$

Under the mentioned assumption of linearity the physical interpretation of $\mathbf{R}$ and $\mathbf{T}$ is fairly straightforward. The coefficients $R_{\alpha\beta}(\mathbf{q}_\parallel|\mathbf{k}_\parallel)$ and $T_{\alpha\beta}(\mathbf{q}_\parallel|\mathbf{k}_\parallel)$, where $\alpha, \beta \in \{p, s\}$, are the field amplitudes for the reflected and transmitted light, respectively, with lateral wave vector $\mathbf{q}_\parallel$ in the polarization state α, generated by a unit incident field with lateral wave vector $\mathbf{k}_\parallel$ in the polarization state β.

3.3 Observables

From the knowledge of the scattering amplitudes $\mathbf{R}$ and $\mathbf{T}$ the mean differential reflection/transmission coefficient, the reflectivity/transmissivity, and the reflectance/transmittance can be calculated. These *observables* represent quantities that are physically observable, which (in principle) can be measured experimentally. We will in the following assume that medium 1

is the medium of incidence, and hence also the medium of reflection. The constant S will be used to denote the area of the x_1x_2-plane covered by the randomly rough interface(s).

3.3.1 The mean DRC/DTC

The differential *reflection* coefficient (DRC) $\partial R/\partial\Omega_r$ is defined such that $(\partial R/\partial\Omega_r)\ \mathrm{d}\Omega_r$ is the fraction of the total time-averaged flux (power) incident on the interface that is scattered in reflection into the element of solid angle $\mathrm{d}\Omega_r$ about the scattering direction defined by the polar and azimuthal scattering angles (θ_r, ϕ_r). For the scattering system geometries presented earlier in this chapter, the lateral wave vectors $\mathbf{k}_\parallel$ and $\mathbf{q}_\parallel$ can be expressed in terms of the polar and azimuthal angles of incidence (θ_0, ϕ_0) and reflection (θ_r, ϕ_r), respectively, by

$$\mathbf{k}_\parallel = \sqrt{\varepsilon_1}\frac{\omega}{c}\sin\theta_0(\cos\phi_0, \sin\phi_0, 0) \tag{3.16a}$$

$$\mathbf{q}_\parallel = \sqrt{\varepsilon_1}\frac{\omega}{c}\sin\theta_r(\cos\phi_r, \sin\phi_r, 0), \tag{3.16b}$$

so that $\mathrm{d}\Omega_r = \sin\theta_r\,\mathrm{d}\theta_r\,\mathrm{d}\phi_r$. As we are dealing with scattering from a randomly rough interface, it is the average of the DRC over the ensemble of realizations of the surface profile function that we need to calculate. This is the *mean* DRC (MDRC), which is defined by

$$\begin{aligned}\left\langle \frac{\partial R_{\alpha\beta}(\mathbf{q}_\parallel|\mathbf{k}_\parallel)}{\partial\Omega_r}\right\rangle &= \frac{1}{S}\varepsilon_1\frac{1}{(2\pi)^2}\left(\frac{\omega}{c}\right)^2\frac{\cos^2\theta_r}{\cos\theta_0}\left\langle\left|R_{\alpha\beta}(\mathbf{q}_\parallel|\mathbf{k}_\parallel)\right|^2\right\rangle \\ &= \frac{1}{S}\sqrt{\varepsilon_1}\frac{1}{(2\pi)^2}\left(\frac{\omega}{c}\right)\frac{\alpha_1(q_\parallel)^2}{\alpha_1(k_\parallel)}\left\langle\left|R_{\alpha\beta}(\mathbf{q}_\parallel|\mathbf{k}_\parallel)\right|^2\right\rangle,\end{aligned} \tag{3.17}$$

where the full derivation is given in the papers included as Refs. 2 and 5.

The differential *transmission* coefficient (DTC) $\partial T/\partial\Omega_t$ is defined in a completely analogous fashion; $(\partial T/\partial\Omega_t)\ \mathrm{d}\Omega_t$ is the fraction of the total time-average flux (power) incident on the interface that is scattered in transmission into the element of solid angle $\mathrm{d}\Omega_t$ about the scattering direction defined by the polar and azimuthal scattering angles (θ_t, ϕ_t). For the case when we are interested in the MDTC Eq. (3.16a) still holds true, but we now have that

$$\mathbf{q}_\parallel = \sqrt{\varepsilon_t}\frac{\omega}{c}\sin\theta_t(\cos\phi_t, \sin\phi_t, 0), \tag{3.18}$$

where ε_t is the dielectric constant in the semi-infinite medium of transmission, so that $\mathrm{d}\Omega_t = \sin\theta_t \,\mathrm{d}\theta_t \,\mathrm{d}\phi_t$. For this and several other reasons we tend to use lateral wave vectors in our equations rather than angles. The mean DTC is defined by

$$\left\langle \frac{\partial T_{\alpha\beta}(\mathbf{q}_\parallel|\mathbf{k}_\parallel)}{\partial \Omega_t} \right\rangle = \frac{1}{S}\frac{\varepsilon_t^{3/2}}{\varepsilon_1^{1/2}}\frac{1}{(2\pi)^2}\left(\frac{\omega}{c}\right)^2 \frac{\cos^2\theta_t}{\cos\theta_0}\left\langle \left|T_{\alpha\beta}(\mathbf{q}_\parallel|\mathbf{k}_\parallel)\right|^2 \right\rangle$$
$$= \frac{1}{S}\sqrt{\varepsilon_t}\frac{1}{(2\pi)^2}\left(\frac{\omega}{c}\right)\frac{\alpha_t(q_\parallel)^2}{\alpha_1(k_\parallel)}\left\langle \left|T_{\alpha\beta}(\mathbf{q}_\parallel|\mathbf{k}_\parallel)\right|^2 \right\rangle, \qquad (3.19)$$

where the full derivation is given in the papers included as Refs 4 and 5.

If we write the scattering amplitude $X_{\alpha\beta}(\mathbf{q}_\parallel|\mathbf{k}_\parallel)$, where X is R or T, as the sum of its mean value and the fluctuation from this mean,

$$X_{\alpha\beta}(\mathbf{q}_\parallel|\mathbf{k}_\parallel) = \left\langle X_{\alpha\beta}(\mathbf{q}_\parallel|\mathbf{k}_\parallel)\right\rangle + \left[X_{\alpha\beta}(\mathbf{q}_\parallel|\mathbf{k}_\parallel) - \left\langle X_{\alpha\beta}(\mathbf{q}_\parallel|\mathbf{k}_\parallel)\right\rangle\right], \qquad (3.20)$$

then each of these two terms contributes separately to the mean DRC/DTC:

$$\left\langle \frac{\partial X_{\alpha\beta}(\mathbf{q}_\parallel|\mathbf{k}_\parallel)}{\partial \Omega} \right\rangle = \left\langle \frac{\partial X_{\alpha\beta}(\mathbf{q}_\parallel|\mathbf{k}_\parallel)}{\partial \Omega} \right\rangle_{\mathrm{coh}} + \left\langle \frac{\partial X_{\alpha\beta}(\mathbf{q}_\parallel|\mathbf{k}_\parallel)}{\partial \Omega} \right\rangle_{\mathrm{incoh}}, \qquad (3.21)$$

where the former term describes the coherent (specular) contribution and the latter term describes the incoherent (diffuse) contribution.

3.3.2 Reflectivity and reflectance

We define the reflectivity, $\mathcal{R}_\alpha(\theta_0)$, for polar angle of incidence θ_0 and light of α polarization to be the co-polarized light reflected coherently by the rough interface:

$$\mathcal{R}_\alpha(\theta_0) = \int_0^{\frac{\pi}{2}} \mathrm{d}\theta_r \,\sin\theta_r \int_{-\pi}^{\pi} \mathrm{d}\phi_r \left\langle \frac{\partial R_{\alpha\alpha}(\mathbf{q}_\parallel|\mathbf{k}_\parallel)}{\partial \Omega_r} \right\rangle_{\mathrm{coh}} = \left|R_\alpha(k_\parallel)\right|^2. \qquad (3.22)$$

The function $R_\alpha(k_\parallel)$ can be obtained via the following result:

$$\langle R_{\alpha\beta}(\mathbf{q}_\parallel|\mathbf{k}_\parallel)\rangle = (2\pi)^2\delta(\mathbf{q}_\parallel - \mathbf{k}_\parallel)\delta_{\alpha\beta}R_\alpha(k_\parallel), \qquad (3.23)$$

where the presence of the delta function is due to the stationarity of the randomly rough surface; the Kronecker symbol $\delta_{\alpha\beta}$ arises from the conservation of angular momentum in the scattering process; and the result that $R_\alpha(k_\parallel)$ depends on $\mathbf{k}_\parallel$ only through its magnitude is due to the isotropy of

the random roughness. We then obtain $R_\alpha(k_\parallel)$ with the aid of the result that $(2\pi)^2\delta(\mathbf{0}) = S$ (for a surface of finite area), in the form

$$R_\alpha(k_\parallel) = R_\alpha\left(\sqrt{\varepsilon_1}\frac{\omega}{c}\sin\theta_0\right) = \frac{1}{S}\left\langle R_{\alpha\alpha}(\mathbf{k}_\parallel|\mathbf{k}_\parallel)\right\rangle. \tag{3.24}$$

In addition to the reflectivity (3.22) it is also of interest to introduce the *reflectance* for β-polarized light defined as

$$\mathscr{R}_\beta(\theta_0) = \sum_{\alpha=p,s}\mathscr{R}_{\alpha\beta}(\theta_0), \tag{3.25a}$$

where

$$\mathscr{R}_{\alpha\beta}(\theta_0) = \int_0^{\frac{\pi}{2}}\mathrm{d}\theta_r\,\sin\theta_r\int_{-\pi}^{\pi}\mathrm{d}\phi_r\left\langle\frac{\partial R_{\alpha\beta}(\mathbf{q}_\parallel|\mathbf{k}_\parallel)}{\partial\Omega_r}\right\rangle. \tag{3.25b}$$

In short, the reflectance measures the fraction of the power flux incident on the rough surface that was reflected by it, taking both specularly and diffusely reflected light into account. In view of Eq. (3.21), the reflectance is the sum of a contribution from light that has been reflected coherently and a contribution from light that has been reflected incoherently by the rough interface, $\mathscr{R}_\beta(\theta_0) = \mathscr{R}_\beta(\theta_0)_{\mathrm{coh}} + \mathscr{R}_\beta(\theta_0)_{\mathrm{incoh}}$, and both co- and cross-polarized reflected light contribute. Since cross-polarized coherently reflected light is not allowed the coherent contribution to the reflectance for β-polarized light equals the reflectivity for β-polarized light; $\mathscr{R}_\beta(\theta_0)_{\mathrm{coh}} = \mathcal{R}_\beta(\theta_0)$. Equation (3.25a) can therefore also be written in the form

$$\mathscr{R}_\beta(\theta_0) = \mathcal{R}_\beta(\theta_0) + \sum_{\alpha=p,s}\mathscr{R}_{\alpha\beta}(\theta_0)_{\mathrm{incoh}}. \tag{3.26}$$

If the incident light is not purely p- or s-polarized, the reflectance and the reflectivity of the rough surface will have to be calculated on the basis of weighted sums of the expressions in Eqs. (3.22) and (3.26), where the weights reflect the fractions of the different polarizations contained within the incident light.

In an analogous fashion we may also define the *transmittance*, $\mathscr{T}_{\alpha\beta}(\theta_0)$ as the fraction of the power flux incident on the rough surface that is transmitted through it, and *transmissivity*, $\mathcal{T}_\alpha(\theta_0)$, as the fraction of the power flux incident on the rough surface that is transmitted coherently and co-polarized through it. The full derivations of these latter observables can be found in the paper included as Ref. [4].

3.4 Conservation of energy

In all cases of scattering systems where all media are lossless, the total energy scattered in both reflection and transmission relative to the incident wave should be preserved [14]. While we emphasize that this is a necessary, but not sufficient, condition for the correctness of our numerical calculations, it is nevertheless a useful and practical sanity check that is easy to perform.

The fraction of the incident power, as light of polarization β, that is scattered in reflection and transmission in polarization α, is given by the integrals of the DRC/DTC over the two semi-infinite upper and lower hemispheres:

$$\mathcal{U}_{\alpha\beta} = \int \mathrm{d}\Omega_r \frac{\partial R_{\alpha\beta}}{\partial \Omega_r} + \int \mathrm{d}\Omega_t \frac{\partial T_{\alpha\beta}}{\partial \Omega_t}. \tag{3.27}$$

If now all media in the system are non-absorbing and the incident light has polarization β, one should have

$$\mathcal{U}_\beta = \sum_\alpha \mathcal{U}_{\alpha\beta} = 1, \tag{3.28}$$

since energy is conserved in the scattering process. The first term in Eq. (3.27) represents the energy scattered in reflections, so for a system where the semi-infinite medium of the substrate is a lossless metal [Re $\varepsilon_t < 0$] or a perfect electric conductor this term is the only term contributing to $\mathcal{U}$. If then all other media in the system are also lossless, we have a condition called *unitarity*, where Eq. (3.28) should sum to one based on reflection alone.

If not all media in the system are lossless, one might correct Eq. (3.28) to include an absorption term. This term is, however, not straightforward to obtain in a rigorous way [7].

3.5 Solving the scattering problem

The review article by Elfouhaily *et al.* [15], written in 2004, is an excellent source for a thorough and consistent comparison of a wide range of scattering approximations. They include tables that compare ≈ 20 different methods. They interestingly, but maybe not surprisingly, conclude that there is no one method that stands out — they all have strengths and weaknesses. Hence,

they also state that the work on good approximative scattering methods is far from concluded.

The remainder of this thesis will primarily rely on methods based on the Rayleigh equations.

Chapter 4

The reduced Rayleigh equation

> “The history of science teaches only too plainly the lesson that no single method is absolutely to be relied upon, that sources of error lurk where they are least expected, and that they may escape the notice of the most experienced and conscientious worker.
>
> — Lord Rayleigh

The Rayleigh hypothesis is, and has been, a successful cornerstone approximation in several models and methods used for the calculation of wave scattering from rough surfaces, both perturbative and non-perturbative. Historically it is maybe best known from one of the oldest and most popular methods, namely the expansion of the scattering amplitudes to an arbitrary order in a small height parameter. This method is often termed the *Small Perturbation Method (SPM)* or the *Rayleigh method*, but it exists in a myriad of varieties and is known under many names [15]. The *Rayleigh equations* are at the origin of this method. They are a set of coupled integral equations that under the Rayleigh hypothesis connect the (known) boundary conditions, our knowledge of the exciting field (the incident light), the scatterers and the materials with the unknown: the scattering amplitudes of reflection and transmission in the different propagating and non-propagating directions possible. The Rayleigh equations are the starting point for many different perturbative methods, but they can also be used to obtain numerical methods that are non-perturbative. They are themselves

only approximative due to their dependence on the Rayleigh hypothesis, which we will describe in detail later in this chapter.

The *reduced Rayleigh equations* are a rewriting of the Rayleigh equations that allows us to calculate *either* the reflection amplitudes *or* the transmission amplitudes directly, without caring about the *other* quantity explicitly. They were first proposed by Toigo *et al.* in 1977 [16], where they were derived with the help of, and also extensively compared to, the exact method based on the Ewald-Oseen extinction theorem [17–19]. This work was further developed by Brown *et al.* in 1985 [20]. The equations were later re-derived for the case of a multi-layered stack of rough surface slabs by Soubret *et al.* [21]. They used these equations to obtain more compact formulations of the scattering amplitudes under the Rayleigh method to third order, and solved these for the case of a single randomly rough interface separating a metal or dielectric and vacuum. In the last three decades numerous works have been based on the reduced Rayleigh equations, both through their perturbative expansions but also through their direct numerical solution. The review article by Simonsen [7] gives a thorough overview of their use leading up to 2009, while some more recent works in two dimensions can be found in e.g. Refs. 2–4, 12, 22–26.

In the following we will first summarize the main assumptions made in the Rayleigh hypothesis, followed by a summary of the derivation of the reduced Rayleigh equations for the system configurations relevant to this thesis. These equations serve as an excellent starting point for perturbative methods, and two such methods will be introduced in Sections 4.3 and 4.4. Finally, we end the chapter with an introduction to the non-perturbative method based on the reduced Rayleigh equations and some discussions on its accuracy, limitations and computational requirements.

4.1 The Rayleigh Hypothesis

There are a plethora of theories and assumptions available to choose from when studying light scattering from rough interfaces, but a common one is the *Rayleigh hypothesis* [27, 28]. It serves as a simplifying link between the (exact) boundary conditions at the scattering interface and the (easy to handle) asymptotic, far-field, outgoing representations of the plane wave electromagnetic fields. Below the highest point of our interface $x_3 = \max \zeta(\mathbf{x}_\parallel)$ and above the lowest point on the same interface $x_3 = \min \zeta(\mathbf{x}_\parallel)$, the region called the *selvedge* region, we are at risk of having the different plane waves

interact in such a way that we need to let our scattered waves propagate both upward and downward in both the medium of incidence and transmission. The Rayleigh hypothesis simply lets us assume that it is *good enough* to let the incident plane wave(s) be the *only* plane wave(s) propagating towards the interface from infinity. It then follows to assume that the scattered field in transmission or reflection is sufficiently described through a superposition of plane waves propagating *away* from the top/bottom interface(s).

The Rayleigh hypothesis is a widely used assumption, in the sense that it has been applied to a rich variety of scattering problems yielding correct results [7, 14]. For many methods, especially those designed to rely on it, it provides a significant mathematical and numerical simplification. It does, however, introduce an assumption into the scattering model which is challenging to quantify. Much work and attention has been given to the discussion of the exact limits of validity of the Rayleigh hypothesis, and while a full discussion on this topic is well outside the scope of this thesis we believe that Refs. 29–37, and recently also Ref. 38, might serve as good starting points for the interested reader. Historically the hypothesis has been much discussed in relation to the various perturbative methods that rely on it, such as the small amplitude perturbation method and its cousins, and some references for the validity discussion is therefore given in Sec. 4.3. In general, and irrespective of material, there is some consensus on the "safe" criterion

$$\frac{\delta}{a} \ll 1 \tag{4.1}$$

for the validity of the Rayleigh hypothesis, where δ is the rms height and a is the transverse correlation length of a given interface. Some authors prefer the essentially similar condition on the gradient of the interface profile function

$$\nabla\zeta(\mathbf{x}_\parallel) \ll 1. \tag{4.2}$$

Both of these formulations of the condition of validity depend on the *slopes* of the interface profile.

We would like to mention that most attempts at a circumvention of the Rayleigh hypothesis, for similar scattering problems as the ones presented in this thesis, are mainly based on the Ewald-Oseen extinction theorem and therefore lead to integral equation methods that are in principle similar to each other [39]. Interestingly, when these integral equations are evaluated in a perturbative manner it has been verified that they, to second order in the

small roughness parameter, are identical to the more classical perturbation method described in Sec. 4.3 which is indeed dependent on the Rayleigh hypothesis [40]. This fact has been used to lend credibility to the argument that the Rayleigh hypothesis can lead to methods with wider applicability than the strict correctness of the hypothesis itself, at least in an asymptotical sense.

Recent contributions by A. V. Tishchenko, summarized in Ref. 35 and written in a popular form in Ref. 41, has carried the title "Rayleigh was right". In this work it is argued that, based on investigations of diffraction gratings, the Rayleigh hypothesis has been underestimated and slightly misunderstood during the last fifty years. A main takeaway from these discussions might be that the Rayleigh hypothesis rarely is the only assumption and approximation made in scattering studies, especially numerical studies, so that the physical validity of the hypothesis itself is a question difficult to untangle. We will not delve any further into this interesting discussion here, but rather treat the Rayleigh hypothesis as an assumption that we handle with care.

4.2 Brief derivation of the reduced Rayleigh equations

We will now use the boundary equations to link the total field expansions in two media separated by an (infinite) interface. This is a step in the direction of the Rayleigh equations, and whether this step in itself requires the Rayleigh hypothesis (Sec. 4.1) is an unresolved topic of scientific discussion. Following this first step we will make some definitions on what we call the *incident* field in our model, and obtain relations for the reflection and transmission amplitudes followed by the reduced Rayleigh equations that enable their calculation separately.

4.2.1 The plane wave transfer equations

Following the general method by Soubret *et al.* [21], we now substitute the field expansion given by Eq. (3.10) into the boundary conditions given by Eq. (3.12b) through the use of a linear integral combination of the boundary conditions. The combinations necessary to obtain the final result were inspired by the extinction theorem [19], which in turn has been proven to

be a consequence of Maxwell's equations themselves [18]. The end result, connecting the general plane waves represented by Eq. (3.10) in medium j and medium $j+1$ across an interface with no overhangs is

$$\sum_{a_j=\pm}\int\frac{\mathrm{d}^2q_\parallel}{(2\pi)^2}\,\mathcal{J}_{j+1,j}^{a_{j+1},a_j}(\mathbf{p}_\parallel|\mathbf{q}_\parallel)\mathbf{M}_{j+1,j}^{a_{j+1},a_j}(\mathbf{p}_\parallel|\mathbf{q}_\parallel)\boldsymbol{\mathcal{E}}_j^{a_j}(\mathbf{q}_\parallel) = \frac{2a_{j+1}\sqrt{\varepsilon_j\varepsilon_{j+1}}\alpha_{j+1}(\mathbf{p}_\parallel)}{\varepsilon_{j+1}-\varepsilon_j}\boldsymbol{\mathcal{E}}_{j+1}^{a_{j+1}}(\mathbf{p}_\parallel). \tag{4.3}$$

Here $\mathbf{p}_\parallel$ is an arbitrary vector in the plane of the interface, and $\boldsymbol{\mathcal{E}}_j^a(\mathbf{q}_\parallel) = (\mathcal{E}_{j,p}^a(\mathbf{q}_\parallel),\mathcal{E}_{j,s}^a(\mathbf{q}_\parallel))^{\mathrm{T}}$ denotes a column vector of the polarization components of the field amplitude in medium j. The matrix $\mathbf{M}_{l,m}^{b,a}(\mathbf{p}_\parallel|\mathbf{q}_\parallel)$ is a 2×2 matrix which originates from a change of coordinate system between the local polarization basis $(\hat{\mathbf{e}}_{p,l}^b(\mathbf{p}_\parallel),\hat{\mathbf{e}}_s(\mathbf{p}_\parallel))$ and $(\hat{\mathbf{e}}_{p,m}^a(\mathbf{q}_\parallel),\hat{\mathbf{e}}_s(\mathbf{q}_\parallel))$, defined for $a=\pm$, $b=\pm$ and $l,m\in\{j,j+1\}$ such that $l\neq m$ as

$$\mathbf{M}_{l,m}^{b,a}(\mathbf{p}_\parallel|\mathbf{q}_\parallel) = \sqrt{\varepsilon_1\varepsilon_2}\,\frac{\omega^2}{c^2}\begin{pmatrix}\hat{\mathbf{e}}_{p,l}^b(\mathbf{p}_\parallel)\cdot\hat{\mathbf{e}}_{p,m}^a(\mathbf{q}_\parallel) & \hat{\mathbf{e}}_{p,l}^b(\mathbf{p}_\parallel)\cdot\hat{\mathbf{e}}_s(\mathbf{q}_\parallel)\\ \hat{\mathbf{e}}_s(\mathbf{p}_\parallel)\cdot\hat{\mathbf{e}}_{p,m}^a(\mathbf{q}_\parallel) & \hat{\mathbf{e}}_s(\mathbf{p}_\parallel)\cdot\hat{\mathbf{e}}_s(\mathbf{q}_\parallel)\end{pmatrix}. \tag{4.4}$$

The kernel scalar factor $\mathcal{J}_{l,m}^{b,a}(\mathbf{p}_\parallel|\mathbf{q}_\parallel)$ encodes the surface geometry and is defined as

$$\mathcal{J}_{l,m}^{b,a}(\mathbf{p}_\parallel|\mathbf{q}_\parallel) = \big(b\alpha_l(\mathbf{p}_\parallel)-a\alpha_m(\mathbf{q}_\parallel)\big)^{-1} \times\int\mathrm{d}^2x_\parallel\exp\Big[-i(\mathbf{q}_l^b(\mathbf{p}_\parallel)-\mathbf{q}_m^a(\mathbf{q}_\parallel))\cdot(\mathbf{x}_\parallel+\zeta_j(\mathbf{x}_\parallel)\hat{\mathbf{x}}_3)\Big], \tag{4.5}$$

where we have again used several definitions from Eqs. (3.11). The interface profile function $\zeta(\mathbf{x}_\parallel)$, and thereby also any information regarding the interface roughness, enters Eq. (4.3) solely through the kernel scalar factor. The numerator in Eq. (4.5) is called the *I-integral* in some of the papers included in this thesis.

In Eq. (4.3) the field amplitude under the integral is the amplitude in medium j. We will see later that this equation therefore is best suited for the calculation of *reflection* amplitudes. However, due to the symmetry in the boundary conditions [21] one may also show that

$$\sum_{a_{j+1}=\pm}\int\frac{\mathrm{d}^2q_\parallel}{(2\pi)^2}\,\mathcal{J}_{j,j+1}^{a_j,a_{j+1}}(\mathbf{p}_\parallel|\mathbf{q}_\parallel)\mathbf{M}_{j,j+1}^{a_j,a_{j+1}}(\mathbf{p}_\parallel|\mathbf{q}_\parallel)\boldsymbol{\mathcal{E}}_{j+1}^{a_{j+1}}(\mathbf{p}_\parallel) = \frac{2a_j\sqrt{\varepsilon_j\varepsilon_{j+1}}\alpha_j(\mathbf{p}_\parallel)}{\varepsilon_j-\varepsilon_{j+1}}\boldsymbol{\mathcal{E}}_j^{a_j}(\mathbf{p}_\parallel), \tag{4.6}$$

which is similar to Eq. (4.3) but with an interchange of j and $j+1$. Equation (4.6) is best suited for the calculation of *transmission* amplitudes.

Equations (4.3) and (4.6) can be combined to represent transfers of plane waves through systems made up of an arbitrary number of layers. In Ref. 5 this is done for a film geometry in such a way that the field amplitudes in the film itself becomes implicit in the equations, enabling the calculation of reflection and transmission amplitudes from the system as a whole. In the following we will keep the equations as general as practically possible with respect to the two system geometries mentioned in Secs. 3.1.2 and 3.1.3, but in order to maintain readability we will primarily discuss the single interface case. For specifics on the equations related to film geometries, see Refs. 3 and 5 (included in this thesis).

4.2.2 The incident field, reflection and transmission

The way they stand, Eqs. (4.3) and (4.6) offer no unique solutions for the field amplitudes in either medium. We have assumed that we can satisfy the boundary conditions at an (infinite) interface through an expansion in plane waves, where we include both propagating and non-propagating waves. A suitable constraint on the equations is needed, and in our case we achieve this by introducing a simple plane wave as our incident field. Under the Rayleigh hypothesis we may assume this plane wave to be the *only* plane wave *approaching* the interface, forcing all other field amplitudes to describe plane waves *leaving* the interface. This is a significant simplification, which is only valid for weakly rough interfaces as discussed in Sec. 4.1.

In our investigations we define the following incident field, a plane wave incident in medium 1:

$$\mathbf{E}_0(\mathbf{x}) = \left[\mathcal{E}_{0,p}\,\hat{\mathbf{e}}^-_{p,1}(\mathbf{k}_\parallel) + \mathcal{E}_{0,s}\,\hat{\mathbf{e}}_s(\mathbf{k}_\parallel)\right] \exp\left(\mathrm{i}\mathbf{k}^-_1(\mathbf{k}_\parallel)\cdot\mathbf{x}\right), \tag{4.7}$$

where $\mathbf{k}^-_1$ is the wave vector of the incident plane wave and $\mathbf{k}_\parallel$ is its projection onto the plane of the mean interface. We now ensure that this incident plane wave is the *only* wave approaching the rough interface in our model by defining the field amplitudes

$$\mathcal{E}^-_1(\mathbf{q}_\parallel) = (2\pi)^2\delta(\mathbf{q}_\parallel - \mathbf{k}_\parallel)\mathcal{E}_0 \tag{4.8a}$$

$$\mathcal{E}^+_2(\mathbf{q}_\parallel) = \mathbf{0}, \tag{4.8b}$$

where $\mathcal{E}_0 = (\mathcal{E}_{0,p}, \mathcal{E}_{0,s})^{\mathrm{T}}$. We would like to reiterate on an important point: the Rayleigh hypothesis is explicitly invoked when we now assume that it is

physically correct still, even after the above assumptions, to use Eqs. (4.3) and (4.6).

Now, in the current context we are not as interested in the field amplitudes as we are in the *ratios* of the field amplitudes, and to this end we assume that the scattered field amplitudes are linearly related to the incident field amplitude $\mathcal{E}$ via the reflection and transmission amplitudes. These are $\mathbf{R}(\mathbf{q}_\parallel|\mathbf{k}_\parallel)$ and $\mathbf{T}(\mathbf{q}_\parallel|\mathbf{k}_\parallel)$ from Sec. 3.2.3, defined as

$$\boldsymbol{\mathcal{E}}_1^+(\mathbf{q}_\parallel) = \mathbf{R}(\mathbf{q}_\parallel|\mathbf{k}_\parallel)\boldsymbol{\mathcal{E}}_0 \tag{4.9a}$$

$$\boldsymbol{\mathcal{E}}_t^-(\mathbf{q}_\parallel) = \mathbf{T}(\mathbf{q}_\parallel|\mathbf{k}_\parallel)\boldsymbol{\mathcal{E}}_0, \tag{4.9b}$$

where we recall from Sec. 3.2.3 that the amplitude matrices $\mathbf{R}$ and $\mathbf{T}$ essentially tell us how the scattered field originating from an incident plane wave with wavenumber $\mathbf{k}_\parallel$ is reflected and transmitted, respectively. Under the assumptions made so far and when the incident field is known, the scattering amplitude $\mathbf{R}$ ($\mathbf{T}$) completely specifies the field above (below) the maximum (minimum) point on the first (last) interface.

These amplitudes are the unknowns we seek, since they easily can be converted into physically observable quantities like the mean differential reflection and transmission coefficients (MDRC/MDTC), as presented in Sec. 3.3.1.

4.2.3 The Reduced Rayleigh Equations

We are now ready to obtain the final equations of interest, relating the geometry, materials and incident plane wave to *either* the reflection *or* transmission amplitudes directly. In order to obtain the reflection amplitudes for a single rough interface, we merely choose $a_{j+1} = a_2 = +$ in Eq. (4.3) and apply the assumptions given by Eqs. (4.8) and (4.9). If we are interested in the transmission amplitudes for a single rough interface we choose $a_j = a_1 = -$ in Eq. (4.6) and again apply the assumptions given by Eqs. (4.8) and (4.9). The end result is the *reduced Rayleigh equations* (RREs), two decoupled integral equations which for $\mathbf{X} = \mathbf{R}$ or $\mathbf{T}$ can be written in the following form:

$$\int \frac{\mathrm{d}^2 q_\parallel}{(2\pi)^2}\, \mathbf{M}_\mathbf{X}(\mathbf{p}_\parallel|\mathbf{q}_\parallel)\mathbf{X}(\mathbf{q}_\parallel|\mathbf{k}_\parallel) = -\mathbf{N}_\mathbf{X}(\mathbf{q}_\parallel|\mathbf{k}_\parallel), \tag{4.10}$$

where in the current notation the matrices $\mathbf{M_X}$ and $\mathbf{N_X}$ are given by

$$\mathbf{M_R}(\mathbf{p}_\parallel|\mathbf{q}_\parallel) = \mathcal{J}^{+,+}_{2,1}(\mathbf{p}_\parallel|\mathbf{q}_\parallel)\mathbf{M}^{+,+}_{2,1}(\mathbf{p}_\parallel|\mathbf{q}_\parallel) \tag{4.11a}$$

$$\mathbf{M_T}(\mathbf{p}_\parallel|\mathbf{q}_\parallel) = \mathcal{J}^{-,-}_{1,2}(\mathbf{p}_\parallel|\mathbf{q}_\parallel)\mathbf{M}^{-,-}_{1,2}(\mathbf{p}_\parallel|\mathbf{q}_\parallel) \tag{4.11b}$$

$$\mathbf{N_R}(\mathbf{p}_\parallel|\mathbf{q}_\parallel) = \mathcal{J}^{+,-}_{2,1}(\mathbf{p}_\parallel|\mathbf{q}_\parallel)\mathbf{M}^{+,-}_{2,1}(\mathbf{p}_\parallel|\mathbf{q}_\parallel) \tag{4.11c}$$

$$\mathbf{N_T}(\mathbf{p}_\parallel|\mathbf{q}_\parallel) = \frac{2\sqrt{\varepsilon_1\varepsilon_2}\alpha_1(\mathbf{p}_\parallel)}{\varepsilon_2 - \varepsilon_1}(2\pi)^2\delta(\mathbf{p}_\parallel - \mathbf{q}_\parallel)\mathbf{I}_2, \tag{4.11d}$$

where $\mathbf{I}_2$ is the 2×2 identity matrix.

Within the Rayleigh hypothesis and the validity of the expansion of the fields in plane waves, Eq. (4.10) is the exact equation for the scattering amplitudes for an arbitrary surface profile. It is valid also for a multilayer system, like the film system described in Sec. 3.1.3, used in Ref. 3. However, multiple interfaces will increase the complexity of the matrices given in Eq. (4.11), even if still only one of the multiple interfaces is non-planar.

4.2.4 Taylor expansion of $\mathcal{J}$

The kernel factor $\mathcal{J}^{b,a}_{l,m}$, as given in Eq. (4.5), is only practical to solve analytically for a limited variety of interface profile functions $\zeta_j(\mathbf{x}_\parallel)$. It contains a so-called Fourier integral, and the oscillating integrands necessitates careful evaluation [42, p. 693]. In order to facilitate a numerical solution of the RREs for randomly rough interface profiles we therefore need a more accessible form of this kernel factor. The most common approach, which is also a critical part of the most common perturbative solution of the RREs, is to expand the kernel factor in an infinite Taylor series about the Fourier transforms of the power of a given interface profile function ζ_j:

$$\mathcal{J}^{b,a}_{l,m}(\mathbf{p}_\parallel|\mathbf{q}_\parallel) = \gamma^{b,a}_{l,m}(\mathbf{p}_\parallel|\mathbf{q}_\parallel)\int \mathrm{d}^2x_\parallel\, \mathrm{e}^{-\mathrm{i}(\mathbf{p}_\parallel-\mathbf{q}_\parallel)\cdot\mathbf{x}_\parallel}\, \mathrm{e}^{-\mathrm{i}\gamma^{b,a}_{l,m}(\mathbf{p}_\parallel|\mathbf{q}_\parallel)\zeta_j(\mathbf{x}_\parallel)} \tag{4.12a}$$

$$= \sum_{n=0}^{\infty} \frac{(-\mathrm{i})^n}{n!}\left[\gamma^{b,a}_{l,m}(\mathbf{p}_\parallel|\mathbf{q}_\parallel)\right]^{n-1}\hat{\zeta}^{(n)}_j(\mathbf{p}_\parallel - \mathbf{q}_\parallel) \tag{4.12b}$$

where we have defined

$$\gamma^{b,a}_{l,m}(\mathbf{p}_\parallel|\mathbf{q}_\parallel) = b\alpha_l(\mathbf{p}_\parallel) - a\alpha_m(\mathbf{q}_\parallel), \tag{4.13}$$

and $\hat{\zeta}_j^{(n)}$ represents the Fourier transform of the n^{th} power of ζ_j, similar to Eq. (3.4):

$$\hat{\zeta}_j^{\,(n)}(\mathbf{Q}_\parallel) = \int \mathrm{d}^2 x_\parallel \, \mathrm{e}^{-\mathrm{i}\mathbf{Q}_\parallel \cdot \mathbf{x}_\parallel} \, \zeta_j^n(\mathbf{x}_\parallel)$$
$$\hat{\zeta}_j^{\,(0)}(\mathbf{Q}_\parallel) = (2\pi)^2 \, \delta(\mathbf{Q}_\parallel). \tag{4.14}$$

It should be noted that the Taylor expansion in Eq. (4.12b) requires that $|\gamma_{l,m}^{b,a}(\mathbf{p}_\parallel|\mathbf{q}_\parallel)\zeta_j(\mathbf{x}_\parallel)| \ll 1$ for the series to converge sufficiently fast. Also, even though this series expansion should then in theory always converge, the oscillatory nature of the series might still prevent numerical convergence when Re $\gamma\zeta < 0$. The end result is that the expansion in Eq. (4.12b) might, in some cases, impose more restrictive constraints on the limits of the interface roughness than the Rayleigh hypothesis itself. An additional point to be made in this regard is that while the Rayleigh hypothesis in essence places a limit on the *slope* of the interface roughness, the practically achievable numerical procedure for evaluating Eq. (4.12b) directly limits the *amplitude* of the interface roughness.

The profile function(s) ζ_j enters the reduced Rayleigh equations *exclusively* through the kernel factors $\mathcal{J}$. Through the Taylor expansion we now also recognize that the RRE, in this form, only sees the Fourier transforms of the profile functions. This fact is well known, and it has had a big impact on the interpretation of scattering phenomena like the ones discussed in this thesis. A direct consequence is that the average of the absolute square of the first order term of the Taylor expansion of $\mathcal{J}$ is directly proportional to the power spectrum [Eq. (3.6)] of the j-th interface. We will soon see that this fact is one of the main lessons taught by small amplitude perturbation theories.

In practice it is not feasible to calculate the sum in Eq. (4.12b) for randomly rough interface profiles to infinite order, and so a truncation of the series is needed. This cutoff and its consequence will be discussed in Secs. 4.5 and 4.5.4.

4.3 Small amplitude perturbation theory

Probably the most common and popular approximate solution of Eq. (4.10) is based on a perturbative expansion of the solutions in the reflection and transmission amplitudes in orders of the interface profile functions [13].

Originally developed by Lord Rayleigh himself at the end of the 19th century [27] for sound waves on sinusoidally corrugated surfaces, the *small amplitude perturbation theory* (SAPT) has shown that it is able to obtain solutions of the RRE of high qualitative and quantitative predictive power, for interfaces with sufficiently small slopes and amplitudes.

The method has a long and rich history, and the details are outside of the scope of this summary. However, some selected pieces of information can be useful. The method is also, in some forms, known as the *small perturbation method* (SPM) or Bragg theory, and the perturbative expansion has also become known as the *Rayleigh method* or the Rayleigh-Rice or Rayleigh-Fano procedure [15]. The early history starts with the work by Lord Rayleigh in 1896, whose method was adapted to the problem of optical gratings by Fano in 1941 [43]. The method was then further developed by Rice in 1951 [44] and 1963 [45]. Navigating the exact history of this collection of methods is challenging, and it can also be difficult to cleanly separate the history of what is by us called the Rayleigh equations, historically the starting point for the RREs, from the perturbative expansions of these equations. Overall it is clear that there are "many roads to Rome", and what is most important for the current work is the assumptions and methods we have used in order to arrive at the reduced Rayleigh equations presented as Eq. (4.10).

We showed how the kernel factors $\mathcal{J}$ can be expanded in a Taylor series in the preceding section. The basic principle of the method is then to expand the unknown reflection and transmission amplitudes in similar series:

$$\mathbf{R}(\mathbf{q}_\parallel|\mathbf{k}_\parallel) = \sum_{n=0}^{\infty} \frac{(-\mathrm{i})^n}{n!} \mathbf{R}^{(n)}(\mathbf{q}_\parallel|\mathbf{k}_\parallel) \tag{4.15a}$$

$$\mathbf{T}(\mathbf{q}_\parallel|\mathbf{k}_\parallel) = \sum_{n=0}^{\infty} \frac{(-\mathrm{i})^n}{n!} \mathbf{T}^{(n)}(\mathbf{q}_\parallel|\mathbf{k}_\parallel), \tag{4.15b}$$

and then match terms of corresponding order in $\zeta(\mathbf{x}_\parallel)$, based on Eq. (4.12b). As an example of the end result, the reflection amplitude for a single interface system to first order in $\zeta(\mathbf{x}_\parallel)$ is

$$\mathbf{R}(\mathbf{q}_\parallel|\mathbf{k}_\parallel) \approx \mathbf{R}^{(0)}(\mathbf{q}_\parallel|\mathbf{k}_\parallel) - \mathrm{i}\mathbf{R}^{(1)}(\mathbf{q}_\parallel|\mathbf{k}_\parallel), \tag{4.16}$$

$$\tag{4.17}$$

where

$$\mathbf{R}^{(0)}(\mathbf{q}_\parallel|\mathbf{k}_\parallel) = (2\pi)^2 \delta(\mathbf{q}_\parallel - \mathbf{k}_\parallel) \boldsymbol{\rho}^{(0)}(\mathbf{k}_\parallel) \tag{4.18a}$$

$$\mathbf{R}^{(1)}(\mathbf{q}_\parallel|\mathbf{k}_\parallel) = \hat{\zeta}(\mathbf{q}_\parallel - \mathbf{k}_\parallel) \boldsymbol{\rho}^{(1)}(\mathbf{q}_\parallel|\mathbf{k}_\parallel). \tag{4.18b}$$

In the expression for $\mathbf{R}^{(0)}(\mathbf{q}_\parallel|\mathbf{k}_\parallel)$, $\boldsymbol{\rho}^{(0)}$ is a diagonal matrix containing the zero-order reflection amplitudes, essentially describing the expected reflection amplitude for a system with all-planar interfaces. For a single interface system, $\boldsymbol{\rho}^{(0)}$ therefore contains the well known Fresnel amplitudes[1], and the delta-term ensures that light is reflected in the specular direction only. The average of the absolute square of the first order term, given in Eq. (4.18b), is clearly directly proportional to the power spectrum [Eq. (3.6)] of the interface profile function. It also depends on the matrix $\boldsymbol{\rho}^{(1)}$, which in this case is given by

$$\begin{aligned}\boldsymbol{\rho}^{(1)}(\mathbf{q}_\parallel|\mathbf{k}_\parallel) =&(\alpha_1(\mathbf{q}_\parallel) - \alpha_2(\mathbf{q}_\parallel)) \left[\mathbf{M}^{+,+}_{2,1}(\mathbf{q}_\parallel|\mathbf{q}_\parallel)\right]^{-1} \\ &\times \left[\mathbf{M}^{+,-}_{2,1}(\mathbf{q}_\parallel|\mathbf{k}_\parallel) + \boldsymbol{\rho}^{(0)}\mathbf{M}^{+,+}_{2,1}(\mathbf{q}_\parallel|\mathbf{k}_\parallel)\right]. \end{aligned} \tag{4.19}$$

We will not discuss this expression here, but refer to the papers included in this thesis where the constituents of SAPT, and especially the first order terms, have been investigated in great detail. The papers included as Refs. 2 and 4 feature derivations of SAPT where the notation is less scattering system agnostic, and therefore is made simpler by fewer indices in the equations.

To first order in $\zeta(\mathbf{x}_\parallel)$ for the reflection and transmission amplitudes, this perturbative method is often interpreted as a *single scattering approximation*. From a physical point of view, it has been common to interpret this first order term as the diffuse contribution to the scattering intensity, while the second order term, usually negative, describes the intensity diminution of the specular intensity caused by the surface roughness [39]. When implemented to the complete fourth order for the intensity, i.e. involving terms up to third order in the amplitude, the method has been used to obtain reliable results that also correctly include multiple scattering effects, most notably the backscattering peaks observed in reflection from metallic surfaces [7, 46–48].

This specific perturbative method has been of great aid in the interpretations of several scattering phenomena, and has played a central part in most of the work included in this thesis. To first order in $\zeta(\mathbf{x}_\parallel)$, SAPT is easy to decompose mathematically. This fact has enabled its use as a tool in the understanding of the underlying mechanisms that lead to a wide range of scattering phenomena, but with some slippery limitations – even for weakly rough interfaces. In passing, we note that our work has indicated that SAPT to first order is not a *complete* description of so-called

[1]The Fresnel power coefficients for air-glass interfaces are illustrated in Fig. 5.1.

single scattering processes, usually interpreted as wave-surface interactions (for interfaces with planar average roughness) that involve a single transfer of momentum $\mathbf{Q}$. SAPT to first order indicates that the scattering distributions are proportional to the power spectrum $g(\mathbf{Q}_{\|})$, and as such it represents an excellent approximation, but not a complete description, of single scattering phenomena.

When SAPT is utilized to get an approximation for the reflection and transmission amplitudes, the most important requirement on the scattering system is that the diffuse component of the scattered light is small [14]. The more exact limits of validity of the method are themselves diffuse, and a full discussion will not be given here. SAPT is in general safe to utilize for sufficiently weakly rough interfaces, for example characterized by the Rayleigh parameter – a value proportional to the ratio of roughness heights to the incident wave length [13]. In this sense the method and its dependence on the Rayleigh hypothesis can also be seen as a low frequency asymptotic solution to the scattering problem. Some selected sources for quantitative discussions on validity are Millar [49–51], Wirgin [52, 53], Soto-Crespo, Friberg and Nieto-Vesperinas [54] and Sánchez-Gil, Mendez and Maradudin [55].

4.4 Phase perturbation theory

Contrary to the case for SAPT, in *phase perturbation theory* (PPT) it is the *phase* of the scattered field that is calculated perturbatively as an expansion in powers of the interface profile function $\zeta(\mathbf{x}_{\|})$ [40, 56, 57]. In essence, the implementation of the method leads to the scattering amplitudes being written as a product between the equivalent planar system Fresnel coefficients and an exponential function of the interface profile function. It is then the exponent in the latter factor that is calculated perturbatively. Interestingly, even in the lowest non-zero order of this expansion phase perturbation theory yields results that represent an infinite summation of some subset of terms in SAPT [55, 58].

As an example of PPT, we will show the expansion to first non-zero order in reflection, similar to what we did in the previous section. In order to be consistent with the work done in Ref. 1, we to this end introduce the well

known *scattering matrix* $\mathbf{S}(\mathbf{q}_\parallel|\mathbf{k}_\parallel)$, given by

$$\mathbf{S}(\mathbf{q}_\parallel|\mathbf{k}_\parallel) = \frac{\sqrt{\alpha_1(q_\parallel)}}{\sqrt{\alpha_1(k_\parallel)}}\mathbf{R}(\mathbf{q}_\parallel|\mathbf{k}_\parallel). \tag{4.20}$$

It is clear that the scattering matrix is closely related to the reflection amplitudes $\mathbf{R}(\mathbf{q}_\parallel|\mathbf{k}_\parallel)$. The perturbative expansion then takes on the following form:

$$\mathbf{S}(\mathbf{q}_\parallel|\mathbf{k}_\parallel) = \sum_{n=0}^{\infty} \frac{(-\mathrm{i})^n}{n!}\mathbf{S}^{(n)}(\mathbf{q}_\parallel|\mathbf{k}_\parallel), \tag{4.21}$$

$$\tag{4.22}$$

where $\mathbf{S}^{(n)}(\mathbf{q}_\parallel|\mathbf{k}_\parallel)$ depends on orders of $\mathbf{R}^{(n)}(\mathbf{q}_\parallel|\mathbf{k}_\parallel)$ as given by Eq. (4.20) but order-by-order. The elements of $\mathbf{S}^{(n)}$ for s-polarized incident light reflected into s-polarized scattered light to first order, for a system with a single rough interface and where $\varepsilon_1 = 1$, are [1]:

$$S_{ss}^{(0)}(\mathbf{q}_\parallel|\mathbf{k}_\parallel) = (2\pi)^2\delta(\mathbf{q}_\parallel - \mathbf{k}_\parallel)\frac{\alpha_1(k_\parallel) - \alpha_2(k_\parallel)}{\alpha_1(k_\parallel) + \alpha_2(k_\parallel)} \tag{4.23a}$$

$$\begin{aligned} S_{ss}^{(1)}(\mathbf{q}_\parallel|\mathbf{k}_\parallel) = 2(1-\varepsilon_2)\left(\frac{\omega}{c}\right)^2 (\hat{\mathbf{q}}_\parallel \cdot \hat{\mathbf{k}}_\parallel)\hat{\zeta}(\mathbf{q}_\parallel - \mathbf{k}_\parallel) \\ \times \frac{\alpha_1^{1/2}(q_\parallel)\alpha_1^{1/2}(k_\parallel)}{[\alpha_1(q_\parallel) + \alpha_2(q_\parallel)][\alpha_1(k_\parallel) + \alpha_2(k_\parallel)]}. \end{aligned} \tag{4.23b}$$

The full derivation of PPT to second order in $S_{ss}(\mathbf{q}_\parallel|\mathbf{k}_\parallel)$ is given in Ref. 1, where the theory is used to successfully obtain a wide range of system parameters through an inversion of light-scattering data.

4.5 Non-perturbative solution of the RREs

Solving the reduced Rayleigh equations in a direct manner, without resorting to perturbation theory, has repeatedly proved to be a valuable compromise between the less computationally demanding low-order perturbative approach and the fully rigorous approach based on the extinction theorem [7]. This non-perturbative method is the main tool of investigation in several of the papers included in this thesis, and the continued development and extension of the corresponding simulation code RAYLEIGH2D [25] is one of the main outputs of the thesis work.

Many details regarding the practical and actual implementation in software for obtaining non-perturbative solutions of the RRE(s), Eq. (4.10), can be found in Ref. 25. We still find it appropriate to summarize here some selected aspects of the implementation used in obtaining the results presented in this thesis, both for convenience and completeness, but also because the capabilities of the software has been extended since the publication of Ref. 25.

4.5.1 Summary of the numerical method

In order to solve the RRE in a non-perturbative manner, we begin by generating one realization of the interface profile function $\zeta_j(\mathbf{x}_\parallel)$ for each interface j in the system. This is done using the Fourier filtering method [11] on a square grid of $N_x \times N_x$ surface points, covering an area of $S = L^2$ in the $(\hat{\mathbf{e}}_1, \hat{\mathbf{e}}_2)$-plane. These profile functions enter Eq. (4.10) through the functions $\mathcal{J}^{b,a}_{l,m}(\mathbf{p}_\parallel|\mathbf{q}_\parallel)$, which is implemented utilizing the Taylor expansion detailed in Sec. 4.2.4 [2] as Eq. (4.12b). On evaluating these kernel scalar factors $\mathcal{J}^{b,a}_{l,m}(\mathbf{p}_\parallel|\mathbf{q}_\parallel)$, we first expand the integrand in powers of $\zeta_j(\mathbf{x}_\parallel)$, truncate this expansion after N_T terms, and integrate the resulting sum term-by-term. The Fourier integral of $\zeta^n_j(\mathbf{x}_\parallel)$ that remains now only depends on the interface profile function and the difference in lateral wave vectors $\mathbf{p}_\parallel - \mathbf{q}_\parallel$, and not on $\alpha_l(\mathbf{p})$ and $\alpha_m(\mathbf{q})$. These Fourier integrals are therefore calculated only once, on a $\mathbf{p}_\parallel - \mathbf{q}_\parallel$ grid, for every interface realization by the use of the fast Fourier transform [42, p. 600]. A typical value for N_T is 20, since this truncation marks a practical limit in the calculation of the factorial function to single precision and this number of terms guarantees convergence for the roughness parameters assumed in the current work [36].

On evaluation of the $\mathbf{q}_\parallel$ integral in Eq. (4.10), the infinite limits of integration are replaced by the finite limits $|\mathbf{q}_\parallel| = \sqrt{q_1^2 + q_2^2} \leq \mathcal{Q}/2$, and the integration is carried out by a two-dimensional version of the extended midpoint rule [42, p. 161]. The finite limits of integration forms a circular subsection of a grid of $N_q \times N_q$ points in the q_1q_2-plane, whose size and discretization is determined by the Nyquist sampling theorem [42, p. 605] and the properties of the discrete Fourier transform [25]. In momentum space, these considerations in short lead to discretization intervals of $\Delta q = 2\pi/L$ along the orthogonal axes of the q_1q_2-plane, and upper limits on the magnitude

[2] The reason why this expansion is vital for the current numerical method is explained in detail in Ref. 25.

of resolved wave vectors are given by $\mathcal{Q} = \Delta q \lfloor N_x/2 \rfloor$, where $\lfloor \cdot \rfloor$ denotes the floor function [59, p. 948]. A more detailed description of the derivation of these limits, and the chosen discretization of all variables, can be found in Ref. 25.

The resulting linear system of equations is solved by LU factorization and back substitution [42, p. 48]. These calculations are then typically performed simultaneously for incident light of both p- and s-polarization, and are performed for a large number N_p of realizations of the model (new realizations of the interface profile functions $\zeta_j(\mathbf{x}_\parallel)$). The resulting scattering amplitude $\mathbf{X}(\mathbf{q}_\parallel|\mathbf{k}_\parallel)$ and its squared modulus $|\mathbf{X}(\mathbf{q}_\parallel|\mathbf{k}_\parallel)|^2$, where X is either $\mathbf{R}$ or $\mathbf{T}$, were obtained for each realization. An arithmetic average of the N_p results for these quantities then yield the mean values $\langle \mathbf{X}(\mathbf{q}_\parallel|\mathbf{k}_\parallel)\rangle$ and $\langle |\mathbf{X}(\mathbf{q}_\parallel|\mathbf{k}_\parallel)|^2\rangle$ that enter Eq. (3.17) and similar for estimates of the observables of interest.

In passing we note that the various combinations of the scattering amplitudes $\mathbf{X}$ that are necessary for the full calculation of the Mueller matrix [24] are also obtained in a trivial manner from the non-perturbative method. All the information about the polarization transformations light undergoes when scattered from rough surfaces is contained in the Mueller matrix, and these matrices were obtained in full for all systems investigated in this thesis.

An example of a typical result is presented in Fig. 4.1, showing results from Ref. 5 where the upper half of each subfigure was obtained using SAPT to first non-trivial order, and the lower half was obtained using the non-perturbative method described in this section. It is clear from the figure that there is some noise in the latter results, stemming from the fact that we average over a limited number of realizations of the randomly rough interfaces.

4.5.2 Computational requirements and limitations

For the interested reader, this section is an attempt at a mention of some of the practical aspects of the use of the non-perturbative RRE method on current hardware, with some added thoughts on the computational limits relevant for the method.

In the majority of the presented work, the non-perturbative solutions of the RRE have been obtained using the software “Rayleigh2D”, implemented in FORTRAN and compiled with a recent Intel compiler. The main depen-

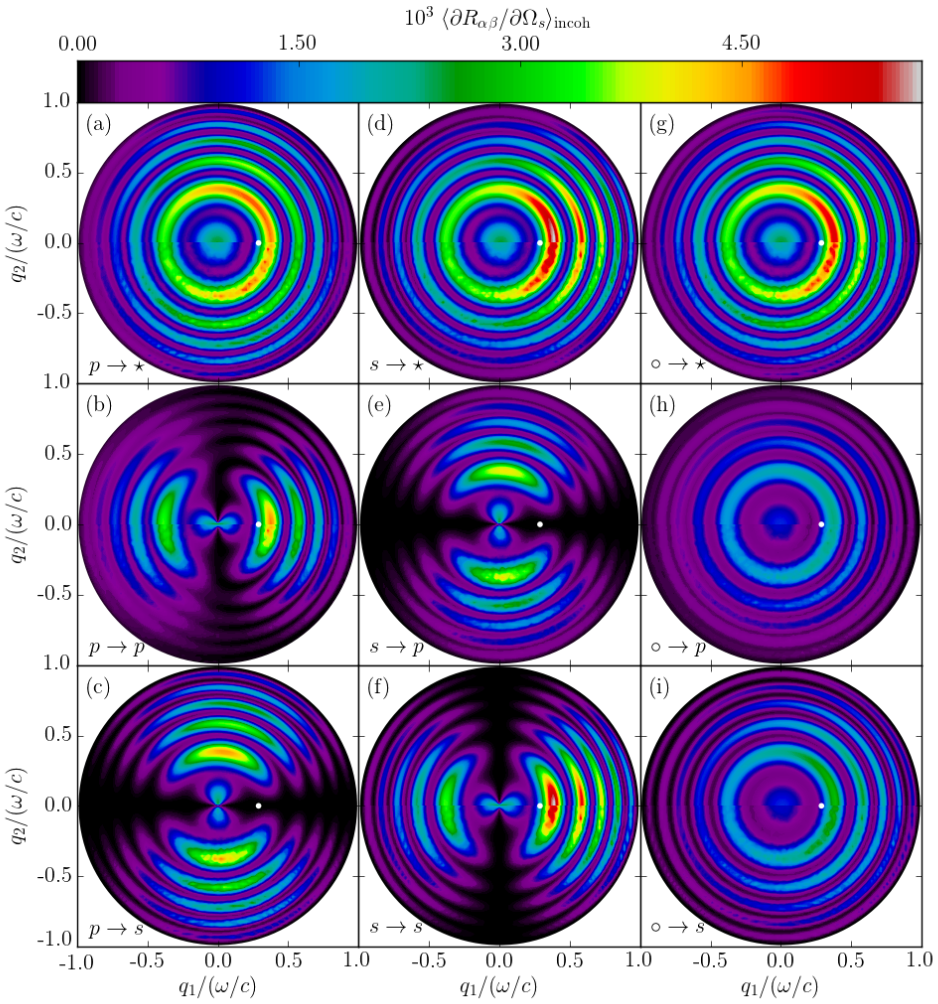

Figure 4.1: The full angular distribution of the incoherent component of the mean DRC, $\langle \partial R_{\alpha\beta}/\partial\Omega_s \rangle_{\rm incoh}$, as function of the lateral wave vector $\mathbf{q}_\parallel$ of the light that is scattered from a rough film where the top interface is rough and the other interface of the film is planar. The light of wavelength $\lambda = 632.8$ nm was incident from vacuum on the rough photoresist film supported by a silicon substrate [$\varepsilon_1 = 1.0$, $\varepsilon_2 = 2.69$, $\varepsilon_3 = 15.08 + 0.15$i]. The rms-roughness of the rough film interface was $\sigma_1 = \lambda/30$, $\sigma_2 = 0$. The surface-height correlation length was $a = 211$nm $= \lambda/3$, the film thickness was $d = 5062.4$nm $= 8\lambda$ and the angles of incidence were $(\theta_0, \phi_0) = (16.8°, 0°)$ for all panels. The positions of the specular directions in reflection are indicated by white dots. The upper halves of all panels are results from the small amplitude perturbation method to leading order, while the lower halves show results obtained through the non-perturbative solutions of the RRE. The sub-figures in Figs. 4.1(a)–(i) are organized in the same manner and show how incident β-polarized light is scattered by the one-rough-interface film geometry into α-polarized light [with $\alpha = p, s$ and $\beta = p, s$] and denoted $\beta \to \alpha$. The full figure caption and details can be found in the paper included as Ref. 5.

dencies were resolved through the use of OpenMPI [60] or Intel MPI for inter-process communication, a parallel version of HDF5 [61] for efficient data storage, Intel Math Kernel Library (MKL) for fast Fourier transforms (FFTs) and the MKL-contained version of ScaLAPACK [62] for efficient LU-decomposition and back-substitution in parallel. Post-processing of the results were accomplished with the use of Python. The Norwegian (NOTUR) national HPC (High Performance Computing) systems "Vilje" and "Stallo", both CPU-based, were used for all computations.

In practice the limiting factor in the numerical solution of the RRE is the number of wave vectors we solve for, mainly due to the associated memory requirements but also the computational load. For our circular domain of integration and N_q wave vectors along each of the two q-axes, the total number of wave vectors in the system is $\approx (\pi/4)N_q^2$. In the case of a single rough interface, irrespective of whether a film geometry is present, the computational requirement for solving the RRE scales with N_q^4 [25]. The aggressive computational scaling of the problem is one of the reasons why numerical solutions of the RRE for two-dimensional interfaces have been available only in the last decade or so.

The time spent on obtaining results for a single system realization are split between two parts: the set-up process of obtaining the matrices involved in the RRE (Eq. (4.10)) and the solving of the resulting linear system of equations using the LU (non-iterative) method. These two processes are of different nature. The set-up part has the property of being "embarrassingly" parallel, meaning that inter-process communication is near-zero across the distributed computing resource. It therefore scales perfectly with increasing parallelism, and the requirement on available memory is minimal since the matrix elements are computed one at a time. The other process, that of solving the linear system of equations, naturally requires the entire linear system to be contained in (distributed) memory for efficient LU-decomposition. For scattering systems where only one interface is randomly rough and the other interfaces, if any, are planar, the practical limitations on the use of the non-perturbative RRE method on systems of size and resolution typical for the papers included in this thesis ($161 < N_q < 225$) are equally split between the two parts, with single-precision memory requirement for the second part at 20-70GB. However, when we employ the non-perturbative RRE method on systems with multiple rough interfaces the computational requirements on the set-up part increases significantly. For the system used in Ref. 5 when both interfaces are rough, almost all CPU-time required in obtaining results for a single system realization is spent in the set-up part

of the problem. A very small system where $N_q = 51$ already requires CPU-time corresponding to $N_q \approx 200$ for a single-rough interface system. In this situation we are therefore not memory limited, and the problem might be much better suited for GPU-based hardware.

Rigorous methods for obtaining the scattering amplitudes and other observables exist, for relevance to the current work the best known such methods are based on the *extinction theorem*. These methods normally make *no approximations* in their modeling of the scattering problem, and are as such only limited by the finite capabilities of computational hardware. These limits are, however, even today severely limiting what systems may be investigated using this class of methods. An example is the study of far-propagating surface plasmon polaritons for weakly rough interfaces. In modeling such a study the non-rigorous method of this chapter may handle vastly larger systems than corresponding exact methods. To this end the non-perturbative solution of the RRE serves to bridge the gap in the possibilities offered by rigorous methods on one side and simple perturbative methods on the other [7].

4.5.3 Notes on some numerical challenges

Alpha-cancellation

Given the practical and efficient implementation of the software for the non-perturbative solution of the RRE, the magnitudes of the lateral vectors $\mathbf{p}_\parallel, \mathbf{q}_\parallel$ and $\mathbf{k}_\parallel$ are all discretized as the midpoint of N_q intervals on the same numerical grid ranging from $[-\mathcal{Q}, \mathcal{Q}]$. In the calculation of Eq. (4.12b) we divide by the factor γ given by Eq. (4.13), which in turn is a difference in values of the normal wave vector components α. These are given by

$$\begin{aligned}\alpha_j(\mathbf{q}_\parallel) &= \sqrt{\varepsilon_j \frac{\omega^2}{c^2} - {q_\parallel}^2} \\ &= \sqrt{\varepsilon_j \frac{\omega^2}{c^2} - (n_1^2 + n_2^2)\Delta q^2},\end{aligned} \tag{4.24}$$

where n_1 and n_2 denotes the indices of some value of $\mathbf{q}_\parallel$ in the numerical grid it is resolved on. The equation above clearly shows that the difference in α given as the factor γ may very well become zero, even for differing values of ε_j. In the current implementation of Rayleigh2D this issue is avoided through the addition of a random value smaller than $\varepsilon_j/10^4$ to ε_j.

Film thickness induced instabilities

When the system of interest is a multi-layered system, as in Refs. 3, 5 and as described for a film system in Sec. 3.1.3, the RRE will always contain factors $\exp(-\mathrm{i}\alpha_2(\mathbf{q}_\parallel)d)$ or $\exp(-\mathrm{i}\alpha_2(\mathbf{p}_\parallel)d)$ where medium 2 is the film medium and d is the film thickness. Numerically, these factors tend to lead to instabilities since their values may grow exponentially for evanescent waves inside the film. This technical issue is resolved by using the following two ideas: (i) expanding the two terms in the kernels (i.e. for $a_2 = \pm$) and factorizing out the troublesome exponential factor and canceling it on both sides of the reduced Rayleigh equation (if the exponential factor is a function of the variable $\mathbf{p}_\parallel$) or (ii) making a change of variable such that the troublesome exponential factor is absorbed into the reflection or transmission amplitudes (if the exponential factor is a function of the variable $\mathbf{q}_\parallel$). One may also shift the x_3-axis in order to facilitate the aforementioned steps. We chose here not to give more details on the explicit implementation, as these modifications are to be done in a case by case basis depending on which surface is planar and whether the reflected or transmitted light is considered.

The exact thickness limits depend on the materials in the system, but the ideas mentioned in the above allowed us to model films with thickness sufficient for the analysis of the Selényi phenomenon in Ref. 5.

4.5.4 Accuracy of the non-perturbative Rayleigh method

The reduced Rayleigh equations rely on a number of approximations and assumptions, most of which have already been discussed. The non-perturbative method of solving the RRE also introduces a number of limitations and approximations. The aim of this section is to obtain a more organized overview over (most) of these. To that end we start with an itemized list over the main talking points:

- The plane wave expansion
- The Rayleigh hypothesis
- Expansion method used for the I-integral,
- Truncation of the Taylor expansion of the I-integral
- Finite size of the rough interface, $L \times L$

- Discretization of the integrals in the RRE over $\mathbf{q}_{\parallel}$
- Finite cut-off in the sum over q (circular region in wave-space)

The plane wave expansion and the implications of the Rayleigh hypothesis have already been discussed in a fair amount of detail, especially in Sec. 4.1. Conservation of energy, as explained in Sec. 3.4, was verified to be satisfactory in all results presented in this thesis.

Solving the I-integrals, Eq. (4.5), by the use of the Fourier method in addition to a Taylor series expansion has fairly important implications on the limits of validity of the current approach to the solution of the RRE. These implications were discussed in Sec. 4.2.4.

As we adhere to the Nyquist limit in our transitions from real space to wave space, a finite sized interface of area $L \times L$ and discretization Δx is intimately linked to the limits in wave space $\pm\mathcal{Q}$ and its discretization Δq, as explained in Sec. 4.5.1. Details regarding these relations are given in Ref. 25. The discretization of the RRE main integrals into sums, in addition to the truncation of these sums, can be expected to introduce some numerical inaccuracy, and possibly errors, into the solutions of the RRE. Physically, the scattering amplitudes $\mathbf{X}(\mathbf{q}_{\parallel}|\mathbf{k}_{\parallel})$ are expected to approach zero as $\mathbf{q}_{\parallel}$ enters the evanescent region. However, for certain geometries and materials these evanescent waves may couple into guided modes and/or surface plasmon polaritons, observable as localized peaks in the scattering amplitudes. We therefore have to make sure that the the limit $\mathcal{Q}$ is large enough to include these phenomena. In all results presented in this thesis, the stability of the results were verified both for an increase in system size and decrease in sampling interval.

In conclusion, as long as we choose systems with sufficient size and discretization for (i) the statistical properties of the interfaces to be valid, (ii) the results to be free from edge-effects and (iii) the limit $\mathcal{Q}$ in wave space to be large enough that evanescent waves of physical importance are included, we may assume that the finite size of the system will still provide results that mimic an infinite system.

Chapter 5

Physical phenomena in scattering from dielectric weakly rough interfaces

We have in the preceding chapters developed some models and methods that might be used to investigate a range of light scattering systems, both theoretically and numerically. Although these models and methods are more than means to an end, the main motivation for developing them was to investigate a selection of little studied light scattering phenomena. This chapter will introduce the phenomena most novel and important in the thesis papers, and will be kept brief since the basic exploration of these phenomena is an actual part of the papers themselves.

When light is scattered in either reflection or transmission from or through a single weakly and randomly rough dielectric interface, two phenomena of interest stand out in the observation of the scattering intensity distributions for the diffusely scattered light. These are the *Yoneda phenomenon*, relatable to the idea of total internal reflection, and the *Brewster scattering phenomenon*, relatable to the polarizing angle. These two phenomena have only been studied to a very limited extent in the past. The exploration and investigation of these phenomena are at the core of the papers included in this thesis, since they together explain most, if not all, deviations in the presented results from more "standard" scattering investigations of systems consisting of incidence in vacuum and a metallic substrate. These phenom-

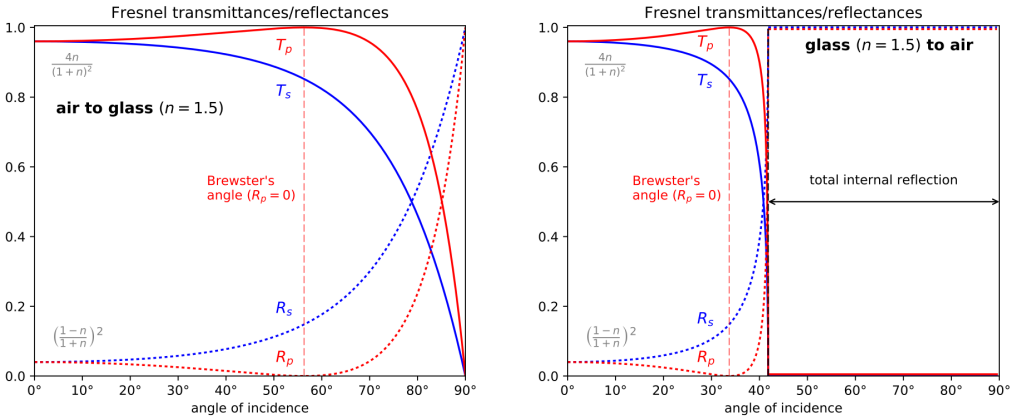

Figure 5.1: Fresnel power coefficients in transmission and reflection. [Left] Air-to-glass interface. [Right] Glass-to-air interface. By Sbergjohansen [CC BY-SA 4.0], via Wikimedia Commons.

ena also explain some interesting and semi-novel behaviors in the scattering interference phenomenon known as "Selényi rings", which we will also introduce in this chapter.

5.1 The Brewster scattering phenomenon

When light is scattered by a randomly rough surface it is well known that the *polarization* of the incident light influences the angular distribution of the diffusely scattered light. Why is that? We will in this section introduce the *Brewster scattering phenomenon* for diffusely scattered light, which fully answers the question, at least for weakly rough dielectric systems. This phenomenon is intimately related to the well-known Brewster angle for planar surfaces, so we will start with a summary of this high-school topic before we return to the Brewster scattering phenomenon.

> "When a pencil of light is incident upon a transparent body at an angle, whose tangent is equal to the index of refraction, the reflected portion will be either wholly polarized, or the quantity of polarized light which it contains will be a maximum.
>
> — Sir David Brewster (1815)

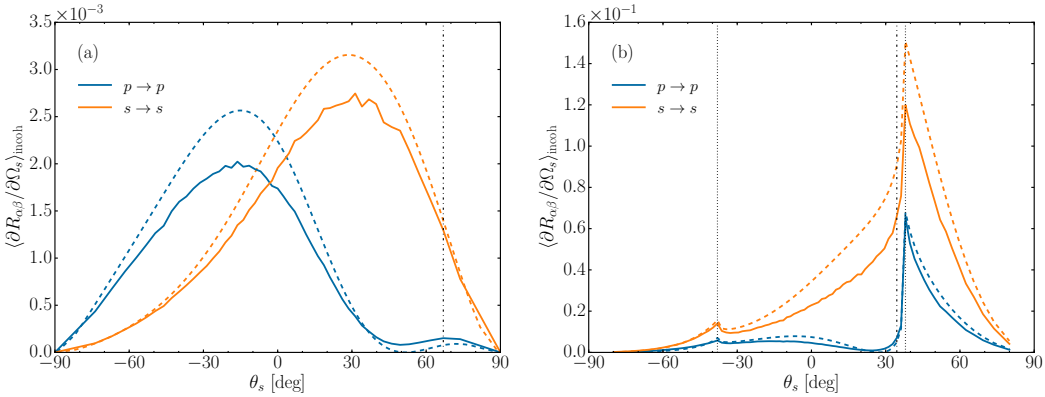

Figure 5.2: The contribution to the incoherent component of the MDRC from the in-plane, co-polarized scattering of p- and s-polarized light incident on (a) a random vacuum-dielectric interface [$\varepsilon_1 = 1.0$, $\varepsilon_2 = 2.64$] at the angle $\theta_0 = 66.9°$ and (b) a dielectric-vacuum interface [$\varepsilon_1 = 2.64$, $\varepsilon_2 = 1.0$] at the angle $\theta_0 = 34.5°$ as a function of the polar angle of scattering θ_s. The solid curves were obtained on the basis of numerically solving the reduced Rayleigh equations, Eq. (4.10), for an ensemble of 4500 surface realizations. The dashed curves are results from small amplitude perturbation theory, Eq. (4.17). The specular direction of reflection is in each figure indicated by a vertical dash-dotted line, and in Fig. 5.2(b), the dotted lines at $|\theta_s| = \theta_c = \sin^{-1}\sqrt{\varepsilon_2/\varepsilon_1} \approx 38.0°$ indicate the positions of the critical angle for total internal reflection (as expected for a flat surface system). Full figure description can be found in the paper included as Ref. 2.

The Brewster angle, also called the polarizing angle, is commonly defined to be the angle of incidence of light onto a planar, dielectric surface for which the specularly reflected light is linearly s-polarized[1]. For light that is incident on a planar non-exotic dielectric surface, the boundary-condition physics represented by the Brewster angle phenomenon is the *only* source of differences in how s- and p-polarized light are reflected and transmitted. This difference is easy to explore through the Fresnel coefficients, for convenience illustrated in Fig. 5.1 since they are central to the work presented in this thesis. Somewhat more surprising to some is that a complete physical understanding of the Brewster phenomenon is, at best, non trivial. The most common explanation for the gradual disappearance of the reflection amplitude for p-polarized light is based on the radiation pattern of dipoles induced in the scattering substrate [64, 65]. This idea is not new, and can be traced back to investigations by e.g. Sommerfeld [66]. A better understand-

[1]The exact definition compatible with exotic materials and modern physics however, is a matter of slight debate [63].

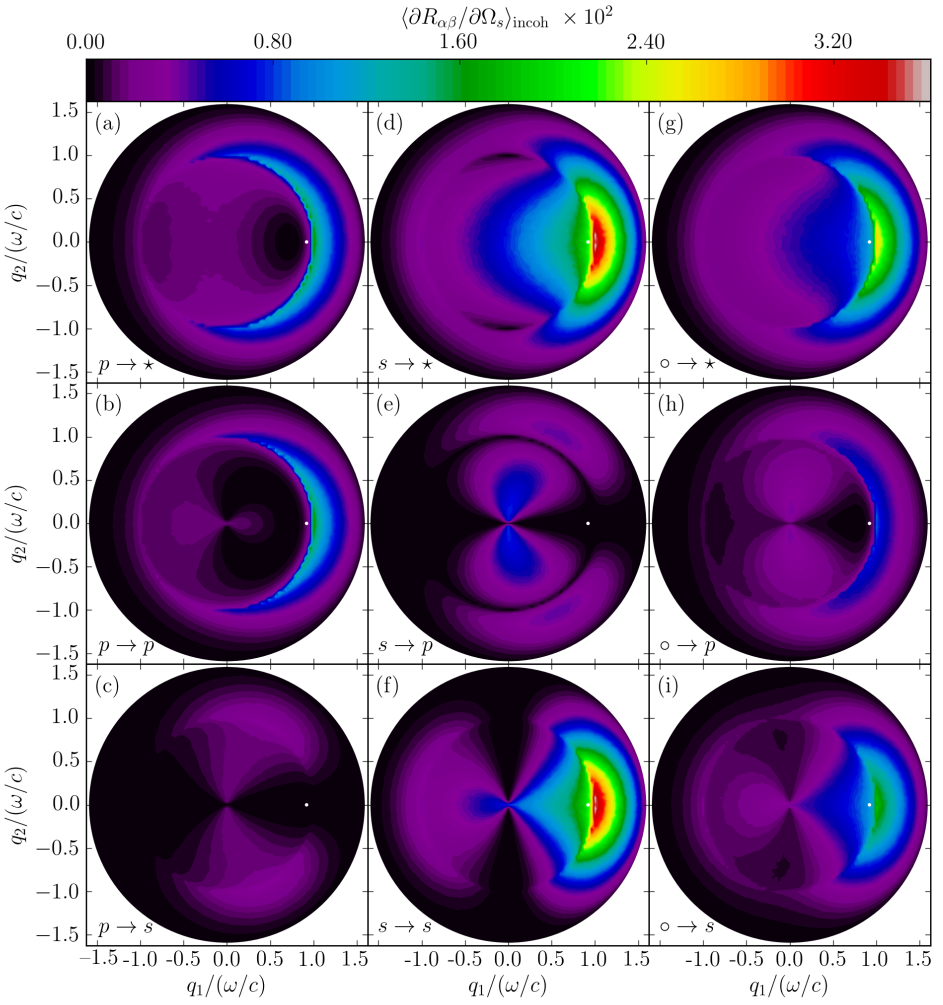

Figure 5.3: The full angular dependence of the contribution to the incoherent component of the MDRC from the scattering of p- and s-polarized light incident on a random dielectric-vacuum interface [$\varepsilon_1 = 2.64$, $\varepsilon_2 = 1.0$] at the angle $\theta_0 = 34.5°$. Figure 5.2(b) consists of in-plane cuts through panels (b) and (f) in this figure. For a brief description of the figure structure, see Fig.4.1. Full figure description can be found in the paper included as Ref. 2.

ing of the physics behind the well known Brewster phenomenon turns out to be a vital part of understanding the scattering distributions of diffuse light discussed in-depth in our paper included as Ref. 6. A more detailed account of the interesting century long journey to understand the phenomenon can be found there.

It has been known for a long time that the scattering distributions for light scattered from randomly rough dielectric surfaces are different for light of different (linear) polarization, a main characteristic being partial suppression of p-polarized scattered light for a wide range of scattering angles. To our knowledge it was still not until Kawanishi *et al.* [67] observed angles of zero scattering intensity to first order in their approach for p-polarized light that a phenomenon central to this difference got a name. Due to these angles' resemblance to the Brewster angle in the reflectivity from a planar interface, Kawanishi *et al.* dubbed these angles the "Brewster *scattering* angles". These angles were observed in both reflection *and* transmission, for light incident from either medium. While Kawanishi *et al.* emphasized the dip to *zero* scattering intensity, we have chosen to expand the terminology somewhat in the current work. By Brewster scattering *angles* we generally mean the angles for which the scattering intensity drops to zero in a *single scattering approximation*. As we include higher-order scattering processes in parts of our work, we have observed that the Brewster scattering angles generally describe local minima rather than dips to zero. In addition, our latest published work [6] shows that the underlying physical origin also underpins all[2] differences between the distributions of p- and s-polarized diffusely scattered light, in the sense that s-polarized light scatters similar to scalar waves contrary to the case for p-polarized light. This has motivated us to use the term "Brewster scattering *phenomenon*" for the broader consequences of the non-scalar-wave diffuse scattering behavior of p-polarized light.

The Brewster scattering phenomenon has been observed and thoroughly discussed in several papers included in this thesis. In Refs. 2 and 4 its impact on scattering distributions from single randomly rough dielectric interfaces is investigated through perturbative and non-perturbative approaches. In this context the impact of the phenomenon is clearly visible, e.g. in the MDRC distributions displayed in Fig. 5.2 for incidence in both vacuum and dielectric. For the angles of incidence used in producing Fig. 5.2 we also clearly observe the Brewster scattering angles themselves, and in Fig. 5.3 we see that these in-plane distributions are part of much more complex

[2]Given the materials and assumptions that work is based on.

and interesting scattering distributions. Figures 5.2 and 5.3 are discussed in-depth in Ref. 2.

While we do not explicitly point it out in "Experimental and numerical studies of the scattering of light from a two-dimensional randomly rough interface in the presence of total internal reflection: optical Yoneda peaks" [3], our comparison between experiment and simulations presented in that paper clearly shows that the real-world consequences of the Brewster scattering phenomenon are accurately captured in our simulations.

For a film geometry we in Ref. 5 claim that the phase shifts associated with the Brewster scattering phenomenon impact the angular positions of interference rings of diffusely scattered light, known as Selényi rings.

Finally, in Ref. 6 we further investigate the phenomenon of Brewster scattering angles and more generally identify the fundamental mechanisms at play in the scattering of polarized light by a weakly rough dielectric surface. We study the Brewster scattering phenomenon for outgoing evanescent waves and circularly-polarized waves, and describe the underpinning physical mechanisms in terms of simple notions such as scalar waves, oscillating and rotating dipoles and geometrical arguments.

In summary, the work included in this thesis attempts to both thoroughly describe and also explain the Brewster scattering phenomenon. While the physical arguments are valid mainly in a single scattering approximation, the computational and experimental results indicate that this understanding might be sufficient for weakly rough interfaces.

5.2 The Yoneda phenomenon

Another phenomenon at the heart of this thesis is what we have come to denote the *Yoneda phenomenon*. It is closely linked with the phenomena commonly known as *total internal and external reflection*, so we will start with a (slightly untraditional) introduction into these phenomena before we continue with Yoneda's 1963 discovery.

5.2.1 Total internal and external reflection

While a well-polished metallic mirror can reflect almost all the visible light that is incident upon it, several technologies we use daily make use of an

even more reflective configuration: the total internal reflection experienced by electromagnetic waves when they are unable to escape the dielectric they propagate in. In its simplest form the dispersion relation (Eq. (2.10), and we will make the same assumptions and simplifications here as were made in deriving that equation) tells us that an electromagnetic wave can only propagate in a certain material if its wavenumber $|\mathbf{k}|$ in that material is proportional to its angular frequency ω. The proportionality factor is given by the material properties through ε and μ, and the speed of light in vacuum c. While the dispersion relation can be expressed in a variety of ways, it basically expresses a forced[3] relation between an electromagnetic wave's oscillations in time and space for a given material and a given energy. When we combine this limitation with the appropriate boundary conditions (e.g. Eq. (3.12b)) valid at an interface between two dielectrics we find that there are limits to which waves are able to propagate across the interface into the other material. When light propagating in a non-magnetic material with permittivity ε_1 is completely reflected from an interface with a material with smaller permittivity ε_2 due to these limitations we call it "total internal reflection". This optical phenomenon has been a cornerstone in many optical technologies for a long time, today exemplified by optical fibers used in high-speed digital communication as well as light guides and reflectors in cameras, displays and LED light sources.

More generally we may say that total reflection is a process that occurs when Snell's law of refraction cannot be solved for real angles. For x-rays most solid materials have a refractive index[4] smaller than unity. Total reflection will then occur as the x-ray impinges on a solid surface from vacuum or similar at grazing angles of incidence, and we therefore call this process total *external* reflection. It is this process that allows us to efficiently focus x-rays in x-ray telescopes [68].

5.2.2 Yoneda peaks and the Yoneda phenomenon

In their original x-ray context, *Yoneda peaks* express themselves as sharp, asymmetric peaks in the rough surface diffuse scattering distributions of x-rays occurring at the critical angle for total external reflection for a fixed angle of incidence. These peaks are notable because they are observed in the *diffusely* scattered light [from an experimental point of view we then observe scattered light for which $\theta_s \neq \theta_0$]. They were first observed exper-

[3] Or natural, depending on the point of view.

[4] For non-magnetic materials the refractive index is $\sqrt{\varepsilon}$.

imentally in the scattering of x-rays incident from air on a metal surface by Y. Yoneda [69] and have subsequently been studied in the context of the scattering of x-rays from both metallic [70–74] and non-metallic [75–78] surfaces, and also for neutrons [71] scattered from rough surfaces.

In an optical context these peaks were first observed as "sidelobes" in the one-dimensional numerical investigations by Nieto-Vesperinas and Sánchez-Gil [79]. These authors did not at the time associate the observation with Yoneda peaks, and did not pursue the observation. The peaks were then later described as "quasi-anomalous scattering peaks" and were thoroughly investigated in the work by Kawanishi *et al.* [67] based on the stochastic functional approach [80]. Kawanishi *et al.* studied the coherent and incoherent scattering of an electromagnetic wave from a two-dimensional randomly rough interface separating two different dielectric media. The light could be incident on the interface from either medium. Yoneda peaks, albeit more spread out than they were in the x-ray experiments, were observed in the angular dependence of the intensity of the light scattered into the optically more dense medium. Their observations therefore showed that the peaks could appear in both reflection and transmission. As an interpretation of their results, the authors suggested that the Yoneda peaks may be associated with the presence of lateral waves [81] propagating along the interface in the optically less dense medium. There have been several other contributions to the physical interpretation of the Yoneda peaks, especially in the x-ray context, in the past. We provide a short overview over these in the paper included as Ref. 2.

The peaks observed for $\theta_s \geq \theta_c$ in Fig. 5.2(b) where $\varepsilon_1 > \varepsilon_2$ are examples of optical analogues of the Yoneda peaks observed in reflection by Y. Yoneda in the scattering of x-rays. The Yoneda peaks were originally observed in x-ray scattering as sharp peaks for incidence close to the grazing angle, as the difference in the dielectric constants of the two scattering media is very small at x-ray frequencies. In our optical work, by Yoneda *peaks* we mean well-defined maxima in the angular distribution of the intensity of the scattered light at, or slightly above, the critical polar angle for total reflection, when $\varepsilon_1 > \varepsilon_2$. In our work on the interpretation of these peaks we also found it necessary to expand this terminology somewhat, since film interference effects and similar makes the use of the word "peaks" too ambiguous. Irrespective of the polarization of the incident and scattered light, what we have termed the *Yoneda phenomenon* is characterized as an enhancement of the intensity of the diffuse light when the light is observed in the optically denser medium. The intensity enhancement occurs above a critical angle

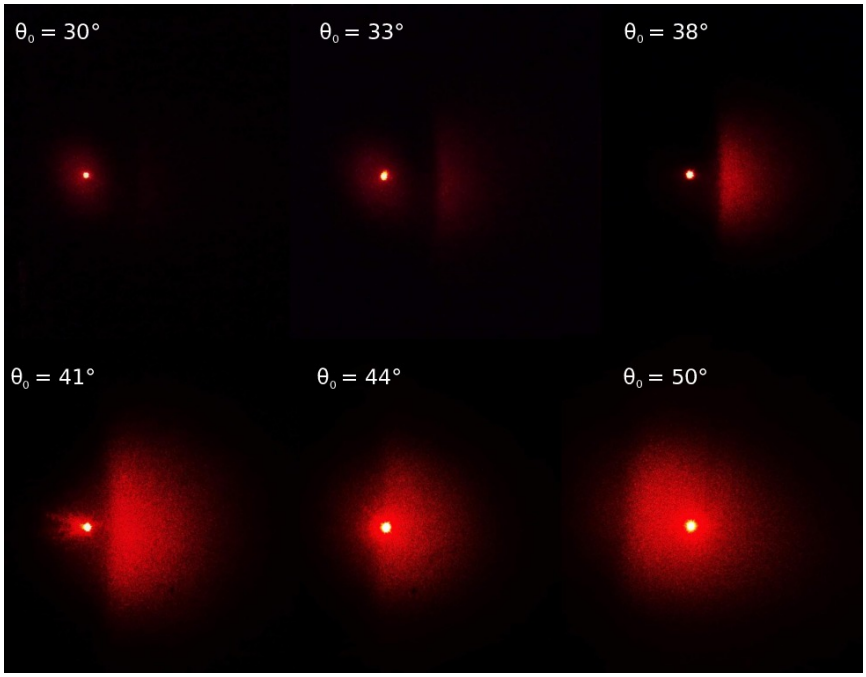

Figure 5.4: Photographs showing the spatial intensity distributions formed on a screen [see Fig. 6 in Ref. 3] for a set of polar angles of incidence, θ_0, as indicated in the figure. See full explanation in the text and in Ref. 3.

of scattering which is independent of the angle of incidence of the excitation. This critical angle is always the polar angle, in the denser medium, for which the wavenumber of a plane wave turns non-propagating in the less dense medium [2, 4]. The scattering distributions in Fig. 5.3 serve as good illustrations of the need for the more general terminology. Since the angle of incidence ($\theta_0 = 34.5°$) is close to the critical polar angle of total internal reflection (for a corresponding flat surface system) it is easy to observe both the Yoneda peaks and the bigger intensity enhancement regions.

Figure 5.4, from the paper included as Ref. 3, shows a purely experimental demonstration of the Yoneda phenomenon as a photo of a scattering intensity distribution. While the full experimental set-up is described in the paper, what we see is at first (top left) only the laser specular reflection peak as a point of high intensity, and some diffusely (incoherently) reflected light surrounding it. The laser has been reflected from a randomly rough dielectric interface in such a way that the scattering we see mimics internal reflection in a dense medium. In the figure, the angle of scattering increases

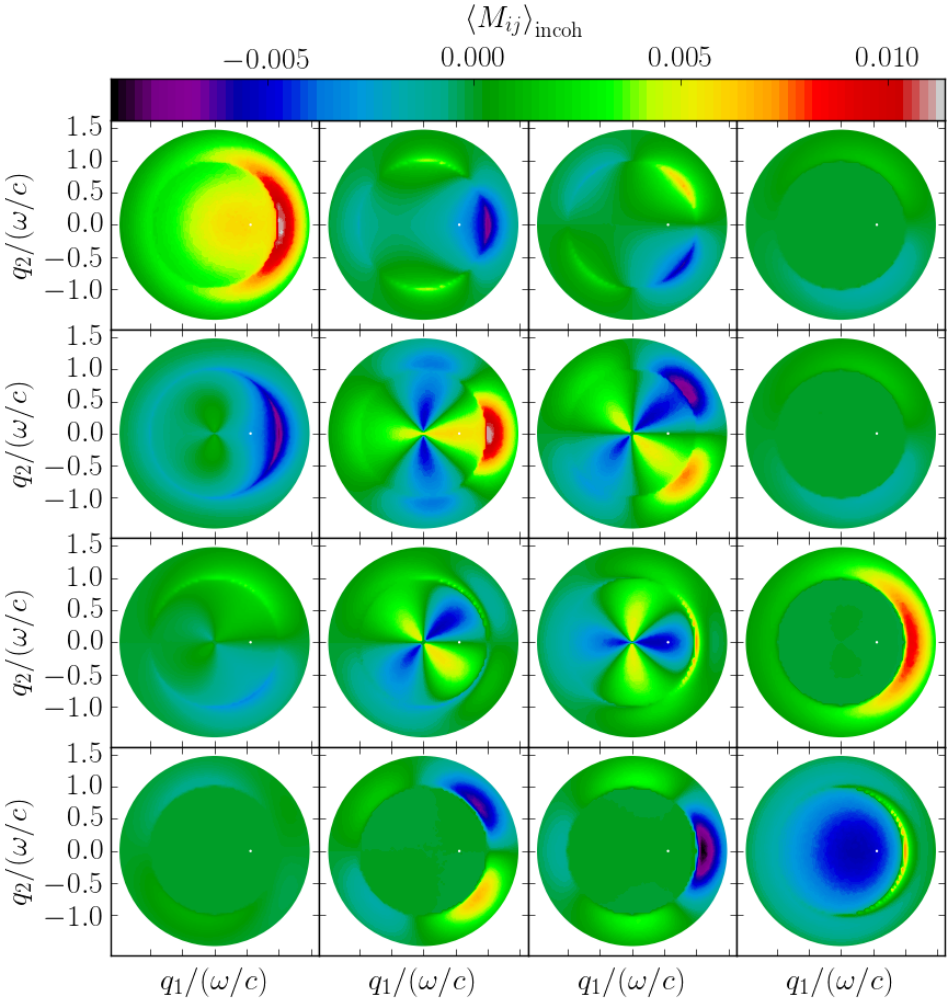

Figure 5.5: The full angular distribution of the Mueller matrix for the scattering of p- and s-polarized light incident on a randomly rough dielectric-vacuum interface [$\varepsilon_1 = 2.64$, $\varepsilon_2 = 1.0$] at the angle $(\theta_0, \phi_0) = (34.5°, 0°)$. The scattering system is identical to the one in Fig. 5.3. The calculation of the Mueller matrix elements is done according to the method described in detail in Ref. 24.

to the right in each subfigure. Therefore, what we observe at the right side in e.g. the subfigure for $\theta_0 = 38°$ is the sudden intensity enhancement in the diffusely reflected light due to the Yoneda phenomenon. For a full explanation of the figure, and the underlying distributions which the photograph is roughly depicting, see Ref. 3. In this paper we present the first experimental demonstration of the optical Yoneda phenomenon in reflection together with matching simulations based on the reduced Rayleigh equations.

A big emphasis in the papers included with this thesis has been on the role of polarization in the light scattered by rough surfaces. It is well known that all the information about the polarization properties of light scattered from two-dimensional rough surfaces is contained in the Mueller matrix [82–84]. Even if none of the current thesis papers explicitly utilize the Mueller matrix, it is still of interest, especially in order to inspire further work, to present an example of all the elements of the Mueller matrix for diffusely scattered light subject to the phenomena of both Brewster scattering and Yoneda enhancement. Figure 5.5 presents such an example, for the system assumed in obtaining the results presented in Figs. 5.2(b) and 5.3. The calculation of the Mueller matrix elements is done according to the method described in detail in Ref. 24.

We thoroughly study the behaviors and consequences of the Yoneda phenomenon in our work included as Refs. 2–6, and the discussions contained in those papers will not be repeated here. However, it may be of interest to summarize our conclusions from the analysis in Ref. 6, since we there claim that the Yoneda phenomenon can be understood through a very simple hypothesis. Through a factorization of a first order perturbative solution to the RREs into a scalar component and a polarization component, we show that the phenomenon results from a so-called single scattering mechanism, and that it is not associated with surface (eigen) modes. The phenomenon is explainable through a pure scalar wave approach, as an intensity enhancement induced by the evanescence of one out of two components making up a scattered couple mode (representing a single wavenumber). All the energy allocated to a given couple mode is then radiated away by the component existing in the denser medium. As such, the phenomenon can be seen as a continuous analogue of a Rayleigh anomaly for periodic dielectric gratings.

5.3 Selényi rings

When we observe rainbow-like color play in soap bubbles or in oil spills on water this is due to thin-film interference effects in the mainly coherently reflected light. We all observe these and other consequences of light interference from time to time. Less well known to most of us are similarly perceived interference effects that occur in the light scattered *diffusely* from some film-like system; specifically the scattering of light from a slightly rough, thin dielectric layer overlying a reflective surface. Roughly speaking, the rough film-like system gives a multitude of different optical paths that the light can traverse before it leaves the system. These paths introduce different phase factors to the scattered light, which results in interference effects that can be observed as bright and dark rings, or sections of rings.

These interference effects actually have a long and rich history [85]. They were formally first described in modern times as "colorful rings" in the diffusely scattered light originating from a dusty back-silvered mirror by Newton [86], and are today best known as Quételet-rings [87] and Selényi-rings [88]. Both kinds of "rings" have a long history of scientific investigation, maybe because they were considered somewhat unavoidable (even unwanted) in any optical system that involved reflecting surfaces [85]. Today we have learned to deal with these phenomena wherever they are unwanted, but they have still received renewed interest due to numerous applications in modern optics [89].

An example of a non-laboratory situation where one may observe the Quételet rings is in light reflections from bodies of water if appropriate algae are present on the water surface. Another is in the image of a strong light source as it is reflected from the surface of a cup of hot tea (or similar). This phenomenon, modeled as a thin layer of spherical scatterers suspended on a reflecting planar surface, was investigated (in a recommended read) by Suhr and Schlichting [90].

The Selényi rings can behave quite differently from their Quételet siblings, but the transition between the two phenomena is somewhat gradual and not well defined. In a theoretical study of the scattering from one-dimensional randomly rough surfaces ruled on dielectric films on perfectly conducting substrates, Lu *et al.* [91] concluded that the degree of surface roughness had the biggest impact on which of the two mentioned interference phenomena could be observed. The patterns in the diffusely scattered light were shown to undergo a transition, with increasing surface roughness, from an inten-

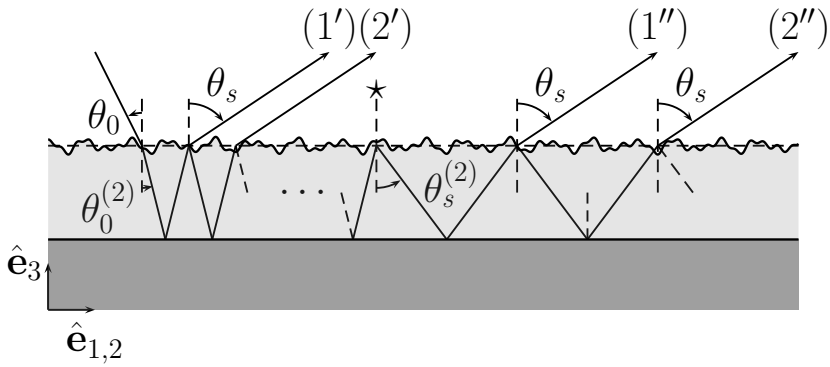

Figure 5.6: Sketch of some of the optical paths involved in the single scattering model in the case of scattering from a randomly rough film system. The light is incident from the top left. In this optical path approximation the light may interact with the film interfaces in a variety of ways, giving rise to rich interference patterns in the diffusely scattered light. See the discussion associated with Fig. 4 in Ref. 5 for a full figure caption and explanation.

sity pattern exhibiting fringes whose angular positions are independent of the angle of incidence (Selényi rings) to one with fringes whose angular positions depend on the angle of incidence (Quételet rings) and eventually into a fringeless pattern with a backscattering peak, which is a signature of multiple scattering [7]. Although the Selényi rings are centered around the mean surface normal, with their position being independent of the angle of incidence, their amplitude, however, is modulated by the angle of incidence.

Figure 4.1 shows the scattering intensity distributions via the MDRC for light scattered from a weakly and randomly rough dielectric film ruled on top of a silicon substrate, with the Selényi rings clearly visible. For simulation method comparison the upper half of each subfigure is obtained through small amplitude perturbation theory (SAPT), while the lower halves are results from full non-perturbative solutions of the RREs. The polar angle of incidence is 16.8° (the white dot indicate the specular reflective peak), but we observe that the rings are still centered around the mean surface normal even if more than half of the scattered intensity is now going into the forward direction (the right half of each subfigure). The figure is from the paper included as Ref. 5, where we continue the work of Lu *et al.* and others in the interpretation of the interference ring phenomenon. We also explore the previously unexplored case when the rough surface is shifted to the non-incident face of the film. According to the traditional understanding of the Selényi rings, their main origin is due to the interference between

light scattered back directly from the top scattering layer and light reflected by the film after being scattered within it. Our studies indicate that this explanation seems to hold true, but only if one carefully considers all possible optical paths (in a single scattering model) both before and after any given scattering event inside and outside the film [5]. However, when we do so we obtain a simple model that is able to exactly predict both the angular positions of the rings and the expected difference in contrast of the rings for film geometries where either the top or the bottom interface of the film is rough. Figure 5.6 shows some of the optical path alternatives that are included in the full model described in Ref. 5.

In the context of this thesis, the exploration of the Selényi interference phenomenon requires all the before mentioned optical phenomena and methods. Building an understanding and a complete single scattering model for the film geometry is made possible through the numerical and analytical results from SAPT, and higher-order effects are considered using the non-perturbative solutions of the RREs with the necessary consideration of the numerical challenges presented in Sec. 4.5.3. Since these are rough dielectric films, both the Yoneda and Brewster scattering phenomena also affect the interference patterns.

Chapter 6

Conclusions and future work

To understand and predict the diffuse scattering of electromagnetic waves through randomly rough surfaces is a relevant problem in many branches of science and engineering. In summary, we have in this thesis investigated the scattering of polarized light from two-dimensional randomly rough dielectric interfaces in order to look for scattering patterns of interest in the angular intensity distributions of the diffusely scattered light. The basis for our investigations has been the so-called reduced Rayleigh equations and their numerical solutions. Our overall scientific contribution is an increased understanding of diffuse scattering from randomly rough surfaces, especially for three-dimensional systems where we allow for cross-polarized scattering. This can be useful in a wide range of optical systems, since the non-invasive method of surface characterization through the analysis of scattering data is interesting for both industry and research.

The Fresnel equations are remarkable in their ability to predict exactly the specular reflectivity and transmissivity of planar interfaces between dielectric media. They accurately describe the three optical phenomena we all learn in high school: refraction, total internal reflection and Brewster's angle (polarizing angle). Largely considered to be manifestations of the wave properties of light, the consequences of these phenomena surround us even if no real surface or interface is perfectly planar. In addition, these phenomena serve as fundamental tools in the optical characterization of any dielectric. When light is scattered diffusely in both reflection and transmission from weakly and randomly rough dielectric interfaces, we find two scattering phenomena that are strongly linked with their more classical cousins. These are

the *Yoneda phenomenon*, relatable to the idea of total internal reflection, and the *Brewster scattering phenomenon*, relatable to the polarizing angle. These scattering phenomena have only partially been investigated in the past, and their study has been the core of this thesis.

The Yoneda phenomenon is characterized as an enhancement of the intensity of the light scattered diffusely by a weakly and randomly rough interface between two dielectric media when the light is observed in the optically denser medium. The intensity enhancement occurs above a critical angle of scattering which is independent of the angle of incidence of the excitation. This critical angle is always the polar angle, in the denser medium, for which the wavenumber of a plane wave turns non-propagating in the less dense medium.

The Brewster scattering phenomenon is characterized by directions for which we observe zero, or near-zero, scattered intensity in either the diffusely reflected or diffusely transmitted p-polarized light. These scattering angles depend on the angle of incidence. A consequence of the directionality of electromagnetic fields, the Brewster scattering phenomenon has been shown to represent the major difference in the scattering distributions of diffusely scattered s- and p-polarized light.

In this thesis we have investigated these phenomena thoroughly through perturbative and non-perturbative numerical and theoretical work [2, 4], also with the aid of new experimental results [3]. We have shown, described, explained and predicted the behavior of both phenomena based on a lowest non-zero order perturbative approach, and as such we have concluded that they are so-called single-scattering phenomena. We have also investigated the physical mechanisms that underpin these phenomena, and have attempted to describe them in terms of simple notions such as scalar waves, oscillating and rotating dipoles and geometrical arguments [6].

For a system of randomly rough dielectric film configurations on a substrate, we have also investigated the appearance of *Selényi interference rings* in the diffusely reflected and transmitted light [5]. We showed how the interference rings can be explained using simple sums of optical paths, and provided a more complete model than what is currently available in the literature. This work also ties in with the Yoneda and Brewster scattering phenomena, since they explain some of the observed results. Theory was developed and presented that can treat an arbitrary number of rough interfaces in a stack, which is a system configuration that can often be found naturally. This theory was employed numerically to show how the interface roughness cross-

correlation between two interfaces may selectively enhance and attenuate the Selényi rings.

Lastly, when medium interfaces are randomly rough, it is of value if we can infer the statistical properties of the roughness along with the properties of the scattering media based purely on the non-invasive scattering of light. Through the use of numerical phase perturbation theory based on the reduced Rayleigh equations, we investigated the reconstruction of such properties through a minimization method based on the reflected intensity distributions [1].

6.1 Directions for further research

What are the exact limitations of the Rayleigh hypothesis? The Rayleigh hypothesis is, and has been, a successful cornerstone in several methods used for the calculation of wave scattering. Although a lot of work has been done towards an understanding of the exact implications of using the Rayleigh hypothesis, there are still several unanswered questions [see Sec. 4.1], especially for randomly rough surfaces. While some aspects of the hypothesis has been discussed in this thesis, a thorough investigation of the Rayleigh equations and hypothesis has recently become available through the PhD thesis of J.-P. Banon [38]. This work is an inspiring step in the direction of a more complete understanding of the Rayleigh hypothesis.

Can the non-perturbative method of solving the RREs employed in this thesis be used effectively also for studying film systems where multiple interfaces are rough? In the paper included as Ref. 5 we investigated light scattering from films with multiple rough interfaces through small amplitude perturbation theory, and this work has also been continued by us for the non-perturbative method. The computational requirements for such an endeavor are very high however, since in short the integral equation kernels become nested. We implemented the possibility of simulating the scattering of light from n-multiple-rough-layered films, but the publication of results based on this expansion of the non-perturbative method will hopefully be part of a future project.

Can the non-perturbative method of solving the RREs be used for simulation of the scattering of surface plasmon polaritons (SPPs) from arbitrarily designed metallic surface roughness? Simulations of the scattering of SPPs incident on various surface bumps and indentations has been done using

a variety of approximate methods in the past [See e.g. Refs. 92–94]. In preliminary work we were able to use the non-perturbative RRE method to recreate some past published results [especially those in Refs. 92 and 94], where our use of fully discretized surface profiles additionally allowed us to perform arbitrary modifications on the roughness profiles. While the results were very interesting, we found it challenging to fully understand the exact interactions between the SPPs and specifics of our implementation of the numerical method. In short, the handling of the incident field becomes more difficult when we want a system with a well-defined SPP incident on a finite surface structure instead of a plane wave incident on the entire surface. It was not possible to include this work in this thesis due to time constraints, but it is an exciting topic for further study.

Can complete Mueller matrices for the incoherently scattered light help us better understand the results discussed in this thesis? While an example of such a Mueller matrix is shown in Fig. 5.5, the insights that these matrix elements provide did not become part of any work published in this thesis. This is in part due to the challenges associated with proper use of this rather complex tool. The complete Mueller matrices are however easily available for all scattering simulations conducted in relation to the current work, and it would be interesting to see what they can provide of further insight into the currently studied phenomena.

Lastly, we mention the concept of the "Depolarization Index" (DI), which was introduced by Gil and Bernabeu in 1985 [95, 96]. It is a single-number metric that can provide interesting insight into the (de)polarizing effect of surface roughness [97]. Calculations of the DI for all scattering angles for some of the systems investigated in this thesis revealed some interesting visual patterns, and might also contribute to a better understanding of rough surface scattering if used in combination with the Mueller matrices.

Bibliography

[1] I. Simonsen, Ø. S. Hetland, J. B. Kryvi, and A. A. Maradudin, "Determination of the normalized-surface-height autocorrelation function of a two-dimensional randomly rough dielectric surface by the inversion of light-scattering data," *Phys. Rev. A*, vol. 93, no. 4, p. 043829, 2016.

[2] Ø. S. Hetland, A. A. Maradudin, T. Nordam, and I. Simonsen, "Numerical studies of the scattering of light from a two-dimensional randomly rough interface between two dielectric media," *Phys. Rev. A*, vol. 93, no. 5, p. 053819, 2016.

[3] A. K. González-Alcalde, J.-P. Banon, Ø. S. Hetland, A. A. Maradudin, E. R. Méndez, T. Nordam, and I. Simonsen, "Experimental and numerical studies of the scattering of light from a two-dimensional randomly rough interface in the presence of total internal reflection: optical Yoneda peaks," *Opt. Express*, vol. 24, no. 23, pp. 25995–26005, 2016.

[4] Ø. S. Hetland, A. A. Maradudin, T. Nordam, P. A. Letnes, and I. Simonsen, "Numerical studies of the transmission of light through a two-dimensional randomly rough interface," *Phys. Rev. A*, vol. 95, no. 4, p. 043808, 2017.

[5] J.-P. Banon, Ø. S. Hetland, and I. Simonsen, "Selective enhancement of Selényi rings induced by the cross-correlation between the interfaces of a two-dimensional randomly rough dielectric film," *Ann. Phys. (N.Y.)*, vol. 389, pp. 352 – 382, 2018.

[6] J.-P. Banon, Ø. S. Hetland, and I. Simonsen, "On the physics of polarized light scattering from weakly rough dielectric surfaces: Yoneda

and Brewster scattering phenomena," *arXiv:1804.07507 (Accepted for publication in Phys. Rev. A)*, 2018.

[7] I. Simonsen, "Optics of surface disordered systems," *Eur. Phys. J.-Spec. Top.*, vol. 181, no. 1, pp. 1–103, 2010.

[8] J. C. Maxwell, "A dynamical theory of the electromagnetic field," *Phil. Trans. R. Soc. Lond.*, vol. 155, p. 459, 1865.

[9] B. Hunt, *The Maxwellians*. Cornell History of Science Series, Cornell University Press, 1991.

[10] J. D. Jackson, *Classical Electrodynamics*. New York: John Wiley & Sons, 3rd ed. ed., 2007.

[11] A. A. Maradudin, T. Michel, A. R. McGurn, and E. Mendez, "Enhanced backscattering of light from a random grating," *Ann. Phys. (N.Y.)*, vol. 203, no. 2, pp. 255 – 307, 1990.

[12] I. Simonsen, J. B. Kryvi, A. A. Maradudin, and T. A. Leskova, "Light scattering from anisotropic, randomly rough, perfectly conducting surfaces," *Comput. Phys. Commun.*, vol. 182, no. 9, pp. 1904 – 1908, 2011.

[13] A. G. Voronovich, *Wave scattering from Rough Surfaces*. Berlin: Springer Verlag, 2nd ed. ed., 1999.

[14] M. Nieto-Vesperinas, *Scattering and Diffraction in Physical Optics*. Singapore: World Scientific Publishing Company, 2nd ed., 2006.

[15] T. M. Elfouhaily and C.-A. Guérin, "A critical survey of approximate scattering wave theories from random rough surfaces," *Wave. Random Media*, vol. 14, no. 4, pp. R1–R40, 2004.

[16] F. Toigo, A. Marvin, V. Celli, and N. R. Hill, "Optical properties of rough surfaces: General theory and the small roughness limit," *Phys. Rev. B*, vol. 15, no. 12, pp. 5618–5626, 1977.

[17] P. P. Ewald, "Zur Begründung der Kristalloptik," *Annalen der Physik*, vol. 354, no. 1, pp. 1–38, 1916.

[18] J. J. Sein, "A note on the Ewald-Oseen extinction theorem," *Opt. Commun.*, vol. 2, no. 4, pp. 170–172, 1970.

[19] D. Pattanayak and E. Wolf, "General form and a new interpretation of the Ewald-Oseen extinction theorem," *Opt. Commun.*, vol. 6, no. 3, pp. 217–220, 1972.

[20] G. Brown, V. Celli, M. Haller, and A. Marvin, "Vector theory of light scattering from a rough surface: Unitary and reciprocal expansions," *Surf. Sci.*, vol. 136, no. 2-3, pp. 381–397, 1984.

[21] A. Soubret, G. Berginc, and C. Bourrely, "Application of reduced Rayleigh equations to electromagnetic wave scattering by two-dimensional randomly rough surfaces," *Phys. Rev. B*, vol. 63, p. 245411, 2001.

[22] T. A. Leskova, P. A. Letnes, A. A. Maradudin, T. Nordam, and I. Simonsen, "The scattering of light from two-dimensional randomly rough surfaces," *Proc. SPIE*, vol. 8172, 2011.

[23] T. Nordam, P. A. Letnes, I. Simonsen, and A. A. Maradudin, "Satellite peaks in the scattering of light from the two-dimensional randomly rough surface of a dielectric film on a planar metal surface," *Opt. Express*, vol. 20, no. 10, pp. 11336–11350, 2012.

[24] P. A. Letnes, A. A. Maradudin, T. Nordam, and I. Simonsen, "Calculation of the mueller matrix for scattering of light from two-dimensional rough surfaces," *Phys. Rev. A*, vol. 86, p. 031803, 2012.

[25] T. Nordam, P. A. Letnes, and I. Simonsen, "Numerical simulations of scattering of light from two-dimensional rough surfaces using the reduced Rayleigh equation," *Front. Phys.*, vol. 1, pp. 1–15, 2013.

[26] T. Nordam, P. A. Letnes, I. Simonsen, and A. A. Maradudin, "Numerical solutions of the Rayleigh equations for the scattering of light from a two-dimensional randomly rough perfectly conducting surface," *J. Opt. Soc. Am. A*, vol. 31, no. 5, p. 1126, 2014.

[27] Lord Rayleigh, *The theory of sound*. London: Macmillan, 1896.

[28] Lord Rayleigh, "On the incidence of aerial and electric waves upon small obstacles in the form of ellipsoids or elliptic cylinders, and on the passage of electric waves through a circular aperture in a conducting screen," *Lond. Edinb. Dubl. Phil. Mag.*

[29] N. R. Hill and V. Celli, "Limits of convergence of the Rayleigh method for surface scattering," *Phys. Rev. B*, vol. 17, pp. 2478–2481, 1978.

[30] J.-J. Greffet, "Scattering of electromagnetic waves by rough dielectric surfaces," *Phys. Rev. B*, vol. 37, no. 11, pp. 6436–6441, 1988.

[31] T. Watanabe, Y. Choyal, K. Minami, and V. L. Granatstein, "Range of validity of the rayleigh hypothesis," *Phys. Rev. E*, vol. 69, p. 056606, 2004.

[32] T. Elfouhaily and T. Hahn, "Rayleigh's Hypothesis and the Geometrical Optics Limit," *Phys. Rev. Lett.*, vol. 97, no. 12, p. 120404, 2006.

[33] A. G. Voronovich, "Rayleigh hypothesis," in *Light Scattering and Nanoscale Surface Roughness* (A. A. Maradudin, ed.), pp. 93–105, Boston, MA: Springer US, 2007.

[34] J. Wauer and T. Rother, "Considerations to Rayleigh's hypothesis," *Opt. Commun.*, vol. 282, no. 3, pp. 339–350, 2009.

[35] A. V. Tishchenko, "Numerical demonstration of the validity of the Rayleigh hypothesis.," *Opt. Express*, vol. 17, no. 19, pp. 17102–17, 2009.

[36] T. Nordam, P. A. Letnes, and I. Simonsen, "Validity of the Rayleigh hypothesis for two-dimensional randomly rough metal surfaces," *J. Phys.: Conf. Ser.*, vol. 454, p. 012033, 2013.

[37] A. V. Tishchenko and A. A. Shcherbakov, "General analytical solution for the electromagnetic grating diffraction problem," *Opt. Express*, vol. 25, no. 12, p. 13435, 2017.

[38] J.-P. Banon, *On the simulation of electromagnetic wave scattering by periodic and randomly rough layered structures based on the reduced Rayleigh equations*. PhD thesis, NTNU – Norwegian University of Science and Technology, 2018.

[39] R. Schiffer, "Reflectivity of a slightly rough surface," *Applied Optics*, vol. 26, no. 4, pp. 704–712, 1987.

[40] D. Winebrenner and A. Ishimaru, "Investigation of a surface field phase perturbation technique for scattering from rough surfaces," *Radio Sci.*, vol. 20, no. 2, pp. 161–170, 1985.

[41] A. V. Tishchenko, "Rayleigh was right: Electromagnetic fields and corrugated interfaces," *Opt. Photonics News*, vol. 21, no. 7, p. 50, 2010.

[42] W. H. Press, S. A. Teukolsky, W. T. Vetterling, and B. P. Flannery, *Numerical Recipes 3rd Edition: The Art of Scientific Computing*. Cambridge University Press, 3rd ed., 2007.

[43] U. Fano, "The theory of anomalous diffraction gratings and of quasi-stationary waves on metallic surfaces (Sommerfeld's waves)," *J. Opt. Soc. Am.*, vol. 31, no. 3, pp. 213–222, 1941.

[44] S. O. Rice, "Reflection of electromagnetic waves from slightly rough surfaces," *Commun. Pure Appl. Math.*, vol. 4, pp. 351–378, 1951.

[45] S. O. Rice, "Reflection of em waves by slightly rough surfaces," in *The theory of electromagnetic waves* (M. Kline, ed.), pp. 351–378, Interscience, New York, 1963.

[46] A. A. Maradudin and E. R. Méndez, "Enhanced backscattering of light from weakly rough, random metal surfaces," *Appl. Opt.*, vol. 32, no. 19, p. 3335, 1993.

[47] A. A. Maradudin, A. R. McGurn, and E. R. Méndez, "Surface plasmon polariton mechanism for enhanced backscattering of light from one-dimensional randomly rough metal surfaces," *J. Opt. Soc. Am. A*, vol. 12, no. 11, p. 2500, 1995.

[48] A. R. McGurn and A. A. Maradudin, "Perturbation theory results for the diffuse scattering of light from two-dimensional randomly rough metal surfaces," *Wave. Random Media*, vol. 6, no. 3, pp. 251–267, 1996.

[49] R. F. Millar, "On the Rayleigh assumption in scattering by a periodic surface," *Math. Proc. Cambridge*, vol. 65, pp. 773–791, 1969.

[50] R. F. Millar, "On the Rayleigh assumption in scattering by a periodic surface. ii," *Math. Proc. Cambridge*, vol. 69, pp. 217–225, 1971.

[51] R. F. Millar, "The Rayleigh hypothesis and a related least-squares solution to scattering problems for periodic surfaces and other scatterers," *Radio Sci.*, vol. 8, no. 8-9, pp. 785–796, 1973.

[52] A. Wirgin, "Reflection from a corrugated surface," *J. Acoust. Soc. Am.*, vol. 68, no. 2, p. 692, 1980.

[53] A. Wirgin, "Scattering from sinusoidal gratings: an evaluation of the Kirchhoff approximation," *J. Opt. Soc. Am.*, vol. 73, no. 8, p. 1028, 1983.

[54] J. M. Soto-Crespo, A. T. Friberg, and M. Nieto-Vesperinas, "Scattering from slightly rough random surfaces: a detailed study on the validity of the small perturbation method," *J. Opt. Soc. Am. A*, vol. 7, no. 7, p. 1185, 1990.

[55] J. A. Sánchez-Gil, E. R. Méndez, and A. A. Maradudin, "Limits of validity of three perturbation theories of the specular scattering of light from one-dimensional, randomly rough, dielectric surfaces," *J. Opt. Soc. Am. A*, vol. 12, no. 7, p. 1547, 1995.

[56] J. Shen and A. A. Maradudin, "Multiple scattering of waves from random rough surfaces," *Phys. Rev. B*, vol. 22, no. 9, pp. 4234–4240, 1980.

[57] D. P. Winebrenner and A. Ishimaru, "Application of the phase-perturbation technique to randomly rough surfaces," *J. Opt. Soc. Am. A*, vol. 2, no. 12, p. 2285, 1985.

[58] A. G. Navarrete Alcalá, E. I. Chaikina, E. R. Méndez, T. A. Leskova, and A. A. Maradudin, "Specular and diffuse scattering of light from two-dimensional randomly rough metal surfaces: experimental and theoretical results," *Wave. Random Media*, vol. 19, no. 4, pp. 600–636, 2009.

[59] W. H. Press, S. A. Teukolsky, W. T. Vetterling, and B. P. Flannery, *Numerical Recipes in Fortran 90 : The Art of Parallel Scientific Computing*. Cambridge University Press, 1996.

[60] E. Gabriel, G. E. Fagg, G. Bosilca, T. Angskun, J. J. Dongarra, J. M. Squyres, V. Sahay, P. Kambadur, B. Barrett, A. Lumsdaine, R. H. Castain, D. J. Daniel, R. L. Graham, and T. S. Woodall, "Open MPI: Goals, concept, and design of a next generation MPI implementation," in *Proceedings, 11th European PVM/MPI Users' Group Meeting*, (Budapest, Hungary), pp. 97–104, 2004.

[61] The HDF Group, "Hierarchical Data Format, version 5." `http://www.hdfgroup.org/HDF5/`, 1997-2018.

[62] L. S. Blackford, J. Choi, A. Cleary, E. D'Azevedo, J. Demmel, I. Dhillon, J. Dongarra, S. Hammarling, G. Henry, A. Petitet, K. Stanley, D. Walker, and R. C. Whaley, *ScaLAPACK Users' Guide*. Philadelphia, PA: Society for Industrial and Applied Mathematics, 1997.

[63] A. Lakhtakia, "Would Brewster recognize today's Brewster angle?," *Opt. News*, vol. 15, no. 6, p. 14, 1989.

[64] J. D. Jackson, *Classical Electrodynamics*. John Wiley & Sons, New York, 3rd ed., 1999.

[65] E. Hecht, *Optics*. Addison-Wesley, 2002.

[66] A. Sommerfeld, "Note on brewster's law," *J. Opt. Soc. Am.*, vol. 7, no. 7, pp. 501–502, 1923.

[67] T. Kawanishi, H. Ogura, and Z. L. Wang, "Scattering of an electromagnetic wave from a slightly random dielectric surface: Yoneda peak and brewster angle in incoherent scattering," *Wave. Random Media*, vol. 7, no. 3, pp. 351–384, 1997.

[68] "NASA Imagine The Universe: X-ray Telescopes." `https://imagine.gsfc.nasa.gov/science/toolbox/xray_telescopes1.html`. Accessed: 2018-01-15.

[69] Y. Yoneda, "Anomalous surface reflection of x rays," *Phys. Rev.*, vol. 131, pp. 2010–2013, 1963.

[70] G. H. Vineyard, "Grazing-incidence diffraction and the distorted-wave approximation for the study of surfaces," *Physical Review B*, vol. 26, pp. 4146–4159, 1982.

[71] S. K. Sinha, E. B. Sirota, S. Garoff, and H. B. Stanley, "X-ray and neutron scattering from rough surfaces," *Phys. Rev. B*, vol. 38, pp. 2297–2311, 1988.

[72] E. E. Gorodnichev, S. L. Dudarev, D. B. Rogozkin, and M. I. Ryazanov, "Nature of anomalous x-ray reflection from a surface," *Sov. Phys. JETP Lett.*, vol. 48, no. 3, pp. 147–150, 1988.

[73] T. A. Leskova and A. A. Maradudin, "X-ray scattering from a randomly rough surface," *Wave. Random Media*, vol. 7, no. 3, pp. 395–434, 1997.

[74] G. Renaud, R. Lazzari, and F. Leroy, "Probing surface and interface morphology with grazing incidence small angle x-ray scattering," *Surf. Sci. Rep.*, vol. 64, no. 8, pp. 255 – 380, 2009.

[75] H. Dosch, "Evanescent absorption in kinematic surface bragg diffraction," *Phys. Rev. B*, vol. 35, pp. 2137–2143, 1987.

[76] S. Stepanov, "X-ray Diffuse Scattering from Interfaces in Semiconductor Multilayers," in *Exploration of Subsurface Phenomena by Particle Scattering* (N. Lam, C. Melendres, and S. Sinha, eds.), pp. 119–137, International Advanced Studies Institute Press, North East, Maryland, 2000.

[77] A. Kitahara, K. Inoue, H. Kikkawa, K. Matsushita, and I. Takahashi, "X-ray Reflectivity study on polymeric surfaces near glass transition temperature," Photon Factory Activity Report No. 20, Part B, p. 83, 2002 (unpublished).

[78] J.-C. Gasse, D. Lützenkirchen-Hecht, R. Wagner, and R. Frahm, "Yoneda-xafs with area x-ray detectors," *J. Phys.: Conf. Ser.*, vol. 712, no. 1, p. 012028, 2016.

[79] M. Nieto-Vesperinas and J. A. Sánchez-Gil, "Light scattering from a random rough interface with total internal reflection," *J. Opt. Soc. Am. A*, vol. 9, no. 3, pp. 424–436, 1992.

[80] J. Nakayama, H. Ogura, and B. Matsumoto, "A probabilistic theory of scattering from a random rough surface," *Radio Science*, vol. 15, no. 6, pp. 1049–1057, 1980.

[81] T. Tamir, "The lateral wave," in *Electromagnetic Surface Modes* (A. D. Boardman, ed.), ch. 13, New York: John Wiley & Sons, 1982.

[82] H. Mueller, "The foundations of optics," *J. Opt. Soc. Am.*, vol. 38, p. 661, 1948.

[83] W. S. Bickel and W. M. Bailey, "Stokes vectors, Mueller matrices, and polarized scattered light," *Am. J. Phys.*, vol. 53, no. 5, pp. 468–478, 1985.

[84] R. A. Chipman, *Handbook of Optics.* New York: McGraw–Hill, 1994.

[85] A. J. de Witte, "Interference in Scattered Light," *Am. J. Phys.*, vol. 35, no. 4, pp. 301–313, 1967.

[86] I. Newton, *Opticks, Or a Treatise of the Reflections, Refractions, Inflections and Colours of Light*, vol. 678. William Innys, 1730.

[87] C. V. Raman and G. L. Datta, "XC. On Quetelet's rings and other allied phenomena," *Philos. Mag.*, vol. 42, no. 251, pp. 826–840, 1921.

[88] P. Selényi, "Über Lichtzerstreuung im Raume Wienerscher Interferenzen und neue, diesen reziproke Interferenzerscheinungen," *Ann. Phys.*, vol. 340, no. 8, pp. 444–460, 1911.

[89] Y. S. Kaganovskii, V. D. Freilikher, E. Kanzieper, Y. Nafcha, M. Rosenbluh, and I. M. Fuks, "Light scattering from slightly rough dielectric films," *J. Opt. Soc. Am. A*, vol. 16, no. 2, p. 331, 1999.

[90] W. Suhr and H. J. Schlichting, "Quételet's fringes due to scattering by small spheres just above a reflecting surface.," *Appl. Opt.*, vol. 48, no. 26, pp. 4978–84, 2009.

[91] J. Q. Lu, J. A. Sánchez-Gil, E. R. Méndez, Z.-H. Gu, and A. A. Maradudin, "Scattering of light from a rough dielectric film on a reflecting substrate: diffuse fringes," *J. Opt. Soc. Am. A*, vol. 15, no. 1, p. 185, 1998.

[92] A. V. Shchegrov, I. V. Novikov, and A. A. Maradudin, "Scattering of surface plasmon polaritons by a circularly symmetric surface defect," *Phys. Rev. Lett.*, vol. 78, no. 22, pp. 4269–4272, 1997.

[93] B. Baumeier, F. Huerkamp, T. A. Leskova, and A. A. Maradudin, "Scattering of surface-plasmon polaritons by a localized dielectric surface defect studied using an effective boundary condition," *Phys. Rev. A*, vol. 84, no. 1, pp. 1–8, 2011.

[94] R. E. Arias and A. A. Maradudin, "Scattering of a surface plasmon polariton by a localized dielectric surface defect," *Opt. Express*, vol. 21, no. 8, p. 9734, 2013.

[95] J. J. Gil and E. Bernabeu, "A Depolarization Criterion in Mueller Matrices," *Opt. Acta Int. J. Opt.*, vol. 32, no. 3, pp. 259–261, 1985.

[96] J. J. Gil and E. Bernabeu, "Depolarization and Polarization Indices of an Optical System," *Opt. Acta Int. J. Opt.*, vol. 33, no. 2, pp. 185–189, 1986.

[97] R. A. Chipman, "Depolarization index and the average degree of polarization," *Appl. Opt.*, vol. 44, no. 13, p. 2490, 2005.

Appendix A

Papers

Paper 1:

I. Simonsen, Ø. S. Hetland, J. B. Kryvi, and A. A. Maradudin, "Determination of the normalized-surface-height autocorrelation function of a two-dimensional randomly rough dielectric surface by the inversion of light-scattering data," *Phys. Rev. A*, vol. 93, no. 4, p. 043829, 2016

Determination of the normalized-surface-height autocorrelation function of a two-dimensional randomly rough dielectric surface by the inversion of light-scattering data

I. Simonsen,[1,*] Ø. S. Hetland,[1] J. B. Kryvi,[1] and A. A. Maradudin[2,†]
[1]*Department of Physics, NTNU Norwegian University of Science and Technology, NO-7491 Trondheim, Norway*
[2]*Department of Physics and Astronomy, University of California, Irvine, California 92697, USA*
(Received 31 December 2015; published 18 April 2016)

An expression is obtained on the basis of phase perturbation theory for the contribution to the mean differential reflection coefficient from the in-plane co-polarized component of the light scattered diffusely from a two-dimensional randomly rough dielectric surface when the latter is illuminated by *s*-polarized light. This result forms the basis for an approach to inverting experimental light-scattering data to obtain the normalized-surface-height autocorrelation function of the surface. Several parametrized forms of this correlation function, and the minimization of a cost function with respect to the parameters defining these representations, are used in the inversion scheme. This approach also yields the rms height of the surface roughness, and the dielectric constant of the dielectric substrate if it is not known in advance. The input data used in validating this inversion consist of computer simulation results for surfaces defined by exponential and Gaussian surface-height correlation functions, without and with the addition of multiplicative noise, for a single or multiple angles of incidence. The reconstructions obtained by this approach are quite accurate for weakly rough surfaces, and the proposed inversion scheme is computationally efficient.

DOI: 10.1103/PhysRevA.93.043829

I. INTRODUCTION

Statistical information about the roughness of a surface is contained in its rms height and in its normalized-surface-height autocorrelation function. Efforts to obtain these properties of rough surfaces from measurements of light scattered into the far field from them are of interest because of the contactless nature of this approach, and because measurements in the far field are easier to carry out than measurements in the near field.

This problem has been studied in the past by several authors. In the case of a one-dimensional randomly rough dielectric surface, Chakrabarti *et al.* [1] inverted by a Fourier transformation an expression for the contribution to the mean differential reflection coefficient, obtained in the Kirchhoff approximation, from light scattered diffusely from the surface. The incident light was *s*-polarized and the plane of incidence was perpendicular to the generators of the surface. Good agreement with numerically generated scattering data was obtained for weakly rough surfaces.

The case of a two-dimensional randomly rough surface was studied by Chandley [2], and by Marx and Vorburger [3]. Chandley used scalar diffraction theory and a thin random phase screen approximation [4] to model the interaction of light with the randomly rough surface. A thin phase screen may be regarded as a layer of negligible thickness that alters the phase of the wave scattered from it but does not change its magnitude. It is derived from simple optical path length and geometrical optics arguments. He used the angular dependence of the mean intensity of the scattered light in the far field as the experimental quantity to be inverted. The nature of his scattering model allowed this inversion to be carried out by means of a Fourier transformation. The dielectric constant of the scattering medium does not appear explicitly in Chandley's theory which means that it is impossible to use it to recover the dielectric constant of the scattering medium from the experimental scattering data if it is not known in advance.

In their study of this problem, Marx and Vorburger applied the Kirchhoff approximation for the scattering of a scalar plane wave from a two-dimensional randomly rough perfectly conducting surface to obtain the mean intensity of the scattered field. The determination of the rms height of the surface and the normalized-surface-height autocorrelation function was achieved by assuming an expression for the latter function of a particular analytic form and by the determination of the parameters defining it by a least-squares fit of the theoretical mean intensity to the experimental result.

In contrast to these studies, in this paper we present an approach to the determination of the rms height and the normalized-surface-height autocorrelation function of a two-dimensional randomly rough penetrable surface, in particular a dielectric surface, from the inversion of optical scattering data. It is based on a vector theory of rough surface scattering rather than on a scalar theory, namely phase perturbation theory [5]. The dielectric constant of the medium is taken into account in this approach. This version of rough-surface-scattering theory was chosen in this study because in a recent comparison between experimental data and the predictions of three perturbation theories for the scattering of electromagnetic radiation from two-dimensional randomly rough metal surfaces, it produced the best results [5]. We expect it to be equally accurate in describing the scattering of visible light from a two-dimensional randomly rough dielectric surface. Specifically, we use the expression for the contribution to the mean differential reflection coefficient from the in-plane, co-polarized component of the light scattered incoherently when the dielectric surface is illuminated at normal or non-normal incidence by *s*-polarized light.

This expression is evaluated with the use of an expression for the normalized-surface-height autocorrelation function that contains adjustable parameters. The values of these parameters

*ingve.simonsen@ntnu.no
†aamaradu@uci.edu

are then determined by a least-squares fit of the resulting expression to the corresponding experimental scattering data. The reconstruction of the parameters is performed using scattering data for both a single and several angles of incidence, and the sensitivity to noise of the reconstructed parameters is investigated. We note that the contribution to the mean differential reflection coefficient from the in-plane co-polarized component of the light scattered incoherently when the surface is illuminated by p-polarized light can also be used for this purpose. However, the expression one works with to effect this inversion is somewhat simpler in s polarization than in p polarization. In addition, there is no Brewster effect in s polarization, so that a smoother function of the scattering angle is being inverted in s polarization than in p polarization. It is for these reasons that we have chosen to work with s polarization.

This paper is organized as follows: First, the scattering system is presented (Sec. II) followed by elements of scattering theory (Sec. III) that will be useful for the subsequent discussion. Then in Sec. IV, we present the inversion scheme that will be used to reconstruct the surface-height autocorrelation function. The results obtained by the use of this procedure are presented in Sec. V for a set of different correlation functions and scattering geometries. Section VI presents discussions of these results and the conclusions that can be drawn from this study. The paper ends with an appendix detailing the derivation of expressions, central to the present work, for the first few moments of the scattering matrix for s-to-s scattering obtained on the basis of phase perturbation theory.

II. THE PHYSICAL SYSTEM STUDIED

The physical system we study in this paper consists of vacuum in the region $x_3 > \zeta(\mathbf{x}_\parallel)$, and a dielectric medium, characterized by a dielectric constant ε that is real, positive, and frequency independent, in the region $x_3 < \zeta(\mathbf{x}_\parallel)$ (Fig. 1). Here $\mathbf{x}_\parallel = (x_1, x_2, 0)$ is a position vector in the plane $x_3 = 0$. The surface profile function $\zeta(\mathbf{x}_\parallel)$ is assumed to be a single-valued function of $\mathbf{x}_\parallel$ that is differentiable with respect to x_1 and x_2. It is also assumed to constitute a stationary, zero-mean, isotropic, Gaussian random process defined by

$$\langle \zeta(\mathbf{x}_\parallel)\zeta(\mathbf{x}'_\parallel)\rangle = \delta^2 W(|\mathbf{x}_\parallel - \mathbf{x}'_\parallel|), \tag{1a}$$

$$\langle \zeta^2(\mathbf{x}_\parallel)\rangle = \delta^2, \tag{1b}$$

where the angle brackets denote an average over the ensemble of realizations of $\zeta(\mathbf{x}_\parallel)$, δ is the rms height of the surface, and $W(|\mathbf{x}_\parallel|)$ is the *normalized-surface-height autocorrelation function*, with the property that $W(0) = 1$.

The surface profile function has a Fourier integral representation,

$$\zeta(\mathbf{x}_\parallel) = \int \frac{d^2Q_\parallel}{(2\pi)^2}\, \hat{\zeta}(\mathbf{Q}_\parallel) \exp(i\mathbf{Q}_\parallel \cdot \mathbf{x}_\parallel), \tag{2}$$

where $\mathbf{Q}_\parallel = (Q_1, Q_2, 0)$ is a two-dimensional wave vector, so that

$$\hat{\zeta}(\mathbf{Q}_\parallel) = \int d^2x_\parallel\, \zeta(\mathbf{x}_\parallel) \exp(-i\mathbf{Q}_\parallel \cdot \mathbf{x}_\parallel). \tag{3a}$$

We also introduce the notation

$$\hat{\zeta}^{(n)}(\mathbf{Q}_\parallel) = \int d^2x_\parallel\, \zeta^n(\mathbf{x}_\parallel) \exp(-i\mathbf{Q}_\parallel \cdot \mathbf{x}_\parallel). \tag{3b}$$

The Fourier coefficient $\hat{\zeta}(\mathbf{Q}_\parallel)$ is also a zero-mean Gaussian random process defined by

$$\langle \hat{\zeta}(\mathbf{Q}_\parallel)\hat{\zeta}(\mathbf{Q}'_\parallel)\rangle = (2\pi)^2 \delta(\mathbf{Q}_\parallel + \mathbf{Q}'_\parallel)\, \delta^2 g(|\mathbf{Q}_\parallel|), \tag{4}$$

where $g(|\mathbf{Q}_\parallel|)$, the *power spectrum* of the surface roughness, is defined by

$$g(|\mathbf{Q}_\parallel|) = \int d^2x_\parallel\, W(|\mathbf{x}_\parallel|)\, \exp(-i\mathbf{Q}_\parallel \cdot \mathbf{x}_\parallel). \tag{5}$$

It follows from Eqs. (1) and (5) that $g(|\mathbf{Q}_\parallel|)$ is normalized to unity,

$$\int \frac{d^2Q_\parallel}{(2\pi)^2} g(|\mathbf{Q}_\parallel|) = 1. \tag{6}$$

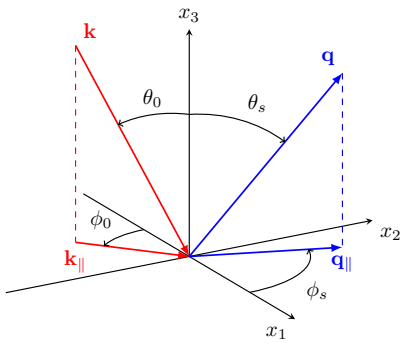

FIG. 1. Schematics of the scattering geometry considered in this work.

III. SCATTERING THEORY

The surface $x_3 = \zeta(\mathbf{x}_\parallel)$ is illuminated from the vacuum by an electromagnetic field of frequency ω. The electric field in the vacuum above the surface is the sum of an incident and a scattered field, $\mathbf{E}(\mathbf{x};t) = \mathbf{E}^{(i)}(\mathbf{x};t) + \mathbf{E}^{(s)}(\mathbf{x};t)$, where

$$\mathbf{E}^{(i)}(\mathbf{x};t) = \Big\{ -\frac{c}{\omega}[\hat{\mathbf{k}}_\parallel \alpha_0(k_\parallel) + \hat{\mathbf{x}}_3 k_\parallel] B_p(\mathbf{k}_\parallel) + (\hat{\mathbf{x}}_3 \times \hat{\mathbf{k}}_\parallel) \times B_s(\mathbf{k}_\parallel) \Big\} \exp\{i[\mathbf{k}_\parallel - \hat{\mathbf{x}}_3 \alpha_0(k_\parallel)] \cdot \mathbf{x} - i\omega t\}, \tag{7a}$$

$$\mathbf{E}^{(s)}(\mathbf{x};t) = \int \frac{d^2q_\parallel}{(2\pi)^2} \Big\{ \frac{c}{\omega}[\hat{\mathbf{q}}_\parallel \alpha_0(q_\parallel) - \hat{\mathbf{x}}_3 q_\parallel] A_p(\mathbf{q}_\parallel) + (\hat{\mathbf{x}}_3 \times \hat{\mathbf{q}}_\parallel) \times A_s(\mathbf{q}_\parallel) \Big\} \exp\{i[\mathbf{q}_\parallel + \hat{\mathbf{x}}_3 \alpha_0(q_\parallel)] \cdot \mathbf{x} - i\omega t\}. \tag{7b}$$

The subscripts p and s denote the p-polarized (TM) and s-polarized (TE) components of each of these fields, respectively.

The function $\alpha_0(q_\parallel)$ in Eqs. (7) is defined as

$$\alpha_0(q_\parallel) = \left[\left(\frac{\omega}{c}\right)^2 - q_\parallel^2\right]^{1/2}, \quad \mathrm{Re}\,\alpha_0(q_\parallel) > 0,\ \mathrm{Im}\,\alpha_0(q_\parallel) > 0. \tag{8}$$

Maxwell's equations imply linear relations between $A_\alpha(\mathbf{q}_\parallel)$ and $B_\beta(\mathbf{q}_\parallel)$, which we write in the form ($\alpha = p,s, \beta = p,s$)

$$A_\alpha(\mathbf{q}_\parallel) = \sum_\beta R_{\alpha\beta}(\mathbf{q}_\parallel|\mathbf{k}_\parallel) B_\beta(\mathbf{k}_\parallel). \tag{9}$$

The scattering amplitudes $\{R_{\alpha\beta}(\mathbf{q}_\parallel|\mathbf{k}_\parallel)\}$ play a significant role in the present theory because the mean differential reflection coefficient is given in terms of them. The differential reflection coefficient $[\partial R_{\alpha\beta}(\mathbf{q}_\parallel|\mathbf{k}_\parallel)/\partial\Omega_s]$ is defined such that $[\partial R_{\alpha\beta}(\mathbf{q}_\parallel|\mathbf{k}_\parallel)/\partial\Omega_s]d\Omega_s$ is the fraction of the total time-averaged flux in an incident field of β polarization the projection of whose wave vector on the mean scattering plane is $\mathbf{k}_\parallel$, that is scattered into a field of α polarization, the projection of whose wave vector on the mean scattering plane is $\mathbf{q}_\parallel$, within an element of solid angle $d\Omega_s$ about the scattering direction defined by the polar and azimuthal angles (θ_s,ϕ_s). It is given by [6,7]

$$\frac{\partial R_{\alpha\beta}(\mathbf{q}_\parallel|\mathbf{k}_\parallel)}{\partial\Omega_s} = \frac{1}{S}\left(\frac{\omega}{2\pi c}\right)^2 \frac{\cos^2\theta_s}{\cos\theta_0} |R_{\alpha\beta}(\mathbf{q}_\parallel|\mathbf{k}_\parallel)|^2, \tag{10}$$

with (see Fig. 1)

$$\mathbf{k}_\parallel = \frac{\omega}{c}\sin\theta_0(\cos\phi_0, \sin\phi_0, 0), \tag{11a}$$

$$\mathbf{q}_\parallel = \frac{\omega}{c}\sin\theta_s(\cos\phi_s, \sin\phi_s, 0), \tag{11b}$$

where (θ_0,ϕ_0) and (θ_s,ϕ_s) are the polar and azimuthal angles of incidence and scattering, respectively. S is the area of the plane $x_3 = 0$ covered by the rough surface. As we are dealing with scattering from a randomly rough surface, it is the average of this function over the ensemble of realizations of the surface profile function that we have to calculate. The contribution to this average from the light scattered incoherently is

$$\left\langle \frac{\partial R_{\alpha\beta}(\mathbf{q}_\parallel|\mathbf{k}_\parallel)}{\partial\Omega_s}\right\rangle_{\mathrm{incoh}} = \frac{1}{S}\left(\frac{\omega}{2\pi c}\right)^2 \frac{\cos^2\theta_s}{\cos\theta_0}[\langle|R_{\alpha\beta}(\mathbf{q}_\parallel|\mathbf{k}_\parallel)|^2\rangle - |\langle R_{\alpha\beta}(\mathbf{q}_\parallel|\mathbf{k}_\parallel)\rangle|^2]. \tag{12}$$

Closely related to the matrix of scattering amplitudes $\mathbf{R}(\mathbf{q}_\parallel|\mathbf{k}_\parallel)$ is the scattering matrix $\mathbf{S}(\mathbf{q}_\parallel|\mathbf{k}_\parallel)$ whose elements $\{S_{\alpha\beta}(\mathbf{q}_\parallel|\mathbf{k}_\parallel)\}$ are given by

$$S_{\alpha\beta}(\mathbf{q}_\parallel|\mathbf{k}_\parallel) = \frac{\alpha_0^{1/2}(q_\parallel)}{\alpha_0^{1/2}(k_\parallel)} R_{\alpha\beta}(\mathbf{q}_\parallel|\mathbf{k}_\parallel). \tag{13}$$

These elements satisfy the reciprocity relations [8]

$$S_{pp}(\mathbf{q}_\parallel|\mathbf{k}_\parallel) = S_{pp}(-\mathbf{k}_\parallel| - \mathbf{q}_\parallel), \tag{14a}$$

$$S_{ss}(\mathbf{q}_\parallel|\mathbf{k}_\parallel) = S_{ss}(-\mathbf{k}_\parallel| - \mathbf{q}_\parallel), \tag{14b}$$

$$S_{ps}(\mathbf{q}_\parallel|\mathbf{k}_\parallel) = -S_{sp}(-\mathbf{k}_\parallel| - \mathbf{q}_\parallel), \tag{14c}$$

which serve as a check on the correctness of their derivation. In terms of the elements of the scattering matrix, Eq. (10) takes the form

$$\left\langle \frac{\partial R_{\alpha\beta}(\mathbf{q}_\parallel|\mathbf{k}_\parallel)}{\partial\Omega_s}\right\rangle_{\mathrm{incoh}} = \frac{1}{S}\left(\frac{\omega}{2\pi c}\right)^2 \cos\theta_s[\langle|S_{\alpha\beta}(\mathbf{q}_\parallel|\mathbf{k}_\parallel)|^2\rangle - |\langle S_{\alpha\beta}(\mathbf{q}_\parallel|\mathbf{k}_\parallel)\rangle|^2]. \tag{15}$$

This is the definition we will work with.

In the Appendix it is shown that the ss element of the expression given by Eq. (15) obtained on the basis of second-order phase perturbation theory can be written as

$$\left\langle \frac{\partial R_{ss}(\mathbf{q}_\parallel|\mathbf{k}_\parallel)}{\partial\Omega_s}\right\rangle_{\mathrm{incoh}} = \frac{(\varepsilon-1)^2}{(2\pi)^2}\left(\frac{\omega}{c}\right)^6 \frac{\cos\theta_s}{[d_s(q_\parallel)d_s(k_\parallel)]^2} \exp[-2M(\mathbf{q}_\parallel|\mathbf{k}_\parallel)] \times \sum_{n=1}^{\infty} \frac{[4\delta^2\alpha_0(q_\parallel)\alpha_0(k_\parallel)(\hat{\mathbf{q}}_\parallel\cdot\hat{\mathbf{k}}_\parallel)^2]^n}{n!} \times \int d^2u_\parallel\, W^n(|\mathbf{u}_\parallel|)\exp[-i(\mathbf{q}_\parallel - \mathbf{k}_\parallel)\cdot\mathbf{u}_\parallel]. \tag{16}$$

In writing this expression we have introduced the functions

$$d_p(q_\parallel) = \varepsilon\alpha_0(q_\parallel) + \alpha(q_\parallel), \tag{17a}$$

$$d_s(q_\parallel) = \alpha_0(q_\parallel) + \alpha(q_\parallel), \tag{17b}$$

where

$$\alpha(q_\parallel) = \left[\varepsilon\left(\frac{\omega}{c}\right)^2 - q_\parallel^2\right]^{1/2} \quad \mathrm{Re}\,\alpha(q_\parallel) > 0,\ \mathrm{Im}\,\alpha(q_\parallel) > 0. \tag{18}$$

The function $M(\mathbf{q}_\parallel|\mathbf{k}_\parallel)$ is given by (see the Appendix)

$$M(\mathbf{q}_\parallel|\mathbf{k}_\parallel) = 2\delta^2\alpha_0^{1/2}(q_\parallel)\alpha_0^{1/2}(k_\parallel) \times \int \frac{d^2p_\parallel}{(2\pi)^2}\,\mathrm{Re}\,F(\mathbf{q}_\parallel|\mathbf{p}_\parallel|\mathbf{k}_\parallel)g(|\mathbf{p}_\parallel - \mathbf{k}_\parallel|), \tag{19}$$

where

$$F(\mathbf{q}_\parallel|\mathbf{p}_\parallel|\mathbf{k}_\parallel) = \mathrm{sgn}(\hat{\mathbf{q}}_\parallel\cdot\hat{\mathbf{k}}_\parallel)\left\{\frac{1}{2}[\alpha(q_\parallel) + \alpha(k_\parallel)](\hat{\mathbf{q}}_\parallel\cdot\hat{\mathbf{k}}_\parallel) + (\varepsilon-1)(\hat{\mathbf{q}}_\parallel\times\hat{\mathbf{p}}_\parallel)_3\frac{\alpha_0(p_\parallel)\alpha(p_\parallel)}{d_p(p_\parallel)}(\hat{\mathbf{p}}_\parallel\times\hat{\mathbf{k}}_\parallel)_3 - (\varepsilon-1)\left(\frac{\omega}{c}\right)^2\frac{(\hat{\mathbf{q}}_\parallel\cdot\hat{\mathbf{p}}_\parallel)(\hat{\mathbf{p}}_\parallel\cdot\hat{\mathbf{k}}_\parallel)}{d_s(p_\parallel)}\right\}, \tag{20}$$

with $\mathrm{sgn}(\cdot)$ denoting the sign function.

We now turn to an evaluation of the ingredients in Eq. (16). We begin with the expression for $2M(\mathbf{q}_\parallel|\mathbf{k}_\parallel)$ given by Eqs. (19)–(20). With the use of Eqs. (5)–(6) we rewrite it in terms of $W(\mathbf{x}_\parallel)$:

$$2M(\mathbf{q}_\parallel|\mathbf{k}_\parallel) = \delta^2\alpha_0^{1/2}(q_\parallel)\alpha_0^{1/2}(k_\parallel)\,\mathrm{sgn}(\hat{\mathbf{q}}_\parallel\cdot\hat{\mathbf{k}}_\parallel)\Big\{2[\alpha(q_\parallel)+\alpha(k_\parallel)](\hat{\mathbf{q}}_\parallel\cdot\hat{\mathbf{k}}_\parallel) + \frac{(\varepsilon-1)}{\pi^2}\mathrm{Re}\int_0^\infty dp_\parallel\, p_\parallel\int_{-\pi}^{\pi}d\phi_p\int_0^\infty dx_\parallel\, x_\parallel W(x_\parallel)$$
$$\times\int_{-\pi}^{\pi}d\phi_x\,\exp[-ip_\parallel x_\parallel\cos(\phi_p-\phi_x)]\exp[ik_\parallel x_\parallel\cos(\phi_k-\phi_x)]$$
$$\times\left[\frac{\alpha_0(p_\parallel)\alpha(p_\parallel)}{d_p(p_\parallel)}\sin(\phi_p-\phi_q)\sin(\phi_k-\phi_p) - \frac{(\omega/c)^2}{d_s(p_\parallel)}\cos(\phi_q-\phi_p)\cos(\phi_p-\phi_k)\right]\Big\}, \tag{21}$$

where ϕ_q, ϕ_p, ϕ_k, and ϕ_x are the azimuthal angles of the unit vectors $\hat{\mathbf{q}}_\parallel$, $\hat{\mathbf{p}}_\parallel$, $\hat{\mathbf{k}}_\parallel$, and $\hat{\mathbf{x}}_\parallel$, respectively, measured from the positive x_1 axis (see Fig. 1). On evaluating the angular integrals this result becomes

$$2M(\mathbf{q}_\parallel|\mathbf{k}_\parallel) = 2\delta^2\alpha_0^{1/2}(q_\parallel)\alpha_0^{1/2}(k_\parallel)|\hat{\mathbf{q}}_\parallel\cdot\hat{\mathbf{k}}_\parallel|\Big\{\alpha(q_\parallel)+\alpha(k_\parallel)-(\varepsilon-1)\,\mathrm{Re}\Big[\int_0^\infty dp_\parallel\, p_\parallel\left(\frac{\alpha_0(p_\parallel)\alpha(p_\parallel)}{d_p(p_\parallel)}+\frac{(\omega/c)^2}{d_s(p_\parallel)}\right)\int_0^\infty dx_\parallel\, x_\parallel$$
$$\times W(x_\parallel)J_0(p_\parallel x_\parallel)J_0(k_\parallel x_\parallel) + \int_0^\infty dp_\parallel\, p_\parallel\left(-\frac{\alpha_0(p_\parallel)\alpha(p_\parallel)}{d_p(p_\parallel)}+\frac{(\omega/c)^2}{d_s(p_\parallel)}\right)\int_0^\infty dx_\parallel\, x_\parallel W(x_\parallel)J_2(p_\parallel x_\parallel)J_2(k_\parallel x_\parallel)\Big]\Big\}, \tag{22}$$

where $J_n(z)$ is a Bessel function of the first kind and order n, and we have used the relation $x\,\mathrm{sgn}(x)=|x|$. Finally, due to the circular symmetry of $W(|\mathbf{u}_\parallel|)$ we obtain the result

$$\int d^2u_\parallel\, W^n(|\mathbf{u}_\parallel|)\exp[-i(\mathbf{q}_\parallel-\mathbf{k}_\parallel)\cdot\mathbf{u}_\parallel] = 2\pi\int_0^\infty du_\parallel\, u_\parallel W^n(u_\parallel)J_0(|\mathbf{q}_\parallel-\mathbf{k}_\parallel|u_\parallel). \tag{23}$$

In the case of normal incidence ($\mathbf{k}_\parallel=\mathbf{0}$) and in-plane ($\hat{\mathbf{q}}_\parallel\parallel\hat{\mathbf{k}}_\parallel$) scattering, Eq. (16) becomes

$$\left\langle\frac{\partial R_{ss}(\mathbf{q}_\parallel|\mathbf{0})}{\partial\Omega_s}\right\rangle_{\mathrm{incoh}} = \frac{(\varepsilon-1)^2}{(2\pi)^2}\left(\frac{\omega}{c}\right)^6\frac{\cos\theta_s}{[d_s(q_\parallel)d_s(0)]^2}\exp[-2M(\mathbf{q}_\parallel|\mathbf{0})]\sum_{n=1}^\infty\frac{[4\delta^2\alpha_0(q_\parallel)\alpha_0(0)]^n}{n!}\int d^2u_\parallel\, W^n(|\mathbf{u}_\parallel|)\exp(-i\mathbf{q}_\parallel\cdot\mathbf{u}_\parallel), \tag{24}$$

and Eq. (22) can be written as

$$2M(\mathbf{q}_\parallel|\mathbf{0}) = 2\delta^2\alpha_0^{1/2}(q_\parallel)\alpha_0^{1/2}(0)\Big\{\alpha(q_\parallel)+\alpha(0)-(\varepsilon-1)\,\mathrm{Re}\int_0^\infty dp_\parallel\, p_\parallel\left[\frac{\alpha_0(p_\parallel)\alpha(p_\parallel)}{d_p(p_\parallel)}+\frac{(\omega/c)^2}{d_s(p_\parallel)}\right]\int_0^\infty dx_\parallel\, x_\parallel W(x_\parallel)J_0(p_\parallel x_\parallel)\Big\}. \tag{25}$$

From Eq. (11) it is noted that for normal incidence $\hat{\mathbf{k}}_\parallel = (\cos\phi_0, \sin\phi_0, 0)$, even if $\mathbf{k}_\parallel/k_\parallel$ is not well defined in this case. Moreover, for scattering into directions that are normal to the mean surface we have $\hat{\mathbf{q}}_\parallel=\hat{\mathbf{k}}_\parallel$, so for all directions $\mathbf{q}_\parallel$ corresponding to in-plane scattering $|\hat{\mathbf{q}}_\parallel\cdot\hat{\mathbf{k}}_\parallel|=1$. These results were used in arriving at the expressions presented in Eqs. (24) and (25).

IV. THE INVERSE PROBLEM

To determine the function $W(x_\parallel)$ from *in-plane* scattering data defined as

$$\left\langle\frac{\partial R_{ss}(\theta_s)}{\partial\Omega_s}\right\rangle_{\mathrm{incoh,input}} \equiv \left\langle\frac{\partial R_{ss}(\mathbf{q}_\parallel|\mathbf{k}_\parallel)}{\partial\Omega_s}\right\rangle_{\mathrm{incoh}}\Bigg|_{|\hat{\mathbf{q}}_\parallel\cdot\hat{\mathbf{k}}_\parallel|=1},$$

we assume an analytic form for it that contains adjustable parameters. The values of these parameters, together with the rms height δ, are determined by minimizing a cost function with respect to variations of these parameters. The cost function we use is

$$\chi^2(\mathcal{P}) = \int_{-\frac{\pi}{2}}^{\frac{\pi}{2}}d\theta_s\left[\left\langle\frac{\partial R_{ss}(\theta_s)}{\partial\Omega_s}\right\rangle_{\mathrm{incoh,input}} - \left\langle\frac{\partial R_{ss}(\theta_s)}{\partial\Omega_s}\right\rangle_{\mathrm{incoh,calc}}\right]^2, \tag{26}$$

where $\mathcal{P}$ denotes the set of variational parameters used to characterize $\langle\partial R_{ss}(\theta_s)/\partial\Omega_s\rangle_{\mathrm{incoh,calc}}$. The minimization of this function with respect to the elements of $\mathcal{P}$ was carried out by the use of the routine "lmdif1" contained in the Fortran package MINPACK which is part of the general purpose mathematical library SLATEC [9]. The routine lmdif1 implements a modified version of the Levenberg-Marquardt algorithm [10,11], and it calculates the Jacobian by a forward-difference approximation.

The function $\langle\partial R_{ss}(\theta_s)/\partial\Omega_s\rangle_{\mathrm{incoh,input}}$ was obtained from rigorous, nonperturbative, purely numerical solutions [8,12] of the reduced Rayleigh equation for the scattering of polarized light from a two-dimensional randomly rough penetrable dielectric surface [13]. These calculations were carried out

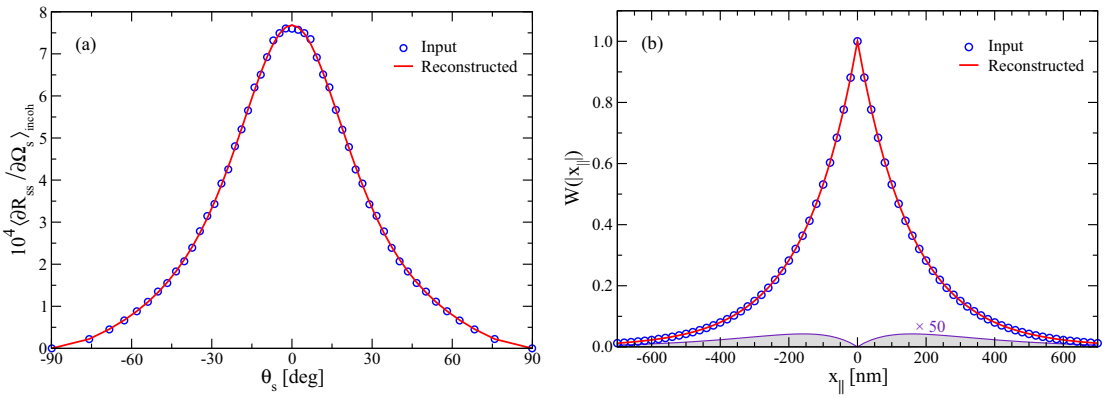

FIG. 2. Reconstruction of the rms roughness $\delta^\star$ and transverse correlation length $a^\star$ from in-plane scattering data obtained for exponentially correlated surfaces. (a) The incoherent component of the in-plane, co-polarized (s-to-s) mean differential reflection coefficient $\langle\partial R_{ss}/\partial\Omega_s\rangle_{\rm incoh}$ as a function of the polar angle of scattering θ_s obtained from computer simulations (open circles), and from second-order phase perturbation theory with the use of the reconstructed surface-roughness parameters (solid curve), for a two-dimensional randomly rough dielectric surface defined by Eq. (28a). The surface-roughness parameters assumed in the computer simulations have the values $\delta = 9.50$ nm and $a = 158.20$ nm, while the reconstructed values of these parameters are $\delta^\star = 9.519$ nm and $a^\star = 158.565$ nm. The dielectric constant of the substrate is $\varepsilon = 2.64$, and the wavelength of the s-polarized light incident normally on the mean surface is $\lambda = 632.8$ nm. (b) The input (open circles) and reconstructed (solid curve) surface-height autocorrelation function $W(|\mathbf{x}_\parallel|)$ for the random surface. The shaded gray region represents the absolute difference between the input and reconstructed surface-height autocorrelation functions.

for an ensemble of random surfaces generated [12] on the basis of expressions for $W(|\mathbf{x}_\parallel|)$ of either the exponential form

$$W(|\mathbf{x}_\parallel|) = \exp\left(-\frac{x_\parallel}{a}\right), \tag{27a}$$

or the Gaussian form

$$W(|\mathbf{x}_\parallel|) = \exp\left\{-\left(\frac{x_\parallel}{a}\right)^2\right\}. \tag{27b}$$

In Eqs. (27), a denotes the transverse correlation length of the surface roughness.

The function $\langle\partial R_{ss}(\theta_s)/\partial\Omega_s\rangle_{\rm incoh,calc}$ was obtained by evaluating the expression for it obtained using phase perturbation theory [Eq. (16)] for the trial function assumed to represent $W(|\mathbf{x}_\parallel|)$. Several forms for this trial function were used in our calculations. In the first set of forms we assumed an exponential or Gaussian trial function, that is,

$$W(|\mathbf{x}_\parallel|) = \exp\left(-\frac{x_\parallel}{a^\star}\right), \tag{28a}$$

or

$$W(|\mathbf{x}_\parallel|) = \exp\left\{-\left(\frac{x_\parallel}{a^\star}\right)^2\right\}. \tag{28b}$$

In this case the variational parameters of the reconstruction are $\delta^\star$,$a^\star$, and potentially also $\varepsilon^\star$.

For the second set of forms for the trial function a stretched exponential was assumed,

$$W(|\mathbf{x}_\parallel|) = \exp\left\{-\left(\frac{x_\parallel}{a^\star}\right)^{\gamma^\star}\right\}, \tag{29}$$

which reduces to the exponential and Gaussian forms when $\gamma^\star = 1$ and $\gamma^\star = 2$, respectively. In this case the variational parameters of the reconstruction are $\delta^\star$,$a^\star$,$\gamma^\star$, and potentially $\varepsilon^\star$.

V. RESULTS

We will now illustrate the inversion method developed here by applying it to the reconstruction of $W(|\mathbf{x}_\parallel|)$, first by the use of one of the trial functions (28) and then by the use of the more general trial function (29).

A. Exponentially correlated surface roughness

For the first scattering system we consider, it is assumed that the surface-height autocorrelation function $W(|\mathbf{x}_\parallel|)$ is *exponential*, Eq. (27a), and characterized by a transverse correlation length $a = 158.20$ nm and an rms height of the surface $\delta = 9.50$ nm. The medium above the surface is vacuum and the dielectric constant of the substrate is $\varepsilon = 2.64$ (photoresist). The wavelength (in vacuum) of the s-polarized incident light is $\lambda = 632.8$ nm. For this geometry and by the method of Ref. [12], we calculated the mean differential reflection coefficients by averaging the results from 5000 realizations of the surface profile function. For normal incidence, the in-plane, s-to-s co-polarized incoherent component of the mean differential reflection coefficient (DRC) obtained in this way is presented as a function of the scattering angle θ_s by open circles in Fig. 2(a) [the same data set also appears in Figs. 3(a)–5(a)]. These data constitute the input function $\langle R_{ss}(\theta_s)/\partial\Omega_s\rangle_{\rm incoh,input}$ for our first set of reconstruction examples.

As our first example of reconstruction based on this data set, we assume that the trial function $W(|\mathbf{x}_\parallel|)$ has the exponential form given by Eq. (28a). The set of variational parameters is therefore $\mathcal{P} = \{\delta^\star, a^\star\}$. The use of a mean differential reflection coefficient generated by the use of a known $W(|\mathbf{x}_\parallel|)$

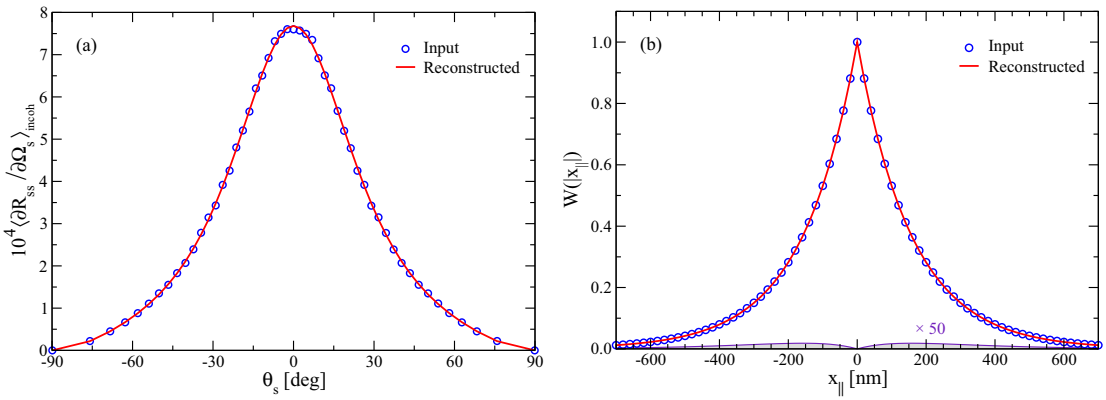

FIG. 3. Reconstruction of the rms roughness $\delta^\star$, the transverse correlation length $a^\star$, and the dielectric constant of the substrate $\varepsilon^\star$ from the in-plane scattering data. This figure is the same as Fig. 2 except now the dielectric constant of the substrate is also reconstructed. The reconstructed surface-roughness parameters are found to be $\delta^\star = 9.272$ nm, $a^\star = 158.042$ nm, and the reconstructed dielectric constant has the value $\varepsilon^\star = 2.718$.

in our inversion approach enables us to assess the quality of the reconstructions we obtain. By starting the minimization procedure with the values $\delta^\star = 2.00$ nm and $a^\star = 75.00$ nm, the values of these parameters that minimize the cost function $\chi^2(\mathcal{P})$, Eq. (26), were found to be $\delta^\star = 9.519$ nm and $a^\star = 158.565$ nm, to be compared with the values $\delta = 9.50$ nm and $a = 158.20$ nm used to generate the input data. In the minimization procedure we assumed that both $\delta^\star$ and $a^\star$ were restricted to positive values. The inversion is quite accurate. The function $\langle\partial R_{ss}(\theta_s)/\partial\Omega_s\rangle_{\text{incoh,calc}}$ calculated with the reconstructed values of $\delta^\star$ and $a^\star$ by means of second-order phase perturbation theory is plotted as the solid curve in Fig. 2(a) while the reconstructed correlation function $W(|\mathbf{x}_\parallel|)$ is plotted as the solid curve in Fig. 2(b). The reconstructed $W(|\mathbf{x}_\parallel|)$ is nearly superimposed on the input $W(|\mathbf{x}_\parallel|)$ [open symbols Fig. 2(b)]. The shaded region in Fig. 2(b), and in the subsequent plots of $W(|\mathbf{x}_\parallel|)$, represents the magnitude of the difference between the input and reconstructed values of this function. This difference is seen to be very small.

In the preceding example it was assumed that the dielectric constant of the scattering medium was known. For our second example we take the input data from our first example, given by the open circles in Fig. 2(a), but now assume that together with the roughness parameters the dielectric constant of the substrate is unknown. Therefore the variational parameter set is now $\mathcal{P} = \{\delta^\star, a^\star, \varepsilon^\star\}$. The results of this inversion are shown in Fig. 3, and it is seen that also in this case a rather good reconstruction is obtained. By starting the minimization procedure with the values $\delta^\star = 2.00$ nm, $a^\star = 75.00$ nm, and $\varepsilon^\star = 2.00$, the values of these parameters that minimize the cost function $\chi^2(\mathcal{P})$ were determined to be $\delta^\star = 9.272$ nm, $a^\star = 158.042$ nm, and $\varepsilon^\star = 2.718$. These are to be compared with the input values $\delta = 9.50$ nm, $a = 158.20$ nm, and $\varepsilon = 2.64$. The function $\langle\partial R_{ss}(\theta_s)/\partial\Omega_s\rangle_{\text{incoh,calc}}$ calculated with the reconstructed values of $\delta^\star, a^\star, \varepsilon^\star$ by means of second-order phase perturbation theory is plotted as the solid curve in Fig. 3(a), while the reconstructed correlation function $W(|\mathbf{x}_\parallel|)$ is plotted as the solid curve in Fig. 3(b). From a comparison of the results presented in Figs. 2 and 3 it is seen that the addition of a single variational parameter changes the reconstruction of $W(|\mathbf{x}_\parallel|)$ only marginally.

A more stringent test of our inversion scheme is obtained when the trial function for $W(|\mathbf{x}_\parallel|)$ has a functional form that differs from the form assumed in generating the input data that the reconstruction is based on. As our third example, we therefore present results of our calculations when the trial $W(|\mathbf{x}_\parallel|)$ is assumed to have the stretched exponential form given by Eq. (29). The set of variational parameters is now $\mathcal{P} = \{\delta^\star, a^\star, \gamma^\star\}$. By starting the minimization procedure with the values $\delta^\star = 2.00$ nm, $a^\star = 75.00$ nm, and $\gamma^\star = 2.00$, the values of these parameters that minimize the cost function were found to be $\delta^\star = 9.425$ nm, $a^\star = 161.717$ nm, and $\gamma^\star = 1.012$. These values are fairly close to the input values $\delta = 9.50$ nm, $a = 158.20$ nm, and $\gamma = 1.0$ used in obtaining the simulation data. However, the importance of this example is to show that our minimization procedure is in fact able to distinguish a Gaussian form for the correlation function from an exponential form. In Fig. 4(a) we plot the function $\langle\partial R_{ss}(\theta_s)/\partial\Omega_s\rangle_{\text{incoh,calc}}$ calculated by means of the second-order phase perturbation theory for the reconstructed values of $\delta^\star, a^\star, \gamma^\star$ (solid curve), together with a plot of the input function (open circles). The agreement between these two results is quite good. In Fig. 4(b) we present plots of the input (open circles) and reconstructed (solid curve) correlation functions $W(|\mathbf{x}_\parallel|)$. The latter curve very nearly coincides with the former curve.

In our final example assuming an exponentially correlated surface, we again use the stretched exponential trial function for $W(|\mathbf{x}_\parallel|)$, but now also assume that the dielectric constant of the scattering medium is unknown. The set of variational parameters is now $\mathcal{P} = \{\delta^\star, a^\star, \varepsilon^\star, \gamma^\star\}$. We start the minimization of the cost function $\chi^2(\mathcal{P})$ with the values $\delta^\star = 2.00$ nm, $a^\star = 75.00$ nm, $\varepsilon^\star = 2.00$, and $\gamma^\star = 2.00$. The values of these parameters that minimize the cost function are found to be $\delta^\star = 9.774$ nm, $a^\star = 166.709$ nm, $\varepsilon^\star = 2.507$, and $\gamma^\star = 1.027$. The proximity of these values to the input values, that

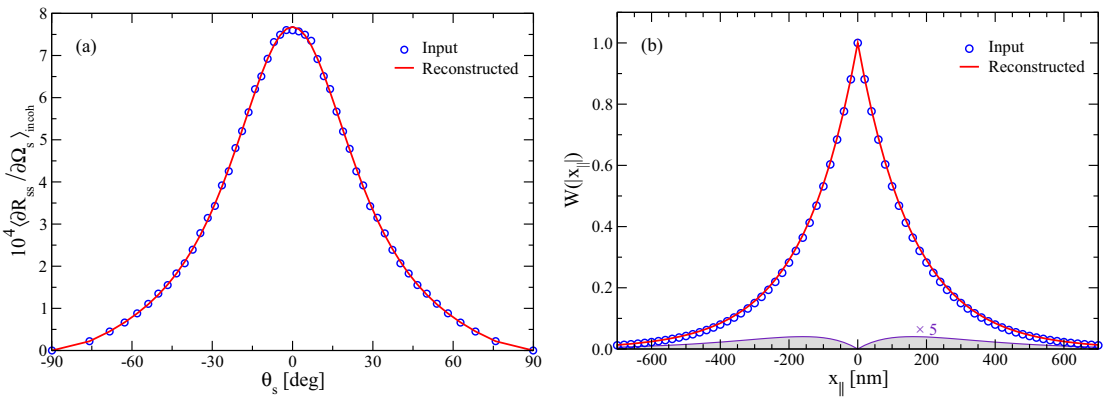

FIG. 4. Reconstruction of the rms roughness $\delta^\star$, the transverse correlation length $a^\star$, and the exponent $\gamma^\star$ from in-plane scattering data. This figure is the same as Fig. 2 except that now the trial function for $W(|\mathbf{x}_\parallel|)$ has the stretched exponential form given by Eq. (29). The reconstructed surface-roughness parameters are found to have the values $\delta^\star = 9.425$ nm, $a^\star = 161.717$ nm, and $\gamma^\star = 1.012$.

are the same as those used previously, is poorer than for the first three examples, but the reconstructed values are still quite satisfactory. The reconstructed function $\langle\partial R_{ss}(\theta_s)/\partial\Omega_s\rangle_{\rm incoh,calc}$ [Fig. 5(a)] and the reconstructed correlation function $W(|\mathbf{x}_\parallel|)$ [Fig. 5(b)] calculated with these reconstructed values are still in good quantitative agreement with the corresponding input functions.

The parameters for the scattering system obtained in the different reconstruction scenarios detailed in this subsection are summarized in Table I.

B. Gaussian-correlated surface roughness

The second scattering system, from which we will use data for the purpose of inversion, is characterized by a *Gaussian* correlation function instead of the exponential correlation function assumed in the earlier set of examples. Compared to the previous scattering system, in addition to the different form of $W(|\mathbf{x}_\parallel|)$, the only parameters that have changed are the rms roughness and the dielectric constant of the substrate; they now take the values $\delta = 15.82$ nm (an increase of more than 65% compared to its previous value) and $\varepsilon = 2.6896$, respectively. Except for the angles of incidence, all other parameters characterizing the scattering system remained unchanged, i.e., $a = 158.20$ nm and $\lambda = 632.8$ nm.

For these parameters, a computer simulation approach [12] was used to generate scattering data that were obtained by averaging the results from 24000 surface realizations. Results obtained this way are presented as open symbols in Fig. 6(a) for the polar angle of incidence $\theta_0 = 50.2^\circ$. It is these data we will base our inversion on in this subsection; that is, here this data set represents $\langle\partial R_{ss}/\partial\Omega_s\rangle_{\rm incoh,input}$.

Motivated by the reconstruction done in Sec. V A using scattering data obtained for the exponentially correlated surface, we will now perform similar inversions for Gaussian-correlated surfaces using various variational parameter sets, $\mathcal{P}$, that are subsets of $\{\delta^\star, a^\star, \varepsilon^\star, \gamma^\star\}$. In such cases, the starting values assumed in the minimization will be $\{2\,\text{nm}, 75\,\text{nm}, 2, 1\}$, respectively, if nothing is said to indicate otherwise.

Figure 6 presents the results of the reconstruction for $\mathcal{P} = \{\delta^\star, a^\star\}$ under the assumption that the trial function used for $W(|\mathbf{x}_\parallel|)$ is of the Gaussian form, Eq. (28b). In this way, the reconstruction procedure resulted in the numerical values $\delta^\star = 15.873$ nm and $a^\star = 158.000$ nm. These values agree rather well with the values assumed in generating the scattering data used in the inversion. Moreover, the input and reconstructed correlation functions, as well as the absolute difference between them, are depicted in Fig. 6(b); the solid red line in Fig. 6(a) represents the mean DRC predicted by the inversion.

We now continue by reconstructing the same variational parameter sets, $\mathcal{P}$, as were used in Sec. V A for the exponential surface roughness; the only difference now is that we will assume the form of the trial function (28b) where we previously used Eq. (28a). A summary of the reconstructed parameters is presented in Table II. Moreover, in Fig. 7 the input and

TABLE I. Summary of the scattering system parameters obtained during the different reconstruction scenarios based on in-plane, s-to-s co-polarized scattering data corresponding to an *exponentially* correlated surface: $\delta^\star$, $a^\star$, $\varepsilon^\star$, and $\gamma^\star$. The scattering system parameters assumed in generating the input data were $\delta = 9.50$ nm, $a = 158.20$ nm, $\varepsilon = 2.64$, and $\theta_0 = 0^\circ$. Note that an exponential correlation function corresponds to the exponent $\gamma = 1$ for the stretched exponential. The last column indicates the relevant figure where the results of the reconstruction in question are presented. The symbol "—" indicates that the corresponding variable was not reconstructed and instead had the value assumed in the input data (numerical simulations). In the two first reconstructions a trial correlation function of the form (28a) was used, while in the last two the form (29) was assumed. The initial values of $\{\delta^\star, a^\star, \varepsilon^\star, \gamma^\star\}$ assumed in the reconstructions were $\{2\,\text{nm}, 75\,\text{nm}, 2, 2\}$, respectively.

$\delta^\star$ (nm)	$a^\star$ (nm)	$\varepsilon^\star$	$\gamma^\star$	Comments
9.519	158.565	–	–	Fig. 2
9.272	158.042	2.718	–	Fig. 3
9.425	161.717	–	1.012	Fig. 4
9.774	166.709	2.507	1.027	Fig. 5

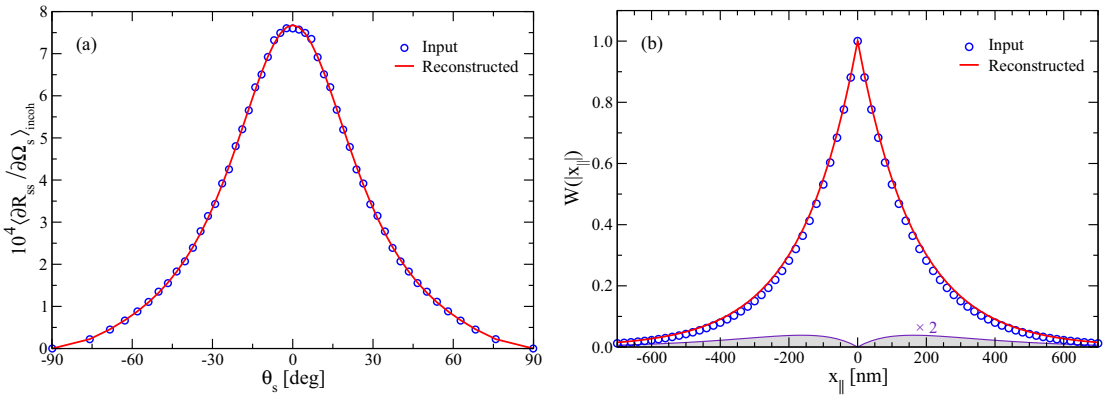

FIG. 5. Reconstruction of the rms roughness $\delta^\star$, the transverse correlation length $a^\star$, the exponent $\gamma^\star$, and the dielectric constant of the substrate $\varepsilon^\star$ from in-plane scattering data. This figure is the same as Fig. 2 except that now the trial function for $W(|\mathbf{x}_\parallel|)$ has the stretched exponential form given by Eq. (29), and the dielectric constant of the scattering medium is assumed to be unknown. The reconstructed surface-roughness parameters are found to have the values $\delta^\star = 9.774$ nm, $a^\star = 166.709$ nm, $\gamma^\star = 1.027$, and the reconstructed value of the dielectric constant is $\varepsilon^\star = 2.507$.

different reconstructed correlation functions obtained in this way are presented, together with comparisons of them. The mean DRCs that result from these reconstructions are visually indistinguishable from those of Fig. 6(a), and such plots have therefore not been presented.

From Figs. 6–7 and Table II we see that the reconstructed results for the Gaussian-correlated surface roughness are in general good, at least for the angle of incidence $\theta_0 = 50.2^\circ$ assumed here. The quality of the results obtained is on a par with the results obtained previously for the exponentially correlated surface roughness, even though in the Gaussian case the rms roughness is significantly larger and the angle of incidence is nonzero.

It should be mentioned that we have also performed reconstructions based on input data corresponding to other polar angles of incidence than $\theta_0 = 50.2^\circ$, and it was found that the values of the reconstructed parameters essentially remained unchanged; if there were any changes at all, the quality of the reconstruction seemed to improve for smaller polar angles of incidence. Assuming different initial values of the parameters of the set $\mathcal{P}$ seemed not to affect the reconstruction. Hence, our results seem to indicate that reconstruction based on different input data, at least for the scattering data that we considered, influences the numerical values of the reconstructed parameters of the surface-height correlation function only to a small extent. Furthermore, the reconstruction seems to be reliable for a wide range of angles of incidence.

C. Sensitivity to noise

Any experimental data set will contain some level of noise. Therefore, it is imperative to have reliable inversion

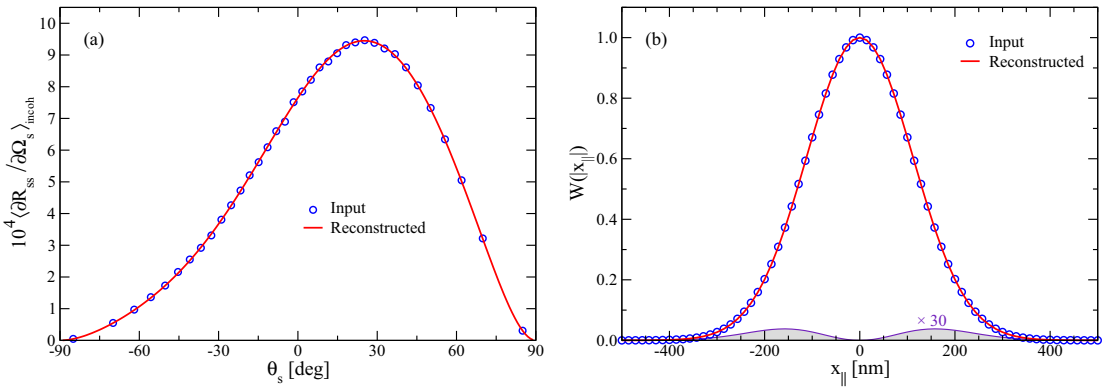

FIG. 6. Same as Fig. 2, but now for a Gaussian-correlated surface where the polar angle of incidence is $\theta_0 = 50.2^\circ$. The trial function assumed in the reconstruction was the Gaussian form (28b), and the values for the parameters obtained were $\delta^\star = 15.873$ nm and $a^\star = 158.000$ nm. The scattering system assumed in generating the input data were characterized by $\delta = 15.82$ nm, $a = 158.20$ nm, $\varepsilon = 2.6896$, and $\lambda = 632.8$ nm.

TABLE II. Summary of the values reconstructed from in-plane scattering data obtained for the polar angle of incidence $\theta_0 = 50.2^\circ$ and corresponding to a Gaussian-correlated surface characterized by $\delta = 15.82$ nm and $a = 158.20$ nm. The dielectric constant of the substrate was $\varepsilon = 2.6896$. Note that a Gaussian correlation function corresponds to an exponent $\gamma = 2.00$ for the stretched exponential. The symbol "—" indicates that the corresponding parameter was not reconstructed and instead had the value assumed in numerically generating the input data. When inverting for any of the parameters in the set $\{\delta^\star, a^\star, \varepsilon^\star, \gamma^\star\}$ the initial values used were $\{2\,\text{nm}, 75\,\text{nm}, 2, 1\}$, respectively.

$\delta^\star$ (nm)	$a^\star$ (nm)	$\varepsilon^\star$	$\gamma^\star$	Comments
15.922	157.928	–	–	Fig. 6
16.161	157.785	2.645	–	Fig. 7(a)
16.170	154.592	–	1.929	Fig. 7(b)
16.180	157.148	2.651	1.986	Fig. 7(c)

approaches that can be applied successfully to data sets containing noise. Until now, we have used simulated data as the basis for the reconstruction, and the only source of uncertainty (or noise) in such simulations results is the finite number of surface realizations used to obtain them. However, since a sufficiently high number of realizations has been used in generating such data, the uncertainty has been modest. To start investigating the sensitivity of the reconstructed parameters to noise, we will, for reasons of comparison, base it on the data set used in Sec. V B [open symbols in Fig. 6(a)] and add noise to it. Due to the way these simulation results were generated [12], only 36 points exist in this data set. However, experimental angular resolved scattering data sets typically will have significantly better angular resolution (and, thus, more points). Therefore, to better mimic the more relevant experimental situation, we have interpolated by splines these simulation results [solid symbols in Fig. 8(a)] to an angular resolution of $\Delta\theta_s = 1^\circ$ for θ_s in the interval from -90° to 90°. Then, to these (locally smooth) interpolated data, we have added *multiplicative Gaussian white noise* of a standard deviation of 5% and zero mean [gray erratic signal oscillating around zero in Fig. 8(a) resulting in the open blue data in Fig. 8(a)]. It is this latter data set that will be used as the *noisy input signal* for the reconstructions to be performed below. In passing, it is noted that additive noise (of constant amplitude) mainly will affect the tails of the in-plane angular intensity distributions of the scattered light due to their typical convex shape. In this study we have chosen to focus on multiplicative noise since it affects the whole intensity distribution and therefore represents a greater challenge for the reconstruction approach.

Results for the reconstructed parameters based on this Gaussian white noisy data set, performed in a fashion identical to what was done in the preceding subsection, are listed in Table III. From this table, we observe that the results obtained are rather good, even for the significant noise level assumed. Moreover, one finds that the quality of the reconstruction is not dramatically degraded compared to what was previously obtained using the non-noisy data set (see Table II). Not surprisingly, the poorest results of the inversion are obtained for the variational parameter set $\mathcal{P}$ of cardinality 4, and this

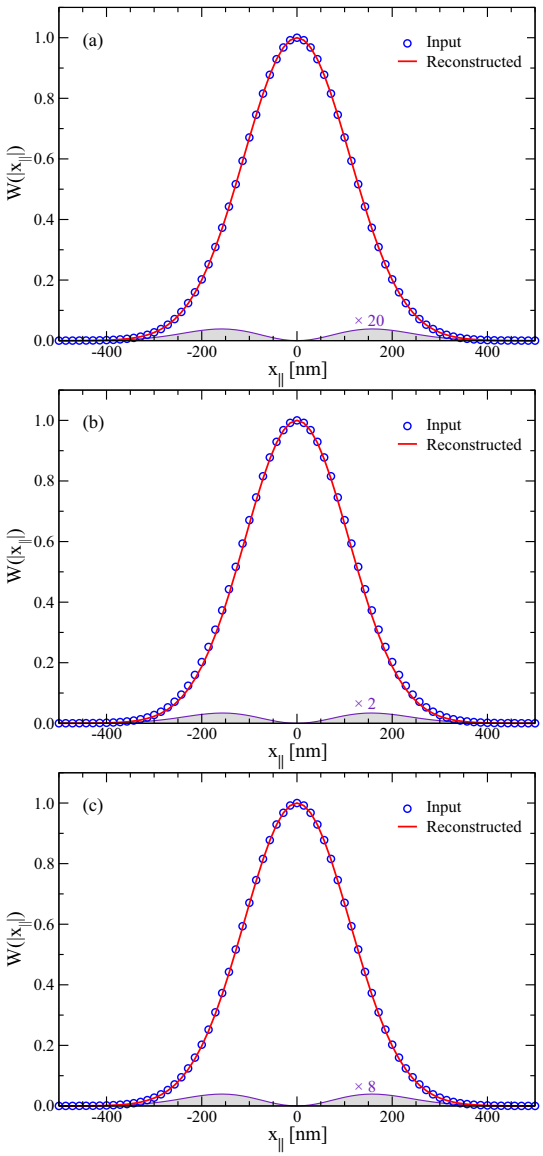

FIG. 7. Correlation functions obtained by reconstructing several variational parameter sets $\mathcal{P}$ for the Gaussian surface roughness parameters defined in Fig. 6: (a) $\mathcal{P} = \{\delta^\star, a^\star, \varepsilon^\star\}$, (b) $\mathcal{P} = \{\delta^\star, a^\star, \gamma^\star\}$, and (c) $\mathcal{P} = \{\delta^\star, a^\star, \varepsilon^\star, \gamma^\star\}$. The numerical values of the reconstructed parameters are listed in Table II. The shaded areas represent the absolute error between the input and reconstructed correlation functions.

"worst case" is presented as solid red lines in Fig. 8. The results presented in Table III and Fig. 8, which for the non-noisy case should be compared to Table II and Fig. 7(c), support the view that the reconstruction approach presented in this paper is able to produce reliable results also when the input data are noisy.

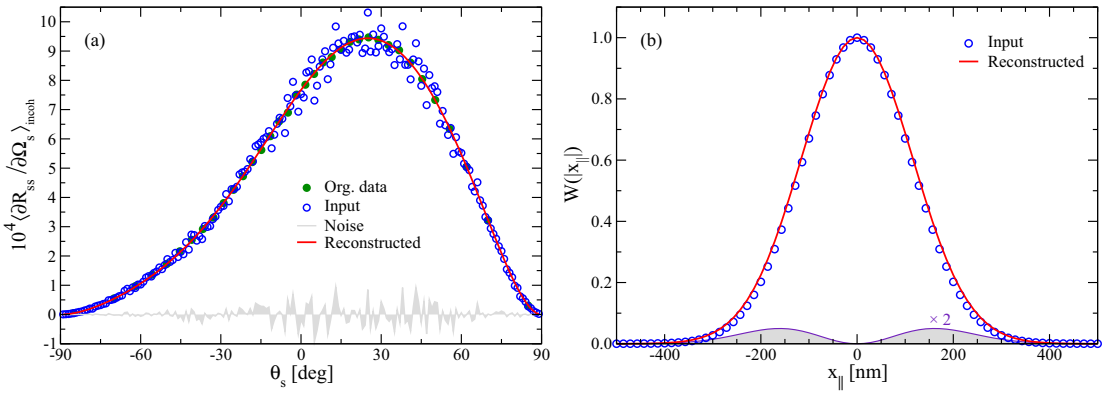

FIG. 8. The sensitivity of the reconstruction to multiplicative Gaussian white noise of 5% standard deviation. (a) The incoherent component of the in-plane mean DRC for s-to-s scattering from a Gaussian-correlated surface roughness. The solid symbols represent the same data set that appears as open symbols in Fig. 6(a). This (smooth) data set was first interpolated to an angular resolution of 1°, and then multiplicative Gaussian white noise of 5% standard deviation was added to it. The open blue symbols represent the resulting noisy signal that the reconstruction is based on; the irregular signal in gray oscillating around zero is the actual noise being added. The (noninterpolated) original data set is indicated by green filled symbols. The solid red line represents the incoherent component of the mean DRC resulting from reconstructing the variational set $\mathcal{P} = \{\delta^\star, a^\star, \varepsilon^\star, \gamma^\star\}$ (actual values given by the last line of Table III). (b) The input and reconstructed correlation function $W(|\mathbf{x}_\parallel|)$ for variational parameter set $\mathcal{P}$; the "non-noisy" equivalent of this graph is presented in Fig. 7(c). It should be noted that reconstruction using any subset of $\mathcal{P}$ results in more accurate results for the correlation function (see Table III), so what is shown here is indeed the "worst case" situation for the cases that we have considered.

For instance, when reconstructing 4 parameters, the relative errors in the reconstructed correlation lengths are about 3.5% and −0.7% for the noisy and non-noisy cases, respectively, which is not dramatic given the level of noise that was added to the input data.

It should be mentioned that we found that if the parameters were estimated using a noisy version of the original scattering data instead of the interpolated data, as done above, the results using the trial function (28b) essentially remained unchanged. However, for the stretched exponential form (29), the results were more sensitive to the initial values used in the minimization, resulting in less robust results than those obtained by the use of the former data set. We will see in the next subsection that this can also be the case when using multiple angles of incidence.

TABLE III. Same as Table II, but now the data set used in the inversion consisted of an interpolated version of the data set used to produce the results of Table II, with added multiplicative Gaussian white noise of a standard deviation of 5% (and mean zero). In Fig. 8, the noisy input data set is depicted as blue open symbols, while the noise appears in gray.

$\delta^\star$ (nm)	$a^\star$ (nm)	$\varepsilon^\star$	$\gamma^\star$	Comments
15.955	157.705	–	–	–
16.151	157.571	2.653	–	–
15.946	157.824	–	2.003	–
15.941	163.661	2.606	2.102	Fig. 8

D. Inversion of data obtained from multiple angles of incidence

When the experimental setup is prepared to measure the in-plane scattering of light for one angle of incidence, it is relatively straightforward to perform additional measurements for other angles of incidence. Therefore, it is of interest to study how the reconstructed parameters will depend on using multiple angles of incidence, and thus several data sets, in the inversion. In order to include, say, N data sets into the reconstruction, the cost function used in the minimization is generalized to

$$\chi^2(\mathcal{P}) = \sum_{n=1}^{N} \chi_n^2(\mathcal{P}), \tag{30}$$

where $\chi_n^2(\mathcal{P})$ is defined by Eq. (26) and corresponds to the contribution to the total cost function $\chi^2(\mathcal{P})$ from a single angle of incidence $\theta_0^{(n)} \in \{\theta_0^{(1)}, \theta_0^{(2)}, \ldots, \theta_0^{(N)}\}$.

Assuming the Gaussian-correlated surface roughness of the previous subsections, in-plane data for the mean DRCs were obtained from computer simulations for the polar angles of incidence $\theta_0 = 1.6°$, 25.3°, and 50.2 [12]. A series of joint inversions were then performed based on the three resulting data sets seen as open symbols in Fig. 9(a). The parameters obtained by such an approach are presented in Table IV and the resulting mean DRCs obtained when reconstructing $\delta^\star$, $a^\star$, and $\varepsilon^\star$ are presented as solid lines in Fig. 9(a). A comparison of the results presented in Tables II and IV reveals that including additional data sets into the inversion scheme, at least for the data sets we used in obtaining these results, did not change the estimates of the parameters in any significant way. If there is any change, it may seem as if a multiangle reconstruction may slightly improve the results when using the trial function

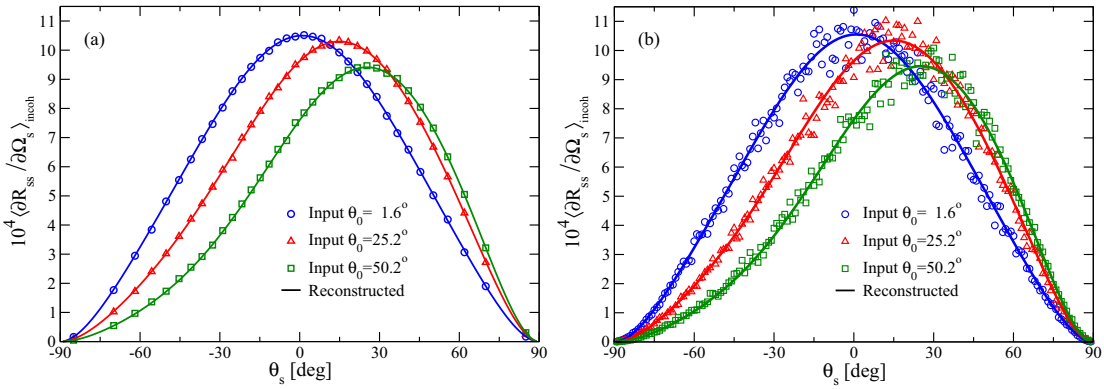

FIG. 9. The same as (a) Fig. 6(a) and (b) Fig. 8(a) but for the polar angles of incidence $\theta_0 = 1{,}6^\circ$, 25.3, and 50.2 and multiangle reconstruction of the data sets corresponding to these angles of incidence assuming the variational parameter set $\mathcal{P} = \{\delta^\star, a^\star, \varepsilon^\star\}$. The solid lines, independent of color, represent the reconstructed mean DRCs. The parameter values obtained from the reconstructions are listed in Tables IV and V.

(28b), while it becomes slightly worse for the trial function (29). However, before one can draw firm conclusions on this issue, proper estimates of the error bars associated with each of these parameters will have to be obtained, something that is outside the scope of the present work.

If now noise is added to these data sets after first interpolating them to a higher angular resolution, as was done above for the single data set corresponding to $\theta_0 = 50.2^\circ$, then on performing multiangle reconstructions based on the resulting data, the values presented in Table V are obtained [see also Fig. 9(b)]. The first thing to observe from Table V is that the multiangle inversions based on the stretched exponential trial function (29) produce rather inaccurate results compared to inversions based on only one of these data sets (see Table III). Potentially one could first estimate the exponent of the stretched exponential from a single data set, since we have found that it does not matter which of the data sets we use, and then use this value for $\gamma^\star$ as a fixed parameter in a multiangle inversion. However, we will not consider this situation farther here, since we feel that it is probably more fruitful to consider alternative forms of the trial functions.

On the other hand, when using the Gaussian trial function (28b) in the minimization, a comparison of the results presented in Tables III and V shows that the multiangle reconstructions are producing more accurate results than those obtained when the inversion is based on the single angle scattering data set corresponding to $\theta_0 = 50.2^\circ$. We have also found this result to be true when any of the other two data sets were used in the single-angle inversion. This is an important result, since it may indicate that including several experimental data sets into the inversion may improve the estimates of the parameters. The results from Table V also hint at the importance of the choice taken for the trial function, since *a priori* it is not known which form of $W(|\mathbf{x}_\parallel|)$ will result in a cost function, $\chi(\mathcal{P})$, that has a deep and well-defined minimum, in contrast to many local minima of comparable depths.

It is also interesting to note that the results obtained for the multiangle noisy case (Table V) seem to be more accurate than those for the corresponding multiangle non-noisy case (Table IV). However, here it is important to recall that significantly more points are used in the inversion in the former than in the latter case, and we speculate that this could be the main reason for the improvement.

E. Computational cost of the inversion scheme

In principle, an inversion scheme, similar to the one proposed in this work, could be based on one of the rigorous simulation approaches that recently have become available to calculate light scattering from two-dimensional

TABLE IV. Same as Table II, but now the reconstruction is based on several data sets corresponding to the polar angles of incidence $\theta_0 = 1.6^\circ$, 25.3°, and 50.2° [open symbols in Fig. 9(a)].

$\delta^\star$ (nm)	$a^\star$ (nm)	$\varepsilon^\star$	$\gamma^\star$	Comments
15.920	157.649	–	–	–
16.074	157.929	2.658	–	Fig. 9(a)
16.308	152.620	–	1.896	–
16.208	155.652	2.665	1.953	–

TABLE V. Same as Table III, but now the reconstruction is based on several data sets obtained for the polar angles of incidence $\theta_0 = 1.6^\circ$, 25.3°, and 50.2°. The data sets with the multiplicative 5% standard deviation Gaussian white noise data added to them, on which the reconstructions are based, are depicted as open symbols in Fig. 9(b).

$\delta^\star$ (nm)	$a^\star$ (nm)	$\varepsilon^\star$	$\gamma^\star$	Comments
15.843	158.694	–	–	–
15.822	158.863	2.669	–	Fig. 9(b)
16.866	145.591	–	1.749	–
17.050	140.664	2.730	1.675	–

randomly rough surfaces [6,7,14]. However, for such an inversion scheme to be practically relevant, it is has to be numerically efficient, since during the inversion process, the forward-scattering problem has to be solved for a large set of parameters. From this perspective, the rigorous numerical simulation approaches mentioned previously fall short since they typically require days of computer time, or more, to run for just one set of parameters.

In contrast, the phase perturbation theoretical approach to the forward scattering problem that we base our inversion scheme on is computationally efficient. For instance, for an angular resolution of 1°, it takes less than 2 s to obtain the mean DRC in the plane of incidence for one set of surface parameters (and one angle of incidence). Furthermore, the CPU times it took to perform the four inversions whose results are given in Table II were 25 s and 140 s when reconstructing 2 and 4 parameters, respectively (initial values as in Sec. V B). The remaining two inversions required CPU times somewhere in between the two previously given CPU times. All reported computer CPU times are based on the use of a single computer core on an Intel i7 960 CPU operating at 3.20 GHz.

Even if such CPU times do depend strongly on the angular resolution of the data set used in the inversion, the amount of noise that it contains, and the initial values from which the reconstruction is started, these numbers for the computational cost do illustrate that the proposed inversion method is rather quick to perform; this, together with its robustness, should make it useful in practical situations.

VI. DISCUSSION AND CONCLUSIONS

In this paper we have shown that second-order phase perturbation theory can be used to model the incoherent scattering of light by a two-dimensional randomly rough dielectric surface and to calculate the mean differential reflection coefficient for such a surface. As a result it has been expected that it should be an effective tool for the inversion of light-scattering data to obtain statistical properties of a random surface on which the mean differential reflection coefficient depends. This expectation has been borne out for weakly rough two-dimensional randomly rough dielectric surfaces. Together with several parametrized forms for the normalized-surface-height autocorrelation function $W(|\mathbf{x}_\parallel|)$, namely an exponential, a Gaussian, and a stretched exponential, and the minimization of a cost function with respect to the parameters defining these forms, phase perturbation theory has been used in this paper to determine $W(|\mathbf{x}_\parallel|)$, the rms height of the surface, the transverse correlation length of the surface roughness, the dielectric constant of the scattering medium when it was not known in advance, as well as the exponent of the stretched exponential. The function $W(|\mathbf{x}_\parallel|)$ has been reconstructed quite accurately. The agreement between the reconstructed values of δ, a, and ε and the input values of these parameters is gratifyingly satisfactory.

This agreement remains very good when significant multiplicative Gaussian white noise is included in the input data. When simulated data for multiple angles of incidence are used in the inversion scheme, it is found that in the absence of noise in the input data the quality of the reconstructions is slightly poorer than when only a single angle of incidence is used. However, when noise is introduced into the input data the use of results obtained from multiple angles of incidence yields slightly better reconstructions than when data from only a single angle of incidence are used. The reasons for this behavior of the reconstructions is not understood, and deserve further study.

An investigation of the computational cost of the inversion approach developed here shows that it is quite computationally efficient compared to the several orders of magnitude higher computational cost of carrying out the inversions by the use of scattering data obtained by rigorous simulations. The CPU times required for carrying out an inversion calculation using our approach for a given angular resolution, one set of surface parameters, and a single angle of incidence, namely seconds, are short enough that this approach can be useful in practical situations.

The inversion approach developed here needs to be explored to determine ranges of roughness, wavelength, and dielectric parameters for which it gives reliable results. Error estimates for the reconstructed values of the roughness and material parameters sought should be obtained. The use of more flexible trial functions for $W(|\mathbf{x}_\parallel|)$ in reconstructions should be explored, as well as the use of more than one wavelength. Reflectivity data can serve as the basis of an inversion scheme based on phase perturbation theory, and its utility for this purpose should be examined. This issue will be explored in subsequent work.

ACKNOWLEDGMENTS

This research was supported in part by NTNU and the Norwegian metacenter for High Performance Computing (NOTUR) by the allocation of computer time. The research of Ø.S.H. and I.S. was supported in part by the Research Council of Norway Contract No. 216699.

APPENDIX: DERIVATION OF EQUATION (16)

Even if we in this work are concerned with a scattering geometry where the substrate is a dielectric, this assumption will not be made in this appendix. Instead, the dielectric function of the substrate will here be assumed complex, so that the substrate can be either a dielectric or a metal. This generalization is done in order to facilitate future reference to the results of this appendix, and because the expressions can be derived simultaneously for a dielectric or metallic substrate with little extra effort.

The starting point for our derivation of Eq. (16) is Eqs. (12), (15), and (16)–(18) of Ref. [15], and the definition of the scattering matrix $\mathbf{S}(\mathbf{q}_\parallel|\mathbf{k}_\parallel)$ in terms of the matrix of the scattering amplitudes $\mathbf{R}(\mathbf{q}_\parallel|\mathbf{k}_\parallel)$, Eq. (13). From these results we obtain for the ss element of the scattering matrix the expansion

$$S_{ss}(\mathbf{q}_\parallel|\mathbf{k}_\parallel) = S_{ss}^{(0)}(\mathbf{q}_\parallel|\mathbf{k}_\parallel) - iS_{ss}^{(1)}(\mathbf{q}_\parallel|\mathbf{k}_\parallel) - \tfrac{1}{2}S_{ss}^{(2)}(\mathbf{q}_\parallel|\mathbf{k}_\parallel) + \cdots, \tag{A1}$$

where the superscript denotes the order of the corresponding term in the surface profile function $\zeta(\mathbf{x}_\parallel)$. The coefficient $S_{ss}^{(0)}(\mathbf{q}_\parallel|\mathbf{k}_\parallel)$ is given by

$$\begin{aligned} S_{ss}^{(0)}(\mathbf{q}_\parallel|\mathbf{k}_\parallel) &= (2\pi)^2\delta(\mathbf{q}_\parallel-\mathbf{k}_\parallel)\frac{\alpha_0(k_\parallel)-\alpha(k_\parallel)}{\alpha_0(k_\parallel)+\alpha(k_\parallel)} \\ &= (2\pi)^2\delta(\mathbf{q}_\parallel-\mathbf{k}_\parallel)\left(\frac{\alpha_0(q_\parallel)-\alpha(q_\parallel)}{\alpha_0(q_\parallel)+\alpha(q_\parallel)}\right)^{1/2}\left(\frac{\alpha_0(k_\parallel)-\alpha(k_\parallel)}{\alpha_0(k_\parallel)+\alpha(k_\parallel)}\right)^{1/2} \\ &= (2\pi)^2\delta(\mathbf{q}_\parallel-\mathbf{k}_\parallel)\frac{\left[\alpha_0^2(q_\parallel)-\alpha^2(q_\parallel)\right]^{1/2}\left[\alpha_0^2(k_\parallel)-\alpha^2(k_\parallel)\right]^{1/2}}{[\alpha_0(q_\parallel)+\alpha(q_\parallel)][\alpha_0(k_\parallel)+\alpha(k_\parallel)]} \\ &= (2\pi)^2\delta(\mathbf{q}_\parallel-\mathbf{k}_\parallel)\frac{(1-\varepsilon)(\omega/c)^2}{[\alpha_0(q_\parallel)+\alpha(q_\parallel)][\alpha_0(k_\parallel)+\alpha(k_\parallel)]}, \end{aligned} \tag{A2a}$$

where the functions $\alpha_0(q_\parallel)$ and $\alpha(q_\parallel)$ are defined by Eqs. (8) and (18), respectively. The coefficient $S_{ss}^{(1)}(\mathbf{q}_\parallel|\mathbf{k}_\parallel)$ is found to be

$$S_{ss}^{(1)}(\mathbf{q}_\parallel|\mathbf{k}_\parallel) = 2(1-\varepsilon)\left(\frac{\omega}{c}\right)^2\frac{\alpha_0^{1/2}(q_\parallel)\alpha_0^{1/2}(k_\parallel)}{[\alpha_0(q_\parallel)+\alpha(q_\parallel)][\alpha_0(k_\parallel)+\alpha(k_\parallel)]}(\hat{\mathbf{q}}_\parallel\cdot\hat{\mathbf{k}}_\parallel)\hat{\zeta}(\mathbf{q}_\parallel-\mathbf{k}_\parallel), \tag{A2b}$$

while the coefficient $S_{ss}^{(2)}(\mathbf{q}_\parallel|\mathbf{k}_\parallel)$ is given by

$$\begin{aligned} S_{ss}^{(2)}(\mathbf{q}_\parallel|\mathbf{k}_\parallel) &= -\frac{4\alpha_0^{1/2}(q_\parallel)\alpha_0^{1/2}(k_\parallel)}{[\alpha_0(q_\parallel)+\alpha(q_\parallel)][\alpha_0(k_\parallel)+\alpha(k_\parallel)]}\Bigg\{-\frac{1}{2}(1-\varepsilon)\left(\frac{\omega}{c}\right)^2[\alpha(q_\parallel)+\alpha(k_\parallel)](\hat{\mathbf{q}}_\parallel\cdot\hat{\mathbf{k}}_\parallel)\hat{\zeta}^{(2)}(\mathbf{q}_\parallel-\mathbf{k}_\parallel) \\ &\quad+\frac{(1-\varepsilon)^2}{\varepsilon}\left(\frac{\omega}{c}\right)^2\int\frac{d^2p_\parallel}{(2\pi)^2}\hat{\zeta}(\mathbf{q}_\parallel-\mathbf{p}_\parallel)(\hat{\mathbf{q}}_\parallel\times\hat{\mathbf{p}}_\parallel)_3\alpha(p_\parallel)(\hat{\mathbf{p}}_\parallel\times\hat{\mathbf{k}}_\parallel)_3\hat{\zeta}(\mathbf{p}_\parallel-\mathbf{k}_\parallel)\Bigg\} \\ &\quad+\frac{4\alpha_0^{1/2}(q_\parallel)\alpha_0^{1/2}(k_\parallel)(1-\varepsilon)(\omega/c)^2}{[\alpha_0(q_\parallel)+\alpha(q_\parallel)][\alpha_0(k_\parallel)+\alpha(k_\parallel)]}\int\frac{d^2p_\parallel}{(2\pi)^2}\hat{\zeta}(\mathbf{q}_\parallel-\mathbf{p}_\parallel) \\ &\quad\times\left\{\frac{1-\varepsilon}{\varepsilon}(\hat{\mathbf{q}}_\parallel\times\hat{\mathbf{p}}_\parallel)_3\frac{\alpha^2(p_\parallel)}{\varepsilon\alpha_0(p_\parallel)+\alpha(p_\parallel)}(\hat{\mathbf{p}}_\parallel\times\hat{\mathbf{k}}_\parallel)_3+(1-\varepsilon)\left(\frac{\omega}{c}\right)^2\frac{(\hat{\mathbf{q}}_\parallel\cdot\hat{\mathbf{p}}_\parallel)(\hat{\mathbf{p}}_\parallel\cdot\hat{\mathbf{k}}_\parallel)}{\alpha_0(p_\parallel)+\alpha(p_\parallel)}\right\}\hat{\zeta}(\mathbf{p}_\parallel-\mathbf{k}_\parallel) \\ &= -4(1-\varepsilon)\left(\frac{\omega}{c}\right)^2\frac{\alpha_0^{1/2}(q_\parallel)\alpha_0^{1/2}(k_\parallel)}{[\alpha_0(q_\parallel)+\alpha(q_\parallel)][\alpha_0(k_\parallel)+\alpha(k_\parallel)]} \\ &\quad\times\int\frac{d^2p_\parallel}{(2\pi)^2}\hat{\zeta}(\mathbf{q}_\parallel-\mathbf{p}_\parallel)\Bigg\{-\frac{1}{2}[\alpha(q_\parallel)+\alpha(k_\parallel)](\hat{\mathbf{q}}_\parallel\cdot\hat{\mathbf{k}}_\parallel)+\frac{1-\varepsilon}{\varepsilon}(\hat{\mathbf{q}}_\parallel\times\hat{\mathbf{p}}_\parallel)_3\alpha(p_\parallel)(\hat{\mathbf{p}}_\parallel\times\hat{\mathbf{k}}_\parallel)_3 \\ &\quad-\frac{1-\varepsilon}{\varepsilon}(\hat{\mathbf{q}}_\parallel\times\hat{\mathbf{p}}_\parallel)_3\frac{\alpha^2(p_\parallel)}{\varepsilon\alpha_0(p_\parallel)+\alpha(p_\parallel)}(\hat{\mathbf{p}}_\parallel\times\hat{\mathbf{k}}_\parallel)_3-(1-\varepsilon)\left(\frac{\omega}{c}\right)^2\frac{(\hat{\mathbf{q}}_\parallel\cdot\hat{\mathbf{p}}_\parallel)(\hat{\mathbf{p}}_\parallel\cdot\hat{\mathbf{k}}_\parallel)}{\alpha_0(p_\parallel)+\alpha(p_\parallel)}\Bigg\}\hat{\zeta}(\mathbf{p}_\parallel-\mathbf{k}_\parallel) \\ &= -4(1-\varepsilon)\left(\frac{\omega}{c}\right)^2\frac{\alpha_0^{1/2}(q_\parallel)\alpha_0^{1/2}(k_\parallel)}{[\alpha_0(q_\parallel)+\alpha(q_\parallel)][\alpha_0(k_\parallel)+\alpha(k_\parallel)]} \\ &\quad\times\int\frac{d^2p_\parallel}{(2\pi)^2}\hat{\zeta}(\mathbf{q}_\parallel-\mathbf{p}_\parallel)\Bigg\{-\frac{1}{2}[\alpha(q_\parallel)+\alpha(k_\parallel)](\hat{\mathbf{q}}_\parallel\cdot\hat{\mathbf{k}}_\parallel)+(1-\varepsilon)(\hat{\mathbf{q}}_\parallel\times\hat{\mathbf{p}}_\parallel)_3\frac{\alpha_0(p_\parallel)\alpha(p_\parallel)}{\varepsilon\alpha_0(p_\parallel)+\alpha(p_\parallel)}(\hat{\mathbf{p}}_\parallel\times\hat{\mathbf{k}}_\parallel)_3 \\ &\quad-(1-\varepsilon)\left(\frac{\omega}{c}\right)^2\frac{(\hat{\mathbf{q}}_\parallel\cdot\hat{\mathbf{p}}_\parallel)(\hat{\mathbf{p}}_\parallel\cdot\hat{\mathbf{k}}_\parallel)}{\alpha_0(p_\parallel)+\alpha(p_\parallel)}\Bigg\}\hat{\zeta}(\mathbf{p}_\parallel-\mathbf{k}_\parallel). \end{aligned} \tag{A2c}$$

In obtaining this expression we have used the result that

$$\hat{\zeta}^{(2)}(\mathbf{q}_\parallel-\mathbf{k}_\parallel) = \int\frac{d^2p_\parallel}{(2\pi)^2}\hat{\zeta}(\mathbf{q}_\parallel-\mathbf{p}_\parallel)\hat{\zeta}(\mathbf{p}_\parallel-\mathbf{k}_\parallel). \tag{A3}$$

When we substitute the results given by Eqs. (A2) into Eq. (A1) we find that through terms of second order in the surface profile function, $S_{ss}(\mathbf{q}_\parallel|\mathbf{k}_\parallel)$ takes the form

$$S_{ss}(\mathbf{q}_\parallel|\mathbf{k}_\parallel) = \mathrm{sgn}(\hat{\mathbf{q}}_\parallel\cdot\hat{\mathbf{k}}_\parallel)\frac{(1-\varepsilon)(\omega/c)^2}{[\alpha_0(q_\parallel)+\alpha(q_\parallel)][\alpha_0(k_\parallel)+\alpha(k_\parallel)s]}\Bigg\{(2\pi)^2\delta(\mathbf{q}_\parallel-\mathbf{k}_\parallel)\,\mathrm{sgn}(\hat{\mathbf{q}}_\parallel\cdot\hat{\mathbf{k}}_\parallel) - 2i\alpha_0^{1/2}(q_\parallel)$$
$$\times\alpha_0^{1/2}(k_\parallel)|\hat{\mathbf{q}}_\parallel\cdot\hat{\mathbf{k}}_\parallel|\hat{\zeta}(\mathbf{q}_\parallel-\mathbf{k}_\parallel) - 2\alpha_0^{1/2}(q_\parallel)\alpha_0^{1/2}(k_\parallel)\,\mathrm{sgn}(\hat{\mathbf{q}}_\parallel\cdot\hat{\mathbf{k}}_\parallel)\int\frac{d^2p_\parallel}{(2\pi)^2}\,\hat{\zeta}(\mathbf{q}_\parallel-\mathbf{p}_\parallel)\Bigg[\frac{1}{2}[\alpha(q_\parallel)+\alpha(k_\parallel)](\hat{\mathbf{q}}_\parallel\cdot\hat{\mathbf{k}}_\parallel)$$
$$+(\varepsilon-1)(\hat{\mathbf{q}}_\parallel\times\hat{\mathbf{p}}_\parallel)_3\frac{\alpha_0(p_\parallel)\alpha(p_\parallel)}{\varepsilon\alpha_0(p_\parallel)+\alpha(p_\parallel)}(\hat{\mathbf{p}}_\parallel\times\hat{\mathbf{k}}_\parallel)_3 - (\varepsilon-1)\left(\frac{\omega}{c}\right)^2\frac{(\hat{\mathbf{q}}_\parallel\cdot\hat{\mathbf{p}}_\parallel)(\hat{\mathbf{p}}_\parallel\cdot\hat{\mathbf{k}}_\parallel)}{\alpha_0(p_\parallel)+\alpha(p_\parallel)}\Bigg]\hat{\zeta}(\mathbf{p}_\parallel-\mathbf{k}_\parallel)\Bigg\}. \tag{A4}$$

This expression for $S_{ss}(\mathbf{q}_\parallel|\mathbf{k}_\parallel)$ is manifestly reciprocal; i.e., it satisfies Eq. (14b). Moreover, for reasons of later convenience, in writing Eq. (A4) we have factored out a phase $\mathrm{sgn}(\hat{\mathbf{q}}_\parallel\cdot\hat{\mathbf{k}}_\parallel)$, where $\mathrm{sgn}(\cdot)$ denotes the sign function defined by $x=\mathrm{sgn}(x)|x|$.

We next express Eq. (A4) in the form of a Fourier integral:

$$S_{ss}(\mathbf{q}_\parallel|\mathbf{k}_\parallel) = \mathrm{sgn}(\hat{\mathbf{q}}_\parallel\cdot\hat{\mathbf{k}}_\parallel)\frac{(1-\varepsilon)(\omega/c)^2}{d_s(q_\parallel)d_s(k_\parallel)}\int d^2x_\parallel\,\exp[-i(\mathbf{q}_\parallel-\mathbf{k}_\parallel)\cdot\mathbf{x}_\parallel]\Bigg\{1-2i\alpha_0^{1/2}(q_\parallel)\alpha_0^{1/2}(k_\parallel)|\hat{\mathbf{q}}_\parallel\cdot\hat{\mathbf{k}}_\parallel|\zeta(\mathbf{x}_\parallel)$$
$$-2\alpha_0^{1/2}(q_\parallel)\alpha_0^{1/2}(k_\parallel)\int\frac{d^2p_\parallel}{(2\pi)^2}\,F(\mathbf{q}_\parallel|\mathbf{p}_\parallel|\mathbf{k}_\parallel)\int d^2u_\parallel\,\exp[-i(\mathbf{p}_\parallel-\mathbf{k}_\parallel)\cdot\mathbf{u}_\parallel]\zeta(\mathbf{x}_\parallel)\zeta(\mathbf{x}_\parallel+\mathbf{u}_\parallel)\Bigg\}, \tag{A5}$$

where

$$F(\mathbf{q}_\parallel|\mathbf{p}_\parallel|\mathbf{k}_\parallel) = \mathrm{sgn}(\hat{\mathbf{q}}_\parallel\cdot\hat{\mathbf{k}}_\parallel)\Bigg\{\frac{1}{2}[\alpha(q_\parallel)+\alpha(k_\parallel)](\hat{\mathbf{q}}_\parallel\cdot\hat{\mathbf{k}}_\parallel)+(\varepsilon-1)(\hat{\mathbf{q}}_\parallel\times\hat{\mathbf{p}}_\parallel)_3\frac{\alpha_0(p_\parallel)\alpha(p_\parallel)}{d_p(p_\parallel)}(\hat{\mathbf{p}}_\parallel\times\hat{\mathbf{k}}_\parallel)_3$$
$$-(\varepsilon-1)\left(\frac{\omega}{c}\right)^2\frac{(\hat{\mathbf{q}}_\parallel\cdot\hat{\mathbf{p}}_\parallel)(\hat{\mathbf{p}}_\parallel\cdot\hat{\mathbf{k}}_\parallel)}{d_s(p_\parallel)}\Bigg\}, \tag{A6}$$

and the functions $d_p(p_\parallel)$ and $d_s(p_\parallel)$ are defined in Eq. (17). One notes from Eq. (A6) that $F(\mathbf{q}_\parallel|\mathbf{p}_\parallel|\mathbf{k}_\parallel)=F(-\mathbf{q}_\parallel|\mathbf{p}_\parallel|\mathbf{k}_\parallel)$ so that the expression inside the curly brackets in Eq. (A5) is a continuous function of the lateral scattering wave vector $\mathbf{q}_\parallel$ (and in particular at $\mathbf{q}_\parallel=\mathbf{0}$).

From Eq. (A5) we find that

$$\langle S_{ss}(\mathbf{q}_\parallel|\mathbf{k}_\parallel)\rangle = \mathrm{sgn}(\hat{\mathbf{q}}_\parallel\cdot\hat{\mathbf{k}}_\parallel)\frac{(1-\varepsilon)(\omega/c)^2}{d_s(q_\parallel)d_s(k_\parallel)}\int d^2x_\parallel\,\exp[-i(\mathbf{q}_\parallel-\mathbf{k}_\parallel)\cdot\mathbf{x}_\parallel]$$
$$\times\left\{1-2\delta^2\alpha_0^{1/2}(q_\parallel)\alpha_0^{1/2}(k_\parallel)\int\frac{d^2p_\parallel}{(2\pi)^2}\,F(\mathbf{q}_\parallel|\mathbf{p}_\parallel|\mathbf{k}_\parallel)g(|\mathbf{p}_\parallel-\mathbf{k}_\parallel|)\right\} \tag{A7a}$$
$$\cong \mathrm{sgn}(\hat{\mathbf{q}}_\parallel\cdot\hat{\mathbf{k}}_\parallel)\frac{(1-\varepsilon)(\omega/c)^2}{d_s(q_\parallel)d_s(k_\parallel)}\int d^2x_\parallel\,\exp[-i(\mathbf{q}_\parallel-\mathbf{k}_\parallel)\cdot\mathbf{x}_\parallel]$$
$$\times\exp\left[-2\delta^2\alpha_0^{1/2}(q_\parallel)\alpha_0^{1/2}(k_\parallel)\int\frac{d^2p_\parallel}{(2\pi)^2}\,F(\mathbf{q}_\parallel|\mathbf{p}_\parallel|\mathbf{k}_\parallel)g(|\mathbf{p}_\parallel-\mathbf{k}_\parallel|)\right]. \tag{A7b}$$

It follows that

$$|\langle S_{ss}(\mathbf{q}_\parallel|\mathbf{k}_\parallel)\rangle|^2 = \left|\frac{(1-\varepsilon)(\omega/c)^2}{d_s(q_\parallel)d_s(k_\parallel)}\right|^2\exp[-2M(\mathbf{q}_\parallel|\mathbf{k}_\parallel)]\int d^2x_\parallel\int d^2x'_\parallel\,\exp[-i(\mathbf{q}_\parallel-\mathbf{k}_\parallel)\cdot(\mathbf{x}_\parallel-\mathbf{x}'_\parallel)], \tag{A8}$$

where

$$2M(\mathbf{q}_\parallel|\mathbf{k}_\parallel) = 4\delta^2\alpha_0^{1/2}(q_\parallel)\alpha_0^{1/2}(k_\parallel)\,\mathrm{Re}\int\frac{d^2p_\parallel}{(2\pi)^2}\,F(\mathbf{q}_\parallel|\mathbf{p}_\parallel|\mathbf{k}_\parallel)g(|\mathbf{p}_\parallel-\mathbf{k}_\parallel|). \tag{A9}$$

We next find that

$$\langle|S_{ss}(\mathbf{q}_\parallel|\mathbf{k}_\parallel)|^2\rangle = \left|\frac{(1-\varepsilon)(\omega/c)^2}{d_s(q_\parallel)d_s(k_\parallel)}\right|^2\int d^2x_\parallel\int d^2x'_\parallel\,\exp[-i(\mathbf{q}_\parallel-\mathbf{k}_\parallel)\cdot(\mathbf{x}_\parallel-\mathbf{x}'_\parallel)]\Bigg\{1-2i\alpha_0^{1/2}(q_\parallel)\alpha_0^{1/2}(k_\parallel)|\hat{\mathbf{q}}_\parallel\cdot\hat{\mathbf{k}}_\parallel|\langle\zeta(\mathbf{x}_\parallel)-\zeta(\mathbf{x}'_\parallel)\rangle$$
$$+4\alpha_0(q_\parallel)\alpha_0(k_\parallel)(\hat{\mathbf{q}}_\parallel\cdot\hat{\mathbf{k}}_\parallel)^2\langle\zeta(\mathbf{x}_\parallel)\zeta(\mathbf{x}'_\parallel)\rangle - 2\alpha_0^{1/2}(q_\parallel)\alpha_0^{1/2}(k_\parallel)\int\frac{d^2p_\parallel}{(2\pi)^2}\int d^2u_\parallel\,[\exp[-i(\mathbf{p}_\parallel-\mathbf{k}_\parallel)\cdot\mathbf{u}_\parallel]$$
$$\times F(\mathbf{q}_\parallel|\mathbf{p}_\parallel|\mathbf{k}_\parallel)\langle\zeta(\mathbf{x}_\parallel)\zeta(\mathbf{x}_\parallel+\mathbf{u}_\parallel)\rangle + \exp[i(\mathbf{p}_\parallel-\mathbf{k}_\parallel)\cdot\mathbf{u}_\parallel]F^*(\mathbf{q}_\parallel|\mathbf{p}_\parallel|\mathbf{k}_\parallel)\langle\zeta(\mathbf{x}'_\parallel)\zeta(\mathbf{x}'_\parallel+\mathbf{u}_\parallel)\rangle]\Bigg\}. \tag{A10}$$

From this result we obtain

$$\begin{aligned}\langle |S_{ss}(\mathbf{q}_\parallel|\mathbf{k}_\parallel)|^2\rangle &= \left|\frac{(1-\varepsilon)(\omega/c)^2}{d_s(q_\parallel)d_s(k_\parallel)}\right|^2 \int d^2x_\parallel \int d^2x'_\parallel \exp\left[-i(\mathbf{q}_\parallel-\mathbf{k}_\parallel)\cdot(\mathbf{x}_\parallel-\mathbf{x}'_\parallel)\right] \\ &\quad\times[1+4\delta^2\alpha_0(q_\parallel)\alpha_0(k_\parallel)(\hat{\mathbf{q}}_\parallel\cdot\hat{\mathbf{k}}_\parallel)^2 W(|\mathbf{x}_\parallel-\mathbf{x}'_\parallel|)-2M(\mathbf{q}_\parallel|\mathbf{k}_\parallel)] \\ &\cong \left|\frac{(1-\varepsilon)(\omega/c)^2}{d_s(q_\parallel)d_s(k_\parallel)}\right|^2 \exp[-2M(\mathbf{q}_\parallel|\mathbf{k}_\parallel)] \int d^2x_\parallel \int d^2x'_\parallel \exp\left[-i(\mathbf{q}_\parallel-\mathbf{k}_\parallel)\cdot(\mathbf{x}_\parallel-\mathbf{x}'_\parallel)\right] \\ &\quad\times \exp[4\delta^2\alpha_0(q_\parallel)\alpha_0(k_\parallel)(\hat{\mathbf{q}}_\parallel\cdot\hat{\mathbf{k}}_\parallel)^2 W(|\mathbf{x}_\parallel-\mathbf{x}'_\parallel|)]. \end{aligned} \tag{A11}$$

Thus, we have finally

$$\begin{aligned}\langle |S_{ss}(\mathbf{q}_\parallel|\mathbf{k}_\parallel)|^2\rangle - |\langle S_{ss}(\mathbf{q}_\parallel|\mathbf{k}_\parallel)\rangle|^2 &= S\left|\frac{(1-\varepsilon)(\omega/c)^2}{d_s(q_\parallel)d_s(k_\parallel)}\right|^2 \exp[-2M(\mathbf{q}_\parallel|\mathbf{k}_\parallel)] \int d^2u_\parallel \exp\left[-i(\mathbf{q}_\parallel-\mathbf{k}_\parallel)\cdot\mathbf{u}_\parallel\right] \\ &\quad\times\{\exp[4\delta^2\alpha_0(q_\parallel)\alpha_0(k_\parallel)(\hat{\mathbf{q}}_\parallel\cdot\hat{\mathbf{k}}_\parallel)^2 W(|\mathbf{u}_\parallel|)]-1\}. \end{aligned} \tag{A12}$$

The substitution of this result into Eq. (15) yields Eq. (16).

[1] S. Chakrabarti, A. A. Maradudin, and E. R. Méndez, Reconstruction of the power spectrum of a randomly rough dielectric surface from reflectivity data, Phys. Rev. A **88**, 013812 (2013).

[2] P. J. Chandley, Determination of the autocorrelation function of height on a rough surface from coherent light scattering, Opt. Quantum Electron. **8**, 329 (1976).

[3] E. Marx and T. Vorburger, Direct and inverse problems for light scattered by rough surfaces, Appl. Opt. **29**, 3613 (1990).

[4] W. T. Welford, Optical estimation of statistics of surface roughness from light scattering measurements, Opt. Quantum Electron. **9**, 269 (1977).

[5] A. G. Navarrete Alcala, E. I. Chaikina, E. R. Mendez, T. A. Leskova, and A. A. Maradudin, Specular and diffuse scattering of light from two-dimensional randomly rough metal surfaces: experimental and theoretical results, Wave. Random Complex **19**, 600 (2009).

[6] I. Simonsen, A. A. Maradudin, and T. A. Leskova, The scattering of electromagnetic waves from two-dimensional randomly rough perfectly conducting surfaces: The full angular intensity distribution, Phys. Rev. A **81**, 013806 (2010).

[7] I. Simonsen, Optics of surface disordered systems: A random walk through rough surface scattering phenomena, Eur. Phys. J. Special Topics **181**, 1 (2010).

[8] T. A. Leskova, P. A. Letnes, A. A. Maradudin, T. Nordam, and I. Simonsen, The scattering of light from two-dimensional randomly rough metal surfaces, Proc. SPIE **8172**, 817209 (2011).

[9] SLATEC Common Mathematical Library, Version 4.1, www.netlib.org/slatec/ (also see http://people.sc.fsu.edu/~jburkardt/f_src/slatec/slatec.html).

[10] K. Levenberg, A method for the solution of certain problems in least squares, Q. Appl. Math. **2**, 164 (1944).

[11] D. W. Marquardt, An algorithm for least squares estimation of nonlinear parameters, J. Soc. Ind. Appl. Math. **11**, 431 (1963).

[12] T. Nordam, P. A. Letnes, and I. Simonsen, Numerical simulations of scattering of light from two-dimensional surfaces using the reduced Rayleigh equation, Front. Phys. **1**, 8 (2013).

[13] G. C. Brown, V. Celli, M. Haller and A. Marvin, Vector theory of light scattering from a rough surface: unitary and reciprocal expansions, Surf. Sci. **136**, 381 (1984).

[14] I. Simonsen, A. A. Maradudin, and T. A. Leskova, The Scattering of Electromagnetic Waves from Two-Dimensional Randomly Rough Penetrable Surfaces, Phys. Rev. Lett. **104**, 223904 (2010).

[15] A. R. McGurn and A. A. Maradudin, Perturbation theory results for the diffuse scattering of light from two-dimensional randomly rough metal surfaces, Waves in Random Media **6**, 251 (1996).

Paper 2:

Ø. S. Hetland, A. A. Maradudin, T. Nordam, and I. Simonsen, "Numerical studies of the scattering of light from a two-dimensional randomly rough interface between two dielectric media," *Phys. Rev. A*, vol. 93, no. 5, p. 053819, 2016

Numerical studies of the scattering of light from a two-dimensional randomly rough interface between two dielectric media

Ø. S. Hetland,[1,*] A. A. Maradudin,[2] T. Nordam,[1] and I. Simonsen[1]

[1]*Department of Physics, NTNU Norwegian University of Science and Technology, NO-7491 Trondheim, Norway*

[2]*Department of Physics and Astronomy, University of California, Irvine California 92697, USA*

(Received 16 February 2016; published 12 May 2016)

The scattering of polarized light incident from one dielectric medium on its two-dimensional randomly rough interface with a second dielectric medium is studied. A reduced Rayleigh equation for the scattering amplitudes is derived for the case where p- or s-polarized light is incident on this interface, with no assumptions being made regarding the dielectric functions of the media. Rigorous, purely numerical, nonperturbative solutions of this equation are obtained. They are used to calculate the reflectivity and reflectance of the interface, the mean differential reflection coefficient, and the full angular distribution of the intensity of the scattered light. These results are obtained for both the case where the medium of incidence is the optically less dense medium and in the case where it is the optically more dense medium. Optical analogs of the Yoneda peaks observed in the scattering of x rays from metal surfaces are present in the results obtained in the latter case. Brewster scattering angles for diffuse scattering are investigated, reminiscent of the Brewster angle for flat-interface reflection, but strongly dependent on the angle of incidence. When the contribution from the transmitted field is added to that from the scattered field it is found that the results of these calculations satisfy unitarity with an error smaller than 10^{-4}.

DOI: 10.1103/PhysRevA.93.053819

I. INTRODUCTION

In the great majority of the theoretical studies of the scattering of light from a two-dimensional randomly rough surface of a dielectric medium, the medium of incidence has been vacuum. Recent reviews of such studies can be found in Refs. [1] and [2]. As a result of this restriction, effects associated with total internal reflection, which requires that the medium of incidence be optically more dense than the scattering medium, were not considered in these studies. There have been exceptions to this general practice, however.

By the use of the stochastic functional approach [3], Kawanishi *et al.* [4] studied the coherent and incoherent scattering of an electromagnetic wave from a two-dimensional randomly rough interface separating two different dielectric media. The light could be incident on the interface from either medium. The theoretical approach used in this work [4] is perturbative in nature and applicable only to weakly rough interfaces. Nevertheless, its use yielded interesting results, including the presence of Yoneda peaks in the angular dependence of the intensity of the light scattered back into the medium of incidence when the latter was the optically more dense medium. These are sharp, asymmetric peaks occurring at the critical angle for total internal reflection for a fixed angle of incidence for both p- and s polarization of the incident light. These peaks were first observed experimentally in the scattering of x rays incident from air on a metal surface [5] and have subsequently been studied theoretically in the context of the scattering of x rays [6–8] and neutrons [7] from rough surfaces.

In Ref. [4], Kawanishi *et al.* also observed angles of zero scattering intensity, to first order in their approach, in the distributions of the intensity of the incoherently scattered light, when the incident light was p polarized. Due to their resemblance to the Brewster angle in the reflectivity from a flat interface, they dubbed these angles the "Brewster scattering angles." These were observed, in both reflection and transmission, for light incident from either medium.

Both the Yoneda peaks and the Brewster scattering angles seem to have had their first appearance in optics in the paper by Kawanishi *et al.* [4]. They have yet to be observed experimentally in this context. It should be mentioned that in an earlier numerical investigation of light scattering from one-dimensional dielectric rough surfaces, Nieto-Vesperinas and Sánchez-Gil [9] observed "sidelobes" in the angular intensity distributions. However, these authors did not associate these features with the Yoneda peak phenomenon, even though we believe doing so would have been correct.

In a subsequent paper Soubret *et al.* [10] derived a reduced Rayleigh equation for the scattering amplitudes when an electromagnetic wave is incident from one dielectric medium on its two-dimensional randomly rough interface with a second dielectric medium. The solution of this equation was obtained in the form of expansions of the scattering amplitudes in powers of the surface profile function through terms of third order. However, in obtaining the numerical results presented in this paper [10], the medium of incidence was assumed to be vacuum.

In this paper we present a study of this problem free from some of the restrictive assumptions and approximations present in the earlier studies of scattering of polarized light from two-dimensional randomly rough dielectric surfaces. We first derive a reduced Rayleigh equation for the scattering amplitudes when p- or s-polarized light is incident from a dielectric medium whose dielectric constant is ε_1 on its two-dimensional randomly rough interface with a dielectric medium whose dielectric constant is ε_2. The dielectric constant ε_1 can be smaller or larger than ε_2. This equation is then solved by a rigorous, purely numerical, nonperturbative approach.

*oyvind.hetland@ntnu.no

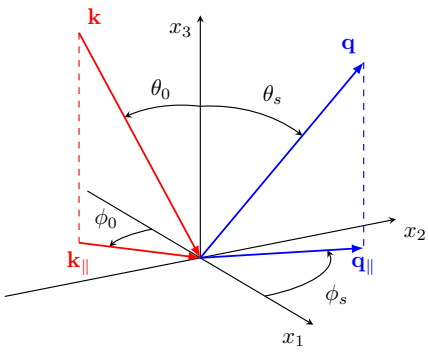

FIG. 1. A sketch of the scattering geometry assumed in this work. The figure also shows the coordinate system used, angles of incidence (θ_0,ϕ_0) and scattering (θ_s,ϕ_s), and the corresponding lateral wave vectors $\mathbf{k}_\parallel$ and $\mathbf{q}_\parallel$, respectively.

The scattering amplitudes obtained in this way are then used to calculate the reflectivity and reflectance of the interface as functions of the angle of incidence and also the effect of surface roughness on the contribution to the mean differential reflection coefficient from the light scattered incoherently (diffusely) and the full angular dependence of the intensity of the incoherently scattered light. It is hoped that the presentation of these results will stimulate and motivate experimental studies of such scattering systems.

II. THE SCATTERING SYSTEM

The system we study in this paper consists of a dielectric medium (medium 1), whose dielectric constant is ε_1, in the region $x_3 > \zeta(\mathbf{x}_\parallel)$, and a dielectric medium (medium 2), whose dielectric constant is ε_2, in the region $x_3 < \zeta(\mathbf{x}_\parallel)$ (Fig. 1). Here $\mathbf{x}_\parallel = (x_1,x_2,0)$ is an arbitrary vector in the plane $x_3 = 0$ and we assume that both ε_1 and ε_2 are real and positive. The surface profile function $\zeta(\mathbf{x}_\parallel)$ is assumed to be a single-valued function of $\mathbf{x}_\parallel$ that is differentiable with respect to x_1 and x_2 and constitutes a stationary, zero-mean, isotropic, Gaussian random process defined by

$$\langle \zeta(\mathbf{x}_\parallel)\zeta(\mathbf{x}'_\parallel)\rangle = \delta^2 W(|\mathbf{x}_\parallel - \mathbf{x}'_\parallel|), \tag{1}$$

where $W(x_\parallel)$ is the *normalized surface height autocorrelation function*, with the property that $W(0) = 1$. The angle brackets here and in all that follows denote an average over the ensemble of realizations of the surface profile function. The root-mean-square height of the surface is given by

$$\delta = \langle \zeta^2(\mathbf{x}_\parallel)\rangle^{\frac{1}{2}}. \tag{2}$$

The power spectrum of the surface roughness $g(k_\parallel)$ is defined by

$$g(k_\parallel) = \int d^2x_\parallel W(x_\parallel)\exp(-i\mathbf{k}_\parallel\cdot\mathbf{x}_\parallel). \tag{3}$$

For $W(x_\parallel)$ we assume the Gaussian function $W(x_\parallel) = \exp(-x_\parallel^2/a^2)$, where the characteristic length a is the transverse correlation length of the surface roughness. The corresponding power spectrum is given by

$$g(k_\parallel) = \pi a^2 \exp\left(-\frac{a^2k_\parallel^2}{4}\right). \tag{4}$$

III. THE REDUCED RAYLEIGH EQUATION

The interface $x_3 = \zeta(\mathbf{x}_\parallel)$ is illuminated from the region $x_3 > \zeta(\mathbf{x}_\parallel)$ (medium 1) by an electromagnetic wave of frequency ω. The total electric field in this region is the sum of an incoming incident field and an outgoing scattered field,

$$\mathbf{E}^>(\mathbf{x}|\omega) = \mathbf{E}_0(\mathbf{k}_\parallel)\exp[i\mathbf{Q}_0(\mathbf{k}_\parallel)\cdot\mathbf{x}] + \int \frac{d^2q_\parallel}{(2\pi)^2}\,\mathbf{A}(\mathbf{q}_\parallel)\exp[i\mathbf{Q}_1(\mathbf{q}_\parallel)\cdot\mathbf{x}], \tag{5}$$

while the electric field in the region $x_3 < \zeta(\mathbf{x}_\parallel)$ is an outgoing transmitted field,

$$\mathbf{E}^<(\mathbf{x}|\omega) = \int \frac{d^2q_\parallel}{(2\pi)^2}\,\mathbf{B}(\mathbf{q}_\parallel)\exp[i\mathbf{Q}_2^-(\mathbf{q}_\parallel)\cdot\mathbf{x}]. \tag{6}$$

In writing these equations we have introduced the functions

$$\mathbf{Q}_0(\mathbf{k}_\parallel) = \mathbf{k}_\parallel - \alpha_1(k_\parallel)\hat{\mathbf{x}}_3, \tag{7a}$$

$$\mathbf{Q}_1(\mathbf{q}_\parallel) = \mathbf{q}_\parallel + \alpha_1(q_\parallel)\hat{\mathbf{x}}_3, \tag{7b}$$

$$\mathbf{Q}_2^\pm(\mathbf{q}_\parallel) = \mathbf{q}_\parallel \pm \alpha_2(q_\parallel)\hat{\mathbf{x}}_3, \tag{7c}$$

where $(i = 1,2)$

$$\alpha_i(q_\parallel) = \left[\varepsilon_i\left(\frac{\omega}{c}\right)^2 - q_\parallel^2\right]^{\frac{1}{2}} \quad \mathrm{Re}\,\alpha_i(q_\parallel) > 0, \quad \mathrm{Im}\,\alpha_i(q_\parallel) > 0. \tag{8}$$

Here $\mathbf{k}_\parallel = (k_1,k_2,0)$, and a caret over a vector indicates that it is a unit vector. A frequency dependence of the field of the form $\exp(-i\omega t)$ has been assumed, but not indicated explicitly.

The boundary conditions satisfied by these fields at the interface $x_3 = \zeta(\mathbf{x}_\parallel)$ are the continuity of the tangential components of the electric field,

$$\mathbf{n}\times\mathbf{E}_0(\mathbf{k}_\parallel)\exp[i\mathbf{k}_\parallel\cdot\mathbf{x}_\parallel - i\alpha_1(k_\parallel)\zeta(\mathbf{x}_\parallel)] + \int \frac{d^2q_\parallel}{(2\pi)^2}\,\mathbf{n}\times\mathbf{A}(\mathbf{q}_\parallel)\exp[i\mathbf{q}_\parallel\cdot\mathbf{x}_\parallel + i\alpha_1(q_\parallel)\zeta(\mathbf{x}_\parallel)] = \int \frac{d^2q_\parallel}{(2\pi)^2}\,\mathbf{n}\times\mathbf{B}(\mathbf{q}_\parallel)\exp[i\mathbf{q}_\parallel\cdot\mathbf{x}_\parallel - i\alpha_2(q_\parallel)\zeta(\mathbf{x}_\parallel)], \tag{9}$$

the continuity of the tangential components of the magnetic field,

$$\mathbf{n}\times[i\mathbf{Q}_0(\mathbf{k}_\parallel)\times\mathbf{E}_0(\mathbf{k}_\parallel)]\exp[i\mathbf{k}_\parallel\cdot\mathbf{x}_\parallel-i\alpha_1(k_\parallel)\zeta(\mathbf{x}_\parallel)]+\int\frac{d^2q_\parallel}{(2\pi)^2}\,\mathbf{n}\times[i\mathbf{Q}_1(\mathbf{q}_\parallel)\times\mathbf{A}(\mathbf{q}_\parallel)]\exp[i\mathbf{q}_\parallel\cdot\mathbf{x}_\parallel+i\alpha_1(q_\parallel)\zeta(\mathbf{x}_\parallel)]$$
$$=\int\frac{d^2q_\parallel}{(2\pi)^2}\,\mathbf{n}\times[i\mathbf{Q}_2^-(\mathbf{q}_\parallel)\times\mathbf{B}(\mathbf{q}_\parallel)]\exp[i\mathbf{q}_\parallel\cdot\mathbf{x}_\parallel-i\alpha_2(q_\parallel)\zeta(\mathbf{x}_\parallel)], \tag{10}$$

and the continuity of the normal component of the electric displacement,

$$\varepsilon_1\mathbf{n}\cdot\mathbf{E}_0(\mathbf{k}_\parallel)\exp[i\mathbf{k}_\parallel\cdot\mathbf{x}_\parallel-i\alpha_1(k_\parallel)\zeta(\mathbf{x}_\parallel)]+\varepsilon_1\int\frac{d^2q_\parallel}{(2\pi)^2}\,\mathbf{n}\cdot\mathbf{A}(\mathbf{q}_\parallel)\exp[i\mathbf{q}_\parallel\cdot\mathbf{x}_\parallel+i\alpha_1(q_\parallel)\zeta(\mathbf{x}_\parallel)]$$
$$=\varepsilon_2\int\frac{d^2q_\parallel}{(2\pi)^2}\,\mathbf{n}\cdot\mathbf{B}(\mathbf{q}_\parallel)\exp[i\mathbf{q}_\parallel\cdot\mathbf{x}_\parallel-i\alpha_2(q_\parallel)\zeta(\mathbf{x}_\parallel)]. \tag{11}$$

The vector $\mathbf{n}\equiv\mathbf{n}(\mathbf{x}_\parallel)$ entering these equations is a vector normal to the surface $x_3=\zeta(\mathbf{x}_\parallel)$ at each point of it, directed into medium 1:

$$\mathbf{n}(\mathbf{x}_\parallel)=\left[-\frac{\partial\zeta(\mathbf{x}_\parallel)}{\partial x_1},-\frac{\partial\zeta(\mathbf{x}_\parallel)}{\partial x_2},1\right]. \tag{12}$$

Equation (11) is redundant, but its inclusion simplifies the subsequent analysis. We now proceed to eliminate the transmission amplitude $\mathbf{B}(\mathbf{q}_\parallel)$ from this set of equations to obtain an equation that relates the scattering amplitude $\mathbf{A}(\mathbf{q}_\parallel)$ to the amplitude of the incident field $\mathbf{E}_0(\mathbf{k}_\parallel)$.

We begin by taking the vector cross product of Eq. (9) with $\varepsilon_2\mathbf{Q}_2^+(\mathbf{p}_\parallel)\exp[-i\mathbf{Q}_2^+(\mathbf{p}_\parallel)\cdot\{\mathbf{x}_\parallel+\hat{\mathbf{x}}_3\zeta(\mathbf{x}_\parallel)\}]$; we next multiply Eq. (10) by $-i\varepsilon_2\exp[-i\mathbf{Q}_2^+(\mathbf{p}_\parallel)\cdot\{\mathbf{x}_\parallel+\hat{\mathbf{x}}_3\zeta(\mathbf{x}_\parallel)\}]$; and finally we multiply Eq. (11) by $-\mathbf{Q}_2^+(\mathbf{p}_\parallel)\exp[-i\mathbf{Q}_2^+(\mathbf{p}_\parallel)\cdot\{\mathbf{x}_\parallel+\hat{\mathbf{x}}_3\zeta(\mathbf{x}_\parallel)\}]$, where $\mathbf{p}_\parallel=(p_1,p_2,0)$ is an arbitrary wave vector in the plane $x_3=0$. When we add the three equations obtained in this way, and integrate the sum over $\mathbf{x}_\parallel$ we obtain an equation that can be written in the form

$$\varepsilon_2\mathbf{Q}_2^+(\mathbf{p}_\parallel)\times[\mathbf{V}_E(\mathbf{p}_\parallel|\mathbf{k}_\parallel)\times\mathbf{E}_0(\mathbf{k}_\parallel)]+\varepsilon_2\mathbf{V}_E(\mathbf{p}_\parallel|\mathbf{k}_\parallel)\times[\mathbf{Q}_0(\mathbf{k}_\parallel)\times\mathbf{E}_0(\mathbf{k}_\parallel)]-\varepsilon_1\mathbf{Q}_2^+(\mathbf{p}_\parallel)[\mathbf{V}_E(\mathbf{p}_\parallel|\mathbf{k}_\parallel)\cdot\mathbf{E}_0(\mathbf{k}_\parallel)]$$
$$+\int\frac{d^2q_\parallel}{(2\pi)^2}\,\{\varepsilon_2\mathbf{Q}_2^+(\mathbf{p}_\parallel)\times[\mathbf{V}_A(\mathbf{p}_\parallel|\mathbf{q}_\parallel)\times\mathbf{A}(\mathbf{q}_\parallel)]+\varepsilon_2\mathbf{V}_A(\mathbf{p}_\parallel|\mathbf{q}_\parallel)\times[\mathbf{Q}_1(\mathbf{q}_\parallel)\times\mathbf{A}(\mathbf{q}_\parallel)]-\varepsilon_1\mathbf{Q}_2^+(\mathbf{p}_\parallel)[\mathbf{V}_A(\mathbf{p}_\parallel|\mathbf{q}_\parallel)\cdot\mathbf{A}(\mathbf{q}_\parallel)]\}$$
$$=\varepsilon_2\int\frac{d^2q_\parallel}{(2\pi)^2}\,\{\mathbf{Q}_2^+(\mathbf{p}_\parallel)\times[\mathbf{V}_B(\mathbf{p}_\parallel|\mathbf{q}_\parallel)\times\mathbf{B}(\mathbf{q}_\parallel)]+\mathbf{V}_B(\mathbf{p}_\parallel|\mathbf{q}_\parallel)\times[\mathbf{Q}_2^-(\mathbf{q}_\parallel)\times\mathbf{B}(\mathbf{q}_\parallel)]-\mathbf{Q}_2^+(\mathbf{p}_\parallel)[\mathbf{V}_B(\mathbf{p}_\parallel|\mathbf{q}_\parallel)\cdot\mathbf{B}(\mathbf{q}_\parallel)]\}, \tag{13}$$

where

$$\mathbf{V}_E(\mathbf{p}_\parallel|\mathbf{k}_\parallel)=\int d^2x_\parallel\;\mathbf{n}(\mathbf{x}_\parallel)\exp\{-i(\mathbf{p}_\parallel-\mathbf{k}_\parallel)\cdot\mathbf{x}_\parallel-i[\alpha_2(p_\parallel)+\alpha_1(k_\parallel)]\zeta(\mathbf{x}_\parallel)\}, \tag{14a}$$

$$\mathbf{V}_A(\mathbf{p}_\parallel|\mathbf{q}_\parallel)=\int d^2x_\parallel\;\mathbf{n}(\mathbf{x}_\parallel)\exp\{-i(\mathbf{p}_\parallel-\mathbf{q}_\parallel)\cdot\mathbf{x}_\parallel-i[\alpha_2(p_\parallel)-\alpha_1(q_\parallel)]\zeta(\mathbf{x}_\parallel)\}, \tag{14b}$$

$$\mathbf{V}_B(\mathbf{p}_\parallel|\mathbf{q}_\parallel)=\int d^2x_\parallel\;\mathbf{n}(\mathbf{x}_\parallel)\exp\{-i(\mathbf{p}_\parallel-\mathbf{q}_\parallel)\cdot\mathbf{x}_\parallel-i[\alpha_2(p_\parallel)+\alpha_2(q_\parallel)]\zeta(\mathbf{x}_\parallel)\}. \tag{14c}$$

At this point it is convenient to introduce the representation

$$\exp[-i\gamma\zeta(\mathbf{x}_\parallel)]=\int\frac{d^2Q_\parallel}{(2\pi)^2}\,I(\gamma|\mathbf{Q}_\parallel)\exp(i\mathbf{Q}_\parallel\cdot\mathbf{x}_\parallel). \tag{15}$$

On differentiating both sides of Eq. (15) with respect to $x_j\,(j=1,2)$ we obtain the result

$$-\frac{\partial\zeta(\mathbf{x}_\parallel)}{\partial x_j}\exp[-i\gamma\zeta(\mathbf{x}_\parallel)]=\int\frac{d^2Q_\parallel}{(2\pi)^2}\,\frac{Q_j}{\gamma}I(\gamma|\mathbf{Q}_\parallel)\exp(i\mathbf{Q}_\parallel\cdot\mathbf{x}_\parallel). \tag{16}$$

Finally, to be able to evaluate the function $I(\gamma|\mathbf{Q}_\parallel)$ we need the inverse of Eq. (15), namely,

$$I(\gamma|\mathbf{Q}_\parallel)=\int d^2x_\parallel\;\exp(-i\mathbf{Q}_\parallel\cdot\mathbf{x}_\parallel)\exp[-i\gamma\zeta(\mathbf{x}_\parallel)]=\sum_{n=0}^{\infty}\frac{(-i\gamma)^n}{n!}\hat{\zeta}^{(n)}(\mathbf{Q}_\parallel), \tag{17}$$

where

$$\hat{\zeta}^{(0)}(\mathbf{Q}_\parallel)=(2\pi)^2\delta(\mathbf{Q}_\parallel), \tag{18a}$$

$$\hat{\zeta}^{(n)}(\mathbf{Q}_\parallel)=\int d^2x_\parallel\;\zeta^n(\mathbf{x}_\parallel)\exp(-i\mathbf{Q}_\parallel\cdot\mathbf{x}_\parallel),\quad n\geqslant 1. \tag{18b}$$

On combining Eqs. (14)–(17) with Eqs. (7) and (12) we obtain the results

$$\mathbf{V}_E(\mathbf{p}_\parallel|\mathbf{k}_\parallel) = [\mathbf{Q}_2^+(\mathbf{p}_\parallel) - \mathbf{Q}_0(\mathbf{k}_\parallel)] \times \frac{I(\alpha_2(p_\parallel)+\alpha_1(k_\parallel)|\mathbf{p}_\parallel-\mathbf{k}_\parallel)}{\alpha_2(p_\parallel)+\alpha_1(k_\parallel)}, \tag{19a}$$

$$\mathbf{V}_A(\mathbf{p}_\parallel|\mathbf{q}_\parallel) = [\mathbf{Q}_2^+(\mathbf{p}_\parallel) - \mathbf{Q}_1(\mathbf{q}_\parallel)] \times \frac{I(\alpha_2(p_\parallel)-\alpha_1(q_\parallel)|\mathbf{p}_\parallel-\mathbf{q}_\parallel)}{\alpha_2(p_\parallel)-\alpha_1(q_\parallel)}, \tag{19b}$$

$$\mathbf{V}_B(\mathbf{p}_\parallel|\mathbf{q}_\parallel) = [\mathbf{Q}_2^+(\mathbf{p}_\parallel) - \mathbf{Q}_2^-(\mathbf{q}_\parallel)] \times \frac{I(\alpha_2(p_\parallel)+\alpha_2(q_\parallel)|\mathbf{p}_\parallel-\mathbf{q}_\parallel)}{\alpha_2(p_\parallel)+\alpha_2(q_\parallel)}. \tag{19c}$$

When the results given by Eq. (19) are substituted into Eq. (13), the latter becomes

$$\mathbf{Q}_2^+(\mathbf{p}_\parallel)\times[\mathbf{Q}_2^+(\mathbf{p}_\parallel)\cdot\mathbf{E}_0(\mathbf{k}_\parallel)]\frac{I(\alpha_2(p_\parallel)+\alpha_1(k_\parallel)|\mathbf{p}_\parallel-\mathbf{k}_\parallel)}{\alpha_2(p_\parallel)+\alpha_1(k_\parallel)} + \int\frac{d^2q_\parallel}{(2\pi)^2}\,\mathbf{Q}_2^+(\mathbf{p}_\parallel)\times[\mathbf{Q}_2^+(\mathbf{p}_\parallel)\cdot\mathbf{A}(\mathbf{q}_\parallel)] \times\frac{I(-\alpha_1(q_\parallel)+\alpha_2(p_\parallel)|\mathbf{p}_\parallel-\mathbf{q}_\parallel)}{-\alpha_1(q_\parallel)+\alpha_2(p_\parallel)} = 0. \tag{20}$$

Thus, the amplitude of the transmitted field $\mathbf{B}(\mathbf{q}_\parallel)$ has been eliminated from the problem and we have obtained an equation for the scattering amplitude $\mathbf{A}(\mathbf{q}_\parallel)$ alone.

To transform Eq. (20) into a more useful form, we first introduce three mutually perpendicular unit vectors:

$$\hat{\mathbf{a}}_0(\mathbf{p}_\parallel) = \frac{c}{\sqrt{\varepsilon_2}\omega}[\mathbf{p}_\parallel + \hat{\mathbf{x}}_3\alpha_2(p_\parallel)] = \frac{c}{\sqrt{\varepsilon_2}\omega}\mathbf{Q}_2^+(\mathbf{p}_\parallel), \tag{21a}$$

$$\hat{\mathbf{a}}_1(\mathbf{p}_\parallel) = \frac{c}{\sqrt{\varepsilon_2}\omega}[\hat{\mathbf{p}}_\parallel\alpha_2(p_\parallel) - \hat{\mathbf{x}}_3 p_\parallel], \tag{21b}$$

$$\hat{\mathbf{a}}_2(\mathbf{p}_\parallel) = \hat{\mathbf{x}}_3\times\hat{\mathbf{p}}_\parallel. \tag{21c}$$

In terms of these vectors Eq. (20) becomes

$$\{[\hat{\mathbf{a}}_0(\mathbf{p}_\parallel)\cdot\mathbf{E}_0(\mathbf{k}_\parallel)]\hat{\mathbf{a}}_0(\mathbf{p}_\parallel) - \mathbf{E}_0(\mathbf{k}_\parallel)\}\frac{I(\alpha_2(p_\parallel)+\alpha_1(k_\parallel)|\mathbf{p}_\parallel-\mathbf{k}_\parallel)}{\alpha_2(p_\parallel)+\alpha_1(k_\parallel)} + \int\frac{d^2q_\parallel}{(2\pi)^2}\,\{[\hat{\mathbf{a}}_0(\mathbf{p}_\parallel)\cdot\mathbf{A}(\mathbf{q}_\parallel)]\hat{\mathbf{a}}_0(\mathbf{p}_\parallel) - \mathbf{A}(\mathbf{q}_\parallel)\} \times\frac{I(\alpha_2(p_\parallel)-\alpha_1(q_\parallel)|\mathbf{p}_\parallel-\mathbf{q}_\parallel)}{\alpha_2(p_\parallel)-\alpha_1(q_\parallel)} = 0. \tag{22}$$

We now write the vectors $\mathbf{E}_0(\mathbf{k}_\parallel)$ and $\mathbf{A}(\mathbf{q}_\parallel)$ in the forms

$$\mathbf{E}_0(\mathbf{k}_\parallel) = \hat{\mathbf{e}}_p^{(i)}(\mathbf{k}_\parallel)E_{0p}(\mathbf{k}_\parallel) + \hat{\mathbf{e}}_s^{(i)}(\mathbf{k}_\parallel)E_{0s}(\mathbf{k}_\parallel), \tag{23a}$$

with

$$\hat{\mathbf{e}}_p^{(i)}(\mathbf{k}_\parallel) = \frac{c}{\sqrt{\varepsilon_1}\omega}[\hat{\mathbf{k}}_\parallel\alpha_1(k_\parallel) + \hat{\mathbf{x}}_3 k_\parallel], \tag{23b}$$

$$\hat{\mathbf{e}}_s^{(i)}(\mathbf{k}_\parallel) = \hat{\mathbf{k}}_\parallel\times\hat{\mathbf{x}}_3, \tag{23c}$$

and

$$\mathbf{A}(\mathbf{q}_\parallel) = \hat{\mathbf{e}}_p^{(s)}(\mathbf{q}_\parallel)A_p(\mathbf{q}_\parallel) + \hat{\mathbf{e}}_s^{(s)}(\mathbf{q}_\parallel)A_s(\mathbf{q}_\parallel), \tag{24a}$$

with

$$\hat{\mathbf{e}}_p^{(s)}(\mathbf{q}_\parallel) = \frac{c}{\sqrt{\varepsilon_1}\omega}[-\hat{\mathbf{q}}_\parallel\alpha_1(q_\parallel) + \hat{\mathbf{x}}_3 q_\parallel], \tag{24b}$$

$$\hat{\mathbf{e}}_s^{(s)}(\mathbf{q}_\parallel) = \hat{\mathbf{q}}_\parallel\times\hat{\mathbf{x}}_3. \tag{24c}$$

In these expressions $E_{0p}(\mathbf{k}_\parallel)$ and $E_{0s}(\mathbf{k}_\parallel)$ are the amplitudes of the p-and s-polarized components of the incident field with respect to the plane of incidence, defined by the vectors $\hat{\mathbf{k}}_\parallel$ and $\hat{\mathbf{x}}_3$. Similarly, $A_p(\mathbf{q}_\parallel)$ and $A_s(\mathbf{q}_\parallel)$ are the amplitudes of the p- and s-polarized components of the scattered field with respect to the plane of scattering, defined by the vectors $\hat{\mathbf{q}}_\parallel$ and $\hat{\mathbf{x}}_3$.

Equation (22) is a vector equation: It is a set of three coupled equations. However, there are only two unknowns, namely $A_p(\mathbf{q}_\parallel)$ and $A_s(\mathbf{q}_\parallel)$. Consequently, one of these equations is redundant. To obtain $A_p(\mathbf{q}_\parallel)$ and $A_s(\mathbf{q}_\parallel)$ in terms of $E_{0p}(\mathbf{k}_\parallel)$ and $E_{0s}(\mathbf{k}_\parallel)$, we proceed as follows. We take the scalar product of Eq. (22) with each of the three unit vectors given by Eq. (21) in turn. The results are

$$\hat{\mathbf{a}}_0(\mathbf{p}_\parallel)\cdot\big[\text{Eq. (22)}\big]: \qquad 0 = 0; \tag{25a}$$

$$\hat{\mathbf{a}}_1(\mathbf{p}_\parallel)\cdot\big[\text{Eq. (22)}\big]: \quad -\hat{\mathbf{a}}_1(\mathbf{p}_\parallel)\cdot\mathbf{E}_0(\mathbf{k}_\parallel)\frac{I(\alpha_2(p_\parallel)+\alpha_1(k_\parallel)|\mathbf{p}_\parallel-\mathbf{k}_\parallel)}{\alpha_2(p_\parallel)+\alpha_1(k_\parallel)} = \int\frac{d^2q_\parallel}{(2\pi)^2}\,\hat{\mathbf{a}}_1(\mathbf{p}_\parallel)\cdot\mathbf{A}(\mathbf{q}_\parallel)\frac{I(\alpha_2(p_\parallel)-\alpha_1(q_\parallel)|\mathbf{p}_\parallel-\mathbf{q}_\parallel)}{\alpha_2(p_\parallel)-\alpha_1(q_\parallel)}; \tag{25b}$$

$$\hat{\mathbf{a}}_2(\mathbf{p}_\parallel)\cdot\big[\text{Eq. (22)}\big]: \quad -\hat{\mathbf{a}}_2(\mathbf{p}_\parallel)\cdot\mathbf{E}_0(\mathbf{k}_\parallel)\frac{I(\alpha_2(p_\parallel)+\alpha_1(k_\parallel)|\mathbf{p}_\parallel-\mathbf{k}_\parallel)}{\alpha_2(p_\parallel)+\alpha_1(k_\parallel)} = \int\frac{d^2q_\parallel}{(2\pi)^2}\,\hat{\mathbf{a}}_2(\mathbf{p}_\parallel)\cdot\mathbf{A}(\mathbf{q}_\parallel)\frac{I(\alpha_2(p_\parallel)-\alpha_1(q_\parallel)|\mathbf{p}_\parallel-\mathbf{q}_\parallel)}{\alpha_2(p_\parallel)-\alpha_1(q_\parallel)}. \tag{25c}$$

Equations (25b) and (25c) are the two equations we seek.

With the use of Eqs. (21) and (23)–(24), Eqs. (25b) and (25c) can be rewritten in the form ($\alpha = p,s$, $\beta = p,s$)

$$A_\alpha(\mathbf{q}_\parallel) = \sum_\beta R_{\alpha\beta}(\mathbf{q}_\parallel|\mathbf{k}_\parallel)E_{0\beta}(\mathbf{k}_\parallel). \tag{26}$$

On combining Eqs. (25b) and (25c) with Eq. (26) we find that the scattering amplitudes $\{R_{\alpha\beta}(\mathbf{q}_\parallel|\mathbf{k}_\parallel)\}$ are the solutions of the equation

$$\int \frac{d^2q_\parallel}{(2\pi)^2}\,\frac{I(\alpha_2(p_\parallel)-\alpha_1(q_\parallel)|\mathbf{p}_\parallel-\mathbf{q}_\parallel)}{\alpha_2(p_\parallel)-\alpha_1(q_\parallel)}\mathbf{M}^+(\mathbf{p}_\parallel|\mathbf{q}_\parallel)\mathbf{R}(\mathbf{q}_\parallel|\mathbf{k}_\parallel) = -\frac{I(\alpha_2(p_\parallel)+\alpha_1(k_\parallel)|\mathbf{p}_\parallel-\mathbf{k}_\parallel)}{\alpha_2(p_\parallel)+\alpha_1(k_\parallel)}\mathbf{M}^-(\mathbf{p}_\parallel|\mathbf{k}_\parallel), \tag{27}$$

where

$$\mathbf{M}^\pm(\mathbf{p}_\parallel|\mathbf{q}_\parallel) = \begin{pmatrix} \frac{1}{\sqrt{\varepsilon_1\varepsilon_2}}[p_\parallel q_\parallel \pm \alpha_2(p_\parallel)\,\hat{\mathbf{p}}_\parallel\cdot\hat{\mathbf{q}}_\parallel\,\alpha_1(q_\parallel)] & -\frac{1}{\sqrt{\varepsilon_2}}\frac{\omega}{c}\alpha_2(p_\parallel)\,[\hat{\mathbf{p}}_\parallel\times\hat{\mathbf{q}}_\parallel]_3 \\ \pm\frac{1}{\sqrt{\varepsilon_1}}\frac{\omega}{c}[\hat{\mathbf{p}}_\parallel\times\hat{\mathbf{q}}_\parallel]_3\,\alpha_1(q_\parallel) & \frac{\omega^2}{c^2}\,\hat{\mathbf{p}}_\parallel\cdot\hat{\mathbf{q}}_\parallel \end{pmatrix} \tag{28a}$$

and

$$\mathbf{R}(\mathbf{q}_\parallel|\mathbf{k}_\parallel) = \begin{pmatrix} R_{pp}(\mathbf{q}_\parallel|\mathbf{k}_\parallel) & R_{ps}(\mathbf{q}_\parallel|\mathbf{k}_\parallel) \\ R_{sp}(\mathbf{q}_\parallel|\mathbf{k}_\parallel) & R_{ss}(\mathbf{q}_\parallel|\mathbf{k}_\parallel) \end{pmatrix}. \tag{28b}$$

Equation (27) is the reduced Rayleigh equation for the scattering amplitudes.

IV. THE MEAN DIFFERENTIAL REFLECTION COEFFICIENT

From the knowledge of the scattering amplitudes the mean differential reflection coefficient, the reflectivity, and the reflectance can be calculated. The differential reflection coefficient $\partial R/\partial\Omega_s$ is defined such that $(\partial R/\partial\Omega_s)d\Omega_s$ is the fraction of the total time-averaged flux incident on the interface that is scattered into the element of solid angle $d\Omega_s$ about the scattering direction defined by the polar and azimuthal scattering angles (θ_s,ϕ_s). To obtain the mean differential reflection coefficient, we first note that the magnitude of the total time-averaged flux incident on the interface is given by

$$\begin{aligned} P_{\rm inc} &= -\mathrm{Re}\,\frac{c}{8\pi}\int d^2x_\parallel\left\{\mathbf{E}_0^*(\mathbf{k}_\parallel)\times\left[\frac{c}{\omega}\mathbf{Q}_0(\mathbf{k}_\parallel)\times\mathbf{E}_0(\mathbf{k}_\parallel)\right]\right\}_3\exp\{[-i\mathbf{Q}_0^*(\mathbf{k}_\parallel)+i\mathbf{Q}_0(\mathbf{k}_\parallel)]\cdot\mathbf{x}\} \\ &= -\mathrm{Re}\,\frac{c^2}{8\pi\omega}\int d^2x_\parallel\,\{|\mathbf{E}_0(\mathbf{k}_\parallel)|^2\mathbf{Q}_0(\mathbf{k}_\parallel)-[\mathbf{E}_0^*(\mathbf{k}_\parallel)\cdot\mathbf{Q}_0(\mathbf{k}_\parallel)]\mathbf{E}_0(\mathbf{k}_\parallel)\}_3 \\ &= \mathrm{Re}\,\frac{c^2}{8\pi\omega}\int d^2x_\parallel\,\alpha_1(k_\parallel)|\mathbf{E}_0(\mathbf{k}_\parallel)|^2 \\ &= S\frac{c^2}{8\pi\omega}\alpha_1(k_\parallel)|\mathbf{E}_0(\mathbf{k}_\parallel)|^2. \end{aligned} \tag{29}$$

In this result S is the area of the x_1x_2 plane covered by the randomly rough surface. The minus sign on the right-hand side of the first equation compensates for the fact that the 3-component of the incident flux is negative, and we have used the fact that $\alpha_1(k_\parallel)$ is real, so that $\mathbf{Q}_0(\mathbf{k}_\parallel)$ is real, and $\mathbf{E}_0^*(\mathbf{k}_\parallel)\cdot\mathbf{Q}_0(\mathbf{k}_\parallel)=0$.

In a similar fashion we note that the total time-averaged scattered flux is given by

$$\begin{aligned} P_{\rm sc} &= \mathrm{Re}\,\frac{c}{8\pi}\int d^2x_\parallel\int\frac{d^2q_\parallel}{(2\pi)^2}\int\frac{d^2q'_\parallel}{(2\pi)^2}\left\{\mathbf{A}^*(\mathbf{q}_\parallel)\times\left[\frac{c}{\omega}\mathbf{Q}_1(\mathbf{q}_\parallel)\times\mathbf{A}(\mathbf{q}'_\parallel)\right]\right\}_3\exp[-i\{\mathbf{Q}_1^*(\mathbf{q}_\parallel)-\mathbf{Q}_1(\mathbf{q}'_\parallel)\}\cdot\mathbf{x}] \\ &= \mathrm{Re}\,\frac{c^2}{8\pi\omega}\int\frac{d^2q_\parallel}{(2\pi)^2}\,\{|\mathbf{A}(\mathbf{q}_\parallel)|^2\mathbf{Q}_1(\mathbf{q}_\parallel)-[\mathbf{A}^*(\mathbf{q}_\parallel)\cdot\mathbf{Q}_1(\mathbf{q}_\parallel)]\mathbf{A}(\mathbf{q}_\parallel)\}_3\exp[-2\mathrm{Im}\,\alpha_1(q_\parallel)x_3] \\ &= \mathrm{Re}\,\frac{c^2}{8\pi\omega}\int\frac{d^2q_\parallel}{(2\pi)^2}\left\{\alpha_1(q_\parallel)|\mathbf{A}(\mathbf{q}_\parallel)|^2-\frac{c}{\sqrt{\varepsilon_1}\omega}q_\parallel[\mathbf{A}^*(\mathbf{q}_\parallel)\cdot\mathbf{Q}_1(\mathbf{q}_\parallel)]A_p(q_\parallel)\right\}\exp[-2\mathrm{Im}\,\alpha_1(q_\parallel)x_3] \\ &= \mathrm{Re}\,\frac{c^2}{8\pi\omega}\int\frac{d^2q_\parallel}{(2\pi)^2}\,\alpha_1(q_\parallel)|\mathbf{A}(\mathbf{q}_\parallel)|^2\exp[-2\mathrm{Im}\,\alpha_1(q_\parallel)x_3] \\ &\quad -\mathrm{Re}\,\frac{c^2}{8\pi\omega}\int\frac{d^2q_\parallel}{(2\pi)^2}\,[\alpha_1(q_\parallel)-\alpha_1^*(q_\parallel)]\frac{c^2}{\varepsilon_1\omega^2}q_\parallel^2|A_p(q_\parallel)|^2\exp[-2\mathrm{Im}\,\alpha_1(q_\parallel)x_3]. \end{aligned} \tag{30}$$

The integral in the second term is purely imaginary. Thus, we have

$$P_{\rm sc} = \frac{c^2}{32\pi^3\omega}\int_{q_\parallel<\sqrt{\varepsilon_1}\frac{\omega}{c}} d^2q_\parallel\,\alpha_1(q_\parallel)|\mathbf{A}(\mathbf{q}_\parallel)|^2. \tag{31}$$

The wave vectors $\mathbf{k}_\parallel$ and $\mathbf{q}_\parallel$ can be expressed in terms of the polar and azimuthal angles of incidence (θ_0,ϕ_0) and scattering (θ_s,ϕ_s), respectively, by

$$\mathbf{k}_\parallel = \sqrt{\varepsilon_1}\frac{\omega}{c}\sin\theta_0(\cos\phi_0, \sin\phi_0, 0), \tag{32a}$$

$$\mathbf{q}_\parallel = \sqrt{\varepsilon_1}\frac{\omega}{c}\sin\theta_s(\cos\phi_s, \sin\phi_s, 0). \tag{32b}$$

From these results it follows that

$$d^2q_\parallel = \varepsilon_1\left(\frac{\omega}{c}\right)^2\cos\theta_s\, d\Omega_s, \tag{33}$$

where $d\Omega_s = \sin\theta_s d\theta_s d\phi_s$. The total time-averaged scattered flux therefore becomes

$$P_{\rm sc} = \frac{\varepsilon_1^{3/2}\omega^2}{32\pi^3 c}\int d\Omega_s\ \cos^2\theta_s[|A_p(\mathbf{q}_\parallel)|^2 + |A_s(\mathbf{q}_\parallel)|^2]. \tag{34}$$

Similarly, the total time-averaged incident flux [Eq. (29)] becomes

$$P_{\rm inc} = S\frac{\sqrt{\varepsilon_1}c}{8\pi}\cos\theta_0[|E_{0p}(\mathbf{k}_\parallel)|^2 + |E_{0s}(\mathbf{k}_\parallel)|^2]. \tag{35}$$

Thus, by definition, the differential reflection coefficient is given by

$$\frac{\partial R}{\partial\Omega_s} = \frac{1}{S}\varepsilon_1\left(\frac{\omega}{2\pi c}\right)^2\frac{\cos^2\theta_s}{\cos\theta_0}\frac{|A_p(\mathbf{q}_\parallel)|^2 + |A_s(\mathbf{q}_\parallel)|^2}{|E_{0p}(\mathbf{k}_\parallel)|^2 + |E_{0s}(\mathbf{k}_\parallel)|^2}. \tag{36}$$

From this result and Eq. (26) we find that the contribution to the differential reflection coefficient when an incident plane wave of polarization β, the projection of whose wave vector on the mean scattering plane is $\mathbf{k}_\parallel$, is reflected into a plane wave of polarization α, the projection of whose wave vector on the mean scattering plane is $\mathbf{q}_\parallel$, is given by

$$\frac{\partial R_{\alpha\beta}(\mathbf{q}_\parallel|\mathbf{k}_\parallel)}{\partial\Omega_s} = \frac{1}{S}\varepsilon_1\left(\frac{\omega}{2\pi c}\right)^2\frac{\cos^2\theta_s}{\cos\theta_0}|R_{\alpha\beta}(\mathbf{q}_\parallel|\mathbf{k}_\parallel)|^2. \tag{37}$$

As we are dealing with scattering from a randomly rough interface, it is the average of this function over the ensemble of realizations of the surface profile function that we need to calculate. This is the mean differential reflection coefficient, which is defined by

$$\left\langle\frac{\partial R_{\alpha\beta}(\mathbf{q}_\parallel|\mathbf{k}_\parallel)}{\partial\Omega_s}\right\rangle = \frac{1}{S}\varepsilon_1\left(\frac{\omega}{2\pi c}\right)^2\frac{\cos^2\theta_s}{\cos\theta_0}\langle|R_{\alpha\beta}(\mathbf{q}_\parallel|\mathbf{k}_\parallel)|^2\rangle. \tag{38}$$

If we write the scattering amplitude $R_{\alpha\beta}(\mathbf{q}_\parallel|\mathbf{k}_\parallel)$ as the sum of its mean value and the fluctuation from this mean,

$$R_{\alpha\beta}(\mathbf{q}_\parallel|\mathbf{k}_\parallel) = \langle R_{\alpha\beta}(\mathbf{q}_\parallel|\mathbf{k}_\parallel)\rangle + [R_{\alpha\beta}(\mathbf{q}_\parallel|\mathbf{k}_\parallel) - \langle R_{\alpha\beta}(\mathbf{q}_\parallel|\mathbf{k}_\parallel)\rangle], \tag{39}$$

then each of these two terms contributes separately to the mean differential reflection coefficient,

$$\left\langle\frac{\partial R_{\alpha\beta}(\mathbf{q}_\parallel|\mathbf{k}_\parallel)}{\partial\Omega_s}\right\rangle = \left\langle\frac{\partial R_{\alpha\beta}(\mathbf{q}_\parallel|\mathbf{k}_\parallel)}{\partial\Omega_s}\right\rangle_{\rm coh} + \left\langle\frac{\partial R_{\alpha\beta}(\mathbf{q}_\parallel|\mathbf{k}_\parallel)}{\partial\Omega_s}\right\rangle_{\rm incoh}, \tag{40}$$

where

$$\left\langle\frac{\partial R_{\alpha\beta}(\mathbf{q}_\parallel|\mathbf{k}_\parallel)}{\partial\Omega_s}\right\rangle_{\rm coh} = \frac{1}{S}\varepsilon_1\left(\frac{\omega}{2\pi c}\right)^2\frac{\cos^2\theta_s}{\cos\theta_0}|\langle R_{\alpha\beta}(\mathbf{q}_\parallel|\mathbf{k}_\parallel)\rangle|^2 \tag{41}$$

and

$$\begin{aligned}\left\langle\frac{\partial R_{\alpha\beta}(\mathbf{q}_\parallel|\mathbf{k}_\parallel)}{\partial\Omega_s}\right\rangle_{\rm incoh} &= \frac{1}{S}\varepsilon_1\left(\frac{\omega}{2\pi c}\right)^2\frac{\cos^2\theta_s}{\cos\theta_0}\langle|R_{\alpha\beta}(\mathbf{q}_\parallel|\mathbf{k}_\parallel) - \langle R_{\alpha\beta}(\mathbf{q}_\parallel|\mathbf{k}_\parallel)\rangle|^2\rangle] \\ &= \frac{1}{S}\varepsilon_1\left(\frac{\omega}{2\pi c}\right)^2\frac{\cos^2\theta_s}{\cos\theta_0}[\langle|R_{\alpha\beta}(\mathbf{q}_\parallel|\mathbf{k}_\parallel)|^2\rangle - |\langle R_{\alpha\beta}(\mathbf{q}_\parallel|\mathbf{k}_\parallel)\rangle|^2].\end{aligned} \tag{42}$$

The former contribution describes the coherent (specular) reflection of the incident field from a randomly rough surface, while the latter contribution describes the incoherent (diffuse) component of the scattered light.

Reflectivity and reflectance

Equation (41) is the starting point for obtaining the reflectivity of the two-dimensional randomly rough interface. We begin with the result that

$$\langle R_{\alpha\beta}(\mathbf{q}_\parallel|\mathbf{k}_\parallel)\rangle = (2\pi)^2\delta(\mathbf{q}_\parallel - \mathbf{k}_\parallel)\delta_{\alpha\beta}R_\alpha(k_\parallel). \tag{43}$$

The presence of the δ function is due to the stationarity of the randomly rough surface; the Kronecker symbol $\delta_{\alpha\beta}$ arises from the conservation of angular momentum in the scattering process; and the result that $R_\alpha(k_\parallel)$ depends on $\mathbf{k}_\parallel$ only through its magnitude is due to the isotropy of the random roughness.

With the result given by Eq. (43), the expression for $\langle\partial R_{\alpha\beta}(\mathbf{q}_\parallel|\mathbf{k}_\parallel)/\partial\Omega_s\rangle_{\rm coh}$ given by Eq. (41), becomes

$$\left\langle\frac{\partial R_{\alpha\alpha}(\mathbf{q}_\parallel|\mathbf{k}_\parallel)}{\partial\Omega_s}\right\rangle_{\rm coh} = \varepsilon_1\left(\frac{\omega}{c}\right)^2\frac{\cos^2\theta_s}{\cos\theta_0}\left|R_\alpha(k_\parallel)\right|^2\delta(\mathbf{q}_\parallel - \mathbf{k}_\parallel), \tag{44}$$

where we have used the result

$$\begin{aligned}[(2\pi)^2\delta(\mathbf{q}_\parallel - \mathbf{k}_\parallel)]^2 &= (2\pi)^2\delta(\mathbf{0})\,(2\pi)^2\delta(\mathbf{q}_\parallel - \mathbf{k}_\parallel) \\ &= S(2\pi)^2\delta(\mathbf{q}_\parallel - \mathbf{k}_\parallel)\end{aligned} \tag{45}$$

in obtaining this expression. We next use the relation

$$\delta(\mathbf{q}_\parallel - \mathbf{k}_\parallel) = \frac{1}{k_\parallel}\delta(q_\parallel - k_\parallel)\,\delta(\phi_s - \phi_0) \tag{46}$$

together with the relations

$$k_\parallel = \sqrt{\varepsilon_1}\frac{\omega}{c}\sin\theta_0, \quad q_\parallel = \sqrt{\varepsilon_1}\frac{\omega}{c}\sin\theta_s, \tag{47}$$

to obtain

$$\left\langle \frac{\partial R_{\alpha\alpha}(\mathbf{q}_\parallel|\mathbf{k}_\parallel)}{\partial\Omega_s}\right\rangle_{\rm coh} = \sqrt{\varepsilon_1}\left(\frac{\omega}{c}\right)\frac{\cos^2\theta_s}{\cos\theta_0}\frac{1}{k_\parallel}|R_\alpha(k_\parallel)|^2 \times \delta(\sin\theta_s-\sin\theta_0)\delta(\phi_s-\phi_0) = \frac{\cos^2\theta_s}{\cos^2\theta_0}\left|R_\alpha(k_\parallel)\right|^2\frac{\delta(\theta_s-\theta_0)\delta(\phi_s-\phi_0)}{\sin\theta_0} = |R_\alpha(k_\parallel)|^2\frac{\delta(\theta_s-\theta_0)\delta(\phi_s-\phi_0)}{\sin\theta_0}. \quad (48)$$

The reflectivity, $\mathcal{R}_\alpha(\theta_0)$, for light of α polarization is defined by

$$\mathcal{R}_\alpha(\theta_0) = \int_0^{\frac{\pi}{2}} d\theta_s\sin\theta_s\int_{-\pi}^{\pi}d\phi_s\left\langle\frac{\partial R_{\alpha\alpha}(\mathbf{q}_\parallel|\mathbf{k}_\parallel)}{\partial\Omega_s}\right\rangle_{\rm coh} = |R_\alpha(k_\parallel)|^2. \quad (49)$$

The function $R_\alpha(k_\parallel)$ is obtained from Eq. (43), with the aid of the result that $(2\pi)^2\delta(\mathbf{0}) = S$, in the form

$$R_\alpha(k_\parallel) = R_\alpha\left(\sqrt{\varepsilon_1}\frac{\omega}{c}\sin\theta_0\right) = \frac{1}{S}\langle R_{\alpha\alpha}(\mathbf{k}_\parallel|\mathbf{k}_\parallel)\rangle. \quad (50)$$

In addition to the reflectivity (49) that depends only on the co-polarized light reflected coherently by the rough interface, it is also of interest to introduce the *reflectance* for β-polarized light defined as

$$\mathscr{R}_\beta(\theta_0) = \sum_{\alpha=p,s}\mathscr{R}_{\alpha\beta}(\theta_0), \quad (51a)$$

where

$$\mathscr{R}_{\alpha\beta}(\theta_0) = \int_0^{\frac{\pi}{2}} d\theta_s\sin\theta_s\int_{-\pi}^{\pi}d\phi_s\left\langle\frac{\partial R_{\alpha\beta}(\mathbf{q}_\parallel|\mathbf{k}_\parallel)}{\partial\Omega_s}\right\rangle. \quad (51b)$$

In short, the reflectance measures the fraction of the power flux incident on the rough surface that was reflected by it, taking both specularly and diffusely reflected light into account: In view of Eq. (40), the reflectance is the sum of a contribution from light that has been reflected coherently and a contribution from light that has been reflected incoherently by the rough interface, $\mathscr{R}_\beta(\theta_0) = \mathscr{R}_\beta(\theta_0)_{\rm coh} + \mathscr{R}_\beta(\theta_0)_{\rm incoh}$, and both co- and cross-polarized reflected light contribute. Since cross-polarized coherently reflected light is not allowed [see Eq. (43)], the coherent contribution to the reflectance for β-polarized light equals the reflectivity for β-polarized light; $\mathscr{R}_\beta(\theta_0)_{\rm coh} = \mathcal{R}_\beta(\theta_0)$. Equation (51a) can therefore also be written in the form

$$\mathscr{R}_\beta(\theta_0) = \mathcal{R}_\beta(\theta_0) + \sum_{\alpha=p,s}\mathscr{R}_{\alpha\beta}(\theta_0)_{\rm incoh}. \quad (52)$$

If the incident light is not purely p- or s-polarized, the reflectance and the reflectivity of the rough surface will have to be calculated on the basis of weighted sums of the expressions in Eqs. (49) and (52), where the weights reflect the fractions of the different polarizations contained within the incident light.

V. NUMERICAL SOLUTION OF THE REDUCED RAYLEIGH EQUATION

The simulation results to be presented in this work were obtained by a nonperturbative numerical solution of the reduced Rayleigh equation (27), which was carried out in the following manner. A realization of the surface profile function was generated on a grid of $N_x \times N_x$ points within a square region of the x_1x_2 plane of edges L. This surface profile enters Eq. (27) through the function $I(\gamma|\mathbf{Q}_\parallel)$, given by Eq. (17). Utilizing the Taylor expansion detailed in Eq. (17), the Fourier transform of $\zeta^n(\mathbf{x}_\parallel)$ was calculated by use of the fast Fourier transform [2], and the Taylor series was truncated at the finite order N_T. In evaluating the $\mathbf{q}_\parallel$ integral in Eq. (27), the infinite limits of integration were replaced by finite limits $|\mathbf{q}_\parallel| < \mathcal{Q}/2$, and the integration was carried out by a two-dimensional version of the extended midpoint rule [11, p. 135] applied to a circular subsection of a grid of $N_q \times N_q$ points in the q_1q_2 plane, whose size and discretization was determined by the Nyquist sampling theorem [11, p. 494] and the properties of the discrete Fourier transform [2]. In momentum space, these limits lead to discretization intervals of $\Delta q = 2\pi/L$ along the orthogonal axes of the q_1q_2 plane, and upper limits on the magnitude of resolved wave vectors are given by $\mathcal{Q} = \Delta q\lfloor N_x/2\rfloor$, where $\lfloor\cdot\rfloor$ denotes the floor function [11, p. 948]. The resulting linear system of equations was solved by LU factorization and back substitution.

These calculations were performed simultaneously for incident light of both p- and s-polarization, and they were performed for a large number N_p of realizations of the surface profile function $\zeta(\mathbf{x}_\parallel)$. The resulting scattering amplitude $R_{\alpha\beta}(\mathbf{q}_\parallel|\mathbf{k}_\parallel)$ and its squared modulus $|R_{\alpha\beta}(\mathbf{q}_\parallel|\mathbf{k}_\parallel)|^2$ were obtained for each realization. An arithmetic average of the N_p results for these quantities yielded the mean values $\langle R_{\alpha\beta}(\mathbf{q}_\parallel|\mathbf{k}_\parallel)\rangle$ and $\langle|R_{\alpha\beta}(\mathbf{q}_\parallel|\mathbf{k}_\parallel)|^2\rangle$ that enter Eqs. (50), (51), and (42) for the reflectivity, reflectance, and mean differential reflection coefficient, respectively. A more detailed description of the numerical method can be found in Ref. [2].

VI. RESULTS AND DISCUSSIONS

The two-dimensional randomly rough dielectric interfaces we study in this work were defined by isotropic Gaussian height distributions of rms heights $\delta = \lambda/40$ and $\delta = \lambda/20$, and an isotropic Gaussian correlation function of transverse correlation length $a = \lambda/4$ [Eq. (4)]. They covered a square region of the x_1x_2 plane of edge $L = 25\lambda$, giving an area $S = L^2 = 25\lambda \times 25\lambda$. The incident light was assumed to be a p- or s-polarized plane wave of wavelength λ in vacuum. One of the two media in our configuration was assumed to be vacuum with a dielectric constant $\varepsilon = 1.0$, and the other medium was assumed to be a photoresist defined by the dielectric constant $\varepsilon = 2.64$. Since the dielectric constants entering the calculations are independent of the wavelength, all lengths appearing in them can be scaled with respect to λ. The angles of incidence were (θ_0,ϕ_0), where the azimuthal angle of incidence was set to $\phi_0 = 0^\circ$, without loss of generality. We remark that this value of ϕ_0 was chosen since it coincided with one of the two axes of the numerical grid, but that it is, due to the isotropy of the roughness, an arbitrary choice in the sense that results for any other value of ϕ_0 can be obtained from the results presented through a trivial rotation. The surface profiles were generated by the Fourier filtering method (see Refs. [12] and [13]) on a grid of $N_x \times N_x = 321 \times 321$ points. The values used for N_x and L correspond to $\mathcal{Q} = 6.4\,\omega/c$, where $\mathcal{Q}$ is the limit in the $I(\gamma|\mathbf{Q}_\parallel)$ integrals [Eq. (17)], and we used the first

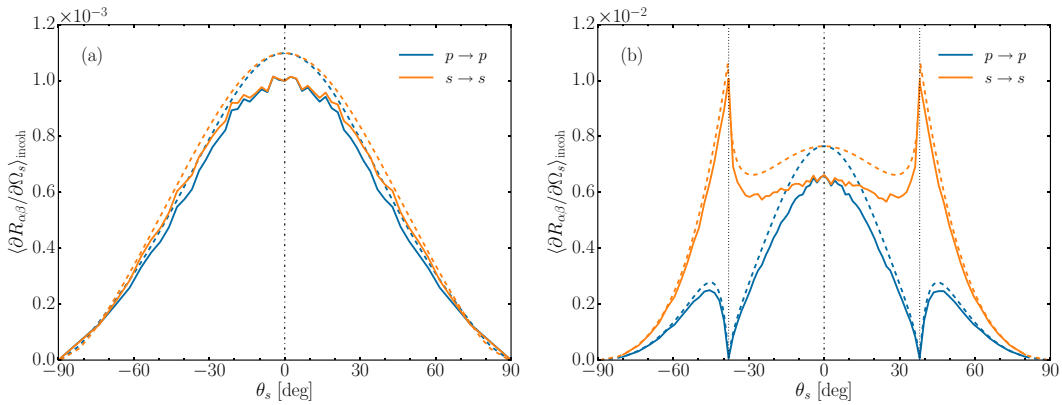

FIG. 2. The contribution to the incoherent component of the mean differential reflection coefficient from the in-plane, co-polarized scattering of p- and s-polarized light incident normally [$\theta_0 = 0^\circ$] on (a) a random vacuum-dielectric interface [$\varepsilon_1 = 1.0, \varepsilon_2 = 2.64$] and (b) a dielectric-vacuum interface [$\varepsilon_1 = 2.64, \varepsilon_2 = 1.0$] as a function of the polar angle of scattering θ_s. The solid curves were obtained on the basis of numerically solving the reduced Rayleigh equations [Eq. (27)] for an ensemble of 4500 surface realizations. The dashed curves are results from small-amplitude perturbation theory [Eq. (53)], included for comparison. The specular direction of reflection is indicated by the vertical dash-dotted line at $\theta_s = 0^\circ$, and in (b) the dotted lines at $|\theta_s| = \theta_c = \sin^{-1}\sqrt{\varepsilon_2/\varepsilon_1} \approx 38.0^\circ$ indicate the positions of the critical angle for total internal reflection (as expected for a flat surface system). Results for cross-polarized scattering have not been indicated since they are generally suppressed in the plane of incidence. The wavelength of the incident light in vacuum was λ. The rough interface was assumed to have a root-mean-square roughness of $\delta = \lambda/40$, and it was characterized by an isotropic Gaussian power spectrum [Eq. (4)] of transverse correlation length $a = \lambda/4$. In the numerical calculations it was assumed that the surface covered an area $L \times L$, with $L = 25\lambda$, and the surface was discretized on a grid of 321×321 points.

$N_T = 18$ terms of the Taylor expansion in the calculation of these integrals.

Investigating the energy conservation of our simulation results can be a useful test of their accuracy. In combining simulation results from the current work with corresponding results obtained for the mean differential transmission coefficient $\langle \partial T_{\alpha\beta}/\partial\Omega_t \rangle$ through the use of computationally similar methods [14,15], we may add the total reflected and transmitted power for any lossless system. When the reflectance is added to the transmittance for any of the systems investigated in the current work, it is found that the results of these calculations satisfy unitarity [14], a measure of energy conservation, with an error smaller than 10^{-4}. This testifies to the accuracy of the approach used, and it is also a good indicator of satisfactory discretization. It should be noted, however, that unitarity is a necessary, but not sufficient, condition for the correctness of the presented results. In a separate investigation [16], unitarity was found to be satisfied to a satisfactory degree for surfaces with a root-mean-square roughness up to about three times larger than the roughness used in obtaining the results presented in this paper.

A. Normal incidence

In Fig. 2 we display the contribution to the in-plane ($\hat{\mathbf{q}}_\parallel \parallel \hat{\mathbf{k}}_\parallel$) incoherent components of the mean differential reflection coefficient (DRC) as a function of the polar angle of scattering when the random surface is illuminated from the vacuum side at normal incidence by p- and s-polarized light [Fig. 2(a)] and when it is illuminated from the dielectric medium side [Fig. 2(b)]. Notice that the unit vectors $\hat{\mathbf{q}}_\parallel = \mathbf{q}_\parallel/q_\parallel$ and $\hat{\mathbf{k}}_\parallel = \mathbf{k}_\parallel/k_\parallel$ are well defined also for $\theta_s = 0^\circ$ and $\theta_0 = 0^\circ$, respectively, as follows from Eqs. (32) and (47). Only results for in-plane co-polarized scattering are presented, since in-plane cross-polarized scattering is suppressed due to the absence of contribution from single-scattering processes. An ensemble of 4500 realizations of the surface profile function was used to produce the numerical results that this figure is based on. This ensemble size is more than adequate in terms of the interpretation of the results and their features, but we note that a larger ensemble size would have reduced the jaggedness that can be observed in all the (solid line) results presented in this work.

From Fig. 2(a) it is observed that the curves corresponding to the two polarizations are featureless and are nearly identical. In contrast, the curves presented in Fig. 2(b) are rather different for the two polarizations; they display both peaks and dips in $p \to p$ scattering and peaks in $s \to s$ scattering. The origins of these features can be understood through small-amplitude perturbation theory (SAPT). The contribution to the mean differential reflection coefficients from light scattered incoherently can to the lowest nonzero order in the surface profile function $\zeta(\mathbf{x}_\parallel)$ be expressed as (see the Appendix for details)

$$\left\langle \frac{\partial R_{pp}(\mathbf{q}_\parallel|\mathbf{k}_\parallel)}{\partial\Omega_s} \right\rangle_{\text{incoh}} = \frac{\delta^2}{\pi^2}\varepsilon_1(\varepsilon_2-\varepsilon_1)^2\left(\frac{\omega}{c}\right)^2\frac{\cos^2\theta_s}{\cos\theta_0}g(|\mathbf{q}_\parallel-\mathbf{k}_\parallel|)\frac{1}{|d_p(q_\parallel)|^2}|\varepsilon_2 q_\parallel k_\parallel - \varepsilon_1\alpha_2(q_\parallel)(\hat{\mathbf{q}}_\parallel\cdot\hat{\mathbf{k}}_\parallel)\alpha_2(k_\parallel)|^2\frac{\alpha_1^2(k_\parallel)}{|d_p(k_\parallel)|^2}, \quad (53a)$$

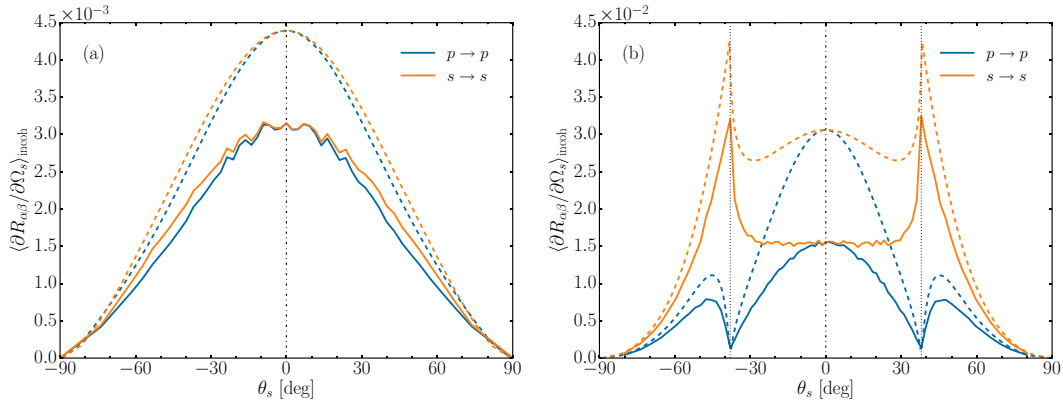

FIG. 3. Same as Fig. 2, but for the root-mean-square roughness $\delta = \lambda/20$.

$$\left\langle \frac{\partial R_{sp}(\mathbf{q}_\parallel|\mathbf{k}_\parallel)}{\partial\Omega_s} \right\rangle_{\rm incoh} = \frac{\delta^2}{\pi^2}\varepsilon_1^2(\varepsilon_2-\varepsilon_1)^2\left(\frac{\omega}{c}\right)^4 \frac{\cos^2\theta_s}{\cos\theta_0} g(|\mathbf{q}_\parallel - \mathbf{k}_\parallel|)\frac{\alpha_2^2(k_\parallel)}{|d_s(q_\parallel)|^2}([\hat{\mathbf{q}}_\parallel \times \hat{\mathbf{k}}_\parallel]_3)^2 \frac{\alpha_1^2(k_\parallel)}{|d_p(k_\parallel)|^2}, \tag{53b}$$

$$\left\langle \frac{\partial R_{ps}(\mathbf{q}_\parallel|\mathbf{k}_\parallel)}{\partial\Omega_s} \right\rangle_{\rm incoh} = \frac{\delta^2}{\pi^2}\varepsilon_1^2(\varepsilon_2-\varepsilon_1)^2\left(\frac{\omega}{c}\right)^4 \frac{\cos^2\theta_s}{\cos\theta_0} g(|\mathbf{q}_\parallel - \mathbf{k}_\parallel|)\frac{\alpha_2^2(q_\parallel)}{|d_p(q_\parallel)|^2}([\hat{\mathbf{q}}_\parallel \times \hat{\mathbf{k}}_\parallel]_3)^2 \frac{\alpha_1^2(k_\parallel)}{|d_s(k_\parallel)|^2}, \tag{53c}$$

$$\left\langle \frac{\partial R_{ss}(\mathbf{q}_\parallel|\mathbf{k}_\parallel)}{\partial\Omega_s} \right\rangle_{\rm incoh} = \frac{\delta^2}{\pi^2}\varepsilon_1(\varepsilon_2-\varepsilon_1)^2\left(\frac{\omega}{c}\right)^6 \frac{\cos^2\theta_s}{\cos\theta_0} g(|\mathbf{q}_\parallel - \mathbf{k}_\parallel|)\frac{1}{|d_s(q_\parallel)|^2}(\hat{\mathbf{q}}_\parallel \cdot \hat{\mathbf{k}}_\parallel)^2 \frac{\alpha_1^2(k_\parallel)}{|d_s(k_\parallel)|^2}, \tag{53d}$$

where the functions $d_\alpha(q_\parallel)$ and $d_\alpha(k_\parallel)$ for $\alpha = p,s$ are presented in Eq. (A5) as $d_\alpha^+(q_\parallel)$ and $d_\alpha^+(k_\parallel)$.

The results of a numerical evaluation of Eq. (53) for normal incidence and in-plane scattering $[\hat{\mathbf{q}}_\parallel \parallel \hat{\mathbf{k}}_\parallel]$ are displayed as dashed curves in Fig. 2. By comparing the curves obtained from small-amplitude perturbation theory to the results obtained from a purely numerical solution of the reduced Rayleigh equation (RRE) [Eq. (27)] we conclude that SAPT for the considered level of roughness, even to lowest nonzero order in the surface profile function as in Eq. (53), reproduces all the important features found in the mean differential reflection coefficients fairly well, but with a discrepancy in the amplitudes. This discrepancy decreases with decreasing surface roughness (results not shown). For example, similar comparisons for surfaces with an rms roughness of $\delta = \lambda/80$, but with the same correlation length $a = \lambda/4$, show that the ability of Eq. (53) to reproduce the results based on the RRE is excellent for such weakly rough surfaces. However, for surfaces of rms roughness $\delta = \lambda/20$ and the same correlation length, significant discrepancies are observed in both intensity (or amplitude) and angular dependence between the curves obtained on the basis of SAPT and the corresponding curves resulting from a numerical solution of the RRE (Fig. 3). For instance, from Fig. 3(b) it is observed that the angular dependence of the $s \to s$ scattered intensity around the normal scattering direction is not correctly reproduced by SAPT; in this angular interval the numerical simulation results are almost constant and therefore essentially independent of θ_s. These results illustrate the importance and necessity of going beyond lowest-order SAPT or of performing numerical simulations. We therefore stress the point that even if we in the following often turn to SAPT for interpretation of the nonperturbative solutions to the RRE, any conclusion drawn on the basis of Eq. (53) is correct only to the lowest nonzero order in the surface profile function.

Results similar to those presented in Figs. 2 and 3 but for scattering *out-of-plane* $[\hat{\mathbf{q}}_\parallel \cdot \hat{\mathbf{k}}_\parallel = 0]$ are not presented, since, for normal incidence, the results for co-polarized in-plane scattering are the same as the results for cross-polarized out-of-plane scattering when the polarization of the scattered light is the same in the two cases. This symmetry is expected for isotropic surfaces like the ones we are investigating when the lateral momentum of the incident light is zero, supported by the observation that Eq. (53a) evaluated in-plane equals Eq. (53c) evaluated out of plane, and correspondingly for Eqs. (53d) and (53b), when $k_\parallel = 0$ and $\theta_0 = 0$.

In order to simplify the subsequent discussion, we here express $d_\alpha(q_\parallel)$ and $d_\alpha(k_\parallel)$ in terms of the polar angles of incidence and scattering using the relations in Eq. (47):

$$d_p(q_\parallel) = \sqrt{\varepsilon_1}\frac{\omega}{c}\left\{\varepsilon_2\cos\theta_s + \varepsilon_1\left[\frac{\varepsilon_2}{\varepsilon_1} - \sin^2\theta_s\right]^{\frac{1}{2}}\right\}, \tag{54a}$$

$$d_s(q_\parallel) = \sqrt{\varepsilon_1}\frac{\omega}{c}\left\{\cos\theta_s + \left[\frac{\varepsilon_2}{\varepsilon_1} - \sin^2\theta_s\right]^{\frac{1}{2}}\right\}, \tag{54b}$$

$$d_p(k_\parallel) = \sqrt{\varepsilon_1}\frac{\omega}{c}\left\{\varepsilon_2\cos\theta_0 + \varepsilon_1\left[\frac{\varepsilon_2}{\varepsilon_1} - \sin^2\theta_0\right]^{\frac{1}{2}}\right\}, \tag{54c}$$

$$d_s(k_\parallel) = \sqrt{\varepsilon_1}\frac{\omega}{c}\left\{\cos\theta_0 + \left[\frac{\varepsilon_2}{\varepsilon_1} - \sin^2\theta_0\right]^{\frac{1}{2}}\right\}. \tag{54d}$$

We see from Eq. (54) that when ε_2 is greater than ε_1, both $d_p(q_\parallel)$ and $d_s(q_\parallel)$ are real continuous functions of θ_s in the interval $0 < |\theta_s| < \pi/2$, and so therefore are $|d_p(q_\parallel)|^2$ and $|d_s(q_\parallel)|^2$. Hence, no features are introduced into the corresponding mean differential reflection coefficients by these functions. However, when ε_1 is greater than ε_2, the function $[(\varepsilon_2/\varepsilon_1) - \sin^2\theta_s]^{\frac{1}{2}}$ present in $d_p(q_\parallel)$ and $d_s(q_\parallel)$ vanishes when $|\theta_s|$ equals the critical angle $\theta_c = \sin^{-1}\sqrt{\varepsilon_2/\varepsilon_1}$ for total internal reflection for the corresponding flat-surface system, and becomes purely imaginary as $|\theta_s|$ increases beyond this angle. The functions $|d_p(q_\parallel)|^2$ and $|d_s(q_\parallel)|^2$, therefore, both have minima at $|\theta_s| = \theta_c$. In the case of $s \to s$ in-plane scattering at normal incidence, the minima in the function $|d_s(q_\parallel)|^2$ for $\varepsilon_1 > \varepsilon_2$ lead to sharp peaks at $|\theta_s| = \theta_c$ in $\langle \partial R_{ss}(\mathbf{q}_\parallel|\mathbf{k}_\parallel)/\partial\Omega_s\rangle_{\rm incoh}$, as displayed in Fig. 2(b). These same peaks will then also be present for $p \to s$ out-of-plane scattering at normal incidence. However, for $p \to p$ in-plane scattering, while there are still minima in the function $|d_p(q_\parallel)|^2$, we see from Eq. (53a) that $\langle \partial R_{pp}(\mathbf{q}_\parallel|\mathbf{k}_\parallel)/\partial\Omega_s\rangle_{\rm incoh}$, to lowest order in the surface profile function, vanishes when the function

$$F(\mathbf{q}_\parallel|\mathbf{k}_\parallel) = |\varepsilon_2 q_\parallel k_\parallel - \varepsilon_1\alpha_2(q_\parallel)(\hat{\mathbf{q}}_\parallel\cdot\hat{\mathbf{k}}_\parallel)\alpha_2(k_\parallel)|^2 \qquad (55)$$

vanishes. For normal incidence ($k_\parallel = 0$) and in-plane scattering ($\hat{\mathbf{q}}_\parallel \parallel \hat{\mathbf{k}}_\parallel$), we see from this expression that $\langle \partial R_{pp}(\mathbf{q}_\parallel|\mathbf{k}_\parallel)/\partial\Omega_s\rangle_{\rm incoh}$ will vanish when $\alpha_2(q_\parallel) = 0$, which is when $q_\parallel = \sqrt{\varepsilon_2}\omega/c$ [see Eq. (47)]. This will be the case for $\theta_s < 90^\circ$ only when $\varepsilon_1 > \varepsilon_2$, and the expression for $\langle \partial R_{pp}(\mathbf{q}_\parallel|\mathbf{k}_\parallel)/\partial\Omega_s\rangle_{\rm incoh}$ in Eq. (53a) will in this case be zero for $|\theta_s| = \theta_c$, explaining the dips shown in Fig. 2(b) for $p \to p$ scattering. We note in passing that the out-of-plane distribution of $\langle \partial R_{ps}(\mathbf{q}_\parallel|\mathbf{k}_\parallel)/\partial\Omega_s\rangle_{\rm incoh}$ also shows dips at the same polar angles, due to the factor $\alpha_2(q_\parallel)$ in Eq. (53c), but these dips will be present regardless of the angle of incidence.

The peaks observed for $\theta_s \geqslant \theta_c$ in Figs. 2 and 3 for $\varepsilon_1 > \varepsilon_2$ are optical analogs of the *Yoneda peaks* observed by Yoneda in the scattering of x-rays from a metal surface [5] and described as "quasi-anomalous scattering peaks" in the two-dimensional work by Kawanishi *et al.* [4]. The Yoneda peaks were originally observed as sharp peaks for incidence close to the grazing angle, as the difference in the dielectric constants of the two scattering media is very small at x-ray frequencies. In the following, by Yoneda peaks we mean well-defined maxima in the angular distribution of the intensity of the scattered light at, or slightly above, the critical polar angle for total internal reflection, when $\varepsilon_1 > \varepsilon_2$.

Although the mathematical origin of the Yoneda peaks is clear from Eqs. (53) and (54)—namely, they are associated with the minimum of the functions $|d_{p,s}(q_\parallel)|^2$ and $|d_{p,s}(k_\parallel)|^2$—a physical interpretation of them is still under discussion. Thus, Warren and Clarke [17], in a study of the reflection of x rays from a polished surface (mirror), proposed that these peaks arise when the incident beam at a grazing angle of incidence θ_0 that is greater than the grazing critical angle for total internal reflection θ_c is scattered through a small angle β by something just above the mirror surface. The scattered field falls upon the mirror at a grazing angle α, and strong reflection occurs when $\alpha < \theta_c$. This reflection is cut off sharply for $\alpha > \theta_c$ and less sharply for $\alpha < \theta_c$ by the rapidly decreasing intensity of small-angle scattering. This produces an asymmetric peak in the intensity of the scattered field, whose maximum occurs at the critical angle. It was suggested that the scatterer could be a projection on an irregular surface.

In a subsequent study of the grazing-angle reflection of x rays from rough metal surfaces with the use of the distorted-wave Born approximation [18], Vineyard [6] noted from an examination of the angular dependence of the magnitude of the Fresnel coefficient for transmission through a planar vacuum-metal interface, that it produces a transmitted field on the surface whose angular dependence has the form of an asymmetric peak. The peak maximum occurs at the critical angle and has a magnitude that is twice that of the incident electric field on the surface, leading to enhanced diffuse scattering at this angle. This "Vineyard effect" was invoked by Sinha *et al.* [7] as the origin of the Yoneda peaks. This result is mathematically similar to the explanation provided by Eqs. (53) and (54), but it is not a physical explanation for these peaks.

Such an interpretation was offered by Kawanishi *et al.* [4], who suggested that the Yoneda peaks may be associated with the presence of lateral waves [19] propagating along the interface in the optically less dense medium. This wave satisfies the condition for refraction back into the optically more dense medium, and it therefore leaks energy at every position along the interface, along rays whose scattering angle θ_s equals θ_c [20]. This radiation is restricted to the range $\theta_c < \theta_s < \pi/2$. This is an attractive explanation, but it needs to be explored more through additional calculations.

We have also calculated the full angular intensity distributions of the reflected light. Figures 4 and 5 present such simulation results for the contribution to the mean differential reflection coefficient from the light that has been scattered incoherently by the randomly rough interface. The angles of incidence were set to $(\theta_0,\phi_0) = (0^\circ,0^\circ)$; it was cross-sectional cuts along the plane of incidence of these angular intensity distributions that resulted in the solid curves presented in Fig. 2. The parameters assumed in producing the results of Figs. 2(a) and 4, and Figs. 2(b) and 5 are therefore identical.

Figures 4 and 5 and all following full angular intensity distributions are organized with a similar layout: They are arranged in 3×3 subfigures where each row and column of the array correspond to the angular distribution of the incoherent component of the mean differential reflection coefficient for a given state of polarization of the scattered and incident light, respectively. The lower left 2×2 corner of such figures corresponds to the cases where β-polarized incident light is reflected by the rough interface into α-polarized light, denoted $\beta \to \alpha$ in the lower left corner of each subfigure, where $\alpha = p,s$ and the same for β. Moreover, the first row corresponds to results where the polarization of the reflected light was not recorded (indicated by $\star$); such results are obtained by adding the other two results from the same column. The rightmost column presents results for which the incident light is *unpolarized* (indicated by an open circle, $\circ$); these results are obtained by taking the arithmetic average of the other two results present in the same row.

The lower left 2×2 corners of Figs. 4 and 5 display dipole-like patterns oriented along the plane of incidence for co polarization and perpendicular to it for cross polarization.

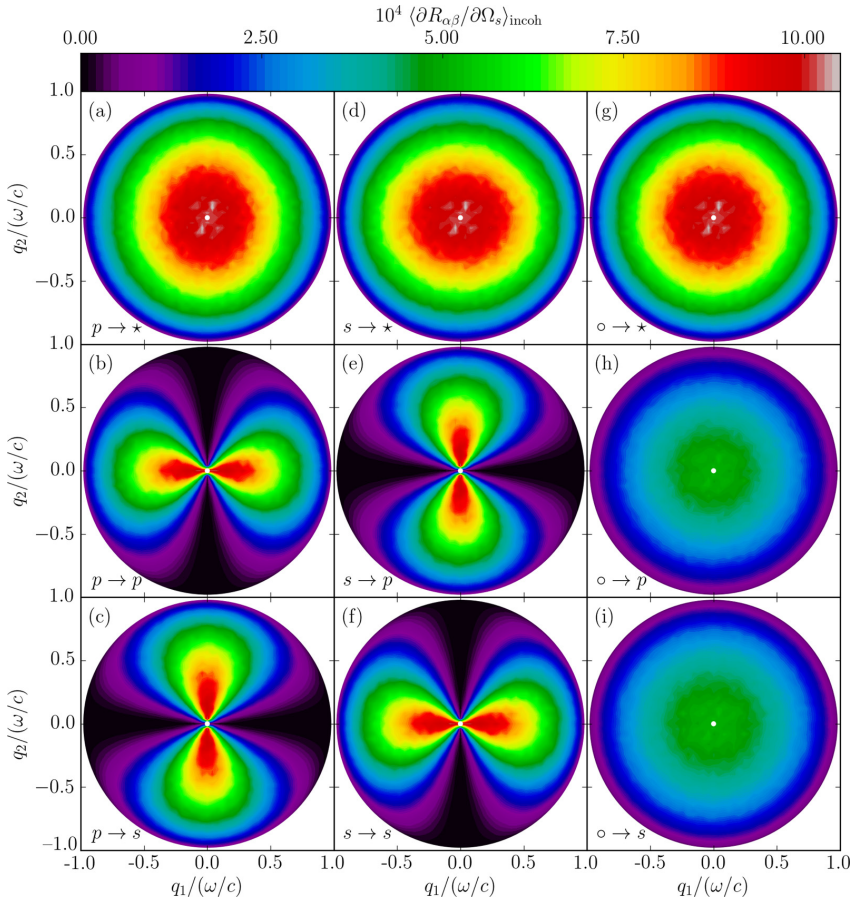

FIG. 4. The incoherent component of the mean differential reflection coefficient, showing the full angular intensity distribution as a function of the lateral wave vector of the light scattered by a rough interface between vacuum and a dielectric. The light was incident on the surface from the vacuum, $[\varepsilon_1 = 1.0, \varepsilon_2 = 2.64]$. The angles of incidence were $(\theta_0, \phi_0) = (0^\circ, 0^\circ)$. The position of the specular direction in reflection is indicated by white dots. The parameters assumed for the scattering geometry and used in performing the numerical simulations had values that are identical to those assumed in obtaining the results of Fig. 2(a). The in-plane intensity variations in panels (b) and (f) are the curves depicted in Fig. 2(a). The star notation, e.g., $p \to \star$, indicates that the polarization of the scattered light was not recorded; hence, panel (a) is the sum of panels (b) and (c), and panel (d) is the sum of panels (e) and (f). Furthermore, for the subfigures in the third column the open circle in, e.g. $\circ \to \star$ symbolizes that the incident light was unpolarized; these simulation results were obtained by taking the arithmetic average of the other two subfigures in the same row. The roughness parameters assumed in obtaining these results were $\delta = \lambda/40$ and $a = \lambda/4$.

This is a consequence of the definition used for the polarization vectors in our system. Moreover, Figs. 4(g)–4(i) and 5(g)–5(i) show that for unpolarized incident light at normal incidence, the scattering distributions are independent of the azimuthal angle of scattering ϕ_s. This rotational symmetry is expected for isotropic surfaces like the ones we are investigating when the lateral momentum of the unpolarized incident light is zero. However, for $\varepsilon_1 < \varepsilon_2$ and when the incident light is linearly polarized but the polarization of the reflected light is not recorded [Figs. 4(a) and 4(d)], we observe a slight skew in the distributions. This is similar to results presented in other, similar work [2,21] and is due to the subtle differences between the distributions of $p \to p$ and $s \to s$ scattered light, as presented for in-plane scattering in Fig. 2.

When $\varepsilon_1 > \varepsilon_2$ the Yoneda peaks form a circle of equal intensity at the polar angle $\theta_s = \theta_c$ [or $q_\parallel = \sqrt{\varepsilon_2}\omega/c$] in Fig. 5(i), where unpolarized incident light is scattered by the surface into s-polarized light. Similarly, a circular groove of close-to-zero intensity [exactly zero according to SAPT, Eq. (53)] can be found at $\theta_s = \theta_c$ in Fig. 5(h). The position and circular symmetry of this groove can be understood through the previously mentioned factors of $\alpha_2(q_\parallel)$ and $k_\parallel$ present in Eq. (53a) for $p \to p$ polarization and the factor $\alpha_2(q_\parallel)$ present in Eq. (53c) for $s \to p$ polarization, since $\alpha_2(q_\parallel)$ becomes zero when $q_\parallel = \sqrt{\varepsilon_2}\omega/c$ and $k_\parallel$ is zero for normal incidence. It can be of interest to note that we also, as a consequence, observe a ϕ_s-independent peak in Fig. 5(h) at a polar scattering angle significantly larger than θ_c: the same peak as seen for $p \to p$

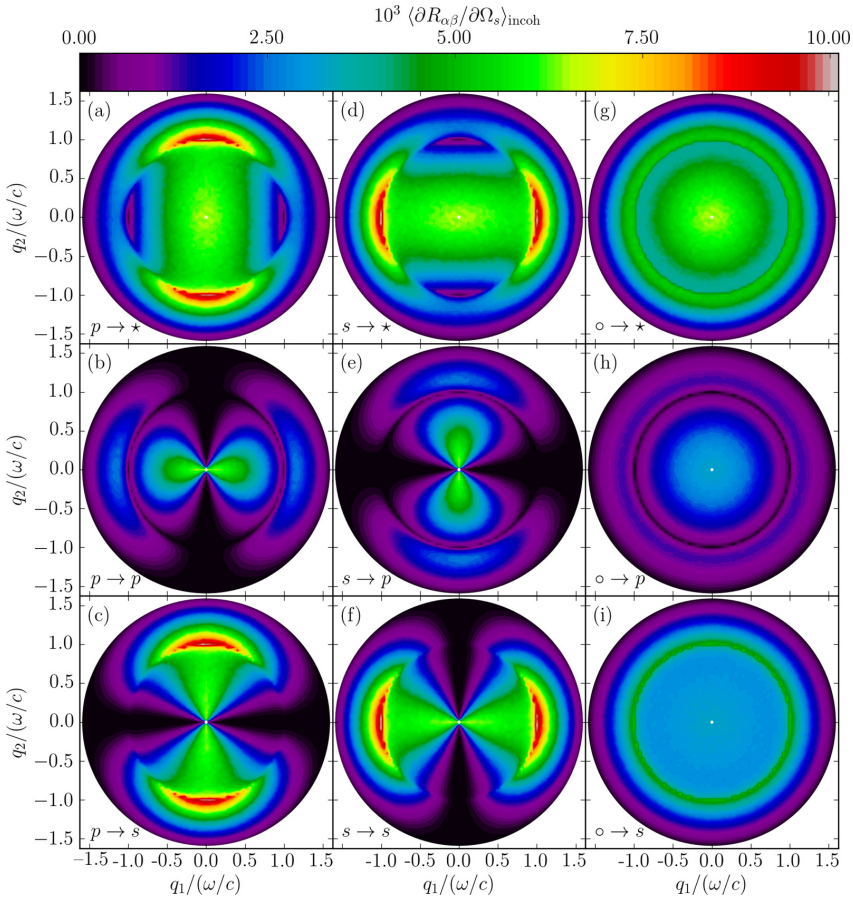

FIG. 5. The same as Fig. 4, but for light incident from the dielectric side onto the interface with vacuum, [$\varepsilon_1 = 2.64$; $\varepsilon_2 = 1.0$]. The in-plane intensity variations in panels (b) and (f) are the curves depicted in Fig. 2(b). Notice the rapid changes in intensity around the polar angle $\theta_s = \theta_c = \sin^{-1}\sqrt{\varepsilon_1/\varepsilon_2}$ [or $q_\parallel = \sqrt{\varepsilon_2}\omega/c$].

scattering in Fig. 2(b). However, this peak is not as sharp as the peak found at θ_c in Fig. 5(i), and, according to our definition, it is not a Yoneda peak.

Equations (53) demonstrate that the angular intensity distributions we are investigating can, to lowest order in the surface profile function, be explained through different factors in these equations with good approximation. As an aid in the interpretation of the results presented here and in the following, we notice that the power spectrum of the surface, $g(|\mathbf{q}_\parallel - \mathbf{k}_\parallel|)$ is common for all equations in Eq. (53). As such, the mean DRC in SAPT to lowest order is essentially a distorted Gaussian on which critical angle effects are superposed.

B. Non-normal incidence

As a starting point for our discussion of results for non-normal incidence, in Fig. 6(a) we present the angular dependence of the light scattered incoherently for a grazing angle of incidence from vacuum: $\theta_0 = 66.9^\circ$. The scattering distribution for $s \to s$ scattered light can be seen to have retained its general shape from Fig. 2(a), but for $p \to p$ scattering we now observe a new feature: a local minimum at $\theta_s \approx 50^\circ$. In the case of small-amplitude perturbation theory, represented in Fig. 6(a) by dashed curves, $\langle \partial R_{pp}(\mathbf{q}_\parallel|\mathbf{k}_\parallel)/\partial\Omega_s \rangle_{\text{incoh}}$ goes to zero at the position of this minimum.

In order to explain this minimum for $p \to p$ scattering in Fig. 6(a), we again turn to Eq. (53). For non-normal incidence ($k_\parallel \neq 0$), the function $F(\mathbf{q}_\parallel|\mathbf{k}_\parallel)$ in Eq. (55) can only cause $\langle \partial R_{pp}(\mathbf{q}_\parallel|\mathbf{k}_\parallel)/\partial\Omega_s \rangle_{\text{incoh}}$ to vanish when $\hat{\mathbf{q}}_\parallel \cdot \hat{\mathbf{k}}_\parallel$ is positive (forward scattering). Specifically, for in-plane forward-scattering [$\hat{\mathbf{q}}_\parallel \cdot \hat{\mathbf{k}}_\parallel = 1$], $\langle \partial R_{pp}(\mathbf{q}_\parallel|\mathbf{k}_\parallel)/\partial\Omega_s \rangle_{\text{incoh}}$ will vanish at a polar angle Θ_B given by

$$\Theta_B(\theta_0) = \sin^{-1}\left[\sqrt{\frac{\varepsilon_2(\varepsilon_2 - \varepsilon_1\sin^2\theta_0)}{(\varepsilon_2^2 - \varepsilon_1^2)\sin^2\theta_0 + \varepsilon_1\varepsilon_2}}\right]. \tag{56}$$

The scattering intensity $\langle \partial R_{pp}(\mathbf{q}_\parallel|\mathbf{k}_\parallel)/\partial\Omega_s \rangle_{\text{incoh}}$ will therefore, to lowest nonzero order in SAPT, have a zero when $\varepsilon_1 < \varepsilon_2$ and θ_0 is in the interval $\sin^{-1}[\varepsilon_2(\varepsilon_2 - \varepsilon_1)/(\varepsilon_2^2 + \varepsilon_2\varepsilon_1 - \varepsilon_1^2)]^{\frac{1}{2}}$

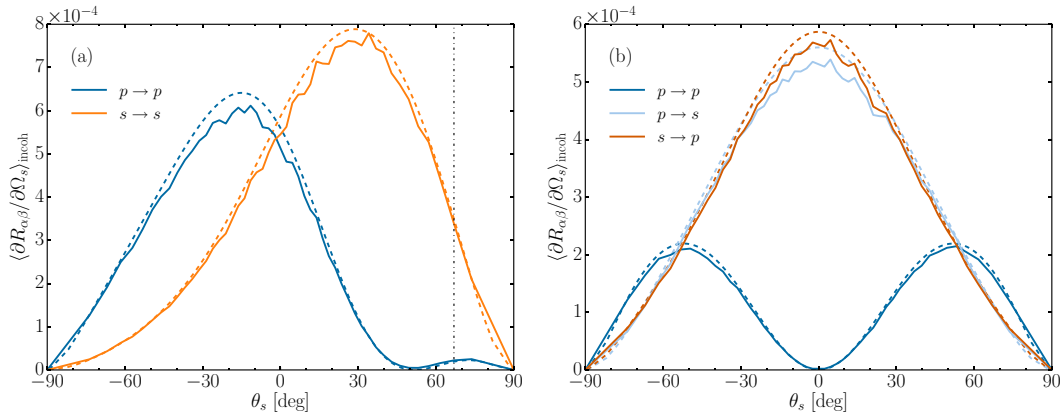

FIG. 6. (a) Same as Fig. 2(a), but for angles of incidence $(\theta_0,\phi_0) = (66.9^\circ,0^\circ)$. (b) Same as panel 6(a), but for out-of-plane scattering $[\phi_s = \pm 90^\circ]$. Results for combinations of the polarizations of the incident and scattered light for which the scattered intensity was everywhere negligible have been omitted. Parameters: $\varepsilon_1 = 1.0$, $\varepsilon_2 = 2.64$; $\delta = \lambda/40$, $a = \lambda/4$.

$< \theta_0 < \pi/2$. For $\theta_0 = 66.9^\circ$, as assumed in producing Fig. 6(a), we therefore expect a local minimum in $\langle \partial R_{pp}(\mathbf{q}_\parallel|\mathbf{k}_\parallel)/\partial\Omega_s \rangle_{\rm incoh}$ at $\theta_s = \Theta_B(66.9^\circ) = 51.7^\circ$, which is in good agreement with the observed value.

The scattering angles defined by Θ_B were first mentioned in the literature by Kawanishi *et al.* [4], where the angular values of Θ_B were explored through a stochastic functional approach for two-dimensional surfaces. They chose to call the angles at which the first-order contribution (according to their approach) to $\langle \partial R_{\alpha p}(\mathbf{q}_\parallel|\mathbf{k}_\parallel)/\partial\Omega_s \rangle_{\rm incoh}$ vanishes the *Brewster scattering angles*, as a generalization of the Brewster angle for a flat surface. In what follows, following Kawanishi *et al.*, we call the polar angles of scattering in the plane of incidence at which p- and s-polarized light is scattered diffusely (incoherently) into light of any polarization with zero, or nearly zero, intensity, the Brewster scattering angles.

The Brewster angle θ_B is defined by the zero in the reflectivity from a flat surface (coherent reflection in the specular direction) for p-polarization at the angle of incidence given by $\theta_0 = \theta_B = \tan^{-1}(\sqrt{\varepsilon_2/\varepsilon_1})$. For one set of $\{\varepsilon_1,\varepsilon_2\}$, there is hence only one Brewster angle for incidence in a given medium. However, in contrast, we would like to stress the fact that the Brewster scattering angles for $p \to p$ scattering are present for a wide range of angles of incidence, given by Eq. (56) for in-plane scattering. From Eq. (56) it is also of interest to note that for light *incident* at the Brewster angle (for the corresponding flat-surface system), $\theta_0 = \theta_B$, we find that $\Theta_B(\theta_B) = \theta_B$; the scattering intensity for light scattered incoherently vanishes for a scattering angle equal to the Brewster angle. This attests to the close relation between the Brewster angle for coherent reflection and the Brewster scattering angle Θ_B for diffuse reflection and is consistent with the findings of Kawanishi *et al.* [4].

Figure 6(b) presents simulation results for the same configuration as in Fig. 6(a), but for light scattered out-of-plane $[\hat{\mathbf{q}}_\parallel \cdot \hat{\mathbf{k}}_\parallel = 0]$. The dot product $\hat{\mathbf{q}}_\parallel \cdot \hat{\mathbf{k}}_\parallel$ in Eq. (53d) indicates that, to lowest nonzero order in SAPT, we should not expect any contribution to the mean DRC from $s \to s$ out-of-plane incoherently scattered light. However, this is not the case for $p \to p$ scattered light, where, even for $\hat{\mathbf{q}}_\parallel \cdot \hat{\mathbf{k}}_\parallel = 0$, a closer look at Eq. (53a) indicates that the out-of-plane scattered intensity is zero only for $\theta_s = 0\,[q_\parallel = 0]$. This is precisely what we observe for $\langle \partial R_{pp}(\mathbf{q}_\parallel|\mathbf{k}_\parallel)/\partial\Omega_s \rangle_{\rm incoh}$ in Fig. 6(b).

Figure 7 depicts results similar to those presented in Fig. 6 but for an increased surface rms roughness of $\delta = \lambda/20$ with the remaining parameters unchanged. As for normal incidence, it is found, not surprisingly, that small-amplitude perturbation theory is most accurate for the smallest surface roughness. However, the most interesting feature to notice from Fig. 7(a), as compared to Fig. 6(a), is the angular position and amplitude of the local minimum of the in-plane $p \to p$ intensity distribution. In the former figure [Fig. 7(a)], the intensity at the position of the minimum is nonzero and it is located at an angle that is smaller than the Brewster scattering angle $\Theta_B(\theta_0)$ predicted by Eq. (56). We speculate that this shift in the Brewster scattering angle is roughness induced in a way similar to how the "normal" Brewster angle is shifted by the introduction of surface roughness.

The results presented in Fig. 6 are in-plane and out-of-plane cuts from Fig. 8, which presents the full angular distribution of the contributions to the mean DRC from incoherently scattered light for the angles of incidence $(\theta_0,\phi_0) = (66.9^\circ,0^\circ)$. Here the white dots indicate the lateral wave vector of the specular reflection, $\mathbf{k}_\parallel$. Compared to the results presented in Fig. 4, Fig. 8 displays many interesting features that are strongly dependent on both incoming and outgoing polarization, and we are in Fig. 8 left with symmetry in the distributions only about the plane of incidence. For $p \to p$ polarized reflection [Fig. 8(b)] we observe that a significant fraction of the incoherently scattered light has shifted into the backscattering portion of the $q_\parallel$ plane as the angle of incidence has increased. The opposite is true for $s \to s$ polarized reflection, Fig. 8(f), where the majority of the incoherently scattered light is scattered into the forward portion of the $q_\parallel$ plane. This can be understood through small-amplitude perturbation theory: In Eq. (53), the function

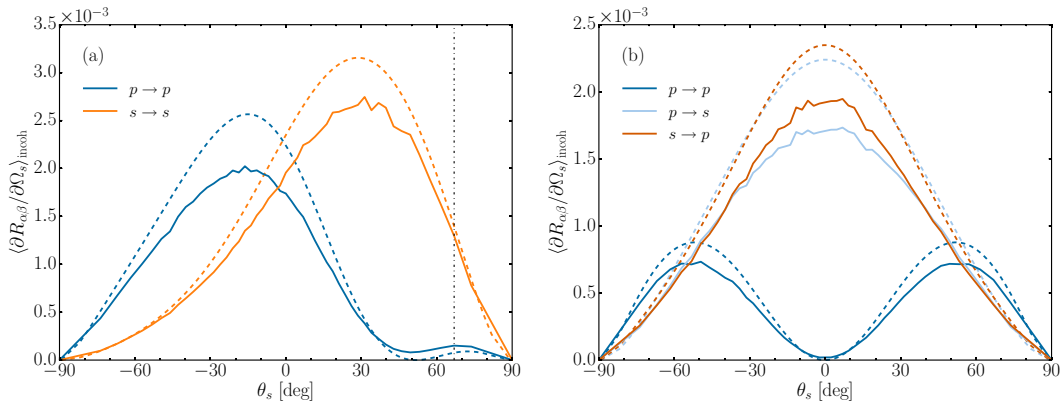

FIG. 7. Same as Fig. 6, but for root-mean-square roughness $\delta = \lambda/20$.

$F(\mathbf{q}_\parallel|\mathbf{k}_\parallel)$ [Eq. (55)] constitutes the main difference between $s \to s$ and $p \to p$ polarized scattering, and it is easy to see that this term will enhance the backward scattering and reduce the forward scattering for $p \to p$ polarization. Additionally, the Brewster scattering angle, which for $\theta_0 = 66.9^\circ$ was given by Eq. (56) and found to be at $\theta_s = 51.7^\circ$ for the parameters

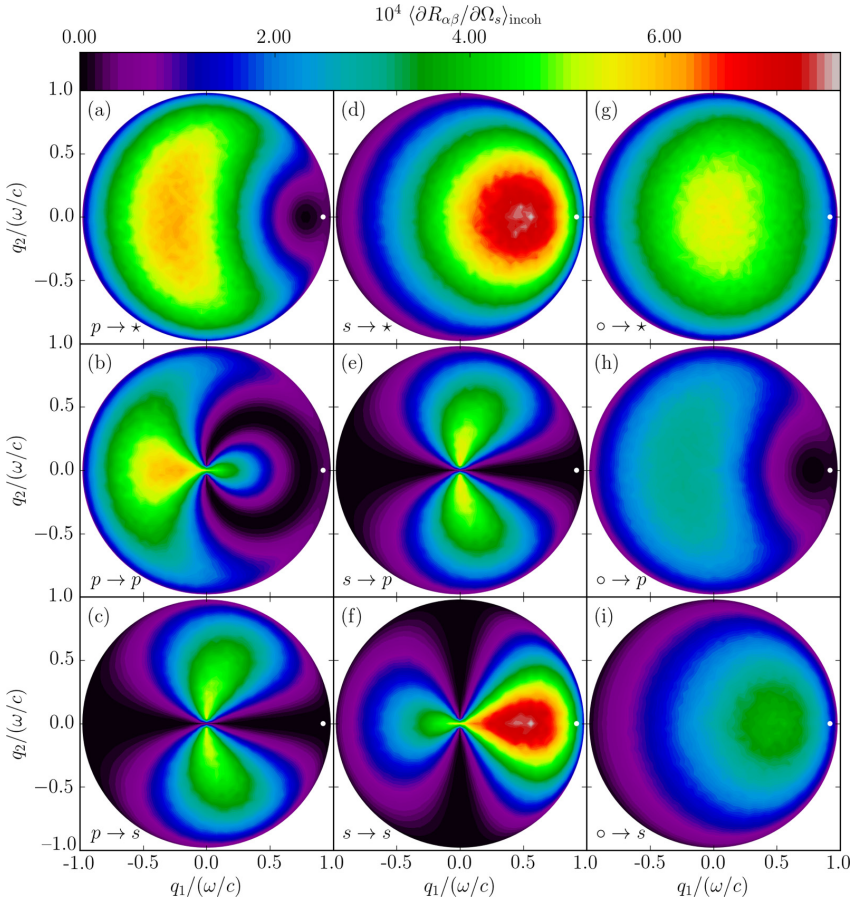

FIG. 8. Same as Fig. 4, but for the angles of incidence $(\theta_0, \phi_0) = (66.9^\circ, 0^\circ)$. Parameters: $\varepsilon_1 = 1.0$, $\varepsilon_2 = 2.64$; $\delta = \lambda/40$, $a = \lambda/4$.

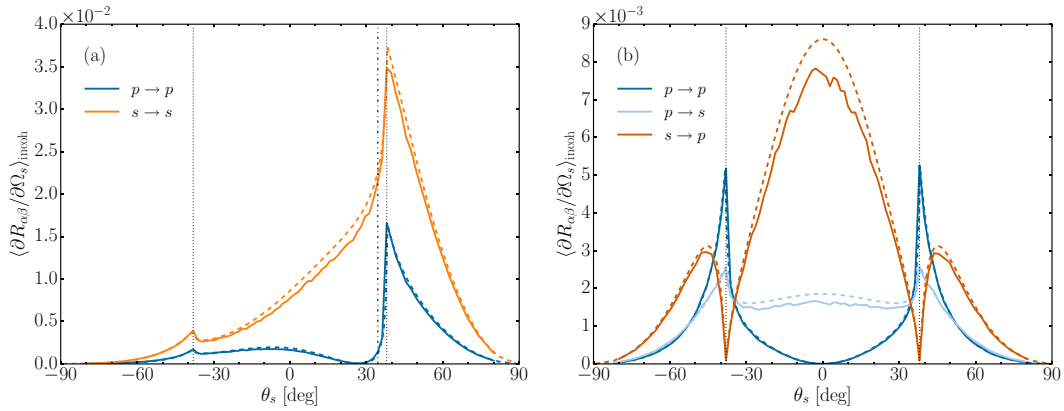

FIG. 9. (a) Same as Fig. 2(b), but for angles of incidence $(\theta_0,\phi_0) = (34.5^\circ,0^\circ)$. (b) Same as panel (a), but for out-of-plane scattering [$\phi_s = \pm 90^\circ$]. Results for combinations of the polarizations of the incident and scattered light for which the scattered intensity was everywhere negligible have been omitted. Parameters: $\varepsilon_1 = 2.64$, $\varepsilon_2 = 1.0$; $\delta = \lambda/40$, $a = \lambda/4$.

assumed, can now be seen to be part of a more general but still localized minimum in both Fig. 8(a) and Fig. 8(h), i.e., for $p \to \star$ and $\circ \to p$ scattering, respectively. Figure 8(b) shows that the Brewster scattering angle for $p \to p$ polarized scattering can be found to be part of an interestingly shaped minimum in the $q_\parallel$ plane. The shape of this minimum can, however, be extracted in a straightforward manner from Eq. (55).

More interesting still is scattering in the inverse configuration, where light is incident from the dielectric side of the rough interface [$\varepsilon_1 = 2.64, \varepsilon_2 = 1.0$]: Solutions of the RRE for this configuration and angles of incidence $(\theta_0,\phi_0) = (34.5^\circ,0^\circ)$, but for otherwise identical parameters as in Figs. 6 and 8, are presented in Fig. 9. Analogous with Fig. 6, Fig. 9(a) shows the incoherent component of the mean DRC for in-plane scattering, and Fig. 9(b) shows the corresponding curves for out-of-plane scattering.

In Fig. 9(a), we now observe that the two dips in $\langle \partial R_{pp}(\mathbf{q}_\parallel|\mathbf{k}_\parallel)/\partial\Omega_s \rangle_{\text{incoh}}$ at $|\theta_s| = \theta_c$ observed in Fig. 2(b) have both turned into Yoneda peaks, albeit with different peak intensities, and that the sharp dip at the same angle for forward scattering have turned into a less sharp local minimum at $\theta_s \approx 27^\circ$. In order to understand these features, we see from Eq. (56) that, for $\varepsilon_1 > \varepsilon_2$, $\langle \partial R_{pp}(\mathbf{q}_\parallel|\mathbf{k}_\parallel)/\partial\Omega_s \rangle_{\text{incoh}}$ vanishes for $\theta_s = \Theta_B(\theta_0)$ when θ_0 is in the interval $0 < \theta_0 < \sin^{-1}\sqrt{\varepsilon_2/\varepsilon_1}$. This minimum in $\langle \partial R_{pp}(\mathbf{q}_\parallel|\mathbf{k}_\parallel)/\partial\Omega_s \rangle_{\text{incoh}}$ will shift its polar position towards $\theta_s = 0^\circ$ for increasing θ_0, eventually "releasing" the Yoneda peaks in the forward-scattering plane originating in the $|d_\alpha(q_\parallel)|^2$ functions also for $p \to p$ scattering. In the backscattering plane, we observe through the function given in (55) that the negative sign of $(\hat{\mathbf{q}}_\parallel \cdot \hat{\mathbf{k}}_\parallel)$ will lead to a monotonic increase in the contribution from Eq. (55) to Eq. (53a) as θ_0 increases, eventually producing a Yoneda peak also for $\hat{\mathbf{q}}_\parallel \cdot \hat{\mathbf{k}}_\parallel < 0$. The overall distribution of $s \to s$ incoherent scattering in Fig. 9(a) also shows a strong forward shift in its scattering intensities, which, as we look to Eq. (53d), can be attributed solely to the shifted power spectrum $g(|\mathbf{q}_\parallel - \mathbf{k}_\parallel|)$.

Looking at Fig. 9(b), we observe several features for out-of-plane scattering that warrant a comment. Overall, we observe that the scattering distributions are again symmetric about $\theta_s = 0$, as is expected for out-of-plane scattering when the surface roughness is isotropic. Moreover, the distribution of $\langle \partial R_{ps}(\mathbf{q}_\parallel|\mathbf{k}_\parallel)/\partial\Omega_s \rangle_{\text{incoh}}$ appears similar in shape to the distribution of $\langle \partial R_{pp}(\mathbf{q}_\parallel|\mathbf{k}_\parallel)/\partial\Omega_s \rangle_{\text{incoh}}$ in Fig. 2(b). Their similarity can, to lowest nonzero order in SAPT, be attributed to their shared factor of $\alpha_2(q_\parallel)$ in Eqs. (53a) and (53c), which in both cases vanishes for $q_\parallel = \sqrt{\varepsilon_2}\omega/c$, thereby suppressing the Yoneda peaks at this polar angle. There are no such suppressing factors present in Eq. (53b), and the distribution of $\langle \partial R_{sp}(\mathbf{q}_\parallel|\mathbf{k}_\parallel)/\partial\Omega_s \rangle_{\text{incoh}}$ therefore displays Yoneda peaks at $|\theta_s| = \theta_c$. Similar to what we observed in Fig. 6(b), we see that the distribution of $\langle \partial R_{pp}(\mathbf{q}_\parallel|\mathbf{k}_\parallel)/\partial\Omega_s \rangle_{\text{incoh}}$ has a local minimum at $\theta_s = 0$; both this minimum and the Yoneda peaks found at $|\theta_s| = \theta_c$ are readily understood through the function in Eq. (55) and the factor $|d_\alpha(q_\parallel)|^2$, respectively.

We now turn to a scattering system for which the rms roughness of the surface is increased to $\delta = \lambda/20$, i.e., twice the roughness assumed in obtaining the results of Fig. 9. Results for the in-plane and out-of-plane scattered intensity distributions for different combinations of the polarizations of the incident and scattered light are presented in Fig. 10. Overall the results in Fig. 10 are in qualitative agreement with those of Fig. 9 for the equivalent but less rough scattering system. In general, the increase in surface roughness is again found to result in a poorer agreement between the results obtained on the basis of SAPT and those obtained by a direct numerical solution of the RRE. However, it is interesting to observe that for the case of in-plane as well as out-of-plane $p \to p$ scattering, SAPT seems to give a fair representation of the simulated scattered intensity distributions for both levels of roughness considered in Figs. 9 and 10. For other combinations of the polarizations of the incident and scattered light this is not the case.

The results presented in Fig. 9 are, as for Fig. 6, in-plane and out-of-plane cuts from Fig. 11, which displays the full angular distribution of the contribution to the mean DRC from the incoherently scattered light for the angles of incidence $(\theta_0,\phi_0) = (34.5^\circ,0^\circ)$. In contrast to what was observed in

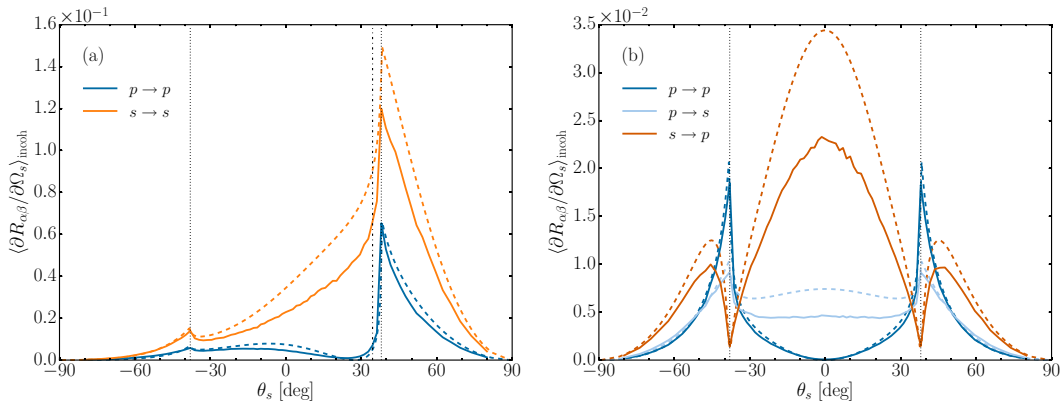

FIG. 10. Same as Fig. 9, but for root-mean-square roughness $\delta = \lambda/20$.

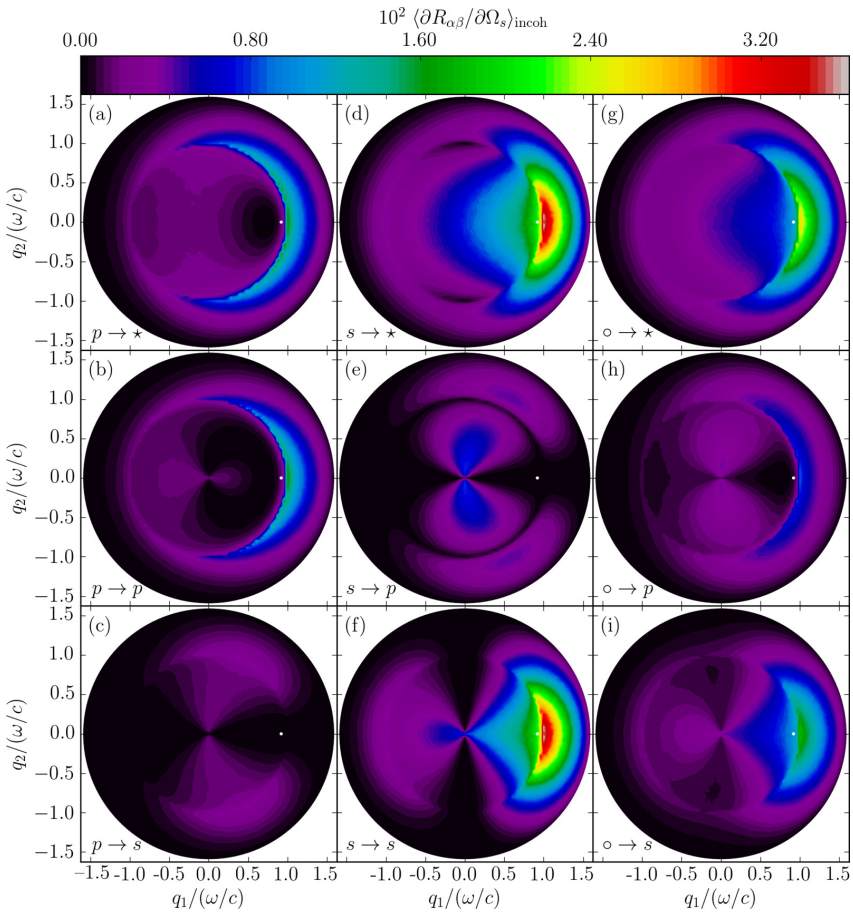

FIG. 11. Same as Fig. 5, but for the angles of incidence $(\theta_0,\phi_0) = (34.5^\circ, 0^\circ)$. As can be seen from the position of the white dot, this figure captures the scattering distribution when the polar angle of incidence θ_0 is close to the critical angle $\theta_c = \sin^{-1}\sqrt{\varepsilon_2/\varepsilon_1}$ for a corresponding flat-interface system. Parameters: $\varepsilon_1 = 2.64$; $\varepsilon_2 = 1.0$; $\delta = \lambda/40$, $a = \lambda/4$.

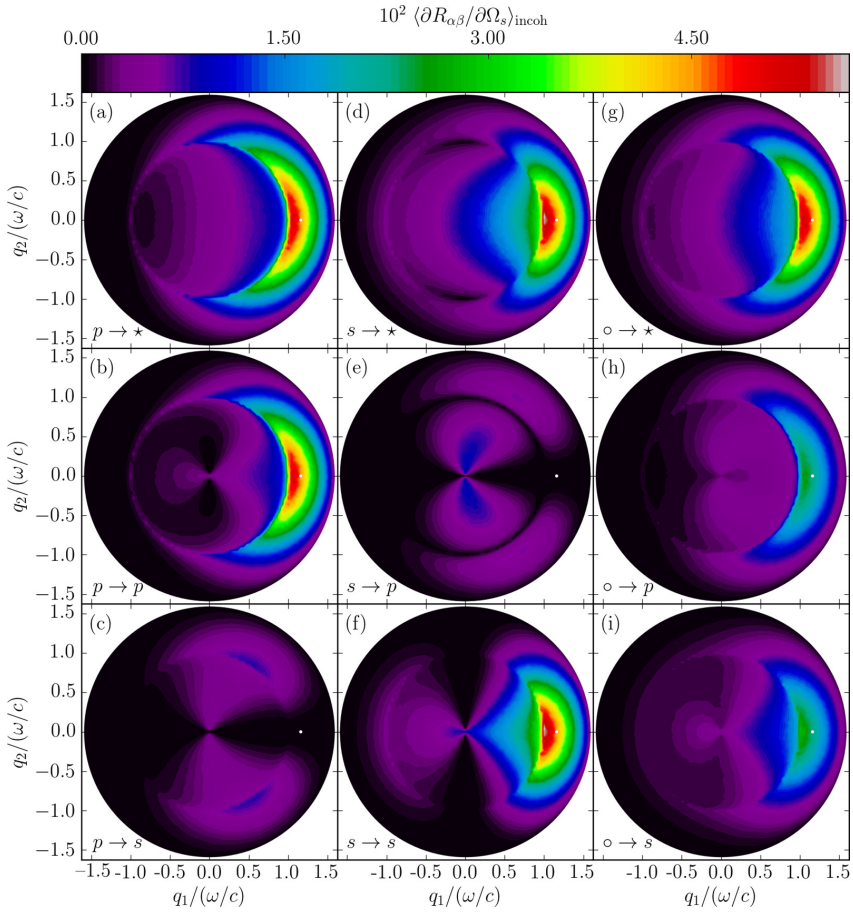

FIG. 12. Same as Fig. 11, but for the angles of incidence $(\theta_0,\phi_0) = (45.5^\circ,0^\circ)$. Parameters: $\varepsilon_1 = 2.64$, $\varepsilon_2 = 1.0$; $\delta = \lambda/40$, $a = \lambda/4$.

Fig. 8, all four of the lower left 2×2 subfigures in Fig. 11 now have significantly differing appearances. Similar to our observations in the case of incidence from vacuum, we observe that the Brewster scattering angle described by Eq. (56) can be seen to be part of a more general but still localized minimum in both Fig. 11(a) and Fig. 11(h), for $p \to \star$ and $\circ \to p$ scattering, respectively. Further, we still, as in Fig. 5, observe Yoneda peaks for all azimuthal angles of scattering. The intensities of these peaks are now, however, significantly stronger in the forward-scattering plane, closer to the direction of specular reflection.

We now turn to Fig. 12, which is identical to Fig. 11 but for the angles of incidence $(\theta_0,\phi_0) = (45.5^\circ,0^\circ)$. For these angles of incidence, the light incident on a flat surface would exhibit total internal reflection. Incoherent scattering is, as before, greatly enhanced for $q_\parallel \geqslant \sqrt{\varepsilon_2}\omega/c$, the part of wave-vector-space that is evanescent in the medium of transmission. The intensity of the light scattered diffusely into this region is now comparable for s- and p-polarized light, and we see Yoneda peaks in both forward and backward scattering, for a fairly wide range of azimuthal angles. This can, as before, be understood to lowest nonzero order in SAPT through Eqs. (53) and (54). The factors $|d_p(k_\parallel)|^{-2}$ and $|d_s(k_\parallel)|^{-2}$ will both have their maxima at $\theta_0 = \sin^{-1}(\sqrt{\varepsilon_2/\varepsilon_1})$, maxima that coincide with the corresponding maxima for the previously mentioned factors $|d_p(q_\parallel)|^{-2}$ and $|d_s(q_\parallel)|^{-2}$. The contribution from these factors will be the same for all ϕ_s, but common for all combinations of polarized scattering in Eq. (53) is that the multiplicative factor of the power spectrum will have its principal weight at $|\mathbf{q}_\parallel - \mathbf{k}_\parallel| = 0$; explaining the asymmetry about $q_1 = 0$ and the consequent shift of scattering to the forward-scattering portion of the $q_\parallel$ plane.

While there is no Brewster scattering angle for the angle of incidence in Fig. 12, we still observe a local minimum in the backward scattering direction close to the critical angle for p-polarized incident light, Fig. 12(a).

C. Reflectivity and reflectance

The reflectivities for the two configurations of media are presented in Fig. 13. Both Fig. 13(a) and Fig. 13(b) show only small deviations from the Fresnel reflection coefficients for a

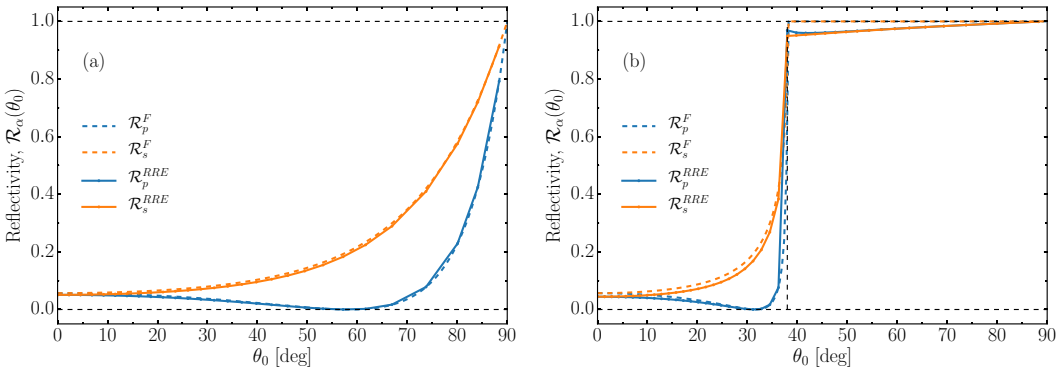

FIG. 13. (a) The reflectivities $\mathcal{R}_\alpha(\theta_0)$ of a two-dimensional randomly rough vacuum-dielectric interface $[\varepsilon_1 = 1.0, \varepsilon_2 = 2.64]$ for p- and s-polarized light as functions of the polar angle of incidence. (b) The same as in panel (a), but for a dielectric-vacuum interface $[\varepsilon_1 = 2.64, \varepsilon_2 = 1.0]$. The quantity $\mathcal{R}_\alpha^F(\theta_0)$ indicates the Fresnel reflection coefficient (flat surface reflectivity). The critical angle $\theta_0 = \theta_c = \sin^{-1}\sqrt{\varepsilon_2/\varepsilon_1}$ for total internal reflection for an equivalent flat-interface system is indicated by a vertical dashed line in panel (b). Several simulations were run with small perturbations in the surface length L in order to obtain reflectivity data with higher angular resolution. The roughness parameters assumed in obtaining these results were $\delta = \lambda/40$ and $a = \lambda/4$.

corresponding flat-surface system, the only notable difference being in Fig. 13(b), where the surface roughness prevents total internal reflection for incoming light with θ_0 larger than $\theta_c = \sin^{-1}\sqrt{\varepsilon_2/\varepsilon_1} \approx 38.0^\circ$, the critical angle corresponding to the values of the dielectric constants assumed in these simulations. The overall reflectivities for both systems are slightly smaller in all cases than the corresponding Fresnel coefficients, which is expected for a rough-surface system since some light is scattered diffusely away from the specular direction. The rough-surface analogs of the Brewster angles for corresponding flat-interface systems, called analogs because the reflectivity does not reach strict zero in the case of surface roughness, are clearly seen for p-polarized light in both figures.

The differences between the presented results for the reflectivity and the corresponding Fresnel coefficients can be better understood through Fig. 14, which presents the contribution to the reflectance from the light that has been reflected incoherently by the interface: $\mathscr{R}_\beta(\theta_0)_{\text{incoh}}$ [see Eq. (52)]. In both subfigures in Fig. 14 we see that the amount of diffusely scattered light in general decreases with an increasing angle of incidence if we ignore the effects of total internal reflection.

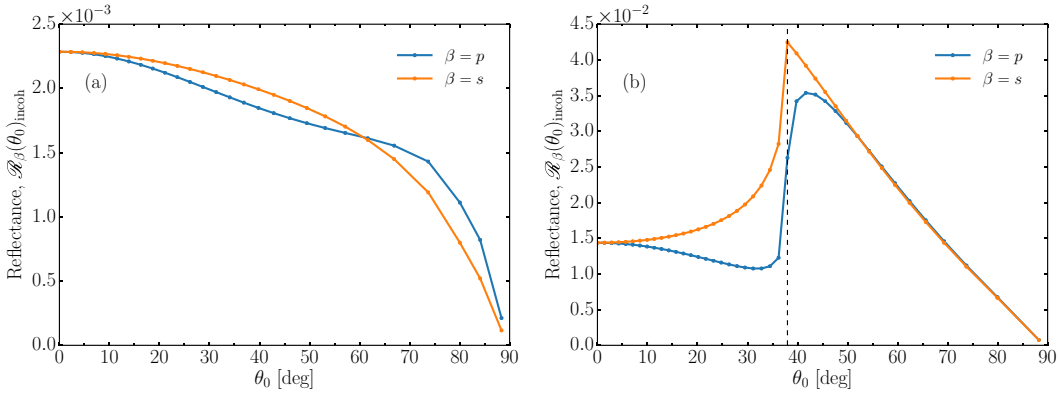

FIG. 14. The θ_0 dependence of the contribution to the reflectance from p- and s-polarized incident light that has been scattered incoherently from a two-dimensional randomly rough surface. This quantity is for β-polarized incident light defined as $\mathscr{R}_\beta(\theta_0)_{\text{incoh}} = \mathscr{R}_\beta(\theta_0) - \mathcal{R}_\beta(\theta_0)$. (a) The reflectances for a vacuum-dielectric interface $[\varepsilon_1 = 1.0, \varepsilon_2 = 2.64]$ for p- and s-polarized light as functions of the polar angle of incidence. (b) Same as panel (a), but for a dielectric-vacuum interface $[\varepsilon_1 = 2.64, \varepsilon_2 = 1.0]$. As in Fig. 13, the critical angle for total internal reflection in a corresponding flat-interface system, θ_c, is indicated by a vertical dashed line in Fig. 14(b). Several simulations were run with small perturbations in the surface length L in order to obtain reflectance data with higher angular resolution. The roughness parameters assumed in obtaining these results were $\delta = \lambda/40$ and $a = \lambda/4$.

This is consistent with the general notion that a rough surface is perceived as less rough for large angles of incidence [14].

Figure 14(a) shows that the incoherent part of the reflectance for the vacuum-dielectric configuration is a monotonically decreasing function of θ_0 for both polarizations, as expected by inspection of Eqs. (53) and (54), for $\varepsilon_1 < \varepsilon_2$. The functions $|d_p(k_\parallel)|^{-2}$ and $|d_s(k_\parallel)|^{-2}$ and the factor $1/\cos(\theta_0)$ are all monotonically increasing functions of $k_\parallel$ (or θ_0), but they do not increase rapidly enough to compensate for the monotonically decreasing factor of $\alpha_1^2(k_\parallel)$. A closer inspection of the numerical results and a more careful evaluation of the different factors in Eq. (53) have shown that the more rapid initial decrease of $\mathscr{R}_p(\theta_0)_{\rm incoh}$ is due to the contribution from its cross-polarized term, while its copolarized term is responsible for the eventual less rapid decrease compared to $\mathscr{R}_s(\theta_0)_{\rm incoh}$.

The incoherent part of the reflectance for the dielectric-vacuum configuration is displayed in Fig. 14(b). We can find here the explanation for why the curve for p-polarization in Fig. 13(b) showed a stronger peak for θ_0 just beyond the critical angle θ_c than the curve for s-polarization: less light is scattered incoherently for these angles when the incident light is p-polarized than when it is s-polarized. We can also see that the contribution to the reflectance from the light scattered incoherently increases more than two-fold at the critical angle relative to the contribution at normal incidence. This behavior can, again, be understood in terms of small-amplitude perturbation theory to lowest order in the surface profile function [Eqs. (53) and (54)]. The functions $|d_p(k_\parallel)|^{-2}$ and $|d_s(k_\parallel)|^{-2}$ will each have their maximum at the critical angle θ_c, but while $\mathscr{R}_s(\theta_0)_{\rm incoh}$ will get monotonically increasing contributions from its co- and cross-polarized components for $0 < \theta_0 < \theta_c$, for $\mathscr{R}_p(\theta_0)_{\rm incoh}$ the cross-polarized component will go to zero due to the $\alpha_2(k_\parallel)$ factor present in Eq. (53b). This dip in $\langle \partial R_{sp}(\mathbf{q}_\parallel|\mathbf{k}_\parallel)/\partial\Omega_s\rangle_{\rm incoh}$ is hence the main reason for the differences in the incoherent component of the reflectance for this configuration of media.

VII. CONCLUSIONS

We have presented a derivation of the RRE for the reflection amplitudes of light scattered from a two-dimensional, randomly rough, surface. These equations enable a nonperturbative solution of the scattering problem based on the Rayleigh hypothesis. As an example of its solution by purely numerical means, the full angular distributions for both co- and cross-polarized incoherent components of the mean differential reflection coefficients were reported for configurations of vacuum and an absorptionless dielectric with a Gaussian surface power spectrum and correlation function.

It was shown that a configuration of reflection within the optically denser medium leads to Yoneda peaks in the angular distributions of the diffusely scattered light, namely peaks at the critical angle for total internal reflection in the denser medium. The behavior and development of these peaks for a wide range of angles of incidence and scattering were investigated, and the lack of such peaks for light scattered into p-polarization for polar angles of incidence smaller than the critical angle were explained through SAPT.

Brewster scattering angles, angles where scattering into p-polarization is suppressed to strict zero in SAPT to lowest nonzero order in the surface profile function, were found to explain many of the differences in scattering into s- and p-polarization for the scattering systems investigated in the current work. These angles were first mentioned in the literature by Kawanishi *et al.* in Ref. [4]. Our results are in good agreement with their findings.

Small-amplitude perturbation theory, to lowest nonzero order in the surface profile function, was overall shown to reproduce our numerical results qualitatively to a fairly high degree of accuracy through both analytical arguments and a numerical implementation of that theory. This leads us to believe that the features presented in the results are single-scattering effects.

The scattering of light from a transparent dielectric is well described by solutions obtained by means of small-amplitude perturbation theory, including the full angular distribution of the mean DRC for all combinations of the polarizations of the incident and scattered light. The reduced Rayleigh equation is a powerful starting point for studies of higher-order scattering features, such as enhanced backscattering, for example. The results presented here show that for the degree of surface roughness and the values of the dielectric constants assumed in this work no higher-order features are observed. Nevertheless, the RRE still gives more accurate numerical results for the mean DRC than does SAPT to lowest nonzero order in the surface profile function when the surface roughness is increased.

As an investigation of the quality of the results, energy conservation (unitarity) was found to be satisfied within 10^{-4} when the total scattered energies from both reflection and transmission were added together for the roughness parameters and configurations used in this paper. An investigation similar to the present one but for light *transmitted* through the dielectric rough interface will be presented in a separate publication [15].

ACKNOWLEDGMENTS

The authors would like to thank J.-P. Banon for helpful discussions. The research of Ø.S.H. and I.S. was supported in part by The Research Council of Norway Contract No. 216699. This work received support from NTNU and the Norwegian metacenter for High Performance Computing (NOTUR) by an allocation of computer time.

APPENDIX: EXPANSION OF $R(\mathbf{q}_\parallel|\mathbf{k}_\parallel)$ IN POWERS OF THE SURFACE PROFILE FUNCTION

In this Appendix we outline the derivation of Eq. (53). To this end, we begin with the expansion

$$\mathbf{R}(\mathbf{q}_\parallel|\mathbf{k}_\parallel) = \sum_{n=0}^{\infty} \frac{(-i)^n}{n!}\mathbf{R}^{(n)}(\mathbf{q}_\parallel|\mathbf{k}_\parallel), \tag{A1}$$

where the superscript n denotes the order of the corresponding term in powers of $\zeta(\mathbf{x}_\parallel)$. When Eqs. (17) and (A1) are substituted into Eq. (27), the latter becomes

$$\sum_{m=0}^{\infty}\sum_{n=0}^{m}\frac{(-i)^m}{m!}\binom{m}{n}\int\frac{d^2q_\parallel}{(2\pi)^2}[-\alpha_1(q_\parallel)+\alpha_2(p_\parallel)]^{n-1}\hat{\zeta}^{(n)}(\mathbf{p}_\parallel-\mathbf{q}_\parallel)\mathbf{M}^+(\mathbf{p}_\parallel|\mathbf{q}_\parallel)\,\mathbf{R}^{(m-n)}(\mathbf{q}_\parallel|\mathbf{k}_\parallel)$$
$$=\sum_{n=0}^{m}-\frac{(-i)^n}{n!}[\alpha_1(k_\parallel)+\alpha_2(p_\parallel)]^{n-1}\hat{\zeta}^{(n)}(\mathbf{p}_\parallel-\mathbf{k}_\parallel)\mathbf{M}^-(\mathbf{p}_\parallel|\mathbf{k}_\parallel). \tag{A2}$$

When we equate terms of zero order in $\zeta(\mathbf{x}_\parallel)$ on both sides of this equation, we obtain

$$\frac{1}{-\alpha_1(p_\parallel)+\alpha_2(p_\parallel)}\mathbf{M}^+(\mathbf{p}_\parallel|\mathbf{p}_\parallel)\,\mathbf{R}^{(0)}(\mathbf{p}_\parallel|\mathbf{k}_\parallel)=-(2\pi)^2\delta(\mathbf{p}_\parallel-\mathbf{k}_\parallel)\frac{1}{\alpha_1(p_\parallel)+\alpha_2(p_\parallel)}\mathbf{M}^-(\mathbf{p}_\parallel|\mathbf{p}_\parallel), \tag{A3}$$

which, if we solve for $\mathbf{R}^{(0)}(\mathbf{q}_\parallel|\mathbf{k}_\parallel)$, gives

$$\begin{pmatrix}R^{(0)}_{pp}(\mathbf{q}_\parallel|\mathbf{k}_\parallel) & R^{(0)}_{ps}(\mathbf{q}_\parallel|\mathbf{k}_\parallel)\\ R^{(0)}_{sp}(\mathbf{q}_\parallel|\mathbf{k}_\parallel) & R^{(0)}_{ss}(\mathbf{q}_\parallel|\mathbf{k}_\parallel)\end{pmatrix}=(2\pi)^2\delta(\mathbf{q}_\parallel-\mathbf{k}_\parallel)\begin{pmatrix}\frac{d_p^-(k_\parallel)}{d_p^+(k_\parallel)} & 0\\ 0 & \frac{d_s^-(k_\parallel)}{d_s^+(k_\parallel)}\end{pmatrix}, \tag{A4}$$

where

$$d_p^\pm(k_\parallel)=\varepsilon_2\alpha_1(k_\parallel)\pm\varepsilon_1\alpha_2(k_\parallel), \tag{A5a}$$

$$d_s^\pm(k_\parallel)=\alpha_1(k_\parallel)\pm\alpha_2(k_\parallel). \tag{A5b}$$

Equation (A4) essentially represents the Fresnel coefficients for specular reflection from a flat interface.

For $m=1$, Eq. (A2) can be simplified to

$$\frac{1}{-\alpha_1(p_\parallel)+\alpha_2(p_\parallel)}\mathbf{M}^+(\mathbf{p}_\parallel|\mathbf{p}_\parallel)\mathbf{R}^{(1)}(\mathbf{p}_\parallel|\mathbf{k}_\parallel)+\int\frac{d^2q_\parallel}{(2\pi)^2}\hat{\zeta}^{(1)}(\mathbf{p}_\parallel-\mathbf{q}_\parallel)\mathbf{M}^+(\mathbf{p}_\parallel|\mathbf{q}_\parallel)\,\mathbf{R}^{(0)}(\mathbf{q}_\parallel|\mathbf{k}_\parallel)=-\hat{\zeta}^{(1)}(\mathbf{p}_\parallel-\mathbf{k}_\parallel)\mathbf{M}^-(\mathbf{p}_\parallel|\mathbf{k}_\parallel). \tag{A6}$$

If we now use the result that the matrix $\mathbf{M}^+(\mathbf{p}_\parallel|\mathbf{p}_\parallel)$ is diagonal and hence readily inverted and that the matrix $\mathbf{R}^{(0)}(\mathbf{q}_\parallel|\mathbf{k}_\parallel)$ is given by Eq. (A4), we can simplify Eq. (A6) into

$$\mathbf{R}^{(1)}(\mathbf{q}_\parallel|\mathbf{k}_\parallel)=-(\varepsilon_2-\varepsilon_1)\hat{\zeta}^{(1)}(\mathbf{q}_\parallel-\mathbf{k}_\parallel)$$
$$\times\begin{pmatrix}\frac{\sqrt{\varepsilon_1\varepsilon_2}}{d_p^+(q_\parallel)d_p^+(k_\parallel)}[d_p^-(k_\parallel)M_{pp}^+(\mathbf{q}_\parallel|\mathbf{k}_\parallel)+d_p^+(k_\parallel)M_{pp}^-(\mathbf{q}_\parallel|\mathbf{k}_\parallel)] & \frac{\sqrt{\varepsilon_1\varepsilon_2}}{d_p^+(q_\parallel)d_s^+(k_\parallel)}M_{ps}^\pm(\mathbf{q}_\parallel|\mathbf{k}_\parallel)[d_s^-(k_\parallel)+d_s^+(k_\parallel)]\\ \frac{1}{d_s^+(q_\parallel)d_p^+(k_\parallel)}[d_p^-(k_\parallel)M_{sp}^+(\mathbf{q}_\parallel|\mathbf{k}_\parallel)+d_p^+(k_\parallel)M_{sp}^-(\mathbf{q}_\parallel|\mathbf{k}_\parallel)] & \frac{1}{d_s^+(q_\parallel)d_s^+(k_\parallel)}M_{ss}^\pm(\mathbf{q}_\parallel|\mathbf{k}_\parallel)[d_s^-(k_\parallel)+d_s^+(k_\parallel)]\end{pmatrix}. \tag{A7}$$

where the matrix elements $\{M^\pm_{\alpha\beta}(\mathbf{q}_\parallel|\mathbf{k}_\parallel)\}$ are given by Eq. (28a). This ultimately gives

$$\mathbf{R}^{(1)}(\mathbf{q}_\parallel|\mathbf{k}_\parallel)=-(\varepsilon_2-\varepsilon_1)\hat{\zeta}^{(1)}(\mathbf{q}_\parallel-\mathbf{k}_\parallel)$$
$$\times\begin{pmatrix}\frac{1}{d_p^+(q_\parallel)d_p^+(k_\parallel)}[\varepsilon_2 q_\parallel k_\parallel-\varepsilon_1\alpha_2(q_\parallel)(\hat{\mathbf{q}}_\parallel\cdot\hat{\mathbf{k}}_\parallel)\alpha_2(k_\parallel)] & -\frac{\sqrt{\varepsilon_1}}{d_p^+(q_\parallel)d_s^+(k_\parallel)}\frac{\omega}{c}\alpha_2(q_\parallel)\,[\hat{\mathbf{q}}_\parallel\times\hat{\mathbf{k}}_\parallel]_3\\ -\frac{\sqrt{\varepsilon_1}}{d_s^+(q_\parallel)d_p^+(k_\parallel)}\frac{\omega}{c}[\hat{\mathbf{q}}_\parallel\times\hat{\mathbf{k}}_\parallel]_3\,\alpha_2(k_\parallel) & \frac{1}{d_s^+(q_\parallel)d_s^+(k_\parallel)}\frac{\omega^2}{c^2}(\hat{\mathbf{q}}_\parallel\cdot\hat{\mathbf{k}}_\parallel)\end{pmatrix}2\alpha_1(k_\parallel). \tag{A8}$$

In view of Eq. (A1) we find that through terms linear in the surface profile function

$$\mathbf{R}(\mathbf{q}_\parallel|\mathbf{k}_\parallel)=\mathbf{R}^{(0)}(\mathbf{q}_\parallel|\mathbf{k}_\parallel)-i\mathbf{R}^{(1)}(\mathbf{q}_\parallel|\mathbf{k}_\parallel)+O(\zeta^2). \tag{A9}$$

The substitution of these results in Eq. (42) and use of the result that $\langle\hat{\zeta}(\mathbf{Q}_\parallel)\hat{\zeta}(\mathbf{Q}_\parallel)^*\rangle=S\delta^2 g(|\mathbf{Q}_\parallel|)$ yields Eq. (53).

[1] T. A. Leskova, P. A. Letnes, A. A. Maradudin, T. Nordam, and I. Simonsen, Proc. SPIE **8172**, 817209 (2011).

[2] T. Nordam, P. A. Letnes, and I. Simonsen, Front. Phys. **1**, 1 (2013).

[3] J. Nakayama, H. Ogura, and B. Matsumoto, Radio Sci. **15**, 1049 (1980).

[4] T. Kawanishi, H. Ogura, and Z. L. Wang, Wave. Random Media **7**, 351 (1997).

[5] Y. Yoneda, Phys. Rev. **131**, 2010 (1963).

[6] G. H. Vineyard, Phys. Rev. B **26**, 4146 (1982).

[7] S. K. Sinha, E. B. Sirota, S. Garoff, and H. B. Stanley, Phys. Rev. B **38**, 2297 (1988).

[8] T. A. Leskova and A. A. Maradudin, Wave. Random Media **7**, 395 (1997).
[9] M. Nieto-Vesperinas and J. A. Sánchez-Gil, J. Opt. Soc. Am. A **9**, 424 (1992).
[10] A. Soubret, G. Berginc, and C. Bourrely, Phys. Rev. B **63**, 245411 (2001).
[11] W. H. Press, S. A. Teukolsky, W. T. Vetterling, and B. P. Flannery, *Numerical Recipes in Fortran 90: The Art of Parallel Scientific Computing* (Cambridge University Press, Cambridge, UK, 1996).
[12] A. A. Maradudin, T. Michel, A. R. McGurn, and E. R. Méndez, Ann. Phys. (NY) **203**, 255 (1990).
[13] I. Simonsen, J. B. Kryvi, A. A. Maradudin, and T. A. Leskova, Comput. Phys. Commun. **182**, 1904 (2011).
[14] I. Simonsen, Eur. Phys. J.-Spec. Top. **181**, 1 (2010).
[15] Ø. S. Hetland, A. A. Maradudin, T. Nordam, P. A. Letnes, and I. Simonsen (unpublished).
[16] T. Nordam, P. A. Letnes, and I. Simonsen, J. Phys.: Conf. Ser. **454**, 012033 (2013).
[17] B. E. Warren and J. S. Clarke, J. Appl. Phys. **36**, 324 (1965).
[18] L. I. Schiff, *Quantum Mechanics* (McGraw-Hill, New York, 1968).
[19] T. Tamir, in *Electromagnetic Surface Modes*, edited by A. D. Boardman (Wiley & Sons, New York, 1982), Chap. 13 .
[20] T. Tamir and A. A. Oliner, J. Opt. Soc. Am. **59**, 942 (1969).
[21] T. Nordam, P. A. Letnes, I. Simonsen, and A. A. Maradudin, J. Opt. Soc. Am. A **31**, 1126 (2014).

Paper 3:

A. K. González-Alcalde, J.-P. Banon, Ø. S. Hetland, A. A. Maradudin, E. R. Méndez, T. Nordam, and I. Simonsen, "Experimental and numerical studies of the scattering of light from a two-dimensional randomly rough interface in the presence of total internal reflection: optical Yoneda peaks," *Opt. Express*, vol. 24, no. 23, pp. 25995–26005, 2016

Research Article | Vol. 24, No. 23 | 14 Nov 2016 | OPTICS EXPRESS 25995

Optics EXPRESS

Experimental and numerical studies of the scattering of light from a two-dimensional randomly rough interface in the presence of total internal reflection: optical Yoneda peaks

ALMA K. GONZÁLEZ-ALCALDE,[1] JEAN-PHILIPPE BANON,[2] ØYVIND S. HETLAND,[2] ALEXEI A. MARADUDIN,[3] EUGENIO R. MÉNDEZ,[1] TOR NORDAM,[2] AND INGVE SIMONSEN[2,4,*]

[1]*División de Física Aplicada, Centro de Investigación Científica y de Educación Superior de Ensenada, Carretera Ensenada-Tijuana No. 3918, Ensenada B.C., 22860, México*
[2]*Department of Physics, NTNU Norwegian University of Science and Technology, NO-7491 Trondheim, Norway*
[3]*Department of Physics and Astronomy, University of California, Irvine, CA 92697, USA*
[4]*Surface du Verre et Interfaces, UMR 125 CNRS/Saint-Gobain, F-93303 Aubervilliers, France*
[*]*ingve.simonsen@ntnu.no*

Abstract: The scattering of polarized light from a dielectric film sandwiched between two different semi-infinite dielectric media is studied experimentally and theoretically. The illuminated interface is planar, while the back interface is a two-dimensional randomly rough interface. We consider here only the case in which the medium of incidence is optically more dense than the substrate, in which case effects due to the presence of a critical angle for total internal reflection occur. A reduced Rayleigh equation for the scattering amplitudes is solved by a rigorous, purely numerical, nonperturbative approach. The solutions are used to calculate the reflectivity of the structure and the mean differential reflection coefficient. Optical analogues of Yoneda peaks are present in the results obtained. The computational results are compared with experimental data for the in-plane mean differential reflection coefficient, and good agreement between theory and experiment is found.

OCIS codes: (240.0240) Optics at surfaces; (290.5880) Scattering, rough surfaces; (260.6970) Total internal reflection.

References and links

1. J. Nakayama, H. Ogura, and B. Matsumoto, "A probabilistic theory of scattering from a random rough surface," Radio Sci. **15**, 1049–1057 (1980).
2. T. Kawanishi, H. Ogura, and Z. L. Wang, "Scattering of an electromagnetic wave from a slightly random dielectric surface: Yoneda peak and Brewster angle in incoherent scattering," Wave. Random Media **7**, 351–384 (1997).
3. Y. Yoneda, "Anomalous Surface Reflection of X Rays," Phys. Rev. **131**, 2010–2013 (1963).
4. A. Soubret, G. Berginc, and C. Bourrely, "Application of reduced Rayleigh equations to electromagnetic wave scattering by two-dimensional randomly rough surfaces," Phys. Rev. B **63**, 245411 (2001).
5. T. Nordam, P. A. Letnes, and I. Simonsen, "Numerical simulations of scattering of light from two-dimensional rough surfaces using the reduced Rayleigh equation," Front. Phys. **1**, 8 (2013).
6. Ø. S. Hetland, A. A. Maradudin, T. Nordam, and I. Simonsen, "Numerical studies of the scattering of light from a two-dimensional randomly rough interface between two dielectric media," Phys. Rev. A **93**, 053819 (2016).
7. E. R. Méndez, G. D. Jiménez, and A. A. Maradudin, "A simple model of a one-dimensional, randomly rough, non-Gaussian surface," Proc. SPIE **9961**, 99610D (2016).
8. P. F. Gray, "A method of forming optical diffusers of simple known statistical properties," Opt. Acta **25**, 765–775 (1978).
9. B. E. Warren and J. S. Clarke, "Interpretation of the Anomalous Surface Reflection of X Rays," J. Appl. Phys. **36**, 324–325 (1965).
10. G. H. Vineyard, "Grazing-incidence diffraction and the distorted-wave approximation for the study of surfaces," Phys. Rev. B **26**, 4146–4159 (1982).
11. S. K. Sinha, E. B. Sirota, S. Garoff, and H. B. Stanley, "X-ray and neutron scattering from rough surfaces," Phys. Rev. B **38**, 2297–2311 (1988).
12. For reasons of convenience, a negative value of the polar angle of scattering, θ_s, is used to denote the case $\hat{\mathbf{q}}_{\parallel} = -\hat{\mathbf{k}}_{\parallel}$.

#272997 http://dx.doi.org/10.1364/OE.24.025995
Journal © 2016 Received 18 Aug 2016; revised 15 Oct 2016; accepted 16 Oct 2016; published 1 Nov 2016

Optics EXPRESS

1. Introduction

In many theoretical and experimental studies of the scattering of light from randomly rough surfaces the medium of incidence is vacuum. In the case that the scattering medium is a dielectric, this choice for the medium of incidence rules out investigations of interesting single- and multiple-scattering effects associated with the phenomenon of total internal reflection, which occurs when the medium of incidence is optically more dense than the scattering medium.

By use of the stochastic functional approach [1] Kawanishi *et al*. studied the coherent and incoherent scattering of an electromagnetic wave from a two-dimensional interface separating two different dielectric media [2]. The medium of incidence could be either medium. The theoretical approach used in this work was perturbative, and applicable only to weakly rough interfaces. Nevertheless it yielded interesting results, including the presence of Yoneda peaks in the angular dependence of the intensity of the light scattered back into the medium of incidence, when the latter is the optically more dense medium. These are sharp asymmetric peaks occurring at the critical angle for total internal reflection, for a fixed angle of incidence, for either p- or s-polarization of the incident light. These peaks were first observed experimentally in the scattering of x-rays incident from air on a metal surface [3]. Until now they have not been observed in optical experiments.

In subsequent work Soubret *et al*. [4] derived a reduced Rayleigh equation for the scattering amplitudes when an electromagnetic wave is incident from one dielectric medium on its two-dimensional randomly rough interface with a second dielectric medium. They obtained a solution of this equation as an expansion in powers of the surface profile through terms of third order, but in obtaining the numerical results presented in the paper the medium of incidence was assumed to be vacuum.

In this paper we remove two limitations present in earlier studies of the scattering of light from dielectric structures possessing one two-dimensional interface. The first constraint we remove is the lack of experimental results for scattering from two-dimensional randomly rough interfaces in the presence of total internal reflection. We present experimental results for the contribution to the mean differential reflection coefficient (DRC) from in-plane co-polarized scattering. These are the first experimental studies of such scattering, and they demonstrate the existence of Yoneda peaks at optical frequencies.

The second limitation we remove is the absence of nonperturbative solutions of the equations of scattering theory. We solve a reduced Rayleigh equation for the scattering amplitudes for the dielectric structure studied experimentally, by a rigorous, purely numerical, nonperturbative approach. The solutions are used to calculate the reflectivity and the mean DRC of the structure, the latter of which is compared with the experimental results.

2. Theoretical formulation

The scattering system we consider consists of a dielectric medium whose dielectric constant is ε_1 in the region $x_3 > 0$, a dielectric medium whose dielectric constant is ε_2 in the region $-d + \zeta(\mathbf{x}_\parallel) < x_3 < 0$, where $\mathbf{x}_\parallel = (x_1, x_2, 0)$, and a dielectric medium whose dielectric constant is ε_3 in the region $x_3 < -d + \zeta(\mathbf{x}_\parallel)$ [see Fig. 1]. The dielectric constants ε_1, ε_2, and ε_3 are all real and positive. The surface profile function $\zeta(\mathbf{x}_\parallel)$ is assumed to be a single-valued function of $\mathbf{x}_\parallel$ that is differentiable with respect to x_1 and x_2, and constitutes a stationary, zero-mean, isotropic, Gaussian random process. This random process is defined by the surface height autocorrelation function $\langle \zeta(\mathbf{x}_\parallel)\zeta(\mathbf{x}'_\parallel)\rangle = \delta^2 W(|\mathbf{x}_\parallel - \mathbf{x}'_\parallel|)$. The angle brackets here and in all that follows denote an average over the ensemble of realizations of the surface profile function, and $\delta = \langle \zeta^2(\mathbf{x}_\parallel)\rangle^{\frac{1}{2}}$ is the rms height of the surface.

Optics EXPRESS

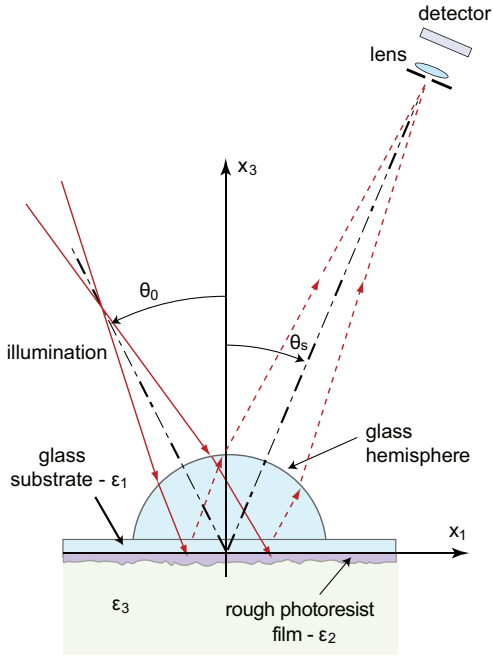

Fig. 1. Schematic diagram of the sample geometry.

We have chosen to study this structure instead of the simpler system of a single two-dimensional randomly rough interface separating two different dielectric media because it is the one employed in the experimental work whose results will be compared with the results of our calculations.

The interface $x_3 = 0$ is illuminated from the region $x_3 > 0$ by a plane wave of angular frequency ω. We write the electric field in this region as the sum of an incident field and a scattered field, $\mathbf{E}(\mathbf{x};t) = [\mathbf{E}(\mathbf{x}|\omega)_{\rm inc} + \mathbf{E}(\mathbf{x}|\omega)_{\rm sc}]\exp(-{\rm i}\omega t)$, where

$$\mathbf{E}(\mathbf{x}|\omega)_{\rm inc} = \left[\hat{\mathbf{e}}_p^{(i)}(\mathbf{k}_\parallel)E_{0p}(\mathbf{k}_\parallel) + \hat{\mathbf{e}}_s^{(i)}(\mathbf{k}_\parallel)E_{0s}(\mathbf{k}_\parallel)\right]\exp\left[{\rm i}\mathbf{k}_\parallel\cdot\mathbf{x}_\parallel - {\rm i}\alpha_1(k_\parallel)x_3\right] \tag{1a}$$

$$\mathbf{E}(\mathbf{x}|\omega)_{\rm sc} = \int \frac{{\rm d}^2 q_\parallel}{(2\pi)^2}\left[\hat{\mathbf{e}}_p^{(s)}(\mathbf{q}_\parallel)A_p(\mathbf{q}_\parallel) + \hat{\mathbf{e}}_s^{(s)}(\mathbf{q}_\parallel)A_s(\mathbf{q}_\parallel)\right]\exp\left[{\rm i}\mathbf{q}_\parallel\cdot\mathbf{x}_\parallel + {\rm i}\alpha_1(q_\parallel)x_3\right], \tag{1b}$$

where $\alpha_i(q_\parallel) = [\varepsilon_i(\omega/c)^2 - q_\parallel^2]^{\frac{1}{2}}$ $(i = 1, 2, 3)$, with ${\rm Re}\,\alpha_i(q_\parallel) > 0$, ${\rm Im}\,\alpha_i(q_\parallel) > 0$, while

$$\hat{\mathbf{e}}_p^{(i)}(\mathbf{k}_\parallel) = \frac{\hat{\mathbf{k}}_\parallel\alpha_1(k_\parallel) + \hat{\mathbf{x}}_3 k_\parallel}{\sqrt{\varepsilon_1}\frac{\omega}{c}} \tag{2a}$$

$$\hat{\mathbf{e}}_s^{(i)}(\mathbf{k}_\parallel) = \hat{\mathbf{k}}_\parallel \times \hat{\mathbf{x}}_3 \tag{2b}$$

and

$$\hat{\mathbf{e}}_p^{(s)}(\mathbf{q}_\parallel) = \frac{-\hat{\mathbf{q}}_\parallel\alpha_1(q_\parallel) + \hat{\mathbf{x}}_3 q_\parallel}{\sqrt{\varepsilon_1}\frac{\omega}{c}} \tag{3a}$$

$$\hat{\mathbf{e}}_s^{(s)}(\mathbf{q}_\parallel) = \hat{\mathbf{q}}_\parallel \times \hat{\mathbf{x}}_3. \tag{3b}$$

Optics EXPRESS

A caret over a vector indicates that it is a unit vector. In Eq. (1) $E_{0p}(\mathbf{k}_\parallel)$ and $E_{0s}(\mathbf{k}_\parallel)$ are the amplitudes of the p- and s-polarized components of the incident field with respect to the plane of incidence, defined by the vectors $\hat{\mathbf{k}}_\parallel$ and $\hat{\mathbf{x}}_3$. Similarly, $A_p(\mathbf{q}_\parallel)$ and $A_s(\mathbf{q}_\parallel)$ are the amplitudes of the p- and s-polarized components of the scattered field with respect to the plane of scattering, defined by the vectors $\hat{\mathbf{q}}_\parallel$ and $\hat{\mathbf{x}}_3$.

Maxwell's equations and the associated boundary conditions at the interfaces $x_3 = 0$ and $x_3 = -d + \zeta(\mathbf{x}_\parallel)$ imply a linear relation between $A_p(\mathbf{q}_\parallel)$, $A_s(\mathbf{q}_\parallel)$ and $E_{0p}(\mathbf{k}_\parallel)$, $E_{0s}(\mathbf{k}_\parallel)$, which we write as ($\alpha = p, s$, $\beta = p, s$)

$$A_\alpha(\mathbf{q}_\parallel) = \sum_\beta R_{\alpha\beta}(\mathbf{q}_\parallel|\mathbf{k}_\parallel) E_{0\beta}(\mathbf{k}_\parallel). \tag{4}$$

The equations satisfied by the scattering amplitudes $\{R_{\alpha\beta}(\mathbf{q}_\parallel|\mathbf{k}_\parallel)\}$ can be written in the form

$$\int \frac{\mathrm{d}^2 q_\parallel}{(2\pi)^2}\, \mathbf{M}^+(\mathbf{p}_\parallel|\mathbf{q}_\parallel)\mathbf{R}(\mathbf{q}_\parallel|\mathbf{k}_\parallel) = -\mathbf{M}^-(\mathbf{p}_\parallel|\mathbf{k}_\parallel), \tag{5}$$

where

$$\mathbf{R}(\mathbf{q}_\parallel|\mathbf{k}_\parallel) = \begin{pmatrix} R_{pp}(\mathbf{q}_\parallel|\mathbf{k}_\parallel) & R_{ps}(\mathbf{q}_\parallel|\mathbf{k}_\parallel) \\ R_{sp}(\mathbf{q}_\parallel|\mathbf{k}_\parallel) & R_{ss}(\mathbf{q}_\parallel|\mathbf{k}_\parallel) \end{pmatrix} \tag{6}$$

$$\mathbf{M}^\pm(\mathbf{p}_\parallel|\mathbf{q}_\parallel) = \begin{pmatrix} M^\pm_{pp}(\mathbf{p}_\parallel|\mathbf{q}_\parallel) & M^\pm_{ps}(\mathbf{p}_\parallel|\mathbf{q}_\parallel) \\ M^\pm_{sp}(\mathbf{p}_\parallel|\mathbf{q}_\parallel) & M^\pm_{ss}(\mathbf{p}_\parallel|\mathbf{q}_\parallel) \end{pmatrix}, \tag{7}$$

and the matrix elements are expressed as [4]

$$\begin{aligned}\mathbf{M}^\pm_{pp}(\mathbf{p}_\parallel|\mathbf{q}_\parallel) =& \frac{1}{\alpha_2(q_\parallel)}\Big\{ I_-(\mathbf{p}_\parallel|\mathbf{q}_\parallel)\left[p_\parallel q_\parallel + \alpha_3(p_\parallel)\hat{\mathbf{p}}_\parallel\cdot\hat{\mathbf{q}}_\parallel\alpha_2(q_\parallel)\right]\left[\varepsilon_1\alpha_2(q_\parallel) \pm \varepsilon_2\alpha_1(q_\parallel)\right] \\ &+ I_+(\mathbf{p}_\parallel|\mathbf{q}_\parallel)\left[p_\parallel q_\parallel - \alpha_3(p_\parallel)\hat{\mathbf{p}}_\parallel\cdot\hat{\mathbf{q}}_\parallel\alpha_2(q_\parallel)\right]\left[\varepsilon_1\alpha_2(q_\parallel) \mp \varepsilon_2\alpha_1(q_\parallel)\right]\Big\} \end{aligned} \tag{8a}$$

$$\begin{aligned}\mathbf{M}^\pm_{sp}(\mathbf{p}_\parallel|\mathbf{q}_\parallel) =& \sqrt{\varepsilon_3}\frac{\omega}{c}\left[\hat{\mathbf{p}}_\parallel\times\hat{\mathbf{q}}_\parallel\right]_3 \\ &\times\Big\{ I_-(\mathbf{p}_\parallel|\mathbf{q}_\parallel)\left[\varepsilon_1\alpha_2(q_\parallel) \pm \varepsilon_2\alpha_1(q_\parallel)\right] - I_+(\mathbf{p}_\parallel|\mathbf{q}_\parallel)\left[\varepsilon_1\alpha_2(q_\parallel) \mp \varepsilon_2\alpha_1(q_\parallel)\right]\Big\} \end{aligned} \tag{8b}$$

$$\begin{aligned}\mathbf{M}^\pm_{ps}(\mathbf{p}_\parallel|\mathbf{q}_\parallel) =& -\sqrt{\varepsilon_1}\varepsilon_2\frac{\omega}{c}\left[\hat{\mathbf{p}}_\parallel\times\hat{\mathbf{q}}_\parallel\right]_3\frac{\alpha_3(p_\parallel)}{\alpha_2(q_\parallel)} \\ &\times\Big\{ I_-(\mathbf{p}_\parallel|\mathbf{q}_\parallel)\left[\alpha_2(q_\parallel) \pm \alpha_1(q_\parallel)\right] + I_+(\mathbf{p}_\parallel|\mathbf{q}_\parallel)\left[\alpha_2(q_\parallel) \mp \alpha_1(q_\parallel)\right]\Big\} \end{aligned} \tag{8c}$$

$$\begin{aligned}\mathbf{M}^\pm_{ss}(\mathbf{p}_\parallel|\mathbf{q}_\parallel) =& \sqrt{\varepsilon_1}\varepsilon_2\sqrt{\varepsilon_3}\left(\frac{\omega}{c}\right)^2\hat{\mathbf{p}}_\parallel\cdot\hat{\mathbf{q}}_\parallel\frac{1}{\alpha_2(q_\parallel)} \\ &\times\Big\{ I_-(\mathbf{p}_\parallel|\mathbf{q}_\parallel)\left[\alpha_2(q_\parallel) \pm \alpha_1(q_\parallel)\right] + I_+(\mathbf{p}_\parallel|\mathbf{q}_\parallel)\left[\alpha_2(q_\parallel) \mp \alpha_1(q_\parallel)\right]\Big\}. \end{aligned} \tag{8d}$$

In writing Eq. (8) we have defined

$$I_\pm(\mathbf{p}_\parallel|\mathbf{q}_\parallel) = \exp\{\mathrm{i}[\alpha_3(p_\parallel) \pm \alpha_2(q_\parallel)]d\}\frac{I(\alpha_3(p_\parallel) \pm \alpha_2(q_\parallel)|\mathbf{p}_\parallel - \mathbf{q}_\parallel)}{\alpha_3(p_\parallel) \pm \alpha_2(q_\parallel)}, \tag{9}$$

where d is the mean thickness of the film, and

$$I(\gamma|\mathbf{Q}_\parallel) = \int \mathrm{d}^2 x_\parallel\, \exp\left[-\mathrm{i}\gamma\zeta(\mathbf{x}_\parallel)\right]\exp\left(-\mathrm{i}\mathbf{Q}_\parallel\cdot\mathbf{x}_\parallel\right). \tag{10}$$

Optics EXPRESS

The contribution to the mean DRC from the light that has been scattered incoherently (diffusely), and the reflectivity of the scattering system can be expressed in terms of the scattering amplitudes $\{R_{\alpha\beta}(\mathbf{q}_\parallel|\mathbf{k}_\parallel)\}$. Thus, the fraction of the total time-averaged flux in an incident wave of polarization β, the projection of whose wave vector on the mean scattering plane is $\mathbf{k}_\parallel$ that is scattered incoherently into a wave of α polarization, the projection of whose wave vector on the mean scattering plane is $\mathbf{q}_\parallel$, within an element of solid angle $\mathrm{d}\Omega_s$ about the scattering direction defined by the polar and azimuthal scattering angles (θ_s, ϕ_s), is given by

$$\left\langle \frac{\partial R_{\alpha\beta}(\mathbf{q}_\parallel|\mathbf{k}_\parallel)}{\partial\Omega_s} \right\rangle_{\text{incoh}} = \frac{\varepsilon_1}{S}\left(\frac{\omega}{2\pi c}\right)^2 \frac{\cos^2\theta_s}{\cos\theta_0}\left[\langle|R_{\alpha\beta}(\mathbf{q}_\parallel|\mathbf{k}_\parallel)|^2\rangle - |\langle R_{\alpha\beta}(\mathbf{q}_\parallel|\mathbf{k}_\parallel)\rangle|^2\right]. \tag{11}$$

Here S is the area of the plane $x_3 = 0$ covered by the random surface, and we have used the relations $\mathbf{k}_\parallel = \sqrt{\varepsilon_1}(\omega/c)\sin\theta_0(\cos\phi_0, \sin\phi_0, 0)$ and $\mathbf{q}_\parallel = \sqrt{\varepsilon_1}(\omega/c)\sin\theta_s(\cos\phi_s, \sin\phi_s, 0)$. Similarly, the reflectivity for light of polarization α incident on the surface with a polar angle of incidence θ_0 is

$$\mathcal{R}_\alpha(\theta_0) = \left|R_\alpha(k_\parallel)\right|^2 = \left|R_\alpha(\sqrt{\varepsilon_1}(\omega/c)\sin\theta_0)\right|^2, \tag{12}$$

where $R_\alpha(k_\parallel) = \langle R_{\alpha\alpha}(\mathbf{k}_\parallel|\mathbf{k}_\parallel)\rangle/S$.

The numerical solution of equations like Eq. (5) is described in detail in [5].

The theoretical results given by Eqs. (5)–(7) are valid both when the medium of incidence is optically more dense than the substrate and when it is optically less dense. However, in this paper we will present computational and experimental results only for the former case, because it is only in that case that effects due to total internal reflection occur. Results for the latter case will be presented elsewhere [6].

3. Experimental details

We have conducted angular scattering experiments with specially fabricated randomly rough surfaces. They were fabricated by exposing photoresist-coated plates (Shipley 1805) to statistically independent speckle patterns [8]. The speckle patterns were produced by passing a He-Cd laser beam ($\lambda = 442\,\text{nm}$) through a ground glass plate. The samples consist then of a glass substrate ($\varepsilon_1 = 2.25$), covered with a randomly rough film of photoresist ($\varepsilon_2 = 2.69$) in contact with air ($\varepsilon_3 = 1$), see Fig. 1.

Due to the exposure characteristics, the surfaces should have approximately Gaussian statistics and a Gaussian correlation function. They were characterized optically (by the strength of the coherent component) and by means of a mechanical profilometer. We present scattering data obtained from a surface whose rms height is $\delta = 22\,\text{nm}$ and its transverse correlation length $a = 1.9\,\mu\text{m}$. In the visible region of the spectrum, theories based on the reduced Rayleigh equation are adequate to deal with surfaces with such characteristic parameters. The mean film thickness of the sample is $d = 0.6\,\mu\text{m}$.

The experimental arrangement is shown in Fig. 1. The intensity was measured as a function of angle using a scatterometer that consists of an illumination and a detection system whose angular position can be controlled by a computer using two rotary stages with an angular resolution of 0.25 degrees. The illumination system consists of a HeNe laser beam ($\lambda = 632.8\,\text{nm}$) and a series of mirrors, diaphragms and lenses. The intensity and polarization of the illumination were controlled by placing, in series, a circular and a linear polarizer.

In order to illuminate the surface from the optically denser medium with angles of incidence close to the total internal reflection angle, the substrate was put in optical contact with a glass hemisphere (about 3.7 cm in diameter) using index matching oil [see Fig. 1]. A converging beam was focused a couple of centimeters before the glass hemisphere so that, after refraction at the hemisphere, the photoresist-air interface was illuminated by a diverging beam. The scattered

Optics EXPRESS

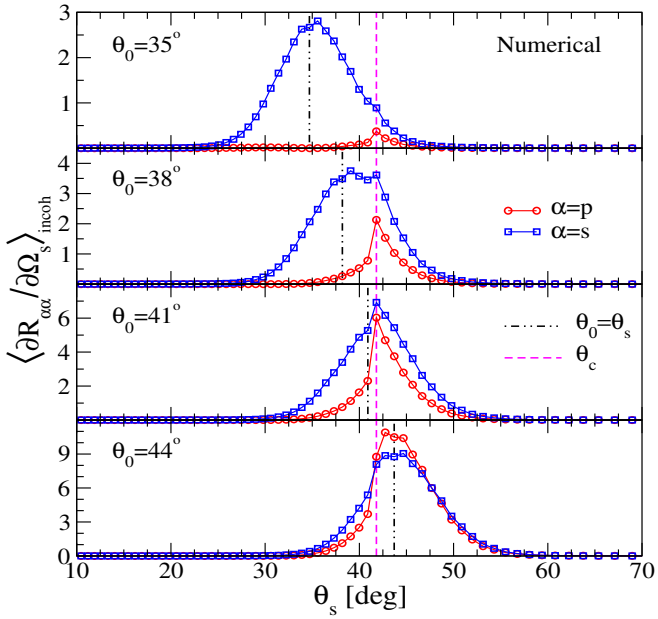

Fig. 2. The in-plane angular dependence of $\langle \partial R_{\alpha\alpha}/\partial\Omega_s \rangle_{\text{incoh}}$ for a set of θ_0 obtained by the numerical approach outlined in the text. The open symbols represents the data points obtained in the simulations, while the lines connecting them, are only included as a guide to the eye. Notice how the amplitudes of the data vary from panel to panel.

light passed again through the glass hemisphere and was collected by the detection system, about 30 cm away, in what is, effectively, the far field of the rough photoresist-air interface. The detection system consisted, basically, of a lens and a silicon detector. To reduce noise in the measurements, the detected signal was processed using lock-in detection techniques. For this, a mechanical chopper and a lock-in amplifier were used in the illumination and detection systems, respectively.

The use of the hemisphere permits the illumination of the rough interface with angles of incidence beyond the critical angle and simplifies the measurements of the angular distribution of scattered light. On the other hand, it introduces some experimental difficulties. First of all, the light has to pass twice through an interface with high optical power and, in a symmetric system (equal distances to the point source and to its image, obtained by specular reflection from the photoresist-air interface), the conjugate distances are practically equal to the diameter of the hemisphere. To facilitate the measurements, the first conjugate (source of the diverging beam) must be placed close to the hemisphere, so that the second conjugate point moves away from the sample, as shown in Fig. 1. The detection system moves then in a circle whose radius is determined by the position where the light that is specularly reflected by the rough photoresist-air interface is focused.

The alignment of the whole system is quite demanding. It is hard to make the center of curvature of the glass hemisphere coincide with the center of rotation of the sample, which makes it difficult to establish the angles of incidence and scattering with precision. However, since the critical angle is determined solely by the dielectric constants of the flat photoresist-air interface, this difficulty was circumvented by making the critical angle observed in the measurements coincide with the theoretical value of the critical angle. The other issue worth mentioning is

Optics EXPRESS

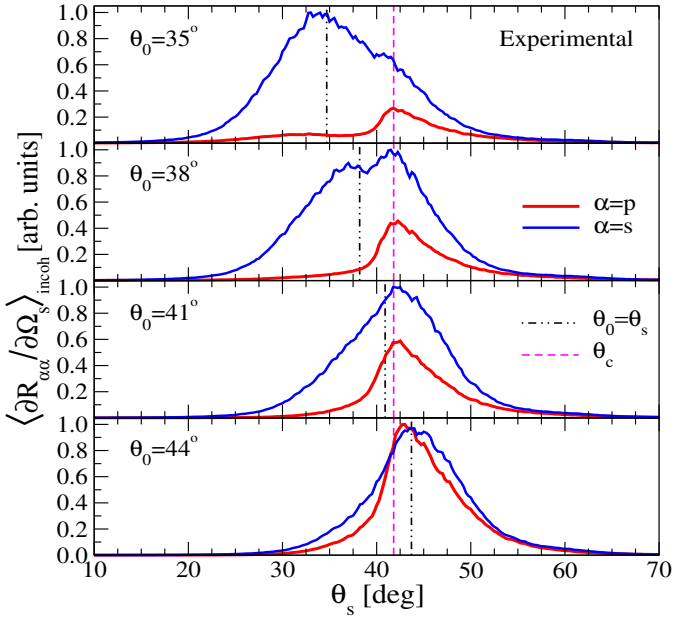

Fig. 3. Same as Fig. 2 but now presenting experimental measurements. The data sets in each panel were scaled by a common factor so that a unit amplitude corresponds to the maximum value of the corresponding numerical simulation results presented in Fig. 2.

that, since it is not possible to measure directly the light incident on the rough photoresist-air interface, it is difficult to obtain scattering data normalized by the incident power.

4. Results and discussion

Numerical and experimental results for the contribution to the mean DRC from in-plane co-polarized light scattered incoherently by the rough surface, $\langle \partial R_{\alpha\alpha}/\partial\Omega_s \rangle_{\text{incoh}}$, are presented in Figs. 2 and 3, respectively, for the same values of θ_0. By also calculating the transmitted intensity, energy conservation was found to be satisfied in our calculations with an error smaller than 10^{-3} (see [6] for details). For polar angles of incidence $\theta_0 \lesssim \theta_0^\star = 30°$, no pronounced Yoneda peaks are observed, either in the experimental or numerical data; at least, this is true for the structure that we considered. However, when the angle of incidence is increased towards the critical angle for total internal reflection $\theta_c = 41.89°$ [$\theta_0^\star \lesssim \theta_0 < \theta_c$], Yoneda peaks gradually start to develop around $\theta_s = \theta_c$ [Figs. 2 and 3; panels $\theta_0 = 35°, 38°$]. Initially these peaks are most readily observed in p-to-p scattering, but for an angle of incidence in the vicinity of the critical angle, $\theta_0 \lesssim \theta_c$, Yoneda peaks are also clearly identifiable in s-to-s scattering. Finally, for $\theta_0 > \theta_c$, Yoneda peaks are no longer observed either in the numerical or experimental data, and the signal amplitude at their position starts to drop off as one approaches grazing incidence [see Fig. 4].

There is a good quantitative agreement between the predicted angular positions of the Yoneda peaks presented in Fig. 2, and the experimental positions presented in Fig. 3. There is qualitative agreement about how these peaks develop with an increase of the polar angle of incidence. However, the experimental distributions $\langle \partial R_{\alpha\alpha}/\partial\Omega_s \rangle_{\text{incoh}}$ are broader then their numerical counterparts, and the ratio of the amplitudes of the two co-polarized experimental intensity distributions are not consistently reproduced by the numerical simulation results. We attribute

Optics EXPRESS

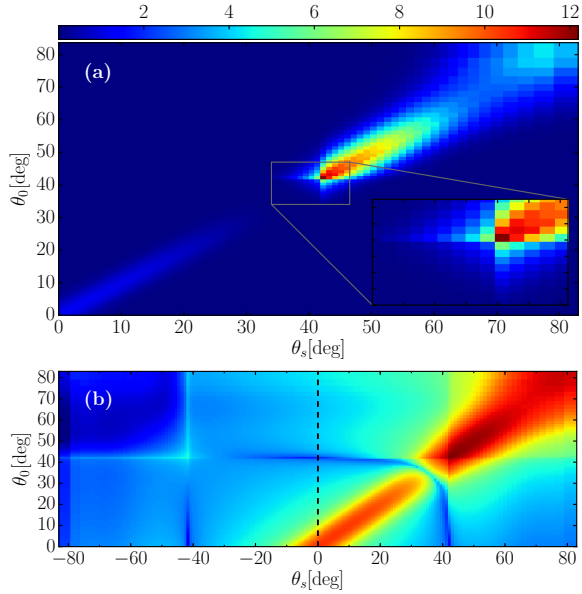

Fig. 4. Contour maps of the in-plane dependence of the raw simulation data for the co-polarized mean DRC as functions of θ_s and θ_0. Figure 4(a) represents the contour map of $\langle \partial R_{pp}/\partial \Omega_s \rangle_{\text{incoh}}$ and its inset details the behavior around $(\theta_s, \theta_0) = (\theta_c, \theta_c)$. In Fig. 4(b) the logarithm of the same data, $\log\langle \partial R_{pp}/\partial \Omega_s \rangle_{\text{incoh}}$, are presented but over the full range of polar scattering angles $-90° < \theta_s < 90°$. The vertical dashed center line (black) indicates $\theta_s = 0°$.

these differences between the experimental and numerical results in part to deviations of the statistical properties of the fabricated randomly rough surface used in the experiments from those assumed in performing the numerical calculations [7].

To better represent the dependence of the incoherently scattered light on the polar angles of incidence and scattering, in Fig. 4 we present contour maps of the angular dependence of the computational results for the in-plane, p-to-p incoherent scattering contribution to the mean DRC. The inset in Fig. 4(a) details the region around $(\theta_s, \theta_0) = (\theta_c, \theta_c)$ and explicitly shows the asymmetric character of the Yoneda peak phenomenon. To more readily inspect the local variations of this data set, Fig. 4(b) presents a contour plot of $\log\langle \partial R_{pp}/\partial \Omega_s \rangle_{\text{incoh}}$ as a function of θ_s and θ_0 for $-90° < \theta_s < 90°$ [12]. Several features of the scattered intensity should be noted from the results presented in Fig. 4(b). The first feature is the rapid intensity variations in the angular region around $\theta_0 = \theta_c$ or $\theta_s = \pm\theta_c$. For instance, at normal incidence [$\theta_0 = 0°$], local minima in the p-to-p scattered intensity distributions are observed around $\theta_s \approx \pm\theta_c$ [seen as the dark blue vertical structures in Fig. 4(b)]. As the polar angle of incidence is increased, the scattered intensity distribution is transformed from displaying local *minima* around $\theta_s \approx \pm\theta_c$ to displaying local *maxima* around the same angles. Only in the latter case does the scattered intensity distribution show Yoneda peaks, the phenomenon that we study experimentally in this work. It should be mentioned that in a recent numerical study of a related scattering system, a similar variation of the in-plane, p-to-p scattered intensity around $\theta_s \approx \pm\theta_c$ was observed and explained theoretically [6]. In this publication it was also shown that the in-plane, s-to-s scattered intensity displays Yoneda peaks independent of the value of the polar angle of incidence.

Optics EXPRESS

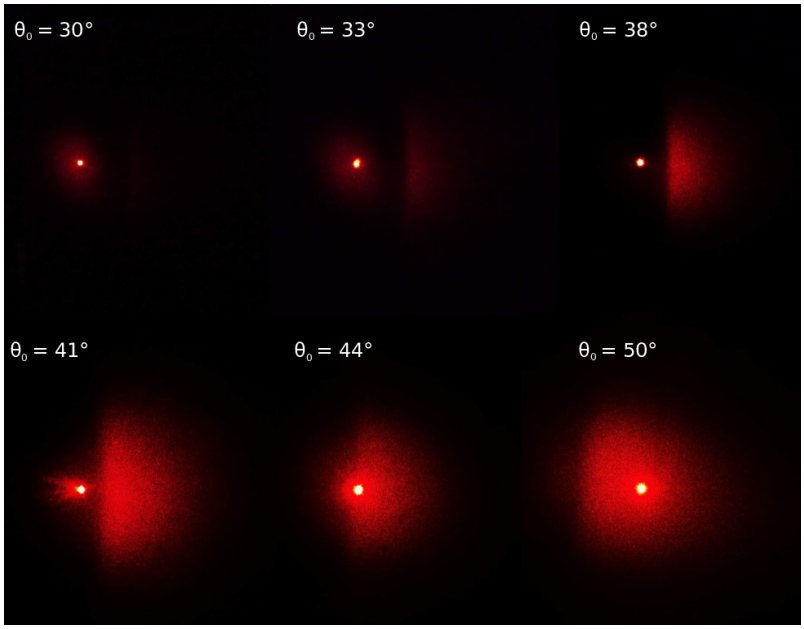

Fig. 5. Photographs showing the spatial intensity distributions formed on the rough aluminum screen [see Fig. 6] for a set of polar angles of incidence, $\theta_0 = \theta_s$, as indicated in the figure.

Figure 5 presents experimental results for the *angular dependence* of the intensity distributions of the light scattered also outside the plane of incidence; as such, these results complement the measured in-plane intensity distributions reported in Fig. 3.

The photographs of the scattered intensity patterns depicted in Fig. 5, were obtained with the arrangement illustrated in Fig. 6. As in the scattering measurements reported in Fig. 3, the sample is illuminated through a glass hemisphere, and the light is scattered back from the rough back surface of the sample through the glass hemisphere. However, in contrast to how the scattering measurements were preformed to produce the results of Fig. 3, a rough aluminum screen was placed about 45 cm from the sample so that the light would rescatter from it and form an image on the screen. A digital camera was then used to take photographs of the scattering patterns observed on the aluminum screen. It is in this way that the photographs shown in Fig. 5 were obtained.

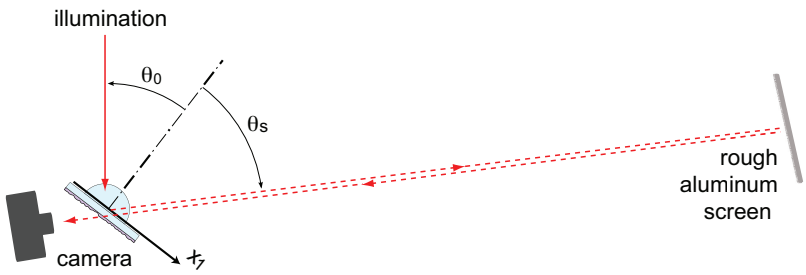

Fig. 6. Schematics of the geometry used to take the photographs presented in Fig. 5.

Optics EXPRESS

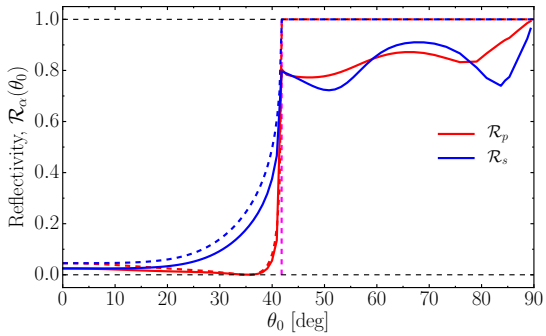

Fig. 7. The reflectivity, $\mathcal{R}_\alpha(\theta_0)$, of the scattering system studied. The dashed lines denotes the Fresnel reflection coefficient, *i.e.* the reflectivity of a corresponding film with planar surfaces.

The specular direction is represented by the bright red circular spots readily observed in the results presented in Fig. 5. As the polar angle of incidence is approaching the critical angle for total internal reflection $\theta_c = 41.89°$, the Yoneda peaks start to appear. In particular, for the intensity distributions presented in Fig. 5 corresponding to the polar angles of incidence 38° and 41°, the Yoneda phenomenon is clearly seen. It is manifested by an abrupt increase in the intensity of the scattered light in directions parallel to the plane of incidence. This results in a "ridge" of high intensity that locally is oriented almost perpendicular to the plane of incidence. This finding is consistent with the theoretical prediction for the full angular intensity distribution of the light scattered from a sample of similar geometry [6].

Although small amplitude perturbation theory predicts that the Yoneda peaks occur in the contribution to the scattering amplitudes $\{R_{\alpha\beta}(\mathbf{q}_\parallel|\mathbf{k}_\parallel)\}$ of first order in the surface profile function [6], and so are single-scattering phenomena, their physical interpretation has been the subject of discussion for five decades. In a study of the reflection of x-rays from a polished surface Warren and Clark [9] proposed that these peaks can be interpreted in terms of a small angle scattering from a projection on an irregular surface followed by total reflection. In a subsequent study of grazing-angle reflection of x-rays from rough metal surfaces, Vineyard [10] noted that the angular dependence of the Fresnel coefficient for transmission through a planar vacuum-metal interface produces a transmitted field on the surface whose angular dependence has the form of an asymmetric peak. The maximum of this peak occurs at the critical angle for total internal reflection and has a magnitude that is twice that of the incident electric field on the surface, which leads to an enhanced diffuse scattering at this angle. This effect was invoked by Sinha *et al.* [11] as the origin of the Yoneda peaks. However, it is not a physical explanation for the origin of these peaks. Kawanishi *et al.* [2] suggested that the Yoneda peaks may be due to the presence of lateral waves, excited through the roughness, propagating along the interface in the optically less dense medium. This wave satisfies the condition for refraction back into the optically more dense medium, and therefore leaks energy at each point along the interface along rays whose scattering angle equals θ_c. This explanation is attractive, but should be explored more through additional calculations.

Finally, in Fig. 7 we present the calculated reflectivity of our structure for p- and s-polarized incident light. The effect of total internal reflection is clearly seen in these results. For $\theta_c < \theta_0 < 90°$ the reflectivity in each polarization decreases by approximately 20% from the corresponding Fresnel reflectivity in much of this interval, a significant change for the degree of roughness possessed by this surface.

Optics EXPRESS

5. Conclusions

In this paper we have presented the first experimental results for the scattering of p- and s-polarized light from a dielectric structure with a two-dimensional randomly rough interface that can display effects associated with total internal reflection. In particular, we have shown the existence of Yoneda peaks in the angular dependence of the mean differential reflection coefficient. The experimental results are supported by the results of rigorous, purely numerical, nonperturbative solutions of the reduced Rayleigh equation for scattering from this structure. These features are already present in single-scattering calculations of the mean differential reflection coefficient. It will be of interest to see how they develop in the presence of strong multiple scattering and in transmission. Finally, we find that even a small degree of roughness significantly depresses the reflection of p- and s-polarized light for scattering angles greater than the critical angle for total internal reflection.

Funding

Consejo Nacional de Ciencia y Tecnología (CONACYT) (180654); The Research Council of Norway (RCN) (216699); The French National Research Agency (ANR) (ANR-15-CHIN-0003-01).

Acknowledgments

This research was supported in part by NTNU and the Norwegian metacenter for High Performance Computing (NOTUR) by the allocation of computer time.

Paper 4:

Ø. S. Hetland, A. A. Maradudin, T. Nordam, P. A. Letnes, and I. Simonsen, "Numerical studies of the transmission of light through a two-dimensional randomly rough interface," *Phys. Rev. A*, vol. 95, no. 4, p. 043808, 2017

Numerical studies of the transmission of light through a two-dimensional randomly rough interface

Ø. S. Hetland,[1,*] A. A. Maradudin,[2] T. Nordam,[1] P. A. Letnes,[1] and I. Simonsen[1,3]
[1]*Department of Physics, NTNU Norwegian University of Science and Technology, NO-7491 Trondheim, Norway*
[2]*Department of Physics and Astronomy, University of California, Irvine, California 92697, USA*
[3]*Surface du Verre et Interfaces, UMR 125 CNRS/Saint-Gobain, F-93303 Aubervilliers, France*
(Received 14 December 2016; published 7 April 2017)

The transmission of polarized light through a two-dimensional randomly rough interface between two dielectric media has been much less studied, by any approach, than the reflection of light from such an interface. We have derived a reduced Rayleigh equation for the transmission amplitudes when *p*- or *s*-polarized light is incident on this type of interface, and have obtained rigorous, purely numerical, nonperturbative solutions of it. The solutions are used to calculate the transmissivity and transmittance of the interface, the mean differential transmission coefficient, and the full angular distribution of the intensity of the transmitted light. These results are obtained for both the case where the medium of incidence is the optically less dense medium and in the case where it is the optically more dense medium. Optical analogs of Yoneda peaks observed in the scattering of x rays from metallic and nonmetallic surfaces are present in the results obtained in the former case. For *p*-polarized incident light we observe Brewster scattering angles, angles at which the diffuse transmitted intensity is zero in a single-scattering approximation, which depend on the angle of incidence in contrast to the Brewster angle for flat-surface reflection.

DOI: 10.1103/PhysRevA.95.043808

I. INTRODUCTION

In the theoretical and experimental studies of the interaction of an electromagnetic wave with a two-dimensional randomly rough dielectric surface, the great majority have been devoted to the reflection problem [1–3], and less attention has been paid to studies of the transmission of light through such surfaces. Greffet [4] obtained a reduced Rayleigh equation for the transmission amplitudes in the case where light incident from vacuum is transmitted through a two-dimensional randomly rough interface into a dielectric medium, and obtained a recursion relation for the successive terms in the expansions of the amplitudes in powers of the surface profile function. Kawanishi *et al.* [5], by the use of the stochastic functional approach, studied the case where a two-dimensional randomly rough interface between two dielectric media is illuminated by *p*- and *s*-polarized light from either medium. Properties of the light transmitted through, as well as reflected from, the interface were examined. This theoretical approach is perturbative in nature and can be applied only to weakly rough surfaces. Nevertheless, Kawanishi *et al.* obtained several interesting properties of the transmitted light that are associated with the phenomenon of total internal reflection when the medium of transmission is the optically denser medium. These include the appearance of Yoneda peaks in the intensity of the transmitted light as a function of the angle of transmission for a fixed value of the angle of incidence. Yoneda peaks are sharp asymmetric peaks at the critical polar angle of transmission for which the wave number of incidence turns nonpropagating when the medium of transmission is the optically more dense medium. Although well known in the scattering of x rays from both metallic [6–9] and nonmetallic [10–13] surfaces, the paper by Kawanishi *et al.* apparently marks their first explicit appearance in optics. Yoneda peaks were recently observed experimentally for a configuration of reflection from a randomly rough dielectric interface, when the medium of incidence was the optically denser medium [14]. The physical origin of the Yoneda peak phenomenon is not clear [15].

For *p*-polarized incident light Kawanishi *et al.* also observed angles of zero scattering intensity, to first order in their approach, in the distributions of the intensity of the incoherently reflected and transmitted light. Due to their resemblance to the Brewster angle in the reflectivity from a flat interface, they dubbed these angles the "Brewster scattering angles." These were observed, in both reflection and transmission, for light incident from either medium, and were found to be strongly dependent on the angle of incidence. The Brewster scattering angles can be observed to be part of the mechanisms that result in a strong dependence on polarization in the scattering distributions of incoherently scattered light. Nieto-Vesperinas and Sánchez-Gil [16] observed this strong dependence on polarization in their numerical investigations of incoherent transmission through one-dimensional dielectric surfaces, but they did not investigate this dependence any further.

Soubret *et al.* [17] also obtained a reduced Rayleigh equation for the transmission amplitudes in the case where light incident from one dielectric medium is transmitted into a second dielectric medium through a two-dimensional randomly rough interface. However, only perturbative solutions of this equation were obtained by them, and only for vacuum as the medium of incidence.

In this paper we present a theoretical study of the transmission of light through a two-dimensional randomly rough interface between two dielectric media, free from some of the limitations and approximations present in the earlier studies of this problem. We obtain a reduced Rayleigh equation for

*oyvind.hetland@ntnu.no

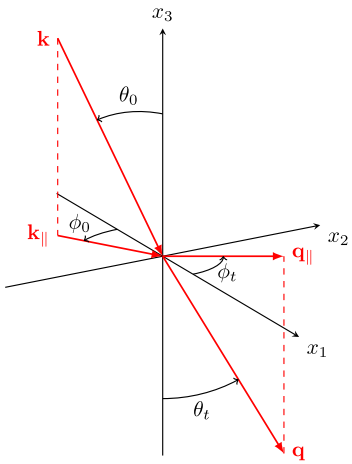

FIG. 1. Sketch of the scattering geometry assumed in this work. The figure also shows the coordinate system used, angles of incidence (θ_0,ϕ_0) and transmission (θ_t,ϕ_t), and the corresponding lateral wave vectors $\mathbf{k}_\parallel$ and $\mathbf{q}_\parallel$.

the transmission amplitudes in the case where light incident from a dielectric medium whose dielectric constant is ε_1 is transmitted through a two-dimensional randomly rough interface into a dielectric medium whose dielectric constant is ε_2. The dielectric constant ε_1 can be larger or smaller than the dielectric constant ε_2. Thus effects associated with total internal reflection are included in the solutions of this equation. Instead of solving the reduced Rayleigh equation as an expansion in powers of the surface profile function, in this work we obtain a rigorous, purely numerical, nonperturbative solution of it. This approach enables us to calculate the transmissivity and transmittance of the system studied, the in-plane co- and cross-polarized, and the out-of-plane co- and cross-polarized incoherent (diffuse) scattering contributions to the mean differential transmission coefficient, and the full angular dependence of the total scattered intensity, all in a nonperturbative fashion.

Numerical studies of similar systems and phenomena, obtained through a corresponding numerical method but in reflection, have previously been reported in Refs. [14,15]. Both Yoneda peaks and Brewster scattering angles were reported and discussed in-depth in Ref. [15], and an experimental observation of Yoneda peaks were presented in Ref. [14]. As such, the currently presented work serves to add to the fuller understanding of the scattering behavior of randomly rough dielectric interfaces.

II. SCATTERING SYSTEM

The system we study in this paper consists of a dielectric medium (medium 1), whose dielectric constant is ε_1, in the region $x_3 > \zeta(\mathbf{x}_\parallel)$, and a dielectric medium (medium 2), whose dielectric constant is ε_2, in the region $x_3 < \zeta(\mathbf{x}_\parallel)$ (Fig. 1). Here $\mathbf{x}_\parallel = (x_1,x_2,0)$ is an arbitrary vector in the plane $x_3 = 0$, and we assume that both ε_1 and ε_2 are real and positive.

The surface profile function $\zeta(\mathbf{x}_\parallel)$ is assumed to be a single-valued function of $\mathbf{x}_\parallel$ that is differentiable with respect to x_1 and x_2, and constitutes a stationary, zero-mean, isotropic, Gaussian random process defined by

$$\langle\zeta(\mathbf{x}_\parallel)\zeta(\mathbf{x}'_\parallel)\rangle = \delta^2 W(|\mathbf{x}_\parallel - \mathbf{x}'_\parallel|), \tag{1}$$

where $W(x_\parallel)$ is the normalized surface height autocorrelation function, with the property that $W(0) = 1$. The angle brackets here and in all that follows denote an average over the ensemble of realizations of the surface profile function. The root-mean-square height of the surface is given by

$$\delta = \langle\zeta^2(\mathbf{x}_\parallel)\rangle^{\frac{1}{2}}. \tag{2}$$

The power spectrum of the surface roughness $g(k_\parallel)$ is defined by

$$g(k_\parallel) = \int d^2x_\parallel W(x_\parallel)\exp(-\mathrm{i}\mathbf{k}_\parallel\cdot\mathbf{x}_\parallel), \tag{3}$$

where $\mathbf{k}_\parallel = (k_1,k_2,0)$ is a lateral wave vector, $k_\parallel = |\mathbf{k}_\parallel|$, and $x_\parallel = |\mathbf{x}_\parallel|$. We will assume for the normalized surface height autocorrelation function $W(x_\parallel)$ the Gaussian function

$$W(x_\parallel) = \exp\left(-\frac{x_\parallel^2}{a^2}\right), \tag{4}$$

where the characteristic length a is the transverse correlation length of the surface roughness. The corresponding power spectrum is given by

$$g(k_\parallel) = \pi a^2\exp\left(-\frac{k_\parallel^2 a^2}{4}\right). \tag{5}$$

III. REDUCED RAYLEIGH EQUATION

The interface $x_3 = \zeta(\mathbf{x}_\parallel)$ is illuminated from the region $x_3 > \zeta(\mathbf{x}_\parallel)$ (medium 1) by an electromagnetic wave of frequency ω. The total electric field in this region is the sum of an incoming incident field and an outgoing scattered field,

$$\mathbf{E}^>(\mathbf{x}|\omega) = \mathbf{E}_0(\mathbf{k}_\parallel)\exp[i\mathbf{Q}_0(\mathbf{k}_\parallel)\cdot\mathbf{x}] + \int\frac{d^2q_\parallel}{(2\pi)^2}\,\mathbf{A}(\mathbf{q}_\parallel)\exp[i\mathbf{Q}_1(\mathbf{q}_\parallel)\cdot\mathbf{x}], \tag{6}$$

while the electric field in the region $x_3 < \zeta(\mathbf{x}_\parallel)$ is an outgoing transmitted field,

$$\mathbf{E}^<(\mathbf{x}|\omega) = \int\frac{d^2q_\parallel}{(2\pi)^2}\,\mathbf{B}(\mathbf{q}_\parallel)\exp[i\mathbf{Q}_2(\mathbf{q}_\parallel)\cdot\mathbf{x}]. \tag{7}$$

In writing these equations we have introduced the functions

$$\mathbf{Q}_0(\mathbf{k}_\parallel) = \mathbf{k}_\parallel - \alpha_1(k_\parallel)\hat{\mathbf{x}}_3, \tag{8a}$$

$$\mathbf{Q}_1(\mathbf{q}_\parallel) = \mathbf{q}_\parallel + \alpha_1(q_\parallel)\hat{\mathbf{x}}_3, \tag{8b}$$

$$\mathbf{Q}_2(\mathbf{q}_\parallel) = \mathbf{q}_\parallel - \alpha_2(q_\parallel)\hat{\mathbf{x}}_3, \tag{8c}$$

where ($i = 1,2$)

$$\alpha_i(q_\parallel) = \begin{cases} \sqrt{\varepsilon_i\left(\frac{\omega}{c}\right)^2 - q_\parallel^2}, & q_\parallel \leqslant \sqrt{\varepsilon_i}\,\omega/c, \\ i\sqrt{q_\parallel^2 - \varepsilon_i\left(\frac{\omega}{c}\right)^2}, & q_\parallel > \sqrt{\varepsilon_i}\,\omega/c. \end{cases} \tag{9}$$

Here $\mathbf{q}_\parallel = (q_1,q_2,0)$, $q_\parallel = |\mathbf{q}_\parallel|$, and a caret over a vector indicates that it is a unit vector. A time dependence of the field of the form $\exp(-i\omega t)$ has been assumed, but not indicated explicitly.

The boundary conditions satisfied by these fields at the interface $x_3 = \zeta(\mathbf{x}_\parallel)$ are the continuity of the tangential components of the electric field,

$$\begin{aligned} &\mathbf{n}\times\mathbf{E}_0(\mathbf{k}_\parallel)\exp[i\mathbf{k}_\parallel\cdot\mathbf{x}_\parallel - i\alpha_1(k_\parallel)\zeta(\mathbf{x}_\parallel)] \\ &\quad + \int \frac{d^2q_\parallel}{(2\pi)^2}\,\mathbf{n}\times\mathbf{A}(\mathbf{q}_\parallel)\exp[i\mathbf{q}_\parallel\cdot\mathbf{x}_\parallel + i\alpha_1(q_\parallel)\zeta(\mathbf{x}_\parallel)] \\ &= \int \frac{d^2q_\parallel}{(2\pi)^2}\,\mathbf{n}\times\mathbf{B}(\mathbf{q}_\parallel)\exp[i\mathbf{q}_\parallel\cdot\mathbf{x}_\parallel - i\alpha_2(q_\parallel)\zeta(\mathbf{x}_\parallel)], \end{aligned} \tag{10}$$

the continuity of the tangential components of the magnetic field,

$$\begin{aligned} &\mathbf{n}\times[i\mathbf{Q}_0(\mathbf{k}_\parallel)\times\mathbf{E}_0(\mathbf{k}_\parallel)]\exp[i\mathbf{k}_\parallel\cdot\mathbf{x}_\parallel - i\alpha_1(k_\parallel)\zeta(\mathbf{x}_\parallel)] \\ &\quad + \int \frac{d^2q_\parallel}{(2\pi)^2}\,\mathbf{n}\times[i\mathbf{Q}_1(\mathbf{q}_\parallel)\times\mathbf{A}(\mathbf{q}_\parallel)] \\ &\quad \times \exp[i\mathbf{q}_\parallel\cdot\mathbf{x}_\parallel + i\alpha_1(q_\parallel)\zeta(\mathbf{x}_\parallel)] \\ &= \int \frac{d^2q_\parallel}{(2\pi)^2}\,\mathbf{n}\times[i\mathbf{Q}_2(\mathbf{q}_\parallel)\times\mathbf{B}(\mathbf{q}_\parallel)] \\ &\quad \times \exp[i\mathbf{q}_\parallel\cdot\mathbf{x}_\parallel - i\alpha_2(q_\parallel)\zeta(\mathbf{x}_\parallel)], \end{aligned} \tag{11}$$

and the continuity of the normal component of the electric displacement,

$$\begin{aligned} &\varepsilon_1\mathbf{n}\cdot\mathbf{E}_0(\mathbf{k}_\parallel)\exp[i\mathbf{k}_\parallel\cdot\mathbf{x}_\parallel - i\alpha_1(k_\parallel)\zeta(\mathbf{x}_\parallel)] \\ &\quad + \varepsilon_1\int \frac{d^2q_\parallel}{(2\pi)^2}\,\mathbf{n}\cdot\mathbf{A}(\mathbf{q}_\parallel)\exp[i\mathbf{q}_\parallel\cdot\mathbf{x}_\parallel + i\alpha_1(q_\parallel)\zeta(\mathbf{x}_\parallel)] \\ &= \varepsilon_2\int \frac{d^2q_\parallel}{(2\pi)^2}\,\mathbf{n}\cdot\mathbf{B}(\mathbf{q}_\parallel)\exp[i\mathbf{q}_\parallel\cdot\mathbf{x}_\parallel - i\alpha_2(q_\parallel)\zeta(\mathbf{x}_\parallel)]. \end{aligned} \tag{12}$$

The vector $\mathbf{n} \equiv \mathbf{n}(\mathbf{x}_\parallel)$ entering these equations is a vector normal to the surface $x_3 = \zeta(\mathbf{x}_\parallel)$ at each point of it, directed into medium 1:

$$\mathbf{n}(\mathbf{x}_\parallel) = \left(-\frac{\partial\zeta(\mathbf{x}_\parallel)}{\partial x_1}, -\frac{\partial\zeta(\mathbf{x}_\parallel)}{\partial x_2}, 1\right). \tag{13}$$

Strictly speaking the continuity of the tangential components of the electric and magnetic fields across the interface, Eqs. (10) and (11), are sufficient (and necessary) boundary conditions on electromagnetic fields [18]. Hence the continuity of the normal components of the electric displacement [Eq. (12)] and the magnetic induction are redundant. However, the inclusion of Eq. (12) enables us to eliminate the scattering amplitude $\mathbf{A}(\mathbf{q}_\parallel)$ from consideration, and thus to obtain an equation that relates the transmission amplitude $\mathbf{B}(\mathbf{q}_\parallel)$ to the amplitude of the incident field $\mathbf{E}_0(\mathbf{k}_\parallel)$. This we do in the following manner.

We take the vector cross product of Eq. (10) with $\varepsilon_1\mathbf{Q}_0(\mathbf{p}_\parallel)\exp[-i\mathbf{p}_\parallel\cdot\mathbf{x}_\parallel + i\alpha_1(p_\parallel)\zeta(\mathbf{x}_\parallel)]$, then multiply Eq. (11) by $-i\varepsilon_1\exp[-i\mathbf{p}_\parallel\cdot\mathbf{x}_\parallel + i\alpha_1(p_\parallel)\zeta(\mathbf{x}_\parallel)]$, and finally multiply Eq. (12) by $-\mathbf{Q}_0(\mathbf{p}_\parallel)\exp[-i\mathbf{p}_\parallel\cdot\mathbf{x}_\parallel + i\alpha_1(p_\parallel)\zeta(\mathbf{x}_\parallel)]$, where $\mathbf{p}_\parallel$ is an arbitrary wave vector in the plane $x_3 = 0$. When we add the three equations obtained in this way, and integrate the sum over $\mathbf{x}_\parallel$ we obtain an equation that can be written in the form

$$\begin{aligned} &\varepsilon_1\{\mathbf{Q}_0(\mathbf{p}_\parallel)\times[\mathbf{V}_E(\mathbf{p}_\parallel|\mathbf{k}_\parallel)\times\mathbf{E}_0(\mathbf{k}_\parallel)] + \mathbf{V}_E(\mathbf{p}_\parallel|\mathbf{k}_\parallel)\times[\mathbf{Q}_0(\mathbf{k}_\parallel)\times\mathbf{E}_0(\mathbf{k}_\parallel)] - \mathbf{Q}_0(\mathbf{p}_\parallel)[\mathbf{V}_E(\mathbf{p}_\parallel|\mathbf{k}_\parallel)\cdot\mathbf{E}_0(\mathbf{k}_\parallel)]\} \\ &\quad + \varepsilon_1\int \frac{d^2q_\parallel}{(2\pi)^2}\,\{\mathbf{Q}_0(\mathbf{p}_\parallel)\times[\mathbf{V}_A(\mathbf{p}_\parallel|\mathbf{q}_\parallel)\times\mathbf{A}(\mathbf{q}_\parallel)] + \mathbf{V}_A(\mathbf{p}_\parallel|\mathbf{q}_\parallel)\times[\mathbf{Q}_1(\mathbf{q}_\parallel)\times\mathbf{A}(\mathbf{q}_\parallel)] - \mathbf{Q}_0(\mathbf{p}_\parallel)[\mathbf{V}_A(\mathbf{p}_\parallel|\mathbf{q}_\parallel)\cdot\mathbf{A}(\mathbf{q}_\parallel)]\} \\ &= \int \frac{d^2q_\parallel}{(2\pi)^2}\,\{\varepsilon_1\mathbf{Q}_0(\mathbf{p}_\parallel)\times[\mathbf{V}_B(\mathbf{p}_\parallel|\mathbf{q}_\parallel)\times\mathbf{B}(\mathbf{q}_\parallel)] + \varepsilon_1\mathbf{V}_B(\mathbf{p}_\parallel|\mathbf{q}_\parallel)\times[\mathbf{Q}_2(\mathbf{q}_\parallel)\times\mathbf{B}(\mathbf{q}_\parallel)] - \varepsilon_2\mathbf{Q}_0(\mathbf{p}_\parallel)[\mathbf{V}_B(\mathbf{p}_\parallel|\mathbf{q}_\parallel)\cdot\mathbf{B}(\mathbf{q}_\parallel)]\}, \end{aligned} \tag{14}$$

where we define

$$\mathbf{V}_E(\mathbf{p}_\parallel|\mathbf{k}_\parallel) = \mathbf{V}(-\alpha_1(p_\parallel) + \alpha_1(k_\parallel)|\mathbf{p}_\parallel - \mathbf{k}_\parallel), \tag{15a}$$

$$\mathbf{V}_A(\mathbf{p}_\parallel|\mathbf{q}_\parallel) = \mathbf{V}(-\alpha_1(p_\parallel) - \alpha_1(q_\parallel)|\mathbf{p}_\parallel - \mathbf{q}_\parallel), \tag{15b}$$

$$\mathbf{V}_B(\mathbf{p}_\parallel|\mathbf{q}_\parallel) = \mathbf{V}(-\alpha_1(p_\parallel) + \alpha_2(q_\parallel)|\mathbf{p}_\parallel - \mathbf{q}_\parallel), \tag{15c}$$

with

$$\mathbf{V}(\gamma|\mathbf{Q}_\parallel) = \int d^2x_\parallel\mathbf{n}(\mathbf{x}_\parallel)\exp(-i\mathbf{Q}_\parallel\cdot\mathbf{x}_\parallel)\exp[-i\gamma\zeta(\mathbf{x}_\parallel)]. \tag{16a}$$

It is shown in Appendix A that

$$\mathbf{V}(\gamma|\mathbf{Q}_\parallel) = \frac{I(\gamma|\mathbf{Q}_\parallel)}{\gamma}(\mathbf{Q}_\parallel + \gamma\hat{\mathbf{x}}_3) - (2\pi)^2\delta(\mathbf{Q}_\parallel)\frac{\mathbf{Q}_\parallel}{\gamma}, \tag{16b}$$

where

$$I(\gamma|\mathbf{Q}_\parallel) = \int d^2x_\parallel\exp(-i\mathbf{Q}_\parallel\cdot\mathbf{x}_\parallel)\exp[-i\gamma\zeta(\mathbf{x}_\parallel)]. \tag{17}$$

When Eqs. (15) and (16) are substituted into Eq. (14), the latter becomes

$$\begin{aligned} &(2\pi)^2\delta(\mathbf{p}_\parallel - \mathbf{k}_\parallel)2\varepsilon_1\frac{\mathbf{k}_\parallel\cdot(\mathbf{p}_\parallel - \mathbf{k}_\parallel)}{-\alpha_1(p_\parallel) + \alpha_1(k_\parallel)}\mathbf{E}_0(\mathbf{k}_\parallel) \\ &= (\varepsilon_1 - \varepsilon_2)\int \frac{d^2q_\parallel}{(2\pi)^2}\,\frac{I(-\alpha_1(p_\parallel) + \alpha_2(q_\parallel)|\mathbf{p}_\parallel - \mathbf{q}_\parallel)}{-\alpha_1(p_\parallel) + \alpha_2(q_\parallel)} \\ &\quad \times\left\{-\varepsilon_1\left(\frac{\omega}{c}\right)^2\mathbf{B}(\mathbf{q}_\parallel) + [\mathbf{Q}_0(\mathbf{p}_\parallel)\cdot\mathbf{B}(\mathbf{q}_\parallel)]\mathbf{Q}_0(\mathbf{p}_\parallel)\right\}. \end{aligned} \tag{18}$$

In obtaining this result we have used the result that the singular term of $\mathbf{V}_B(\mathbf{p}_\parallel|\mathbf{q}_\parallel)$ does not contribute to the right-hand side of Eq. (14), since $\mathbf{p}_\parallel = \mathbf{q}_\parallel$ leaves $-\alpha_1(p_\parallel) + \alpha_2(q_\parallel)$ nonzero (see Appendix A). If we note that

$$-\alpha_1(p_\parallel) + \alpha_1(k_\parallel) = \frac{\mathbf{k}_\parallel \cdot (\mathbf{p}_\parallel - \mathbf{k}_\parallel)}{\alpha_1(k_\parallel)} + O((\mathbf{p}_\parallel - \mathbf{k}_\parallel)^2), \quad (19)$$

the left-hand side of Eq. (18) becomes $(2\pi)^2\delta(\mathbf{p}_\parallel - \mathbf{k}_\parallel)2\varepsilon_1\alpha_1(k_\parallel)\mathbf{E}_0(\mathbf{k}_\parallel)$. Thus we have an equation for the transmission amplitude $\mathbf{B}(\mathbf{q}_\parallel)$ alone:

$$\begin{aligned}\mathbf{t} = &\int \frac{d^2q_\parallel}{(2\pi)^2}\, \frac{I(-\alpha_1(p_\parallel) + \alpha_2(q_\parallel)|\mathbf{p}_\parallel - \mathbf{q}_\parallel)}{-\alpha_1(p_\parallel) + \alpha_2(q_\parallel)} \\ &\times \left\{-\varepsilon_1\left(\frac{\omega}{c}\right)^2 \mathbf{B}(\mathbf{q}_\parallel) + [\mathbf{Q}_0(\mathbf{p}_\parallel)\cdot\mathbf{B}(\mathbf{q}_\parallel)]\mathbf{Q}_0(\mathbf{p}_\parallel)\right\} \\ &= (2\pi)^2\delta(\mathbf{p}_\parallel - \mathbf{k}_\parallel)\frac{2\varepsilon_1\alpha_1(k_\parallel)}{\varepsilon_1 - \varepsilon_2}\mathbf{E}_0(\mathbf{k}_\parallel). \quad (20)\end{aligned}$$

We now write the vectors $\mathbf{E}_0(\mathbf{k}_\parallel)$ and $\mathbf{B}(\mathbf{q}_\parallel)$ in the forms

$$\mathbf{E}_0(\mathbf{k}_\parallel) = \hat{\mathbf{e}}_p^{(i)}(\mathbf{k}_\parallel)E_{0p}(\mathbf{k}_\parallel) + \hat{\mathbf{e}}_s^{(i)}(\mathbf{k}_\parallel)E_{0s}(\mathbf{k}_\parallel), \quad (21a)$$

where

$$\hat{\mathbf{e}}_p^{(i)}(\mathbf{k}_\parallel) = \frac{c}{\sqrt{\varepsilon_1}\omega}[\hat{\mathbf{k}}_\parallel\alpha_1(k_\parallel) + \hat{\mathbf{x}}_3 k_\parallel], \quad (21b)$$

$$\hat{\mathbf{e}}_s^{(i)}(\mathbf{k}_\parallel) = \hat{\mathbf{x}}_3 \times \hat{\mathbf{k}}_\parallel, \quad (21c)$$

and

$$\mathbf{B}(\mathbf{q}_\parallel) = \hat{\mathbf{e}}_p^{(t)}(\mathbf{q}_\parallel)B_p(\mathbf{q}_\parallel) + \hat{\mathbf{e}}_s^{(t)}(\mathbf{q}_\parallel)B_s(\mathbf{q}_\parallel), \quad (22a)$$

where

$$\hat{\mathbf{e}}_p^{(t)}(\mathbf{q}_\parallel) = \frac{c}{\sqrt{\varepsilon_2}\omega}[\hat{\mathbf{q}}_\parallel\alpha_2(q_\parallel) + \hat{\mathbf{x}}_3 q_\parallel], \quad (22b)$$

$$\hat{\mathbf{e}}_s^{(t)}(\mathbf{q}_\parallel) = \hat{\mathbf{x}}_3 \times \hat{\mathbf{q}}_\parallel. \quad (22c)$$

In these expressions $E_{0p}(\mathbf{k}_\parallel)$ and $E_{0s}(\mathbf{k}_\parallel)$ are the amplitudes of the p- and s-polarized components of the incident field with respect to the plane of incidence, defined by the vectors $\hat{\mathbf{k}}_\parallel$ and $\hat{\mathbf{x}}_3$. Similarly, $B_p(\mathbf{q}_\parallel)$ and $B_s(\mathbf{q}_\parallel)$ are the amplitudes of the p- and s-polarized components of the transmitted field with respect to the plane of transmission defined by the vectors $\hat{\mathbf{q}}_\parallel$ and $\hat{\mathbf{x}}_3$.

Our goal is to express $B_p(\mathbf{q}_\parallel)$ and $B_s(\mathbf{q}_\parallel)$ in terms of $E_{0p}(\mathbf{k}_\parallel)$ and $E_{0s}(\mathbf{k}_\parallel)$. To this end we introduce three mutually perpendicular unit vectors:

$$\hat{\mathbf{a}}_0(\mathbf{p}_\parallel) = \frac{c}{\sqrt{\varepsilon_1}\omega}[\hat{\mathbf{p}}_\parallel - \hat{\mathbf{x}}_3\alpha_1(p_\parallel)], \quad (23a)$$

$$\hat{\mathbf{a}}_1(\mathbf{p}_\parallel) = \frac{c}{\sqrt{\varepsilon_1}\omega}[\hat{\mathbf{p}}_\parallel\alpha_1(p_\parallel) + \hat{\mathbf{x}}_3 p_\parallel], \quad (23b)$$

$$\hat{\mathbf{a}}_2(\mathbf{p}_\parallel) = \hat{\mathbf{x}}_3 \times \hat{\mathbf{p}}_\parallel. \quad (23c)$$

We now take the scalar product of Eq. (20) with each of these three unit vectors in turn, after $\mathbf{E}_0(\mathbf{k}_\parallel)$ and $\mathbf{B}(\mathbf{q}_\parallel)$ have been replaced by the right-hand sides of Eq. (21a) and (22a), respectively. The results are

$$\hat{\mathbf{a}}_0(\mathbf{p}_\parallel)\cdot\mathbf{t}: \quad 0 = 0, \quad (24a)$$

$$\begin{aligned}&\hat{\mathbf{a}}_1(\mathbf{p}_\parallel)\cdot\mathbf{t}: \\ &\int \frac{d^2q_\parallel}{(2\pi)^2}\, \frac{I(-\alpha_1(p_\parallel) + \alpha_2(q_\parallel)|\mathbf{p}_\parallel - \mathbf{q}_\parallel)}{-\alpha_1(p_\parallel) + \alpha_2(q_\parallel)} \\ &\times\left\{-\sqrt{\frac{\varepsilon_1}{\varepsilon_2}}[\alpha_1(p_\parallel)\hat{\mathbf{p}}_\parallel\cdot\hat{\mathbf{q}}_\parallel\,\alpha_2(q_\parallel) + p_\parallel q_\parallel]B_p(\mathbf{q}_\parallel) + \sqrt{\varepsilon_1}\frac{\omega}{c}\alpha_1(p_\parallel)[\hat{\mathbf{p}}_\parallel\times\hat{\mathbf{q}}_\parallel]_3\, B_s(\mathbf{q}_\parallel)\right\} \\ &= (2\pi)^2\delta(\mathbf{p}_\parallel - \mathbf{k}_\parallel)\frac{2\varepsilon_1\alpha_1(k_\parallel)}{\varepsilon_1 - \varepsilon_2}E_{0p}(\mathbf{k}_\parallel), \quad (24b)\end{aligned}$$

$$\begin{aligned}&\hat{\mathbf{a}}_2(\mathbf{p}_\parallel)\cdot\mathbf{t}: \\ &\int \frac{d^2q_\parallel}{(2\pi)^2}\, \frac{I(-\alpha_1(p_\parallel) + \alpha_2(q_\parallel)|\mathbf{p}_\parallel - \mathbf{q}_\parallel)}{-\alpha_1(p_\parallel) + \alpha_2(q_\parallel)}\left\{-\frac{\varepsilon_1}{\sqrt{\varepsilon_2}}\frac{\omega}{c}\,[\hat{\mathbf{p}}_\parallel\times\hat{\mathbf{q}}_\parallel]_3\,\alpha_2(q_\parallel)B_p(\mathbf{q}_\parallel) - \varepsilon_1\frac{\omega^2}{c^2}\hat{\mathbf{p}}_\parallel\cdot\hat{\mathbf{q}}_\parallel B_s(\mathbf{q}_\parallel)\right\} \\ &= (2\pi)^2\delta(\mathbf{p}_\parallel - \mathbf{k}_\parallel)\frac{2\varepsilon_1\alpha_1(k_\parallel)}{\varepsilon_1 - \varepsilon_2}E_{0s}(\mathbf{k}_\parallel). \quad (24c)\end{aligned}$$

These equations represent linear relations between $B_{p,s}(\mathbf{q}_\parallel)$ and $E_{0p,s}(\mathbf{k}_\parallel)$ which we write in the form ($\alpha = p,s$, $\beta = p,s$)

$$B_\alpha(\mathbf{q}_\parallel) = \sum_\beta T_{\alpha\beta}(\mathbf{q}_\parallel|\mathbf{k}_\parallel)E_{0\beta}(\mathbf{k}_\parallel). \quad (25)$$

On combining Eqs. (24) and (25) we find that the transmission amplitudes $\{T_{\alpha\beta}(\mathbf{q}_\parallel|\mathbf{k}_\parallel)\}$ are the solutions of the equation

$$\int \frac{d^2q_\parallel}{(2\pi)^2}\, \frac{I(-\alpha_1(p_\parallel) + \alpha_2(q_\parallel)|\mathbf{p}_\parallel - \mathbf{q}_\parallel)}{-\alpha_1(p_\parallel) + \alpha_2(q_\parallel)}\mathbf{M}(\mathbf{p}_\parallel|\mathbf{q}_\parallel)\mathbf{T}(\mathbf{q}_\parallel|\mathbf{k}_\parallel) = (2\pi)^2\delta(\mathbf{p}_\parallel - \mathbf{k}_\parallel)\frac{2\alpha_1(k_\parallel)}{\varepsilon_2 - \varepsilon_1}\mathbf{I}_2, \quad (26)$$

where

$$\mathbf{M}(\mathbf{p}_\parallel|\mathbf{q}_\parallel) = \begin{pmatrix} \frac{1}{\sqrt{\varepsilon_1\varepsilon_2}}[\alpha_1(p_\parallel)\,\hat{\mathbf{p}}_\parallel\cdot\hat{\mathbf{q}}_\parallel\,\alpha_2(q_\parallel) + p_\parallel q_\parallel] & -\frac{1}{\sqrt{\varepsilon_1}}\frac{\omega}{c}\alpha_1(p_\parallel)\,[\hat{\mathbf{p}}_\parallel\times\hat{\mathbf{q}}_\parallel]_3 \\ \frac{1}{\sqrt{\varepsilon_2}}\frac{\omega}{c}[\hat{\mathbf{p}}_\parallel\times\hat{\mathbf{q}}_\parallel]_3\,\alpha_2(q_\parallel) & \frac{\omega^2}{c^2}\,\hat{\mathbf{p}}_\parallel\cdot\hat{\mathbf{q}}_\parallel \end{pmatrix}, \tag{27a}$$

$$\mathbf{T}(\mathbf{q}_\parallel|\mathbf{k}_\parallel) = \begin{pmatrix} T_{pp}(\mathbf{q}_\parallel|\mathbf{k}_\parallel) & T_{ps}(\mathbf{q}_\parallel|\mathbf{k}_\parallel) \\ T_{sp}(\mathbf{q}_\parallel|\mathbf{k}_\parallel) & T_{ss}(\mathbf{q}_\parallel|\mathbf{k}_\parallel) \end{pmatrix}, \tag{27b}$$

and

$$\mathbf{I}_2 = \begin{pmatrix} 1 & 0 \\ 0 & 1 \end{pmatrix}. \tag{27c}$$

Equation (26) is the reduced Rayleigh equation for the transmission amplitudes.

IV. MEAN DIFFERENTIAL TRANSMISSION COEFFICIENT

The differential transmission coefficient $\partial T/\partial\Omega_t$ is defined such that $(\partial T/\partial\Omega_t)d\Omega_t$ is the fraction of the total time-averaged flux incident on the interface that is transmitted into the element of solid angle $d\Omega_t$ about the direction of transmission (θ_t,ϕ_t). To obtain the mean differential transmission coefficient we first note that the magnitude of the total time-averaged flux incident on the interface is given by

$$\begin{aligned} P_{\rm inc} &= -{\rm Re}\,\frac{c}{8\pi}\int d^2x_\parallel\left\{\mathbf{E}_0^*(\mathbf{k}_\parallel)\times\left[\frac{c}{\omega}\mathbf{Q}_0(\mathbf{k}_\parallel)\times\mathbf{E}_0(\mathbf{k}_\parallel)\right]\right\}_3 \exp\{[-i\mathbf{Q}_0^*(\mathbf{k}_\parallel)+i\mathbf{Q}_0(\mathbf{k}_\parallel)]\cdot\mathbf{x}\} \\ &= -{\rm Re}\,\frac{c^2}{8\pi\omega}\int d^2x_\parallel\{|\mathbf{E}_0(\mathbf{k}_\parallel)|^2\mathbf{Q}_0(\mathbf{k}_\parallel)-[\mathbf{E}_0^*(\mathbf{k}_\parallel)\cdot\mathbf{Q}_0(\mathbf{k}_\parallel)]\mathbf{E}_0(\mathbf{k}_\parallel)\}_3 \\ &= {\rm Re}\,\frac{c^2}{8\pi\omega}\int d^2x_\parallel\alpha_1(k_\parallel)|\mathbf{E}_0(\mathbf{k}_\parallel)|^2 \\ &= S\frac{c^2}{8\pi\omega}\alpha_1(k_\parallel)|\mathbf{E}_0(\mathbf{k}_\parallel)|^2. \end{aligned} \tag{28}$$

In this result S is the area of the x_1x_2 plane covered by the randomly rough surface, and the integrand in the first line is the time-averaged three-component of the complex Poynting vector [19]. The minus sign on the right-hand side of the first equation compensates for the fact that the three-component of the incident flux is negative, and we have used the fact that $\alpha_1(k_\parallel)$ is real, so that $\mathbf{Q}_0(\mathbf{k}_\parallel)$ is real, and $\mathbf{E}_0^*(\mathbf{k}_\parallel)\cdot\mathbf{Q}_0(\mathbf{k}_\parallel)=0$.

In a similar fashion we note that the total time-averaged transmitted flux is given by

$$\begin{aligned} P_{\rm trans} &= -{\rm Re}\,\frac{c}{8\pi}\int d^2x_\parallel\int\frac{d^2q_\parallel}{(2\pi)^2}\int\frac{d^2q'_\parallel}{(2\pi)^2}\left\{\mathbf{B}^*(\mathbf{q}_\parallel)\times\left[\frac{c}{\omega}\mathbf{Q}_2(\mathbf{q}'_\parallel)\times\mathbf{B}(\mathbf{q}'_\parallel)\right]\right\}_3 \\ &\quad\times\exp\{-i(\mathbf{q}_\parallel-\mathbf{q}'_\parallel)\cdot\mathbf{x}_\parallel - i[\alpha_2(q'_\parallel)-\alpha_2^*(q_\parallel)]x_3\} \\ &= -{\rm Re}\,\frac{c^2}{8\pi\omega}\int\frac{d^2q_\parallel}{(2\pi)^2}\{\mathbf{B}^*(\mathbf{q}_\parallel)\times[\mathbf{Q}_2(\mathbf{q}_\parallel)\times\mathbf{B}(\mathbf{q}_\parallel)]\}_3\,\exp[2\,{\rm Im}\,\alpha_2(q_\parallel)x_3] \\ &= -{\rm Re}\,\frac{c^2}{8\pi\omega}\int\frac{d^2q_\parallel}{(2\pi)^2}\{|\mathbf{B}(\mathbf{q}_\parallel)|^2\mathbf{Q}_2(\mathbf{q}_\parallel)-[\mathbf{B}^*(\mathbf{q}_\parallel)\cdot\mathbf{Q}_2(\mathbf{q}_\parallel)]\mathbf{B}(\mathbf{q}_\parallel)\}_3\exp[2\,{\rm Im}\,\alpha_2(q_\parallel)x_3] \\ &= {\rm Re}\,\frac{c^2}{32\pi^3\omega}\int d^2q_\parallel|\mathbf{B}(\mathbf{q}_\parallel)|^2\alpha_2(q_\parallel)\exp[2\,{\rm Im}\,\alpha_2(q_\parallel)x_3] \\ &\quad -{\rm Re}\,\frac{ic^4}{16\pi^2\varepsilon_2\omega^3}\int d^2q_\parallel{\rm Im}\,\alpha_2(q_\parallel)q_\parallel^2|B_p(\mathbf{q}_\parallel)|^2\exp[2\,{\rm Im}\,\alpha_2(q_\parallel)x_3]. \end{aligned} \tag{29}$$

The second term vanishes since it is the real part of a pure imaginary number. Thus we have

$$P_{\rm trans} = \frac{c^2}{32\pi^3\omega}\int_{q_\parallel<\sqrt{\varepsilon_2}\frac{\omega}{c}} d^2q_\parallel\alpha_2(q_\parallel)|\mathbf{B}(\mathbf{q}_\parallel)|^2. \tag{30}$$

The vectors $\mathbf{k}_\parallel$ and $\mathbf{q}_\parallel$ can be expressed in terms of the polar and azimuthal angles of incidence (θ_0,ϕ_0) and transmission (θ_t,ϕ_t), respectively, by

$$\mathbf{k}_\parallel = \sqrt{\varepsilon_1}\frac{\omega}{c}\sin\theta_0(\cos\phi_0,\sin\phi_0,0), \tag{31a}$$

$$\mathbf{q}_\parallel = \sqrt{\varepsilon_2}\frac{\omega}{c}\sin\theta_t(\cos\phi_t,\sin\phi_t,0). \tag{31b}$$

From these results it follows that

$$d^2q_\parallel = \varepsilon_2\left(\frac{\omega}{c}\right)^2 \cos\theta_t d\Omega_t, \tag{32}$$

where $d\Omega_t = \sin\theta_t d\theta_t d\phi_t$. The total time-averaged transmitted flux becomes

$$P_{\rm trans} = \frac{\varepsilon_2^{3/2}\omega^2}{32\pi^3 c}\int d\Omega_t \cos^2\theta_t [|B_p(\mathbf{q}_\parallel)|^2 + |B_s(\mathbf{q}_\parallel)|^2]. \tag{33}$$

Similarly, the total time-averaged incident flux, Eq. (28), becomes

$$P_{\rm inc} = S\frac{\sqrt{\varepsilon_1}c}{8\pi}\cos\theta_0[|E_{0p}(\mathbf{k}_\parallel)|^2 + |E_{0s}(\mathbf{k}_\parallel)|^2]. \tag{34}$$

Thus, by definition, the differential transmission coefficient is given by

$$\frac{\partial T}{\partial\Omega_t} = \frac{1}{S}\frac{\varepsilon_2^{3/2}}{\varepsilon_1^{1/2}}\left(\frac{\omega}{2\pi c}\right)^2 \frac{\cos^2\theta_t}{\cos\theta_0}\frac{|B_p(\mathbf{q}_\parallel)|^2 + |B_s(\mathbf{q}_\parallel)|^2}{|E_{0p}(\mathbf{k}_\parallel)|^2 + |E_{0s}(\mathbf{k}_\parallel)|^2}. \tag{35}$$

When we combine this result with Eq. (25) we find that the contribution to the differential transmission coefficient when an incident plane wave of polarization β, the projection of whose wave vector on the mean scattering plane is $\mathbf{k}_\parallel$, is transmitted into a plane wave of polarization α, the projection of whose wave vector on the mean scattering plane is $\mathbf{q}_\parallel$, is given by

$$\frac{\partial T_{\alpha\beta}(\mathbf{q}_\parallel|\mathbf{k}_\parallel)}{\partial\Omega_t} = \frac{1}{S}\frac{\varepsilon_2^{3/2}}{\varepsilon_1^{1/2}}\left(\frac{\omega}{2\pi c}\right)^2 \frac{\cos^2\theta_t}{\cos\theta_0}|T_{\alpha\beta}(\mathbf{q}_\parallel|\mathbf{k}_\parallel)|^2. \tag{36}$$

Since we are considering the transmission of light through a randomly rough interface, it is the average of this function over an ensemble of realizations of the surface profile function that we need to calculate. This is the mean differential transmission coefficient, which is defined by

$$\left\langle\frac{\partial T_{\alpha\beta}(\mathbf{q}_\parallel|\mathbf{k}_\parallel)}{\partial\Omega_t}\right\rangle = \frac{1}{S}\frac{\varepsilon_2^{3/2}}{\varepsilon_1^{1/2}}\left(\frac{\omega}{2\pi c}\right)^2 \frac{\cos^2\theta_t}{\cos\theta_0}\langle|T_{\alpha\beta}(\mathbf{q}_\parallel|\mathbf{k}_\parallel)|^2\rangle. \tag{37}$$

If we write the transmission amplitude $T_{\alpha\beta}(\mathbf{q}_\parallel|\mathbf{k}_\parallel)$ as the sum of its mean value and the fluctuation from this mean,

$$T_{\alpha\beta}(\mathbf{q}_\parallel|\mathbf{k}_\parallel) = \langle T_{\alpha\beta}(\mathbf{q}_\parallel|\mathbf{k}_\parallel)\rangle + [T_{\alpha\beta}(\mathbf{q}_\parallel|\mathbf{k}_\parallel) - \langle T_{\alpha\beta}(\mathbf{q}_\parallel|\mathbf{k}_\parallel)\rangle], \tag{38}$$

then each of these two terms contributes separately to the mean differential transmission coefficient,

$$\left\langle\frac{\partial T_{\alpha\beta}(\mathbf{q}_\parallel|\mathbf{k}_\parallel)}{\partial\Omega_t}\right\rangle = \left\langle\frac{\partial T_{\alpha\beta}(\mathbf{q}_\parallel|\mathbf{k}_\parallel)}{\partial\Omega_t}\right\rangle_{\rm coh} + \left\langle\frac{\partial T_{\alpha\beta}(\mathbf{q}_\parallel|\mathbf{k}_\parallel)}{\partial\Omega_t}\right\rangle_{\rm incoh}, \tag{39}$$

where

$$\left\langle\frac{\partial T_{\alpha\beta}(\mathbf{q}_\parallel|\mathbf{k}_\parallel)}{\partial\Omega_t}\right\rangle_{\rm coh} = \frac{1}{S}\frac{\varepsilon_2^{3/2}}{\varepsilon_1^{1/2}}\left(\frac{\omega}{2\pi c}\right)^2 \frac{\cos^2\theta_t}{\cos\theta_0}|\langle T_{\alpha\beta}(\mathbf{q}_\parallel|\mathbf{k}_\parallel)\rangle|^2 \tag{40}$$

and

$$\begin{aligned}\left\langle\frac{\partial T_{\alpha\beta}(\mathbf{q}_\parallel|\mathbf{k}_\parallel)}{\partial\Omega_t}\right\rangle_{\rm incoh} &= \frac{1}{S}\frac{\varepsilon_2^{3/2}}{\varepsilon_1^{1/2}}\left(\frac{\omega}{2\pi c}\right)^2 \frac{\cos^2\theta_t}{\cos\theta_0}[\langle|T_{\alpha\beta}(\mathbf{q}_\parallel|\mathbf{k}_\parallel) - \langle T_{\alpha\beta}(\mathbf{q}_\parallel|\mathbf{k}_\parallel)\rangle|^2\rangle] \\ &= \frac{1}{S}\frac{\varepsilon_2^{3/2}}{\varepsilon_1^{1/2}}\left(\frac{\omega}{2\pi c}\right)^2 \frac{\cos^2\theta_t}{\cos\theta_0}[\langle|T_{\alpha\beta}(\mathbf{q}_\parallel|\mathbf{k}_\parallel)|^2\rangle - |\langle T_{\alpha\beta}(\mathbf{q}_\parallel|\mathbf{k}_\parallel)\rangle|^2].\end{aligned} \tag{41}$$

The first contribution describes the refraction of the incident field, while the second contribution describes the diffuse transmission.

V. TRANSMISSIVITY AND TRANSMITTANCE

In the following we will refer to *transmittance* as the fraction of the power flux incident on the rough surface that is transmitted through it, and *transmissivity* as the fraction of the power flux incident on the rough surface that is transmitted coherently and copolarized through it. To obtain the transmissivity of the two-dimensional randomly rough interface we start with the result that

$$\langle T_{\alpha\beta}(\mathbf{q}_\parallel|\mathbf{k}_\parallel)\rangle = (2\pi)^2\delta(\mathbf{q}_\parallel - \mathbf{k}_\parallel)\delta_{\alpha\beta}T_\alpha(k_\parallel). \tag{42}$$

The presence of the δ function is due to the stationarity of the randomly rough surface, the Kronecker symbol $\delta_{\alpha\beta}$ arises from the conservation of angular momentum in the transmission process, and the result that $T_\alpha(k_\parallel)$ depends on $\mathbf{k}_\parallel$ only through its magnitude is due to the isotropy of the random roughness.

With the result given by Eq. (42), the expression for $\langle\partial T_{\alpha\beta}(\mathbf{q}_\parallel|\mathbf{k}_\parallel)/\partial\Omega_t\rangle_{\rm coh}$ given by Eq. (40) becomes

$$\left\langle\frac{\partial T_{\alpha\alpha}(\mathbf{q}_\parallel|\mathbf{k}_\parallel)}{\partial\Omega_t}\right\rangle_{\rm coh} = \frac{\varepsilon_2^{3/2}}{\varepsilon_1^{1/2}}\left(\frac{\omega}{c}\right)^2 \frac{\cos^2\theta_t}{\cos\theta_0}|T_\alpha(k_\parallel)|^2\,\delta(\mathbf{q}_\parallel - \mathbf{k}_\parallel), \tag{43}$$

where we have used the result

$$\begin{aligned}[(2\pi)^2\delta(\mathbf{q}_\parallel - \mathbf{k}_\parallel)]^2 &= (2\pi)^2\delta(\mathbf{0})(2\pi)^2\delta(\mathbf{q}_\parallel - \mathbf{k}_\parallel) \\ &= S(2\pi)^2\delta(\mathbf{q}_\parallel - \mathbf{k}_\parallel)\end{aligned} \tag{44}$$

in obtaining this expression. We next use the result

$$\begin{aligned}\delta(\mathbf{q}_\parallel - \mathbf{k}_\parallel) &= \frac{1}{k_\parallel}\delta(q_\parallel - k_\parallel)\,\delta(\phi_t - \phi_0) \\ &= \frac{1}{\sqrt{\varepsilon_1\varepsilon_2}}\left(\frac{c}{\omega}\right)^2 \frac{\delta(\theta_t - \Theta_t)\,\delta(\phi_t - \phi_0)}{\sin\theta_0\cos\Theta_t}\end{aligned} \tag{45}$$

to obtain

$$\left\langle\frac{\partial T_{\alpha\alpha}(\mathbf{q}_\parallel|\mathbf{k}_\parallel)}{\partial\Omega_t}\right\rangle_{\rm coh} = \frac{\varepsilon_2}{\varepsilon_1}\frac{\cos\Theta_t}{\sin\theta_0\cos\theta_0}|T_\alpha(k_\parallel)|^2\delta(\theta_t - \Theta_t)\,\delta(\phi_t - \phi_0), \tag{46}$$

where the polar angle for the specular direction of transmission has, according to Snell's law, been denoted

$$\Theta_t \equiv \sin^{-1}\left(\sqrt{\frac{\varepsilon_1}{\varepsilon_2}}\sin\theta_0\right). \tag{47}$$

The transmissivity, $\mathcal{T}_\alpha(\theta_0)$, for light of α polarization is defined by

$$\begin{aligned}\mathcal{T}_\alpha(\theta_0) &= \int_0^{\frac{\pi}{2}} d\theta_t \sin\theta_t \int_{-\pi}^{\pi} d\phi_t \left\langle \frac{T_{\alpha\alpha}(\mathbf{q}_\parallel|\mathbf{k}_\parallel)}{\partial\Omega_t} \right\rangle_{\rm coh} \\ &= \frac{\varepsilon_2}{\varepsilon_1}\frac{\cos\Theta_t \sin\Theta_t}{\sin\theta_0\cos\theta_0}|T_\alpha(k_\parallel)|^2 \int_0^{\frac{\pi}{2}} d\theta_t \delta(\theta_t-\Theta_t) \\ &= \begin{cases} \sqrt{\frac{\varepsilon_2}{\varepsilon_1}}\frac{\cos\Theta_t}{\cos\theta_0}|T_\alpha(k_\parallel)|^2, & 0 < \sqrt{\varepsilon_1/\varepsilon_2}\sin\theta_0 < 1, \\ 0, & \text{otherwise.} \end{cases}\end{aligned} \tag{48}$$

In writing this expression we have used the result that $\sin\Theta_t = \sqrt{\varepsilon_1/\varepsilon_2}\sin\theta_0$, and that $\sin\theta_0$ is a monotonically increasing function of θ_0 for $0^\circ < \theta_0 < 90^\circ$, and so therefore is $\sin\Theta_t$. We see from Eq. (48) that when $\varepsilon_1 > \varepsilon_2$ the transmissivity is nonzero for angles of incidence satisfying $0 < \theta_0 < \sin^{-1}(\sqrt{\varepsilon_2/\varepsilon_1})$, and vanishes for angles of incidence satisfying $\sin^{-1}(\sqrt{\varepsilon_2/\varepsilon_1}) < \theta_0 < \pi/2$. This result is a consequence for transmission of the existence of a critical angle for total internal reflection, namely $\theta_0^\star = \sin^{-1}(\sqrt{\varepsilon_2/\varepsilon_1})$. In the case where $\varepsilon_1 < \varepsilon_2$, the transmissivity is nonzero in the entire range of angles of incidence, $0 < \theta_0 < \pi/2$.

The function $T_\alpha(k_\parallel)$ is obtained from Eq. (42), with the aid of the result that $(2\pi)^2\delta(\mathbf{0}) = S$, in the form

$$T_\alpha(k_\parallel) = T_\alpha\left(\sqrt{\varepsilon_1}\frac{\omega}{c}\sin\theta_0\right) = \frac{1}{S}\langle T_{\alpha\alpha}(\mathbf{k}_\parallel|\mathbf{k}_\parallel)\rangle. \tag{49}$$

In addition to the transmissivity (48) that depends only on the copolarized light transmitted coherently by the rough interface, it is also of interest to introduce the transmittance for light of β polarization defined as

$$\mathscr{T}_\beta(\theta_0) = \sum_{\alpha=p,s} \mathscr{T}_{\alpha\beta}(\theta_0), \tag{50a}$$

where

$$\mathscr{T}_{\alpha\beta}(\theta_0) = \int_0^{\frac{\pi}{2}} d\theta_t \sin\theta_t \int_{-\pi}^{\pi} d\phi_t \left\langle \frac{T_{\alpha\beta}(\mathbf{q}_\parallel|\mathbf{k}_\parallel)}{\partial\Omega_t} \right\rangle. \tag{50b}$$

In light of Eq. (39), the transmittance obtains contributions from light that have been transmitted coherently as well as incoherently through the rough interface, $\mathscr{T}_\beta(\theta_0) = \mathscr{T}_\beta(\theta_0)_{\rm coh} + \mathscr{T}_\beta(\theta_0)_{\rm incoh}$, and both co- and cross-polarized transmitted light contribute to it. Moreover, with Eq. (48), and since cross-polarized coherently transmitted light is not allowed [see Eq. (42)], the coherent contribution to transmittance for light of β polarization equals the transmissivity for light of β polarization: $\mathscr{T}_\beta(\theta_0)_{\rm coh} = \mathcal{T}_\beta(\theta_0)$. Therefore, Eq. (50a) can be written in the form

$$\mathscr{T}_\beta(\theta_0) = \mathcal{T}_\beta(\theta_0) + \sum_{\alpha={\rm p,s}} \mathscr{T}_{\alpha\beta}(\theta_0)_{\rm incoh}. \tag{51}$$

It remains to remark that in cases where the incident light is not purely p or s polarized, the transmittance and transmissivity of the optical system will have to be calculated on the basis of weighted sums of the expressions in Eqs. (48) and (50) where the weights reflect the fraction of p and s polarization associated with the incident light.

VI. RESULTS AND DISCUSSIONS

Calculations were carried out for two-dimensional randomly rough dielectric surfaces defined by an isotropic Gaussian height distribution of rms height $\delta = \lambda/20$ and an isotropic Gaussian correlation function of transverse correlation length $a = \lambda/4$. The incident light consisted of a p- or s-polarized plane wave of wavelength λ (in vacuum) and well-defined angles of incidence (θ_0,ϕ_0). The dielectric medium was assumed to be a photoresist defined by the dielectric constant $\varepsilon = 2.6896$. The azimuthal angle of incidence was $\phi_0 = 0^\circ$ in all simulation results presented in this work; this choice for ϕ_0 is somewhat arbitrary, since, due to the isotropy of the roughness, results for another choice of ϕ_0 can be obtained from the results presented here by a trivial rotation. Realizations of the surface profile function $\zeta(\mathbf{x}_\parallel)$ were generated [1,20] on a grid of $N_x \times N_x = 321\times321$ points. The surfaces covered a square region of the x_1x_2 plane of edge $L = 25\lambda$, giving an area $S = L^2$. With these spatial parameters, the corresponding momentum space parameters used in the simulations were $\Delta q = 2\pi/L$ for the discretization intervals in momentum space, and the largest momentum value that was resolved was $\mathcal{Q} = 6.4\omega/c$.

The reduced Rayleigh equation (26) was solved numerically by the method described in detail in Ref. [2], so only a summary of this method will be presented here. In evaluating the $\mathbf{q}_\parallel$ integral in Eq. (26), the infinite limits of integration were replaced by finite limits $|\mathbf{q}_\parallel| < \mathcal{Q}/2$, and the integration was carried out by a two-dimensional version of the extended midpoint rule [21, p. 161] applied to the circular subsection of a grid in the q_1q_2 plane which is determined by the Nyquist sampling theorem [21, p. 605] and the properties of the discrete Fourier transform [2]. The function $I(\gamma|\mathbf{q}_\parallel)$ was evaluated by expanding the integrand in Eq. (17) in powers of $\zeta(\mathbf{x}_\parallel)$ and calculating the Fourier transform of $\zeta^n(\mathbf{x}_\parallel)$ by the fast Fourier transform [2]. For these expansions we used the first $\mathcal{N} = 18$ terms. The resulting matrix equations were solved by LU factorization and back substitution, using the ScaLAPACK library [22].

These calculations were carried out for a large number N_p of realizations of the surface profile function $\zeta(\mathbf{x}_\parallel)$ for an incident plane wave of p or s polarization. For each surface realization the transmission amplitude $T_{\alpha\beta}(\mathbf{q}_\parallel|\mathbf{k}_\parallel)$ and its squared modulus $|T_{\alpha\beta}(\mathbf{q}_\parallel|\mathbf{k}_\parallel)|^2$ were obtained. An arithmetic average of the N_p results for these quantities yielded the mean values $\langle T_{\alpha\beta}(\mathbf{q}_\parallel|\mathbf{k}_\parallel)\rangle$ and $\langle|T_{\alpha\beta}(\mathbf{q}_\parallel|\mathbf{k}_\parallel)|^2\rangle$ entering Eq. (41) for the mean differential transmission coefficient, and related quantities [see Eqs. (49) and (51)].

Investigating the energy conservation of our simulation results can be a useful test of their accuracy. In combining simulation results from the current work with corresponding results obtained for the mean differential reflection coefficient $\langle\partial R_{\alpha\beta}/\partial\Omega_s\rangle$ through the use of the computationally similar methods presented in Ref. [15], we may add the total reflected and transmitted power for any lossless system. When the reflectance is added to the transmittance for any of the systems investigated in the current work, it is found that the results of these calculations satisfy unitarity with an error smaller than 10^{-4}. This testifies to the accuracy of the approach used, and it is also a good indicator for satisfactory discretization.

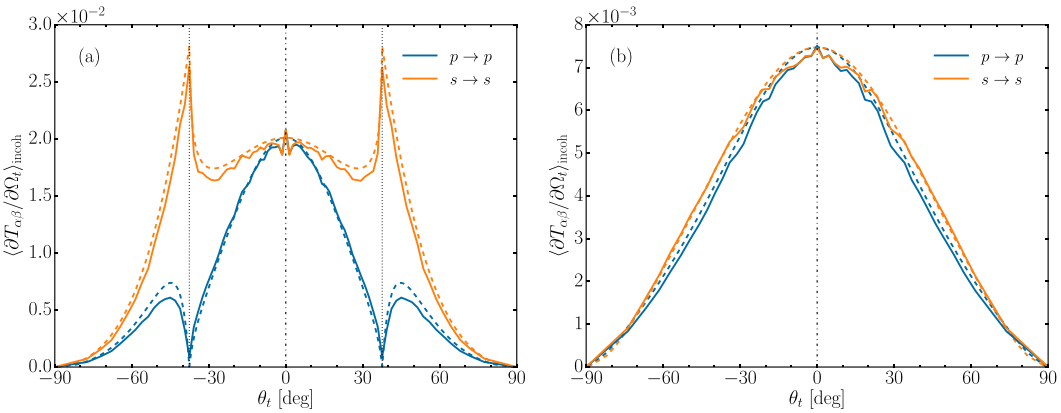

FIG. 2. Contribution to the incoherent component of the mean differential transmission coefficient from the in-plane, copolarized transmission of p- and s-polarized light incident normally $[(\theta_0,\phi_0) = (0^\circ,0^\circ)]$ on the random vacuum-dielectric interface, as a function of the angle of transmission θ_t. (a) The medium of incidence is vacuum $[\varepsilon_1 = 1; \varepsilon_2 = 2.6896]$; (b) the medium of incidence is the dielectric $[\varepsilon_1 = 2.6896; \varepsilon_2 = 1]$. Negative values of θ_t correspond to light transmitted in the azimuthal direction of $\phi_t = 180^\circ$. Results for (in-plane) cross-polarized transmission have not been indicated since they are generally suppressed in the plane of incidence. The results presented as solid lines were obtained on the basis of numerical solutions of the reduced Rayleigh equation (26) for an ensemble of 5000 surface realizations. The dashed curves represent the result of the small amplitude perturbation theory (52) to first order, assuming polarization as indicated for the solid lines of the same color. The specular direction of transmission is indicated by the vertical dash-dotted line at $\theta_t = 0^\circ$, and in Fig. 2(a), the vertical dotted lines at $\theta_t = \pm\theta_t^\star$ indicate the position of the critical angle where $\theta_t^\star = \sin^{-1}(\sqrt{\varepsilon_1/\varepsilon_2}) \approx 37.6^\circ$ for the parameters assumed. The wavelength of the incident light in vacuum was λ. The rough interface was assumed to have a root-mean-square roughness of $\delta = \lambda/20$, and it was characterized by an isotropic Gaussian power spectrum (3) of transverse correlation length $a = \lambda/4$. In the numerical calculations it was assumed that the surface covered an area $L \times L$, with $L = 25\lambda$, and the surface was discretized on a grid of 321×321 points.

It should be noted, however, that unitarity is a necessary, but not sufficient, condition for the correctness of the presented results. Through a preliminary investigation, unitarity seemed to be satisfied to a satisfactory degree for surfaces with a root mean square roughness up to about two times larger than the roughness used in obtaining the results presented in this paper, if the correlation function was kept the same.

A. Normal incidence

In Fig. 2 we display the mean differential transmission coefficient (MDTC) in the plane of incidence as a function of the polar angle of transmission when the random surface is illuminated from the vacuum at normal incidence by p- and s-polarized light, Fig. 2(a), and when it is illuminated from the dielectric medium, Fig. 2(b). Only results for in-plane $[\mathbf{q}_\parallel \parallel \mathbf{k}_\parallel]$ copolarized transmission are presented, since in-plane cross-polarized transmission is suppressed due to the absence of a contribution from single-scattering processes. An ensemble of 5000 realizations of the surface profile function was used to produce the averaged results presented in each of these figures.

From Fig. 2(a) it is observed that the curves display both maxima and minima in the $p \to p$ transmission spectrum, and peaks in the $s \to s$ transmission spectrum. In contrast, the curves presented in Fig. 2(b) are featureless, and are nearly identical. The presence of these features, and others in subsequent figures, can be understood if we calculate the contribution to the MDTC from the light transmitted incoherently through the random interface as an expansion in powers of the surface profile function. This calculation, outlined in Appendix B, yields the result that to lowest nonzero order in $\zeta(\mathbf{x}_\parallel)$ we have

$$\left\langle \frac{\partial T_{pp}(\mathbf{q}_\parallel|\mathbf{k}_\parallel)}{\partial\Omega_t} \right\rangle_{\text{incoh}} = \frac{\delta^2}{\pi^2}(\varepsilon_2-\varepsilon_1)^2\varepsilon_1^{1/2}\varepsilon_2^{5/2}\left(\frac{\omega}{c}\right)^2\frac{\cos^2\theta_t}{\cos\theta_0}g(|\mathbf{q}_\parallel-\mathbf{k}_\parallel|)\frac{1}{|d_p(q_\parallel)|^2}|\alpha_1(q_\parallel)(\hat{\mathbf{q}}_\parallel\cdot\hat{\mathbf{k}}_\parallel)\alpha_2(k_\parallel)+q_\parallel k_\parallel|^2\frac{\alpha_1^2(k_\parallel)}{|d_p(k_\parallel)|^2}, \tag{52a}$$

$$\left\langle \frac{\partial T_{ps}(\mathbf{q}_\parallel|\mathbf{k}_\parallel)}{\partial\Omega_t} \right\rangle_{\text{incoh}} = \frac{\delta^2}{\pi^2}(\varepsilon_2-\varepsilon_1)^2\frac{\varepsilon_2^{5/2}}{\varepsilon_1^{1/2}}\left(\frac{\omega}{c}\right)^4\frac{\cos^2\theta_t}{\cos\theta_0}g(|\mathbf{q}_\parallel-\mathbf{k}_\parallel|)\frac{|\alpha_1(q_\parallel)|^2}{|d_p(q_\parallel)|^2}([\hat{\mathbf{q}}_\parallel\times\hat{\mathbf{k}}_\parallel]_3)^2\frac{\alpha_1^2(k_\parallel)}{|d_s(k_\parallel)|^2}, \tag{52b}$$

$$\left\langle \frac{\partial T_{sp}(\mathbf{q}_\parallel|\mathbf{k}_\parallel)}{\partial\Omega_t} \right\rangle_{\text{incoh}} = \frac{\delta^2}{\pi^2}(\varepsilon_2-\varepsilon_1)^2\frac{\varepsilon_2^{1/2}}{\varepsilon_1^{1/2}}\left(\frac{\omega}{c}\right)^4\frac{\cos^2\theta_t}{\cos\theta_0}g(|\mathbf{q}_\parallel-\mathbf{k}_\parallel|)\frac{1}{|d_s(q_\parallel)|^2}([\hat{\mathbf{q}}_\parallel\times\hat{\mathbf{k}}_\parallel]_3)^2\frac{\alpha_1^2(k_\parallel)|\alpha_2(k_\parallel)|^2}{|d_p(k_\parallel)|^2}, \tag{52c}$$

$$\left\langle \frac{\partial T_{ss}(\mathbf{q}_\parallel|\mathbf{k}_\parallel)}{\partial\Omega_t} \right\rangle_{\text{incoh}} = \frac{\delta^2}{\pi^2}(\varepsilon_2-\varepsilon_1)^2\frac{\varepsilon_2^{3/2}}{\varepsilon_1^{1/2}}\left(\frac{\omega}{c}\right)^6\frac{\cos^2\theta_t}{\cos\theta_0}g(|\mathbf{q}_\parallel-\mathbf{k}_\parallel|)\frac{1}{|d_s(q_\parallel)|^2}(\hat{\mathbf{q}}_\parallel\cdot\hat{\mathbf{k}}_\parallel)^2\frac{\alpha_1^2(k_\parallel)}{|d_s(k_\parallel)|^2}, \tag{52d}$$

where the functions $d_\alpha(q_\parallel)$ and $d_\alpha(k_\parallel)$ for $\alpha = p,s$ are presented in Eqs. (B11) and (53). In the following we will refer to Eq. (52) as the results of *small amplitude perturbation theory* (SAPT) to first order. Results from numerical evaluations of Eq. (52) for normal incidence and in-plane transmission [$\hat{\mathbf{q}}_\parallel \parallel \hat{\mathbf{k}}_\parallel$] are displayed as dashed lines in Fig. 2 and several figures to follow. For Fig. 2 we have not included results for transmission *out of plane* [$\hat{\mathbf{q}}_\parallel \cdot \hat{\mathbf{k}}_\parallel = 0$], since, for normal incidence, the results for copolarized in-plane transmission are identical with the results for cross-polarized out-of-plane transmission. We notice in passing that the unit vectors $\hat{\mathbf{q}}_\parallel = \mathbf{q}_\parallel/q_\parallel$ and $\hat{\mathbf{k}}_\parallel = \mathbf{k}_\parallel/k_\parallel$ are well defined also for $\theta_t = 0^\circ$ and $\theta_0 = 0^\circ$, respectively, as follows from Eq. (31).

From Fig. 2 it is observed that the single-scattering perturbation theory reproduces fairly well the overall shape of the MDTC for in-plane copolarized transmission, at least for the level of roughness assumed in producing these results. However, there is a difference in amplitude between the simulation results and the curves produced from perturbation theory, in particular when $\varepsilon_1 < \varepsilon_2$.

The results from SAPT can be further analyzed in order to understand all features seen in Fig. 2. With the aid of $q_\parallel = \sqrt{\varepsilon_2}(\omega/c)\sin\theta_t$, $d_\alpha(q_\parallel)$ can be written in the form

$$d_p(q_\parallel) = \sqrt{\varepsilon_2}\frac{\omega}{c}\left\{\varepsilon_2\left[\left(\frac{\varepsilon_1-\varepsilon_2}{\varepsilon_2}\right)+\cos^2\theta_t\right]^{\frac{1}{2}}+\varepsilon_1\cos\theta_t\right\}, \tag{53a}$$

$$d_s(q_\parallel) = \sqrt{\varepsilon_2}\frac{\omega}{c}\left\{\left[\left(\frac{\varepsilon_1-\varepsilon_2}{\varepsilon_2}\right)+\cos^2\theta_t\right]^{\frac{1}{2}}+\cos\theta_t\right\}, \tag{53b}$$

and from $k_\parallel = \sqrt{\varepsilon_1}(\omega/c)\sin\theta_0$, $d_\alpha(k_\parallel)$ can be expressed as

$$d_p(k_\parallel) = \sqrt{\varepsilon_1}\frac{\omega}{c}\left\{\varepsilon_1\left[\left(\frac{\varepsilon_2-\varepsilon_1}{\varepsilon_1}\right)+\cos^2\theta_0\right]^{\frac{1}{2}}+\varepsilon_2\cos\theta_0\right\}, \tag{53c}$$

$$d_s(k_\parallel) = \sqrt{\varepsilon_1}\frac{\omega}{c}\left\{\left[\left(\frac{\varepsilon_2-\varepsilon_1}{\varepsilon_1}\right)+\cos^2\theta_0\right]^{\frac{1}{2}}+\cos\theta_0\right\}. \tag{53d}$$

We see from Eqs. (53a) and (53b) that when ε_1 is greater than ε_2, both $d_p(q_\parallel)$ and $d_s(q_\parallel)$ are real continuous monotonically decreasing functions of θ_t, and so therefore are $|d_p(q_\parallel)|^2$ and $|d_s(q_\parallel)|^2$. This leads to smooth dependencies of the MDTC on the angle of transmission [Fig. 2(b)]. However, when ε_1 is smaller than ε_2, the first term in the expressions for $d_p(q_\parallel)$ and $d_s(q_\parallel)$ vanishes for a polar angle of transmission $\theta_t = \theta_t^\star$ defined by $\cos\theta_t^\star = [(\varepsilon_2-\varepsilon_1)/\varepsilon_2]^{\frac{1}{2}}$, or, equivalently, when $\sin\theta_t^\star = \sqrt{\varepsilon_1/\varepsilon_2}$, and becomes pure imaginary as θ_t increases beyond the angle

$$\theta_t^\star = \sin^{-1}\sqrt{\frac{\varepsilon_1}{\varepsilon_2}}, \tag{54}$$

which is the critical angle for total internal reflection in the corresponding, inverse, flat-surface system where $\varepsilon_1 \to \varepsilon_2$ and $\varepsilon_2 \to \varepsilon_1$. The functions $|d_p(q_\parallel)|^{-2}$ and $|d_s(q_\parallel)|^{-2}$ in Eq. (52) therefore display asymmetric peaks at the polar angle of transmission $\theta_t = \theta_t^\star$. For $s \to s$ copolarized in-plane (incoherent) transmission at normal incidence we therefore see sharp peaks in the MDTC at this polar angle both for forward and backward scattered light [Fig. 2(a)]. The same peaks will then also be visible for $p \to s$ cross-polarized out-of-plane transmission at normal incidence. However, in the case of $p \to p$ copolarized transmission we instead see dips at $\theta_t^\star$ in Fig. 2(a). In the case of the first-order SAPT results, the MDTC does indeed go to zero at this "critical" polar angle. This is due to the zeros in Eq. (52a), specifically the zeros in the function

$$F(\mathbf{q}_\parallel|\mathbf{k}_\parallel) = |\alpha_1(q_\parallel)(\hat{\mathbf{q}}_\parallel \cdot \hat{\mathbf{k}}_\parallel)\alpha_2(k_\parallel) + q_\parallel k_\parallel|^2. \tag{55}$$

For normal incidence [$k_\parallel = 0$] and in-plane transmission [$\mathbf{q}_\parallel \parallel \mathbf{k}_\parallel$], the function $F(\mathbf{q}_\parallel|\mathbf{k}_\parallel)$ is zero for $\alpha_1(q_\parallel) = 0$. This is the case for $q_\parallel = \sqrt{\varepsilon_1}\omega/c$ [Eq. (9)], which corresponds to $\theta_t = \theta_t^\star$ in the medium of transmission when ε_2 is greater than ε_1. Finally, in the case of $s \to p$ cross-polarized transmission, we will also see dips at $\theta_t^\star$ due to the simple factor $\alpha_1(q_\parallel)$ in Eq. (52b), but this factor is zero at this angle of transmission regardless of the angle of incidence.

The peaks observed in Fig. 2(a) where $\varepsilon_1 < \varepsilon_2$ are the optical analogs of the *Yoneda peaks* observed in the scattering (in reflection) of x rays from both metallic [6–9] and nonmetallic [10–13] surfaces, later described as "quasi-anomalous scattering peaks" in the two-dimensional numerical work by Kawanishi *et al.* [5]. The Yoneda peaks were originally observed as sharp peaks for incidence close to the grazing angle, as the difference in the dielectric constants of the two scattering media is very small at x-ray frequencies. In the following, by Yoneda peaks we will mean well-defined maxima in the angular distribution of the intensity of the transmitted light at, or slightly above, the critical polar angle in the medium of transmission for which the wave number turns nonpropagating in the medium of incidence, when $\varepsilon_1 < \varepsilon_2$. A more detailed discussion on Yoneda peaks in reflection and in general can be found in Ref. [15].

Because the Yoneda peaks and the minima given by Eq. (55) are present in the expressions for the MDTC obtained in the lowest order in the surface profile function, the second, they can be interpreted as single-scattering phenomena, not multiple-scattering effects. This is supported by the qualitative similarity between the plots presented in Fig. 2. We specify that the polar angle of transmission where the Yoneda phenomenon can be observed is determined only by the ratio of the dielectric constants of the two media; it does not, for instance, depend on the polar angle of incidence.

We now turn to the angular intensity distributions of the transmitted light. In Figs. 3 and 4 we present simulation results for the contribution to the MDTC from the light that has been transmitted incoherently through the randomly rough interface, that display the full angular distribution of this contribution. These two figures were obtained under the assumption that the angles of incidence were $(\theta_0,\phi_0) = (0^\circ,0^\circ)$; cuts along the plane of incidence of these angular intensity distributions result in the curves presented in Fig. 2. Therefore, the parameters assumed in producing the results of Figs. 2(a) and 3 are identical, and so are the parameters assumed in obtaining Figs. 2(b) and 4.

All angular intensity distributions presented in this work, including those in Figs. 3 and 4, are organized in the same fashion. They are arranged in 3×3 subfigures where each row and column of the array correspond to the angular distribution of the incoherent component of the mean differential

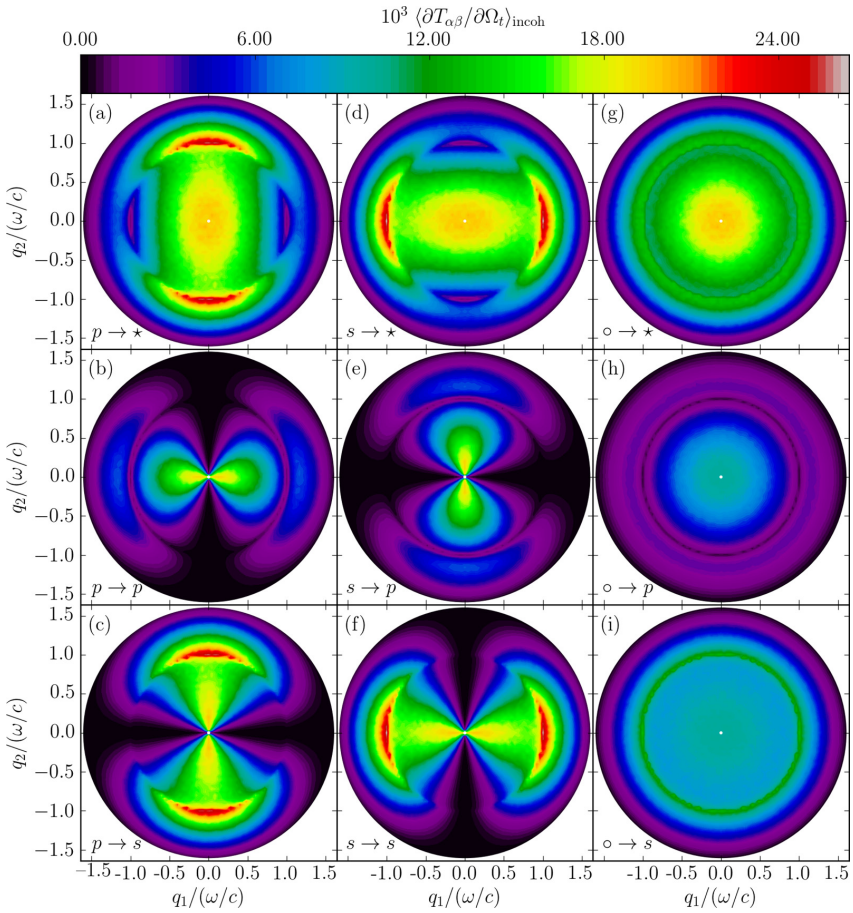

FIG. 3. Incoherent component of the mean differential transmission coefficient, showing the full angular intensity distribution as a function of the lateral wave vector of the light transmitted from vacuum into a dielectric medium separated by a rough interface. The angles of incidence are $(\theta_0,\phi_0) = (0^\circ,0^\circ)$. Notice the rapid changes in intensity around the polar angle $\theta_t = \theta_t^\star = \sin^{-1}(\sqrt{\varepsilon_1/\varepsilon_2})$ corresponding to $q_\parallel = \sqrt{\varepsilon_1}\omega/c$. The position of the specular direction in transmission is indicated by white dots. The parameters assumed for the scattering geometry and used in performing the numerical simulations have values that are identical to those assumed in obtaining the results of Fig. 2(a). The in-plane intensity variations in Figs. 3(b) and 3(f) are the curves depicted in Fig. 2(a). The star notation, e.g., $p \to \star$, indicates that the polarization of the transmitted light was not recorded. Furthermore, in, e.g., Fig. 3(g), the open circle in $\circ \to \star$ symbolizes that the incident light was unpolarized; this simulation result was obtained by adding *half* of the results from Figs. 3(a) and 3(d). [Parameters: $\varepsilon_1 = 1.0$, $\varepsilon_2 = 2.6896$; $\delta = \lambda/20$, $a = \lambda/4$.]

transmission coefficient for a given state of polarization of the transmitted and incident light, respectively. The lower left 2×2 corner of such figures corresponds to the cases where β-polarized incident light is transmitted by the rough interface into α-polarized light, denoted $\beta \to \alpha$ in the lower left corner of each subfigure, where $\alpha = p,s$ and the same for β. Moreover, the first row corresponds to results where the polarization of the transmitted light was not recorded (indicated by $\star$); such results are obtained by adding the other two results from the same column. The last column of the angular intensity distribution figures corresponds to the situation when the incident light is *unpolarized* (indicated by an open circle, $\circ$); these results are obtained by adding *half* of the other two results present in the same row. For instance, the subfigure in the upper right corner, labeled $\circ \to \star$, refers to unpolarized light (the open circle) transmitted by the surface into light for which we do not record the polarization (the star). It should be stressed that even if the polarization of the transmitted light is not recorded, it does not mean that the transmitted light is unpolarized; in general this is not the case as can be seen by, for instance, inspecting Fig. 3.

When both the incident and transmitted light are linearly polarized, the lower left 2×2 corners of Figs. 3 and 4 show that the angular distributions of the incoherent component of the

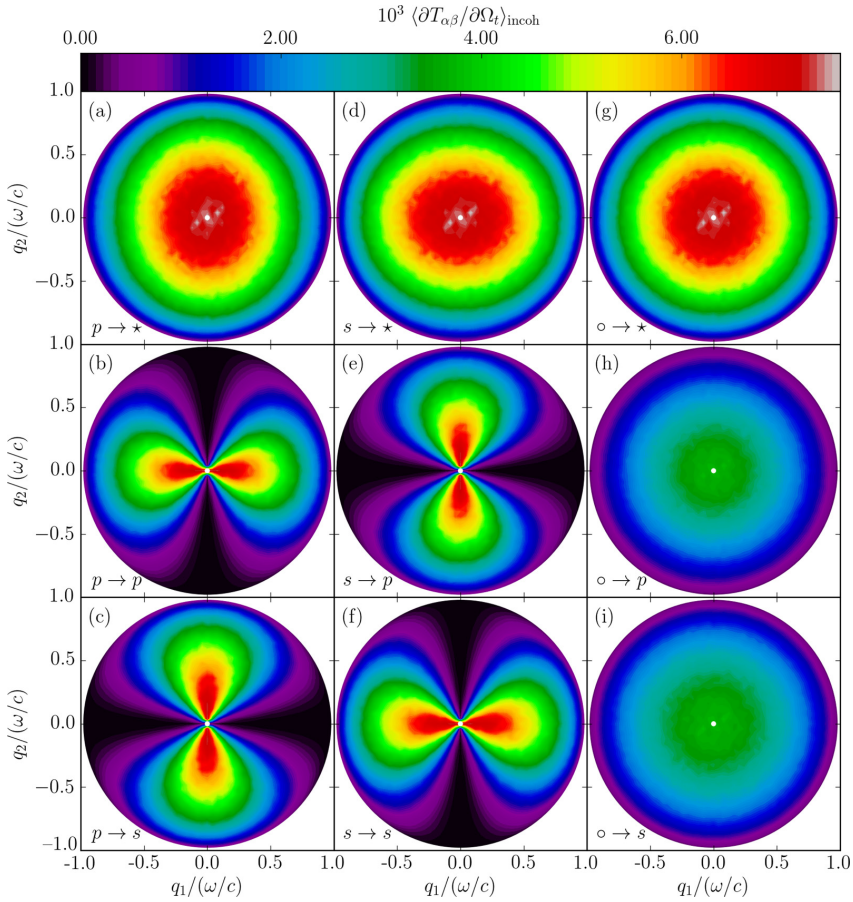

FIG. 4. Same as Fig. 3, but for light incident from the dielectric side onto the interface with vacuum. The in-plane intensity variations in Figs. 4(b) and 4(f) are the curves depicted in Fig. 2(b). [Parameters: $\varepsilon_1 = 2.6896$, $\varepsilon_2 = 1.0$; $\delta = \lambda/20$, $a = \lambda/4$.]

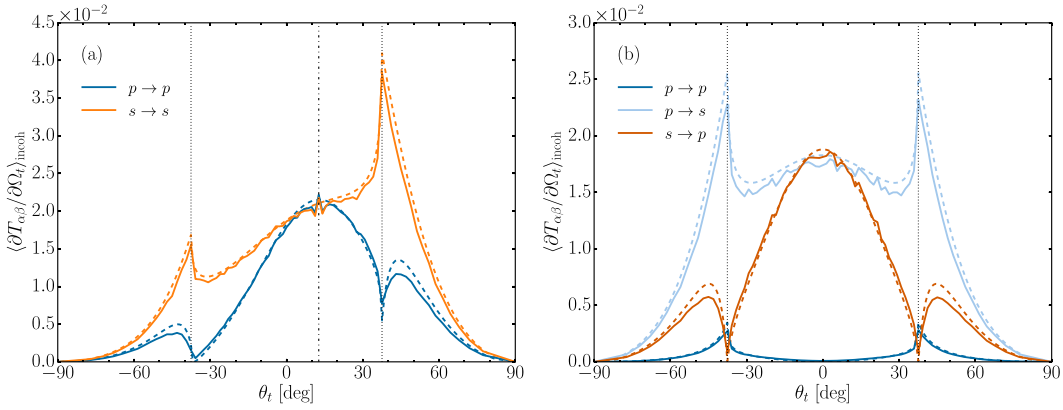

FIG. 5. (a) Same as Fig. 2(a) but for angles of incidence $(\theta_0, \phi_0) = (21.1^\circ, 0^\circ)$. (b) Same as (a) but for out-of-plane scattering [$\phi_t = \pm 90^\circ$]. Results for combinations of the polarizations of the incident and scattered light for which the scattered intensity was everywhere negligible have been omitted. [Parameters: $\varepsilon_1 = 1.0$, $\varepsilon_2 = 2.6896$; $\delta = \lambda/20$, $a = \lambda/4$.]

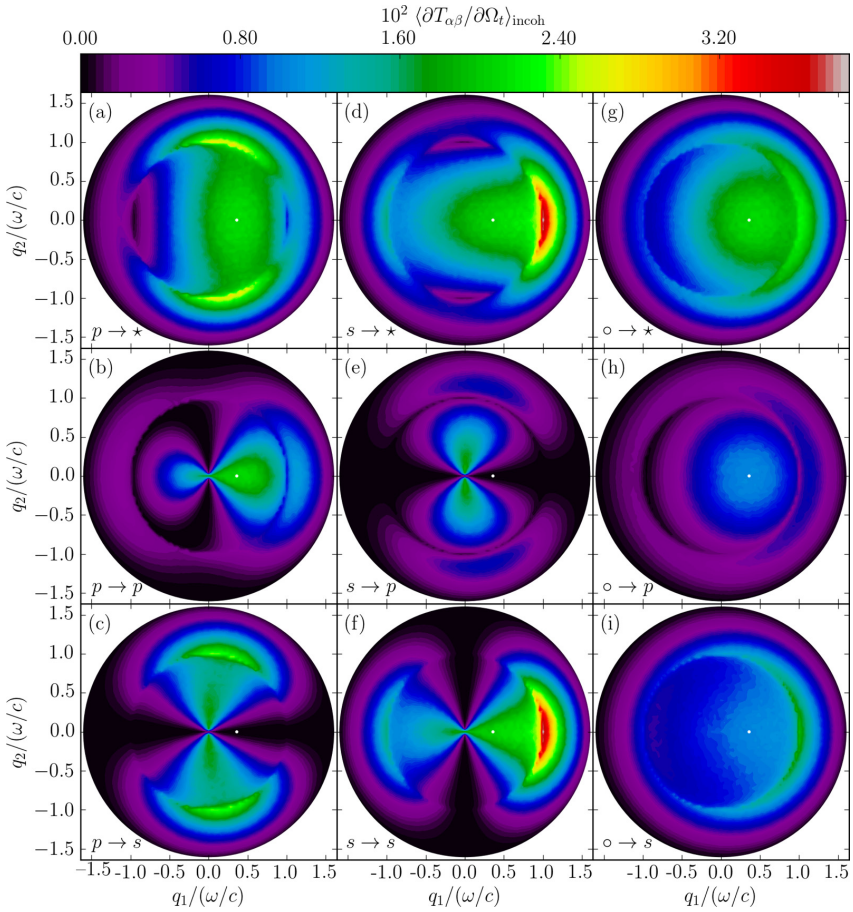

FIG. 6. Same as Fig. 3, but for the angles of incidence $(\theta_0,\phi_0) = (21.1^\circ,0^\circ)$.

mean differential transmission coefficients take on dipolelike patterns oriented along the plane of incidence for copolarization and perpendicular to it for cross polarization. We note that such patterns are a consequence of our definitions of the polarization vectors, and that similar patterns have recently been observed in reflection [2,15,23]. It was already concluded based on Fig. 2 that the in-plane, copolarized transmission is rather different for p and s polarization when the medium of incidence is vacuum, and rather similar when the medium of incidence is the dielectric. Not surprisingly, a similar conclusion can be drawn by inspecting the copolarized angular intensity distributions depicted in the $\beta \to \beta$ subfigures of Figs. 3 and 4 ($\beta = p,s$). For normal incidence, the angular intensity distributions for cross- and copolarized transmission are intimately related to each other, but only if they share the same polarization state of the transmitted light; in fact, the former distributions are 90° rotations of the latter. For instance, for scattering into s-polarized light, this can be understood if we note from Eqs. (52c), (52d), and (27) [see also Eq. (B13) of Appendix B] that to the lowest nonzero order in $\zeta(\mathbf{x}_\parallel)$ we have

$$\left\langle \frac{\partial T_{sp}(\mathbf{q}_\parallel|\mathbf{k}_\parallel)}{\partial\Omega_t} \right\rangle_{\text{incoh}} = \frac{\delta^2}{\pi^2}(\varepsilon_2-\varepsilon_1)^2\varepsilon_1^{1/2}\varepsilon_2^{5/2}\left(\frac{\omega}{c}\right)^2\frac{\cos^2\theta_t}{\cos\theta_0} \times g(|\mathbf{q}_\parallel-\mathbf{k}_\parallel|)\frac{|M_{sp}(\mathbf{q}_\parallel|\mathbf{k}_\parallel)|^2\alpha_1^2(k_\parallel)}{|d_s(q_\parallel)|^2|d_p(k_\parallel)|^2}, \tag{56a}$$

$$\left\langle \frac{\partial T_{ss}(\mathbf{q}_\parallel|\mathbf{k}_\parallel)}{\partial\Omega_t} \right\rangle_{\text{incoh}} = \frac{\delta^2}{\pi^2}(\varepsilon_2-\varepsilon_1)^2\frac{\varepsilon_2^{3/2}}{\varepsilon_1^{1/2}}\left(\frac{\omega}{c}\right)^2\frac{\cos^2\theta_t}{\cos\theta_0} \times g(|\mathbf{q}_\parallel-\mathbf{k}_\parallel|)\frac{|M_{ss}(\mathbf{q}_\parallel|\mathbf{k}_\parallel)|^2\alpha_1^2(k_\parallel)}{|d_s(q_\parallel)|^2|d_s(k_\parallel)|^2}, \tag{56b}$$

where the matrix elements $M_{sp}(\mathbf{q}_\parallel|\mathbf{k}_\parallel)$ and $M_{ss}(\mathbf{q}_\parallel|\mathbf{k}_\parallel)$ are presented in Eq. (27). For normal incidence, $d_p(0)/\sqrt{\varepsilon_1\varepsilon_2} = d_s(0)$ and $M_{sp}(\mathbf{q}_\parallel|\mathbf{0})$ out of plane equals $M_{ss}(\mathbf{q}_\parallel|\mathbf{0})$ in plane. This means that $\langle\partial T_{sp}(\mathbf{q}_\parallel|\mathbf{0})/\partial\Omega_t\rangle_{\text{incoh}}$ will equal

$\langle \partial T_{ss}(\mathbf{q}'_\parallel|\mathbf{0})/\partial\Omega_t\rangle_{\rm incoh}$ if $\mathbf{q}_\parallel$, after a rotation by an angle of 90°, equals $\mathbf{q}'_\parallel$. A similar argument can be used to relate the angular distribution of $\langle \partial T_{ps}(\mathbf{q}_\parallel|\mathbf{0})/\partial\Omega_t\rangle_{\rm incoh}$ to a 90° rotation of the angular distribution of $\langle \partial T_{pp}(\mathbf{q}_\parallel|\mathbf{0})/\partial\Omega_t\rangle_{\rm incoh}$. This symmetry property of the angular intensity distributions at normal incidence is readily observed in Figs. 3 and 4. Hence we conclude that the regions of high intensity observed in the cross-polarized angular intensity distribution in Fig. 3(c) around the out-of-plane direction are also Yoneda peaks; their origin is due to the peaking factor $|d_s(q_\parallel)|^{-2}$ versus transmitted wave number, identical to what we found for the in-plane peaks in the copolarized transmitted light.

When $\varepsilon_1 < \varepsilon_2$, Yoneda peaks may actually be observed for a wide range of azimuthal angles of transmission. For instance, at normal incidence, and when unpolarized incident light is transmitted through the surface into s-polarized light, the Yoneda peaks occur around $\theta_t = \theta_t^\star$ (or $q_\parallel = \sqrt{\varepsilon_1}\omega/c$) independent of the value of the azimuthal angle of transmission ϕ_t, and they will have constant height [Fig. 3(i)]. Similarly, when unpolarized light is transmitted into p-polarized light for the same scattering system, one observes from Fig. 3(h) that a circular groove exists at $q_\parallel = \sqrt{\varepsilon_1}\omega/c$. For normal incidence ($k_\parallel = 0$), the amplitudes of $\langle \partial T_{pp}(\mathbf{q}_\parallel|\mathbf{k}_\parallel)/\partial\Omega_t\rangle_{\rm incoh}$ and $\langle \partial T_{ps}(\mathbf{q}_\parallel|\mathbf{k}_\parallel)/\partial\Omega_t\rangle_{\rm incoh}$ at the position of the groove will be zero according to (52a) and (52b). As mentioned earlier, this is due to the factor $\alpha_1(q_\parallel)$, which vanishes when $q_\parallel = \sqrt{\varepsilon_1}\omega/c$.

It should be observed from Figs. 3(g)–3(i) and 4(g)–4(i), that at normal incidence, and due to the isotropy of the surface, unpolarized incident light will be transmitted by the surface into rotationally symmetric intensity distributions independent of whether the transmitted light is p or s polarized. When unpolarized light is incident from the dielectric, there are only minor differences in the intensity distributions of the p- and s-polarized transmitted light [Figs. 4(h) and 4(i)]. However, when the light is incident from vacuum, Figs. 3(h) and 3(i) show pronounced differences in their intensity distributions.

B. Non-normal incidence

We now address the situation when $\theta_0 \neq 0°$, and we start our discussion by assuming that the light is incident from vacuum onto its rough interface with the dielectric. In Fig. 5 we present the MDTC for light that has been transmitted incoherently (a) in plane and (b) out of plane by the surface for $\theta_0 = 21.1°$, and in Fig. 6 we present the corresponding full angular intensity distributions. Figures 5 and 6 show that the Yoneda peaks are still prominent, but their amplitudes are no longer independent of the azimuthal angle of transmission, as was found for normal incidence. For $s \to s$ transmission, Figs. 5(a) and 6(f), it is found that the Yoneda peak amplitudes are higher in the forward transmission plane than in the backward plane, and the former peaks have a higher amplitude than they had for normal incidence. Moreover, the Yoneda peaks visible in cross-polarized $p \to s$ transmission, Fig. 6(c), that for normal incidence were located symmetrically out of plane, are now moving into the forward transmission plane. The amplitude of $\langle \partial T_{p\alpha}(\mathbf{q}_\parallel|\mathbf{k}_\parallel)/\partial\Omega_t\rangle_{\rm incoh}$ when $q_\parallel = \sqrt{\varepsilon_1}\omega/c$, which was essentially zero for normal incidence, no longer vanishes everywhere as can be seen in Fig. 5 and the second row of subfigures in Fig. 6, but we do still observe a local minimum in the transmitted intensity into p-polarized light at the position of the Yoneda peaks, and this intensity is, in the plane of incidence, substantially lower than the corresponding intensity for transmission into s-polarized light.

Further inspection of Fig. 5 for $p \to p$ copolarized transmission reveals that the local minimum found in plane in the backscattering direction ($\phi_t = 180°$), has shifted its position away from the critical polar angle of $\theta_t^\star$. To first order in SAPT, for which the transmitted intensity at this local minimum is zero, this shift is due to behavior in the function $F(\mathbf{q}_\parallel|\mathbf{k}_\parallel)$ [Eq. (55)] that deserves a more thorough discussion. When $k_\parallel \neq 0$, $F(\mathbf{q}_\parallel|\mathbf{k}_\parallel)$ can only cause $\langle \partial T_{pp}(\mathbf{q}_\parallel|\mathbf{k}_\parallel)/\partial\Omega_t\rangle_{\rm incoh}$ to vanish for $\mathbf{q}_\parallel \cdot \mathbf{k}_\parallel < 0$ (backward scattering). Specifically, for in-plane backward scattering $[\hat{\mathbf{q}}_\parallel \cdot \hat{\mathbf{k}}_\parallel = -1]$, $\langle \partial T_{pp}(\mathbf{q}_\parallel|\mathbf{k}_\parallel)/\partial\Omega_t\rangle_{\rm incoh}$ will be zero for angles of transmission

$$\Theta_B(\theta_0) = \sin^{-1}\left(\frac{\varepsilon_1}{\varepsilon_2}\sqrt{\frac{\varepsilon_2}{\varepsilon_1} - \sin^2\theta_0}\right). \tag{57}$$

Note that for normal incidence, $\theta_0 = 0°$, Eq. (57) reduces to $\Theta_B(0°) = \sin^{-1}\sqrt{\varepsilon_1/\varepsilon_2}$, which becomes $\theta_t^\star$ when $\varepsilon_1 < \varepsilon_2$. Figure 7 shows the dependence of Θ_B on θ_0 for both configurations of the dielectric and vacuum, provided that $\phi_t = 180°$. In this figure, the critical angle $\theta_t^\star$ has been indicated on both axes as black dash-dotted lines. Corresponding plots of Θ_B but for incoherent *reflection* from the rough interface [Eq. (56) in Ref. [15]] have been included in the figure as thicker colored dashed lines. For $\varepsilon_1 = 1.0$, $\varepsilon_2 = 2.6896$, and $\theta_0 = 21.1°$, Eq. (57) gives $\Theta_B(21.1°) \approx 36.5°$, in good agreement with what we observe in Fig. 5.

The transmission angles defined by Θ_B were first mentioned in the literature by Kawanishi *et al.* [5], where the angular values of Θ_B in both reflection and transmission were explored through a stochastic functional approach for two-dimensional surfaces. They chose to call the angles at

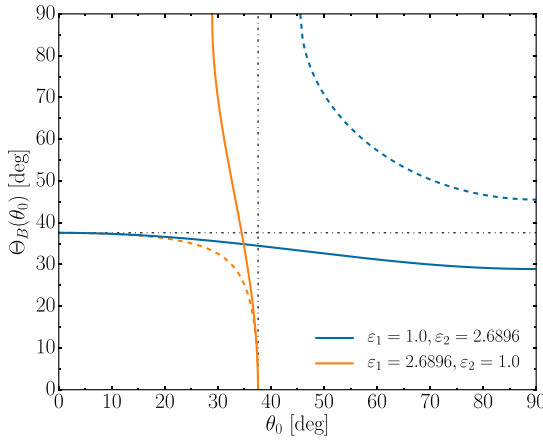

FIG. 7. Dependence of the in-plane Brewster scattering angle Θ_B on the polar angle of incidence θ_0 for $\phi_t = 180°$ [Eq. (57)]. Corresponding results, but for Θ_B in reflection and $\phi_s = 0°$ as provided by Eq. (56) in Ref. [15], are included as dashed lines for completeness. The critical angle $\theta_t^\star$ has been indicated on both axes as black dash-dotted lines.

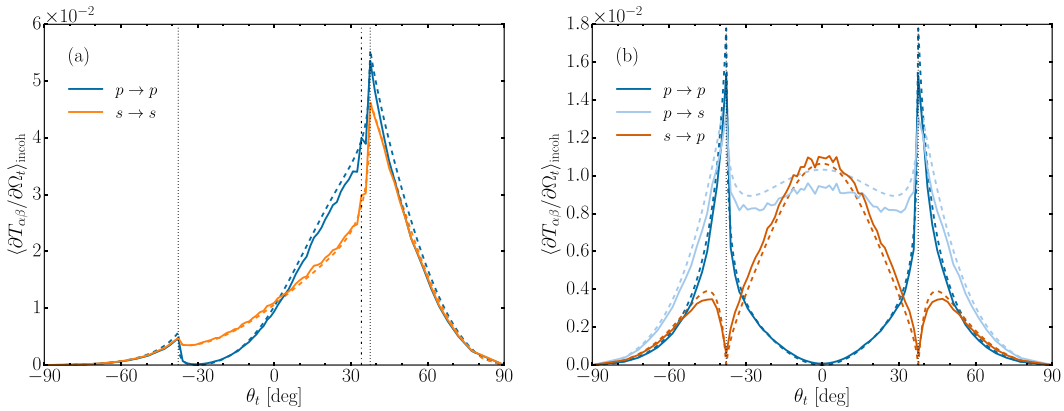

FIG. 8. (a) Same as Fig. 2(a) but for angles of incidence $(\theta_0,\phi_0) = (66.9^\circ,0^\circ)$. (b) Same as (a) but for out-of-plane scattering [$\phi_t = \pm 90^\circ$]. Results for combinations of the polarizations of the incident and scattered light for which the scattered intensity was everywhere negligible have been omitted. [Parameters: $\varepsilon_1 = 1.0$, $\varepsilon_2 = 2.6896$; $\delta = \lambda/20$, $a = \lambda/4$.]

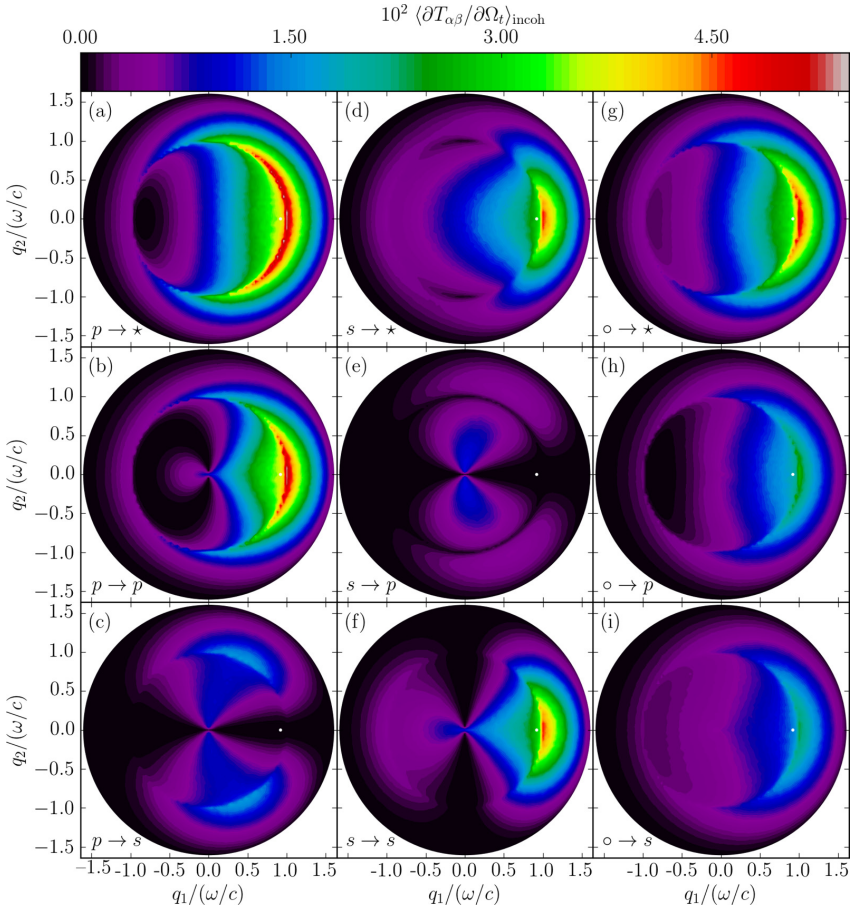

FIG. 9. Same as Fig. 3, but for the angles of incidence $(\theta_0,\phi_0) = (66.9^\circ,0^\circ)$.

which the first-order contribution (according to their approach) to $\langle \partial T_{p\alpha}(\mathbf{q}_\parallel|\mathbf{k}_\parallel)/\partial\Omega_t\rangle_{\text{incoh}}$ vanishes the *Brewster scattering angles*, as a generalization of the Brewster angle (polarizing angle) in reflection for a flat surface. In what follows, following Kawanishi *et al.*, we will refer to the polar angles of transmission in the plane of incidence at which p- and s-polarized light is transmitted diffusely (incoherently) into light of any polarization with zero, or nearly zero, intensity, the Brewster scattering angles. This is consistent with our previous investigation into the Brewster scattering angles in reflection, as presented in Ref. [15].

The Brewster angle θ_B is defined by the zero in the reflectivity from a flat surface, for p polarization at the angle of incidence given by $\theta_0 = \theta_B = \tan^{-1}(\sqrt{\varepsilon_2/\varepsilon_1})$. For one set of $\{\varepsilon_1,\varepsilon_2\}$, there is hence only one Brewster angle for incidence in a given medium. However, in contrast, we would like to stress the fact that the Brewster scattering angles for $p \to p$ scattering are present for a wide range of angles of incidence, given by Eq. (57) for in-plane transmission.

We now let the polar angle of incidence increase to $\theta_0 = 66.9^\circ$, as presented in Figs. 8 and 9. These figures show that p-polarized transmitted light gives a significant, maybe even dominant, contribution to the in-plane transmitted intensity at the position of the Yoneda peak in the forward transmission plane ($\phi_t = \phi_0$). This is in sharp contrast to what was found when $\theta_0 = 0^\circ$ and $\theta_0 = 21.1^\circ$, where s-polarized transmitted light gave the most significant contribution to the in-plane transmitted intensity at the position of the Yoneda peaks. To explain this behavior in the current context, we will again be assisted by Eq. (52a), from which it follows that at the position of the Yoneda peaks

$$\left\langle \frac{\partial T_{pp}(\mathbf{q}_\parallel|\mathbf{k}_\parallel)}{\partial\Omega_t}\right\rangle_{\text{incoh}}\Bigg|_{q_\parallel=\sqrt{\varepsilon_1}\omega/c} \propto \frac{k_\parallel^2}{|d_p(k_\parallel)|^2}, \tag{58}$$

where we used $\alpha_1(\sqrt{\varepsilon_1}\omega/c) = 0$ in obtaining this result. For normal incidence, Eq. (58) predicts that the $p \to p$ transmission should go to zero, consistent with what we have seen. However, as the polar angle of incidence is increased, the function on the right-hand side of Eq. (58) will grow quickly, particularly as one approaches grazing incidence. This has the consequence that $\langle \partial T_{pp}(\mathbf{q}_\parallel|\mathbf{k}_\parallel)/\partial\Omega_t\rangle_{\text{incoh}}$, for increasing polar angle of incidence, will go from dipping to peaking at the position of the Yoneda peaks, $q_\parallel = \sqrt{\varepsilon_1}\omega/c$. This will not happen for the $s \to p$ transmitted light since to lowest order in the surface profile function its intensity is proportional to $\alpha_1(q_\parallel)$, which will always be zero at the position of the Yoneda peaks [see Eq. (52c)].

To illustrate this behavior, we study the copolarized transmitted intensity at the position of the Yoneda peak in the forward transmission plane, $(\theta_t,\phi_t) = (\theta_t^\star,\phi_0)$, by defining the quantity

$$Y_\alpha(\theta_0) \equiv \left\langle \frac{\partial T_{\alpha\alpha}(\mathbf{q}_\parallel|\mathbf{k}_\parallel)}{\partial\Omega_t}\right\rangle_{\text{incoh}}\Bigg|_{\mathbf{q}_\parallel=\sqrt{\varepsilon_1}\frac{\omega}{c}\hat{\mathbf{k}}_\parallel}. \tag{59}$$

Figure 10 presents simulation results for $Y_\alpha(\theta_0)$ as a function of polar angle of incidence for transmission through the vacuum-dielectric system. This figure shows, as is consistent with the preceding discussion, that $Y_p(\theta_0)$ increases more rapidly than $Y_s(\theta_0)$ for moderate angles of incidence; moreover, for an angle

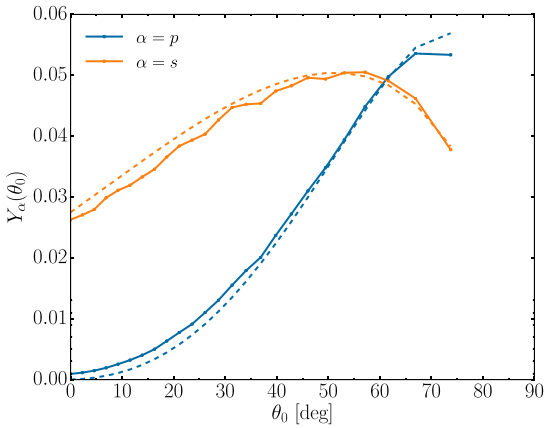

FIG. 10. Simulation results for the in-plane, copolarized contribution to the mean DTC at the Yoneda peak in the forward transmission plane as measured by the function $Y_\alpha(\theta_0)$ defined in Eq. (59). Results for the same angles of incidence, but obtained through SAPT, are included as dashed lines. [Parameters: $\varepsilon_1 = 1.0$, $\varepsilon_2 = 2.6896$; $\delta = \lambda/20$, $a = \lambda/4$.]

of incidence of about 62° and greater, we find that $Y_p(\theta_0) \geqslant Y_s(\theta_0)$ for the dielectric constants assumed in the current work. The reason for the nonzero $Y_p(\theta_0 = 0^\circ)$ is multiple scattering effects which were included consistently in the nonperturbative simulation technique used to obtain the solid-line results of Fig. 10.

Also of interest in the figures presented for $\theta_0 = 66.9^\circ$ is the position of the Brewster scattering angle Θ_B, which is now shifted even farther away from the critical angle $\theta_t^\star$. From Eq. (57) we calculate that $\Theta_B(66.9^\circ) \approx 30.3^\circ$, in good agreement with the observed value in Fig. 8. This Brewster scattering angle is close to its limiting value for grazing incidence for the dielectric constants currently investigated: $\Theta_B(90^\circ) \approx 28.9^\circ$ [Fig. 7].

We now turn our attention to the inverse system where light is again incident from the dielectric side of the rough interface. For this system, Fig. 11 presents the (a) in-plane and (b) out-of-plane distributions of the MDTC for a polar angle of incidence $\theta_0 = 34.1^\circ$. As we compare Figs. 11 to 2(b), the observation made for the vacuum-dielectric system that an increase in θ_0 will result in the majority of the light being transmitted into the forward transmission plane seems also to hold true for the dielectric-vacuum system. This is expected for weakly rough surfaces like the ones we are investigating, as the main weight of the MDTC to first order in SAPT depends on the power-spectrum factor in Eq. (52), a modified Gaussian centered at the angular position of the coherently transmitted light.

The Brewster scattering angle can be found also when the light is incident from the dielectric side. For the parameters in Fig. 11, we find that $\langle \partial T_{pp}(\mathbf{q}_\parallel|\mathbf{k}_\parallel)/\partial\Omega_t\rangle_{\text{incoh}}$, to first order in SAPT, vanishes at the polar angle of $\Theta_B(34.1^\circ) \approx 40.2^\circ$ for $\phi_t = 180^\circ$. A similar result is presented in the work by Nieto-Vesperinas and Sánchez-Gil [Fig. 12 in Ref. [16]], but the Brewster scattering phenomenon is not mentioned explicitly in this work.

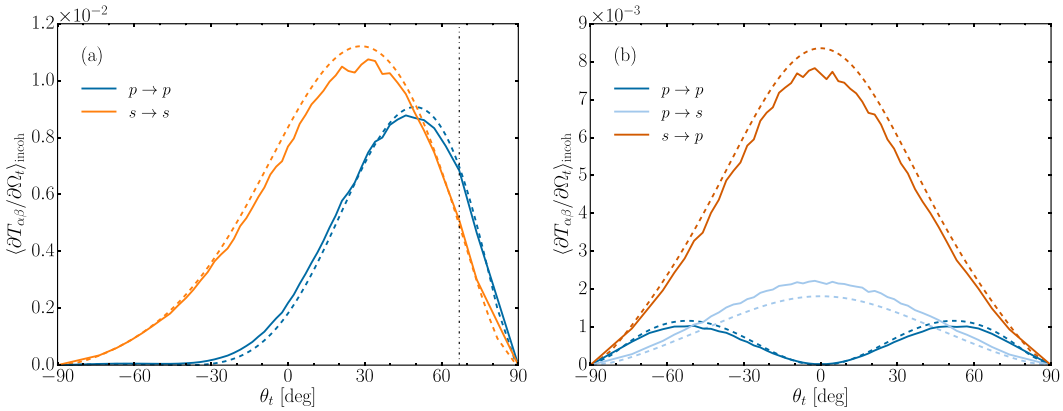

FIG. 11. (a) Same as Fig. 2(b) but for angles of incidence $(\theta_0,\phi_0) = (34.1^\circ, 0^\circ)$. (b) Same as (a) but for out-of-plane scattering [$\phi_t = \pm 90^\circ$]. Results for combinations of the polarizations of the incident and scattered light for which the scattered intensity was everywhere negligible have been omitted. [Parameters: $\varepsilon_1 = 2.6896$, $\varepsilon_2 = 1.0$; $\delta = \lambda/20$, $a = \lambda/4$.]

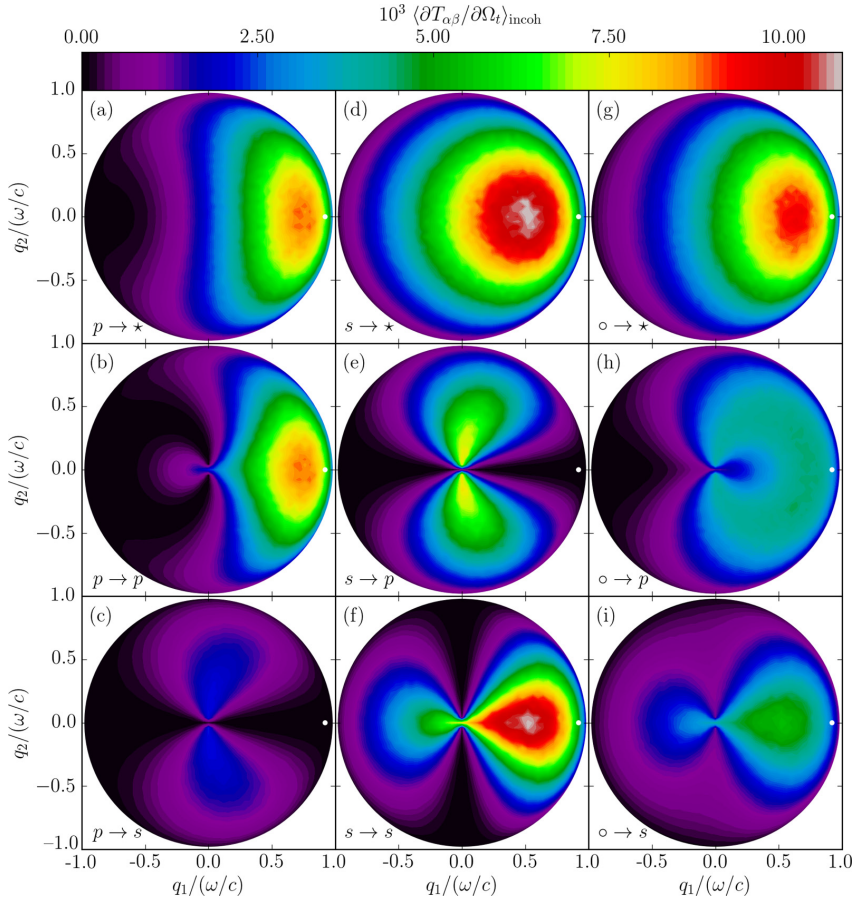

FIG. 12. Same as Fig. 4, but for the angles of incidence $(\theta_0,\phi_0) = (34.1^\circ, 0^\circ)$.

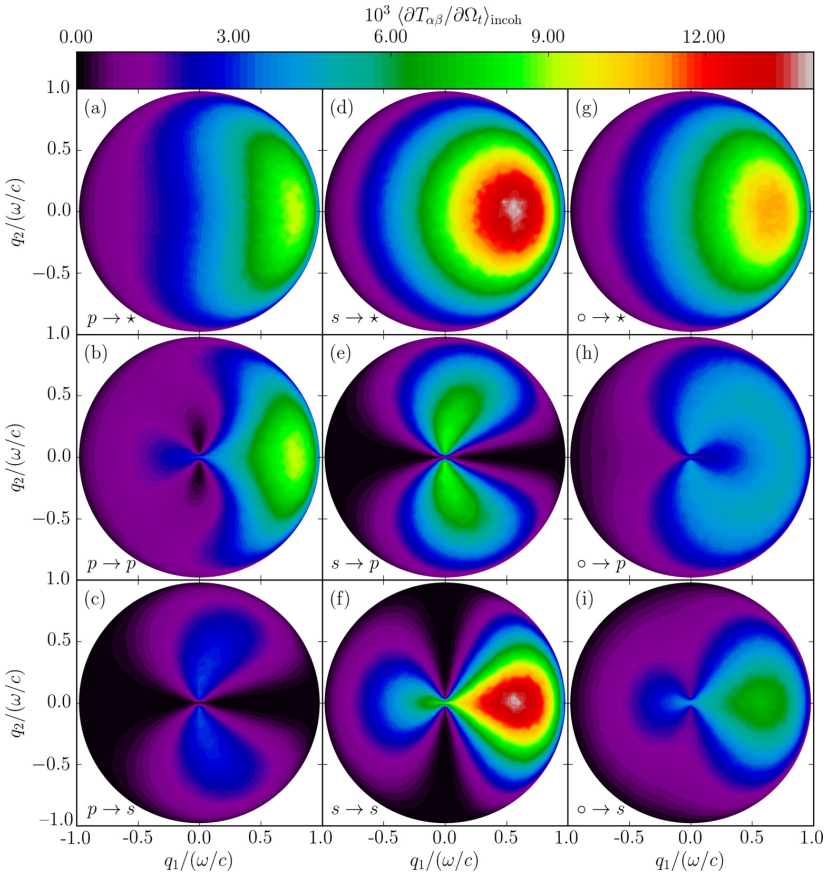

FIG. 13. Same as Fig. 4, but for the angles of incidence $(\theta_0,\phi_0) = (45.0^\circ,0^\circ)$. Note that for the corresponding flat interface system there would have been zero transmission, since the incident field will experience total internal reflection due to $\theta_0 > \theta_t^\star \approx 37.6^\circ$. For this reason there is no white dot indicating the specular direction of transmission in this case. For this rough interface system, the light that is transmitted is induced by the surface roughness.

Figures 12 and 13 present the full angular distributions of the MDTC for angles of incidence $(\theta_0,\phi_0) = (34.1^\circ,0^\circ)$ and $(\theta_0,\phi_0) = (45.0^\circ,0^\circ)$, respectively. The distributions in Figs. 12 and 13 are rather smooth with few, if any, surprising characteristics. It should be noted that the polar angle of incidence $\theta_0 = 45.0^\circ$ is larger than the critical angle for total internal reflection, $\theta_0^\star = \sin^{-1}(\sqrt{\varepsilon_2/\varepsilon_1}) \approx 37.6^\circ$, so, for the equivalent planar system, no light would have been transmitted at all; the nonzero intensity distributions observed in Fig. 13 are therefore all roughness induced.

C. Transmissivity and transmittance

Turning now to the transmissivity [defined in Eq. (48)] of the randomly rough interface, we present in Fig. 14(a) the transmissivity as a function of the polar angle of incidence θ_0 when the interface is illuminated from vacuum by p- and s-polarized light. The transmissivity when the interface is illuminated from the dielectric is presented in Fig. 14(b). In Fig. 14(a), the transmissivity for incident light of both polarizations is nonzero for all values of θ_0, and tends to zero at a grazing angle of incidence $\theta_0 \approx 90^\circ$. In contrast, the vanishing of the transmissivity for incident light of both polarizations for angles of incidence greater than the critical angle for total internal reflection, $\theta_0^\star = \sin^{-1}(\sqrt{\varepsilon_2/\varepsilon_1})$, which evaluates to $\theta_0^\star \approx 37.6^\circ$ for the assumed values of the dielectric constants, is clearly seen in Fig. 14(b). The transmissivity is larger for p-polarized light than it is for s-polarized light, irrespective of the medium of incidence. This is consistent with the result that the reflectivity of a dielectric surface is larger for s-polarized light than for p-polarized light [15]. Even if the transmissivity curves presented in Fig. 14 closely resemble the functional form of the transmissivity obtained for equivalent flat interface systems (the Fresnel transmission coefficients, quantified by the dashed lines in Fig. 14), we remark that there are differences. For instance, from Fig. 14 one observes that $\mathcal{T}_p(\theta_0) < 1$ for all angles of incidence, while

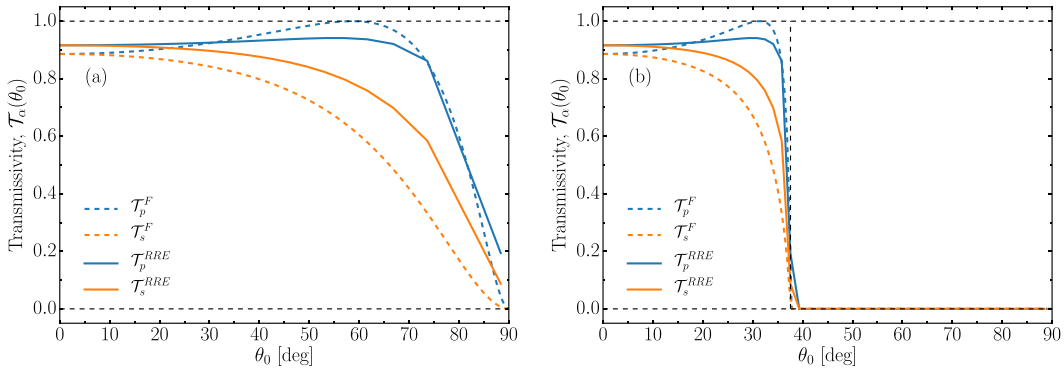

FIG. 14. (a) Transmissivities $\mathcal{T}_\alpha(\theta_0)$ of a two-dimensional randomly rough vacuum-dielectric interface ($\varepsilon_1 = 1$, $\varepsilon_2 = 2.6896$) for p- and s-polarized light as functions of the polar angle of incidence. (b) The same as in 14(a), but for a dielectric-vacuum interface ($\varepsilon_1 = 2.6896$, $\varepsilon_2 = 1$). The quantity $\mathcal{T}_\alpha^F(\theta_0)$ indicates the Fresnel transmission coefficient (flat surface transmissivity). The critical angle $\theta_0 = \theta_0^\star = \sin^{-1}(\sqrt{\varepsilon_2/\varepsilon_1})$ for total internal reflection for the equivalent planar dielectric-vacuum system is indicated by the vertical dashed line, with the values assumed for the dielectric constants $\theta_0^\star \approx 37.6^\circ$. The roughness parameters assumed in obtaining these results are the same as in Fig. 2.

for the equivalent flat interface systems the transmissivity will be unity at the Brewster angle located around the maxima of $\mathcal{T}_p(\theta_0)$ in Fig. 14.

We now focus on the contribution to the transmittance from the light that has been transmitted incoherently through the surface; in Eq. (51), this is the last term denoted by $\mathcal{T}_\beta(\theta_0)_{\rm incoh}$ for incident light of β polarization. Small amplitude perturbation theory, through Eq. (52), will again assist us in the interpretation of the results. The transmittance from vacuum into the dielectric is depicted in Fig. 15(a). In this situation, for which $\varepsilon_1 < \varepsilon_2$, the functions $|d_p(k_\parallel)|^{-2}$ and $|d_s(k_\parallel)|^{-2}$ are both monotonically increasing functions of $k_\parallel$ (or θ_0), and the transmittances $\mathcal{T}_\beta(\theta_0)_{\rm incoh}$ ($\beta = p,s$) are hence slowly varying functions of the angles of incidence, consistent with what is observed in Fig. 15(a).

Figure 15(b) presents the transmittance $\mathcal{T}_\beta(\theta_0)_{\rm incoh}$ as a function of the polar angle of incidence when the incident medium is the dielectric, and it is found that this quantity displays interesting features. For instance, in s polarization, a sharp maximum is observed for an angle of incidence a little smaller than 40°, and for this angle of incidence the contribution to the transmittance from the light being transmitted incoherently is about twice the value at normal incidence. This behavior can be understood on the basis of Eq. (52d). As a function of the polar angle of incidence (or $k_\parallel$), the expression for $\langle \partial T_{ss}(\mathbf{q}_\parallel|\mathbf{k}_\parallel)/\partial\Omega_t\rangle_{\rm incoh}$ in this equation

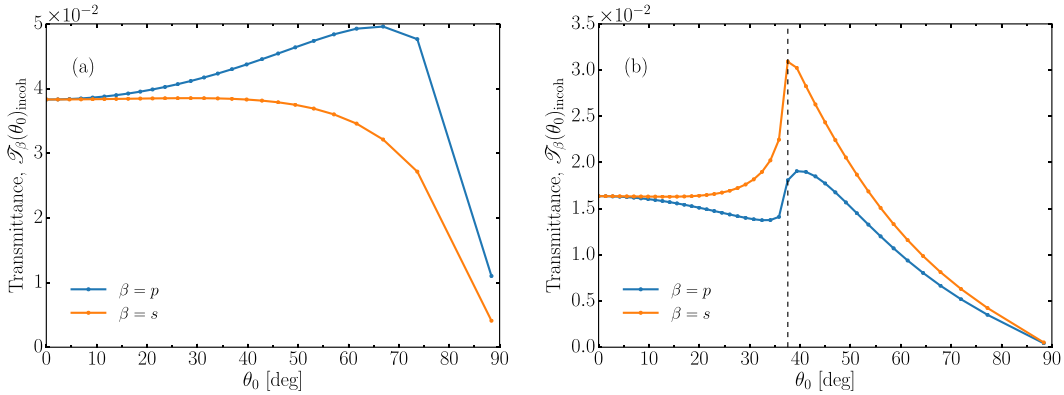

FIG. 15. θ_0 dependence of the contribution to the transmittance from p- and s-polarized incident light that has been transmitted incoherently through a two-dimensional randomly rough surface. This quantity is for β-polarized incident light defined by the last term of Eq. (51), i.e., $\mathcal{T}_\beta(\theta_0)_{\rm incoh} = \mathcal{T}_\beta(\theta_0) - \mathcal{T}_\beta(\theta_0)$. The scattering systems assumed in obtaining these results were (a) vacuum dielectric ($\varepsilon_1 = 1$, $\varepsilon_2 = 2.6896$) and (b) dielectric vacuum ($\varepsilon_1 = 2.6896$, $\varepsilon_2 = 1$). The critical angle $\theta_0 = \theta_0^\star$ for total internal reflection in the equivalent flat dielectric-vacuum system is indicated by the vertical dashed line. The roughness parameters assumed were the same as in Fig. 2. Several simulations were run with small perturbations in the surface length L in order to obtain transmittance data with higher angular resolution (data points are indicated by the solid dots).

will have a maximum when $|d_s(k_\parallel)|^{-2}$ is peaking. This happens when $k_\parallel = \sqrt{\varepsilon_2}\omega/c$, or equivalently, when $\theta_0 = \theta_0^\star$. The expression for the $s \to p$ cross-polarized MDTC will also go through a maximum at the same critical angle [see Eq. (52b)], and so, therefore, will $\mathcal{T}_s(\theta_0)_{\text{incoh}}$. This explains the functional dependence of $\mathcal{T}_s(\theta_0)_{\text{incoh}}$ on the angle of incidence. From Fig. 15(b) it is also observed that the two curves behave differently around $\theta_0 = \theta_0^\star$. While the transmittance $\mathcal{T}_s(\theta_0)_{\text{incoh}}$ is monotonically increasing in the interval $0^\circ < \theta_0 < \theta_0^\star$ and monotonically decreasing in the interval $\theta_0^\star < \theta_0 < 90^\circ$, this is not the case for the transmittance of p-polarized incident light. Similar to the case of s-polarized incident light, the rapid dependence on the angle of incidence of $\mathcal{T}_p(\theta_0)_{\text{incoh}}$ around $\theta_0 = \theta_0^\star$ is due to the factor $|d_p(k_\parallel)|^{-2}$ present in Eqs. (52a) and (52c). However, unlike in the case of s-polarized incident light, the cross-polarized contribution to the MDTC, $\langle \partial T_{sp}(\mathbf{q}_\parallel|\mathbf{k}_\parallel)/\partial\Omega_t\rangle_{\text{incoh}}$, Eq. (52c), will go to zero at the critical angle $\theta_0 = \theta_0^\star$ due to the factor $\alpha_2(k_\parallel)$ that is present in the expression for it. Therefore, for p-polarized incident light, the transmittance will have a contribution from copolarized transmission which peaks at the critical angle of incidence, and a contribution from cross polarization that has a dip down to zero at the critical angle, and it is the sum of the two that results in the functional form observed in Fig. 15(b).

VII. CONCLUSIONS

In the current work we have investigated the transmission of light through a two-dimensional, randomly rough interface between two semi-infinite dielectric media. A derivation of the reduced Rayleigh equation for the amplitudes of light transmitted both coherently and incoherently was presented together with expressions for the mean differential transmission coefficient, transmissivity and transmittance. The RRE enables a nonperturbative, purely numerical solution of the surface scattering problem, under the Rayleigh hypothesis. As an example of the numerical implementation of the RRE, the full angular distribution for both co- and cross-polarized incoherent components of the MDTC were reported together with a discussion on the angular dependence of the transmissivity and transmittance, for configurations of vacuum and an absorptionless dielectric separated by a randomly rough interface with a Gaussian power spectrum and correlation function.

Yoneda peaks, peaks in the incoherent MDTC at the critical polar angle in the medium of transmission where the wave number in the medium of incidence turns nonpropagating, were shown in all cases of transmission into the denser medium. These peaks are a dominating feature in the distribution of s-polarized diffusely transmitted light for a wide range of azimuthal angles of scattering, but are suppressed for the p-polarized counterpart when the angle of incidence is at, or close to, normal incidence. The suppression of p-polarized incoherent scattering in plane in the backscattering direction ($\phi_t = 180^\circ$) was found to be of special interest, since the angular position of the local scattering minimum in the MDTC was shown to be dependent on the angle of incidence. This phenomenon, called the "Brewster scattering angle" due to its similarity with the flat-surface Brewster angle, was also observed when the medium of incidence was the dielectric. This is consistent with the findings of Kawanishi *et al.* [5]. The development and behavior of both Yoneda peaks and Brewster scattering angles were investigated over a wide range of angular parameters, and all observed features were explored through small amplitude perturbation theory.

Small amplitude perturbation theory, to lowest order in the surface profile function, was shown to reproduce our numerical results qualitatively to a high degree of accuracy, both through analytical arguments and a numerical implementation of that theory. This leads us to believe that the features presented in the results can be interpreted as single-scattering effects.

The physical origin of the Yoneda peak phenomenon is still not clear, neither from the existing literature on the topic nor from the results obtained in the present detailed study of it. We have concluded that it is a single-scattering phenomenon. In addition, our results contradict the explanation for the existence of the Yoneda peaks given by Gorodnichev *et al.* [8], who argue that the peaks arise from the multiscale roughness of the surface, which requires that the surface height autocorrelation function should be modeled by a sum of Gaussian functions, rather than by just one. In contrast, the numerical results of the present study, as well as the results of first-order small-amplitude perturbation theory, show explicitly that the representation of $W(x_\parallel)$ by a single Gaussian function, Eq. (4), is sufficient to produce the Yoneda peaks. Therefore, a systematic study of the physical origin of the Yoneda peaks, and their dependence on polarization, will be left for subsequent work.

As an investigation of the quality of the numerical results presented in this paper, unitarity (energy conservation) [19] was found to be satisfied with an error smaller than 10^{-4} when the scattered energies from both reflection and transmission were added, for the roughness parameters and configurations used.

Calculations of the transmission of light through two-dimensional randomly rough surfaces are challenging, and hence they are still often carried out by means of perturbative and approximate methods. Our approach, through the reduced Rayleigh equations, represents a step towards more accurate but still computationally viable solutions of the problem. This paper complements our previously published work [15] on the *reflection* of light from a randomly rough dielectric interface.

ACKNOWLEDGMENTS

The authors would like to thank Jean-Philippe Banon for valuable discussions and contributions to the presented work. The research of Ø.S.H. and I.S. was supported in part by The Research Council of Norway Contract No. 216699. In addition, I.S. acknowledges financial support from the French National Research Agency (ANR) under Contract No. ANR-15-CHIN-0003-01. This research was supported in part by NTNU and the Norwegian metacenter for High Performance Computing (NOTUR) by the allocation of computer time.

APPENDIX A: EVALUATION OF $\mathbf{V}(\gamma|\mathbf{Q}_\parallel)$

In this Appendix we outline the calculation of the vector $\mathbf{V}(\gamma|\mathbf{Q}_\parallel)$ defined by Eq. (16a). From Eqs. (16a) and (17) it

follows immediately that

$$V_3(\gamma|\mathbf{Q}_\parallel) = I(\gamma|\mathbf{Q}_\parallel). \tag{A1}$$

The remaining two components of $\mathbf{V}(\gamma|\mathbf{Q}_\parallel)$ can be obtained by expanding $\exp(-i\gamma\zeta(\mathbf{x}_\parallel))$ in powers of the surface profile function and integrating the resulting series term by term ($\alpha = 1,2$)

$$\begin{aligned} V_\alpha(\gamma|\mathbf{Q}_\parallel) &= -\int d^2x_\parallel \exp(-i\mathbf{Q}_\parallel\cdot\mathbf{x}_\parallel)\zeta_\alpha(\mathbf{x}_\parallel)\exp[-i\gamma\zeta(\mathbf{x}_\parallel)] \\ &= -\int d^2x_\parallel \exp(-i\mathbf{Q}_\parallel\cdot\mathbf{x}_\parallel)\zeta_\alpha(\mathbf{x}_\parallel)\sum_{n=0}^{\infty}\frac{(-i\gamma)^n}{n!}\zeta^n(\mathbf{x}_\parallel) \\ &= -\sum_{n=0}^{\infty}\frac{(-i\gamma)^n}{(n+1)!}\int d^2x_\parallel \exp(-i\mathbf{Q}_\parallel\cdot\mathbf{x}_\parallel)\frac{\partial\zeta^{n+1}(\mathbf{x}_\parallel)}{\partial x_\alpha} \\ &= -\frac{i}{\gamma}\sum_{m=1}^{\infty}\frac{(-i\gamma)^m}{m!}\int d^2x_\parallel \exp(-i\mathbf{Q}_\parallel\cdot\mathbf{x}_\parallel)\frac{\partial\zeta^m(\mathbf{x}_\parallel)}{\partial x_\alpha}. \end{aligned} \tag{A2}$$

Introducing the Fourier representation of the mth power of the surface profile function,

$$\zeta^m(\mathbf{x}_\parallel) = \int \frac{d^2P_\parallel}{(2\pi)^2}\,\hat{\zeta}^{(m)}(\mathbf{P}_\parallel)\exp(i\mathbf{P}_\parallel\cdot\mathbf{x}_\parallel), \quad m \geqslant 1, \tag{A3}$$

into Eq. (A2), and evaluating the two resulting integrals after changing their order, yields

$$\begin{aligned} V_\alpha(\gamma|\mathbf{Q}_\parallel) &= \frac{Q_\alpha}{\gamma}\sum_{m=1}^{\infty}\frac{(-i\gamma)^m}{m!}\hat{\zeta}^{(m)}(\mathbf{Q}_\parallel) \\ &= \frac{Q_\alpha}{\gamma}\left[\sum_{m=0}^{\infty}\frac{(-i\gamma)^m}{m!}\hat{\zeta}^{(m)}(\mathbf{Q}_\parallel) - (2\pi)^2\delta(\mathbf{Q}_\parallel)\right] \\ &= \frac{I(\gamma|\mathbf{Q}_\parallel)}{\gamma}Q_\alpha - (2\pi)^2\delta(\mathbf{Q}_\parallel)\frac{Q_\alpha}{\gamma}. \end{aligned} \tag{A4}$$

In the last step we have used the result that

$$I(\gamma|\mathbf{Q}_\parallel) = \sum_{n=0}^{\infty}\frac{(-i\gamma)^n}{n!}\hat{\zeta}^{(n)}(\mathbf{Q}_\parallel) \tag{A5}$$

and $\hat{\zeta}^{(0)}(\mathbf{Q}_\parallel) = (2\pi)^2\delta(\mathbf{Q}_\parallel)$. Equation (A5) follows readily from Eq. (17) by expanding the latter in powers of the surface profile function and integrating the resulting series term by term.

By combining Eqs. (A1) and (A4) we arrive at the final result

$$\mathbf{V}(\gamma|\mathbf{Q}_\parallel) = \frac{I(\gamma|\mathbf{Q}_\parallel)}{\gamma}(\mathbf{Q}_\parallel + \gamma\hat{\mathbf{x}}_3) - (2\pi)^2\delta(\mathbf{Q}_\parallel)\frac{\mathbf{Q}_\parallel}{\gamma}. \tag{A6}$$

We note that the last term of Eq. (A6), due to the presence of the factor $\delta(\mathbf{Q}_\parallel)\mathbf{Q}_\parallel$, will contribute only if $\mathbf{Q}_\parallel = \mathbf{0}$. Therefore, γ must also be zero; in all other cases this term will vanish. For this reason, we will refer to the second term of Eq. (A6) as the singular contribution to $\mathbf{V}(\gamma|\mathbf{Q}_\parallel)$.

Technically, $\mathbf{V}(\gamma|\mathbf{Q}_\parallel)$ is a distribution [24]; for instance, for the special case $\zeta(\mathbf{x}_\parallel) = 0$ it follows from Eq. (16) that $\mathbf{V}(\gamma|\mathbf{Q}_\parallel) = (2\pi)^2\delta(\mathbf{Q}_\parallel)\hat{\mathbf{x}}_3$ (which is independent of γ). As is true for any distribution, it cannot appear alone in a mathematical expression and should therefore not be evaluated for a single argument as if it were an ordinary function; instead a distribution can only be evaluated after being multiplied by some (test) function. This has the consequence that the singular term of $\mathbf{V}(\gamma|\mathbf{Q}_\parallel)$ may not necessarily lead to a "real" singularity when evaluating the distribution. We will indeed see that this is what happens in our case.

APPENDIX B: EXPANSION OF $T(\mathbf{q}_\parallel|\mathbf{k}_\parallel)$ IN POWERS OF THE SURFACE PROFILE FUNCTION

In this Appendix we outline the derivation of Eq. (52). We begin with the expansions

$$I(\gamma|\mathbf{Q}_\parallel) = \sum_{n=0}^{\infty}\frac{(-i\gamma)^n}{n!}\hat{\zeta}^{(n)}(\mathbf{Q}_\parallel), \tag{B1}$$

where

$$\hat{\zeta}^{(n)}(\mathbf{Q}_\parallel) = \int d^2x_\parallel e^{-i\mathbf{Q}_\parallel\cdot\mathbf{x}_\parallel}\zeta^n(\mathbf{x}_\parallel), \tag{B2a}$$

$$\hat{\zeta}^{(0)}(\mathbf{Q}_\parallel) = (2\pi)^2\delta(\mathbf{Q}_\parallel), \tag{B2b}$$

and

$$\mathbf{T}(\mathbf{q}_\parallel|\mathbf{k}_\parallel) = 2\alpha_1(k_\parallel)\sum_{n=0}^{\infty}\frac{(-i)^n}{n!}\mathbf{t}^{(n)}(\mathbf{q}_\parallel|\mathbf{k}_\parallel). \tag{B3}$$

In the last equation the superscript n denotes the order of the corresponding term in powers of $\zeta(\mathbf{x}_\parallel)$. When Eqs. (B1) and (B3) are substituted into Eq. (26), the latter becomes

$$\sum_{m=0}^{\infty}\sum_{n=0}^{m}\frac{(-i)^m}{m!}\binom{m}{n}\int\frac{d^2q_\parallel}{(2\pi)^2}[-\alpha_1(p_\parallel)+\alpha_2(q_\parallel)]^{n-1}\hat{\zeta}^{(n)}(\mathbf{p}_\parallel-\mathbf{q}_\parallel)\mathbf{M}(\mathbf{p}_\parallel|\mathbf{q}_\parallel)\,\mathbf{t}^{(m-n)}(\mathbf{q}_\parallel|\mathbf{k}_\parallel) = (2\pi)^2\delta(\mathbf{p}_\parallel-\mathbf{k}_\parallel)\frac{1}{\varepsilon_2-\varepsilon_1}\mathbf{I}_2. \tag{B4}$$

When we equate terms of zero order in $\zeta(\mathbf{x}_\parallel)$ on both sides of this equation we obtain

$$\frac{1}{-\alpha_1(p_\parallel)+\alpha_2(p_\parallel)}\mathbf{M}(\mathbf{p}_\parallel|\mathbf{p}_\parallel)\,\mathbf{t}^{(0)}(\mathbf{p}_\parallel|\mathbf{k}_\parallel) = (2\pi)^2\delta(\mathbf{p}_\parallel-\mathbf{k}_\parallel)\frac{1}{\varepsilon_2-\varepsilon_1}\mathbf{I}_2. \tag{B5}$$

With the aid of the relation

$$\frac{1}{-\alpha_1(p_\parallel)+\alpha_2(p_\parallel)} = \frac{\alpha_1(p_\parallel)+\alpha_2(p_\parallel)}{(\omega/c)^2(\varepsilon_2-\varepsilon_1)}, \tag{B6}$$

Eq. (B5) can be rewritten in the form

$$\begin{pmatrix} \frac{1}{\sqrt{\varepsilon_1\varepsilon_2}}[\varepsilon_2\alpha_1(\mathbf{p}_\parallel)+\varepsilon_1\alpha_2(\mathbf{p}_\parallel)] & 0 \\ 0 & \alpha_1(\mathbf{p}_\parallel)+\alpha_2(\mathbf{p}_\parallel) \end{pmatrix} \begin{pmatrix} t_{pp}^{(0)}(\mathbf{p}_\parallel|\mathbf{k}_\parallel) & t_{ps}^{(0)}(\mathbf{p}_\parallel|\mathbf{k}_\parallel) \\ t_{sp}^{(0)}(\mathbf{p}_\parallel|\mathbf{k}_\parallel) & t_{ss}^{(0)}(\mathbf{p}_\parallel|\mathbf{k}_\parallel) \end{pmatrix} = (2\pi)^2\delta(\mathbf{p}_\parallel-\mathbf{k}_\parallel)\mathbf{I}_2, \tag{B7}$$

from which we obtain

$$\begin{pmatrix} t_{pp}^{(0)}(\mathbf{q}_\parallel|\mathbf{k}_\parallel) & t_{ps}^{(0)}(\mathbf{q}_\parallel|\mathbf{k}_\parallel) \\ t_{sp}^{(0)}(\mathbf{q}_\parallel|\mathbf{k}_\parallel) & t_{ss}^{(0)}(\mathbf{q}_\parallel|\mathbf{k}_\parallel) \end{pmatrix} = (2\pi)^2\delta(\mathbf{q}_\parallel-\mathbf{k}_\parallel) \begin{pmatrix} \frac{\sqrt{\varepsilon_1\varepsilon_2}}{\varepsilon_2\alpha_1(\mathbf{k}_\parallel)+\varepsilon_1\alpha_2(\mathbf{k}_\parallel)} & 0 \\ 0 & \frac{1}{\alpha_1(\mathbf{k}_\parallel)+\alpha_2(\mathbf{k}_\parallel)} \end{pmatrix}. \tag{B8}$$

For $m \geqslant 1$, Eq. (B4) can be written as

$$\frac{1}{-\alpha_1(p_\parallel)+\alpha_2(p_\parallel)}\mathbf{M}(\mathbf{p}_\parallel|\mathbf{p}_\parallel)\mathbf{t}^{(m)}(\mathbf{p}_\parallel|\mathbf{k}_\parallel) + \int \frac{d^2q_\parallel}{(2\pi)^2}[-\alpha_1(p_\parallel)+\alpha_2(q_\parallel)]^{m-1}\hat{\zeta}^{(m)}(\mathbf{p}_\parallel-\mathbf{q}_\parallel)\mathbf{M}(\mathbf{p}_\parallel|\mathbf{q}_\parallel)\,\mathbf{t}^{(0)}(\mathbf{q}_\parallel|\mathbf{k}_\parallel)$$
$$+\sum_{n=1}^{m-1}\binom{m}{n}\int \frac{d^2q_\parallel}{(2\pi)^2}[-\alpha_1(p_\parallel)+\alpha_2(q_\parallel)]^{n-1}\hat{\zeta}^{(n)}(\mathbf{p}_\parallel-\mathbf{q}_\parallel)\mathbf{M}(\mathbf{p}_\parallel|\mathbf{q}_\parallel)\,\mathbf{t}^{(m-n)}(\mathbf{q}_\parallel|\mathbf{k}_\parallel) = \mathbf{0}. \tag{B9}$$

If we use the result that the matrix $\mathbf{M}(\mathbf{p}_\parallel|\mathbf{p}_\parallel)$ is diagonal and hence easily inverted, and that the matrix $\mathbf{t}^{(0)}(\mathbf{q}_\parallel|\mathbf{k}_\parallel)$ is given by Eq. (B8), we can simplify Eq. (B9) into

$$\mathbf{t}^{(m)}(\mathbf{p}_\parallel|\mathbf{k}_\parallel) = -(\varepsilon_2-\varepsilon_1)[-\alpha_1(p_\parallel)+\alpha_2(k_\parallel)]^{m-1}\hat{\zeta}^{(m)}(\mathbf{p}_\parallel-\mathbf{k}_\parallel) \begin{pmatrix} \frac{\sqrt{\varepsilon_1\varepsilon_2}}{d_p(p_\parallel)} & 0 \\ 0 & \frac{1}{d_s(p_\parallel)} \end{pmatrix} \begin{pmatrix} \frac{\sqrt{\varepsilon_1\varepsilon_2}M_{pp}(\mathbf{p}_\parallel|\mathbf{k}_\parallel)}{d_p(k_\parallel)} & \frac{M_{ps}(\mathbf{p}_\parallel|\mathbf{k}_\parallel)}{d_s(k_\parallel)} \\ \frac{\sqrt{\varepsilon_1\varepsilon_2}M_{sp}(\mathbf{p}_\parallel|\mathbf{k}_\parallel)}{d_p(k_\parallel)} & \frac{M_{ss}(\mathbf{p}_\parallel|\mathbf{k}_\parallel)}{d_s(k_\parallel)} \end{pmatrix}$$
$$-(\varepsilon_2-\varepsilon_1)\sum_{n=1}^{m-1}\binom{m}{n}\int \frac{d^2q_\parallel}{(2\pi)^2}[-\alpha_1(p_\parallel)+\alpha_2(q_\parallel)]^{n-1}\hat{\zeta}^{(n)}(\mathbf{p}_\parallel-\mathbf{q}_\parallel) \begin{pmatrix} \frac{\sqrt{\varepsilon_1\varepsilon_2}M_{pp}(\mathbf{p}_\parallel|\mathbf{q}_\parallel)}{d_p(p_\parallel)} & \frac{\sqrt{\varepsilon_1\varepsilon_2}M_{ps}(\mathbf{p}_\parallel|\mathbf{q}_\parallel)}{d_p(p_\parallel)} \\ \frac{M_{sp}(\mathbf{p}_\parallel|\mathbf{q}_\parallel)}{d_s(p_\parallel)} & \frac{M_{ss}(\mathbf{p}_\parallel|\mathbf{q}_\parallel)}{d_s(p_\parallel)} \end{pmatrix} \mathbf{t}^{(m-n)}(\mathbf{q}_\parallel|\mathbf{k}_\parallel), \tag{B10}$$

where

$$d_p(p_\parallel) = \varepsilon_2\alpha_1(p_\parallel)+\varepsilon_1\alpha_2(p_\parallel), \tag{B11a}$$
$$d_s(p_\parallel) = \alpha_1(p_\parallel)+\alpha_2(p_\parallel). \tag{B11b}$$

Equation (B10) allows $\mathbf{t}^{(m)}(\mathbf{p}_\parallel|\mathbf{k}_\parallel)$ to be obtained recursively in terms of $\mathbf{t}^{(m-1)}(\mathbf{p}_\parallel|\mathbf{k}_\parallel), \ldots, \mathbf{t}^{(1)}(\mathbf{p}_\parallel|\mathbf{k}_\parallel)$.
When $m = 1$, we obtain from Eq. (B10) the result

$$\mathbf{t}^{(1)}(\mathbf{q}_\parallel|\mathbf{k}_\parallel) = -(\varepsilon_2-\varepsilon_1)\hat{\zeta}^{(1)}(\mathbf{q}_\parallel-\mathbf{k}_\parallel) \begin{pmatrix} \frac{\varepsilon_1\varepsilon_2 M_{pp}(\mathbf{q}_\parallel|\mathbf{k}_\parallel)}{d_p(q_\parallel)d_p(k_\parallel)} & \frac{\sqrt{\varepsilon_1\varepsilon_2}M_{ps}(\mathbf{q}_\parallel|\mathbf{k}_\parallel)}{d_p(q_\parallel)d_s(k_\parallel)} \\ \frac{\sqrt{\varepsilon_1\varepsilon_2}M_{sp}(\mathbf{q}_\parallel|\mathbf{k}_\parallel)}{d_s(q_\parallel)d_p(k_\parallel)} & \frac{M_{ss}(\mathbf{q}_\parallel|\mathbf{k}_\parallel)}{d_s(q_\parallel)d_s(k_\parallel)} \end{pmatrix}. \tag{B12}$$

The matrix elements $\{M_{\alpha\beta}(\mathbf{q}_\parallel|\mathbf{k}_\parallel)\}$ are given by Eq. (27a).

In view of Eq. (B3) we find that through terms linear in the surface profile function

$$\mathbf{T}(\mathbf{q}_\parallel|\mathbf{k}_\parallel) = (2\pi)^2\delta(\mathbf{q}_\parallel-\mathbf{k}_\parallel) \begin{pmatrix} \frac{\sqrt{\varepsilon_1\varepsilon_2}}{d_p(k_\parallel)} & 0 \\ 0 & \frac{1}{d_s(k_\parallel)} \end{pmatrix} 2\alpha_1(k_\parallel)$$
$$+i(\varepsilon_2-\varepsilon_1)\hat{\zeta}^{(1)}(\mathbf{q}_\parallel-\mathbf{k}_\parallel) \begin{pmatrix} \frac{\varepsilon_1\varepsilon_2 M_{pp}(\mathbf{q}_\parallel|\mathbf{k}_\parallel)}{d_p(q_\parallel)d_p(k_\parallel)} & \frac{\sqrt{\varepsilon_1\varepsilon_2}M_{ps}(\mathbf{q}_\parallel|\mathbf{k}_\parallel)}{d_p(q_\parallel)d_s(k_\parallel)} \\ \frac{\sqrt{\varepsilon_1\varepsilon_2}M_{sp}(\mathbf{q}_\parallel|\mathbf{k}_\parallel)}{d_s(q_\parallel)d_p(k_\parallel)} & \frac{M_{ss}(\mathbf{q}_\parallel|\mathbf{k}_\parallel)}{d_s(q_\parallel)d_s(k_\parallel)} \end{pmatrix} 2\alpha_1(k_\parallel) + O(\zeta^2). \tag{B13}$$

The substitution of these results into Eq. (41) and the use of $\langle\hat{\zeta}(\mathbf{Q}_\parallel)\hat{\zeta}(\mathbf{Q}_\parallel)^*\rangle = S\delta^2 g(|\mathbf{Q}_\parallel|)$ yields Eq. (52).

[1] I. Simonsen, J. B. Kryvi, A. A. Maradudin, and T. A. Leskova, Comput. Phys. Commun. **182**, 1904 (2011).
[2] T. Nordam, P. A. Letnes, and I. Simonsen, Front. Phys. **1**, 1 (2013).
[3] T. A. Leskova, P. A. Letnes, A. A. Maradudin, T. Nordam, and I. Simonsen, Proc. SPIE **8172**, 817209 (2011).
[4] J.-J. Greffet, Phys. Rev. B **37**, 6436 (1988).
[5] T. Kawanishi, H. Ogura, and Z. L. Wang, Wave. Random Media **7**, 351 (1997).
[6] Y. Yoneda, Phys. Rev. **131**, 2010 (1963).
[7] S. K. Sinha, E. B. Sirota, S. Garoff, and H. B. Stanley, Phys. Rev. B **38**, 2297 (1988).

[8] E. E. Gorodnichev, S. L. Dudarev, D. B. Rogozkin, and M. I. Ryazanov, Pis'ma Zh. Eksp. Teor. Fiz. **48**, 137 (1988) [Sov. Phys. JETP Lett. **48**, 147 (1988)].
[9] G. Renaud, R. Lazzari, and F. Leroy, Surf. Sci. Rep. **64**, 255 (2009).
[10] H. Dosch, Phys. Rev. B **35**, 2137 (1987).
[11] S. Stepanov, in *Exploration of Subsurface Phenomena by Particle Scattering*, edited by N. Lam, C. Melendres, and S. Sinha (IASI Press, North East, Maryland, 2000), pp. 119–137.
[12] A. Kitahara, K. Inoue, H. Kikkawa, K. Matsushita, and I. Takahashi, X-ray reflectivity study on polymeric surfaces near glass transition temperature, Photon Factory Activity Report No. 20, Part B, 2002 (unpublished), p. 83.
[13] J.-C. Gasse, D. Lützenkirchen-Hecht, R. Wagner, and R. Frahm, J. Phys.: Conf. Ser. **712**, 012028 (2016).
[14] A. K. González-Alcalde, J.-P. Banon, Ø. S. Hetland, A. A. Maradudin, E. R. Méndez, T. Nordam, and I. Simonsen, Opt. Express **24**, 25995 (2016).
[15] Ø. S. Hetland, A. A. Maradudin, T. Nordam, and I. Simonsen, Phys. Rev. A **93**, 053819 (2016).
[16] M. Nieto-Vesperinas and J. A. Sánchez-Gil, J. Opt. Soc. Am. A **9**, 424 (1992).
[17] A. Soubret, G. Berginc, and C. Bourrely, Phys. Rev. B **63**, 245411 (2001).
[18] C. Yeh, Phys. Rev. E **48**, 1426 (1993).
[19] I. Simonsen, Eur. Phys. J. Spec. Top. **181**, 1 (2010).
[20] A. Maradudin, T. Michel, A. McGurn, and E. Mendez, Ann. Phys. (NY) **203**, 255 (1990).
[21] W. H. Press, S. A. Teukolsky, W. T. Vetterling, and B. P. Flannery, *Numerical Recipes in Fortran 90: The Art of Parallel Scientific Computing* (Cambridge University Press, Cambridge, UK, 1996).
[22] L. S. Blackford, J. Choi, A. Cleary, E. D'Azevedo, J. Demmel, I. Dhillon, J. Dongarra, S. Hammarling, G. Henry, A. Petitet, K. Stanley, D. Walker, and R. C. Whaley, *ScaLAPACK Users' Guide* (Society for Industrial and Applied Mathematics, Philadelphia, PA, 1997).
[23] T. Nordam, P. A. Letnes, I. Simonsen, and A. A. Maradudin, J. Opt. Soc. Am. A **31**, 1126 (2014).
[24] I. M. Gelfand and G. E. Shilov, *Generalized Functions, Vol. I: Properties and Operations* (Academic Press, New York, 1964).

Paper 5:

J.-P. Banon, Ø. S. Hetland, and I. Simonsen, "Selective enhancement of Selényi rings induced by the cross-correlation between the interfaces of a two-dimensional randomly rough dielectric film," *Ann. Phys. (N.Y.)*, vol. 389, pp. 352 – 382, 2018

Annals of Physics 389 (2018) 0–30

Contents lists available at ScienceDirect

Annals of Physics

journal homepage: www.elsevier.com/locate/aop

Selective enhancement of Selényi rings induced by the cross-correlation between the interfaces of a two-dimensional randomly rough dielectric film

J.-P. Banon [a,*], Ø.S. Hetland [a], I. Simonsen [a,b]

[a] Department of Physics, NTNU – Norwegian University of Science and Technology, NO-7491 Trondheim, Norway

[b] Surface du Verre et Interfaces, UMR 125 CNRS/Saint-Gobain, F-93303 Aubervilliers, France

ARTICLE INFO

Article history:
Received 6 September 2017
Accepted 9 December 2017
Available online 19 December 2017

Keywords:
Light scattering
Interference
Randomly rough surfaces
Numerical simulation

ABSTRACT

By the use of both perturbative and non-perturbative solutions of the reduced Rayleigh equation, we present a detailed study of the scattering of light from two-dimensional weakly rough dielectric films. It is shown that for several rough film configurations, Selényi interference rings exist in the diffusely scattered light. For film systems supported by dielectric substrates where only one of the two interfaces of the film is weakly rough and the other planar, Selényi interference rings are observed at angular positions that can be determined from simple phase arguments. For such single-rough-interface films, we find and explain by a single scattering model that the contrast in the interference patterns is better when the top interface of the film (the interface facing the incident light) is rough than when the bottom interface is rough. When both film interfaces are rough, Selényi interference rings exist but a potential cross-correlation of the two rough interfaces of the film can be used to selectively enhance some of the interference rings while others are attenuated and might even disappear. This feature may in principle be used in determining the correlation properties of interfaces of films that otherwise would be difficult to access.

* Corresponding author.
E-mail address: jean-philippe.banon@ntnu.no (J.-P. Banon).

https://doi.org/10.1016/j.aop.2017.12.003
0003-4916/

1. Introduction

Interference effects in the diffuse light scattered by thin and rough dielectric films can look both stunning and unexpected, and they have fascinated their observers for centuries. First formally described in modern times as colorful rings in the diffusely scattered light originating from a dusty back-silvered mirror by Newton [1], what is today known as Quételet- and Selényi-rings have been thoroughly analyzed theoretically [2–6] and experimentally [7,8]. An example of a non-laboratory situation where one may observe this phenomenon is in light reflections from bodies of water if appropriate algae are present on the water surface. This phenomenon, modeled as a thin layer of spherical scatterers suspended on a reflecting planar surface, was investigated by Suhr and Schlichting [6].

In a theoretical study of the scattering from one-dimensional randomly rough surfaces ruled on dielectric films on perfectly conducting substrates, Lu et al. [4] concluded that the degree of surface roughness had the biggest impact on which interference phenomena could be observed. For films with a thickness on the order of several wavelengths they were able to explain the periodic fringes they observed in the mean differential reflection coefficient through simple phase arguments. The patterns in the diffusely scattered light were shown to undergo a transition, with increasing surface roughness, from an intensity pattern exhibiting fringes whose angular positions are independent of the angle of incidence (Selényi rings [9]) to one with fringes whose angular positions depend on the angle of incidence (Quételet rings [7]) and eventually into a fringeless pattern with a backscattering peak, which is a signature of multiple scattering [10]. Although the Selényi rings are centered around the mean surface normal, with their position being independent of the angle of incidence, their amplitude, however, is modulated by the angle of incidence. According to the current understanding of the Selényi rings, their main origin is due to the interference between light scattered back directly from the top scattering layer and light reflected by the film after being scattered within it. In this paper we seek to complete this interpretation of the interference phenomena within a single scattering approximation, enabling a sound interpretation of the Selényi rings for the previously unexplored case when the rough surface is shifted to the non-incident face of the film.

A similar system to the one studied by Lu et al. was also thoroughly studied perturbatively and experimentally by Kaganovskii et al. [8]. They concluded that the long-range (smooth) component of the surface roughness, whenever present, can have a deciding effect on the interference pattern observed in the diffusely scattered light.

However, most of the relevant studies conducted on the topic so far have been restricted to investigations of scattering from a single rough interface. Allowing for more than one rough interface significantly increases the complexity of the problem both analytically and computationally, but it also opens a door to a richer set of scattering phenomena. Such stacked, multi-layered systems will in many cases better represent the real-world scattering systems we are attempting to model [2]. Two or more of these randomly rough interfaces in the stack will also often be correlated, either naturally occurring, by design or by method of production [11,12]. Since both Quételet- and Selényi-rings may enable a practical way of remote sensing and surface characterization for certain geometries and layer thicknesses, it is important also to model the impact of such roughness cross-correlation.

In this paper we investigate interference effects in the light scattered diffusely from an optical system composed of two semi-infinite media separated by a single thin dielectric film where both interfaces may be rough [Fig. 1(a)]. After describing the statistical properties of the interfaces in Section 2, we derive, in Section 3, a set of reduced Rayleigh equations (RREs) for the case of electromagnetic scattering from a system with two rough interfaces, inspired by the work of Soubret et al. [13]. Although only the case of reflected light will be analyzed in detail, the RREs for both the reflection and the transmission amplitudes are given for completeness; furthermore, this also serves to show that the presented framework can easily be generalized to an arbitrary number of rough interfaces. A perturbative method and a purely numerical method for solving the RREs are described in Section 4. Since solving the RREs for a set of two, or more, two-dimensional randomly rough surfaces by purely numerical means is a highly computationally intensive task, the perturbative method will be our main investigation tool for simulating and interpreting interference effects in such geometries. In Section 5.1 we discuss rough film geometries where either the top interface or bottom interface of the film is allowed to be randomly rough and the other interface is planar. For

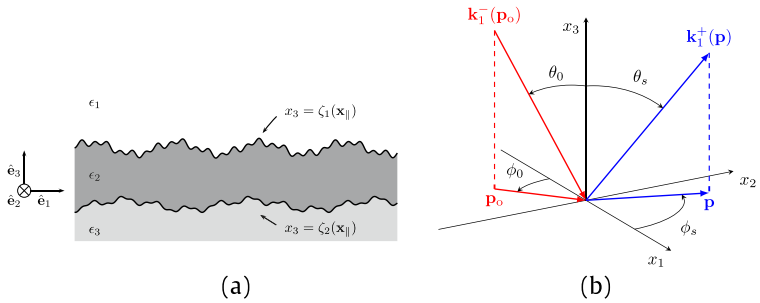

Fig. 1. (a) Layered system with two rough interfaces. (b) Definitions of the angles of incidence and scattering and wave vectors.

such geometries, we compare the predictions for the scattered intensities obtained on the basis of the perturbative and non-perturbative methods. After having established the apparent validity of the perturbative method for the level of roughness assumed, we continue to investigate rough film geometries where both interfaces of the film are randomly rough and have a varying cross-correlation [Section 5.2]. Section 5.3 gives a brief discussion concerning additional effects one expects to observe in transmission. Finally, Section 6 presents the conclusions that we have drawn from this study.

2. Scattering systems

An overview of a typical system geometry is provided in Fig. 1. We consider the case where both interfaces of the film may be randomly rough and possess non-trivial auto- and cross-correlation. Furthermore, we will be interested in scattering systems for which the mean thickness of the film is several wavelengths so that interference fringes can be observed in the diffusely reflected or transmitted intensities. The definition of the geometry is set in the three-dimensional space endowed with a Cartesian coordinate system $(O, \hat{\mathbf{e}}_1, \hat{\mathbf{e}}_2, \hat{\mathbf{e}}_3)$, with the vector plane $(\hat{\mathbf{e}}_1, \hat{\mathbf{e}}_2)$ parallel to the mean plane of the interfaces [Fig. 1(b)]. The origin, O, can be arbitrarily chosen, only affecting the complex reflection and transmission amplitudes by an overall phase factor which plays no role in the intensity of the scattered light. The scattering system splits space into a slab of three domains, or layers, that will be denoted by the indices $j \in \{1, 2, 3\}$. The mean thickness of the film will be denoted $d > 0$, and the jth interface separating media j and $j + 1$ can be described by the equation

$$x_3 = \zeta_j(\mathbf{x}_\parallel) = d_j + h_j(\mathbf{x}_\parallel)\,, \tag{1}$$

for $j \in \{1, 2\}$, where $\mathbf{x}_\parallel = x_1\,\hat{\mathbf{e}}_1 + x_2\,\hat{\mathbf{e}}_2$, $d_j = \langle \zeta_j \rangle$ denotes the average of the jth profile (and we have $d_1 - d_2 = d$), and the term h_j will be assumed to be a continuous, differentiable, single-valued, stationary, isotropic, Gaussian random process with zero mean and given auto-correlation. More specifically, the surface profile functions are assumed to satisfy the following properties

$$\big\langle h_j(\mathbf{x}_\parallel) \big\rangle = 0 \tag{2a}$$

$$\big\langle h_j(\mathbf{x}_\parallel) h_j(\mathbf{x}'_\parallel) \big\rangle = \sigma_j^2\, W(\mathbf{x}_\parallel - \mathbf{x}'_\parallel). \tag{2b}$$

Here and in the following, the angle brackets denote an average over an ensemble of realizations of the stochastic process, σ_j denotes the rms roughness of interface j and $W(\mathbf{x}_\parallel)$ represents the height auto-correlation function normalized so that $W(\mathbf{0}) = 1$. For reasons of simplicity we here restrict ourselves to the situation where both interfaces are characterized by the same form of the correlation function. In particular, we will here assume a Gaussian form of the auto-correlation function that is defined by

$$W(\mathbf{x}_\parallel) = \exp\left(-\frac{|\mathbf{x}_\parallel|^2}{a^2}\right)\,, \tag{3}$$

where a is the correlation length. The corresponding power spectrum (defined as the Fourier transform of W) is then

$$g(\mathbf{p}) = \pi a^2 \exp\left(-\frac{|\mathbf{p}|^2 a^2}{4}\right) , \tag{4}$$

with $\mathbf{p} = p_1\,\hat{\mathbf{e}}_1 + p_2\,\hat{\mathbf{e}}_2$. In addition, the two interfaces will be assumed to be cross-correlated in the following way

$$\left\langle h_1(\mathbf{x}_\parallel) h_2(\mathbf{x}'_\parallel)\right\rangle = \gamma\ \sigma_1\sigma_2\ W(\mathbf{x}_\parallel - \mathbf{x}'_\parallel) , \tag{5}$$

where $\gamma \in [-1, 1]$ is a dimensionless cross-correlation coupling variable. When $\gamma = 0$ the two interfaces are uncorrelated, and the extreme cases $\gamma = \pm 1$ and $\sigma_1 = \sigma_2$ can be viewed respectively as the second interface being a shifted copy of the first one by a vector $-d\,\hat{\mathbf{e}}_3$, or as the second interface being a symmetric copy of the first one with respect to the plane $x_3 = (d_1 + d_2)/2$. We can summarize the correlations expressed by Eqs. (2b) and (5) by the following relation

$$\left\langle h_i(\mathbf{x}_\parallel) h_j(\mathbf{x}'_\parallel)\right\rangle = [\delta_{ij} + \gamma(1 - \delta_{ij})]\ \sigma_i\sigma_j\ W(\mathbf{x}_\parallel - \mathbf{x}'_\parallel) , \tag{6}$$

where δ_{ij} denotes the Kronecker delta.

3. Formulation of the problem

The theoretical approach used in this work to study the scattering of light from the systems of interest is based on the so-called reduced Rayleigh equations. A reduced Rayleigh equation is an integral equation in which the integral kernel encodes the materials and geometry of the scattering system and the unknowns are the reflection or transmission amplitudes for each polarization. In the following, in order to establish the notation and highlight the main assumptions of the method, we will briefly recall the key ideas of the derivation of the reduced Rayleigh equations for a system composed of three media separated by two disjoint rough interfaces. We will use, to our knowledge, the most general form of the reduced Rayleigh equations for a single interface derived by Soubret et al. in Ref. [13] and used by these authors in Refs. [13,14] in the case of a single interface system and a film geometry. Once the general framework is established, we will apply it to the specific geometries of interest.

3.1. The reduced Rayleigh equations

All physical quantities introduced hereafter will be indexed with respect to the medium (domain) they belong to. The electromagnetic response of the media is modeled by non-magnetic, homogeneous, isotropic, linear constitutive relations in the frequency domain, i.e. that *a priori* each medium is characterized by frequency dependent scalar complex dielectric functions, $\epsilon_j(\omega)$, where ω denotes the frequency of the electromagnetic wave excitation. We consider the presence of an electromagnetic field $(\mathbf{E}, \mathbf{H})$ in the whole space. The fields will be denoted by a subscript j depending on their containing medium. As an example, the electric field evaluated at a point $\mathbf{x}$ in medium 1 at time t is denoted $\mathbf{E}_1(\mathbf{x}, t) = \mathbf{E}_1(\mathbf{x}, \omega)\exp(-i\omega t)$. The source free Maxwell equations, together with homogeneous, linear and isotropic constitutive relations in the frequency domain, result in the electric and magnetic fields satisfying the Helmholtz equation in each region. Namely, for all $j \in \{1, 2, 3\}$,

$$\nabla^2\mathbf{E}_j(\mathbf{x}, \omega) + \epsilon_j(\omega)\left(\frac{\omega}{c}\right)^2 \mathbf{E}_j(\mathbf{x}, \omega) = \mathbf{0} , \tag{7}$$

and a similar equation satisfied for $\mathbf{H}$. Here, ∇^2 denotes the Laplace operator and c represents the speed of light in vacuum. In the following, we will drop the time, or frequency, dependence, since we assume a stationary regime where time contributes only by an overall phase factor $\exp(-i\omega t)$. It is known that a solution to the Helmholtz equation can be written as a linear combination of plane waves, thus the representation of the electric field in each region can be written as

$$\mathbf{E}_j(\mathbf{x}) = \sum_{a=\pm} \int_{\mathbb{R}^2} \left[\mathcal{E}^a_{j,p}(\mathbf{q})\ \hat{\mathbf{e}}^a_{p,j}(\mathbf{q}) + \mathcal{E}^a_{j,s}(\mathbf{q})\ \hat{\mathbf{e}}_s(\mathbf{q})\right] \exp\left(i\,\mathbf{k}^a_j(\mathbf{q})\cdot\mathbf{x}\right) \frac{\mathrm{d}^2 q}{(2\pi)^2} , \tag{8}$$

where

$$\alpha_j(\mathbf{q}) = \sqrt{\epsilon_j\left(\frac{\omega}{c}\right)^2 - \mathbf{q}^2}, \qquad \mathrm{Re}\,(\alpha_j), \mathrm{Im}\,(\alpha_j) \geq 0\,, \tag{9a}$$

$$\mathbf{k}_j^{\pm}(\mathbf{q}) = \mathbf{q} \pm \alpha_j(\mathbf{q})\,\hat{\mathbf{e}}_3\,, \tag{9b}$$

$$\hat{\mathbf{e}}_s(\mathbf{q}) = \hat{\mathbf{e}}_3 \times \hat{\mathbf{q}}\,, \tag{9c}$$

$$\hat{\mathbf{e}}_{p,j}^{\pm}(\mathbf{q}) = \frac{c}{\sqrt{\epsilon_j}\omega}\left(\pm\alpha_j(\mathbf{q})\,\hat{\mathbf{q}} - |\mathbf{q}|\,\hat{\mathbf{e}}_3\right). \tag{9d}$$

Here a caret over a vector indicates that the vector is a unit vector. Note that the wave vector $\mathbf{k}_j^{\pm}(\mathbf{q})$ of an elementary plane wave is decomposed into its projection $\mathbf{q}$ in the lateral vector plane $(\hat{\mathbf{e}}_1, \hat{\mathbf{e}}_2)$ and the component $\pm\alpha_j(\mathbf{q})$ along $\hat{\mathbf{e}}_3$. The sum for $a = \pm$ takes into account both upwards and downwards propagating and evanescent (and possibly growing) waves. The field amplitude is decomposed in the *local polarization basis* $(\hat{\mathbf{e}}_{p,j}^{a}(\mathbf{q})\,, \hat{\mathbf{e}}_s(\mathbf{q})\,)$, so that $\mathcal{E}_{j,\alpha}^{a}(\mathbf{q})$ denotes the component of the field amplitude in the polarization state α of the mode characterized by a and $\mathbf{q}$. In this basis, the directions given by $\hat{\mathbf{e}}_{p,j}^{\pm}(\mathbf{q})$, and $\hat{\mathbf{e}}_s(\mathbf{q})$ are respectively the directions of the p- and s-polarization of the electric field amplitude. Furthermore, the electromagnetic fields have to satisfy the boundary conditions ($j \in \{1, 2\}$)

$$\mathbf{n}_j(\mathbf{x}_\parallel) \times \Big[\mathbf{E}_{j+1}(\mathbf{s}_j(\mathbf{x}_\parallel)) - \mathbf{E}_j(\mathbf{s}_j(\mathbf{x}_\parallel))\Big] = \mathbf{0} \tag{10a}$$

$$\mathbf{n}_j(\mathbf{x}_\parallel) \times \Big[\mathbf{H}_{j+1}(\mathbf{s}_j(\mathbf{x}_\parallel)) - \mathbf{H}_j(\mathbf{s}_j(\mathbf{x}_\parallel))\Big] = \mathbf{0}\,, \tag{10b}$$

where $\mathbf{n}_j(\mathbf{x}_\parallel)$ is a vector that is normal to surface j at the surface point $\mathbf{s}_j(\mathbf{x}_\parallel) = \mathbf{x}_\parallel + \zeta_j(\mathbf{x}_\parallel)\hat{\mathbf{e}}_3$, and given by

$$\mathbf{n}_j(\mathbf{x}_\parallel) = \hat{\mathbf{e}}_3 - \frac{\partial\zeta_j}{\partial x_1}(\mathbf{x}_\parallel)\,\hat{\mathbf{e}}_1 - \frac{\partial\zeta_j}{\partial x_2}(\mathbf{x}_\parallel)\,\hat{\mathbf{e}}_2\,. \tag{11}$$

Here, $\partial/\partial x_k$ denotes the partial derivative along the direction $\hat{\mathbf{e}}_k$. Following Soubret et al. [13], for a given surface indexed by j, by substituting the field expansion Eq. (8) into Eq. (10) and by a clever linear integral combination of the boundary conditions, one can show that the upward or downward field amplitudes in medium $j+1$ can be linked to the upward and downward field amplitudes in medium j via the following integral equation defined for $a_{j+1} = \pm$, $j \in \{1, 2\}$, and $\mathbf{p}$ in the vector plane $(\hat{\mathbf{e}}_1, \hat{\mathbf{e}}_2)$:

$$\sum_{a_j=\pm}\int \mathcal{J}_{j+1,j}^{a_{j+1},a_j}(\mathbf{p}\,|\,\mathbf{q})\;\mathbf{M}_{j+1,j}^{a_{j+1},a_j}(\mathbf{p}\,|\,\mathbf{q})\;\boldsymbol{\mathcal{E}}_j^{a_j}(\mathbf{q})\,\frac{\mathrm{d}^2q}{(2\pi)^2} = \frac{2\,a_{j+1}\,\sqrt{\epsilon_j\epsilon_{j+1}}\,\alpha_{j+1}(\mathbf{p})}{\epsilon_{j+1}-\epsilon_j}\,\boldsymbol{\mathcal{E}}_{j+1}^{a_{j+1}}(\mathbf{p})\,. \tag{12}$$

Here $\boldsymbol{\mathcal{E}}_j^{a}(\mathbf{q}) = (\mathcal{E}_{j,p}^{a}(\mathbf{q})\,, \mathcal{E}_{j,s}^{a}(\mathbf{q})\,)^{\mathrm{T}}$ denotes a column vector of the polarization components of the field amplitude in medium j. Moreover, $\mathbf{M}_{l,m}^{b,a}(\mathbf{p}\,|\,\mathbf{q})$ is a $2\times\ 2$ matrix which originates from a change of coordinate system between the local polarization basis $(\hat{\mathbf{e}}_{p,l}^{b}(\mathbf{p})\,, \hat{\mathbf{e}}_s(\mathbf{p})\,)$ and $(\hat{\mathbf{e}}_{p,m}^{a}(\mathbf{q})\,, \hat{\mathbf{e}}_s(\mathbf{q})\,)$, defined for $a = \pm$, $b = \pm$, and $l, m \in \{j, j+1\}$ such that $l \neq m$ as

$$\mathbf{M}_{l,m}^{b,a}(\mathbf{p}\,|\,\mathbf{q}) = \begin{pmatrix} |\mathbf{p}||\mathbf{q}| + ab\,\alpha_l(\mathbf{p})\,\alpha_m(\mathbf{q})\,\hat{\mathbf{p}}\cdot\hat{\mathbf{q}} & -b\,\sqrt{\epsilon_m}\,\dfrac{\omega}{c}\,\alpha_l(\mathbf{p})\,[\hat{\mathbf{p}}\times\hat{\mathbf{q}}]\cdot\hat{\mathbf{e}}_3 \\ a\,\sqrt{\epsilon_l}\,\dfrac{\omega}{c}\,\alpha_m(\mathbf{q})\,[\hat{\mathbf{p}}\times\hat{\mathbf{q}}]\cdot\hat{\mathbf{e}}_3 & \sqrt{\epsilon_l\epsilon_m}\,\dfrac{\omega^2}{c^2}\,\hat{\mathbf{p}}\cdot\hat{\mathbf{q}} \end{pmatrix}. \tag{13}$$

The kernel scalar factor $\mathcal{J}_{l,m}^{b,a}(\mathbf{p}\,|\,\mathbf{q})$ encodes the surface geometry and is defined as

$$\mathcal{J}_{l,m}^{b,a}(\mathbf{p}\,|\,\mathbf{q}) = (b\alpha_l(\mathbf{p}) - a\alpha_m(\mathbf{q}))^{-1}\int \exp\left[-i(\mathbf{k}_l^{b}(\mathbf{p}) - \mathbf{k}_m^{a}(\mathbf{q}))\cdot(\mathbf{x}_\parallel + \zeta_j(\mathbf{x}_\parallel)\,\hat{\mathbf{e}}_3)\right]\mathrm{d}^2x_\parallel. \tag{14}$$

Notice that, as already pointed out in Ref. [13], due to the symmetry of the boundary conditions, one may also show in the same way that

$$\sum_{a_{j+1}=\pm}\int \mathcal{J}_{j,j+1}^{a_j,a_{j+1}}(\mathbf{p}\,|\,\mathbf{q})\;\mathbf{M}_{j,j+1}^{a_j,a_{j+1}}(\mathbf{p}\,|\,\mathbf{q})\;\boldsymbol{\mathcal{E}}_{j+1}^{a_{j+1}}(\mathbf{q})\,\frac{\mathrm{d}^2q}{(2\pi)^2}=\frac{2\,a_j\,\sqrt{\epsilon_j\epsilon_{j+1}}\,\alpha_j(\mathbf{p})}{\epsilon_j-\epsilon_{j+1}}\,\boldsymbol{\mathcal{E}}_j^{a_j}(\mathbf{p})\;, \tag{15}$$

which can be obtained from Eq. (12) by interchanging j and $j+1$. Typically, Eq. (12) is appropriate to solve the problem of reflection whereas Eq. (15) is appropriate to solve the problem of transmission, as we will see later. In the following, it will be convenient to define

$$\boldsymbol{\Theta}_{j+1,j}^{a_{j+1},a_j}(\mathbf{p}\,|\,\mathbf{q})=\alpha_{j+1}^{-1}(\mathbf{p})\mathcal{J}_{j+1,j}^{a_{j+1},a_j}(\mathbf{p}\,|\,\mathbf{q})\;\mathbf{M}_{j+1,j}^{a_{j+1},a_j}(\mathbf{p}\,|\,\mathbf{q}) \tag{16}$$

and

$$\boldsymbol{\Theta}_{j,j+1}^{a_j,a_{j+1}}(\mathbf{p}\,|\,\mathbf{q})=\alpha_j^{-1}(\mathbf{p})\mathcal{J}_{j,j+1}^{a_j,a_{j+1}}(\mathbf{p}\,|\,\mathbf{q})\;\mathbf{M}_{j,j+1}^{a_j,a_{j+1}}(\mathbf{p}\,|\,\mathbf{q}) \tag{17}$$

which we will refer to as the forward and backward *single interface transfer kernels* between media j and $j+1$, respectively. Our aim is to study reflection from and transmission through the whole system, i.e. we need to relate the field amplitudes in regions 1 and 3 without having to explicitly consider the field amplitudes in region 2. To this end, we have to combine Eq. (12) for $j=1$ and $j=2$ in order to eliminate $\boldsymbol{\mathcal{E}}_2^{\pm}$. A systematic way of doing this, and which can be generalized to an arbitrary number of layers, is presented below. The key observation lies in the fact that one can choose the sign a_{j+1} in Eq. (12) and therefore Eq. (12) contains two vector equations for a given j. For reasons that will soon become clear, the variable $\mathbf{p}$ that appears in Eq. (12) is renamed $\mathbf{p}_2$. By left-multiplying both sides of Eq. (12) taken at $j=1$ by $a_2\,\boldsymbol{\Theta}_{3,2}^{a_3,a_2}(\mathbf{p}\,|\,\mathbf{p}_2)$, where $a_3=\pm$ can be arbitrarily chosen, we obtain

$$\sum_{a_1=\pm} a_2\int \boldsymbol{\Theta}_{3,2}^{a_3,a_2}(\mathbf{p}\,|\,\mathbf{p}_2)\,\boldsymbol{\Theta}_{2,1}^{a_2,a_1}(\mathbf{p}_2\,|\,\mathbf{q})\,\boldsymbol{\mathcal{E}}_1^{a_1}(\mathbf{q})\,\frac{\mathrm{d}^2q}{(2\pi)^2}=\frac{2\sqrt{\epsilon_1\epsilon_2}}{\epsilon_2-\epsilon_1}\,\boldsymbol{\Theta}_{3,2}^{a_3,a_2}(\mathbf{p}\,|\,\mathbf{p}_2)\,\boldsymbol{\mathcal{E}}_2^{a_2}(\mathbf{p}_2)\,.$$

By integrating this equation over $\mathbf{p}_2$ divided by $(2\pi)^2$ and summing over $a_2=\pm$, one obtains that the right-hand-side of the resulting equation is, up to a constant factor, equal to the left-hand-side of Eq. (12) evaluated for $j=2$. In this way we obtain

$$\sum_{a_1=\pm}\int \boldsymbol{\Theta}_{3,1}^{a_3,a_1}(\mathbf{p}\,|\,\mathbf{q})\,\boldsymbol{\mathcal{E}}_1^{a_1}(\mathbf{q})\,\frac{\mathrm{d}^2q}{(2\pi)^2}=a_3\,\frac{4\sqrt{\epsilon_1\epsilon_2^2\epsilon_3}}{(\epsilon_3-\epsilon_2)(\epsilon_2-\epsilon_1)}\,\boldsymbol{\mathcal{E}}_3^{a_3}(\mathbf{p})\,, \tag{18}$$

where the *forward two-interface transfer kernel* $\boldsymbol{\Theta}_{3,1}^{a_3,a_1}(\mathbf{p}|\mathbf{q})$ is defined by the composition rule

$$\boldsymbol{\Theta}_{3,1}^{a_3,a_1}(\mathbf{p}\,|\,\mathbf{q})=\sum_{a_2=\pm} a_2\int \boldsymbol{\Theta}_{3,2}^{a_3,a_2}(\mathbf{p}\,|\,\mathbf{p}_2)\,\boldsymbol{\Theta}_{2,1}^{a_2,a_1}(\mathbf{p}_2\,|\,\mathbf{q})\,\frac{\mathrm{d}^2p_2}{(2\pi)^2}. \tag{19}$$

By a similar method and by the use of Eq. (15), we obtain the backward relation

$$\sum_{a_3=\pm}\int \boldsymbol{\Theta}_{1,3}^{a_1,a_3}(\mathbf{p}\,|\,\mathbf{q})\,\boldsymbol{\mathcal{E}}_3^{a_3}(\mathbf{q})\,\frac{\mathrm{d}^2q}{(2\pi)^2}=a_1\,\frac{4\sqrt{\epsilon_1\epsilon_2^2\epsilon_3}}{(\epsilon_1-\epsilon_2)(\epsilon_2-\epsilon_3)}\,\boldsymbol{\mathcal{E}}_1^{a_1}(\mathbf{p})\,, \tag{20}$$

where the *backward two-interface transfer kernel* $\boldsymbol{\Theta}_{1,3}^{a_1,a_3}(\mathbf{p}|\mathbf{q})$ is defined as

$$\boldsymbol{\Theta}_{1,3}^{a_1,a_3}(\mathbf{p}\,|\,\mathbf{q})=\sum_{a_2=\pm} a_2\int \boldsymbol{\Theta}_{1,2}^{a_1,a_2}(\mathbf{p}\,|\,\mathbf{p}_2)\,\boldsymbol{\Theta}_{2,3}^{a_2,a_3}(\mathbf{p}_2\,|\,\mathbf{q})\,\frac{\mathrm{d}^2p_2}{(2\pi)^2}. \tag{21}$$

Let us now make a few remarks on Eqs. (18) and (19). Eq. (18) is an integral equation of the same form as Eq. (12) but it only relates the field amplitudes in medium 1 and 3. Our aim of eliminating the field amplitudes in the intermediary medium is therefore achieved. However, this comes at a cost since the new transfer kernel $\boldsymbol{\Theta}_{3,1}^{a_3,a_1}(\mathbf{p}\,|\,\mathbf{q})$ is defined as an integral of the product of two single interface kernels

as can be seen in Eq. (19). We will see that this pays off in the case where one of the interfaces is flat, but that the cost can be significant in terms of computational load when both interfaces are rough.

So far, we have stayed general and simply assumed the presence of an electromagnetic field decomposed in propagating and non-propagating waves in each region. Therefore, there is no uniqueness in the solutions to the transfer equations, Eqs. (18) and (20). To ensure a unique solution, one needs to impose some constraints on the field. First, we need to introduce an incident field to our model. This will split the field expansion into a sum of an incident field, which is given by our model of the problem, and a scattered field. Note that within this framework, the incident field may be chosen to be in either medium, or to be a combination of excitations incident from different media. Second, we need to impose the Sommerfeld radiation condition at infinity. This implies that the non-propagating waves are indeed only evanescent waves in the media unbounded in the $\hat{\mathbf{e}}_3$-direction and that the propagating ones are directed outwards.

In our case, the incident field will be taken as a plane wave incident from medium 1 and defined as

$$\mathbf{E}_0(\mathbf{x}) = \left[\mathcal{E}_{0,p}\,\hat{\mathbf{e}}^-_{p,1}(\mathbf{p}_0) + \mathcal{E}_{0,s}\,\hat{\mathbf{e}}_s(\mathbf{p}_0)\right] \exp\left(i\mathbf{k}^-_1(\mathbf{p}_0)\cdot\mathbf{x}\right), \tag{22}$$

where $\mathbf{p}_0$ is the projection of the incident wave's wave vector in the $(\hat{\mathbf{e}}_1, \hat{\mathbf{e}}_2)$ plane, with the property $|\mathbf{p}_0| \leq \sqrt{\epsilon_1}\,\omega/c$, i.e. we consider an incident propagating wave. The fact that this is the only incident wave considered, together with the Sommerfeld radiation condition at infinity, gives, apart from the incident field, that the only elementary waves allowed in the scattered field are those with wave vectors of the form $\mathbf{k}^+_1(\mathbf{p})$ and $\mathbf{k}^-_3(\mathbf{p})$ in medium 1 and 3, respectively. This property can be expressed by defining the field amplitudes

$$\boldsymbol{\mathcal{E}}^-_1(\mathbf{q}) = (2\pi)^2\,\delta(\mathbf{q}-\mathbf{p}_0)\,\boldsymbol{\mathcal{E}}_0\,, \tag{23a}$$

$$\boldsymbol{\mathcal{E}}^+_3(\mathbf{q}) = \mathbf{0}\,, \tag{23b}$$

where $\boldsymbol{\mathcal{E}}_0 = (\mathcal{E}_{0,p}, \mathcal{E}_{0,s})^{\mathrm{T}}$. Next, we assume that the scattered field amplitudes are linearly related to the incident field amplitude $\boldsymbol{\mathcal{E}}_0$ via the reflection and transmission amplitudes, $\mathbf{R}(\mathbf{q}\,|\,\mathbf{p}_0)$ and $\mathbf{T}(\mathbf{q}\,|\,\mathbf{p}_0)$, defined as

$$\boldsymbol{\mathcal{E}}^+_1(\mathbf{q}) = \mathbf{R}(\mathbf{q}|\mathbf{p}_0)\boldsymbol{\mathcal{E}}_0, \tag{24a}$$

$$\boldsymbol{\mathcal{E}}^-_3(\mathbf{q}) = \mathbf{T}(\mathbf{q}|\mathbf{p}_0)\boldsymbol{\mathcal{E}}_0. \tag{24b}$$

The reflection and transmission amplitudes are therefore described by 2×2 matrices, i.e. for $\mathbf{X} = \mathbf{R}$ or $\mathbf{T}$

$$\mathbf{X} = \begin{pmatrix} X_{pp} & X_{ps} \\ X_{sp} & X_{ss} \end{pmatrix}. \tag{25}$$

From a physical point of view, the coefficient $R_{\alpha\beta}(\mathbf{q}|\mathbf{p}_0)$ (resp. $T_{\alpha\beta}(\mathbf{q}|\mathbf{p}_0)$) for $\alpha, \beta \in \{p, s\}$ is the field amplitude for the reflected (resp. transmitted) light with lateral wave vector $\mathbf{q}$ in the polarization state α from a unit incident field with lateral wave vector $\mathbf{p}_0$ in the polarization state β. The reflection and transmission amplitudes are then the unknowns in our scattering problem. The equations we need to solve are deduced from the general equations Eqs. (18) and (20) by applying them respectively at $a_3 = +$ and $a_1 = -$ and by using Eqs. (23) and (24) for the model of the field expansion. This yields the following two decoupled integral equations for the reflection or transmission amplitudes, the so-called reduced Rayleigh equations, that can be written in the following general form, for $\mathbf{X} = \mathbf{R}$ or $\mathbf{T}$ [15]

$$\int \mathbf{M}_{\mathbf{X}}(\mathbf{p}|\mathbf{q})\,\mathbf{X}(\mathbf{q}|\mathbf{p}_0)\frac{\mathrm{d}^2q}{(2\pi)^2} = -\mathbf{N}_{\mathbf{X}}(\mathbf{p}|\mathbf{p}_0)\,, \tag{26}$$

where the matrices $\mathbf{M}_{\mathbf{X}}$ and $\mathbf{N}_{\mathbf{X}}$ are given by

$$\mathbf{M}_{\mathbf{R}}(\mathbf{p}|\mathbf{q}) = \boldsymbol{\Theta}^{+,+}_{3,1}(\mathbf{p}|\mathbf{q}) \tag{27a}$$

$$\mathbf{M}_{\mathbf{T}}(\mathbf{p}|\mathbf{q}) = \boldsymbol{\Theta}^{-,-}_{1,3}(\mathbf{p}|\mathbf{q}) \tag{27b}$$

$$\mathbf{N_R}(\mathbf{p}|\mathbf{q}) = \Theta_{3,1}^{+,-}(\mathbf{p}|\mathbf{q}) \tag{27c}$$

$$\mathbf{N_T}(\mathbf{p}|\mathbf{q}) = \frac{4\sqrt{\epsilon_1\epsilon_2^2\epsilon_3}}{(\epsilon_1-\epsilon_2)(\epsilon_2-\epsilon_3)}\,(2\pi)^2\,\delta(\mathbf{p}-\mathbf{q})\,\mathbf{I}_2, \tag{27d}$$

with $\mathbf{I}_2$ denoting the 2×2 identity matrix. In the cases where only one interface is rough and the other interface is planar, the complexity associated with the transfer kernels is equivalent to that of a single rough interface separating two media. For instance, if the second interface is planar and the first interface is rough, we can choose the origin of the coordinate system such that $\zeta_2(\mathbf{x}_\parallel) = d_2 = 0$, and Eq. (14) yields, for $l, m \in \{2, 3\}$ and $l \neq m$,

$$\mathcal{J}_{l,m}^{b,a}(\mathbf{p}\,|\,\mathbf{q}) = \frac{(2\pi)^2\,\delta(\mathbf{p}-\mathbf{q})}{b\alpha_l(\mathbf{p}) - a\alpha_m(\mathbf{q})}. \tag{28}$$

The Dirac distribution then simplifies the wave vector integration present in the two-interface transfer kernels and one gets

$$\Theta_{3,1}^{a_3,a_1}(\mathbf{p}\,|\,\mathbf{q}) = \sum_{a_2=\pm} a_2\,\frac{\mathbf{M}_{3,2}^{a_3,a_2}(\mathbf{p}\,|\,\mathbf{p})\,\Theta_{2,1}^{a_2,a_1}(\mathbf{p}\,|\,\mathbf{q})}{\alpha_3(\mathbf{p})\,[a_3\alpha_3(\mathbf{p}) - a_2\alpha_2(\mathbf{p})\,]}, \tag{29a}$$

and

$$\Theta_{1,3}^{a_1,a_3}(\mathbf{p}\,|\,\mathbf{q}) = \sum_{a_2=\pm} a_2\,\frac{\Theta_{1,2}^{a_1,a_2}(\mathbf{p}\,|\,\mathbf{q})\,\mathbf{M}_{2,3}^{a_2,a_3}(\mathbf{q}\,|\,\mathbf{q})}{\alpha_2(\mathbf{q})\,[a_2\alpha_2(\mathbf{q}) - a_3\alpha_3(\mathbf{q})\,]}. \tag{29b}$$

If the first interface is planar and the second interface rough, we can choose the origin of the coordinate system such that $\zeta_1(\mathbf{x}_\parallel) = d_1 = 0$, and Eq. (28) holds for $l, m \in \{1, 2\}$ and $l \neq m$, and the two-interface transfer kernels read

$$\Theta_{3,1}^{a_3,a_1}(\mathbf{p}\,|\,\mathbf{q}) = \sum_{a_2=\pm} a_2\,\frac{\Theta_{3,2}^{a_3,a_2}(\mathbf{p}\,|\,\mathbf{q})\,\mathbf{M}_{2,1}^{a_2,a_1}(\mathbf{q}\,|\,\mathbf{q})}{\alpha_2(\mathbf{q})\,[a_2\alpha_2(\mathbf{q}) - a_1\alpha_1(\mathbf{q})\,]}, \tag{30a}$$

and

$$\Theta_{1,3}^{a_1,a_3}(\mathbf{p}\,|\,\mathbf{q}) = \sum_{a_2=\pm} a_2\,\frac{\mathbf{M}_{1,2}^{a_1,a_2}(\mathbf{p}\,|\,\mathbf{p})\,\Theta_{2,3}^{a_2,a_3}(\mathbf{p}\,|\,\mathbf{q})}{\alpha_1(\mathbf{p})\,[a_1\alpha_1(\mathbf{p}) - a_2\alpha_2(\mathbf{p})\,]}. \tag{30b}$$

3.2. Observables

The observable of interest in this study is the so-called incoherent (or diffuse) component of the *mean differential reflection coefficient* (DRC) that we denote $\langle \partial R_{\alpha\beta}(\mathbf{p}|\mathbf{p}_0)/\partial\Omega_s\rangle_{\text{incoh}}$. It is defined as the ensemble average over realizations of the surface profile function of the incoherent component of the radiated reflected flux of an α-polarized wave around direction $\hat{\mathbf{k}}_1^+(\mathbf{p})$, per unit incident flux of a β-polarized plane wave of wave vector $\mathbf{k}_1^-(\mathbf{p}_0)$, and per unit solid angle. The precise mathematical definition and the derivation of the expression for the mean DRC as a function of the reflection amplitudes is given in Appendix B.

4. Numerical methods

Solutions of the reduced Rayleigh equation, Eq. (26), are obtained via both a perturbative and a non-perturbative numerical approach. In this work we investigate systems with two interfaces; For the case when one of these interfaces is planar we are able to employ both approaches, but when both interfaces are rough we will exclusively use the perturbative approach due to the high computational cost of the non-perturbative approach.

4.1. Perturbative method

The approximated solution of Eq. (26) for the reflection amplitudes, and to first order in product of surface profiles, obtained by small amplitude perturbation theory (SAPT) is derived in Appendix A and given by

$$\mathbf{R}(\mathbf{p} \mid \mathbf{p}_0) \approx \mathbf{R}^{(0)}(\mathbf{p} \mid \mathbf{p}_0) - i\mathbf{R}^{(1)}(\mathbf{p} \mid \mathbf{p}_0)\,, \tag{31a}$$

$$\mathbf{R}^{(1)}(\mathbf{p} \mid \mathbf{p}_0) = \hat{h}_1(\mathbf{p} - \mathbf{p}_0)\boldsymbol{\rho}_1(\mathbf{p} \mid \mathbf{p}_0) + \hat{h}_2(\mathbf{p} - \mathbf{p}_0)\boldsymbol{\rho}_2(\mathbf{p} \mid \mathbf{p}_0). \tag{31b}$$

Here $\mathbf{R}^{(0)}(\mathbf{p} \mid \mathbf{p}_0)$ is the response from the corresponding system with planar interfaces (i.e. that of a Fabry–Perot interferometer), $\hat{h}_j$ are the Fourier transforms of the stochastic component of the surface profiles and $\boldsymbol{\rho}_j(\mathbf{p} \mid \mathbf{p}_0)$ are matrix-valued amplitudes depending *only* on the mean film thickness, the dielectric constants of all media and the wave vectors of incidence and scattering. The explicit expressions for these matrices are given in Appendix A (see Eq. (A.20)). The corresponding expression for the incoherent component of the mean differential reflection coefficient reads Appendices A and B

$$\left\langle \frac{\partial R_{\alpha\beta}(\mathbf{p}|\mathbf{p}_0)}{\partial \Omega_s} \right\rangle_{\text{incoh}} = \epsilon_1 \left(\frac{\omega}{2\pi c}\right)^2 \frac{\cos^2\theta_s}{\cos\theta_0}\, g(\mathbf{p} - \mathbf{p}_0)\Big[\sigma_1^2\, |\rho_{1,\alpha\beta}(\mathbf{p} \mid \mathbf{p}_0)|^2 + \sigma_2^2\, |\rho_{2,\alpha\beta}(\mathbf{p} \mid \mathbf{p}_0)|^2 + 2\gamma\sigma_1\sigma_2\, \mathrm{Re}\left\{\rho_{1,\alpha\beta}(\mathbf{p} \mid \mathbf{p}_0)\rho^*_{2,\alpha\beta}(\mathbf{p} \mid \mathbf{p}_0)\right\}\Big]\,, \tag{32}$$

where the wave vectors

$$\mathbf{p} = \sqrt{\epsilon_1}\frac{\omega}{c}\sin\theta_s(\cos\phi_s\,\hat{\mathbf{e}}_1 + \sin\phi_s\,\hat{\mathbf{e}}_2) \tag{33a}$$

and

$$\mathbf{p}_0 = \sqrt{\epsilon_1}\frac{\omega}{c}\sin\theta_0(\cos\phi_0\,\hat{\mathbf{e}}_1 + \sin\phi_0\,\hat{\mathbf{e}}_2) \tag{33b}$$

are defined in terms of the angles of scattering (θ_s, ϕ_s) and incidence (θ_0, ϕ_0), respectively [see Fig. 1]. The three terms present in the angular brackets of Eq. (32) can be interpreted as follows. The term containing $\sigma_1^2\, |\rho_{1,\alpha\beta}(\mathbf{p} \mid \mathbf{p}_0)|^2$ (resp. $\sigma_2^2\, |\rho_{2,\alpha\beta}(\mathbf{p} \mid \mathbf{p}_0)|^2$) corresponds to the contribution to the diffuse intensity of the associated system for which the first (resp. second) interface would be rough and the other planar. Indeed, this would be the only remaining term if we were to set $\sigma_2 = 0$ (resp. $\sigma_1 = 0$) in Eq. (32). The sum of the two first terms would correspond to the sum of intensity of the aforementioned associated systems, which would be the expected overall response if the two interface *were not* correlated, i.e. if $\gamma = 0$. The last term in Eq. (32), which does not vanish for $\gamma \neq 0$, can be interpreted physically as taking into account the interference between paths resulting from single scattering events on the top interface and those resulting from single scattering events on the bottom interface. Note that this last term, in contrast to the two first, may take positive *and* negative values as the incident and scattering wave vectors are varied, and hence may result in cross-correlation induced constructive and destructive interference. It is clear from the derivation, however, that the overall incoherent component of the mean differential coefficient remains non-negative, as is required for any intensity.

4.2. Nonperturbative method

Solutions of Eq. (26) were also obtained in a rigorous, purely numerical, nonperturbative manner according to the method described in detail in Ref. [16]; only a brief summary of the method is presented here. This method has previously been used for the investigations of the two-dimensional rough surface scattering of light from metallic or perfectly conducting surfaces [16–18]; from and through single dielectric interfaces [17,19,20] and film geometries [21–23]. In this method, an ensemble of realizations of the surface profile function $\zeta_j(\mathbf{x}_\parallel)$ is generated by the use of the Fourier filtering method [24] on a square grid of $N_x \times N_x$ surface points, covering an area of $S = L^2$ in the $(\hat{\mathbf{e}}_1, \hat{\mathbf{e}}_2)$-plane. The integral equation, Eq. (26), is solved numerically with finite limits $\pm Q$ and

discretization $\Delta q = 2\pi/L$ with $N_q \times N_q$ points in wave vector space according to the Nyquist sampling theorem given the spatial discretization of the surface. On evaluating the kernel scalar factors $\mathcal{J}_{l,m}^{b,a}(\mathbf{p}\,|\,\mathbf{q})$, defined in Eq. (14), we first expand the integrand in powers of $\zeta_j(\mathbf{x}_\parallel)$, truncate this expansion after 20 terms, and integrate the resulting sum term-by-term. The Fourier integral of $\zeta_j^n(\mathbf{x}_\parallel)$ that remains now only depends on the surface profile function and the difference in lateral wave vectors $\mathbf{p}-\mathbf{q}$, and not on $\alpha_l(\mathbf{p})$ and $\alpha_m(\mathbf{q})$. These Fourier integrals are therefore calculated only once, on a $\mathbf{p}-\mathbf{q}$ grid, for every surface realization by the use of the fast Fourier transform. The resulting matrix equations are then solved by LU factorization and back substitution, using the ScaLAPACK library [25]. This process is repeated for a large number N_p of realizations of the surface profile function, enabling the calculation of the ensemble averaged observables of interest; like the mean DRC.

It remains to mention that Eqs. (29) and (30), giving the transfer kernels in the case where only one of the interfaces is rough and the other planar, have been written in a rather compact form. Numerically, these expressions tend to lead to instabilities due to factors of the form $\exp(-i\alpha_2(\mathbf{q})d)$ or $\exp(-i\alpha_2(\mathbf{p})d)$ which grow for evanescent waves inside the film. This technical issue is resolved by using the following two ideas: (i) expanding the two terms in the kernels (i.e. for $a_2 = \pm$) and factorizing out the troublesome exponential factor and canceling it on both sides of the reduced Rayleigh equation (if the exponential factor is a function of the variable $\mathbf{p}$) or (ii) making a change of variable such that the troublesome exponential factor is absorbed into the reflection or transmission amplitudes (if the exponential factor is a function of the variable $\mathbf{q}$). One may also shift the x_3-axis in order to facilitate the aforementioned steps. We chose here not to give more details on the explicit implementation, as these modifications are to be done in a case by case basis depending on which surface is planar and whether the reflected or transmitted light is considered.

5. Results and discussion

5.1. Single rough interface

As a direct comparison between results obtained by the perturbative and nonperturbative solutions of Eq. (26), Fig. 2 shows the angular distributions of the co-polarized ($\alpha = \beta$) incoherent contribution to the mean DRC for light incident from vacuum ($\epsilon_1 = 1$) that is reflected diffusively into the plane of incidence (i.e. $|\hat{\mathbf{p}} \cdot \hat{\mathbf{p}}_0| = 1$) from a randomly rough dielectric film (photoresist, $\epsilon_2 = 2.69$) deposited on a silicon substrate ($\epsilon_3 = 15.08 + 0.15i$) for the cases where only one of the interfaces is rough and the other planar. Results for the case where only the top interface (the interface facing the medium of incidence) is rough ($\sigma_2 = 0$) and where only the bottom interface is rough ($\sigma_1 = 0$) are shown in Figs. 2(a)–(b) and (c)–(d), respectively. Light was incident on the dielectric film from the vacuum side in the form of a plane wave of wavelength $\lambda = 632.8$ nm with angles of incidence $(\theta_0, \phi_0) = (16.8°, 0°)$. The two interfaces were characterized by rms-roughness $\sigma_1 = \lambda/30, \sigma_2 = 0$ [Figs. 2(a)–(b)] or $\sigma_1 = 0, \sigma_2 = \lambda/30$ [Figs. 2(c)–(d)], correlation length $a = \lambda/3$, and the film thickness was assumed to be $d = 8\lambda \approx 5\ \mu$m. The scattering system was chosen in order to highlight the interference phenomena and to purposely deviate from the more historically typical scattering system of a dielectric film on a perfect electric conductor. The dashed curves in Fig. 2 display the results of computations of the perturbative solution of the RRE, Eq. (32), to leading order, while the solid curves in Fig. 2 show the non-perturbative solutions of the RRE, Eq. (26). In obtaining these latter results the following parameters, defined in Section 4.2, were used: $N_x = 449$, $L = 45\lambda$, $N_q = 225$ and $N_p = 325$, implying integration limits in wavevector space $Q = \pm 2.5\omega/c$. Since these non-perturbative results for the mean DRC are obtained through an ensemble average over a finite number of surface realizations, they are less smooth than their perturbative counterparts, for which the averaging is performed analytically. Using a larger number of surface realizations in obtaining the ensemble average would have produced smoother results, but we have chosen not to do so here due to the high associated computational cost.

Figs. 2(a)–(b) show excellent agreement between the results for the mean DRC obtained by the analytical perturbative method and the corresponding results obtained by a full solution of the RRE for the chosen parameters for the case where only the upper interface is rough. In particular, the fringes observed in these figures are consistently predicted by both calculation methods for the set

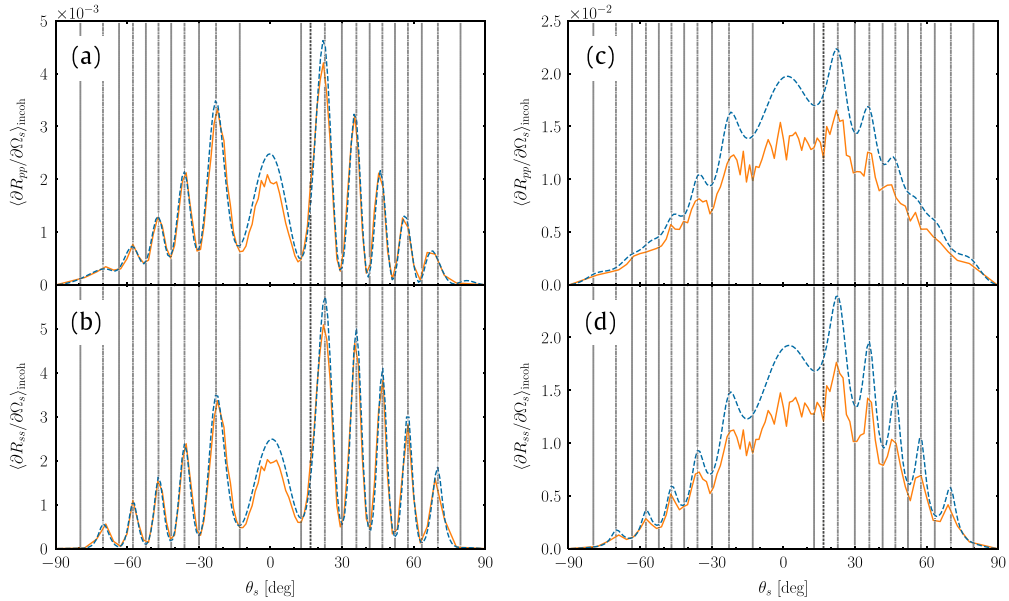

Fig. 2. Incoherent components of the mean DRCs for in-plane co-polarized scattering as functions of the polar angle of scattering, θ_s (note the convention $\theta_s < 0$ for $\phi_s = \phi_0 + 180°$). The light of wavelength $\lambda = 632.8$ nm was incident from vacuum on the rough photoresist film supported by a silicon substrate [$\epsilon_1 = 1.0, \epsilon_2 = 2.69, \epsilon_3 = 15.08 + 0.15i$]. The surface-height correlation length of the rough Gaussian correlated surface was $a = \lambda/3$, the mean film thickness was $d = 8\lambda$, and the angles of incidence were $(\theta_0, \phi_0) = (16.8°, 0°)$ in all cases. Panels (a) and (b) correspond to cases where only the top interface was rough, while panels (c) and (d) present the results for a film where only the bottom interface of the film is rough. In both cases, the rms-roughness of the rough interface was set to $\sigma = \lambda/30$. The results obtained on the basis of the non-perturbative method are shown as solid lines while those obtained with the perturbative method, Eq. (32), are shown as dashed lines. The position of the specular direction in reflection is indicated by the vertical dashed lines. The vertical dash-dotted and dotted lines indicate the angular positions of the maxima and minima predicted by Eq. (36), respectively.

of parameters assumed and their angular positions agree well with the expected angular positions (dashed–dotted vertical lines in Figs. 2(a)–(b)). When the lower surface is rough, the results presented in Figs. 2(c)–(d) show that the agreement between the two calculation methods is still satisfactory, but a larger discrepancy between them is now observed relative to what was found when the upper surface was rough. This larger discrepancy might be due to the fact that the error between the perturbative solution and the exact solution grows with the ratio of the dielectric constants of the media that are separated by the rough interface. Since the dielectric contrast between the silicon substrate and the photoresist film is larger than that between the photoresist film and vacuum, the corresponding error is also larger. Since the perturbative method is employed only to leading order, these agreements overall indicate that the physical phenomena that give rise to the scattered intensity distributions are well approximated as single scattering phenomena, at least for weakly rough surfaces.

We identify the interference fringes in Fig. 2 as in-plane scattering distributions of Selényi rings [9]. These rings are known to be centered around the mean surface normal, with their *angular position* being independent of the angle of incidence. Their *amplitude*, however, is modulated by the angle of incidence. This can indeed be observed if we vary the angle of incidence and record the resulting in-plane co-polarized angular scattering distributions, presented as contour plots in the first two columns of Fig. 3. Figs. 3(a)–(b) present, for *p*-polarized light, contour plots of the (θ_0, θ_s) dependence of the in-plane co-polarized incoherent component of the mean DRC when the top or bottom interface of the film is rough, respectively. Similar results but for *s*-polarized light are presented in Figs. 3(f)–(g). For both configurations, the co-polarized incoherent component of the mean DRC exhibits maxima that occur on a regular grid of (θ_0, θ_s)-points for *s*-polarized light [Figs. 3(f)–(g)]. A similar pattern

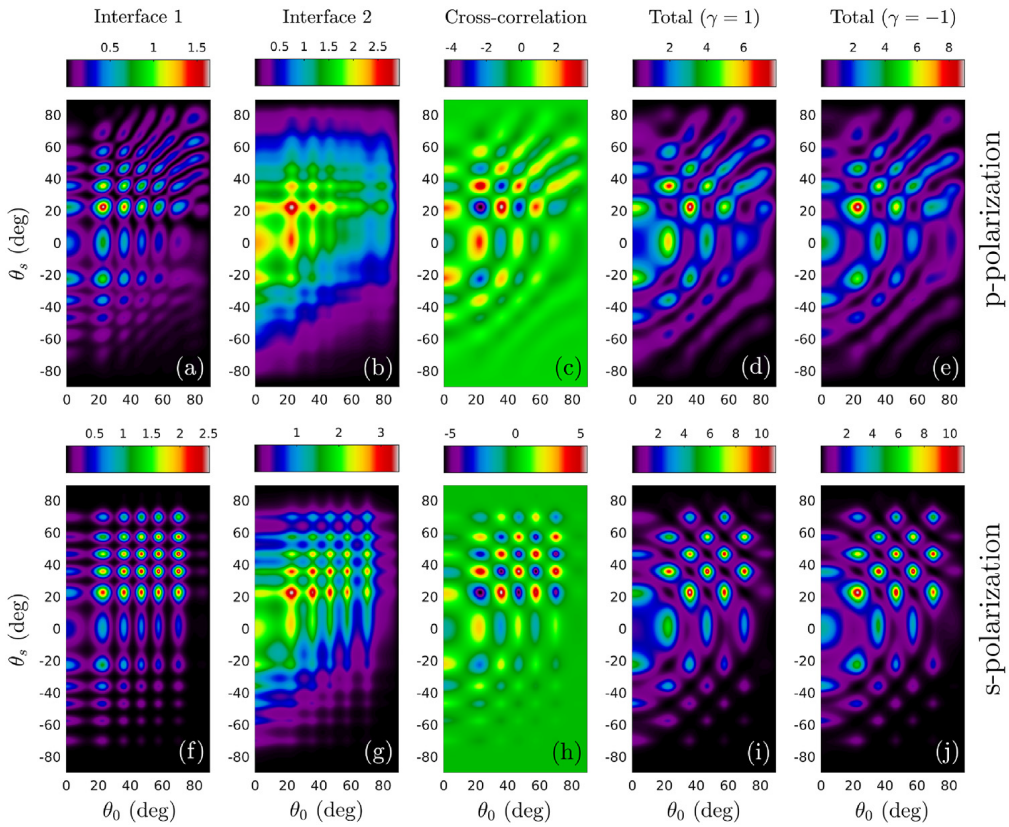

Fig. 3. Scaled incoherent component of the mean DRCs for in-plane co-polarized scattering, $100 \times \langle \partial R_{\alpha\alpha} / \partial \Omega_s \rangle_{\text{incoh}}$, as functions of the polar angle of incidence θ_0 and the polar angle of scattering θ_s obtained on the basis of Eq. (32). The first row of sub-figures [Figs. 3(a)–(e)] corresponds to *p*-polarized light (as marked in the figure), while the second row [Figs. 3(f)–(j)] corresponds to *s*-polarized light. These results were obtained under the assumption that the wavelength in vacuum was $\lambda = 632.8$ nm, the mean film thickness was $d = 8\lambda$., and the dielectric constants of the media were $\epsilon_1 = 1.0$, $\epsilon_2 = 2.69$, $\epsilon_3 = 15.08 + 0.15i$. The rms-roughness of the rough interfaces of the film were assumed to be $\sigma_1 = \sigma_2 = \lambda/30$, and the Gaussian correlation functions were characterized by the correlation length $a = \lambda/3$. The first column of sub-figures presents contour plots of the mean DRCs for a film geometry where only the top interface of the film is rough and the bottom interface planar. The second column shows similar results when the top film interface is planar and the bottom film interface is rough. In the third column, contour plots of *only* the cross-correlation term in Eq. (32) – that is, the contribution to the mean DRC produced by the last term in the square brackets of this equation – are depicted assuming a perfect correlation [$\gamma = 1$] between the rough top and rough bottom interface of the film. Finally, in the fourth and fifth column, contour plots of the total mean DRCs obtained on the basis of Eq. (32) are presented for two-rough-interface film geometries characterized by $\gamma = 1$ and $\gamma = -1$, respectively.

is observed for *p*-polarized light in Figs. 3(a)–(b), although the grid of maxima appears to lose some of its regularity for the larger polar angles of incidence and scattering [Figs. 3(a)–(b)]. We speculate that this is due to a Brewster effect, both in its traditional sense and through the Brewster scattering angles [19,20,26], but we will not delve further on this behavior here. In addition, by comparing the results presented in Figs. 2, 3(a)–(b), and 3(f)–(g), we note that the contrast in the interference pattern is better for the configurations where the top interface is rough than for those where the bottom interface is rough. In the following we will explain these observations in terms of a single scattering model which is an extension of the model previously proposed by Lu and co-workers [4].

Lu et al. suggested that, for sufficiently small roughness, the main effect of the rough interface is to produce scattered waves that cover a wide range of scattering angles both inside and outside the film, and the film may then be considered to approximate a planar waveguide for subsequent reflections and refractions within the film. This claim is supported by the observed agreement between the

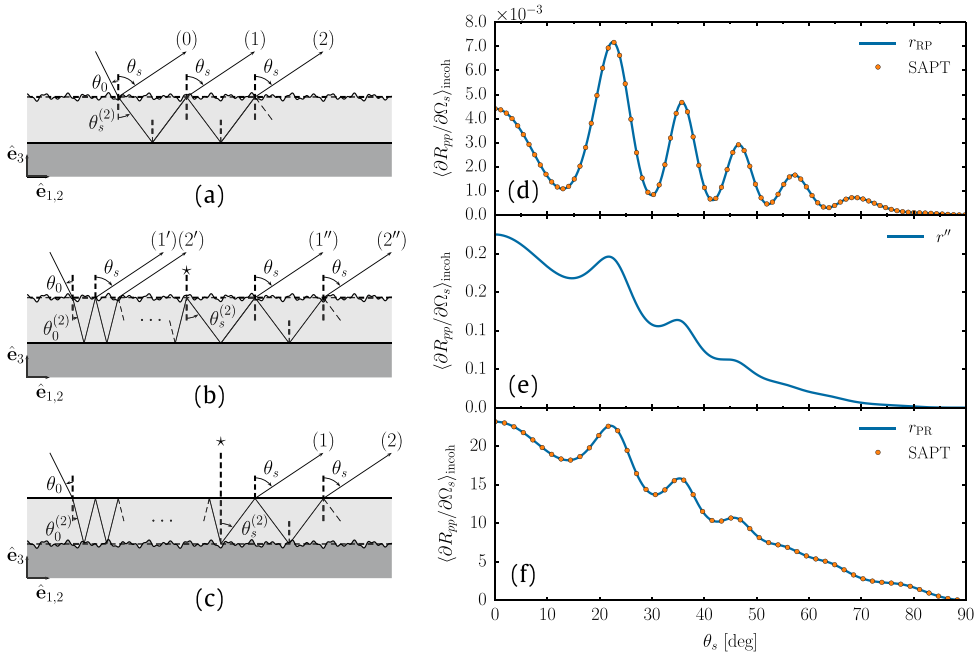

Fig. 4. Sketch of the optical paths involved in the single scattering model in the case of scattering from the top surface (a) and (b), or from the bottom interface (c). Incoherent component of the mean differential reflection coefficient for in-plane co-polarized scattering as a function of the polar angle of scattering for normal incidence for *p*-polarization (d) to (f). Apart from the angle of incidence the remaining parameters are the same as those from Fig. 2. In panels (d) and (f), the results were obtained from SAPT (circles), and from the single scattering model Eqs. (40)(d) and (41)(e) (solid line) respectively for the cases illustrated in (a–b) and (c). In panel (e), only the contribution of r'' (Eq. (39)) to the incoherent component of the mean DRC is shown.

mean DRC distributions obtained through the perturbative solution to leading order, whose physical interpretation is to take only single scattering events into account, and the full solutions of the RRE in Fig. 2, since the latter method allows for the full range of multiple scattering events. As the incident light interacts with the rough interface, whether it is located at the top or bottom interface, multiple wave components are generated in the film. These waves then undergo multiple specular reflections within the film while also being partially refracted back into the medium of incidence. Since Lu et al. only investigated the case where the rough interface is on top, their results were adequately explained under the assumption that the incident light was scattered by the rough interface during its first encounter with the interface. However, a more detailed analysis of the possible optical paths in the system is necessary in order to fully understand the case where the rough interface is at the bottom of the film, as illustrated by the more complete depiction of optical paths in Figs. 4(a)–(c). We will now analyze the different optical paths involving a single scattering event in the two configurations in more detail, and also construct a model for the resulting reflection amplitudes. Let $r_{ji}(\mathbf{p} \mid \mathbf{p}_0)$ and $t_{ji}(\mathbf{p} \mid \mathbf{p}_0)$ denote the reflection and transmission amplitudes obtained by small amplitude perturbation theory to first order in the surface profile separating *two* media with dielectric constants ϵ_i and ϵ_j (with the incident wave in medium i). Note that these amplitudes are different from those obtained for the full system considered in this paper. The expressions for these reflection amplitudes can be found e.g. in Refs. [19,20]. Moreover, let $r_{ji}^{(\mathrm{F})}(\mathbf{p})$ and $t_{ji}^{(\mathrm{F})}(\mathbf{p})$ represent the corresponding Fresnel amplitudes. All the amplitudes considered here may represent either *p*-polarization or *s*-polarization as we treat in-plane co-polarized scattering for simplicity.

In the case where only the top interface is rough the scattering event may occur on the first intersection between the path and the top interface, yielding a reflected scattered path denoted (0) in Fig. 4(a). Alternatively, on the first intersection the scattering event may yield a refracted (and

scattered) wave in the film. Since the single scattering event allowed in our analysis has then occurred, subsequent reflections within the film and refractions through the top interface are treated according to Snell's law of reflection and refraction, resulting in the paths denoted (1) and (2) (and so on) in Fig. 4(a). With each such non-scattering interaction with an interface, the reflection/transmission amplitude associated with the path is given by the Fresnel amplitude. Following the different paths depicted in Fig. 4(a) and summing the corresponding (partial) reflection amplitudes we obtain the following reflection amplitude:

$$\begin{aligned} r(\mathbf{p}|\mathbf{p}_0) &= r_{21}(\mathbf{p}|\mathbf{p}_0) + t_{12}^{(\mathrm{F})}(\mathbf{p})\, r_{32}^{(\mathrm{F})}(\mathbf{p})\, t_{21}(\mathbf{p}|\mathbf{p}_0) \exp(2i\varphi_s) \sum_{n=0}^{\infty} \left[r_{12}^{(\mathrm{F})}(\mathbf{p})\, r_{32}^{(\mathrm{F})}(\mathbf{p})\, \exp(2i\varphi_s) \right]^n \\ &= r_{21}(\mathbf{p}|\mathbf{p}_0) + \frac{t_{12}^{(\mathrm{F})}(\mathbf{p})\, r_{32}^{(\mathrm{F})}(\mathbf{p})\, t_{21}(\mathbf{p}|\mathbf{p}_0)\, \exp(2i\varphi_s)}{1 - r_{12}^{(\mathrm{F})}(\mathbf{p})\, r_{32}^{(\mathrm{F})}(\mathbf{p}) \exp(2i\varphi_s)}\,, \end{aligned} \tag{34}$$

where $\varphi_s = 2\pi\sqrt{\epsilon_2}d\cos\theta_s^{(2)}/\lambda$. The positions of the maxima in the resulting angular intensity distribution $|r(\mathbf{p}|\mathbf{p}_0)|^2$ are consistent with the predictions given by Lu et al. [4]. The difference in optical path length between path (0) and (1), and between (1) and (2), and more generally between two such consecutive paths, can be expressed as

$$\Delta = 2\sqrt{\epsilon_2}d\cos\theta_s^{(2)}, \tag{35}$$

where θ_s in the vacuum is related to $\theta_s^{(2)}$ in the film by $\sqrt{\epsilon_2}\sin\theta_s^{(2)} = \sqrt{\epsilon_1}\sin\theta_s$ according to Snell's law. The polar angles of scattering for which the diffusely scattered intensity has local maxima are given by

$$\frac{2\pi\sqrt{\epsilon_2}d}{\lambda}\,\cos\theta_s^{(2)} = \frac{2\pi d}{\lambda}\left(\epsilon_2 - \epsilon_1\sin^2\theta_s\right)^{1/2} = (\nu + 1/2)\pi\,, \tag{36a}$$

while the positions of the minima are determined from the relation

$$\frac{2\pi\sqrt{\epsilon_2}d}{\lambda}\,\cos\theta_s^{(2)} = \frac{2\pi d}{\lambda}\left(\epsilon_2 - \epsilon_1\sin^2\theta_s\right)^{1/2} = \nu\pi\,, \tag{36b}$$

where $\nu \in \mathbb{Z}$. The angular positions of the maxima and minima predicted by Eq. (36) are indicated by vertical dash-dotted and dotted vertical lines, respectively, in Fig. 2, and these predictions agree well with the maxima and minima that can be observed in the in-plane co-polarized mean DRC. Equation (36) does not depend on the polar angle of incidence θ_0, which supports the observation that the positions of the maxima and minima of the incoherent components of the mean DRC do not move with angle of incidence for weakly rough films. However, the modulation of the fringes with the angle of incidence cannot be explained if we consider solely the paths depicted in Fig. 4(a). Indeed, additional paths involving a single scattering event may be drawn as illustrated in Fig. 4(b). It is possible for the incident path not to experience a scattering event when it encounters the top interface for the first time, and it may also bounce within the film an arbitrary number of times before it experiences a scattering event while finally being refracted into the vacuum. Such paths are denoted (1′) and (2′) in Fig. 4(b). The resulting (partial) reflection amplitude corresponding to the "single-primed" paths in Fig. 4(b) reads

$$\begin{aligned} r'(\mathbf{p}|\mathbf{p}_0) &= t_{12}(\mathbf{p}|\mathbf{p}_0)\, r_{32}^{(\mathrm{F})}(\mathbf{p}_0)\, t_{21}^{(\mathrm{F})}(\mathbf{p}_0) \exp(2i\varphi_0) \sum_{n=0}^{\infty} \left[r_{12}^{(\mathrm{F})}(\mathbf{p}_0)\, r_{32}^{(\mathrm{F})}(\mathbf{p}_0)\, \exp(2i\varphi_0) \right]^n \\ &= \frac{t_{12}(\mathbf{p}|\mathbf{p}_0)\, r_{32}^{(\mathrm{F})}(\mathbf{p}_0)\, t_{21}^{(\mathrm{F})}(\mathbf{p}_0) \exp(2i\varphi_0)}{1 - r_{12}^{(\mathrm{F})}(\mathbf{p}_0)\, r_{32}^{(\mathrm{F})}(\mathbf{p}_0)\, \exp(2i\varphi_0)}, \end{aligned} \tag{37}$$

where $\varphi_0 = 2\pi\sqrt{\epsilon_2}d\cos\theta_0^{(2)}/\lambda$. The difference in optical path length between path (1′) and (2′) is given by

$$\Delta = 2\sqrt{\epsilon_2}d\cos\theta_0^{(2)}, \tag{38}$$

where $\sqrt{\epsilon_2}\sin\theta_0^{(2)} = \sqrt{\epsilon_1}\sin\theta_0$ according to Snell's law. Hence, we again obtain a series of maxima and minima in the mean DRC if we replace $\theta_s^{(2)}$ by $\theta_0^{(2)}$ in Eq. (36), but this time the positions of the maxima and minima are indeed a function of the polar angle of incidence θ_0. This interference phenomenon serves to modulate the intensity of the Selényi interference patterns. The static fringe pattern and the modulation introduced by the angle of incidence is clearly observed in the in-plane scattered intensities displayed in Fig. 3(a) and (f). However, we still have more optical paths to take into account. Indeed, paths yielding outgoing paths of type (1′) and (2′) may experience a scattering event while being reflected on the top surface instead of being refracted into the vacuum. Such a scattering event is indicated by the star in Fig. 4(b), and thereon the path may be reflected within the film an arbitrary number of times before being refracted into the vacuum as depicted by the paths denoted (1″) and (2″) in Fig. 4(b). In order to obtain the reflection amplitudes corresponding to all such paths, it suffices to multiply the overall reflection amplitude for *all* paths bouncing *any* arbitrary number of times with an angle $\theta_0^{(2)}$ within the film before the scattering event, with the overall reflection amplitude of *all* paths starting from the scattering event and bouncing *any* number of times within the film before being refracted into the vacuum. In this way we obtain the reflection amplitude

$$\begin{aligned} r''(\mathbf{p}|\mathbf{p}_0) &= t_{21}^{(\mathrm{F})}(\mathbf{p}_0)\, r_{32}^{(\mathrm{F})}(\mathbf{p}_0)\, \exp(2i\varphi_0) \sum_{n=0}^{\infty} \left[r_{12}^{(\mathrm{F})}(\mathbf{p}_0)\, r_{32}^{(\mathrm{F})}(\mathbf{p}_0)\, \exp(2i\varphi_0) \right]^n \\ &\quad \times t_{12}^{(\mathrm{F})}(\mathbf{p})\, r_{32}^{(\mathrm{F})}(\mathbf{p})\, r_{12}(\mathbf{p}|\mathbf{p}_0)\, \exp(2i\varphi_s) \sum_{n'=0}^{\infty} \left[r_{12}^{(\mathrm{F})}(\mathbf{p})\, r_{32}^{(\mathrm{F})}(\mathbf{p})\, \exp(2i\varphi_s) \right]^{n'} \\ &= \frac{t_{12}^{(\mathrm{F})}(\mathbf{p})\, r_{32}^{(\mathrm{F})}(\mathbf{p})\, r_{12}(\mathbf{p}|\mathbf{p}_0)\, r_{32}^{(\mathrm{F})}(\mathbf{p}_0)\, t_{21}^{(\mathrm{F})}(\mathbf{p}_0)\, \exp(2i(\varphi_0+\varphi_s))}{\left[1 - r_{12}^{(\mathrm{F})}(\mathbf{p})\, r_{32}^{(\mathrm{F})}(\mathbf{p})\, \exp(2i\varphi_s)\right] \left[1 - r_{12}^{(\mathrm{F})}(\mathbf{p}_0)\, r_{32}^{(\mathrm{F})}(\mathbf{p}_0)\, \exp(2i\varphi_0)\right]}. \end{aligned} \tag{39}$$

Note that the paths (1″) and (2″) are somewhat ill-defined in Fig. 4(b). Indeed, each path represents a family of paths with different history prior to the scattering event. For a given path, the path prior to the scattering event consists of a number of specular reflections within the film for which amplitudes dependent on the angle of incidence θ_0, as seen previously for the paths represented by r', while the path that follows after the scattering event consists of a number of specular reflections within the film which are dependent on the angle of scattering θ_s. Therefore, the phase difference between any two such paths will, in general, contain an integer combination of φ_0 and φ_s depending on the number of bounces prior to and after the scattering event. Eq. (39) hence contains both φ_0 and φ_s. The total reflection amplitude for all possible paths involving a single scattering event for the rough-planar (RP) film [Figs. 4(a) and (b)] is obtained by summing the amplitudes obtained from all the previously analyzed diagrams, namely

$$r_{\mathrm{RP}}(\mathbf{p}|\mathbf{p}_0) = r(\mathbf{p}|\mathbf{p}_0) + r'(\mathbf{p}|\mathbf{p}_0) + r''(\mathbf{p}|\mathbf{p}_0). \tag{40}$$

The intensity distribution corresponding to Eq. (40) is shown in Fig. 4(d) for normal incidence and *p*-polarized light, and is compared to results based on small amplitude perturbation theory to leading order, Eq. (32), in the case where only the top interface is rough. The two results are literally indistinguishable. Similar results were also found in the case of *s*-polarized light, but the results are not shown (in order to keep the figure simple). These findings strongly suggest that the two methods are equivalent. In particular, this means that the perturbative solution to leading order derived in Appendix A can indeed be interpreted as a sum of all paths involving a single scattering event, although this was not obvious from the derivation itself. The model presented here thus justifies this physical picture. Fig. 4(e) shows the incoherent contribution to the in-plane co-polarized mean DRC one would obtain if *only* paths of type (1″), (2″), and so on were present, in other words the intensity distribution resulting from Eq. (39). The relative contribution from r'' [Fig. 4(e)] to r_{RP} [Fig. 4(d)] is so small that it to some approximation may be ignored, as it was in Ref. [4], but we will soon see that this path type is crucial in the case of a system with the rough interface shifted to the bottom of the film.

Let us now analyze the case where only the bottom interface is rough, as illustrated in Fig. 4(c). If we follow paths (1) and (2) in Fig. 4(c), it becomes evident that a path must first undergo a Snell refraction

from vacuum into the film before it may interact with the rough interface. Following this refraction into the film a given path may undergo an arbitrary number of Snell reflections within the film, now at a polar angle $\theta_0^{(2)}$ with the normal to the mean film interfaces, before it is scattered by the rough interface as indicated by the star in Fig. 4(c). The path then performs an arbitrary number of Snell reflections within the film, now at a polar angle of scattering $\theta_s^{(2)}$ with the normal to the mean film interfaces, before it exits into the vacuum. All possible paths involving a single scattering event are for the present configuration depicted in Fig. 4(c), and it is now immediately evident that these paths bear close resemblance to those shown in Fig. 4(b) which correspond to the amplitude r''. Consequently the resulting intensity pattern associated with the paths in Fig. 4(c) will exhibit, by construction of the paths, dependencies on *both* the polar angles of incidence and scattering as given by Eqs. (38) and (35). This is supported both by the resulting reflection amplitude [Eq. (41)] and the angular positions of the maxima and minima of the in-plane co-polarized mean DRC displayed in Figs. 2(c) and (d), indicated as vertical dashed–dotted and dotted lines, respectively. Similar to what was done for the paths of type (1″) and (2″) in the configuration depicted in Fig. 4(b), the resulting reflection amplitude for the paths shown in Fig. 4(c) can be expressed as the product of the partial reflection amplitude resulting from all possible paths *prior* to the scattering event and the partial reflection amplitude resulting from all possible paths that may follow *after* the scattering event. The resulting reflection amplitude for the planar-rough (PR) film [Fig. 4(c)] obtained in this way reads

$$\begin{aligned} r_{\mathrm{PR}}(\mathbf{p}|\mathbf{p}_0) &= t_{21}^{(\mathrm{F})}(\mathbf{p}_0)\,\exp(i\varphi_0)\sum_{n=0}^{\infty}\left[r_{12}^{(\mathrm{F})}(\mathbf{p}_0)\,r_{32}^{(\mathrm{F})}(\mathbf{p}_0)\,\exp(2i\varphi_0)\right]^n \\ &\quad\times t_{12}^{(\mathrm{F})}(\mathbf{p})\,r_{32}(\mathbf{p}|\mathbf{p}_0)\,\exp(i\varphi_s)\sum_{n'=0}^{\infty}\left[r_{12}^{(\mathrm{F})}(\mathbf{p})\,r_{32}^{(\mathrm{F})}(\mathbf{p})\,\exp(2i\varphi_s)\right]^{n'} \\ &= \frac{t_{12}^{(\mathrm{F})}(\mathbf{p})\,r_{32}(\mathbf{p}|\mathbf{p}_0)\,t_{21}^{(\mathrm{F})}(\mathbf{p}_0)\,\exp(i(\varphi_0+\varphi_s))}{\left[1-r_{12}^{(\mathrm{F})}(\mathbf{p})\,r_{32}^{(\mathrm{F})}(\mathbf{p})\,\exp(2i\varphi_s)\right]\left[1-r_{12}^{(\mathrm{F})}(\mathbf{p}_0)\,r_{32}^{(\mathrm{F})}(\mathbf{p}_0)\,\exp(2i\varphi_0)\right]}. \end{aligned} \tag{41}$$

The intensity pattern predicted by Eq. (41) is presented as a solid line in Fig. 4(f) for normal incident *p*-polarized light; in the same figure, the filled circles represent the prediction from Eq. (32). As was the case when only the top interface was rough, we find an excellent agreement between the two approaches also when only the bottom interface is rough. A similar agreement was also found when the incident light was *s*-polarized (results not shown). These findings support our single scattering interpretation of the perturbative solution to leading order. We have now explained the angular positions of the Selényi rings and their amplitude modulation with the angle of incidence based on optical path analysis.

It remains to explain the difference in contrast observed in the interference patterns corresponding to the geometries where the rough surface is either located on the top of the film or at the bottom of the film (with the other film interface planar). In providing such an explanation, the expressions given by Eqs. (40) and (41) will prove to be useful alternative representations of the perturbative solutions of the RRE to leading order. Indeed, we can now investigate the relative contribution from each type of path by artificially removing terms. In our analysis of the type of paths in the two configurations, we have identified that paths of type (1″) and (2″), in the configuration where the top interface is rough, are similar to paths (1) and (2) for the configuration where the bottom interface is rough. As was mentioned previously, Fig. 4(e) shows the (diffuse) in-plane mean DRC we would obtain if *only* paths of type (1″), (2″), *etc.* were present; in other words the scattering intensities originating in Eq. (39). We observe that the curve in Fig. 4(e) exhibits poor contrast, and is very similar to the scattering intensities observed in the case where the bottom interface is rough [Fig. 4(f)]. This clearly hints towards the idea that the poor contrast observed when the bottom film interface is rough is intrinsically linked to the nature of the paths. Moreover, we have seen that ignoring the contribution from r'' in Eq. (40) gives a result similar to when all terms of the same equation are included. This indicates that the contribution from r'' can be neglected relative to the other two terms in Eq. (40). However, since paths similar to (1″), (2″), *etc.* are the *only* paths allowed for the configuration where the bottom interface is rough, the contrast is poor by default. In both cases, and as we have seen, a

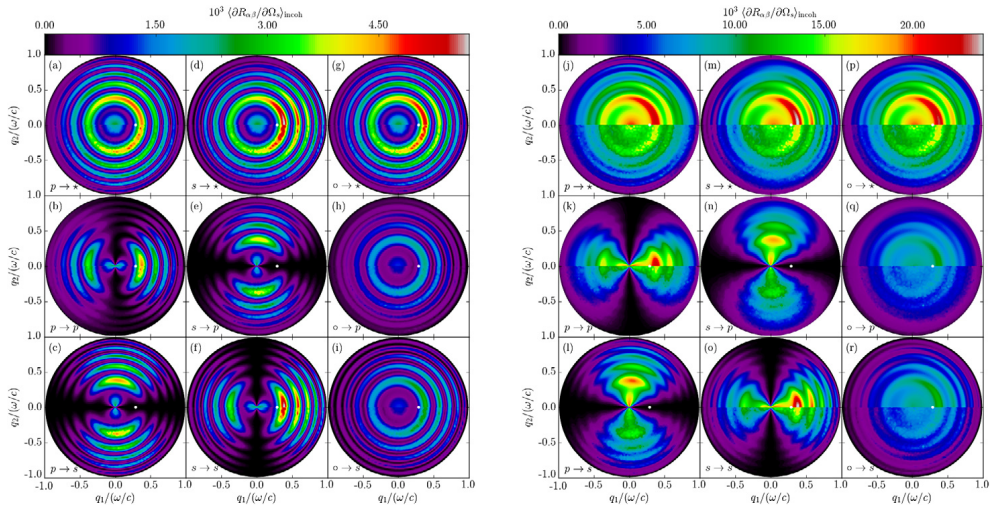

Fig. 5. The full angular distribution of the incoherent component of the mean DRC, $\langle \partial R_{\alpha\beta}/\partial\Omega_s \rangle_{\text{incoh}}$, as function of the lateral wave vector $\mathbf{q}$ of the light that is scattered from a rough film where either the top interface is rough [Figs. 5(a)–(i)] or the bottom interface is rough [Figs. 5(j)–(r)] and the other interface of the film is planar. The light of wavelength $\lambda = 632.8$ nm was incident from vacuum on the rough photoresist film supported by a silicon substrate [$\epsilon_1 = 1.0, \epsilon_2 = 2.69, \epsilon_3 = 15.08 + 0.15i$]. The rms-roughness of the rough film interface was $\sigma_1 = \lambda/30$, $\sigma_2 = 0$ [Figs. 5(a)–(i)] and $\sigma_1 = 0, \sigma_2 = \lambda/30$ [Figs. 5(j)–(r)]. The surface-height correlation length was $a = 211\text{nm} = \lambda/3$, the film thickness was $d = 5062.4\text{nm} = 8\lambda$ and the angles of incidence were $(\theta_0, \phi_0) = (16.8^\circ, 0^\circ)$ for all panels. The positions of the specular directions in reflection are indicated by white dots. The remaining parameters assumed for the scattering geometry and used in performing the numerical simulations had values that are identical to those assumed in obtaining the results of Fig. 2. The upper halves of all panels are results from the small amplitude perturbation method to leading order, while the lower halves show results obtained through the non-perturbative solutions of the RRE. The sub-figures in Figs. 5(a)–(i) and (j)–(r) are both organized in the same manner and show how incident β-polarized light is scattered by the one-rough-interface film geometry into α-polarized light [with $\alpha = p, s$ and $\beta = p, s$] and denoted $\beta \to \alpha$. Moreover, the notation $\circ \to \star$ is taken to mean that the incident light was unpolarized while the polarization of the scattered light was not recorded. For instance, this means that the data shown in Fig. 5(a) are obtained by adding the data sets presented in Figs. 5(b)–(c); similarly, the data shown in Fig. 5(g) result from the addition and division by a factor two of the data sets presented in Figs. 5(a) and (d); *etc.*. Finally, the in-plane intensity variations from Figs. 5(b, f) and (k, o) are the curves depicted in Figs. 2(a)–(b) and (c)–(d), respectively. (For interpretation of the references to color in this figure legend, the reader is referred to the web version of this article.)

typical path must undergo a number of non-scattering reflections within the film both before *and* after the scattering event occurs. Consequently, the phase difference between any two such paths will in general involve integer combinations of φ_0 and φ_s, as can be seen from Eqs. (39) and (41). This phase mixing is the fundamental reason for the difference in contrast found in the contributions to the total intensity r_{RP} from the three components of Eq. (40). The difference in contrast can also be investigated mathematically by estimating the contrast directly, as explained in Appendix C.

We now turn to the full angular distributions for the mean DRC. Figs. 5(a)–(i) and (j)–(r) show the full angular distributions of the incoherent contribution to the mean DRC, for simulation parameters corresponding to those assumed in obtaining the results of Figs. 2(a)–(b) and (c)–(d), respectively. In fact, the non-perturbative results presented in Figs. 2(a)–(b) and (c)–(d) correspond to in-plane cuts along the q_1 axis from Figs. 5(b, f, k, o). The results of Fig. 5 show that, in addition to the interference phenomena already mentioned, the distributions of the incoherent contributions to the mean DRC are also weighted by the shifted power spectrum of the rough interface. In the current work this is a Gaussian envelope centered at the angle of specular reflection, where the width of the envelope is directly influenced by the surface-height correlation length a. This is shown explicitly in the case of small amplitude perturbation theory to leading order as the term $g(\mathbf{p} - \mathbf{p}_0)$ in Eq. (32), and its impact on the scattering distributions should not be confused with the interference phenomena.

The reader may verify that the maxima and minima are located at the same positions as predicted for Fig. 2, as is predicted by Eq. (36). However, for Figs. 5(j)–(r) the contrast in the oscillations of the incoherent contribution to the mean DRC is now less pronounced, as explained for in-plane scattering.

The lower left 2×2 panels in each of the panel collections in Fig. 5 display overall dipole-like patterns oriented along the plane of incidence for co-polarized scattering and perpendicular to it for cross-polarized scattering. These features are consequences of the definition used for the polarization vectors of our system. They are similar to the scattered intensity patterns obtained in recent studies of light scattering from single two-dimensional randomly rough surfaces [16,19,20,27–29].

5.2. Two rough interfaces

We will now turn to the discussion of the geometry where *both* the top and bottom interfaces of the film are rough. In the following it will be assumed that these rough interfaces are characterized by Eq. (6), and for simplicity it will be assumed that their rms-roughness are the same and equal to $\sigma_1 = \sigma_2 = \lambda/30$. The cross-correlation between these two interfaces is characterized by the parameter γ which is allowed to take values in the interval from -1 to 1. All the remaining experimental parameters are identical to those assumed in the preceding sections of this paper.

For the case where only one of the two interfaces of the film was rough, we demonstrated that good agreement exists between the results obtained by a purely numerical solution of the RRE and those obtained on the basis of a perturbative solution of the same equation [SAPT]. A purely numerical solution of the RRE associated with a film geometry where more than one of the interfaces are rough is a challenging task that requires extensive computational resources to obtain, and to the best of our knowledge such a purely numerical solution has not yet been reported. Therefore, for film geometries where both interfaces are rough we will only solve the corresponding RRE through SAPT to obtain the incoherent component of the mean DRC to second order in products of the surface profile functions, for which the relevant expression is given by Eq. (32). In the following it will be assumed that for the level of surface roughness that we consider here, which provided accurate results for the corresponding one-rough-interface film geometry considered in the preceding subsection, such a perturbative solution method is sufficiently accurate to adequately describe the physics of the problem under investigation.

The first set of scattering results for a film bounded by two rough interfaces is presented in Fig. 6. In particular, Figs. 6(a)–(c) present the incoherent component of the mean DRC for in-plane co-polarized scattering (*i.e.* $|\hat{\mathbf{p}} \cdot \hat{\mathbf{p}}_0| = 1$ and $\alpha = \beta$) as a function of the polar angle of scattering θ_s, for given polar angle of incidence equal to $\theta_0 = 0^\circ$, and for three extreme values of the cross-correlation parameter $\gamma \in \{0, 1, -1\}$. These three values of γ physically correspond to the situations of uncorrelated film interfaces; perfectly positively correlated interfaces so that the film thickness measured along any vertical line segment will be constant and equal to d; and perfectly negatively correlated or anti-correlated interfaces, respectively. From Fig. 6(a) one observes that for uncorrelated interfaces of the film [$\gamma = 0$], the number of interference fringes and their angular positions remain unchanged as compared to what was found when only one of the two interfaces of the film was rough. This is found to be the case for both p- and s-polarized incident light. Such behavior can easily be understood in terms of the expression in Eq. (32); when $\gamma = 0$ only the first two terms in the square brackets on the right-hand-side of this equation contribute. These two terms are the only non-zero contributions to the incoherent component of the mean DRC (to second order) for a film system bounded by two *uncorrelated* rough surfaces. Moreover, these two contributions are, respectively, identical to the incoherent component of the mean DRC obtained for film geometries where either the top or the bottom interface of the film is rough and the other planar. Summing these two contributions will hence result in summing two similar interference intensity patterns. Consequently, the resulting interference pattern maintains the same number of fringes at the same positions as the pattern obtained from scattering from the corresponding one-rough interface film geometry. However, by gradually introducing more cross-correlation between the two rough interfaces of the film [$\gamma \neq 0$], one observes that half of the fringes observed for the system for which $\gamma = 0$ are significantly attenuated whereas the other half are enhanced [Figs. 6(b) and (c)]. Furthermore, it is observed from the results in Figs. 6(a)–(c) that the fringes that are enhanced (attenuated) for the case when $\gamma = 1$

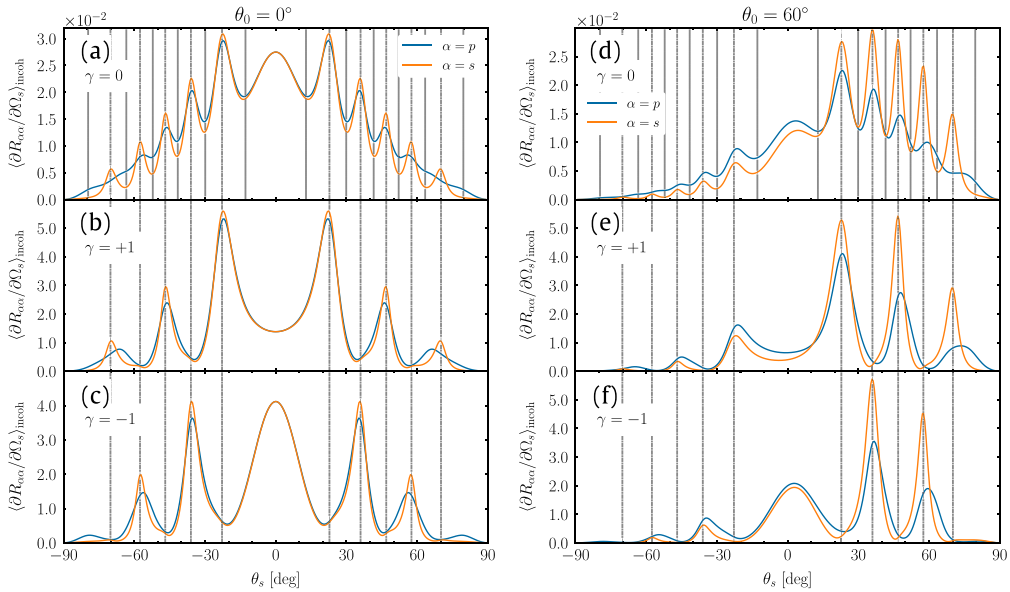

Fig. 6. Incoherent components of the mean differential reflection coefficients $\langle \partial R_{\alpha\alpha}/\partial\Omega_s \rangle_{\text{incoh}}$ for in-plane co-polarized scattering from a two-rough-interface film geometry for the polar angle of incidence $\theta_0 = 0°$ [Figs. 6(a)–(c)] and $\theta_0 = 60°$ [Figs. 6(d)–(e)]. The wavelength of the incident light was $\lambda = 632$ nm, the mean thickness of the film $d = 8\lambda$, and the dielectric constants of the media were $\epsilon_1 = 1.0, \epsilon_2 = 2.69, \epsilon_3 = 15.08 + 0.15i$. The rms-roughness of the interfaces were $\sigma_1 = \sigma_2 = \lambda/30$, and the Gaussian correlation functions of each of the surfaces were characterized by the correlation length $a = \lambda/3$. The cross-correlation function between the rough top and rough bottom interface of the film had the form (5) and was characterized by the parameter γ with values as indicated in each of the panels. The vertical dash-dotted and dotted lines indicate the expected angular positions of the maxima and minima of the scattered intensity as predicted by Eq. (36b), respectively. For reasons of clarity only the expected positions of the minima of the in-plane mean DRCs are indicated in Figs. 6(a) and (d).

are the fringes being attenuated (enhanced) for the case when $\gamma = -1$. This phenomenon can be attributed to the last term in the square brackets in Eq. (32) which is linear in γ and can take both positive and negative values and hence increase or decrease the value of the intensity pattern resulting from the superposition of the scattering amplitudes obtained for the two independent aforementioned one-rough-interface film geometries.

The last term in the square brackets of Eq. (32) is an interference term. Physically it can be interpreted as the interference between a path formed by a single scattering event occurring on the *top* interface of the film such as one depicted in Figs. 4(a–b), and a path consisting of a single scattering event taking place on the *bottom* interface as depicted in Fig. 4(c). When the two interfaces are uncorrelated, the phase difference between these two optical paths will form an uncorrelated random variable so that the ensemble average of the term where it appears in Eq. (32) will be zero and the mean DRC will equal the sum of the intensities of the two corresponding one-rough-interface geometries, i.e. it will be given by the two first terms of Eq. (32). However, when the two interfaces of the film are completely or partially correlated, $|\gamma| > 0$, the phase difference of these two paths becomes a correlated random variable so that the interference term – the last term in (32) – does not average to zero; this results in an optical interference effect. Consequently, the observed interference pattern for $|\gamma| > 0$ will obtain a non-zero contribution from the last term in the square brackets of Eq. (32), which thus will make it different from the pattern obtained for an uncorrelated film geometry that corresponds to $\gamma = 0$.

Figs. 6(d)–(f) present for polar angle of incidence $\theta_0 = 60°$ similar results to those presented in Figs. 6(a)–(c) for normal incidence. Except for the increased intensity of the light scattered into the forward direction defined by $\theta_s > 0°$ relative to what is scattered into angles $\theta_s < 0°$, and the increased contrast of the fringes observed for *s*-polarized light in the forward direction, the behavior of the mean DRC curves is rather similar for the two angles of incidence. In particular, for the same value

of γ, fringes are observed at the same angular positions for the two angles of incidence. Moreover, which of the fringes that are enhanced or attenuated by the introduction of (positive or negative) cross-correlation between the two rough interfaces of the film are also the same for the two angles of incidence. Such behavior is as expected for Selényi fringes.

A close inspection of the perturbative results presented in Fig. 6 reveals that for both $\theta_0 = 0°$ and $\theta_0 = 60°$ the angular positions of the maxima of the in-plane, co-polarized mean DRC curves are more accurately predicted by Eq. (36) for *s*-polarized light than for *p*-polarized light; this seems in particular to be the case for the larger values of $|\theta_s|$. We speculate that such behavior is related to a phase change associated with the Brewster scattering phenomenon [19,20,26] that exists in the case of *p*-polarized light, reminiscent of the well known phase change associated with the Brewster angle found for planar interfaces.

So far in our analysis of the two-rough-interface film geometry, we have observed that the enhancement or attenuation of the diffusely scattered co-polarized intensity are localized to regions around the polar angles determined by Eq. (36a). In order to make this observation more apparent, Figs. 3(a)–(e) present various terms, or combinations of terms, from Eq. (32) when the incident and scattered light is *p*-polarized; Figs. 3(f)–(j) depict similar results for *s*-polarized incident and scattered light. The three first columns of sub-figures that are present in Fig. 3 – labeled "Interface 1", "Interface 2", and "Cross-correlation" – represent the terms in Eq. (32) that contain the factors σ_1^2, σ_2^2, and $\sigma_1\sigma_2$, respectively. The cross-correlation terms, Figs. 3(c) and (h), where obtained from the last term of Eq. (32) with $\gamma = 1$. Furthermore, a contour plot that appears in the 4th column of Fig. 3 [labeled "Total ($\gamma = 1$)"], displays the sum of the data used to produce the three first mean DRC contour plots appearing in the same row. In other words, the results depicted in Figs. 3(d) and (i) are the contour plots of the incoherent component of the mean DRC for a film geometry bounded by two perfectly correlated rough interfaces and therefore given by the expression in Eq. (32) with $\gamma = 1$. Similarly, the incoherent component of the mean DRCs for a geometry where the two rough interfaces of the film are perfectly anti-correlated are displayed in the last column of Fig. 3 [Figs. 3(e) and (j)] and labeled "Total ($\gamma = -1$)". These latter results correspond to Eq. (32) with $\gamma = -1$, and can be obtained by summing the results of the two first columns and subtracting the result of the third column of Fig. 3.

The contour plots of the cross-correlation terms presented in Figs. 3(c) and (h), which are obtained under the assumption that $\gamma = 1$, display extrema localized on the same grid of points in the (θ_0, θ_s)-plane as the extrema of the incoherent component of the mean DRC obtained when only one of the film interfaces is rough [Figs. 3(a)–(b) and (f)–(g)]. An important observation should be made from these results. The minima of the former (the cross-correlation terms) are negative while the latter are always non-negative. Hence, the incoherent component of the mean DRC for $\gamma = 1$, which according to Eq. (32) corresponds to the addition of the results used to produce the three first columns of each row of Fig. 3, will cause fringes localized at the minima of the cross-correlation terms to be *attenuated* (or disappear) and those localized at the maxima of the cross-correlation terms to be *enhanced* [see Figs. 3(d) and (i)].

The preceding discussion stays valid when considering the full angular distribution of the incoherent component of the mean DRC. Fig. 7 presents the full angular distribution of the incoherent component of the mean DRC, obtained on the basis of Eq. (32), for the two polar angles of incidence $\theta_0 = 0°$ [Figs. 7(a)–(f)] and $\theta_0 = 60°$ [Figs. 7(g)–(l)]. In this figure, each column formed by the sub-plots corresponds to either *p*- or *s*-polarized incident light, and in all cases the polarization of the scattered light was not recorded. Moreover, each of the three rows of sub-figures that are present in Fig. 7 corresponds to different values for the cross-correlation parameter $\gamma \in \{0, 1, -1\}$ as indicated in the figure. From the results presented in Fig. 7 it should be apparent that what appear as fringes in the in-plane angular dependence of the mean DRCs indeed are expressed as interference rings in the full-angular distribution of the same quantity; this is particularly apparent for normal incidence where the intensity of the (Selényi) interference rings is independent of the azimuthal angle of scattering ϕ_s (due to the rotational invariance of the system and the source). The angular distributions in Figs. 7(a)–(f) also demonstrate very clearly how the possible interference rings present for uncorrelated interfaces of the film [$\gamma = 0$] are enhanced or attenuated when $|\gamma| \neq 0$, *i.e.* when cross-correlation exists between the two rough interfaces of the film.

Figs. 7(g)–(l) show that interference rings are also present for non-normal incidence and that they are present for the same polar scattering angles θ_s as was found for normal incidence. However, for

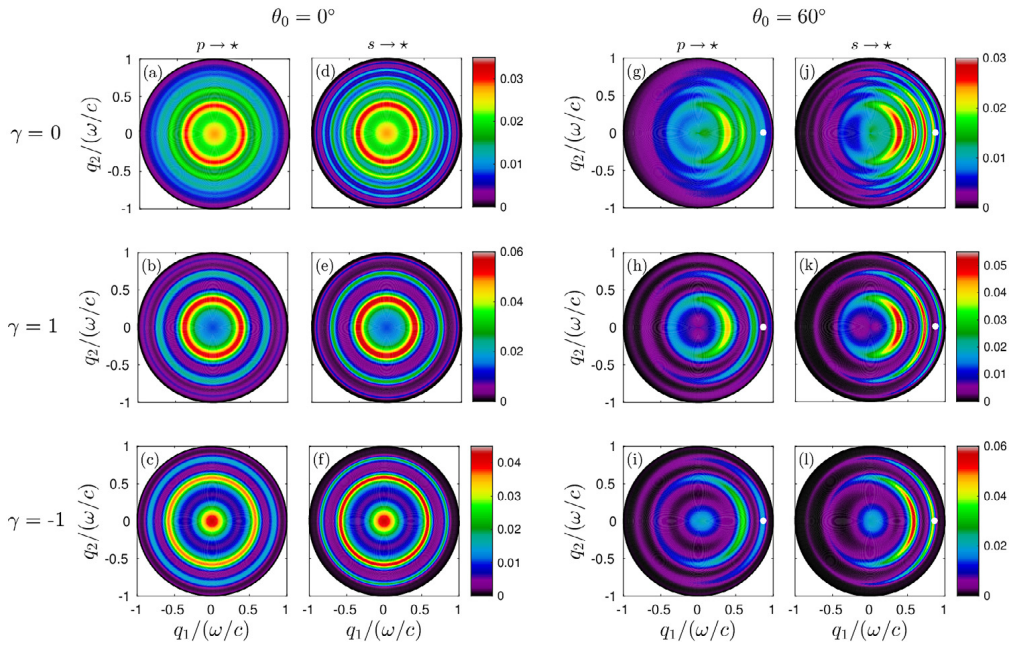

Fig. 7. The full angular distribution of the incoherent component of the mean DRC, $\langle \partial R_{\alpha\beta}/\partial\Omega_s \rangle_{\text{incoh}}$, for incident β-polarized light that is scattered by a two-rough-interface film geometry into α-polarized light [with $\alpha = p, s$ and $\beta = p, s$]. When the polarization of the scattered light is not observed, the relevant mean DRC quantity is $\sum_{\alpha=p,s} \langle \partial R_{\alpha\beta}/\partial\Omega_s \rangle_{\text{incoh}}$ and this situation is labeled as $\beta \to \star$. The reported results were obtained on the basis of SAPT, Eq. (32), and the polar angles of incidence were $\theta_0 = 0°$ [Figs. 7(a)–(f)] and $\theta_0 = 60°$ [Figs. 7(g)–(l)]. The incident in-plane wave vector is indicated by the white dot for non-normal incidence [Figs. 7(g)–(l)]. The cross-correlation function between the rough top and rough bottom interface of the film had the form (5) and was characterized by the parameter γ as indicated in the figure (and constant for each row of sub-figure). The remaining roughness parameters are identical to those assumed in producing the results presented in Fig. 6. (For interpretation of the references to color in this figure legend, the reader is referred to the web version of this article.)

non-normal incidence the intensity of the rings does depend on the azimuthal angle of scattering. It is found that the intensity of the interference rings are concentrated to the forward scattering plane [$|\phi_s - \phi_0| < 90°$].

For normal incidence Fig. 8 presents, for completeness, the full angular distribution of $\langle \partial R_{\alpha\beta}/\partial\Omega_s \rangle_{\text{incoh}}$ for all possible linear polarization couplings, *i.e.* from incident β-polarized light to scattered α-polarized light. The values assumed for the cross-correlation parameter in obtaining these results were $\gamma \in \{0, 1, -1\}$. It should be observed from the results of Fig. 8 that interference structures are observed but they are *not* ring structures of a constant amplitude as was seen in Figs. 7(a)–(f). The reason for this difference is that in the results presented in Fig. 8 only scattered light of a given linear polarization was observed; this contrasts with the situation assumed in producing Fig. 7 where all scattered light was observed and not only scattered light of a given linear polarization.

We have here only shown the extreme cases of cross-correlation, but one may also consider intermediate values for the cross-correlation parameter γ. The effect found for $\gamma = \pm 1$ remains also for $0 < |\gamma| < 1$ but with less pronounced enhancement and attenuation of the rings. The reader is invited to take a look at the animations in the Supplementary Materials, where the contour plots of the incoherent component of the mean DRCs are featured for smoothly varying cross-correlation parameter γ over the interval from -1 to 1, for both normal incidence and for $\theta_0 = 60°$ incidence.

5.3. Transmitted light

Finally, we would like to briefly comment on what would be observed in transmission if a non-absorbing medium was chosen, such as silica. No results will be presented here, but we have observed

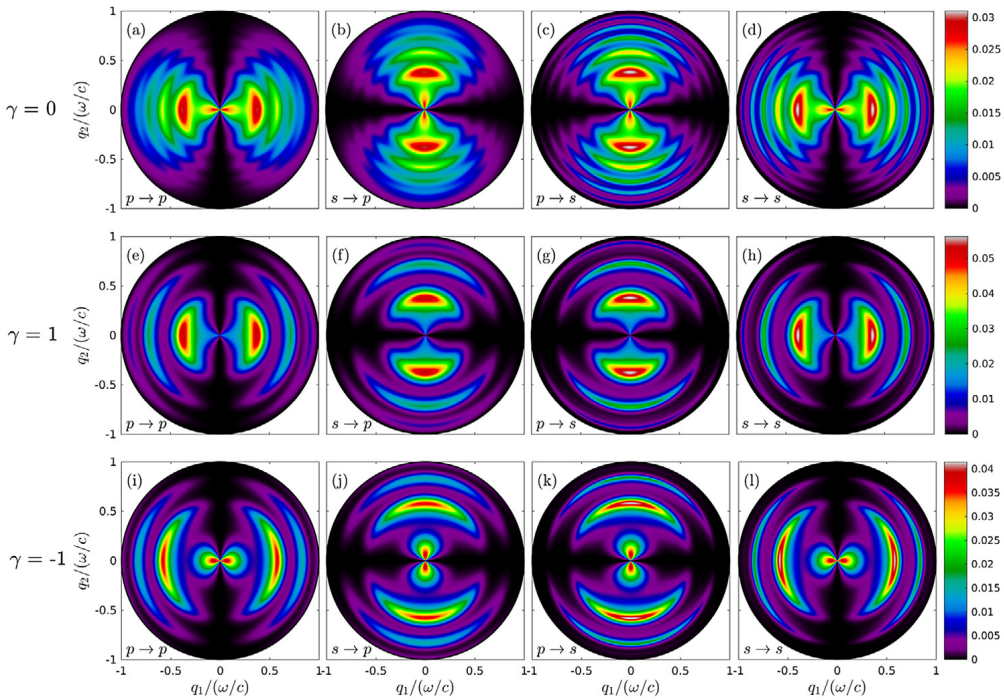

Fig. 8. The full angular distribution of the incoherent component of the mean DRC, $\langle \partial R_{\alpha\beta}/\partial\Omega_s \rangle_{\text{incoh}}$, for incident β-polarized light of polar angle $\theta_0 = 0^\circ$ that is scattered by a two-rough-interface film geometry into α-polarized light [with $\alpha = p, s$ and $\beta = p, s$] and labeled $\beta \to \alpha$ in the sub-figures. The cross-correlation function between the rough top and rough bottom interface of the film had the form (5) and was characterized by the parameter γ as marked in the figure. The reported results were obtained on the basis of SAPT, Eq. (32). The remaining experimental and roughness parameters are identical to those assumed in producing the results presented in Figs. 6 and 7.

that interference rings are also observed in the diffusely transmitted light and that the effect of enhancement and attenuation of the rings induced by the interface cross-correlation still holds. Furthermore, additional features attributed to the so-called Brewster scattering angles and Yoneda effects in the diffusely transmitted light would then be present. As presented in Ref. [20] for scattering systems of comparable surface roughness and materials, the diffusely transmitted intensity as a function of angle of transmission will be modulated by a typical Yoneda intensity pattern. At normal incidence this pattern exhibits a peak at some critical angle of scattering for *s*-polarized light and a vanishing intensity for *p*-polarized light (see Ref. [20] for details). However, we observed that not only did the overall intensity distribution undergo such modulation: the angular positions of the fringes were also affected compared to the predictions provided by naive optical path arguments, analogous to what was presented in this paper for reflection. The angular positions of the fringes predicted by optical path arguments leading to equations similar to Eq. (36) still hold for scattering angles below the Yoneda critical angle, but must be corrected for scattering angles larger than the Yoneda critical angle. We speculate that this is due to a gradual phase shift that occurs above the critical angle, and that it is associated with the Yoneda phenomenon. Note that this phenomenon is also observed in the diffusely reflected light if the medium of incidence has a higher refractive index than that of the substrate (i.e. $\epsilon_1 > \epsilon_3$) [19,22]. Moreover, we have also observed that when scattered to larger polar angles than the Brewster scattering angle the *p*-polarized transmitted light exhibits an additional phase shift, as compared to *s*-polarized transmitted light, resulting in a switch in the positions for the maxima and minima. These and other features of the interference rings in the diffusely transmitted light will be discussed in more detail in a dedicated paper.

6. Conclusion

Based on both non-perturbative and perturbative solutions of the reduced Rayleigh equation, we have in this paper demonstrated that for systems composed of two-dimensional weakly rough dielectric films, Selényi rings can be observed in the diffusely scattered light. These rings make up a static interference pattern that is modulated by the polar angle of incidence. We have illustrated that the interference mechanism at play can be explained by simple optical path arguments, leading to a simple model capable of predicting both the angular positions of the rings and the expected difference in contrast of the rings for film geometries where either the top or the bottom interface of the film is rough (but not both interfaces).

Furthermore, by investigating the influence of the cross-correlation between the film interfaces when both interfaces are rough, we have shown that a selective enhancement or attenuation of the interference rings in the diffusely scattered light can be observed. This suggests that the positions and the amplitudes of Selényi rings can, when combined with reflectivity and/or ellipsometry measurements, in principle enable the determination of the mean film thickness, the dielectric constant of the film material and the statistical properties of the interfaces. In particular, numerical experiments show that the cross-correlation between interfaces can be assessed. Alternatively, film geometries consisting of cross-correlated interfaces can be designed to control the intensity pattern of the diffusely scattered light that they give rise to. Sensors can also be designed in such a way that the interference rings observed for a clean system with known cross-correlated interfaces will be modified by the adsorption of a substance or nano-particles onto the first interface, hence partially destroying the effective cross-correlation between the interfaces. These possibilities are, however, likely to be limited by the ordering of length scales $d > \lambda > \sigma$, which expresses the fact that the film thickness must be on the order of a few wavelengths to observe interference rings in the diffusely scattered light and that the rms-roughness of the interfaces should be small compared to the wavelength. Such a length scale ordering combined with controlled interface cross-correlation may be challenging to achieve experimentally.

While the main results presented in this paper considered the diffusely scattered light, the theoretical framework that it presents also allows for the investigation into the light transmitted diffusely through transparent film structures with one or several rough interfaces. The developed theoretical framework is readily generalized to the case of an arbitrary number of correlated layers and allows, for example, for the study of the effect of gradually changing cross-correlations over many interfaces.

We hope that the results presented in this paper can motivate experimental investigations into the scattering of light from rough film systems so that the predictions that are reported here based on theoretical grounds can be confirmed experimentally.

Acknowledgments

This research was supported in part by The Research Council of Norway Contract No. 216699. The research of I.S. was supported in part by the French National Research Agency (ANR-15-CHIN-0003). This research was supported in part by NTNU and the Norwegian metacenter for High Performance Computing (NOTUR) by the allocation of computer time.

Appendix A. Perturbative solution

We present here a method known as small amplitude perturbation theory that we apply to find an approximate solution of the reduced Rayleigh equations. We will illustrate the method considering a system made of a stack of three media separated by two randomly rough interfaces, like the one depicted in Fig. 1. Using the notation introduced in Section 3, we know that the reduced Rayleigh equations for the reflection amplitude is given by Eqs. (26) and (27)

$$\int \boldsymbol{\Theta}_{3,1}^{+,+}(\mathbf{p} \mid \mathbf{q})\, \mathbf{R}(\mathbf{q} \mid \mathbf{p}_0) \frac{\mathrm{d}^2 q}{(2\pi)^2} = -\boldsymbol{\Theta}_{3,1}^{+,-}(\mathbf{p} \mid \mathbf{p}_0)\,, \tag{A.1}$$

where we recall that the *forward two-interface transfer kernel* is defined as

$$\Theta_{3,1}^{a_3,a_1}(\mathbf{p}_3 \,|\, \mathbf{p}_1) = \sum_{a_2=\pm} a_2 \int \Theta_{3,2}^{a_3,a_2}(\mathbf{p}_3 \,|\, \mathbf{p}_2)\, \Theta_{2,1}^{a_2,a_1}(\mathbf{p}_2 \,|\, \mathbf{p}_1)\, \frac{\mathrm{d}^2 p_2}{(2\pi)^2}\,, \tag{A.2}$$

with the *single-interface kernels* $\Theta_{l,m}^{b,a}$ defined for successive media, i.e. $l, m \in \{1, 3\}$ such that $|l-m| = 1$, $a, b \in \{\pm\}$, as

$$\Theta_{l,m}^{b,a}(\mathbf{p} \,|\, \mathbf{q}) = \alpha_l^{-1}(\mathbf{p}) \mathcal{J}_{l,m}^{b,a}(\mathbf{p} \,|\, \mathbf{q})\, \mathbf{M}_{l,m}^{b,a}(\mathbf{p} \,|\, \mathbf{q}). \tag{A.3}$$

The perturbative method consists in expanding each single-interface kernel in a series of Fourier moments. In order to avoid unnecessary lengthy expansion, we first introduce some notations that will allow us to keep a compact derivation and proved to be useful for generalizing to an arbitrary number of layers and for numerical implementation. We define

$$\begin{aligned}\tilde{\Theta}_{3,1}^{a_3,a_1,(\mathbf{m})}(\mathbf{p}_3 \,|\, \mathbf{p}_2 \,|\, \mathbf{p}_1) = \sum_{a_2=\pm} a_2\, \alpha_3^{-1}(\mathbf{p}_3) \big[a_3\alpha_3(\mathbf{p}_3) - a_2\alpha_2(\mathbf{p}_2)\big]^{m_2-1} \\ \times\ \exp\big[-i\left\{a_3\alpha_3(\mathbf{p}_3) - a_2\alpha_2(\mathbf{p}_2)\right\} d_2\big] \\ \times\ \alpha_2^{-1}(\mathbf{p}_2) \big[a_2\alpha_2(\mathbf{p}_2) - a_1\alpha_1(\mathbf{p}_1)\big]^{m_1-1} \\ \times\ \exp\big[-i\left\{a_2\alpha_2(\mathbf{p}_2) - a_1\alpha_1(\mathbf{p}_1)\right\} d_1\big] \\ \times\ \mathbf{M}_{3,2}^{a_3,a_2}(\mathbf{p}_3 \,|\, \mathbf{p}_2)\, \mathbf{M}_{2,1}^{a_2,a_1}(\mathbf{p}_2 \,|\, \mathbf{p}_1)\,,\end{aligned} \tag{A.4}$$

where $\mathbf{m} = (m_1, m_2) \in \mathbb{N}^2$ is a pair-index (i.e. a two component multi-index). Here, we have made the choice of factorizing the phase factor $e^{-i(a_{j+1}\alpha_{j+1}(\mathbf{p}_{j+1}) - a_j\alpha_j(\mathbf{p}_j))d_j}$, with $d_j = \langle \zeta_j \rangle$ being the offset height of the jth interface, from each factor $\mathcal{J}_{j+1,j}^{a_{j+1},a_j}(\mathbf{p}_{j+1} \,|\, \mathbf{p}_j)$ for later convenience. Given this definition, an expansion of the two-interface kernel in Fourier moments is given by

$$\begin{aligned}\Theta_{3,1}^{a_3,a_1}(\mathbf{p}_3 \,|\, \mathbf{p}_1) &= \sum_{\mathbf{m}=0}^{\infty} \frac{(-i)^{|\mathbf{m}|}}{\mathbf{m}!} \int \hat{h}_2^{(m_2)}(\mathbf{p}_3 - \mathbf{p}_2)\, \hat{h}_1^{(m_1)}(\mathbf{p}_2 - \mathbf{p}_1) \tilde{\Theta}_{3,1}^{a_3,a_1,(\mathbf{m})}(\mathbf{p}_3 \,|\, \mathbf{p}_2 \,|\, \mathbf{p}_1) \frac{\mathrm{d}^2 p_2}{(2\pi)^2} \\ &= \sum_{\mathbf{m}=0}^{\infty} \frac{(-i)^{|\mathbf{m}|}}{\mathbf{m}!}\, \mathbf{Z}_{3,1}^{a_3,a_1,(\mathbf{m})}(\mathbf{p}_3 \,|\, \mathbf{p}_1)\,,\end{aligned} \tag{A.5}$$

where $\sum_{\mathbf{m}=0}^{\infty} \equiv \sum_{m_1=0}^{\infty} \sum_{m_2=0}^{\infty}$, $|\mathbf{m}| = m_1 + m_2$ is the *length* of the pair-index, and $\mathbf{m}! = m_1!\, m_2!$, and for all $j \in \{1, 2\}$,

$$\hat{h}_j^{(m_j)}(\mathbf{q}) = \int \exp\big[-i\mathbf{q}\cdot\mathbf{x}\big]\ \big[\zeta_j(\mathbf{x}) - d_j\big]^{m_j} \mathrm{d}^2 x\,, \tag{A.6}$$

is the Fourier moment of $h_j = \zeta_j - d_j$ of order m_j. It is then clear that $\mathbf{Z}_{3,1}^{a_3,a_1,(\mathbf{m})}(\mathbf{p}_3 \,|\, \mathbf{p}_1)$ is a term of order $|\mathbf{m}|$ in product of surface profiles. The reflection amplitude can be expanded as

$$\mathbf{R}(\mathbf{q} \,|\, \mathbf{p}_0) = \sum_{j=0}^{\infty} \frac{(-i)^j}{j!} \mathbf{R}^{(j)}(\mathbf{q} \,|\, \mathbf{p}_0)\,, \tag{A.7}$$

where the term $\mathbf{R}^{(j)}(\mathbf{q} \,|\, \mathbf{p}_0)$ is of order j in product of surface profiles. We are now ready to start the derivation of the perturbative expansion. By plugging Eqs. (A.5) and (A.7) into Eq. (A.1) we obtain

$$\sum_{\substack{\mathbf{m}'=0 \\ j=0}}^{\infty} \frac{(-i)^{|\mathbf{m}'|+j}}{\mathbf{m}'!\, j!} \int \mathbf{Z}_{3,1}^{+,+,(\mathbf{m}')}(\mathbf{p} \,|\, \mathbf{q})\, \mathbf{R}^{(j)}(\mathbf{q} \,|\, \mathbf{p}_0) \frac{\mathrm{d}^2 q}{(2\pi)^2} = -\sum_{\mathbf{m}=0}^{\infty} \frac{(-i)^{|\mathbf{m}|}}{\mathbf{m}!} \mathbf{Z}_{3,1}^{+,-,(\mathbf{m})}(\mathbf{p} \,|\, \mathbf{p}_0). \tag{A.8}$$

Summing over all multi-index $\mathbf{m}$ is equivalent to summing over subsets $\mathcal{S}_m = \{\mathbf{m} \in \mathbb{N}^2 \,||\mathbf{m}| = m\}$ of multi-index of constant length m, i.e. that we have $\sum_{\mathbf{m}=0}^{\infty} \equiv \sum_{m=0}^{\infty} \sum_{\mathbf{m}\in\mathcal{S}_m}$, therefore the previous

equation can be re-written as

$$\sum_{\substack{m'=0\\ j=0}}^{\infty} \sum_{\mathbf{m}'\in\mathcal{S}_{m'}} \frac{(-i)^{m'+j}}{\mathbf{m}'!\,j!} \int \mathbf{Z}_{3,1}^{+,+,(\mathbf{m}')}(\mathbf{p}\mid\mathbf{q})\,\mathbf{R}^{(j)}(\mathbf{q}\mid\mathbf{p}_0)\frac{\mathrm{d}^2q}{(2\pi)^2} = -\sum_{m=0}^{\infty}\sum_{\mathbf{m}\in\mathcal{S}_m}\frac{(-i)^m}{\mathbf{m}!}\mathbf{Z}_{3,1}^{+,-,(\mathbf{m})}(\mathbf{p}\mid\mathbf{p}_0). \tag{A.9}$$

We then use the definition of the multinomial coefficient in multi-index form as $|\mathbf{m}|!/\mathbf{m}! = \binom{|\mathbf{m}|}{\mathbf{m}}$ to obtain

$$\sum_{\substack{m'=0\\ j=0}}^{\infty} \frac{(-i)^{m'+j}}{m'!\,j!} \sum_{\mathbf{m}'\in\mathcal{S}_{m'}} \binom{m'}{\mathbf{m}'} \int \mathbf{Z}_{3,1}^{+,+,(\mathbf{m}')}(\mathbf{p}\mid\mathbf{q})\,\mathbf{R}^{(j)}(\mathbf{q}\mid\mathbf{p}_0)\frac{\mathrm{d}^2q}{(2\pi)^2} = -\sum_{m=0}^{\infty}\frac{(-i)^m}{m!}\sum_{\mathbf{m}\in\mathcal{S}_m}\binom{m}{\mathbf{m}}\mathbf{Z}_{3,1}^{+,-,(\mathbf{m})}(\mathbf{p}\mid\mathbf{p}_0). \tag{A.10}$$

We now make a change of summation index $j \leftrightarrow m - m'$ on the left hand side of the above equation. This makes clearly appear terms of order m in product of surface profiles. We obtain

$$\sum_{m=0}^{\infty}\sum_{m'=0}^{m} \frac{(-i)^m}{m'!\,(m-m')!} \sum_{\mathbf{m}'\in\mathcal{S}_{m'}} \binom{m'}{\mathbf{m}'} \int \mathbf{Z}_{3,1}^{+,+,(\mathbf{m}')}(\mathbf{p}\mid\mathbf{q})\,\mathbf{R}^{(m-m')}(\mathbf{q}\mid\mathbf{p}_0)\frac{\mathrm{d}^2q}{(2\pi)^2} = -\sum_{m=0}^{\infty}\frac{(-i)^m}{m!}\sum_{\mathbf{m}\in\mathcal{S}_m}\binom{m}{\mathbf{m}}\mathbf{Z}_{3,1}^{+,-,(\mathbf{m})}(\mathbf{p}\mid\mathbf{p}_0)\,, \tag{A.11}$$

which can be re-written with the use of the definition of the binomial coefficient $\binom{m}{m'}$ as

$$\sum_{m=0}^{\infty}\frac{(-i)^m}{m!}\sum_{m'=0}^{m}\binom{m}{m'} \sum_{\mathbf{m}'\in\mathcal{S}_{m'}} \binom{m'}{\mathbf{m}'} \int \mathbf{Z}_{3,1}^{+,+,(\mathbf{m}')}(\mathbf{p}\mid\mathbf{q})\,\mathbf{R}^{(m-m')}(\mathbf{q}\mid\mathbf{p}_0)\frac{\mathrm{d}^2q}{(2\pi)^2} = -\sum_{m=0}^{\infty}\frac{(-i)^m}{m!}\sum_{\mathbf{m}\in\mathcal{S}_m}\binom{m}{\mathbf{m}}\mathbf{Z}_{3,1}^{+,-,(\mathbf{m})}(\mathbf{p}\mid\mathbf{p}_0).$$

It is now time to identify terms of same orders in the left and right hand sides. For $m = 0$, only the term for $\mathbf{m}' = (0, 0)$ remains in the left hand side, only the term $\mathbf{m} = (0, 0)$ remains in the right hand side and we have

$$\int \mathbf{Z}_{3,1}^{+,+,(\mathbf{0})}(\mathbf{p}\mid\mathbf{q})\,\mathbf{R}^{(0)}(\mathbf{q}\mid\mathbf{p}_0)\frac{\mathrm{d}^2q}{(2\pi)^2} = -\mathbf{Z}_{3,1}^{+,-,(\mathbf{0})}(\mathbf{p}\mid\mathbf{p}_0). \tag{A.12}$$

which, when expanded, reads

$$\iint \hat{h}_2^{(0)}(\mathbf{p}-\mathbf{p}_2)\,\hat{h}_1^{(0)}(\mathbf{p}_2-\mathbf{q})\tilde{\mathbf{\Theta}}_{3,1}^{+,+,(\mathbf{0})}(\mathbf{p}\mid\mathbf{p}_2\mid\mathbf{q})\frac{\mathrm{d}^2p_2}{(2\pi)^2}\,\mathbf{R}^{(0)}(\mathbf{q}\mid\mathbf{p}_0)\frac{\mathrm{d}^2q}{(2\pi)^2} = -\int \hat{h}_2^{(0)}(\mathbf{p}-\mathbf{p}_2)\,\hat{h}_1^{(0)}(\mathbf{p}_2-\mathbf{p}_0)\tilde{\mathbf{\Theta}}_{3,1}^{+,-,(\mathbf{0})}(\mathbf{p}\mid\mathbf{p}_2\mid\mathbf{p}_0)\frac{\mathrm{d}^2p_2}{(2\pi)^2}. \tag{A.13}$$

From the definition of the zero order Fourier moment, we have $\hat{h}_j^{(0)}(\mathbf{q}) = (2\pi)^2\,\delta(\mathbf{q})$, which yields

$$\tilde{\mathbf{\Theta}}_{3,1}^{+,+,(\mathbf{0})}(\mathbf{p}\mid\mathbf{p}\mid\mathbf{p})\,\mathbf{R}^{(0)}(\mathbf{p}\mid\mathbf{p}_0) = -(2\pi)^2\tilde{\mathbf{\Theta}}_{3,1}^{+,-,(\mathbf{0})}(\mathbf{p}_0\mid\mathbf{p}_0\mid\mathbf{p}_0)\,\delta(\mathbf{p}-\mathbf{p}_0). \tag{A.14}$$

Here, the reader may recognize the solution of the reflection problem for a stack of layers with flat interfaces, i.e. Fresnel amplitudes

$$\mathbf{R}^{(0)}(\mathbf{p}|\mathbf{p}_0) = -\left[\bar{\Theta}_{3,1}^{+,+}(\mathbf{p}_0)\right]^{-1} \bar{\Theta}_{3,1}^{+,-}(\mathbf{p}_0)\,(2\pi)^2\delta(\mathbf{p}-\mathbf{p}_0) = -\rho_0(\mathbf{p}_0)\,(2\pi)^2\delta(\mathbf{p}-\mathbf{p}_0)\,, \tag{A.15}$$

where $\bar{\Theta}_{3,1}^{+,+}(\mathbf{p}_0) \equiv \tilde{\Theta}_{3,1}^{+,+,(\mathbf{0})}(\mathbf{p}_0\,|\,\mathbf{p}_0\,|\,\mathbf{p}_0)$ and $\bar{\Theta}_{3,1}^{+,-}(\mathbf{p}_0) \equiv \tilde{\Theta}_{3,1}^{+,-,(\mathbf{0})}(\mathbf{p}_0\,|\,\mathbf{p}_0\,|\,\mathbf{p}_0)$. Thus, the order zero of the perturbative expansion corresponds to the Fresnel coefficients for the corresponding system with flat interfaces. For orders $m \geq 1$, we have

$$\begin{aligned}\sum_{m'=0}^{m}\binom{m}{m'}\sum_{\mathbf{m}'\in\mathcal{S}_{m'}}\binom{m'}{\mathbf{m}'}\int \mathbf{Z}_{3,1}^{+,+,(\mathbf{m}')}(\mathbf{p}\,|\,\mathbf{q})\,\mathbf{R}^{(m-m')}(\mathbf{q}\,|\,\mathbf{p}_0)\frac{\mathrm{d}^2q}{(2\pi)^2}\\ = -\sum_{\mathbf{m}\in\mathcal{S}_m}\binom{m}{\mathbf{m}}\mathbf{Z}_{3,1}^{+,-,(\mathbf{m})}(\mathbf{p}\,|\,\mathbf{p}_0).\end{aligned}$$

By isolating the term corresponding to $m' = 0$, hence $\mathbf{m}' = (0, 0)$ and using that for all $j \in \{1, 2\}$ we have $\hat{h}_j^{(0)}(\mathbf{q}) = (2\pi)^2\,\delta(\mathbf{q})$, we obtain

$$\begin{aligned}\mathbf{R}^{(m)}(\mathbf{p}\,|\,\mathbf{p}_0) = -\left[\bar{\Theta}_{3,1}^{+,+}(\mathbf{p})\right]^{-1}\Bigg[\sum_{\mathbf{m}\in\mathcal{S}_m}\binom{m}{\mathbf{m}}\mathbf{Z}_{3,1}^{+,-,(\mathbf{m})}(\mathbf{p}\,|\,\mathbf{p}_0)\\ +\sum_{m'=1}^{m}\binom{m}{m'}\int\sum_{\mathbf{m}'\in\mathcal{S}_{m'}}\binom{m'}{\mathbf{m}'}\mathbf{Z}_{3,1}^{+,+,(\mathbf{m}')}(\mathbf{p}\,|\,\mathbf{q})\mathbf{R}^{(m-m')}(\mathbf{q}\,|\,\mathbf{p}_0)\frac{\mathrm{d}^2q}{(2\pi)^2}\Bigg].\end{aligned} \tag{A.16}$$

We have finally obtained a recursive expression giving the mth order term in the reflection amplitude expansion as a function of lower order terms. For weakly rough surfaces, an approximation based on a truncation of the expansion of the reflection amplitude Eq. (A.7) to the first non-trivial order often yields accurate physical insights. For $m = 1$, we obtain that

$$\begin{aligned}\mathbf{R}^{(1)}(\mathbf{p}\,|\,\mathbf{p}_0) &= -\left[\bar{\Theta}_{3,1}^{+,+}(\mathbf{p})\right]^{-1}\Bigg[\mathbf{Z}_{3,1}^{+,-,(1,0)}(\mathbf{p}\,|\,\mathbf{p}_0)+\mathbf{Z}_{3,1}^{+,-,(0,1)}(\mathbf{p}\,|\,\mathbf{p}_0)\\ &\quad+\int\left(\mathbf{Z}_{3,1}^{+,+,(1,0)}(\mathbf{p}\,|\,\mathbf{q})+\mathbf{Z}_{3,1}^{+,+,(0,1)}(\mathbf{p}\,|\,\mathbf{q})\right)\mathbf{R}^{(0)}(\mathbf{q}\,|\,\mathbf{p}_0)\frac{\mathrm{d}^2q}{(2\pi)^2}\Bigg]\\ &= -\left[\bar{\Theta}_{3,1}^{+,+}(\mathbf{p})\right]^{-1}\Bigg[\mathbf{Z}_{3,1}^{+,-,(1,0)}(\mathbf{p}\,|\,\mathbf{p}_0)+\mathbf{Z}_{3,1}^{+,-,(0,1)}(\mathbf{p}\,|\,\mathbf{p}_0)\\ &\quad-\left(\mathbf{Z}_{3,1}^{+,+,(1,0)}(\mathbf{p}\,|\,\mathbf{p}_0)+\mathbf{Z}_{3,1}^{+,+,(0,1)}(\mathbf{p}\,|\,\mathbf{p}_0)\right)\left[\bar{\Theta}_{3,1}^{+,+}(\mathbf{p}_0)\right]^{-1}\bar{\Theta}_{3,1}^{+,-}(\mathbf{p}_0)\Bigg],\end{aligned} \tag{A.17}$$

where we have used the previously obtained expression for $\mathbf{R}^{(0)}(\mathbf{q}\,|\,\mathbf{p}_0)$ in Eq. (A.15), and in particular the fundamental property of the Dirac delta. From the definition of $\mathbf{Z}_{3,1}^{a_3,a_1,(\mathbf{m})}$ [Eq. (A.5)] it is clear that for $\mathbf{m} = (1, 0)$ or $(0, 1)$ the integration reduces to

$$\mathbf{Z}_{3,1}^{a_3,a_1,(1,0)}(\mathbf{p}\,|\,\mathbf{p}_0) = \hat{h}_1^{(1)}(\mathbf{p}-\mathbf{p}_0)\tilde{\Theta}_{3,1}^{a_3,a_1,(1,0)}(\mathbf{p}\,|\,\mathbf{p}\,|\,\mathbf{p}_0) \tag{A.18a}$$

$$\mathbf{Z}_{3,1}^{a_3,a_1,(0,1)}(\mathbf{p}\,|\,\mathbf{p}_0) = \hat{h}_2^{(1)}(\mathbf{p}-\mathbf{p}_0)\tilde{\Theta}_{3,1}^{a_3,a_1,(0,1)}(\mathbf{p}\,|\,\mathbf{p}_0\,|\,\mathbf{p}_0). \tag{A.18b}$$

It is convenient to group terms with common factor $\hat{h}_j \equiv \hat{h}_j^{(1)}$ in Eq. (A.17), which leads to

$$\mathbf{R}^{(1)}(\mathbf{p}\,|\,\mathbf{p}_0) = \hat{h}_1(\mathbf{p}-\mathbf{p}_0)\rho_1(\mathbf{p}\,|\,\mathbf{p}_0) + \hat{h}_2(\mathbf{p}-\mathbf{p}_0)\rho_2(\mathbf{p}\,|\,\mathbf{p}_0)\,, \tag{A.19}$$

with

$$\rho_1(\mathbf{p}\,|\,\mathbf{p}_0) = \left[\bar{\Theta}_{3,1}^{+,+}(\mathbf{p})\right]^{-1}\left[\tilde{\Theta}_{3,1}^{+,+,(1,0)}(\mathbf{p}\,|\,\mathbf{p}\,|\,\mathbf{p}_0)\rho_0(\mathbf{p}_0) - \tilde{\Theta}_{3,1}^{+,-,(1,0)}(\mathbf{p}\,|\,\mathbf{p}\,|\,\mathbf{p}_0)\right] \tag{A.20a}$$

$$\rho_2(\mathbf{p}\,|\,\mathbf{p}_0) = \left[\bar{\Theta}_{3,1}^{+,+}(\mathbf{p})\right]^{-1}\left[\tilde{\Theta}_{3,1}^{+,+,(0,1)}(\mathbf{p}\,|\,\mathbf{p}_0\,|\,\mathbf{p}_0)\rho_0(\mathbf{p}_0) - \tilde{\Theta}_{3,1}^{+,-,(0,1)}(\mathbf{p}\,|\,\mathbf{p}_0\,|\,\mathbf{p}_0)\right]. \tag{A.20b}$$

We have treated the case of reflection as a representative example, but the same method applies for transmission.

Appendix B. Differential reflection coefficient

Assuming we have obtained the reflection amplitudes $R_{\alpha\beta}(\mathbf{p} \mid \mathbf{p}_0)$ either by using the perturbative approach or by the purely numerical simulation, we can now proceed to express the differential reflection coefficient (DRC) defined as the time-averaged flux radiated around a given scattering direction (θ_s, ϕ_s) per unit solid angle and per unit incident flux and denoted $\partial R/\partial\Omega_s(\mathbf{p} \mid \mathbf{p}_0)$. Let a virtual hemisphere of radius $r \gg c/\omega$ lie on the plane $x_3 = 0$ on top of the scattering system. The support of this hemisphere is a disk of area $S = \pi r^2$. We consider the scattering from a *truncated* version of the scattering system in which the surface profiles are set to be flat outside the disk support. Consequently, the field amplitudes we will manipulate are not strictly speaking those of the full system of interest but will converge to them as $r \to \infty$. We will nevertheless keep the same notations as that from the full system introduced in Section 3 for simplicity. The time-averaged flux incident on this disk is given by

$$\begin{aligned} P_{\mathrm{inc}/S} &= -\mathrm{Re}\frac{c}{8\pi}\int_S \left[\mathbf{E}_0^*(\mathbf{p}_0) \times \left(\frac{c}{\omega}\,\mathbf{k}_1^-(\mathbf{p}_0) \times \mathbf{E}_0(\mathbf{p}_0)\right)\right] \cdot \hat{\mathbf{e}}_3 \;\exp\left[-i(\mathbf{k}_1^{-*}(\mathbf{p}_0) - \mathbf{k}_1^-(\mathbf{p}_0)) \cdot \mathbf{x}\right] \mathrm{d}^2x_\parallel \\ &= -\frac{c^2}{8\pi\omega}\,\mathrm{Re}\int_S \left[|\mathbf{E}_0(\mathbf{p}_0)|^2\,\mathbf{k}_1^-(\mathbf{p}_0) - \left(\mathbf{E}_0^*(\mathbf{p}_0)\cdot\mathbf{k}_1^-(\mathbf{p}_0)\right)\cdot\mathbf{E}_0(\mathbf{p}_0)\right]\cdot\hat{\mathbf{e}}_3\mathrm{d}^2x_\parallel \\ &= S\,\frac{c^2}{8\pi\omega}\,\alpha_1(\mathbf{p}_0)\,|\mathbf{E}_0(\mathbf{p}_0)|^2 \\ &= S\,\frac{c^2}{8\pi\omega}\,\alpha_1(\mathbf{p}_0)\left[\left|\mathcal{E}_{0,p}\right|^2 + \left|\mathcal{E}_{0,s}\right|^2\right]. \end{aligned} \tag{B.1}$$

Here, the * denotes the complex conjugate, and incident field amplitude $\mathbf{E}_0(\mathbf{p}_0) = \mathcal{E}_{0,p}\,\hat{\mathbf{e}}^-_{p,1}(\mathbf{p}_0) + \mathcal{E}_{0,s}\,\hat{\mathbf{e}}_s(\mathbf{p}_0)$ as defined in Eq. (22), the vector identity $\mathbf{a}\times(\mathbf{b}\times\mathbf{c}) = (\mathbf{a}\cdot\mathbf{c})\mathbf{b} - (\mathbf{a}\cdot\mathbf{b})\mathbf{c}$ and the orthogonality between the field and the wave vector $\mathbf{E}_0^*(\mathbf{p}_0)\cdot\mathbf{k}_1^-(\mathbf{p}_0) = 0$ have been used. Note that the flux incident on the disk is proportional to the disk area. Let us now consider the outgoing flux crossing an elementary surface $\mathrm{d}\sigma = r^2\sin\theta_s\mathrm{d}\theta_s\mathrm{d}\phi_s = r^2\mathrm{d}\Omega_s$ around a point $\mathbf{r} = r\,(\sin\theta_s\cos\phi_s\,\hat{\mathbf{e}}_1 + \sin\theta_s\sin\phi_s\,\hat{\mathbf{e}}_2 + \cos\theta_s\,\hat{\mathbf{e}}_3) = r\,\hat{\mathbf{n}}$. The flux crossing this elementary surface is given by

$$P_{\mathrm{d}\sigma} = \frac{c}{8\pi}\,\mathrm{Re}\left[\mathbf{E}_1^{+*}(\mathbf{r}) \times \mathbf{H}_1^+(\mathbf{r})\right]\cdot\hat{\mathbf{n}}\,\mathrm{d}\sigma. \tag{B.2}$$

We then use the well-known asymptotic expansion of the field in the far-field given by (see Refs. [30,31])

$$\mathbf{E}_1^+(\mathbf{r}) \sim -i\,\epsilon_1^{1/2}\,\frac{\omega}{2\pi\,c}\,\cos\theta_s\,\frac{\exp(i\epsilon_1^{1/2}\frac{\omega}{c}r)}{r}\,\mathbf{E}_1^+(\mathbf{p}) \tag{B.3a}$$

$$\mathbf{H}_1^+(\mathbf{r}) \sim -i\,\epsilon_1\,\frac{\omega}{2\pi\,c}\,\cos\theta_s\,\frac{\exp(i\epsilon_1^{1/2}\frac{\omega}{c}r)}{r}\,\hat{\mathbf{n}}\times\mathbf{E}_1^+(\mathbf{p}) \tag{B.3b}$$

where $\mathbf{p} = \sqrt{\epsilon_1}\frac{\omega}{c}(\sin\theta_s\cos\phi_s\,\hat{\mathbf{e}}_1 + \sin\theta_s\sin\phi_s\,\hat{\mathbf{e}}_2)$. This asymptotic approximation will become more and more accurate as we let $r\to\infty$. Plugging Eq. (B.3) into Eq. (B.2) we obtain

$$\begin{aligned} P_{\mathrm{d}\sigma} &= \epsilon_1^{3/2}\left(\frac{\omega}{2\pi\,c}\right)^2\cos^2\theta_s\,\frac{c}{8\pi}\,|\mathbf{E}_1^+(\mathbf{p})|^2\,\mathrm{d}\Omega_s \\ &= \epsilon_1^{3/2}\left(\frac{\omega}{2\pi\,c}\right)^2\cos^2\theta_s\,\frac{c}{8\pi}\,\left(|\mathcal{E}_{1,p}^+(\mathbf{p})|^2 + |\mathcal{E}_{1,s}^+(\mathbf{p})|^2\right)\mathrm{d}\Omega_s. \end{aligned} \tag{B.4}$$

The total differential reflection coefficient is then given by

$$\frac{\partial R}{\partial\Omega_s}(\mathbf{p} \mid \mathbf{p}_0) = \lim_{r\to\infty}\frac{P_{\mathrm{d}\sigma}}{P_{\mathrm{inc}/S}\,\mathrm{d}\Omega_s} = \lim_{r\to\infty}\frac{\epsilon_1}{S}\left(\frac{\omega}{2\pi\,c}\right)^2\frac{\cos^2\theta_s}{\cos\theta_0}\,\frac{|\mathcal{E}_{1,p}^+(\mathbf{p})|^2 + |\mathcal{E}_{1,s}^+(\mathbf{p})|^2}{|\mathcal{E}_{0,p}|^2 + |\mathcal{E}_{0,s}|^2}. \tag{B.5}$$

From the total differential reflection coefficient given by Eq. (B.5), we deduce the differential reflection coefficient when an incident plane wave of polarization β, with in-plane wave vector $\mathbf{p}_0$ is reflected into a plane wave of polarization α with in-plane wave vector $\mathbf{p}$ given as

$$\frac{\partial R_{\alpha\beta}}{\partial \Omega_s}(\mathbf{p} \mid \mathbf{p}_0) = \lim_{r\to\infty} \frac{\epsilon_1}{S}\left(\frac{\omega}{2\pi\, c}\right)^2 \frac{\cos^2\theta_s}{\cos\theta_0} \left|R_{\alpha\beta}(\mathbf{p} \mid \mathbf{p}_0)\right|^2 = \lim_{r\to\infty} \frac{\partial R^{(S)}_{\alpha\beta}}{\partial \Omega_s}(\mathbf{p} \mid \mathbf{p}_0). \tag{B.6}$$

As we are interested in averaging the optical response over realizations of the surface profiles, we consider the following ensemble average

$$\left\langle \frac{\partial R^{(S)}_{\alpha\beta}}{\partial \Omega_s}(\mathbf{p} \mid \mathbf{p}_0) \right\rangle = \frac{\epsilon_1}{S}\left(\frac{\omega}{2\pi\, c}\right)^2 \frac{\cos^2\theta_s}{\cos\theta_0} \left\langle \left|R_{\alpha\beta}(\mathbf{p} \mid \mathbf{p}_0)\right|^2 \right\rangle. \tag{B.7}$$

By decomposing the reflection amplitudes as the sum of the mean and fluctuation (deviation from the mean)

$$R_{\alpha\beta}(\mathbf{p} \mid \mathbf{p}_0) = \left\langle R_{\alpha\beta}(\mathbf{p} \mid \mathbf{p}_0) \right\rangle + \left[R_{\alpha\beta}(\mathbf{p} \mid \mathbf{p}_0) - \left\langle R_{\alpha\beta}(\mathbf{p} \mid \mathbf{p}_0) \right\rangle \right], \tag{B.8}$$

we can decompose the mean differential reflection coefficient as the sum of a coherent term and an incoherent term

$$\left\langle \frac{\partial R^{(S)}_{\alpha\beta}}{\partial \Omega_s}(\mathbf{p} \mid \mathbf{p}_0) \right\rangle = \left\langle \frac{\partial R^{(S)}_{\alpha\beta}}{\partial \Omega_s}(\mathbf{p} \mid \mathbf{p}_0) \right\rangle_{\text{coh}} + \left\langle \frac{\partial R^{(S)}_{\alpha\beta}}{\partial \Omega_s}(\mathbf{p} \mid \mathbf{p}_0) \right\rangle_{\text{incoh}}, \tag{B.9}$$

where

$$\left\langle \frac{\partial R^{(S)}_{\alpha\beta}}{\partial \Omega_s}(\mathbf{p} \mid \mathbf{p}_0) \right\rangle_{\text{coh}} = \frac{\epsilon_1}{S}\left(\frac{\omega}{2\pi\, c}\right)^2 \frac{\cos^2\theta_s}{\cos\theta_0} \left|\left\langle R_{\alpha\beta}(\mathbf{p} \mid \mathbf{p}_0) \right\rangle\right|^2 \tag{B.10a}$$

$$\left\langle \frac{\partial R^{(S)}_{\alpha\beta}}{\partial \Omega_s}(\mathbf{p} \mid \mathbf{p}_0) \right\rangle_{\text{incoh}} = \frac{\epsilon_1}{S}\left(\frac{\omega}{2\pi\, c}\right)^2 \frac{\cos^2\theta_s}{\cos\theta_0} \left[\left\langle \left|R_{\alpha\beta}(\mathbf{p} \mid \mathbf{p}_0)\right|^2 \right\rangle - \left|\left\langle R_{\alpha\beta}(\mathbf{p} \mid \mathbf{p}_0) \right\rangle\right|^2\right]. \tag{B.10b}$$

If we now use the expression found in Appendix A for the reflection amplitudes to first order in the product of surface profiles,

$$\mathbf{R}(\mathbf{p} \mid \mathbf{p}_0) \approx \mathbf{R}^{(0)}(\mathbf{p} \mid \mathbf{p}_0) - i\mathbf{R}^{(1)}(\mathbf{p} \mid \mathbf{p}_0), \tag{B.11}$$

where $\mathbf{R}^{(0)}(\mathbf{p} \mid \mathbf{p}_0)$ is the response from the corresponding system with flat interfaces (i.e. that of a Fabry–Perot interferometer), Eq. (A.15), and $\mathbf{R}^{(1)}(\mathbf{p} \mid \mathbf{p}_0)$ is given in Eq. (A.19), we obtain that the factor in the square bracket in Eq. (B.10b) reads

$$\begin{aligned}
\left\langle \left|R_{\alpha\beta}(\mathbf{p} \mid \mathbf{p}_0)\right|^2 \right\rangle - \left|\left\langle R_{\alpha\beta}(\mathbf{p} \mid \mathbf{p}_0) \right\rangle\right|^2 &= \left\langle \left|R^{(1)}_{\alpha\beta}(\mathbf{p} \mid \mathbf{p}_0)\right|^2 \right\rangle \\
&= \left\langle \left|\hat{h}_{1,S}(\mathbf{p}-\mathbf{p}_0)\right|^2 \right\rangle \left|\rho_{1,\alpha\beta}(\mathbf{p} \mid \mathbf{p}_0)\right|^2 \\
&\quad + \left\langle \left|\hat{h}_{2,S}(\mathbf{p}-\mathbf{p}_0)\right|^2 \right\rangle \left|\rho_{2,\alpha\beta}(\mathbf{p} \mid \mathbf{p}_0)\right|^2 \\
&\quad + 2\,\mathrm{Re}\left\langle \hat{h}_{1,S}(\mathbf{p}-\mathbf{p}_0)\hat{h}^*_{2,S}(\mathbf{p}-\mathbf{p}_0) \right\rangle \\
&\quad \times \left(\rho_{1,\alpha\beta}(\mathbf{p} \mid \mathbf{p}_0)\rho^*_{2,\alpha\beta}(\mathbf{p} \mid \mathbf{p}_0)\right).
\end{aligned} \tag{B.12}$$

Note here that we are still dealing with a scattering system whose surface profiles are flat outside the disk of radius r, hence the subscript S. For the statistical properties attributed to the surface profiles in Section 2, we have

$$\begin{aligned}
\left\langle \hat{h}_{i,S}(\mathbf{q})\hat{h}^*_{j,S}(\mathbf{q}) \right\rangle &= \left\langle \int_S \int_S h_i(\mathbf{x}) h_j(\mathbf{x}') \exp\left[i\mathbf{q}\cdot(\mathbf{x}-\mathbf{x}')\right] \mathrm{d}^2x\, \mathrm{d}^2x' \right\rangle \\
&= \int_S \int_S \left\langle h_i(\mathbf{x}) h_j(\mathbf{x}') \right\rangle \exp\left[i\mathbf{q}\cdot(\mathbf{x}-\mathbf{x}')\right] \mathrm{d}^2x\, \mathrm{d}^2x'
\end{aligned}$$

$$= \int_S \int_S \gamma_{ij}\, W(\mathbf{x}-\mathbf{x}')\, \exp\left[i\mathbf{q}\cdot(\mathbf{x}-\mathbf{x}')\right]\, \mathrm{d}^2x\, \mathrm{d}^2x'. \tag{B.13}$$

Here we have used the definition of the Fourier transform, and the fact that ensemble average commutes with the integration of the surfaces and the definition of the correlation function. We have also introduced the shorthand $\gamma_{ij} = \left[\delta_{ij} + \gamma(1-\delta_{ij})\right]\, \sigma_i\, \sigma_j$. Via the change of variable $\mathbf{u} = \mathbf{x} - \mathbf{x}'$ we obtain

$$\left\langle \hat{h}_{i,S}(\mathbf{q})\hat{h}^*_{j,S}(\mathbf{q})\right\rangle = S\, \gamma_{ij} \int_S W(\mathbf{u})\, \exp(i\mathbf{q}\cdot\mathbf{u})\, \mathrm{d}^2u = S\, \gamma_{ij}\, g_S(\mathbf{q}). \tag{B.14}$$

Thus

$$\left\langle |R_{\alpha\beta}(\mathbf{p}\,|\,\mathbf{p}_0)|^2\right\rangle - \left|\left\langle R_{\alpha\beta}(\mathbf{p}\,|\,\mathbf{p}_0)\right\rangle\right|^2 = S\, g_S(\mathbf{p}-\mathbf{p}_0)\Big[\sigma_1^2\, \left|\rho_{1,\alpha\beta}(\mathbf{p}\,|\,\mathbf{p}_0)\right|^2 + \sigma_2^2\, \left|\rho_{2,\alpha\beta}(\mathbf{p}\,|\,\mathbf{p}_0)\right|^2 + 2\gamma\sigma_1\sigma_2\, \mathrm{Re}\left\{\rho_{1,\alpha\beta}(\mathbf{p}\,|\,\mathbf{p}_0)\rho^*_{2,\alpha\beta}(\mathbf{p}\,|\,\mathbf{p}_0)\right\}\Big]. \tag{B.15}$$

Finally, by plugging the above equation into Eq. (B.10b), the surface area S cancels and letting $r \to \infty$, $g_S \to g$ (where we remind the reader that g is the power spectrum of the surface profiles) and we finally obtain the expression for the incoherent component of the mean differential reflection coefficient for the entire (infinite) system under the first order approximation of the reflected amplitudes in product of the surface profiles

$$\left\langle \frac{\partial R_{\alpha\beta}(\mathbf{p}|\mathbf{p}_0)}{\partial\Omega_s}\right\rangle_{\mathrm{incoh}} = \epsilon_1\Big(\frac{\omega}{2\pi c}\Big)^2\, \frac{\cos^2\theta_s}{\cos\theta_0}\, g(\mathbf{p}-\mathbf{p}_0)\Big[\sigma_1^2\, \left|\rho_{1,\alpha\beta}(\mathbf{p}\,|\,\mathbf{p}_0)\right|^2 + \sigma_2^2\, \left|\rho_{2,\alpha\beta}(\mathbf{p}\,|\,\mathbf{p}_0)\right|^2 + 2\gamma\sigma_1\sigma_2\, \mathrm{Re}\left\{\rho_{1,\alpha\beta}(\mathbf{p}\,|\,\mathbf{p}_0)\rho^*_{2,\alpha\beta}(\mathbf{p}\,|\,\mathbf{p}_0)\right\}\Big]. \tag{B.16}$$

Appendix C. Contrast estimates

We propose here to motivate mathematically that the phase mixing in paths of type (1''), (2'') *etc.*, from Fig. 4(b) and those from Fig. 4(c) intrinsically leads to poorer contrast in the interference pattern found in the incoherent contribution to the mean DRC than, for example, paths of type (1), (2) in Fig. 4(a), where no phase mixing is allowed. As a prototypical reflection amplitude for a sum of paths that involves phase mixing and a sum of paths that does not (and will serve as reference), let us have respectively

$$r_{\mathrm{mix}\varphi} = \frac{\tilde{r}}{[1 - r_0\exp(2i\varphi_0)]\,[1 - r_s\exp(2i\varphi_s)]} \tag{C.1a}$$

$$r_{\mathrm{ref}} = \frac{\tilde{r}}{1 - r_s\exp(2i\varphi_s)}. \tag{C.1b}$$

These reflection amplitudes mimic the structure from Eqs. (41) and Eq. (34) respectively, but we will see that the precise expressions for the numerators do not matter for the contrast, and are hence denoted by the same symbol $\tilde{r}$. Note that all the reflection amplitudes in Eq. (C.1) depend on angles of incidence and scattering, but for clarity we drop these arguments. Our first step consists in taking the square modulus of Eq. (C.1)

$$I_{\mathrm{mix}\varphi} = \frac{|\tilde{r}|^2}{|1 - r_0\exp(2i\varphi_0)|^2\, |1 - r_s\exp(2i\varphi_s)|^2} \tag{C.2a}$$

$$I_{\mathrm{ref}} = \frac{|\tilde{r}|^2}{|1 - r_s\exp(2i\varphi_s)|^2}\,, \tag{C.2b}$$

and in bounding the intensity by using the triangular inequality

$$\frac{|\tilde{r}|^2}{(1+|r_0|)^2\,(1+|r_s|)^2} \quad\leq\quad I_{\mathrm{mix}\varphi} \quad\leq\quad \frac{|\tilde{r}|^2}{(1-|r_0|)^2\,(1-|r_s|)^2} \tag{C.3a}$$

$$\frac{|\tilde{r}|^2}{(1+|r_s|)^2} \quad \leq \quad I_{\text{ref}} \quad \leq \quad \frac{|\tilde{r}|^2}{(1-|r_s|)^2}. \tag{C.3b}$$

It is clear from Eq. (C.3) that the intensity lies between two bounding curves. A fair estimate for the trend, i.e. the intensity without the oscillations would be given by $|\tilde{r}|^2$, and we thus estimate, or rather define, the *inverse contrast* as

$$\eta_{\text{mix}\varphi}^{-1} = (1+|r_0|)^2(1+|r_s|)^2 - (1-|r_0|)^2(1-|r_s|)^2 \tag{C.4a}$$

$$\eta_{\text{ref}}^{-1} = (1+|r_s|)^2 - (1-|r_s|)^2. \tag{C.4b}$$

This may not be the most *natural* definition for the contrast, but we choose this one since it is easier to work with and will not change the conclusion. By re-writing Eq. (C.4) by using straightforward algebra, we obtain

$$\eta_{\text{mix}\varphi}^{-1} = 4|r_s| + 4|r_0| + 4|r_0||r_s| + 4|r_0|^2|r_s| \tag{C.5a}$$

$$\eta_{\text{ref}}^{-1} = 4|r_s|. \tag{C.5b}$$

This shows that the inverse contrast for phase mixing is larger than that of the reference, i.e. that the *contrast* in the case of phase mixing is smaller than that of the reference. Indeed, the two last terms in Eq. (C.5a) are cross-terms resulting directly from the phase mixing nature of the initial reflection amplitude. Note that the choice for the reference was arbitrary and one could choose to study paths of type (1'), (2'), *etc.*, in Fig. 4(b), and hence replace $r_s \exp(2i\varphi_s)$ in Eq. (C.1) by $r_0 \exp(2i\varphi_0)$, and the conclusion would still hold.

Appendix D. Supplementary data

Supplementary material related to this article can be found online at https://doi.org/10.1016/j.aop.2017.12.003.

References

[1] I. Newton, Opticks, Or a Treatise of the Reflections, Refractions, Inflections and Colours of Light, William Innys, 1730.
[2] A.J. de Witte, Amer. J. Phys. 35 (1967) 301–313.
[3] V. Freilikher, V.I. Tatarskii, M. Pustilnik, I. Yurkevich, Opt. Lett. 19 (1994) 1382.
[4] J.Q. Lu, J.A. Sánchez-Gil, E.R. Méndez, Z.-H. Gu, A.A. Maradudin, J. Opt. Soc. Am. A 15 (1998) 185.
[5] O. Calvo-Perez, A. Sentenac, J.J. Greffet, Radio Sci. 34 (1999) 311–335.
[6] W. Suhr, H.J. Schlichting, Appl. Opt. 48 (2009) 4978–4984.
[7] C. Raman, G.L. Datta, Phil. Mag. 42 (1921) 826–840.
[8] Y.S. Kaganovskii, V.D. Freilikher, E. Kanzieper, Y. Nafcha, M. Rosenbluh, I.M. Fuks, J. Opt. Soc. Am. A 16 (1999) 331.
[9] P. Selényi, Ann. Phys. 340 (1911) 444–460.
[10] I. Simonsen, Eur. Phys. J.-Spec. Top. 181 (2010) 1–103.
[11] C. Amra, J.H. Apfel, E. Pelletier, Appl. Opt. 31 (1992) 3134.
[12] Y. Pan, Z. Wu, L. Hang, Appl. Surf. Sci. 256 (2010) 3503–3507.
[13] A. Soubret, G. Berginc, C. Bourrely, Phys. Rev. B 63 (2001) 245411.
[14] A. Soubret, G. Berginc, C. Bourrely, J. Opt. Soc. Am. A 18 (2001) 2778–2788.
[15] G.C. Brown, V. Celli, M. Haller, A. Marvin, Surf. Sci. 136 (1984) 381–397.
[16] T. Nordam, P.A. Letnes, I. Simonsen, Front. Phys. 1 (2013) 1–15.
[17] T.A. Leskova, P.A. Letnes, A.A. Maradudin, T. Nordam, I. Simonsen, Proc. SPIE 8172 (2011) 817209–817209–20.
[18] T. Nordam, P.A. Letnes, I. Simonsen, A.A. Maradudin, J. Opt. Soc. Am. A 31 (2014) 1126–1134.
[19] Ø.S. Hetland, A.A. Maradudin, T. Nordam, I. Simonsen, Phys. Rev. A 93 (2016) 053819.
[20] Ø.S. Hetland, A.A. Maradudin, T. Nordam, P.A. Letnes, I. Simonsen, Phys. Rev. A 95 (2017) 043808.
[21] T. Nordam, P.A. Letnes, I. Simonsen, A.A. Maradudin, Opt. Express 20 (2012) 11336–11350.
[22] A.K. González-Alcalde, J.-P. Banon, Ø.S. Hetland, A.A. Maradudin, E.R. Méndez, T. Nordam, I. Simonsen, Opt. Express 24 (2016) 25995–26005.
[23] J.-P. Banon, T. Nesse, Z. Ghadyani, M. Kildemo, I. Simonsen, Opt. Lett. 42 (2017) 2631–2634.
[24] A. Maradudin, T. Michel, A. McGurn, E. Mendez, Ann. Phys., NY 203 (1990) 255–307.
[25] L.S. Blackford, J. Choi, A. Cleary, E. D'Azevedo, J. Demmel, I. Dhillon, J. Dongarra, S. Hammarling, G. Henry, A. Petitet, K. Stanley, D. Walker, R.C. Whaley, ScaLAPACK Users' Guide, Society for Industrial and Applied Mathematics, Philadelphia, PA, 1997.

[26] T. Kawanishi, H. Ogura, Z.L. Wang, Wave. Random Media 7 (1997) 351–384.
[27] I. Simonsen, A.A. Maradudin, T.A. Leskova, Phys. Rev. A 81 (2010) 013806.
[28] I. Simonsen, J.B. Kryvi, A.A. Maradudin, T.A. Leskova, Comput. Phys. Comm. 182 (2011) 1904–1908.
[29] I. Simonsen, A.A. Maradudin, T. Leskova, Phys. Rev. Lett. 104 (2010) 223904.
[30] G.S. Agarwal, Phys. Rev. B 15 (1977) 2371–2383.
[31] K. Miyamoto, E. Wolf, J. Opt. Soc. Amer. 52 (1962) 615–625.

Paper 6:

J.-P. Banon, Ø. S. Hetland, and I. Simonsen, "On the physics of polarized light scattering from weakly rough dielectric surfaces: Yoneda and Brewster scattering phenomena," *arXiv:1804.07507 (Accepted for publication in Phys. Rev. A)*, 2018

On the physics of polarized light scattering from weakly rough dielectric surfaces: Yoneda and Brewster scattering phenomena

J.-P. Banon[1], Ø. S. Hetland[1], and I. Simonsen[1,2]
[1]*Department of Physics, NTNU Norwegian University of Science and Technology, NO-7491 Trondheim, Norway and*
[2]*Surface du Verre et Interfaces, UMR 125 CNRS/Saint-Gobain, F-93303 Aubervilliers, France*
(Dated: April 20, 2018)

The optical Yoneda and Brewster scattering phenomena are studied theoretically based on pertubative solutions of the reduced Rayleigh equations. The Yoneda phenomenon is characterized as an enhancement of the intensity of the diffuse light scattered by a randomly rough interface between two dielectric media when the light is observed in the optically denser medium. The intensity enhancement occurs above a critical angle of scattering which is independent of the angle of incidence of the excitation. The Brewster scattering phenomenon is characterized by a zero scattered intensity either in the reflected or transmitted light for an angle of scattering which depends on the angle of incidence. We also describe a generalization of the Brewster scattering phenomenon for outgoing evanescent waves and circularly-polarized waves. The physical mechanisms responsible for these phenomena are described in terms of simple notions such as scalar waves, oscillating and rotating dipoles and geometrical arguments, and are valid in a regime of weakly rough interfaces.

I. INTRODUCTION

When light is scattered in either reflection or transmission from or through a weakly rough interface, two phenomena of interest can be observed in the scattered intensity distributions. These are the *Yoneda phenomenon*, relatable to the idea of total internal reflection, and the *Brewster scattering phenomenon*, relatable to the polarizing angle.

The Yoneda phenomenon is characterized as an enhancement of the intensity of the light scattered diffusely by a randomly rough interface between two dielectric media when the light is observed in the optically denser medium. The intensity enhancement occurs above a critical angle of scattering which is independent of the angle of incidence of the excitation. This critical angle is always the polar angle, in the denser medium, for which the wavenumber of a plane wave turns non-propagating in the less dense medium [1, 2]. Although well known in the scattering of x-rays from both metallic [3–8] and non-metallic [9–12] surfaces, a paper by Kawanishi *et al.* [13] marks their first explicit appearance in optics[14]. Kawanishi *et al.*, by the use of the stochastic functional approach, studied the case where a two-dimensional randomly rough interface between two dielectric media is illuminated by p- or s-polarized light from either medium. They obtained several interesting properties of the reflected and transmitted light that are associated with the phenomenon of total internal reflection when the medium of observation is the optically denser medium. These include the appearance of Yoneda peaks, which were described by the authors as "quasi-anomalous scattering peaks." As an interpretation of their results, the authors suggested that the Yoneda peaks may be associated with the presence of lateral waves [15] propagating along the interface in the optically less dense medium. Although the mathematical origin of the Yoneda effect has been shown through various perturbative approaches based on the reduced Rayleigh equations (RRE), a physical interpretation of the effect is still under discussion; a summary of which can be found in Ref. 1. Optical Yoneda peaks were recently observed experimentally for a configuration of reflection from a randomly rough dielectric interface, when the medium of incidence was the optically denser medium [16].

The *Brewster angle* is maybe the best known planar surface reflection effect where the polarization of light plays a major role. Proposed as a *polarizing angle* by Sir David Brewster in 1812 [17], its exact definition has been a slight matter of debate in modern times [18]. For isotropic dielectric non-magnetic materials, however, it may be defined to be the angle of incidence, onto a planar dielectric surface, for which the reflection amplitude for p-polarized light (light polarized in the plane given by the incident light and the surface normal) is zero.

A complete physical understanding of the Brewster phenomenon is, at best, non trivial. The most common explanation for the gradual disappearance of the reflection amplitude is based on the radiation pattern of dipoles induced in the scattering substrate [19, 20]. This idea is not new, and can be traced back to investigations by e.g. Sommerfeld [21]. Modelling the scattering from a rough surface as a layer of polarizable spheres led Greffet and Sentenac [22] to the same conclusion. In a later collaboration with Calvo-Perez, this point of view was reinforced through the development of, and the results given by, the Mean Field Theory (MFT) [23, 24]. However, amongst others Lekner [25] argues that even if the dipole argument holds great explanatory power for a wide range of scattering systems, he challenges the argument for the case of the Brewster angle for dielectric media. His main issue with the argument is that the accelerated electrons cannot oscillate as dipoles in the transmitted medium in the case of the wave approaching an interface with vacuum on the opposing side, since the argument goes that the dipoles are oriented according to the field in the refracted wave. Also, there is an analogue

to Brewster's angle for longitudinal acoustic waves called Green's angle, and in this case the radiation from each scatterer does not have dipole character [25].

These and other conceptual issues in the explanatory model for the Brewster angle are attempted reconciled by Doyle [26] in his work with a factored form of the Fresnel equations. Inspired by the work of Sein [27], and Pattanayak and Wolf [28] on the interpretation and generality of the extinction theorem, Doyle claims that the proper understanding of the Brewster phenomenon has been hampered by the attention given to surface sources through a slightly misunderstood interpretation of the Ewald-Oseen extinction theorem [29]. Doyle emphatizes the participation of the entire media in the creation of the reflected wave, and makes use of Ewald's original concept of "wave triads". Doyle's factored form of the Fresnel equations separately expresses the scattering pattern from individual dipoles and the coherent scattering function of the dipole array, and manages in this way to explain the polarizing angles for any combination of transparent media.

Kawanishi *et al.* [13] observed angles of zero scattering intensity to first order in their approach in the distributions of the intensity of the incoherently scattered light when the incident light was p-polarized. Due to their resemblance to the Brewster angle in the reflectivity from a flat interface, they dubbed these angles the "Brewster scattering angles". These angles were observed in both reflection *and* transmission, for light incident from either medium.

Both the Brewster scattering angles and Yoneda peaks were recently observed and discussed in numerical simulations of scattering in both reflection and transmission from weakly rough surfaces [1, 2], and also in a film geometry [30] where it was claimed that the phase shifts associated with these phenomena impact the angular positions of interference rings of diffusely scattered light, known as Selényi rings.

In this paper we seek to further illuminate the phenomena of Brewster scattering angles and Yoneda peaks and more generally identify the fundamental mechanisms at play in the scattering of polarized light by a weakly rough surface. After describing the statistical properties of the interface in Sec. II, we derive, in Sec. III, a set of reduced Rayleigh equations (RREs) for the case of electromagnetic scattering inspired by the work of Soubret *et al.* [31] and give the corresponding RRE for scalar waves subjected to the continuity of the scalar field and its normal derivatives with respect to the interface. Furthermore, we give an approximate solution of the RREs to first order in the surface profile function in a series expansion of the reflection and transmission amplitudes. The first order perturbative solution will be our main tool of investigation in Sec. IV. Section IV A is devoted to summarizing some phenomenological observations which have been obtained in the literature before embarking in Sec. IV B into a more in-depth analysis of the reflection and transmission amplitudes with special care given to their physical interpretation. In particular, we show how the response can be factorized as a product of a term reminiscent of a scalar wave response and a term encoding the component of the response specific to polarization. Such a factorization is a clear signature of two aspects of scattering by arrays of dipoles; the radiated power is controlled both by the interference of the spherical-like waves emitted by each atomic source and their individual characteristic dipolar radiation. Once the general physical interpretation of the equations is clarified, we explain in detail the origin of the Yoneda phenomenon in Sec. IV C, and show that it is fundamentally a single scattering, scalar wave phenomenon. The Brewster scattering phenomenon, and more generally all polarization induced effects, are then discussed thoroughly in Secs. IV D-IV F. We first restrict the analysis of the Brewster scattering phenomenon to scattering in the plane of incidence and derive a one-line criterion for predicting the Brewster scattering angle which allows for a simple geometrical interpretation. A detour via the analysis of the polarization properties of the radiation of oscillating and rotating dipoles in free space is made in Sec. IV E in order to facilitate the intuitive understanding of the full angular distribution of scattering by a rough surface discussed in Sec. IV F. Finally, Sec. V summarizes the conclusions we have drawn from this study and suggests experimental setups to test some interesting predictions made by the theory.

II. SCATTERING SYSTEMS

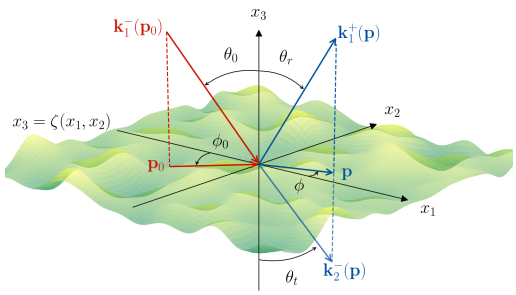

FIG. 1. Definitions of the angles of incidence and scattering, together with the relevant wave vectors.

The system we study in this work consists of a non-magnetic dielectric medium (medium 1), whose dielectric constant is $\epsilon_1 > 0$ (refractive index $n_1 = \sqrt{\epsilon_1}$), in the region $x_3 > \zeta(\mathbf{x}_\parallel)$, and a non-magnetic dielectric medium (medium 2), whose dielectric constant is $\epsilon_2 > 0$ (refractive index $n_2 = \sqrt{\epsilon_2}$), in the region $x_3 < \zeta(\mathbf{x}_\parallel)$ [Fig. 1]. The definition of the geometry is set in the three-dimensional space endowed with a Cartesian coordinate system $(O, \hat{\mathbf{e}}_1, \hat{\mathbf{e}}_2, \hat{\mathbf{e}}_3)$, with the vector plane $(\hat{\mathbf{e}}_1, \hat{\mathbf{e}}_2)$ parallel to the mean plane of the interface. The origin, O,

of the coordinate system can be arbitrarily chosen, only affecting the complex reflection and transmission amplitudes by an overall phase factor which plays no role in the intensity of the scattered light. A point is then represented as $\mathbf{x} = \sum_{i=1}^{3} x_i \hat{\mathbf{e}}_i = \mathbf{x}_\parallel + x_3\,\hat{\mathbf{e}}_3$. An overview of a typical system geometry is provided in Fig. 1. The surface profile function ζ will be assumed to be a realization of a continuous, differentiable, single-valued, stationary, isotropic, Gaussian random process with zero mean and given auto-correlation. More specifically, the surface profile function is assumed to satisfy the following properties:

$$\big\langle \zeta(\mathbf{x}_\parallel) \big\rangle = 0\,, \tag{1a}$$

$$\Big\langle \zeta(\mathbf{x}_\parallel)\zeta(\mathbf{x}'_\parallel) \Big\rangle = \sigma^2\, W(\mathbf{x}_\parallel - \mathbf{x}'_\parallel)\,. \tag{1b}$$

Here and in the following, the angle brackets denote an average over an ensemble of realizations of the stochastic process, σ denotes the rms roughness and W the height auto-correlation function normalized so that $W(\mathbf{0}) = 1$. In particular, we will deal with the special case of a Gaussian auto-correlation function defined by

$$W(\mathbf{x}_\parallel) = \exp\left(-\frac{|\mathbf{x}_\parallel|^2}{a^2}\right)\,, \tag{2}$$

where a is the correlation length. The corresponding power spectrum (defined as the Fourier transform of W) is then

$$g(\mathbf{p}) = \pi a^2 \exp\left(-\frac{|\,\mathbf{p}\,|^2 a^2}{4}\right)\,, \tag{3}$$

with $\mathbf{p} = p_1\,\hat{\mathbf{e}}_1 + p_2\,\hat{\mathbf{e}}_2$.

III. THEORY

The theoretical approach used in this work to study the scattering of light from the systems of interest is based on the so-called reduced Rayleigh equations. A reduced Rayleigh equation is an inhomogeneous integral equation in which the integral kernel encodes the materials and geometry of the scattering system, and the unknowns are the reflection or transmission amplitudes for each polarization. First derived by Brown *et al.* [32], the reduced Rayleigh equation is obtained from the Rayleigh solution to the electromagnetic boundary problem. Using inspiration drawn from the extinction theorem it is possible to "reduce" the full Rayleigh equations through the elimination of either the reflected or transmitted field. In the following, in order to establish the notation and highlight the main assumptions of the method, we will briefly recall the key ideas of the derivation of the reduced Rayleigh equations for a system composed of two media separated by a rough interface. We will use, to our knowledge, the most general form of the reduced Rayleigh equations for a single interface derived by Soubret *et al.* in Ref. 31 and used by these authors in Refs. 31 and 33 in the case of a single interface system and a film geometry.

A. The reduced Rayleigh equations

In this work we assume the electromagnetic response of the media to be modeled by non-magnetic, homogeneous, isotropic, linear constitutive relations in the frequency domain. We consider the presence of an electromagnetic field $(\mathbf{E}, \mathbf{H})$ in the whole space, where their restriction will be denoted by a subscript j depending on the medium in which they are evaluated. As an example, the electric field evaluated at a point $\mathbf{x}$ in medium 1 at time t is denoted $\mathbf{E}_1(\mathbf{x}, t)$. The source free Maxwell equations, together with homogeneous, linear and isotropic constitutive relations in the frequency domain, result in the fact that the electric and magnetic fields satisfy the Helmholtz equation in each region. Namely, for $j \in \{1, 2\}$,

$$\nabla^2 \mathbf{E}_j(\mathbf{x}, \omega) + \epsilon_j(\omega)\,\left(\frac{\omega}{c}\right)^2\,\mathbf{E}_j(\mathbf{x}, \omega) = \mathbf{0}\,, \tag{4}$$

and similarly for $\mathbf{H}$. Here, ∇^2 denotes the vector Laplace operator and c is the speed of light in vacuum. Here onward, we will drop the time, or frequency, dependence, since we assume a stationary regime at a fixed frequency where time contributes only by an overall phase factor $\exp(-i\omega t)$. It is well known that a solution to the Helmholtz equation can be written as a linear combination of plane waves, thus the electric field in each region can be represented as

$$\mathbf{E}_j(\mathbf{x}) = \sum_{a=\pm} \int_{\mathbb{R}^2} \left[\mathcal{E}^a_{j,p}(\mathbf{q})\,\hat{\mathbf{e}}^a_{p,j}(\mathbf{q}) + \mathcal{E}^a_{j,s}(\mathbf{q})\,\hat{\mathbf{e}}_s(\mathbf{q})\right] \times \exp\left(i\;\mathbf{k}^a_j(\mathbf{q})\cdot\;\mathbf{x}\right)\frac{\mathrm{d}^2 q}{(2\pi)^2}\,, \tag{5}$$

where we have defined

$$\mathbf{k}^\pm_j(\mathbf{q}) = \mathbf{q} \pm \alpha_j(\mathbf{q})\,\hat{\mathbf{e}}_3\,, \tag{6a}$$

$$\alpha_j(\mathbf{q}) = \sqrt{k_j^2 - \mathbf{q}^2}, \quad \mathrm{Re}\,(\alpha_j), \mathrm{Im}\,(\alpha_j) \geq 0\,, \tag{6b}$$

$$\hat{\mathbf{e}}_s(\mathbf{q}) = \hat{\mathbf{e}}_3 \times \hat{\mathbf{q}}\,, \tag{6c}$$

$$\hat{\mathbf{e}}^\pm_{p,j}(\mathbf{q}) = k_j^{-1}\,(\pm\alpha_j(\mathbf{q})\,\hat{\mathbf{q}} - |\mathbf{q}|\,\hat{\mathbf{e}}_3) \tag{6d}$$

$$k_j = n_j\frac{\omega}{c} = |\,\mathbf{k}^\pm_j(\mathbf{q})|\,. \tag{6e}$$

In other words, the wave vector $\mathbf{k}^\pm_j(\mathbf{q})$ of an elementary plane wave is decomposed into its projection $\mathbf{q}$ in the lateral vector plane $(\hat{\mathbf{e}}_1, \hat{\mathbf{e}}_2)$ and the component $\pm\alpha_j(\mathbf{q})$ along $\hat{\mathbf{e}}_3$. The sum over $a = \pm$ takes into account both upwards $(+)$ and downwards $(-)$ propagating and evanescent (and possibly growing) waves. The field amplitude is decomposed in the *local polarization basis* $(\hat{\mathbf{e}}^a_{p,j}(\mathbf{q}), \hat{\mathbf{e}}_s(\mathbf{q}))$, hence $\mathcal{E}^a_{j,\alpha}(\mathbf{q})$ denotes the component of the field amplitude in the polarization state α of the mode characterized by a and $\mathbf{q}$. In this basis, the directions given by $\hat{\mathbf{e}}^\pm_{p,j}(\mathbf{q})$, and $\hat{\mathbf{e}}_s(\mathbf{q})$ are the directions of the p- and s-polarization of the electric field amplitude, respectively. Furthermore, the electromagnetic fields have

to satisfy the boundary conditions

$$\mathbf{n}(\mathbf{x}_\parallel) \times \Big[\mathbf{E}_2(\mathbf{s}(\mathbf{x}_\parallel)) - \mathbf{E}_1(\mathbf{s}(\mathbf{x}_\parallel))\Big] = \mathbf{0} \tag{7a}$$

$$\mathbf{n}(\mathbf{x}_\parallel) \times \Big[\mathbf{H}_2(\mathbf{s}(\mathbf{x}_\parallel)) - \mathbf{H}_1(\mathbf{s}(\mathbf{x}_\parallel))\Big] = \mathbf{0}\,, \tag{7b}$$

where $\mathbf{n}(\mathbf{x}_\parallel)$ is a vector normal to the interface at the surface point $\mathbf{s}(\mathbf{x}_\parallel) = \mathbf{x}_\parallel + \zeta(\mathbf{x}_\parallel)\hat{\mathbf{e}}_3$, given by

$$\mathbf{n}(\mathbf{x}_\parallel) = \hat{\mathbf{e}}_3 - \frac{\partial \zeta}{\partial x_1}(\mathbf{x}_\parallel)\,\hat{\mathbf{e}}_1 - \frac{\partial \zeta}{\partial x_2}(\mathbf{x}_\parallel)\,\hat{\mathbf{e}}_2\,. \tag{8}$$

Here, $\partial\cdot/\partial x_k$ denotes the partial derivative along the direction $\hat{\mathbf{e}}_k$. Following Soubret *et al.* [31], by substituting the field expansion Eq. (5) into Eq. (7) and by a clever linear integral combination of the boundary conditions inspired by the extinction theorem [28], one can show that the upward or downward field amplitudes in medium 2 can be linked to the upward and downward field amplitudes in medium 1 via the following integral equation defined for $a_2 = \pm$, and $\mathbf{p}$ in the vector plane $(\hat{\mathbf{e}}_1, \hat{\mathbf{e}}_2)$:

$$\sum_{a_1=\pm} \int \mathcal{J}_{2,1}^{a_2,a_1}(\mathbf{p}\,|\,\mathbf{q})\; \mathbf{M}_{2,1}^{a_2,a_1}(\mathbf{p}\,|\,\mathbf{q})\; \boldsymbol{\mathcal{E}}_1^{a_1}(\mathbf{q})\, \frac{\mathrm{d}^2 q}{(2\pi)^2} = \frac{2\,a_2\,n_1 n_2\,\alpha_2(\mathbf{p})}{\epsilon_2 - \epsilon_1}\; \boldsymbol{\mathcal{E}}_2^{a_2}(\mathbf{p}). \tag{9}$$

Here $\boldsymbol{\mathcal{E}}_j^a(\mathbf{q}) = (\mathcal{E}_{j,p}^a(\mathbf{q}), \mathcal{E}_{j,s}^a(\mathbf{q}))^{\mathrm{T}}$ denotes a column vector of the polarization components of the field amplitude in medium j. Moreover, $\mathbf{M}_{l,m}^{b,a}(\mathbf{p}\,|\,\mathbf{q})$ is the 2×2 matrix

$$\mathbf{M}_{l,m}^{b,a}(\mathbf{p}\,|\,\mathbf{q}) = k_1 k_2 \begin{pmatrix} \hat{\mathbf{e}}_{p,l}^b(\mathbf{p})\cdot\hat{\mathbf{e}}_{p,m}^a(\mathbf{q}) & \hat{\mathbf{e}}_{p,l}^b(\mathbf{p})\cdot\hat{\mathbf{e}}_s(\mathbf{q}) \\ \hat{\mathbf{e}}_s(\mathbf{p})\cdot\hat{\mathbf{e}}_{p,m}^a(\mathbf{q}) & \hat{\mathbf{e}}_s(\mathbf{p})\cdot\hat{\mathbf{e}}_s(\mathbf{q}) \end{pmatrix}, \tag{10}$$

which originates from a change of coordinate system between the local polarization basis $(\hat{\mathbf{e}}_{p,l}^b(\mathbf{p}), \hat{\mathbf{e}}_s(\mathbf{p}))$ and $(\hat{\mathbf{e}}_{p,m}^a(\mathbf{q}), \hat{\mathbf{e}}_s(\mathbf{q}))$, defined for $a = \pm$, $b = \pm$, and $l, m \in \{1, 2\}$ with $l \neq m$. The kernel scalar factor $\mathcal{J}_{l,m}^{b,a}(\mathbf{p}\,|\,\mathbf{q})$ encodes the surface geometry and is defined as

$$\mathcal{J}_{l,m}^{b,a}(\mathbf{p}\,|\,\mathbf{q}) = [b\alpha_l(\mathbf{p}) - a\alpha_m(\mathbf{q})]^{-1} \times \int \exp\left[-i(\mathbf{k}_l^b(\mathbf{p}) - \mathbf{k}_m^a(\mathbf{q}))\cdot\mathbf{s}(\mathbf{x}_\parallel)\right] \mathrm{d}^2 x_\parallel. \tag{11}$$

Notice that, as already pointed out in Ref. 31, due to the symmetry of the boundary conditions, one may also show in the same way that

$$\sum_{a_2=\pm} \int \mathcal{J}_{1,2}^{a_1,a_2}(\mathbf{p}\,|\,\mathbf{q})\; \mathbf{M}_{1,2}^{a_1,a_2}(\mathbf{p}\,|\,\mathbf{q})\; \boldsymbol{\mathcal{E}}_2^{a_2}(\mathbf{q})\, \frac{\mathrm{d}^2 q}{(2\pi)^2} = \frac{2\,a_1\,n_1 n_2\,\alpha_1(\mathbf{p})}{\epsilon_1 - \epsilon_2}\; \boldsymbol{\mathcal{E}}_1^{a_1}(\mathbf{p}), \tag{12}$$

which can be obtained from Eq. (9) by interchanging the subscripts 1 and 2. Typically, Eq. (9) is appropriate to solve the problem of reflection whereas Eq. (12) is appropriate to solve the problem of transmission, as we will see later.

So far, we have stayed general and simply assumed the presence of an electromagnetic field decomposed in propagating and non-propagating waves in each region. Therefore, there is no uniqueness in the solutions to the transfer equations, Eqs. (9) and (12). To ensure a unique solution, one needs to impose some constraints on the field. First, we need to introduce an incident field to our model. This will split the field expansion into a sum of an incident field, which is given by our model of the problem, and a scattered field. Note that within this framework, the incident field may be chosen to be in either medium, or to be a combination of excitations incident from different media.

In our case, the incident field will be taken as a plane wave incident from medium 1 and defined as

$$\mathbf{E}_0(\mathbf{x}) = \big[\mathcal{E}_{0,p}\;\hat{\mathbf{e}}_{p,1}^-(\mathbf{p}_0) + \mathcal{E}_{0,s}\;\hat{\mathbf{e}}_s(\mathbf{p}_0)\big] \times \exp\left(i\,\mathbf{k}_1^-(\mathbf{p}_0)\cdot\mathbf{x}\right), \tag{13}$$

where $\mathbf{p}_0$ is the projection of the wave vector of the incident wave onto the $(\hat{\mathbf{e}}_1, \hat{\mathbf{e}}_2)$ plane, with the property $|\,\mathbf{p}_0\,| \leq k_1$, i.e. we consider an incident propagating wave. The fact that this is the only incident wave considered, together with the Sommerfeld radiation condition at infinity, gives that the only elementary waves allowed in the scattered field are those with wave vectors of the form $\mathbf{k}_1^+(\mathbf{p})$ and $\mathbf{k}_2^-(\mathbf{p})$ in medium 1 and 2, respectively. This property can be expressed by defining the field amplitudes

$$\boldsymbol{\mathcal{E}}_1^-(\mathbf{q}) = (2\pi)^2\,\delta(\mathbf{q} - \mathbf{p}_0)\;\boldsymbol{\mathcal{E}}_0\,, \tag{14a}$$

$$\boldsymbol{\mathcal{E}}_2^+(\mathbf{q}) = \mathbf{0}\,, \tag{14b}$$

where $\boldsymbol{\mathcal{E}}_0 = (\mathcal{E}_{0,p}, \mathcal{E}_{0,s})^{\mathrm{T}}$. Next, we assume that the scattered field amplitudes are linearly related to the incident field amplitude $\boldsymbol{\mathcal{E}}_0$ via the reflection and transmission amplitudes, $\mathbf{R}(\mathbf{q}\,|\,\mathbf{p}_0)$ and $\mathbf{T}(\mathbf{q}\,|\,\mathbf{p}_0)$, defined as

$$\boldsymbol{\mathcal{E}}_1^+(\mathbf{q}) = \mathbf{R}(\mathbf{q}\,|\,\mathbf{p}_0)\,\boldsymbol{\mathcal{E}}_0, \tag{15a}$$

$$\boldsymbol{\mathcal{E}}_2^-(\mathbf{q}) = \mathbf{T}(\mathbf{q}\,|\,\mathbf{p}_0)\,\boldsymbol{\mathcal{E}}_0\,. \tag{15b}$$

The reflection and transmission amplitudes are therefore described by 2×2 matrices of the form,

$$\mathbf{X} = \begin{pmatrix} X_{pp} & X_{ps} \\ X_{sp} & X_{ss} \end{pmatrix}, \tag{16}$$

with $\mathbf{X} = \mathbf{R}$ or $\mathbf{T}$. From a physical point of view, the complex amplitude $R_{\alpha\beta}(\mathbf{q}\,|\,\mathbf{p}_0)$ (resp. $T_{\alpha\beta}(\mathbf{q}\,|\,\mathbf{p}_0)$) for $\alpha, \beta \in \{p, s\}$ is the field amplitude for the reflected light (resp. transmitted) with lateral wave vector $\mathbf{q}$ in the polarization state α from a unit incident field with lateral wave vector $\mathbf{p}_0$ in the polarization state β. The reflection and transmission amplitudes are then the unknowns in our scattering problem. The equations we need to

solve are deduced from the transfer equations, Eqs. (9) and (12), by applying them respectively at $a_2 = +$ and $a_1 = -$ and by using Eqs. (14) and (15) for the model of the field expansion. This yields the following two decoupled integral equations for the reflection and transmission amplitudes, the so-called reduced Rayleigh equations, that can be written in the following general form, for $\mathbf{X} = \mathbf{R}$ or $\mathbf{T}$:

$$\int \mathbf{M}_{\mathbf{X}}(\mathbf{p}\,|\,\mathbf{q})\,\mathbf{X}(\mathbf{q}\,|\,\mathbf{p}_0)\,\frac{\mathrm{d}^2q}{(2\pi)^2} = -\mathbf{N}_{\mathbf{X}}(\mathbf{p}\,|\,\mathbf{p}_0)\,, \quad (17)$$

where the matrices $\mathbf{M}_{\mathbf{X}}$ and $\mathbf{N}_{\mathbf{X}}$ are given by

$$\mathbf{M}_{\mathbf{R}}(\mathbf{p}\,|\,\mathbf{q}) = \mathcal{J}^{+,+}_{2,1}(\mathbf{p}\,|\,\mathbf{q})\;\mathbf{M}^{+,+}_{2,1}(\mathbf{p}\,|\,\mathbf{q}) \quad (18a)$$

$$\mathbf{M}_{\mathbf{T}}(\mathbf{p}\,|\,\mathbf{q}) = \mathcal{J}^{-,-}_{1,2}(\mathbf{p}\,|\,\mathbf{q})\;\mathbf{M}^{-,-}_{1,2}(\mathbf{p}\,|\,\mathbf{q}) \quad (18b)$$

$$\mathbf{N}_{\mathbf{R}}(\mathbf{p}\,|\,\mathbf{q}) = \mathcal{J}^{+,-}_{2,1}(\mathbf{p}\,|\,\mathbf{q})\;\mathbf{M}^{+,-}_{2,1}(\mathbf{p}\,|\,\mathbf{q}) \quad (18c)$$

$$\mathbf{N}_{\mathbf{T}}(\mathbf{p}\,|\,\mathbf{q}) = \frac{2n_1n_2\alpha_1(\mathbf{p})}{\epsilon_2-\epsilon_1}(2\pi)^2\delta(\mathbf{p}-\mathbf{q})\,\mathbf{I}_2, \quad (18d)$$

with $\mathbf{I}_2$ denoting the 2×2 identity matrix.

B. RRE for scalar waves

The reduced Rayleigh equations can also be derived for scalar waves satisfying the scalar Helmholtz equation and subjected to various boundary conditions at the interfaces. Here, we focus on scalar waves subjected to the continuity of the field and its normal derivative at the interface. Under these hypotheses, one can derive the corresponding reduced Rayleigh equations which read

$$\int M_X(\mathbf{p}\,|\,\mathbf{q})\,X(\mathbf{q}\,|\,\mathbf{p}_0)\frac{\mathrm{d}^2q}{(2\pi)^2} = -N_X(\mathbf{p}\,|\,\mathbf{p}_0)\,, \quad (19)$$

where $X = R$ or T is either the scalar reflection or transmission amplitude, and the scalar kernels and right-hand-sides are given by Eq. (18) where all the $\mathbf{M}^{b,a}_{l,m}$ matrices are replaced by the scalar constant $k_1k_2 = n_1n_2\,\omega^2/c^2$ and $\mathbf{I}_2$ is replaced by the scalar constant 1. We would like to stress that the fact that one can go from the electromagnetic RRE to the scalar RRE by simply replacing all the aforementioned matrices by 1 is only true for the case where the scalar field is subjected to the continuity of the field and its normal derivative at the surface. For other types of boundary conditions, as for the case of acoustic waves for example, one would obtain different expressions [25]. The obtained equations could in principle be used for modeling the scattering of a quantum particle by a surface between two regions of constant potential. In this paper, we will use the presented scalar RRE, for which the analysis is simplified compared to the case for electromagnetic waves, to explain the fundamental mechanism of the Yoneda effect. We will show that the Yoneda effect is present for scalar waves (subjected to the aforementioned boundary conditions) and can be decoupled from additional effects induced by the polarization of electromagnetic waves, such as the Brewster scattering effect. The identified mechanism for scalar waves will then be extended to electromagnetic waves.

C. Perturbative method

Probably the most common approximate solution to Eq. (17) is based on a perturbative expansion of the reflection and transmission amplitudes in powers of the interface profile function. This approach, often called "small amplitude perturbation theory" (SAPT) or "small perturbation method" (SPM), has shown that it is capable of obtaining solutions of the RRE of high qualitative and quantitative predictive power, for interfaces with sufficiently small slopes and amplitudes. To first order in ζ for the reflection and transmission amplitudes, the method is often interpreted as a *single scattering approximation*. When implemented to the complete fourth order in the surface profile function for the intensity, i.e. involving terms up to third order in the amplitude, the method has been used to obtain reliable results that also correctly include multiple scattering effects, most notably the backscattering peaks observed in reflection from metallic surfaces [34–37].

To first order in the interface profile function ζ, we have for $\mathbf{X} = \mathbf{R}$ or $\mathbf{T}$ that

$$\mathbf{X}\,(\mathbf{p}\,|\,\mathbf{p}_0) \approx \mathbf{X}^{(0)}\,(\mathbf{p}\,|\,\mathbf{p}_0) - i\,\mathbf{X}^{(1)}\,(\mathbf{p}\,|\,\mathbf{p}_0)\,, \quad (20)$$

where

$$\mathbf{R}^{(0)}\,(\mathbf{p}\,|\,\mathbf{p}_0) = (2\pi)^2\delta(\mathbf{p}-\mathbf{p}_0)\,\boldsymbol{\rho}^{(0)}(\mathbf{p}_0)\,, \quad (21a)$$

$$\mathbf{T}^{(0)}\,(\mathbf{p}\,|\,\mathbf{p}_0) = (2\pi)^2\delta(\mathbf{p}-\mathbf{p}_0)\,\boldsymbol{\tau}^{(0)}(\mathbf{p}_0)\,, \quad (21b)$$

$$\mathbf{R}^{(1)}\,(\mathbf{p}\,|\,\mathbf{p}_0) = \hat{\zeta}(\mathbf{p}-\mathbf{p}_0)\,\boldsymbol{\rho}^{(1)}\,(\mathbf{p}\,|\,\mathbf{p}_0)$$
$$= [\alpha_1(\mathbf{p})-\alpha_2(\mathbf{p})]\,\hat{\zeta}(\mathbf{p}-\mathbf{p}_0)\,\hat{\boldsymbol{\rho}}^{(1)}\,(\mathbf{p}\,|\,\mathbf{p}_0)\,, \quad (21c)$$

$$\mathbf{T}^{(1)}\,(\mathbf{p}\,|\,\mathbf{p}_0) = \hat{\zeta}(\mathbf{p}-\mathbf{p}_0)\,\boldsymbol{\tau}^{(1)}\,(\mathbf{p}\,|\,\mathbf{p}_0)$$
$$= [\alpha_1(\mathbf{p})-\alpha_2(\mathbf{p})]\,\hat{\zeta}(\mathbf{p}-\mathbf{p}_0)\,\hat{\boldsymbol{\tau}}^{(1)}\,(\mathbf{p}\,|\,\mathbf{p}_0)\,. \quad (21d)$$

Here $\hat{\zeta}$ denotes the Fourier transform of ζ, and $\boldsymbol{\rho}^{(0)}(\mathbf{p}_0)$ and $\boldsymbol{\tau}^{(0)}(\mathbf{p}_0)$ are matrix-valued amplitudes for the zero order reflection and transmission amplitudes, respectively. The matrix-valued amplitudes $\boldsymbol{\rho}^{(1)}\,(\mathbf{p}\,|\,\mathbf{p}_0)$, $\hat{\boldsymbol{\rho}}^{(1)}\,(\mathbf{p}\,|\,\mathbf{p}_0)$, $\boldsymbol{\tau}^{(1)}\,(\mathbf{p}\,|\,\mathbf{p}_0)$, and $\hat{\boldsymbol{\tau}}^{(1)}\,(\mathbf{p}\,|\,\mathbf{p}_0)$ for the first order terms are derived in A. In Eqs. (21c) and (21d), we have given two alternative factorizations of the first order reflection and transmission amplitudes. The factorization including the caret amplitudes is the most appropriate for physical interpretation, while the factorization including the non-caret amplitudes simply aims at separating $\hat{\zeta}$, which is the only factor depending on the specific realization of the surface profile, from the remaining profile-independent amplitude factor.

D. Observables

The observables of interest in this study are the so-called *diffuse* or *incoherent component of the mean differential reflection and transmission coefficients* (MDRC and MDTC) denoted $\langle \partial R_{\alpha\beta}(\mathbf{p}|\mathbf{p}_0)/\partial\Omega_r \rangle_{\text{incoh}}$ and $\langle \partial T_{\alpha\beta}(\mathbf{p}|\mathbf{p}_0)/\partial\Omega_t \rangle_{\text{incoh}}$, respectively. They are both defined as the ensemble average over realizations of the surface profile of the incoherent component of the radiated reflected/transmitted flux of an α-polarized wave around a direction given by $\mathbf{k}_1^+(\mathbf{p})/\mathbf{k}_2^-(\mathbf{p})$ per unit incident flux of a β-polarized plane wave with wave vector $\mathbf{k}_1^-(\mathbf{p}_0)$, per unit solid angle. Based on the reflection and transmission amplitudes found to first order in ζ, the incoherent component of the MDRC and MDTC can be expressed as

$$\left\langle \frac{\partial R_{\alpha\beta}}{\partial\Omega_r}(\mathbf{p}\,|\,\mathbf{p}_0) \right\rangle_{\text{incoh}} = \epsilon_1 \left(\frac{\omega}{2\pi c}\right)^2 \frac{\cos^2\theta_r}{\cos\theta_0} \times \sigma^2\, g(\mathbf{p}-\mathbf{p}_0)\, \left|\rho^{(1)}_{\alpha\beta}(\mathbf{p}\,|\,\mathbf{p}_0)\right|^2, \tag{22}$$

and

$$\left\langle \frac{\partial T_{\alpha\beta}}{\partial\Omega_t}(\mathbf{p}\,|\,\mathbf{p}_0) \right\rangle_{\text{incoh}} = \frac{\epsilon_2^{3/2}}{\epsilon_1^{1/2}} \left(\frac{\omega}{2\pi c}\right)^2 \frac{\cos^2\theta_t}{\cos\theta_0} \times \sigma^2\, g(\mathbf{p}-\mathbf{p}_0)\, \left|\tau^{(1)}_{\alpha\beta}(\mathbf{p}\,|\,\mathbf{p}_0)\right|^2. \tag{23}$$

The detailed derivation of the Eqs. (22) and (23) can be found in B. The definition of the angles of incidence and scattering can be deduced from Figure 1.

IV. RESULTS AND DISCUSSION

In order to study the phenomena observed in the scattering of light from weakly rough dielectric interfaces, we choose to base our discussion on results obtained through small amplitude perturbation theory (SAPT) to lowest non-zero order in the interface profile function, Eqs. (21). For sufficiently smooth interfaces this approximation has previously been compared to numerical non-perturbative solutions to the reduced Rayleigh equations, where it has been shown to adequately model the phenomena of both the Brewster scattering angles and the Yoneda peaks [1, 2]. We will start our investigations with a summary of the features observed in the main physical observables, the MDRC and MDTC [Eqs. (22) and (23)], followed by more in-depth analyses and discussions from a physics point of view.

A. Phenomenology of the Yoneda and Brewster scattering effects

The top panel of each subfigure in Fig. 2 presents results based on Eqs. (22) and (23) for the contribution to the co-polarized diffuse component of the MDRC and MDTC in the plane of incidence ($\hat{\mathbf{p}} \parallel \hat{\mathbf{p}}_0$), for a configuration where light is incident from vacuum [$\epsilon_1 = 1$] onto a two-dimensional randomly rough interface with glass [$\epsilon_2 = 2.25$]. The incident light was assumed to be a p- or s-polarized plane wave of wavelength $\lambda = 632.8\,\text{nm}$ in vacuum. In the current work all results presented for randomly rough interfaces consist of interfaces defined by an isotropic Gaussian height distribution with rms height $\sigma = 32\,\text{nm} = \lambda/20$ and an isotropic Gaussian correlation function of transverse correlation length $a = 211\,\text{nm} = \lambda/3$.

For normal incidence [$\theta_0 = 0°$, Fig. 2(a)] the MDRC distributions are nearly featureless. The differences in the scattered intensities observed for p- and s-polarized incident light are very small. Note that the scattered intensity is zero beyond the limit of propagation in the medium of reflection ($|p_1| > k_1$). The overall bell-shape of the distributions can be attributed in part to the Gaussian correlation function for the transverse correlation length in the interface profile together with the $\cos^2\theta_r$ factor of the MDRC, as seen in Eq. (22). The corresponding transmitted intensity (MDTC) shown in Fig. 2(d), however, shows several interesting features. As is detailed in Ref. 2, we now observe pronounced peaks in s-polarization and narrow dips to zero in p-polarization around $|p_1| = k_1$. For normal incidence these features are independent of the azimuthal angle of transmission ϕ. The peaks have become known as "Yoneda peaks", and are always found at the parallel wavevectors $\mathbf{p}$ along the propagation limit in the less dense medium (i.e. $|\mathbf{p}| = \min(k_1, k_2)$). The polar angles corresponding to the dips to zero in the MDTC have been called the "Brewster scattering angles"[13], and are unique to scattered light which is p-polarized. As the polar angle of incidence is increased [$\theta_0 = 35°$ or $70°$ in Fig. 2], we observe that a Brewster scattering angle also appears in the MDRC. In transmission, the distributions of the MDTC behave very predictably in the s-polarized case as the weight of the distribution is shifted to higher polar scattering angles. However, in the case of p-polarization the Brewster scattering angle in the direction of $\phi = 180°$ (negative values of θ_t in Fig. 2(d)) shifts to positions closer to $\theta_t = 0°$ as the angle of incidence is increased, and the dip to zero in the forward scattering direction [$\phi = 0°$] first becomes a non-zero local minimum and is gradually replaced with a Yoneda peak similar to the one found for s-polarization.

Figure 3 presents results similar to those in Fig. 2, but for the situation where the media are interchanged; the light is now incident from glass [$\epsilon = 2.25$] onto a two-dimensional randomly rough interface with vacuum [$\epsilon = 1$]. A closer inspection of the distributions of the MDRC for normal incidence reveals that the distributions are reminiscent of the distributions seen in transmission for the MDTC in Fig. 2, and vice versa. This similarity between intensity distributions for which the media of propagation is the same is an expected symmetry, but as the angle of incidence increases these sim-

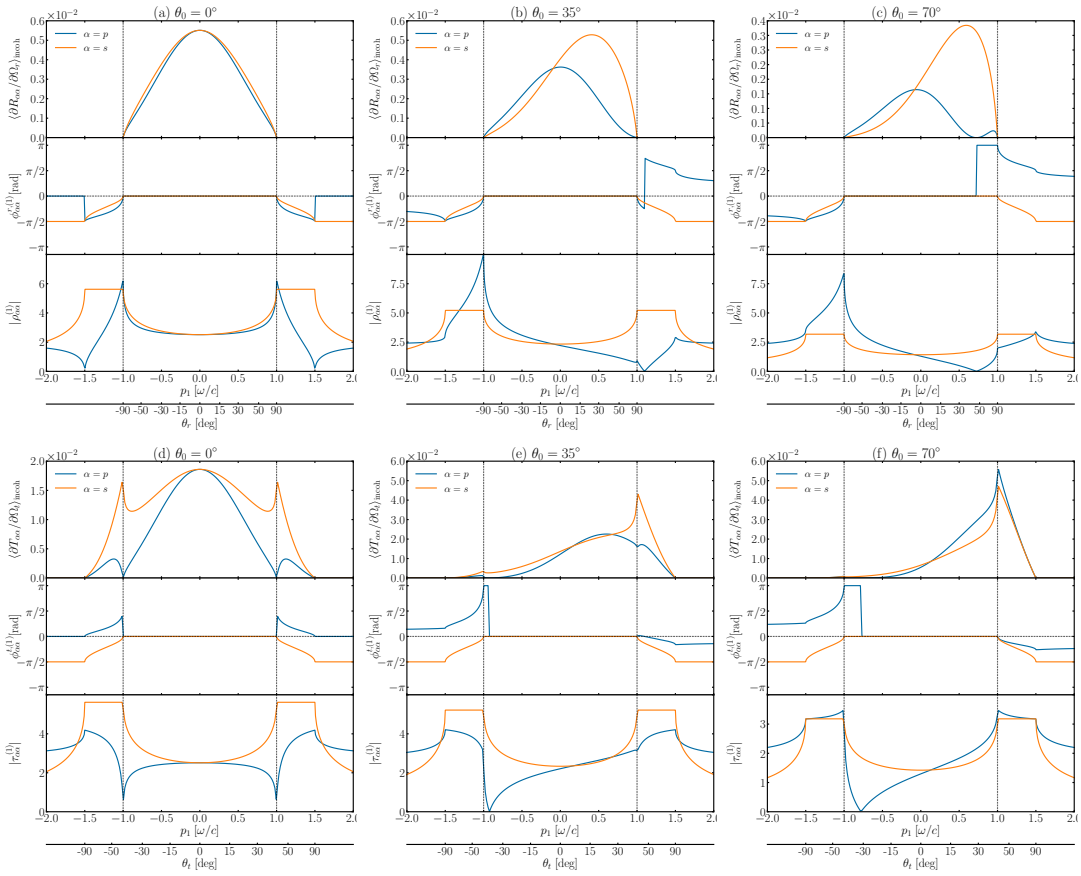

FIG. 2. The incoherent component of the MDRC (top row) and MDTC (bottom row) for light incident from vacuum [$\epsilon_1 = 1.0$] onto a randomly rough interface with glass [$\epsilon_2 = 2.25$], for in-plane co-polarized scattering, as a function of the lateral component of the wave vector of scattering p_1 or polar angle of scattering $\theta_{r,t}$. The polar angle of incidence is indicated on top of each subfigure. The argument and the modulus of $\rho^{(1)}_{\alpha\alpha}$ and $\tau^{(1)}_{\alpha\alpha}$ are indicated in the middle and bottom section of each subfigure respectively. Note that we have adopted here the convention that negative $\theta_{r,t}$ values correspond to $\theta_{r,t} > 0$ according Fig. 1 but for $\phi = 180°$. The vertical lines indicate $|\,\mathbf{p}\,| = k_{\rm min}$.

ilarities gradually fade. For light impinging on the interface at $\theta_0 = 35°$, the Brewster scattering angle for the MDRC is now in the forward scattering direction, and as documented in Ref. 1 it shifts closer to $\theta_r = 0°$ as the angle of incidence increases towards the critical angle given by $\theta_c = \sin^{-1}(n_2/n_1)$. Results for an angle of incidence equal to the critical angle, $\theta_0 = \theta_c$, are presented in Figs. 3(c) and 3(f). For the same system but for polar angles of incidence larger than the critical angle, presented in Fig. 4, the dip to zero MDRC in the forward scattering direction is gradually overtaken by a Yoneda peak for p-polarized light. Contrary to the case for transmission in Fig. 2 however, the peak in p-polarization never grows beyond the peak in s-polarization. For the intensity distributions of the transmitted light we again observe a gradual shift of the weight of the distributions into the forward scattering direction, but the Brewster scattering angle is now only visible (strictly speaking) for $\theta_0 = 35°$ and $\theta_0 = 41.81°$, where it is now found in the backward scattering direction and at $\theta_t = 0°$, respectively.

As an aid in understanding the Brewster scattering angles in Figs. 2, 3 and 4, and also as a support to the further discussion of these angles in both reflection and transmission, Fig. 5 presents an overview of the Brewster scattering angles found in the MDRC/MDTC as derived from first order SAPT. Figure 5 is based on the following

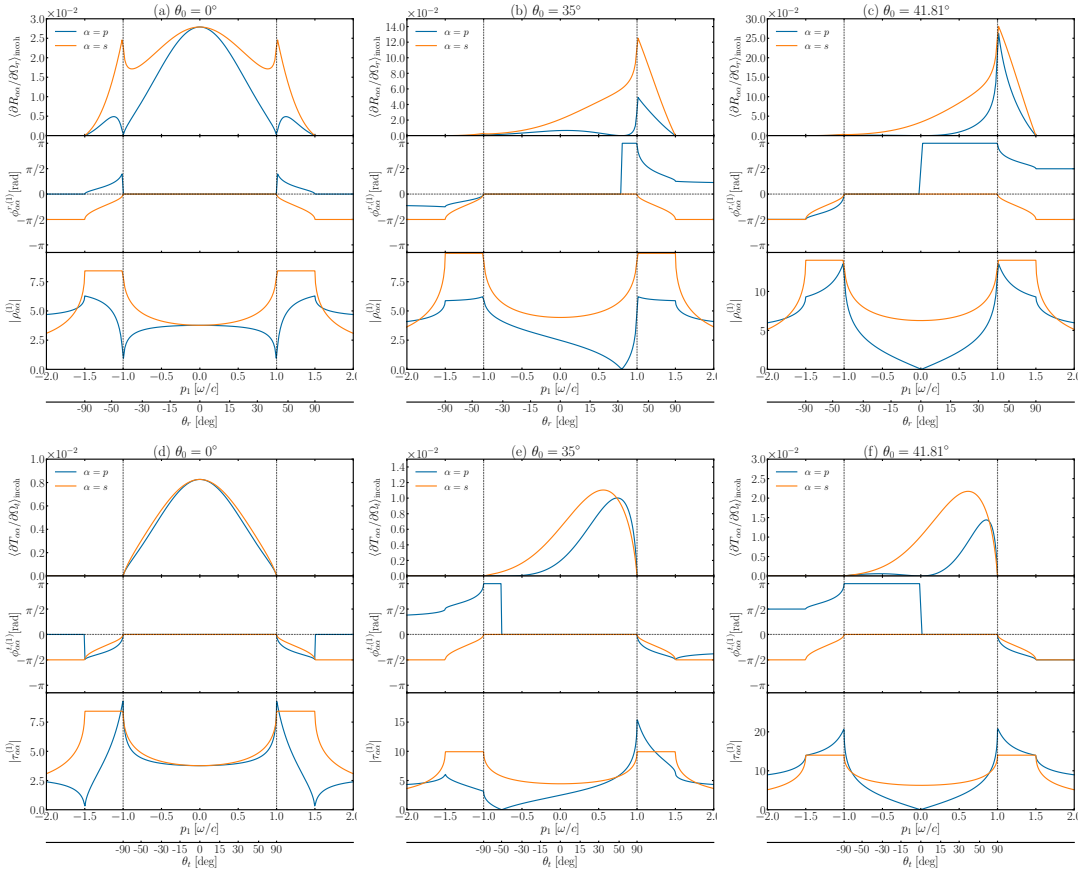

FIG. 3. Same as Fig. 2, but for light incident from glass [$\epsilon_1 = 2.25$] onto a randomly rough interface with vacuum [$\epsilon_2 = 1.0$].

result, obtained from SAPT [1, 2]:

$$\Theta_B(\theta_0) = \sin^{-1}\left(\sqrt{\frac{\epsilon_2(\epsilon_2 - \epsilon_1 \sin^2\theta_0)}{(\epsilon_2^2 - \epsilon_1^2)\sin^2\theta_0 + \epsilon_1\epsilon_2}}\right). \quad (24)$$

for reflection and

$$\Theta_B(\theta_0) = \sin^{-1}\left(\frac{\epsilon_1}{\epsilon_2}\sqrt{\frac{\epsilon_2}{\epsilon_1} - \sin^2\theta_0}\right), \quad (25)$$

for transmission. Here Θ_B indicates the Brewster scattering angle. As can be observed in both Fig. 5 and from Eqs. (24) and (25), Θ_B is not well-defined for all angles of incidence for all ϵ_1 and ϵ_2. These limits will be further explored in Sec. IV D where a clear geometrical interpretation will be given.

The scattering in both reflection and transmission from such a randomly rough interface has been thoroughly studied in the past, and the distributions of the MDRC and MDTC presented in Figs. 2, 3 and 4 were partially explained based on the components of the perturbative approximation in Refs. 1 and 2. However, these publications stopped short of presenting a full physical interpretation of the features seen in these distributions. In the current work we aim to finalize this analysis, and to that end we expand the investigation to include results for the complex amplitudes on which the MDRC and MDTC are based. The center panel of each subfigure in Figs. 2, 3 and 4 presents the average phase, $\phi_{\alpha\alpha}^{r,(1)}$, $\phi_{\alpha\alpha}^{t,(1)}$ of the co-polarized scattered light, obtained from the argument of the complex amplitudes $\rho_{\alpha\alpha}^{(1)}$ or $\tau_{\alpha\alpha}^{(1)}$ for $\alpha \in \{p, s\}$ given in Eqs. (21 d) and (21 e), respectively. The lower panel of each subfigure shows the modulus of $\rho_{\alpha\alpha}^{(1)}$ and $\tau_{\alpha\alpha}^{(1)}$.

In passing we emphasize that even if the results presented are based on a perturbation method to lowest non-zero order in the interface profile function, previous studies have demonstrated their validity for the parameters

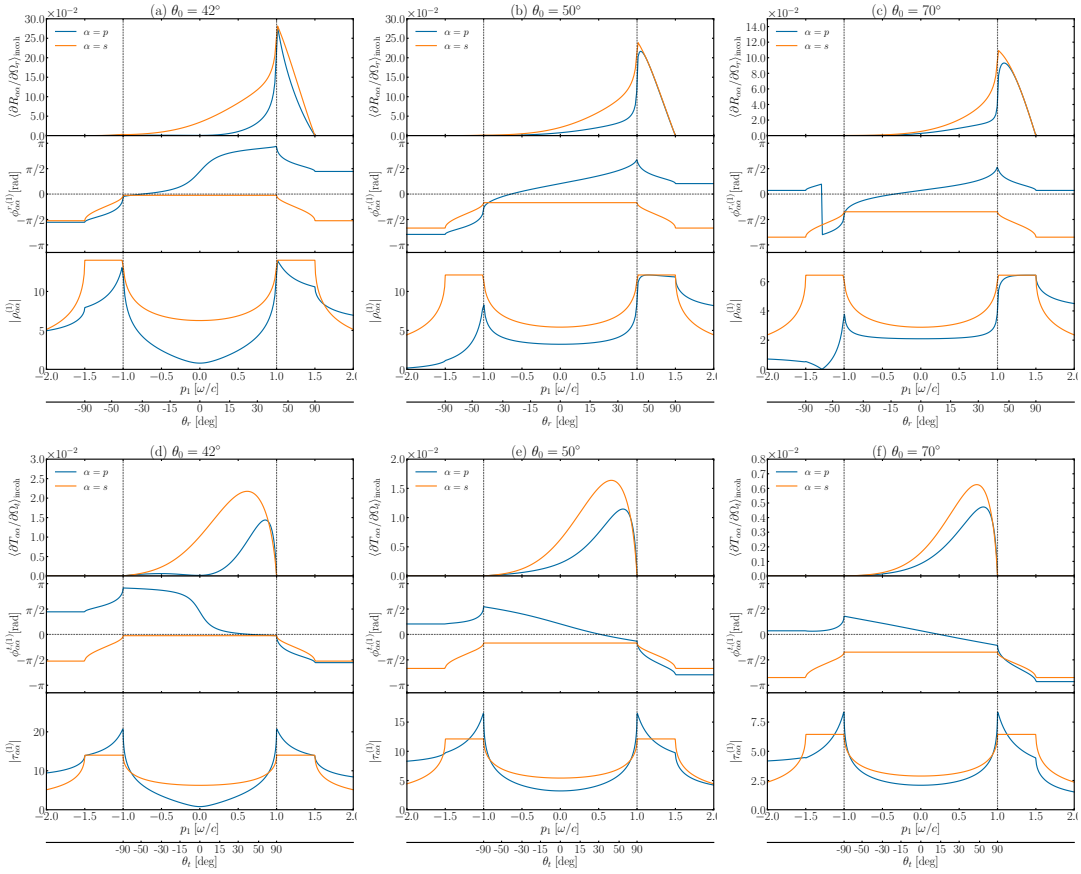

FIG. 4. Same as Fig. 3, but for additional polar angles of incidence θ_0.

and dielectric constants assumed in obtaining them. In addition, the results for both MDRC and MDTC have been compared against numerical results based on the extinction theorem based method described in Ref. 37 for a 1D system, a method known to be rigorous.

[19]

$$r_s^{\mathrm{F}}(\mathbf{p}_0) = \frac{\alpha_1(\mathbf{p}_0) - \alpha_2(\mathbf{p}_0)}{\alpha_1(\mathbf{p}_0) + \alpha_2(\mathbf{p}_0)} \tag{26a}$$

$$r_p^{\mathrm{F}}(\mathbf{p}_0) = \frac{\epsilon_2\alpha_1(\mathbf{p}_0) - \epsilon_1\alpha_2(\mathbf{p}_0)}{\epsilon_2\alpha_1(\mathbf{p}_0) + \epsilon_1\alpha_2(\mathbf{p}_0)}\,, \tag{26b}$$

B. Physical interpretation of SAPT to first order

Order zero, Fresnel amplitudes — First we revisit the interpretation of the Fresnel coefficients which are encoded in the amplitudes $\boldsymbol{\rho}^{(0)}(\mathbf{p}_0)$ and $\boldsymbol{\tau}^{(0)}(\mathbf{p}_0)$ [Eqs. (21a) and (21b)].

We start our analysis looking at the case of reflection. The Fresnel amplitudes for s- and p-polarized waves reflected by a planar surface between two dielectrics read which we have here written in a common form in terms of the components of the wave vectors along $\hat{\mathbf{e}}_3$. It is easy to show by using straightforward algebra that these expressions are equivalent to $\rho_{ss}^{(0)}(\mathbf{p}_0)$ and $\rho_{pp}^{(0)}(\mathbf{p}_0)$ respectively, given by perturbation theory to zero order. An equivalent way of writing the Fresnel amplitudes which follows directly from Eq. (A6) and the definition of the $\mathbf{M}_{l,m}^{b,a}(\mathbf{p}\,|\,\mathbf{q})$ matrix in terms of the polarization vectors,

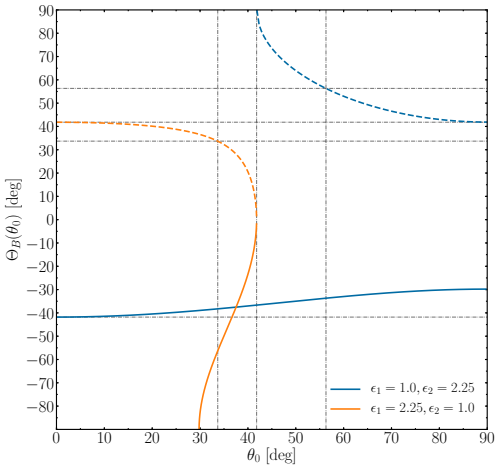

FIG. 5. Dependence of the in-plane Brewster scattering angle Θ_B on the polar angle of incidence θ_0, as given by Eq. (25). $\phi = 180°$ is indicated by negative values of Θ_B and θ_0. Solid lines indicate Θ_B in transmission, while the dashed lines with color corresponding to the values of ϵ indicate Θ_B in reflection. The critical angles and the regular Brewster angles for a corresponding system with a planar interface have been indicated on both axes as black dash-dotted lines.

Eq. (10), is

$$\rho^{(0)}_{ss}(\mathbf{p}_0) = \rho^{(0)}(\mathbf{p}_0)\,\frac{\hat{\mathbf{e}}_s(\mathbf{p}_0)\cdot\hat{\mathbf{e}}_s(\mathbf{p}_0)}{\hat{\mathbf{e}}_s(\mathbf{p}_0)\cdot\hat{\mathbf{e}}_s(\mathbf{p}_0)} \tag{27a}$$

$$\rho^{(0)}_{pp}(\mathbf{p}_0) = \rho^{(0)}(\mathbf{p}_0)\,\frac{\hat{\mathbf{e}}^+_{p,2}(\mathbf{p}_0)\cdot\hat{\mathbf{e}}^-_{p,1}(\mathbf{p}_0)}{\hat{\mathbf{e}}^+_{p,2}(\mathbf{p}_0)\cdot\hat{\mathbf{e}}^+_{p,1}(\mathbf{p}_0)} \tag{27b}$$

$$\rho^{(0)}(\mathbf{p}_0) = \frac{\alpha_1(\mathbf{p}_0)-\alpha_2(\mathbf{p}_0)}{\alpha_1(\mathbf{p}_0)+\alpha_2(\mathbf{p}_0)}\,. \tag{27c}$$

In Eq. (27a), we have intentionally chosen not to simplify the dot products (all equal to 1) to illustrate that the Fresnel amplitudes expressed in the form given by Eqs. (27a) and (27b) exhibit a remarkable factorization which reveals two facets of the physics of scattering from a microscopic point of view. First, both Fresnel amplitudes in Eqs. (27a) and (27b) share the same first factor, $\rho^{(0)}(\mathbf{p}_0)$ defined in Eq. (27c), which corresponds to the reflection amplitude for a scalar plane wave subjected to the continuity of the scalar field and its normal derivative at the surface. In other words, this first factor can be interpreted as the coherent response of arrays of individual scatterers (at the atomic level) which scatter the incident wave as *spherical waves*. The second factor, which differs for each polarization, is the signature of the dipolar nature of the radiation of each individual scatterer. Indeed, for an s-polarized incident wave, the scattering dipoles are excited along the $\hat{\mathbf{e}}_2$-axis and hence re-emit isotropically in the plane of incidence $(\hat{\mathbf{e}}_1, \hat{\mathbf{e}}_3)$. We argue that this is the reason why the second factor is identically equal to 1 for s-polarized light. For p-polarization, the scattering dipoles are excited along some direction in the plane of incidence $(\hat{\mathbf{e}}_1, \hat{\mathbf{e}}_3)$ and therefore the reflection amplitude given by the scattering of spherical waves must be weighted with the second factor in Eq. (27b) in order to take into account the dipole radiation pattern. Such a factorization and interpretation of the Fresnel amplitudes were given and thoroughly discussed by Doyle [26] in light of the Ewald-Oseen extinction theorem and its original derivation by Ewald based on microscopic optics [29].

For a planar surface all scattered waves interfere destructively in all directions but the specular, as indicated by the Dirac distribution in Eqs. (21a) and (21b). This is not the case when the surface is non-planar, and the above interpretation suggests that the spherical-like waves scattered away from the specular direction are then to be weighted by the appropriate dipole factor, even for s-polarized light (as will be the case for the first order term).

From Eq. (27), we can deduce two properties well known for the reflection of a plane wave at a planar interface between two dielectric media. First, for $\epsilon_1 > \epsilon_2$ there exists a critical polar angle $\theta_c = \sin^{-1}(n_2/n_1)$, or equivalently a critical norm of the lateral wave vector $p_c = n_2\,\omega/c$, such that for all angles of incidence larger than θ_c (equivalently for all lateral wave vectors where $|\,\mathbf{p}_0\,| > p_c$), all the incident power is reflected. The phenomenon of total internal reflection is entirely controlled by the factor $\rho^{(0)}(\mathbf{p}_0)$ present for both polarizations, and hence can be analyzed from a scalar wave picture decoupled from polarization effects. From a physical point of view, total internal reflection occurs whenever the refracted wave is evanescent in the medium of transmission, and therefore it cannot transport energy away from the surface. It is instructive to analyze the behavior of the reflection amplitude $\rho^{(0)}(\mathbf{p}_0)$ as the refracted wave turns evanescent in the second medium as one varies the incident lateral wave vector $\mathbf{p}_0$. For $|\,\mathbf{p}_0\,| < p_c$, both $\alpha_1(\mathbf{p}_0)$ and $\alpha_2(\mathbf{p}_0)$ are real. As $|\,\mathbf{p}_0\,| \to p_c$, $\rho^{(0)}(\mathbf{p}_0)$ moves on the real line towards 1 when α_2 vanishes, $\alpha_1(\mathbf{p}_0) = \sqrt{\epsilon_1-\epsilon_2}\;\omega/c$. When $|\,\mathbf{p}_0\,| > p_c$, $\alpha_2(\mathbf{p}_0)$ becomes pure imaginary and $\rho^{(0)}(\mathbf{p}_0)$ starts to trace a circular arc in the lower half of the complex plane (negative imaginary part) with unit modulus (the fact that $|\rho^{(0)}(\mathbf{p}_0)| = 1$ for $|\,\mathbf{p}_0\,| > p_c$ is immediate since then $\rho^{(0)}(\mathbf{p}_0)$ is of the form z^*/z where z is a non-zero complex number). As $|\,\mathbf{p}_0\,| \to n_1\omega/c$, the reflected wave (and the incident wave) reaches the limit of propagation in the first medium and $\alpha_1(\mathbf{p}_0) \to 0$ which makes the reflection amplitude real, negative, equal to -1. Thus, as we go from the critical point to grazing incidence the reflection amplitude traces a half circle in the complex plane with unit modulus. The argument of the reflection amplitude, the phase, hence varies from 0 to $-\pi$ rad. This gradual phase shift is known as the Goos-Hänchen phase shift and can be interpreted as follows. If we regard the reflected

and refracted waves as two components of a single mode, then as the wave enters the second medium the wave oscillates while propagating along the surface before it eventually goes back into the first medium where it can continue to propagate to infinity. As the wave propagates along the surface, while being evanescent in medium 2, it acquires a temporal delay which depends on its wave vector. This delay is translated into a phase shift as the wave oscillates back into medium 1. Geometrically this process is often interpreted as if the wave is reflected from the second medium only after a slight penetration into it [19].

The second phenomenon of interest is that of the polarization angle, or Brewster's angle, which, as the name indicates, requires us to analyze the polarization dependent factor in the reflection amplitudes. For an s-polarized wave the polarization factor is identically equal to 1 and no polarization angle is observed. However, the Fresnel amplitude for p-polarized light, Eq. (27b), is shown to be proportional to $\hat{\mathbf{e}}^{+}_{p,2}(\mathbf{p}_0) \cdot \hat{\mathbf{e}}^{-}_{p,1}(\mathbf{p}_0)$ i.e. it is proportional to the component of the incident electric field (given by $E_0\, \hat{\mathbf{e}}^{-}_{p,1}(\mathbf{p}_0)$) along the direction given by $\hat{\mathbf{e}}^{+}_{p,2}(\mathbf{p}_0)$. We recall that the direction given by $\hat{\mathbf{e}}^{+}_{p,2}(\mathbf{p}_0)$ corresponds to the local p-polarization direction for a wave whose wave vector is given by $\mathbf{k}^{+}_{2}(\mathbf{p}_0)$, in other words, a wave which propagates upwards in the second medium. These factors of the dot products in Eq. (27b) therefore seem to indicate that the reflected amplitude for p-polarized light depends on a projection of the incident field along the polarization vector of a seemingly *nonexisting* wave, propagating along the wave vector $\mathbf{k}^{+}_{2}(\mathbf{p}_0)$. However, such a seemingly virtual wave does have a physical interpretation, based on the mutual interaction between waves propagating in dielectric media. Doyle [26] provided an explanation based on the concept of the *wave triad* originally introduced by Ewald [29]. Ewald considered a dense array of dipole scatterers (the entire dielectric medium) situated in a half space and excited by an incident plane wave incident from the vacuum half-space, filling the whole space between the scatterers. He showed that the dipole scatterers would respond to the excitation in such a way that there exist planes of scatterers of coherent response, meaning that all dipoles within such a plane oscillate in phase. As a consequence of this fact and that the array of scatterers is bounded within a half space, the superposition of all elementary wavelets emitted by each individual scatterer results in the propagation of three plane waves: two waves called *vacuum waves* propagating with a phase velocity equal to c and one wave propagating with phase velocity c/n called *polarization wave*, where n corresponds to the refractive medium made of scatterers within the macroscopic picture. The wave propagating with phase velocity c/n corresponds to the transmitted wave in the macroscopic picture, while one of the waves propagating with phase velocity c serves to exactly cancel the incident wave within the dielectric medium. The other wave propagating with phase velocity c exits the medium and corresponds to the reflected wave. The wave vectors of the different waves are naturally given by Snell's law, and Ewald's derivation can be viewed as a microscopic validation of Snell's law.

When two half-spaces are filled with dipole scatterers of different dipole moments, similar arguments apply with the difference that the superposition of all wavelets emitted by all scatterers (i.e. from both sides of the interface) must be taken into account. This results in three wave triads: one triad associated with the incident wave, one for the reflected wave and one for the refracted wave, which all satisfy the so-called dynamical conditions [26]. To the incident polarization wave in medium 1, propagating with phase velocity c/n_1 and wave vector $\mathbf{k}^{-}_{1}(\mathbf{p}_0)$ are associated two waves propagating with phase velocity c/n_2 with wave vectors $\mathbf{k}^{\pm}_{2}(\mathbf{p}_0)$. Similarly, to the reflected (resp. refracted) polarization wave, whose wave vector is given by $\mathbf{k}^{+}_{1}(\mathbf{p}_0)$ (resp. $\mathbf{k}^{-}_{2}(\mathbf{p}_0)$), are associated two waves propagating with phase velocity c/n_2 (resp. c/n_1) and wave vectors $\mathbf{k}^{\pm}_{2}(\mathbf{p}_0)$ (resp. $\mathbf{k}^{\pm}_{1}(\mathbf{p}_0)$). The dynamical conditions are state that the amplitudes of the different waves are such that (i) the wave associated with the refracted polarization wave and propagating along $\mathbf{k}^{-}_{1}(\mathbf{p}_0)$ in medium 2 cancels the incident wave and (ii) that the superposition of waves associated with the incident and reflected polarization waves and propagating along $\mathbf{k}^{+}_{2}(\mathbf{p}_0)$ vanishes (more details can be found in Refs. 26 and 29).

In the following, we will refer to the wave vectors $\mathbf{k}^{a}_{1}(\mathbf{p})$ and $\mathbf{k}^{a}_{2}(\mathbf{p})$, i.e. wave vectors sharing the same projection in the $(\hat{\mathbf{e}}_1, \hat{\mathbf{e}}_2)$-plane and pointing either both upward or downward, as *Snell-conjugate* wave vectors. When it comes to the polarization dependence of the reflection amplitudes, the fact that $\rho^{(0)}_{pp}(\mathbf{p}_0)$ is proportional to $\hat{\mathbf{e}}^{+}_{p,2}(\mathbf{p}_0) \cdot \hat{\mathbf{e}}^{-}_{p,1}(\mathbf{p}_0)$ indicates that the amplitude of the reflected wave is controlled by the component of the incident field along the p-polarization vector associated with the Snell-conjugate wave vector of the wave vector of the reflected wave. This indicates that the direction of the dipole oscillation is intimately linked to waves in the aforementioned triad.

Equation (27b) provides an interesting condition for the well known Brewster's angle. The Brewster phenomenon for dielectric media is commonly defined as the extinction of the p-polarized reflected wave in the case of a planar interface. From Eq. (27b), it is clear that the Fresnel amplitude vanishes if and only if [38] $\hat{\mathbf{e}}^{+}_{p,2}(\mathbf{p}_0) \cdot \hat{\mathbf{e}}^{-}_{p,1}(\mathbf{p}_0) = 0$. Since $\hat{\mathbf{e}}^{+}_{p,2}(\mathbf{p}_0)$ is orthogonal to $\mathbf{k}^{+}_{2}(\mathbf{p}_0)$, we can restate the condition for Brewster's angle as the polar angle where $\mathbf{k}^{+}_{2}(\mathbf{p}_0) \parallel \hat{\mathbf{e}}^{-}_{p,1}(\mathbf{p}_0)$. This means that we can define Brewster's angle as *the angle of reflection ensuring colinearity between the incident field amplitude and the wave vector which is Snell-conjugate to that of the reflected wave.* Note that we take here a slight change of point of view compared to the common phrasing. One usually refer to Brewster's angle as an angle of incidence, while we prefer to refer to the angle of reflection. Obviously, the two are the same for a planar interface, but the latter point of view is the one which

will hold true for non-planar interfaces. Nevertheless, it is convenient to use the term Brewster's incidence for a planar interface and we can define it as the angle of incidence $\theta_{\rm B} = \arctan(n_2/n_1)$ which yields a Brewster (non-)reflected wave. We will see that this angle of incidence, $\theta_0 = \theta_{\rm B}$, has a remarkable property in the case of scattering by a non-planar interface.

Brewster's angle in the case of non-magnetic media is often said to be the angle of incidence that results in a right angle (90°) between the wave vector of the transmitted wave and that of the (non-)reflected wave. In the case of a planar interface, our new definition of Brewster angle agrees with this explanation. Indeed, if $\hat{\mathbf{e}}^-_{p,1}(\mathbf{p}_0) \cdot \hat{\mathbf{e}}^+_{p,2}(\mathbf{p}_0) = 0$ it is immediate that $\mathbf{k}^+_1(\mathbf{p}_0) \cdot \mathbf{k}^-_2(\mathbf{p}_0) = 0$. However, we will see below that the new geometrical criterion proposed in the above holds when applied with Snell-conjugate wave vector associated with a non-specularly scattered wave, while the "right angle" criterion between wave vectors breaks down.

The Fresnel amplitudes for the *refracted* wave for s- and p-polarized light expressed in terms of polarization vectors, presented in a similar fashion as Eq. (27), read

$$\tau^{(0)}_{ss}(\mathbf{p}_0) = \frac{\tau^{(0)}(\mathbf{p}_0)}{\hat{\mathbf{e}}_s(\mathbf{p}_0) \cdot \hat{\mathbf{e}}_s(\mathbf{p}_0)} \tag{28a}$$

$$\tau^{(0)}_{pp}(\mathbf{p}_0) = \frac{\tau^{(0)}(\mathbf{p}_0)}{\hat{\mathbf{e}}^-_{p,1}(\mathbf{p}_0) \cdot \hat{\mathbf{e}}^-_{p,2}(\mathbf{p}_0)} \tag{28b}$$

$$\tau^{(0)}(\mathbf{p}_0) = \frac{c^2}{\omega^2} \frac{2\alpha_1(\mathbf{p}_0)}{(\epsilon_1 - \epsilon_2)} [\alpha_1(\mathbf{p}_0) - \alpha_2(\mathbf{p}_0)] \,. \tag{28c}$$

From Eq. (28), it is readily observed that neither the s- nor p-polarized zero order transmitted wave vanishes in general, which relates to the common experience that no Brewster angle is known for transmission through a planar interface. This fact does not, however, prevent the existence of Brewster *scattering* angles in the diffusely transmitted light. Equation (28) will therefore be important in the remainder of this paper. Note the presence of the factor $\alpha_1(\mathbf{p}_0) - \alpha_2(\mathbf{p}_0)$ in the transmission amplitude of the scalar wave in Eq. (28c) which is identical to the numerator of the reflection amplitude in Eq. (27c). The analysis of this term on total internal reflection hence leads to a similar behavior for the transmission amplitude, in the sense that $\tau^{(0)}(\mathbf{p}_0)$ leaves the real line and traces a path in the complex plane when total internal reflection occurs. This fact illustrates the coupling between the reflected and the transmitted waves, which may be interpreted as two components of the same mode.

First order — We now turn to the first order amplitudes $\mathbf{R}^{(1)}(\mathbf{p} \,|\, \mathbf{p}_0)$ and $\mathbf{T}^{(1)}(\mathbf{p} \,|\, \mathbf{p}_0)$. The first remarkable point to notice is that, when using the caret amplitudes, *both* the first order reflection and transmission amplitudes are proportional to $[\alpha_1(\mathbf{p}) - \alpha_2(\mathbf{p})]\hat{\zeta}(\mathbf{p} - \mathbf{p}_0)$. By a careful examination of the derivation of Eqs. (21c) and (21d) we note that this factor originates from a Taylor expansion of the term $\exp[-i(b\alpha_l(\cdot) - a\alpha_m(\cdot))\zeta(\cdot)]$ appearing in the $\mathcal{J}^{b,a}_{l,m}$ integral (see A). Intuitively, the $\mathcal{J}^{b,a}_{l,m}$ integral encodes information about the sum of amplitudes of scattering events occurring near the surface. A comparison of the expression for the $\mathcal{J}^{b,a}_{l,m}$ integral and the expression obtained by summing complex amplitudes for single scattering paths scattered at the surface of a perfect conductor supports this analogy. In other words, the integral encodes the resulting interference due to the phase difference between any scattering path occurring along the surface. To be more accurate, if one has the microscopic picture in mind one might say that it corresponds to summing scattering events occurring anywhere in the bulk, but in virtue of the extinction theorem the summation reduces to a sum over the surface [28]. With this picture in mind, the factor $[\alpha_1(\mathbf{p}) - \alpha_2(\mathbf{p})]\hat{\zeta}(\mathbf{p} - \mathbf{p}_0)$ corresponds to the resulting *interference* pattern when the phase factor is linearly approximated. Note that this factor does not contain any information about polarization. It is therefore instructive to consider the first order reflection and transmission amplitudes for scalar waves as a first step in order to obtain a better understanding of the full amplitudes. For scalar waves we set all the $\mathbf{M}^{b,a}_{l,m}$ matrices to unity in Eqs. (21c) and (21d) to obtain

$$R^{(1)}(\mathbf{p} \,|\, \mathbf{p}_0) = [\alpha_1(\mathbf{p}) - \alpha_2(\mathbf{p})]\, \hat{\zeta}(\mathbf{p} - \mathbf{p}_0) \times [1 + \rho^{(0)}(\mathbf{p}_0)] \tag{29a}$$

$$T^{(1)}(\mathbf{p} \,|\, \mathbf{p}_0) = [\alpha_1(\mathbf{p}) - \alpha_2(\mathbf{p})]\, \hat{\zeta}(\mathbf{p} - \mathbf{p}_0)\, \tau^{(0)}(\mathbf{p}_0) \,. \tag{29b}$$

From Eq. (29) it is apparent that the first order amplitudes are equal to the aforementioned interference factor, $[\alpha_1(\mathbf{p}) - \alpha_2(\mathbf{p})]\, \hat{\zeta}(\mathbf{p} - \mathbf{p}_0)$, weighted by the *total scalar zero order field amplitude* in either medium 1 or 2. Indeed, the factor $[1 + \rho^{(0)}(\mathbf{p}_0)]$ in Eq. (29a) represents the sum of the unit incident field amplitude and the amplitude of the reflected zero order field, while $\tau^{(0)}(\mathbf{p}_0)$ is simply the refracted zero order field amplitude; hence the denomination total zero order field.

One may think of the total zero order field as characterizing the state of a background field to which the interference pattern induced by the surface corrugation is superimposed (in a multiplicative sense). One could say that the interference pattern allows to probe the state of the zero order field away from the specular direction. In addition, note that the dependence on the outgoing wave vector $\mathbf{p}$ is entirely encoded in the term $[\alpha_1(\mathbf{p}) - \alpha_2(\mathbf{p})]\hat{\zeta}(\mathbf{p} - \mathbf{p}_0)$ while the state of the zero order field only depends on the incident wave vector $\mathbf{p}_0$. This indicates that the factor $[\alpha_1(\mathbf{p}) - \alpha_2(\mathbf{p})]\, \hat{\zeta}(\mathbf{p} - \mathbf{p}_0)$ can be thought to define a probability measure (by taking its modulus square) for a change of lateral wave vector from $\mathbf{p}_0$ to $\mathbf{p}$ (or its corresponding lateral momentum). Moreover, since the amplitude for a wave scattered with lateral wave vector $\mathbf{p}$ does not, to first order, involve any other wave than the incident one through its wave vector $\mathbf{p}_0$, we can consider a wave with lateral wave vector $\mathbf{p}$ as completely decoupled from a wave with lateral wave vector $\mathbf{q} \neq \mathbf{p}$. However, the wave reflected with lateral wave

vector $\mathbf{p}$ is considered to be coupled to the wave transmitted with the same lateral wave vector. In fact, this point of view is strengthened by the fact that both the reflected and transmitted waves sharing the same lateral wave vector also share exactly the same $\mathbf{p}$-dependence for their amplitude according to Eq. (29). We can interpret this fact by saying that the reflected and transmitted waves sharing the same lateral wave vector are two pieces of *one* mode defined in the whole space, and not solely on a single side of the interface. Note that this point of view is not new. It was adopted by Fano in the early 1940s as a general interpretation of the first order perturbative solution of the Rayleigh equation and used to further deduce the origin of the Wood anomalies [39].

What is now the physical interpretation of the polarization factors $\hat{\boldsymbol{\rho}}^{(1)}(\mathbf{p}\,|\,\mathbf{p}_0)$ and $\hat{\boldsymbol{\tau}}^{(1)}(\mathbf{p}\,|\,\mathbf{p}_0)$? It is clear from the definition of the amplitudes $\hat{\boldsymbol{\rho}}^{(1)}(\mathbf{p}\,|\,\mathbf{p}_0)$ and $\hat{\boldsymbol{\tau}}^{(1)}(\mathbf{p}\,|\,\mathbf{p}_0)$, given in Eqs. (A9) and (A16) respectively, that they are identical for different realizations of the surface profile. This suggests that these amplitudes are, in some sense, rather a signature of the bulk polarization response than the surface scattering properties. In using their definitions together with Eqs. (A9) and (A16) and by expressing the $\mathbf{M}^{b,a}_{l,m}$ matrices as functions of the polarization vectors in the local polarization basis as given in Eq. (10), we obtain the following expressions:

$$\hat{\rho}^{(1)}_{ss}(\mathbf{p}\,|\,\mathbf{p}_0) = \frac{\hat{\mathbf{e}}_s(\mathbf{p})\cdot\hat{\mathbf{e}}_s(\mathbf{p}_0) + \rho^{(0)}_{ss}(\mathbf{p}_0)\;\hat{\mathbf{e}}_s(\mathbf{p})\cdot\hat{\mathbf{e}}_s(\mathbf{p}_0)}{\hat{\mathbf{e}}_s(\mathbf{p})\cdot\hat{\mathbf{e}}_s(\mathbf{p})} = \hat{\mathbf{e}}_s(\mathbf{p})\cdot\mathbf{E}^{(0)}_{1,s}(\mathbf{p}_0) \tag{30a}$$

$$\hat{\rho}^{(1)}_{ps}(\mathbf{p}\,|\,\mathbf{p}_0) = \frac{\hat{\mathbf{e}}^{+}_{p,2}(\mathbf{p})\cdot\hat{\mathbf{e}}_s(\mathbf{p}_0) + \rho^{(0)}_{ss}(\mathbf{p}_0)\,\hat{\mathbf{e}}^{+}_{p,2}(\mathbf{p})\cdot\hat{\mathbf{e}}_s(\mathbf{p}_0)}{\hat{\mathbf{e}}^{+}_{p,2}(\mathbf{p})\cdot\hat{\mathbf{e}}^{+}_{p,1}(\mathbf{p})} = \frac{\hat{\mathbf{e}}^{+}_{p,2}(\mathbf{p})\cdot\mathbf{E}^{(0)}_{1,s}(\mathbf{p}_0)}{\hat{\mathbf{e}}^{+}_{p,2}(\mathbf{p})\cdot\hat{\mathbf{e}}^{+}_{p,1}(\mathbf{p})} \tag{30b}$$

$$\hat{\rho}^{(1)}_{sp}(\mathbf{p}\,|\,\mathbf{p}_0) = \frac{\hat{\mathbf{e}}_s(\mathbf{p})\cdot\hat{\mathbf{e}}^{-}_{p,1}(\mathbf{p}_0) + \hat{\mathbf{e}}_s(\mathbf{p})\cdot\hat{\mathbf{e}}^{+}_{p,1}(\mathbf{p}_0)\rho^{(0)}_{pp}(\mathbf{p}_0)}{\hat{\mathbf{e}}_s(\mathbf{p})\cdot\hat{\mathbf{e}}_s(\mathbf{p})} = \hat{\mathbf{e}}_s(\mathbf{p})\cdot\mathbf{E}^{(0)}_{1,p}(\mathbf{p}_0) \tag{30c}$$

$$\hat{\rho}^{(1)}_{pp}(\mathbf{p}\,|\,\mathbf{p}_0) = \frac{\hat{\mathbf{e}}^{+}_{p,2}(\mathbf{p})\cdot\hat{\mathbf{e}}^{-}_{p,1}(\mathbf{p}_0) + \hat{\mathbf{e}}^{+}_{p,2}(\mathbf{p})\cdot\hat{\mathbf{e}}^{+}_{p,1}(\mathbf{p}_0)\rho^{(0)}_{pp}(\mathbf{p}_0)}{\hat{\mathbf{e}}^{+}_{p,2}(\mathbf{p})\cdot\hat{\mathbf{e}}^{+}_{p,1}(\mathbf{p})} = \frac{\hat{\mathbf{e}}^{+}_{p,2}(\mathbf{p})\cdot\mathbf{E}^{(0)}_{1,p}(\mathbf{p}_0)}{\hat{\mathbf{e}}^{+}_{p,2}(\mathbf{p})\cdot\hat{\mathbf{e}}^{+}_{p,1}(\mathbf{p})} \tag{30d}$$

for the reflection amplitudes and

$$\hat{\tau}^{(1)}_{ss}(\mathbf{p}\,|\,\mathbf{p}_0) = \tau^{(0)}_{ss}(\mathbf{p}_0)\,\frac{\hat{\mathbf{e}}_s(\mathbf{p})\cdot\hat{\mathbf{e}}_s(\mathbf{p}_0)}{\hat{\mathbf{e}}_s(\mathbf{p})\cdot\hat{\mathbf{e}}_s(\mathbf{p})} = \frac{\hat{\mathbf{e}}_s(\mathbf{p})\cdot\mathbf{E}^{(0)}_{2,s}(\mathbf{p}_0)}{\hat{\mathbf{e}}_s(\mathbf{p})\cdot\hat{\mathbf{e}}_s(\mathbf{p})} \tag{31a}$$

$$\hat{\tau}^{(1)}_{ps}(\mathbf{p}\,|\,\mathbf{p}_0) = \tau^{(0)}_{ss}(\mathbf{p}_0)\,\frac{\hat{\mathbf{e}}^{-}_{p,1}(\mathbf{p})\cdot\hat{\mathbf{e}}_s(\mathbf{p}_0)}{\hat{\mathbf{e}}^{-}_{p,1}(\mathbf{p})\cdot\hat{\mathbf{e}}^{-}_{p,2}(\mathbf{p})} = \frac{\hat{\mathbf{e}}^{-}_{p,1}(\mathbf{p})\cdot\mathbf{E}^{(0)}_{2,s}(\mathbf{p}_0)}{\hat{\mathbf{e}}^{-}_{p,1}(\mathbf{p})\cdot\hat{\mathbf{e}}^{-}_{p,2}(\mathbf{p})} \tag{31b}$$

$$\hat{\tau}^{(1)}_{sp}(\mathbf{p}\,|\,\mathbf{p}_0) = \tau^{(0)}_{pp}(\mathbf{p}_0)\,\frac{\hat{\mathbf{e}}_s(\mathbf{p})\cdot\hat{\mathbf{e}}^{-}_{p,2}(\mathbf{p}_0)}{\hat{\mathbf{e}}_s(\mathbf{p})\cdot\hat{\mathbf{e}}_s(\mathbf{p})} = \frac{\hat{\mathbf{e}}_s(\mathbf{p})\cdot\mathbf{E}^{(0)}_{2,p}(\mathbf{p}_0)}{\hat{\mathbf{e}}_s(\mathbf{p})\cdot\hat{\mathbf{e}}_s(\mathbf{p})} \tag{31c}$$

$$\hat{\tau}^{(1)}_{pp}(\mathbf{p}\,|\,\mathbf{p}_0) = \tau^{(0)}_{pp}(\mathbf{p}_0)\,\frac{\hat{\mathbf{e}}^{-}_{p,1}(\mathbf{p})\cdot\hat{\mathbf{e}}^{-}_{p,2}(\mathbf{p}_0)}{\hat{\mathbf{e}}^{-}_{p,1}(\mathbf{p})\cdot\hat{\mathbf{e}}^{-}_{p,2}(\mathbf{p})} = \frac{\hat{\mathbf{e}}^{-}_{p,1}(\mathbf{p})\cdot\mathbf{E}^{(0)}_{2,p}(\mathbf{p}_0)}{\hat{\mathbf{e}}^{-}_{p,1}(\mathbf{p})\cdot\hat{\mathbf{e}}^{-}_{p,2}(\mathbf{p})} \tag{31d}$$

for the transmission amplitudes. Here we have defined the total zero order field amplitudes in media 1 and 2, for s- and p-polarized incident light, as

$$\mathbf{E}^{(0)}_{1,s}(\mathbf{p}_0) = \left[1+\rho^{(0)}_{ss}(\mathbf{p}_0)\right]\,\hat{\mathbf{e}}_s(\mathbf{p}_0) \tag{32a}$$

$$\mathbf{E}^{(0)}_{1,p}(\mathbf{p}_0) = \hat{\mathbf{e}}^{-}_{p,1}(\mathbf{p}_0) + \rho^{(0)}_{pp}(\mathbf{p}_0)\,\hat{\mathbf{e}}^{+}_{p,1}(\mathbf{p}_0) \tag{32b}$$

$$\mathbf{E}^{(0)}_{2,s}(\mathbf{p}_0) = \tau^{(0)}_{ss}(\mathbf{p}_0)\;\hat{\mathbf{e}}_s(\mathbf{p}_0) \tag{32c}$$

$$\mathbf{E}^{(0)}_{2,p}(\mathbf{p}_0) = \tau^{(0)}_{pp}(\mathbf{p}_0)\,\hat{\mathbf{e}}^{-}_{p,2}(\mathbf{p}_0)\,. \tag{32d}$$

The amplitudes given in Eqs. (32) correspond to the sum of the unit incident field and the reflected or transmitted zero order field amplitudes. In other words, they characterize the state of the field given by the superposition of the incident wave and the zero order response of the media. This is analogous to what we found for scalar waves in Eq. (29), with the difference that due to the dipolar nature of the scatterers the state of this zero order background is anisotropic, as indicated by the dependence on $\mathbf{p}$.

An interesting point to notice from Eqs. (30) and (31) is that the amplitude of the first order α-polarized wave scattered with lateral wave vector $\mathbf{p}$ in medium j is proportional to the projection of the total zero order field amplitude in medium j, induced by an incident β-polarized wave with lateral wave vector $\mathbf{p}_0$, on the direction of the polarization vector associated with its Snell-conjugate wave vector (with lateral wave vector $\mathbf{p}$). For s-polarized scattered waves the Snell-conjugate wave vector is not apparent since all s-polarization vectors are in the $(\hat{\mathbf{e}}_1,\hat{\mathbf{e}}_2)$-plane. For p-polarized scattered waves this is clear as is indicated by the vectors $\hat{\mathbf{e}}^{+}_{p,2}(\mathbf{p})$ and $\hat{\mathbf{e}}^{-}_{p,1}(\mathbf{p})$, for the first order amplitudes in reflection and transmis-

sion, respectively. One way of interpreting these equations is to imagine that the wave scattered in one medium is induced by the roughness of the surface in the sense that, contrary to the case of the planar surface, the path issued from a scattering event on the surface will *not* destructively interfere anymore when summed over the surface, and hence probe the underlying polarized radiation pattern induced by arrays of dipole emitters in the bulk. The scattering amplitude of such a scattered wave will be controlled by the polarized state of the media, in such a way that the amplitude is proportional to the total zero order field amplitude in the medium of scattering but projected on the polarization vector the scattered wave would have had, keeping its lateral wave vector and according to Snell's law, if it were incoming from the opposite medium. This is a generalization of Doyle's analysis based on the Ewald triad, although we now have a triad associated with each observed scattered wave.

A more detailed microscopic understanding of this result would require an analysis of the way arrays of dipoles emit when excited by a primary incident wave, and by summing the elementary wavelets emitted by all the dipoles while also taking into account the geometry of the surface. Such an analysis was done by Ewald in his derivation of the extinction theorem for a planar surface [29], and later used by Doyle [26] in interpreting the Fresnel coefficients at a microscopic level, as explained earlier. A Snell-conjugate wave vector can be viewed as the wave vector of one of the waves of the Ewald triad associated to a (first order) scattered wave, in a similar fashion as what we have already encountered when factorizing the Fresnel coefficients for a p-polarized wave in Eq. (27b). Modern derivations of the extinction theorem are directly based on the macroscopic properties of the media, and what we obtain from such formalism can only be the integrated contribution of all the scatterers, as is also the case with the solution of the reduced Rayleigh equations, which can be shown to derive from the extinction theorem. Consequently, we must take our Snell-conjugate wave interpretation as a signature of a more fundamental microscopic view, and consider this concept as a useful short cut for reasoning directly on the integrated response, just as we did for interpreting the Fresnel coefficients following Doyle's interpretation.

We can summarize the interpretations of the first order amplitudes discussed in this section as a factorization of two main mechanisms. All the first order amplitudes can be written as the product of a polarization independent factor, $[\alpha_1(\mathbf{p}) - \alpha_2(\mathbf{p})]\ \hat{\zeta}(\mathbf{p}-\mathbf{p}_0)$, common to all amplitudes sharing the same outgoing lateral wave vector, and a polarization dependent factor. The polarization independent factor encodes the interference pattern of all spherical waves scattered in the vicinity of the non-planar surface, and can be viewed as the scattering or probing mechanism. The polarization dependent factor is controlled by the state of the zero order field, and is always proportional to the projection of the total zero order field amplitude onto the polarization vector of a Snell-conjugate wave associated to the observed scattered wave. This mechanism ensures that the polarization and amplitude of the observed scattered wave is consistent with the polarized dipole radiation characterized by the state of the zero order field. We are now ready for a more in-depth analysis of the Yoneda and Brewster scattering effects based on the physical interpretation and concepts we have developed in the present section.

C. The physical origin of the Yoneda effect

Our observations on the Yoneda and Brewster scattering effects in Section IV A led us to the conclusion that the two effects can be explained independently. The fact that the Brewster scattering angle coincides with the Yoneda critical angle for normal incidence can, for the time being, be considered a simple coincidence. Since the Yoneda phenomenon seems to be independent of polarization we can attempt an explanation solely based on scalar waves and consider Eq. (29) a relevant simplified model, in an analogous fashion as Eq. (27c) was sufficient to explain total internal reflection from a planar surface. In fact, for the scattering of s-polarized waves restricted to the plane of incidence ($\mathbf{p} \parallel \mathbf{p}_0$) the reflection and transmission amplitudes are exactly given by Eq. (29). We will therefore keep to scalar waves for the main analysis, but we will also illustrate our conclusions with results obtained for s-polarized waves. In the following, it will be convenient to refer to the smallest and largest dielectric constant by $\epsilon_{\min}$ and $\epsilon_{\max}$ respectively, and more generally we will index by min and max the quantities corresponding to these media. Our analysis will be independent of the configurations of the media but will require us to distinguish the optically denser medium from the less dense medium for the scattered waves.

We can view the scattering mechanism responsible for the Yoneda peak phenomenon as a two step process for the sake of clarity. First, the incident wave impinges on the surface with an in-plane lateral wave vector $\mathbf{p}_0$ and, within a single scattering point of view, gives rise to a scattered elementary wave reflected with the in-plane lateral wave vector $\mathbf{p}$ and a scattered elementary wave transmitted with the in-plane lateral wave vector $\mathbf{p}$. These are arbitrarily chosen wave vectors; the total scattered field will have components *a priori* for all wave vectors but in our analysis we consider just these two arbitrary waves. One may have in mind the picture of an optical path allowed to be scattered only once in our single scattering view and the total field will be obtained by summing the probability amplitude of all optical paths. As argued in Section **??**, the probability for a change of lateral wave vector from $\mathbf{p}_0$ to $\mathbf{p}$ is controlled by the factor $[\alpha_1(\mathbf{p}) - \alpha_2(\mathbf{p})]\ \hat{\zeta}(\mathbf{p}-\mathbf{p}_0)$ (or its modulus square). This is not sufficient to obtain the complete probability amplitude, which in general and for polarized waves will

depend on the wave vectors, dielectric constants and polarizations of the waves involved in the process. However, we will show that we do not need to analyze the details of these amplitudes in order to investigate the Yoneda phenomenon.

The second step determines whether the intensity is enhanced in the optically denser medium for a given elementary scattered wave. We can view the elementary reflected and transmitted waves as coupled into a single mode as explained in the previous section. We can take this one step further, and interpret the argument based on the probability measure for a change of momentum as a way to allocate part of the energy from the incident wave, to be shared between, and radiated away by, the two scattered waves gathered in a coupled mode with a shared lateral wave vector $\mathbf{p}$.

Let us first consider the situation where the shared lateral wave vector of the scattered waves is restricted to $|\,\mathbf{p}\,| < n_{\min}\omega/c = p_c$, which means that both waves are allowed to propagate to infinity in their respective medium. Under this assumption, the total energy of the two waves will be shared *a priori* non-trivially between the two waves. In particular, for a given $\mathbf{p}$ it is apparent from Eq. (29) that the energy will be split according to the relative amplitudes given by the zero order state since the factor $[\alpha_1(\mathbf{p}) - \alpha_2(\mathbf{p})]\,\hat{\zeta}(\mathbf{p}-\mathbf{p}_0)$ is common to both the reflected and transmitted wave. However, if now the shared lateral wave vector is such that $n_{\min}\omega/c < |\,\mathbf{p}\,| < n_{\max}\omega/c$, the wave scattered in the optically less dense medium will be evanescent. Therefore the total energy for the coupled mode will be carried away solely by the wave which can propagate, namely the one scattered into the dense medium, resulting in the apparent sudden increase of intensity at the transition between propagation and evanescence of the wave scattered in the optically less dense medium. An illustrative way of seeing that the intensity needs to be enhanced is by analyzing the factor $\alpha_1(\mathbf{p})-\alpha_2(\mathbf{p})$ assuming $|\hat{\zeta}|$ to vary slowly. For $|\,\mathbf{p}\,| < p_c$ both $\alpha_1(\mathbf{p})$ and $\alpha_2(\mathbf{p})$ are real. As $|\,\mathbf{p}\,| \to p_c$ from below, $\alpha_{\min}(\mathbf{p}) \to 0$ and $\alpha_1(\mathbf{p}) - \alpha_2(\mathbf{p}) \to \pm\alpha_c$, with $\alpha_c = \sqrt{\epsilon_{\max} - \epsilon_{\min}}\,\omega/c$. By writing $p = |\,\mathbf{p}\,| = p_c - \Delta p$, with $\Delta p > 0$, we can make an asymptotic analysis of $|\alpha_1(\mathbf{p})-\alpha_2(\mathbf{p})|$ as $p \to p_c$ from below. In this way we obtain the following result

$$
\begin{aligned}
&|\alpha_1(\mathbf{p}) - \alpha_2(\mathbf{p})|\frac{c}{\omega} = [\alpha_{\max}(\mathbf{p}) - \alpha_{\min}(\mathbf{p})]\frac{c}{\omega} \\
&= [\epsilon_{\max} - (\tilde{p}_c - \Delta\tilde{p})^2]^{1/2} - [\epsilon_{\min} - (\tilde{p}_c - \Delta\tilde{p})^2]^{1/2} \\
&= [\epsilon_{\max} - \epsilon_{\min} + 2\epsilon_{\min}^{1/2}\Delta\tilde{p} - \Delta\tilde{p}^2]^{1/2} - [2\epsilon_{\min}^{1/2}\Delta\tilde{p} - \Delta\tilde{p}^2]^{1/2} \\
&= \alpha_c\,\frac{c}{\omega} - [2\epsilon_{\min}^{1/2}\Delta\tilde{p}]^{1/2} + o(\Delta\tilde{p}^{1/2})\,. \qquad (33)
\end{aligned}
$$

Here we have chosen to work with unit-less quantities and denoted $\tilde{p} = p\,c/\omega$ for conciseness. From Eq. (33) it then follows that as $\Delta p \to 0$, $|\alpha_1(\mathbf{p}) - \alpha_2(\mathbf{p})|$ must increase towards α_c in an inner-neighborhood of the circle $p = p_c$. Furthermore, the asymptotic expansion reveals that the critical point will be reached with a sharp edge (infinite slope) for $p < p_c$ as can be deduced from the square root behavior in Δp. Note that both the reflection and transmission amplitudes exhibit the same behavior independently of which medium is denser. This is due to the fact that the two waves are part of the same mode. However, as the wave propagating in the less dense medium becomes a grazing wave, the corresponding differential scattering coefficient is forced to vanish due to the angular dependence in $\cos^2\theta_s$ ($\theta_s = \theta_r$ or θ_t depending on the context). The complex amplitude is nevertheless enhanced for both the reflected and transmitted wave. This is illustrated for example in Figs. 2(a) and 2(d), which corresponds to a case for which the medium of incidence is vacuum. From the results presented in these figures, we can see that while the incoherent component of the MDRC is forced to go to zero when $p_1 \to p_c = \omega/c$, the surface-independent part of the reflection amplitude $\rho_{ss}^{(1)}$ exhibits a sharp increase in modulus. Simultaneously, the surface-independent part of the transmission amplitude $\tau_{ss}^{(1)}$ also exhibits a similar sharp increase in modulus as p_1 approaches p_c. Consequently, since the wave can propagate away from the surface in the second medium (which consists of glass in this specific case), the corresponding incoherent component of the MDTC exhibits a similar increase. Note that both the phases associated with $\rho_{ss}^{(1)}$ and $\tau_{ss}^{(1)}$ remain constant and equal to 0 for $p_1 < p_c$ for all θ_0 in Fig. 2, since the complex amplitude stays on the real line in the case where $\epsilon_1 < \epsilon_2$ independent of the angle of incidence.

Figures 3 and 4 support the same conclusion but by interchanging the role of the media. The only difference worth noting is that the phases $\phi_{ss}^{r,(1)}$ and $\phi_{ss}^{t,(1)}$ have a constant plateau for $p_1 < p_c$ which is equal to 0 only for $\theta_0 < \theta_c$. The plateau is offset for $\theta_0 > \theta_c$. This overall phase offset is due to the Goos-Hänchen phase shift associated with total internal reflection of the zero order wave. Indeed, recall that the first order amplitudes are proportional to the total zero order field amplitudes. As a consequence, if the zero order waves exhibit a phase shift, it will affect the first order amplitudes in the form of a constant phase offset for all $\mathbf{p}$.

When $|\,\mathbf{p}\,| > p_c$, $\alpha_{\min}$ becomes purely imaginary and $\alpha_1(\mathbf{p}) - \alpha_2(\mathbf{p})$ thus moves off the real line. For $p_c < |\,\mathbf{p}\,| < n_{\max}\omega/c$, we find that in this regime $\alpha_1(\mathbf{p})-\alpha_2(\mathbf{p})$ keeps a constant modulus equal to α_c. Indeed, by writing $\alpha_{\min}(\mathbf{p}) = i\beta_{\min}(\mathbf{p})$ we have

$$
\begin{aligned}
|\alpha_1(\mathbf{p}) - \alpha_2(\mathbf{p})| &= |\alpha_{\max}(\mathbf{p}) - i\beta_{\min}(\mathbf{p})| \\
&= \left[\alpha_{\max}^2(\mathbf{p}) + \beta_{\min}^2(\mathbf{p})\right]^{1/2} \\
&= \left[\epsilon_{\max} - \tilde{p}^2 + \tilde{p}^2 - \epsilon_{\min}\right]^{1/2}\omega/c \\
&= \alpha_c\,. \qquad (34)
\end{aligned}
$$

The complex number $\alpha_1(\mathbf{p}) - \alpha_2(\mathbf{p})$ thus traces a circular arc of radius α_c in the complex plane. Finally, when $|\,\mathbf{p}\,| > n_{\max}\,\omega/c$, both the reflected and transmitted waves are evanescent, $\alpha_{\max}$ becomes pure imaginary and

hence $\alpha_1(\mathbf{p}) - \alpha_2(\mathbf{p})$ moves along the imaginary axis. The constant value of $|\rho_{ss}^{(1)}|$ and $|\tau_{ss}^{(1)}|$ in the regime $n_{\min}\,\omega/c < \mathbf{p} < n_{\max}\,\omega/c$ can be appreciated for all angles of incidence illustrated in Figs. 2 – 4, while the phases exhibit a smooth variation from their plateau value and decay by a total amount of $-\pi/2$ when reaching $p_1 = n_{\max}\,\omega/c$. Once the threshold of $n_{\max}\,\omega/c$ has been passed, the phases remain constant and the modulii decay towards zero as $|\,\mathbf{p}\,| \to \infty$ (which can easily be deduced from a straightforward asymptotic analysis leading to $\alpha_1(\mathbf{p}) - \alpha_2(\mathbf{p}) \sim i(\epsilon_{\max} - \epsilon_{\min})\omega^2/(2c^2 p)$). The phase change associated with the transition from the real line to the imaginary line in the complex plane is therefore $-\pi/2$. This gradual phase change is similar to that of the Goos-Hänchen phase shift discussed for the reflection by a planar surface. The difference of absolute total phase change, of π for the case of the Fresnel amplitude and $\pi/2$ in the case of the scattered waves, comes mathematically from the fact that in the former case the amplitude is written as the ratio of a complex number and its complex conjugate, while in the latter case there is no such ratio. The phase consequently turns twice as fast in the former case than in the latter. A physical interpretation of this difference is that for the Fresnel amplitude both the incident and outgoing wave vector must vary simultaneously (since they are the same), while in the case of a scattered wave the incident wave vector is fixed while only the outgoing wave vector is allowed to vary. In fact, we have only analyzed the phase associated with the factor $\alpha_1(\mathbf{p}) - \alpha_2(\mathbf{p})$ in Eq. (29). The phase of the overall complex amplitude will be the sum of the aforementioned phase, that given by the argument of $\hat{\zeta}(\mathbf{p} - \mathbf{p}_0)$, and the phase given by the argument of the total zero order amplitude $[1 + \rho^{(0)}(\mathbf{p}_0)]$ or $\tau^{(0)}(\mathbf{p}_0)$. In particular, if the angle of incidence is such that total internal reflection occurs for the zero order field, the overall phase of the scattered amplitude will contain a signature of the Goos-Hänchen phase shift associated with the total internal reflection of the zero order field in addition to the corresponding Goos-Hänchen phase shift associated with the Yoneda effect. Note that when averaged over surface realizations, the phase contribution coming from $\hat{\zeta}$ averages to zero. This supports our choice of limiting the detailed investigation to the surface-independent factors in Eq. (29).

To summarize, let us gather some important results and answer some of the questions which were left unanswered in previous studies. First, we would like to stress that the above analysis predicts a critical angle for the Yoneda phenomenon which is independent both of the angle of incidence and of which medium the incident wave came from. The Yoneda transition will therefore always occur at the same polar angle of scattering: the one given by $|\,\mathbf{p}_c\,| = n_{\min}\,\omega/c$. We also want to emphasize that the approximate solution of the reduced Rayleigh equations obtained via SAPT to first order in the surface profile is commonly accepted as a single scattering approximation. In light of our analysis of the Yoneda phenomenon, it is clear that the analogy of the Yoneda phenomenon with that of total internal reflection put forward in the literature may seem a valid one. There are, however, some comments to be made about this analogy. It is important to emphasize the underlying cause of total internal reflection, namely the impossibility of an evanescent wave to carry energy away from the surface, given the assumed scattering system. Indeed, trying to directly and naively apply the total internal reflection argument would lead one to expect an absence of the Yoneda effect in transmission into the dense medium based on a single scattering picture, as this would require multiple scattering events. Indeed, one could imagine that the incident wave would need to scatter once to a transmitted grazing or evanescent wave and then a second time to be scattered in reflection in the dense medium and therefore follow the rule of total internal reflection. Such a naive picture would be in contradiction with results from numerical experiments based on first order perturbation theory [1, 2], or at least contradict the common single-scattering picture associated with it, and we believe that our interpretation resolves this issue. The results presented in Refs. 1 and 2 validated the qualitative use of SAPT in describing the Yoneda phenomenon, for the roughness parameters assumed in these studies, when compared to numerical results obtained through a non-perturbative solution of the reduced Rayleigh equations. Similar non-perturbative solutions were found to match experimental results showing the Yoneda phenomenon in Ref. 16.

In fact, the Yoneda phenomenon for weakly rough surfaces originates from the same physical mechanism as the Rayleigh anamolies for periodic dielectric gratings. The continuous set of scattered wave vectors in the case of a randomly rough surface can be viewed as probing a diffracted order scattered from a periodic surface with continuously changing lattice constant. It is easy to show numerically and with SAPT to first order, that the behavior of the efficiency of a given diffractive order as the lattice constant is changed exhibits the same characteristic peak as the Yoneda peak when its counter part in the less dense medium becomes evanescent. The perturbative analysis in the case of a periodic grating is exactly the same as in the case of a randomly rough surface with the only difference being that $\mathbf{p}$ must be replaced by the in-plane wave vector of the diffractive order of interest and make the lattice constant vary instead.

As a remark, we would like to point out that since the analysis was carried out for the scattering of a scalar wave subjected to the continuity of the field and its normal derivative with respect to the surface, we predict that the Yoneda phenomenon should also be observed for the scattering of a quantum particle by a rough interface between two regions of constant potential.

In studying the results from Figs. 2 – 4 we avoided a direct discussion for p-polarized waves, for which the re-

sults put forward by the scalar wave analysis seem to be invalidated. The analysis done for scalar waves is, in fact, still valid but must be complemented with additional effects, due to polarization, not only for p-polarized light but also for s-polarized light when the scattering direction is out of the plane of incidence as suggested by Eqs. (30, 31). This is the subject of the following section.

D. Physical and geometrical explanations of the Brewster scattering effect

For a randomly rough surface, we have seen in Figs. 2 – 4 that we may find a Brewster scattering angle for a wide range of angles of incidence if we look at both the reflected and transmitted light (the MDRC and MDTC). We will now see that the general Brewster scattering phenomenon, roughly defined as a wave scattered with zero amplitude in a single scattering approximation, also extends to scattered waves in the evanescent regime. To this end we will continue our dissection of the phenomenon through perturbative theory.

In-plane reflection — Let us focus first on the case of co-polarized scattering in the plane of incidence to fix the ideas. Equation (30a) shows that $\hat{\rho}^{(1)}_{ss}(\mathbf{p}\,|\,\mathbf{p}_0)$ is proportional to $\hat{\mathbf{e}}_s(\mathbf{p})\cdot\mathbf{E}^{(0)}_{s,1}(\mathbf{p}_0)$, where $\mathbf{E}^{(0)}_{s,1}(\mathbf{p}_0)$ is the *total zero order field amplitude* in medium 1 given by the sum of the unit incident field amplitude and the reflected field amplitude given by the Fresnel coefficient for an s-polarized wave. This relation indicates that the field amplitude of the *first order* reflected amplitude for the wave scattered with lateral wave vector $\mathbf{p}$ is proportional to the projection of its polarization vector on the total zero order field. For scattering in the plane of incidence $\hat{\mathbf{e}}_s(\mathbf{p}) = \hat{\mathbf{e}}_s(\mathbf{p}_0)$ and therefore the first order reflection amplitude reduces to that of the scalar wave Eq. (29a). Consequently, there is no extinction for $s \to s$ scattering in the plane of incidence for any angle of incidence. The same analysis and conclusion hold for the transmitted s-polarized wave.

Similarly, for p-polarized light, Eq. (30d) shows that the first order reflection amplitude is proportional to $\hat{\mathbf{e}}^{+}_{p,2}(\mathbf{p})\cdot\mathbf{E}^{(0)}_{1,p}(\mathbf{p}_0)$, where we recall that $\mathbf{E}^{(0)}_{1,p}(\mathbf{p}_0)$ is the total zero order field amplitude given by the sum of the unit incident field amplitude and the reflected field amplitude given by the Fresnel coefficient for p-polarized waves. Equation (30d) states that the *first order* field amplitude is proportional to the projection of the Snell-conjugate wave's polarization vector $\hat{\mathbf{e}}^{+}_{p,2}(\mathbf{p})$ along the direction of the *total zero order field*. Note the similarity with what was found for the Fresnel coefficient for p-polarized light in Eq. (27b). From Eq. (30d) we can deduce a simple geometrical criterion for Brewster scattering within first order perturbation theory: *The lateral wave vector(s)* $\mathbf{p}_{\rm B}$ *of the elementary Brewster scattered wave(s), for which the reflection amplitude for a p-polarized reflected wave vanishes given a p-polarized incident wave with lateral wave vector* $\mathbf{p}_0$ *is given by the condition of orthogonality between the p-polarization vector of the Snell-conjugate scattered wave(s) and the total zero order field in medium 1, i.e.*

$$\hat{\mathbf{e}}^{+}_{p,2}(\mathbf{p}_{\rm B})\cdot\mathbf{E}^{(0)}_{p,1}(\mathbf{p}_0) = 0\,. \tag{35}$$

As a direct consequence, in the case of co-polarized scattering in the plane of incidence, the geometrical condition can be re-stated as a requirement on the colinearity between the Snell-conjugate wave vector and the total zero order field, which is exactly the same geometrical criterion found in the case of reflection from a planar interface. A second corollary is that for in-plane scattering $\Theta_{\rm B}(\theta_{\rm B}) = \theta_{\rm B}$: the *Brewster scattering angle* is equal to the *Brewster angle for a planar interface* when the angle of incidence is equal to the Brewster angle for a planar interface, $\theta_0 = \theta_{\rm B}$ (or so-called Brewster incidence). In other words, the Brewster angle for a planar interface, $\theta_{\rm B}$, is a fixed point for the mapping which associates the angle of incidence to the Brewster scattering angle: $\Theta_{\rm B} : \theta_0 \mapsto \Theta_{\rm B}(\theta_0)$. This is readily understood from the geometrical criterion expressed by Eq. (35). At Brewster incidence the zero order reflected wave vanishes (by definition of Brewster incidence). Thus the total zero field amplitude is simply the incident field amplitude, $\mathbf{E}^{(0)}_{p,1}(\mathbf{p}_0) = \hat{\mathbf{e}}^{-}_{p,1}(\mathbf{p}_0)$, and consequently, the Brewster scattering angle is necessarily equal to $\theta_{\rm B}$.

Let us now apply the above criterion for tracking the Brewster scattering direction while the angle of incidence varies. We start with the case where the incident plane wave is approaching the rough interface from vacuum, and is reflected from a glass substrate [$\epsilon_1 = 1$ and $\epsilon_2 = 2.25$]. Figure 6 presents selected wave vectors for different polar angles of incidence θ_0, highlighting the geometrical relations leading to the Brewster scattering direction. The dashed circles in this figure represent the dispersion relations ($|\,\mathbf{k}^{\pm}_j\,| = k_j = n_j\omega/c$) by indicating the norm of wave vectors allowed to propagate in the two media. The incident wave vector $\mathbf{k}^{-}_1(\mathbf{p}_0)$ is represented pointing towards the origin for clarity while the wave vector for the reflected zero order wave, $\mathbf{k}^{+}_1(\mathbf{p}_0)$, is represented as pointing outwards. The red dashed line corresponds to the direction of the reflected wave vector for Brewster scattering in the case of a planar interface with the purpose of illustrating the aforementioned fixed point property of the Brewster incident angle $\theta_0 = \theta_{\rm B}$. The general construction rules go as follows. First, the wave vectors of the incident and the reflected zero order waves are drawn in black. Second, the direction of the total zero order field given by Eq. (32b) is determined and the wave vector of the virtual wave, which is colinear to the total zero order field (not represented), is drawn as the blue wave vector $\mathbf{k}^{+}_2(\mathbf{p}_{\rm B})$. Note that $\mathbf{k}^{+}_2(\mathbf{p}_{\rm B})$ lies on the circle of radius $n_2\omega/c$. The projection of $\mathbf{k}^{+}_2(\mathbf{p}_{\rm B})$ along $\hat{\mathbf{e}}_1$ gives the Brewster lateral wave vector $\mathbf{p}_{\rm B}$ from which we deduce $\mathbf{k}^{+}_1(\mathbf{p}_{\rm B})$ in red. Note that the reflected wave associated with $\mathbf{k}^{+}_1(\mathbf{p}_{\rm B})$ may be evanescent, and in that case we simply represent its lateral component $\mathbf{p}_{\rm B}$ as its component along $\hat{\mathbf{e}}_3$ is pure imaginary.

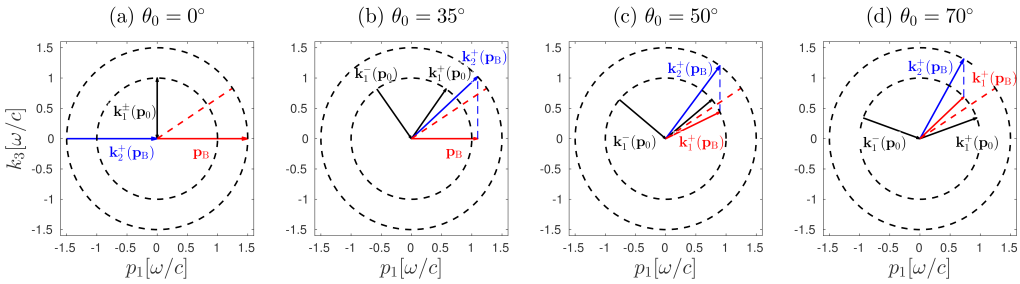

FIG. 6. Illustration of the geometrical criterion for in-plane Brewster scattering for different polar angles of incidence: (a) $\theta_0 = 0°$, (b) $\theta_0 = 35°$, (c) $\theta_0 = 50°$ and (d) $\theta_0 = 70°$. The dashed circles represent the norm of the full wave vectors, given by the dispersion relations, in vacuum ($\epsilon_1 = 1$ inner circle) and glass ($\epsilon_2 = 2.25$ outer circle). The black arrows represent respectively the incident wave vector $\mathbf{k}_1^-(\mathbf{p}_0)$, which is drawn as pointing towards the origin for clarity, and the wave vector of the reflected zero order wave, $\mathbf{k}_1^+(\mathbf{p}_0)$. The blue arrow represents the wave vector of the virtual wave, $\mathbf{k}_2^+(\mathbf{p}_B)$, from which the lateral wave vector of the Brewster wave, $\mathbf{p}_B$, is deduced by projection along $\hat{\mathbf{e}}_1$. From $\mathbf{p}_B$, the full wave vector for the Brewster wave, $\mathbf{k}_1^+(\mathbf{p}_B)$, can be drawn (provided propagation in medium 1) as a red arrow. Note that if the Brewster wave is evanescent, only $\mathbf{p}_B$ is draw in red as the out-of-plane component of $\mathbf{k}_1^+(\mathbf{p}_B)$ is purely imaginary. The red dashed line indicates the Brewster angle for a planar surface approximately equal to 56.3° in this case.

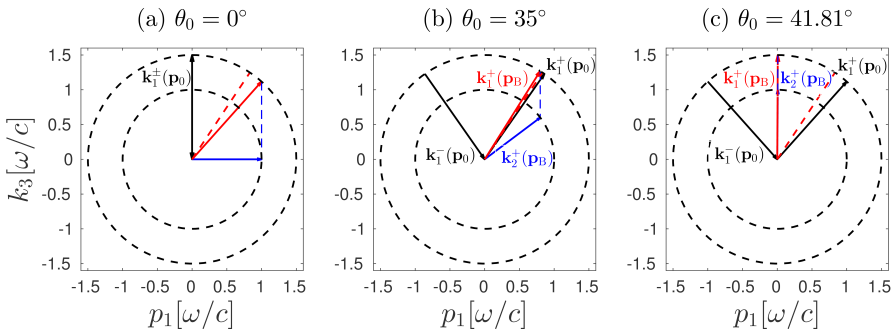

FIG. 7. Illustration of the geometrical criterion for in-plane Brewster scattering for different polar angles of incidence: (a) $\theta_0 = 0°$, (b) $\theta_0 = 35°$ and (c) $\theta_0 = 41.81°$. The dashed circles represent the norm of the full wave vectors, given by the dispersion relations, in glass ($\epsilon_1 = 2.25$ inner circle) and vacuum ($\epsilon_2 = 1$ outer circle). The black arrows represent respectively the incident wave vector $\mathbf{k}_1^-(\mathbf{p}_0)$, which is drawn as pointing towards the origin for clarity, and the wave vector of the reflected zero order wave, $\mathbf{k}_1^+(\mathbf{p}_0)$. The blue arrow represents the wave vector of the virtual wave, $\mathbf{k}_2^+(\mathbf{p}_B)$, from which the lateral wave vector of the Brewster wave, $\mathbf{p}_B$, is deduced by projection along $\hat{\mathbf{e}}_1$. From $\mathbf{p}_B$, the full wave vector for the Brewster wave, $\mathbf{k}_1^+(\mathbf{p}_B)$, can be drawn (provided propagation in medium 1) as a red arrow. Note that if the Brewster wave is evanescent, only $\mathbf{p}_B$ is drawn in red as the out-of-plane component of $\mathbf{k}_1^+(\mathbf{p}_B)$ is purely imaginary. The red dashed line indicates the Brewster angle for a planar surface, approximately equal to 33.7° in this case.

For normal incidence [Fig. 6(a)] the total zero order electric field lies along $\hat{\mathbf{e}}_1$, and consequently, so does $\mathbf{k}_2^+(\mathbf{p}_B)$. In fact, for normal incidence, due to the fact that the total zero order field lies along $\hat{\mathbf{e}}_1$, there are *two* Brewster waves in the plane of incidence with opposite wave vectors $p_1 = \pm n_2\,\omega/c$, but we focus on the one pointing to the right for clarity in Fig. 6(a). It follows from $\mathbf{k}_2^+(\mathbf{p}_B)$ that $|\,\mathbf{p}_B\,| > n_1\,\omega/c$ and the corresponding Brewster (non-) reflected wave is therefore evanescent. Such a case could not be revealed in previous work which focused on the diffusely scattered intensity radiated away from the surface. Nevertheless, the theory suggests that the notion of Brewster scattering should be extended to evanescent waves. This effect is indeed visible by inspection of the modulus of the amplitude $\rho_{pp}^{(1)}$ in Fig. 2(a). Indeed, we observe that for $p_1 = \pm n_2\,\omega/c$, $\rho_{pp}^{(1)}$ vanishes. The corresponding phase $\phi_{pp}^{\mathrm{r},(1)}$ exhibits a jump which is characteristic of the Brewster effect. The phase jump is equal to $\pi/2$ in this case, while in general the phase jump associated with the Brewster effect is equal to π. The $\pi/2$ jump seems to happen only when two Brewster waves with opposite lateral wave vectors are solutions of the criterion Eq. (35), which as far as

we can see only occurs at normal incidence for the systems studied in this paper. It is tempting to interpret the $\pi/2$ jump as actually a π jump evenly shared by the two Brewster waves (although this is over interpreted as we will see later). By progressively increasing the polar angle of incidence, the direction of the total zero order field changes, and so does the wave vector of the Brewster Snell-conjugate wave (which now is unique). For a polar angle of incidence equal to 35°, as sketched in Fig. 6(b), we can observe that the projection of $\mathbf{k}_2^+(\mathbf{p}_\mathrm{B})$ along $\hat{\mathbf{e}}_1$ still yields an evanescent Brewster wave, but the lateral wave vector is now closer to the propagation limit. This case corresponds to the parameters assumed in obtaining the results in Fig. 2(b) and we can observe that $\rho_{pp}^{(1)}$ vanishes indeed for p_1 just above ω/c, and that the corresponding phase exhibits a π jump. By further increasing the polar angle of incidence the Brewster wave is found in the propagating region as $|\,\mathbf{p}_\mathrm{B}\,| < n_1\,\omega/c$, and its full wave vector can now be represented as following the inner dashed circle. As the polar angle of incidence increases towards the Brewster angle for a planar surface, the wave vector associated with the reflected zero order wave $\mathbf{k}_1^+(\mathbf{p}_0)$, drawn in black in Fig. 6, and the wave vector of the Brewster scattered wave both approach the red dashed line from either sides and cross it at the same angle of incidence, namely the Brewster angle for a planar interface, $\theta_0 = \theta_\mathrm{B}$. Figure 6(c) shows the case where $\theta_0 = 50°$ at a slightly lower angle than the Brewster angle of incidence (approximately equal to 56.3°), i.e. just before the cross-over. When θ_0 is further increased the lateral component of the Brewster wave vector continues to decrease. Figure 6(d) assumes $\theta_0 = 70°$ which corresponds to Fig. 2(c) where we now observe that the Brewster wave is indeed in the propagating region as can be seen both from $\rho_{pp}^{(1)}$ and the extinction of the incoherent component of the MDRC. Note also the π jump in the phase. Finally, as the polar angle of incidence approaches 90°, the virtual wave does *not* approach the vertical direction as one might naively expect. Indeed, the total zero order field does not become oriented along $\hat{\mathbf{e}}_3$ but along the direction given by the critical angle for total internal reflection. The change in the expected Brewster scattering angle $\Theta_B(\theta_0)$ for a range of angles of incidence and for the currently discussed system is visible as blue dashed lines in Fig. 5.

We now repeat the analysis but for an incident wave approaching the surface in the denser medium [$\epsilon_1 = 2.25$, $\epsilon_2 = 1.0$]. For normal incidence, the total zero order field is along $\hat{\mathbf{e}}_1$, and yet again we recover two Brewster waves. However, since now the magnitudes of the Snell-conjugate waves are situated on the inner circle ($\epsilon_2 = 1$), the wave vectors $\mathbf{k}_1^+(\pm\,\mathbf{p}_\mathrm{B})$ correspond to propagating waves in glass, and coincide with the Yoneda threshold. This situation is illustrated in Fig. 7(a) and Fig. 3(a). Due to the presence of two Brewster waves, the phase jump is $\pi/2$ [see Fig. 3(a)]. The coincidence of the Yoneda threshold and the Brewster scattering angle for internal reflection for normal incidence is now explained, and we see that although the two effects are of different nature and decoupled, they occur simultaneously in this case simply as a consequence of the geometry imposed by the dispersion relations. As the polar angle of incidence is increased, only one Brewster wave remains, and the corresponding lateral wave vector shrinks [see Fig. 7(b) and Fig. 3(b)]. The wave vectors of the reflected zero order wave and of the Brewster wave cross each other at the Brewster angle of incidence ($\approx 33.7°$). Now comes an interesting effect which was not present when the wave was incident from the less dense medium. As the polar angle of incidence approaches the critical angle of total internal reflection of the zero order reflected wave, the Snell-conjugate wave vector and that of the Brewster wave approach the vertical direction and reach it for $\theta_0 = \theta_c$, as displayed in Fig. 3(c). Then a sudden transition occurs when θ_0 is increased beyond θ_c. In Fig. 4(a), which shows results for θ_0 just above the critical angle, it seems that the Brewster scattering angle is nowhere to be found. However, the Brewster scattering angle now comes back from the left (backscattering) side, visible in the evanescent region of Fig. 4(c) where the polar angle of incidence is 70°. What happened? The overall behaviour of the phase in Figs. 4(a)–(c) gives us a good indication. We have mentioned earlier that for s-polarized light, when the zero order reflected wave undergoes total internal reflection, the central phase plateau must undergo a Goos-Hänchen shift with θ_0 (in fact it is the whole graph which undergoes the shift). Similarly, the p-polarized zero order reflected wave undergoes a Goos-Hänchen shift and, as a consequence, the two terms in Eq. (32b) are *not* any longer in phase. In the case where $\epsilon_1 < \epsilon_2$, the arguments of the two complex amplitudes in Eq. (32b) are always either in phase or are separated by a phase difference of π. Therefore, as time progresses, the *real* total zero order field keeps a fixed direction. When $\epsilon_1 > \epsilon_2$, the Goos-Hänchen phase shift makes the real total zero order field change direction and turn in the plane of incidence as time progresses (it describes an ellipse). Intuitively, this seems to indicate that the corresponding dipole radiation is not expected to be that of an oscillating dipole anymore but that of a *rotating* dipole. It is therefore understandable that the measurement of a propagating p-polarized wave does not yield any direction of extinction when the radiation is emitted from a rotating dipole. Stated in an equivalent way, $\rho_{pp}^{(0)}$ now draws a lower half circle in the complex plane from 1 to -1 as the angle of incidence is varied from the critical angle to 90°, while it previously stayed on the real line. It follows that $\mathbf{E}_{p,1}^{(0)}(\mathbf{p}_0)$ has a complex amplitude with non-zero imaginary part. It is therefore not possible for a propagating Snell-conjugate wave to satisfy the requirement of Eq. (35) since its p-polarization vector would be real. Hence, in order to satisfy Eq. (35) the polarization vector $\hat{\mathbf{e}}_{p,2}^+(\mathbf{p}_\mathrm{B})$ must itself be complex, and the Snell-conjugate wave is now found in the *evanescent* region of medium 2. This is the reason why the Brewster scattering lateral wave vector seems to disappear at the transition $\theta_0 = \theta_c + \Delta\theta_0$ and then come

back from the negative p_1 side as the angle of incidence is increased, which reveals the evanescent nature of the Snell-conjugate wave.

Note that what we have defined as a p-polarized wave, according to the polarization vector $\hat{\mathbf{e}}^{\pm}_{p,j}(\mathbf{p})$ given in Eq. (6d), takes a rather interesting structure when it is evanescent. For an evanescent wave, $\alpha_j(\mathbf{p})$ is pure imaginary and the polarization vector $\hat{\mathbf{e}}^{\pm}_{p,j}(\mathbf{p})$ hence has a real component along $\hat{\mathbf{e}}_3$ and a pure imaginary component along the transverse wave vector direction. This means that the corresponding real electric field is the sum of a wave polarized along $\hat{\mathbf{e}}_3$ and a longitudinal wave (*longitudinal* with respect to the lateral wave vector) dephased by $\pi/2$ radians with respect to the first wave. The resulting field therefore describes an ellipse in the $(\hat{\mathbf{e}}_3, \hat{\mathbf{p}})$-plane.

In-plane transmission — The analysis for the Brewster scattering effect in the transmitted light is similar to that of the reflected light and will not be analyzed in details. One difference worth mentioning, however, is that the Brewster scattering direction is generally found in the backscattering region when the corresponding Brewster scattering for reflection is found in the forward scattering direction. Intuitively, this effect can be related to the emission of an oscillating dipole which yields zero emitted power along the direction of oscillation, hence producing two antipodal zero intensity points when the intensity is mapped onto a sphere. This fact is better illustrated in the next section.

E. Polarization of the radiation of oscillating and rotating dipoles in free space

Before treating the full angular distribution of the light scattered diffusely by a randomly rough surface, we allow ourselves a detour via the analysis of the polarization properties of the radiation emitted by an oscillating dipole or a rotating dipole in free space. The study of the polarization of the radiation in these two cases gives remarkable insight and intuition into the qualitative physical mechanisms at play for the case of the scattering from a random interface, for which a more quantitative analysis requiring Snell-conjugate waves will be given in the next section.

Polarization of the radiation from an oscillating dipole in free space with respect to the local $(\hat{\mathbf{e}}_p, \hat{\mathbf{e}}_s)$ *basis* – We consider first the radiation emitted by a single oscillating dipole in free space. We let this dipole, of dipole moment $\mathbf{D}(\vartheta) = d(\sin\vartheta\ \hat{\mathbf{e}}_1 + \cos\vartheta\ \hat{\mathbf{e}}_3)/2 = d/2\,\hat{\mathbf{e}}_\vartheta$, be tilted from the x_3-axis by an angle of $\vartheta \in [0, \pi/2]$ radians. The dipole is placed in free space at the origin of the coordinate system, where it oscillates with angular frequency ω and radiates the following electric field in the far-field [19]:

$$\mathbf{E}_{\rm dip}(\mathbf{r}, t) = -\frac{\omega^2}{4\pi\varepsilon_0 c^2}\,\frac{\hat{\mathbf{e}}_r \times [\hat{\mathbf{e}}_r \times \mathbf{D}(\vartheta)]}{r}\, e^{-i\omega(t-r/c)}\,, \quad (36)$$

where $\mathbf{r} = r\,\hat{\mathbf{e}}_r = r(\sin\theta\cos\phi\,\hat{\mathbf{e}}_1 + \sin\theta\sin\phi\,\hat{\mathbf{e}}_2 + \cos\theta\,\hat{\mathbf{e}}_3)$ is the point of observation, and $r = |\,\mathbf{r}\,|$. It is well known that no power is radiated along the axis of oscillation of the dipole ($\hat{\mathbf{e}}_r \times \mathbf{D}(\vartheta)$ vanishes in Eq. (36) when $\hat{\mathbf{e}}_r \parallel \hat{\mathbf{e}}_\vartheta$) and that the radiation is polarized in accordance with the cross products in Eq. (36). The electric field is polarized along the vector $\hat{\mathbf{e}}_\theta{}'$, which is the basis vector tangent to a meridian in a spherical coordinate system (r, θ', ϕ') attached to the dipole direction. We are, however, interested in analyzing the polarization of the dipole radiation with respect to the local polarization basis given in Eq. (6), which is defined with respect to the propagation direction of the radiation *and* the plane $x_3 = 0$. Thus we study the following dot products: $\hat{\mathbf{e}}_r \times [\hat{\mathbf{e}}_r \times \hat{\mathbf{e}}_\vartheta] \cdot \hat{\mathbf{e}}_s$ and $\hat{\mathbf{e}}_r \times [\hat{\mathbf{e}}_r \times \hat{\mathbf{e}}_\vartheta] \cdot \hat{\mathbf{e}}_p$ where $\hat{\mathbf{e}}_s = \frac{\hat{\mathbf{e}}_3 \times \hat{\mathbf{e}}_r}{|\,\hat{\mathbf{e}}_3 \times \hat{\mathbf{e}}_r\,|}$ and $\hat{\mathbf{e}}_p = \frac{\hat{\mathbf{e}}_s \times \hat{\mathbf{e}}_r}{|\,\hat{\mathbf{e}}_s \times \hat{\mathbf{e}}_r\,|}$ are defined with respect to $\hat{\mathbf{e}}_r$ in order to mimic the local s- and p-polarization vectors attached to a scattering direction along $\hat{\mathbf{e}}_r$. The unit vectors $\hat{\mathbf{e}}_p = \hat{\mathbf{e}}_\theta = \mathrm{d}\,\hat{\mathbf{e}}_r\,/\mathrm{d}\theta$ and $\hat{\mathbf{e}}_s = \hat{\mathbf{e}}_\phi = 1/\sin\theta\ \mathrm{d}\,\hat{\mathbf{e}}_r\,/\mathrm{d}\phi$ are also the conventional basis vectors in spherical coordinates. First we observe that $\hat{\mathbf{e}}_r \times [\hat{\mathbf{e}}_r \times \hat{\mathbf{e}}_\vartheta] \cdot \hat{\mathbf{e}}_s$ and $\hat{\mathbf{e}}_r \times [\hat{\mathbf{e}}_r \times \hat{\mathbf{e}}_\vartheta] \cdot \hat{\mathbf{e}}_p$ are invariant under the transformation $\hat{\mathbf{e}}_r \mapsto -\,\hat{\mathbf{e}}_r$, and so the s- and p-polarized distributions of the dipole radiation are symmetric with respect to the origin as $\hat{\mathbf{e}}_r$ runs over the unit sphere. Second, for $\vartheta \in (0, \pi/2]$ radians the identity $\mathbf{a} \times [\mathbf{b} \times \mathbf{c}] = (\mathbf{a} \cdot \mathbf{c})\,\mathbf{b} - (\mathbf{a} \cdot \mathbf{b})\,\mathbf{c}$ leads to

$$\hat{\mathbf{e}}_r \times [\hat{\mathbf{e}}_r \times \hat{\mathbf{e}}_\vartheta] = (\hat{\mathbf{e}}_r \cdot \hat{\mathbf{e}}_\vartheta)\,\hat{\mathbf{e}}_r - \hat{\mathbf{e}}_\vartheta\,, \quad (37)$$

hence the projection of the dipole radiation on the local s-polarization basis reads

$$\hat{\mathbf{e}}_r \times [\hat{\mathbf{e}}_r \times \hat{\mathbf{e}}_\vartheta] \cdot \hat{\mathbf{e}}_s = -\,\hat{\mathbf{e}}_\vartheta \cdot \hat{\mathbf{e}}_\phi = -\sin\vartheta\sin\phi\,. \quad (38)$$

A direct consequence of Eq. (38) is that $\hat{\mathbf{e}}_r \times [\hat{\mathbf{e}}_r \times \hat{\mathbf{e}}_\vartheta] \cdot \hat{\mathbf{e}}_s$ vanishes for all $\hat{\mathbf{e}}_r$ in the $(\hat{\mathbf{e}}_1, \hat{\mathbf{e}}_3)$-plane [see Fig. 8(d)]. The corresponding projection on the local p-polarization basis reads

$$\hat{\mathbf{e}}_r \times [\hat{\mathbf{e}}_r \times \hat{\mathbf{e}}_\vartheta] \cdot \hat{\mathbf{e}}_p = -\,\hat{\mathbf{e}}_\vartheta \cdot \hat{\mathbf{e}}_\theta\,, \quad (39)$$

which is a quantity that depends on ϑ, θ, and ϕ. In the particular case where $\hat{\mathbf{e}}_\theta$ belongs to the $(\hat{\mathbf{e}}_1, \hat{\mathbf{e}}_3)$-plane, there are two solutions for Eq.(39) equal to zero: $\hat{\mathbf{e}}_r = \pm\,\hat{\mathbf{e}}_\vartheta$, which correspond to the two intersections of the dipole moment direction with the unit sphere. This is not surprising since we already know that no power is emitted along the direction of oscillation of the dipole, independent of polarization. More interesting are cases for which $\hat{\mathbf{e}}_\theta$, and hence $\hat{\mathbf{e}}_r$, does not belong to the $(\hat{\mathbf{e}}_1, \hat{\mathbf{e}}_3)$-plane. Expanding the dot product in Eq. (39) in terms of the angles ϑ, θ, and ϕ we obtain the following implicit

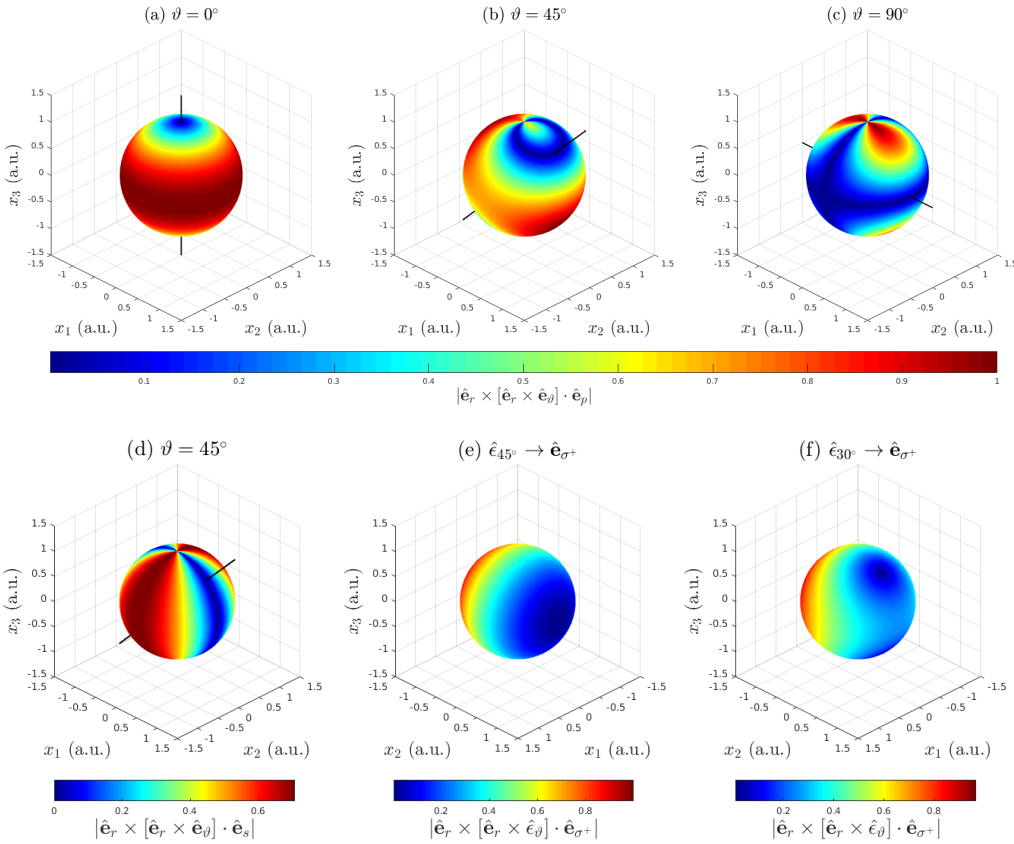

FIG. 8. (a-c) Dependence of the p-polarized radiation of a tilted dipole in free space, $|\,\hat{\mathbf{e}}_r \times [\hat{\mathbf{e}}_r \times \hat{\mathbf{e}}_\vartheta] \cdot \hat{\mathbf{e}}_p\,|$, on the direction of $\hat{\mathbf{e}}_r$ as it runs over the unit sphere for different dipole tilting angles $\vartheta \in \{0°, 45°, 90°\}$. (d) Similar dependence of the s-polarized radiation of a tilted dipole in free space on $\hat{\mathbf{e}}_r$ for $\vartheta = 45°$. The black line in panels (a-d) indicates the direction of the dipole moment. (e-f) Dependence of the σ^+-polarized radiation of a rotating dipole in free space parametrized by $\vartheta = 45°$ and $\vartheta = 30°$ respectively (note the orientation of the coordinate system).

equation for the set of points on the unit sphere where the p-polarization component of the dipole radiation vanishes:

$$\sin\vartheta\,\cos\theta\,\cos\phi - \cos\vartheta\,\sin\theta = 0\,, \tag{40}$$

or equivalently for non-pathologic cases

$$\frac{\tan\vartheta}{\tan\theta} = \frac{1}{\cos\phi}\,. \tag{41}$$

We verify that for the cases $\phi = 0$ and $\phi = \pi$ radians, we recover that $\theta = \vartheta$ and $\theta = \pi - \vartheta$, i.e. the points of intersection of the dipole moment direction and the unit sphere. For $\phi \in (-\pi/2, \pi/2)$, $\cos\phi > 0$, which implies that $\tan\theta > 0$ (recall that $0 < \vartheta < \pi/2$ hence $\tan\vartheta > 0$) and $\tan\vartheta > \tan\theta$. By the monotony of the tangent function, and the continuity of Eq. (41) with respect to the variables, we thus deduce that when ϕ varies in $(-\pi/2, \pi/2)$ the set of the points of zero traces a curve on the unit sphere latitude-bounded by $\theta < \vartheta$. By the aforementioned symmetry of the polarization dependence of the dipole radiation with respect to the origin we immediately deduce that when ϕ varies in $(\pi/2, 3\pi/2)$ the set of the points of zero traces a curve on the unit sphere latitude-bounded by $\theta > \pi - \vartheta$. This is well illustrated in Fig. 8(b) where $|\,\hat{\mathbf{e}}_r \times [\hat{\mathbf{e}}_r \times \hat{\mathbf{e}}_\vartheta] \cdot \hat{\mathbf{e}}_p\,|$ is shown as a color map on a unit sphere. For $\vartheta = 45°$ we here observe that the curve of zero p-polarized radiation passes through both the north pole and the intersection point of the dipole moment direction on the northern hemisphere. The degenerate cases $\vartheta = 0°$ [Fig. 8(a)] and $\vartheta = 90°$ [Fig. 8(c)] are also illustrated. For these cases the curves of zero p-polarized radiation reduces to two points (the poles) in the former case, and the equator

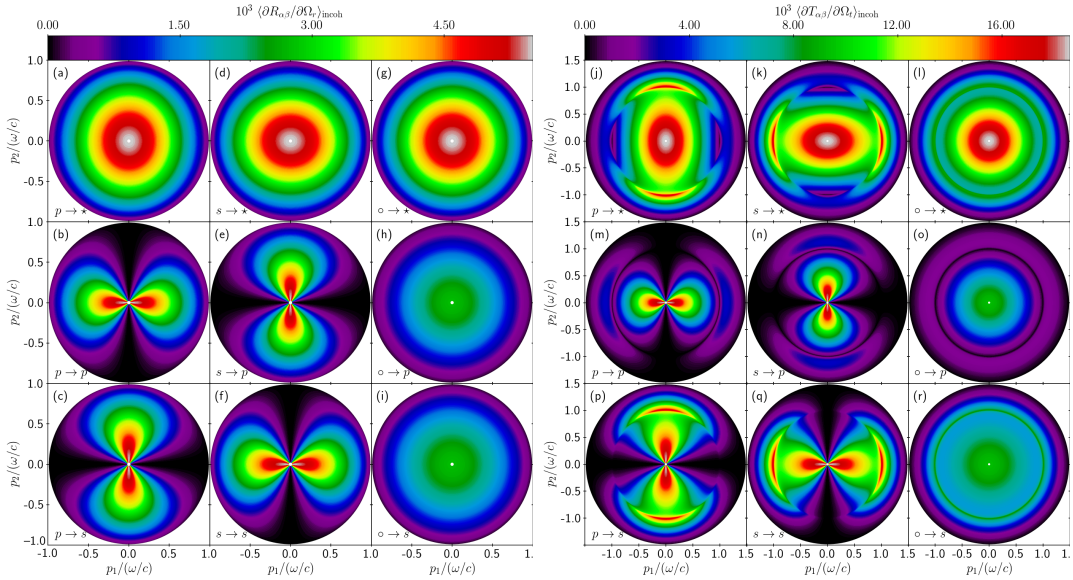

FIG. 9. The full angular distribution of the incoherent component of the MDRC/MDTC, $\langle \partial X_{\alpha\beta}/\partial\Omega_r \rangle_{\rm incoh}$ for $X = R$ or T, as function of the lateral wave vector $\mathbf{q}$ of the light that is scattered from a rough interface where the angle of incidence $\theta_0 = 0^\circ$. The positions of the specular directions in reflection and transmission are indicated by white dots. The parameters assumed for the scattering geometry and used in performing the numerical calculation had values that are identical to those assumed in obtaining the results of Fig. 2. The sub-figures in Figs. 9(a)–(i) and 9(j)–(r) are both organized in the same manner and show how incident β-polarized light is scattered by the one-rough-interface film geometry into α-polarized light [with $\alpha = p, s$ and $\beta = p, s$] and denoted $\beta \to \alpha$. Moreover, the notation $\circ \to \star$ is taken to mean that the incident light was unpolarized while the polarization of the scattered light was not recorded. For instance, this means that the data shown in Fig. 9(a) are obtained by adding the data sets presented in Figs. 9(b)–(c); similarly, the data shown in Fig. 9(g) result from the addition and division by a factor two of the the data sets presented in Figs. 9(a) and 9(d); *etc.* Finally, the in-plane intensity variations from Figs. 9(b, f) and 9(k, o) are the curves depicted in Figs. 2(a) and Figs. 2(d), respectively.

$(\theta = \pi/2)$ and meridians $\phi = \pm\pi/2$ in the latter. Indeed, θ must go to zero when $\vartheta \to 0$ as $\tan\vartheta$ vanishes, and, *either* ϕ must go towards $\pm\pi/2$ *or* θ must go towards $\pi/2$ when $\vartheta \to \pi/2$ as $\tan\vartheta$ diverges.

Polarization of the radiation from a rotating dipole in free space with respect to the local $(\hat{\mathbf{e}}_{\sigma^+}, \hat{\mathbf{e}}_{\sigma^-})$ *basis* – We now consider the radiation of a dipole rotating in the $(\hat{\mathbf{e}}_1, \hat{\mathbf{e}}_3)$-plane. Equation (36) still holds, but we need to modify the dipole moment which now reads

$$\mathbf{D}(\vartheta) = d\,(\sin\vartheta\ \hat{\mathbf{e}}_1 + i\cos\vartheta\ \hat{\mathbf{e}}_3)/2 = d/2\,\hat{\boldsymbol{\epsilon}}_\vartheta\ . \tag{42}$$

The real vector $\mathrm{Re}[\hat{\boldsymbol{\epsilon}}_\vartheta \exp(-i\omega t)]$ hence describes an ellipse in the $(\hat{\mathbf{e}}_1, \hat{\mathbf{e}}_3)$-plane whose excentricity is parametrized by ϑ. In the limiting cases $\vartheta = 0$ and $\vartheta = \pi/2$ radians we obtain an oscillating dipole along $\hat{\mathbf{e}}_3$ and $\hat{\mathbf{e}}_1$ respectively. For $\vartheta = \pi/4$ we obtain a circularly rotating dipole. We now consider the polarization of the radiation from such an elliptically rotating dipole with respect to the local left and right circularly polarized basis $\hat{\mathbf{e}}_{\sigma^+}$ and $\hat{\mathbf{e}}_{\sigma^-}$ defined as

$$\hat{\mathbf{e}}_{\sigma^\pm} = \frac{1}{\sqrt{2}}\,(\hat{\mathbf{e}}_p \pm i\,\hat{\mathbf{e}}_s)\,. \tag{43}$$

The σ^+ polarization component of the rotating dipole radiation is then measured by

$$\hat{\mathbf{e}}_r \times[\hat{\mathbf{e}}_r \times\hat{\boldsymbol{\epsilon}}_\vartheta] \cdot \hat{\mathbf{e}}_{\sigma^+} = -\hat{\boldsymbol{\epsilon}}_\vartheta \cdot \hat{\mathbf{e}}_{\sigma^+}\ , \tag{44}$$

which when expressed in terms of the angles reads[40]

$$\hat{\mathbf{e}}_r \times[\hat{\mathbf{e}}_r \times\hat{\boldsymbol{\epsilon}}_\vartheta] \cdot \hat{\mathbf{e}}_{\sigma^+} = -\frac{1}{\sqrt{2}}\ \sin\vartheta\cos\theta\cos\phi - \frac{i}{\sqrt{2}}\,(\cos\vartheta\sin\theta - \sin\vartheta\sin\phi)\,. \tag{45}$$

The modulus square of Eq. (45) yields

$$|\,\hat{\mathbf{e}}_r \times[\hat{\mathbf{e}}_r \times\hat{\boldsymbol{\epsilon}}_\vartheta] \cdot \hat{\mathbf{e}}_{\sigma^+}\,|^2 = \frac{1}{2}\ \sin^2\vartheta\cos^2\theta\cos^2\phi + \frac{1}{2}\,(\cos\vartheta\sin\theta - \sin\vartheta\sin\phi)^2\,. \tag{46}$$

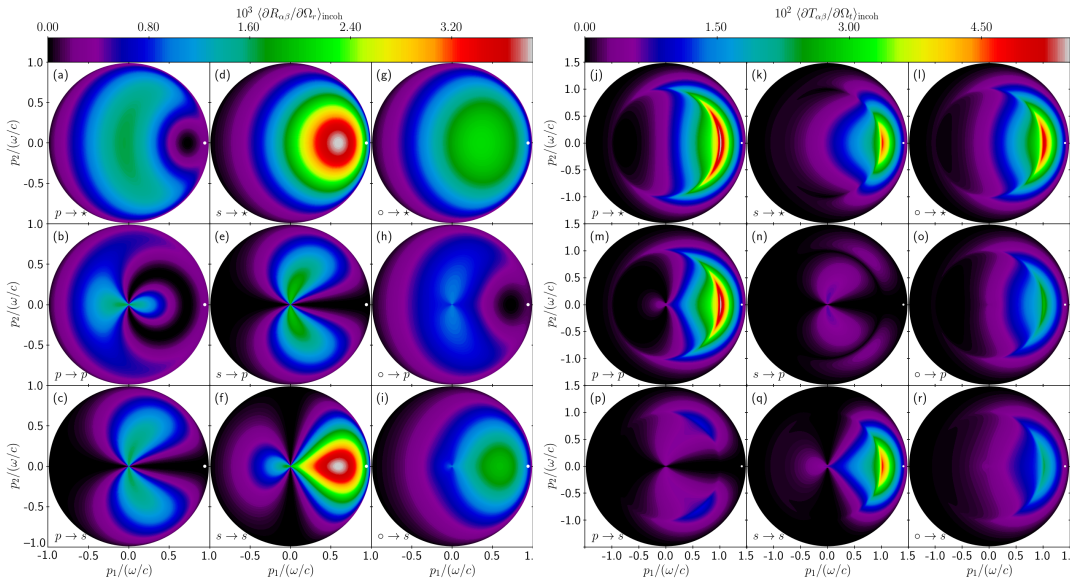

FIG. 10. Same as Fig. 9, but now for the angle of incidence $\theta_0 = 70°$.

The directions of zero σ^+-polarized light radiation are obtained if and only if both terms on the right-hand side of Eq. (46) are zero. The first term vanishes if at least $\sin\vartheta$, $\cos\theta$ or $\sin\phi$ is zero. If we first assume that $\vartheta = 0$, then the second term is zero if and only if the condition $\sin\theta = 0$ is satisfied. Such a case corresponds to a dipole oscillating along the x_3-axis and its radiation vanishes at the poles of the unit sphere. More interesting are the cases for which $\vartheta \neq 0$ and either $\theta = \pi/2$ (recall that $\theta \in (0, \pi)$) or $\phi = \pm\pi/2$. Let us first assume that $\phi = \pm\pi/2$. The second term in Eq. (46) then vanishes if and only if

$$\sin\theta = \pm\tan\vartheta\,. \tag{47}$$

This last condition imposes a constraint on ϑ, which must then have a value between 0 and $\pi/4$ in order for $\tan\vartheta$ (and hence $\sin\theta$) to be less than unity. Since $\theta \in (0, \pi)$, only the case $\phi = \pi/2$ yields two solutions, θ_1 and θ_2, that are symmetric with respect to $\theta = \pi/2$. This is illustrated in Fig. 8(f). Assuming now that $\theta = \pi/2$, the second term in Eq. (46) vanishes if and only if

$$\sin\phi = \operatorname{cotan}\vartheta\,. \tag{48}$$

Since $\sin\phi$ requires $\operatorname{cotan}\vartheta$ to be less than unity the above condition can only be satisfied if $\vartheta \in (\pi/4, \pi/2)$. There are then two solutions for ϕ between 0 and π (since $\sin\phi > 0$ for $\vartheta \in (\pi/4, \pi/2)$), which are symmetric with respect to $\pi/2$. In fact, it can be shown that the polarization of the radiation of the rotating dipole for $\vartheta \in (\pi/4, \pi/2)$ corresponds to that of a rotating dipole for which $\vartheta' = \pi/2 - \vartheta$ (as in Fig. 8(f)) but rotated by 90° with respect to the x_2-axis. These different cases where Eq. (46) vanishes for a given circular polarization have a very simple geometrical interpretation. For $\vartheta < \pi/4$ the rotating dipole describes an ellipse whose long axis is oriented along the x_3-axis. The two directions of zero σ^+-polarized radiation correspond to the two directions from which the ellipse is observed as a circle, with the orientation of the dipole rotation opposite to that of the σ^+ polarization. For these two directions the radiation is therefore purely σ^--polarized, explaining why the zeros of radiation are found on the meridian where $\phi = \pi/2$. For $\vartheta > \pi/4$ the long axis of the ellipse is along the x_1-direction, which explains the fact that the directions where one circular polarization is zero are found at the equator. By symmetry the directions where the σ^--polarized radiation vanishes are symmetric to those of the σ^+-polarized radiation with respect to the $(\hat{\mathbf{e}}_1, \hat{\mathbf{e}}_3)$-plane.

These results, obtained for the polarization of the dipole radiation in free space, will prove to be useful for the qualitative understanding of the full angular distribution of the incoherent component of the MDRC and MDTC in the case of the scattering by a randomly rough dielectric surface.

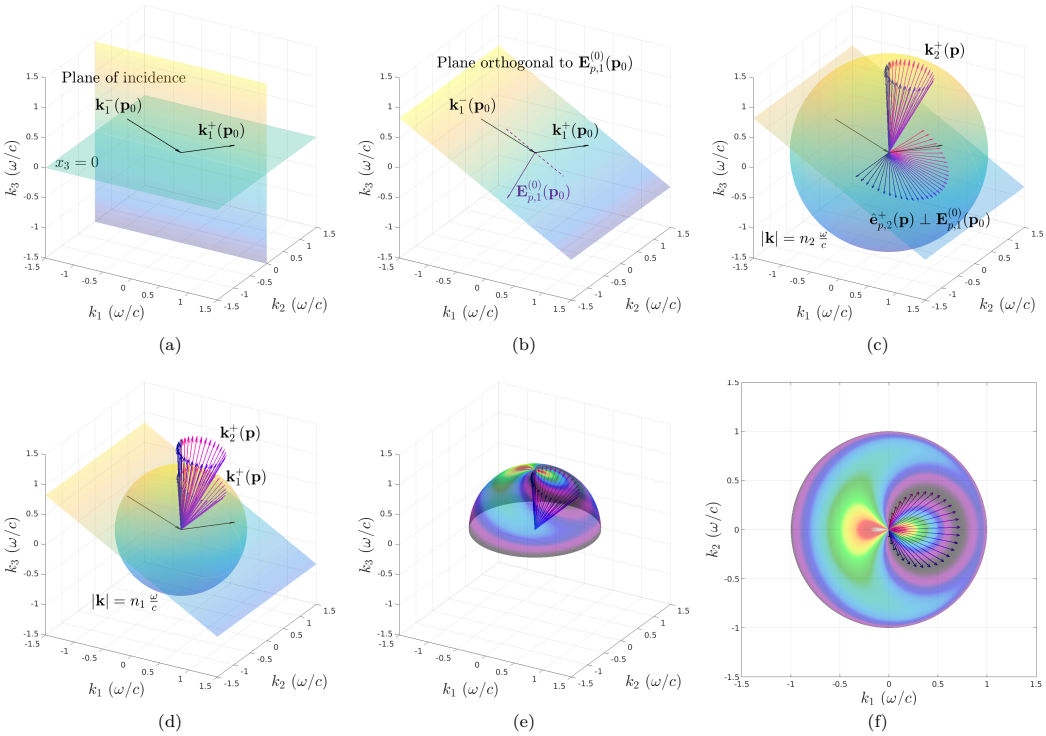

FIG. 11. Illustration of the construction steps leading to the set of directions of zero $p \to p$ reflection for an angle of incidence of $\theta_0 = 70°$. (a) Sketch of the average surface, the plane of incidence and the considered wave vectors of the incident and reflected zero order waves ($\mathbf{k}_1^-(\mathbf{p}_0)$ and $\mathbf{k}_1^-(\mathbf{p}_0)$). (b) Construction of the total zero order field amplitude $\mathbf{E}_{p,1}^{(0)}(\mathbf{p}_0)$ and the plane orthogonal to it. Note that the incident wave vector does not in general belong in this plane as illustrated with the dashed indigo line indicating the intersection of the plane of incidence and the plane $\mathbf{E}_{p,1}^{(0)}(\mathbf{p}_0)^\perp$. (c) Unit vectors belonging to the lower half $\mathbf{E}_{p,1}^{(0)}(\mathbf{p}_0)^\perp$-plane. They correspond to the possible polarization vectors $\hat{\mathbf{e}}_{p,2}^+(\mathbf{p})$ of Eq. (35). The wave vectors $\mathbf{k}_2^+(\mathbf{p})$ associated to the polarization vectors $\hat{\mathbf{e}}_{p,2}^+(\mathbf{p})$ are then constructed according to Eqs. (6). Note that they lie on a sphere of radius $|\,\mathbf{k}\,| = n_2\,\omega/c$. The color associated to the vectors $\hat{\mathbf{e}}_{p,2}^+(\mathbf{p})$ and $\mathbf{k}_2^+(\mathbf{p})$ helps us to identify the $\mathbf{k}_2^+(\mathbf{p})$ associated to each $\hat{\mathbf{e}}_{p,2}^+(\mathbf{p})$ (they share the same color). (d) The wave vectors $\mathbf{k}_2^+(\mathbf{p})$ are projected on the sphere of radius $|\,\mathbf{k}\,| = n_1\,\omega/c$ following the x_3-direction, hence giving the wave vectors $\mathbf{k}_1^+(\mathbf{p})$ of zero $p \to p$ reflection. (e) The incoherent component of the MDRC is shown on the scattering sphere together with the set of wave vectors $\mathbf{k}_1^+(\mathbf{p})$ obtained in (d). (f) Projection of (e) in the $(\hat{\mathbf{e}}_1, \hat{\mathbf{e}}_2)$-plane. We verify in (e) and (f) that the constructed wave vectors indeed follow the curve of zero scattering of the incoherent component of the MDRC.

F. Full angular distributions of the MDRC/MDTC

P-polarized Brewster scattering — Figure 9 presents the full angular distributions of the diffuse contribution to the MDRC and MDTC for $\theta_0 = 0°$ and parameters equivalent to those assumed in Figs. 2(a) and 2(d), respectively. The overall dipole-like appearance of the lower left 2×2 panels in each collection of panels in Fig. 9 is reminiscent of the polarization pattern of the dipole radiation in free space discussed above in the case when the dipole oscillates in the $(\hat{\mathbf{e}}_1, \hat{\mathbf{e}}_2)$-plane. For normal incidence all the zero order waves and the incident wave have an oscillating electric field either along $\hat{\mathbf{e}}_1$ for p polarization or along $\hat{\mathbf{e}}_2$ for s polarization. Thus the dipoles in the media[41] oscillate along the direction of the incident field. For an s-polarized wave (field along $\hat{\mathbf{e}}_2$) we have seen that the dipole radiation in free space yields zero s-polarized emission in the $(\hat{\mathbf{e}}_2, \hat{\mathbf{e}}_3)$-plane and an overall $|\sin(\phi_r - \pi/2)|$ intensity, which is consistent with what is observed in Fig. 9(f). Note that for a given polar angle of reflection θ_r, the variation along ϕ_r of the incoherent component of the MDRC to lowest non-zero order in the surface roughness for $s \to s$ polarized scattering is *exactly*

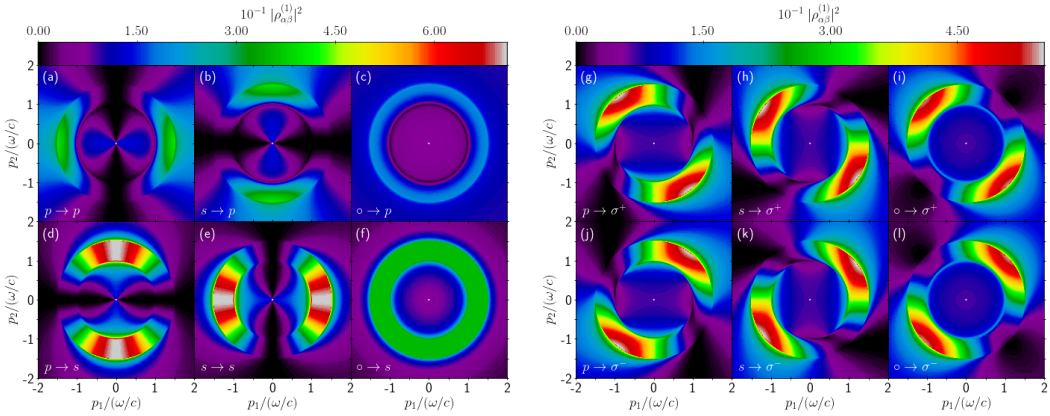

FIG. 12. The full angular distribution of $|\rho^{(1)}_{\alpha\beta}|^2$ for normal incidence, $\theta_0 = 0°$, $\epsilon_1 = 2.25$, $\epsilon_2 = 1$, for incident polarization $\beta \in \{p, s\}$ or unpolarized ($\circ$) and outgoing polarization $\alpha \in \{p, s, \sigma^+, \sigma^-\}$.

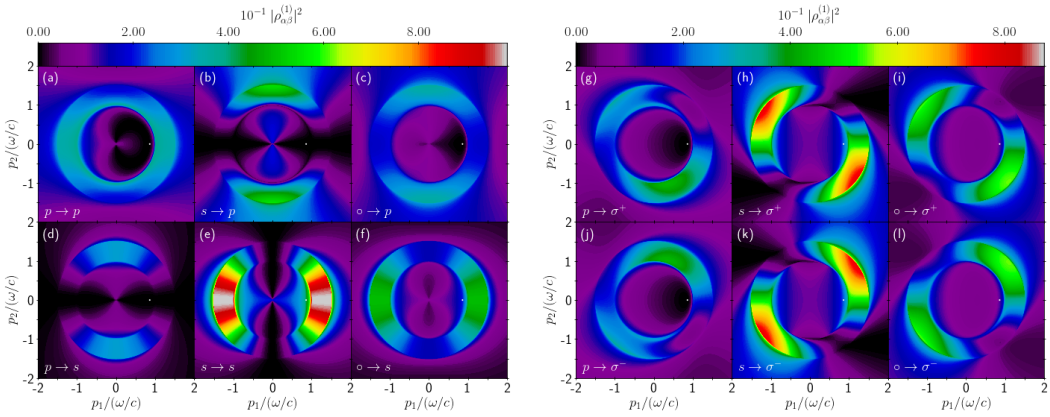

FIG. 13. Same as Fig. 12 but for the angle of incidence $\theta_0 = 35°$.

proportional to $|\sin(\phi_r - \pi/2)|$ since $\rho^{(1)}_{ss}$ is proportional to $\hat{\mathbf{e}}_s(\mathbf{p}) \cdot \hat{\mathbf{e}}_s(\mathbf{p}_0)$, as can be seen from Eq. (30a), and this is the only ϕ_r dependence for normal incidence. This observation holds for all the polarization couplings up to a rotation by $\pi/2$ for cross-polarization. For example, for an s-polarized incident field and p-polarized reflected light the ϕ_r dependence is proportional to $|\sin\phi_r|$. For the transmitted light [Fig. 9(j-r)] the behaviour is similar, but in addition we now observe the Yoneda phenomenon. This is the enhancement of the diffuse contribution to the MDTC intensity above the critical lateral wave vector for the scattered light $|\,\mathbf{p}\,| > p_c$, as discussed extensively in Sec. IV C, which for normal incidence is directly observable for outgoing s-polarized light, especially in Fig. 9(r). For transmitted p-polarized light we observe a black ring of zero scattering intensity along the circle $|\,\mathbf{p}\,| = p_c$. This is the two-dimensional extension of our discussion in Sec. IV D for in-plane scattering, where we found that at normal incidence two Brewster waves with $\mathbf{p}_B = \pm p_c\,\hat{\mathbf{e}}_1$ could be found. Now we see that in two-dimensional $\mathbf{p}$-space the solution to Eq. (35) is in fact given by $|\,\mathbf{p}\,| = p_c$. In terms of dipole radiation in free space this corresponds to the vanishing radiation of p-polarized light in the equatorial plane for the case $\vartheta = 90°$ as illustrated in Fig. 8(c). A ring of zero intensity for the p-polarized *reflected* waves can also be found, but then in the evanescent regime as a two-dimensional extension of the corresponding discussion for in-plane scattering.

The similitude with the polarization of the radiation emitted by an oscillating dipole in free space is clear for

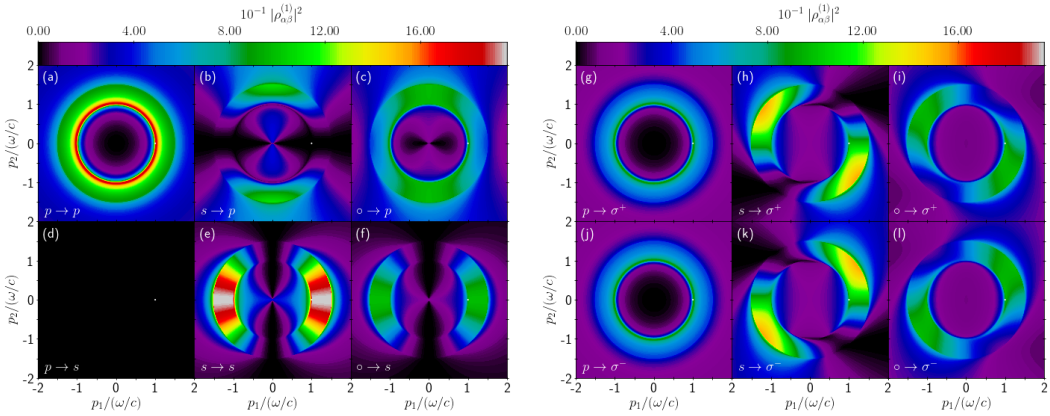

FIG. 14. Same as Fig. 12 but for the angle of incidence equal to the critical angle for total internal reflection, $\theta_0 = \theta_c = 41.81°$.

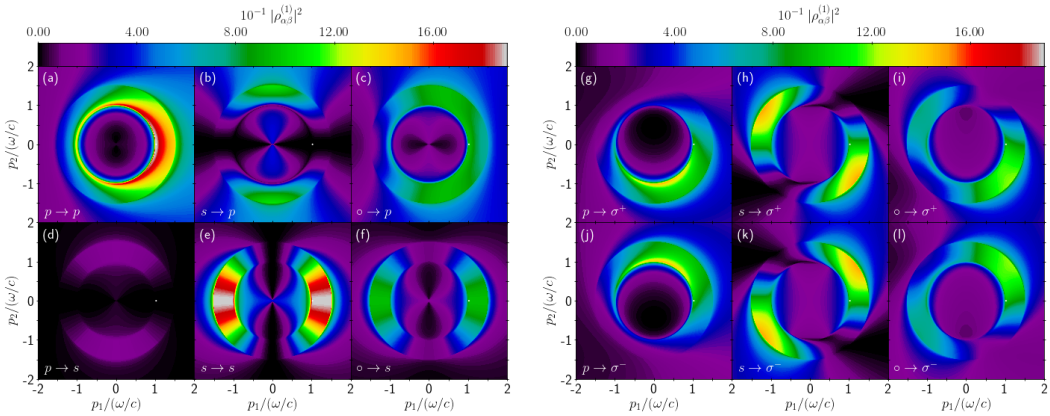

FIG. 15. Same as Fig. 12 but for the angle of incidence $\theta_0 = 43°$.

normal incidence. Let us now consider a larger angle of incidence, $\theta_0 = 70°$, for which the diffuse contributions to the MDRC and MDTC for incidence in vacuum are shown in Fig. 10. First, we observe that for $p \to p$ reflection [Fig. 10(b)], there exists a closed curve of zero intensity in the forward scattering direction. Similarly, we observe a closed curve of zero intensity for $p \to p$ transmission [Fig. 10(k)] but in the backscattering region. These features are analogous to those observed in the case of the p polarization component of the dipole radiation in free space in the case where the dipole tilting angle is such that $0° < \vartheta < 90°$, e.g. as is illustrated in Fig. 8(b) for $\vartheta = 45°$. We can interpret the curves of zero intensity for $p \to p$ scattering in Fig. 10 as the signature of an overall dipole radiation whose dipole moment is tilted from the x_3-axis by some angle ϑ, where the polarization of the reflected light is derived from the northern hemisphere of the radiation polarization pattern while the polarization of the transmitted light is derived from the southern hemisphere of the radiation polarization pattern.

Let us now interpret Eq. (35) geometrically for $p \to p$ scattering for the case of reflection and $\theta_0 = 70°$. This construction is a generalization of the one made for scattering in the plane of incidence presented in Sec. IV D. Figure 11 provides illustrations of the main steps of the geometrical construction of the set of directions of zero $p \to p$ reflection in three dimensions. First, the wave vectors of incidence $\mathbf{k}_1^-(\mathbf{p}_0)$ and of the reflected zero order wave $\mathbf{k}_1^+(\mathbf{p}_0)$ are drawn [Fig. 11(a)]. Second, one determines the direction of the total zero order field amplitude $\mathbf{E}^{(0)}_{p,1}(\mathbf{p}_0)$ which is contained in the plane of incidence. The steps to geometrically construct the total zero order field have been treated in detail for s- and p- polariza-

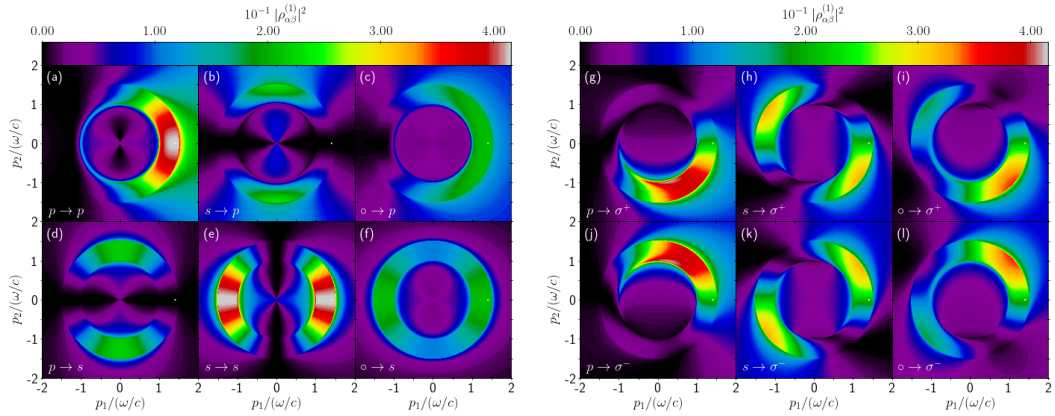

FIG. 16. Same as Fig. 12 but for the angle of incidence $\theta_0 = 70°$.

tions in Ref. 42, and thus we do not show these here for clarity. Once $\mathbf{E}^{(0)}_{p,1}(\mathbf{p}_0)$ is determined, we can construct the plane orthogonal to it: $\mathbf{E}^{(0)}_{p,1}(\mathbf{p}_0)^\perp$ [Fig. 11(b)]. Note that in general this plane does *not* contain the incident wave vector as made clear by the dashed line, showing the intersection of the plane of incidence with the plane $\mathbf{E}^{(0)}_{p,1}(\mathbf{p}_0)^\perp$. According to Eq. (35), all the polarization vectors $\hat{\mathbf{e}}^+_{p,2}(\mathbf{p})$ must be contained in the plane $\mathbf{E}^{(0)}_{p,1}(\mathbf{p}_0)^\perp$. Moreover, since the $\hat{\mathbf{e}}^+_{p,2}(\mathbf{p})$ vectors are normalized their end points are distributed on a circle of unit radius. The set of all $\hat{\mathbf{e}}^+_{p,2}(\mathbf{p})$ vectors satisfying Eq. (35) therefore spans a half circle in the plane $\mathbf{E}^{(0)}_{p,1}(\mathbf{p}_0)^\perp$ as shown on Fig. 11(c), where a sample of polarization vectors are represented. The fact that only the lower half circle is needed comes from the definition[43] of a polarization vector $\hat{\mathbf{e}}^+_{p,2}(\mathbf{p})$. For each polarization vector satisfying Eq. (35) we can construct its corresponding wave vector $\mathbf{k}^+_2(\mathbf{p})$, using for example that the direction is given by $\hat{\mathbf{e}}^+_{p,2}(\mathbf{p}) \times [\hat{\mathbf{e}}^+_{p,2}(\mathbf{p}) \times \hat{\mathbf{e}}_3]$ and that $\mathbf{k}^+_2(\mathbf{p})$ lies on the northern hemisphere of radius $k_2 = n_2\omega/c$. We thus obtain the set of all wave vectors $\mathbf{k}^+_2(\mathbf{p})$ whose corresponding p polarization vector satisfies Eq. (35). A sample of such vectors are represented for $\hat{\mathbf{e}}^+_{p,2}(\mathbf{p})$ and $\mathbf{k}^+_2(\mathbf{p})$ in Fig. 11(c). The last step consists in projecting the vectors $\mathbf{k}^+_2(\mathbf{p})$ along $\hat{\mathbf{e}}_3$ onto the sphere of radius $|\,\mathbf{k}\,| = n_1\,\omega/c$ to obtain the wave vectors $\mathbf{k}^+_1(\mathbf{p})$ of zero $p \to p$ reflection [Fig. 11(d)]. Figures 11(e) and 11(f) show the resulting sampled wave vectors $\mathbf{k}^+_1(\mathbf{p})$ together with the diffuse contribution to the the MDRC, mapped to the hemisphere and its projection in the $(\hat{\mathbf{e}}_1, \hat{\mathbf{e}}_2)$-plane respectively. We verify that the set of constructed wave vectors correspond to the observed curve of zero intensity for $p \to p$ reflection.

Figure 10(n) shows that the $s \to p$ transmitted light exhibits a circle of zero intensity, for $|\,\mathbf{p}\,| = n_1\,\omega/c$ similar to what was observed for normal incidence [Fig. 9(n)]. This feature is also present in reflection but in the evanescent region, and is observed by considering the complex amplitude instead of the MDRC. The reason for the invariance of the circle of zero intensity with the angle of incidence for the $s \to p$ scattering is simple to understand in terms of the dipole radiation in free space. For s-polarized incident light the dipoles in the media are all oriented along $\hat{\mathbf{e}}_2$, independent of the angle of incidence. Thus when measuring the p-polarized component of the radiated light we expect to obtain an underlying pattern of zero intensity consistent with that obtained in the case of the oscillating dipole in free space as illustrated in Fig. 8(c).

Circularly-polarized Brewster scattering — It is instructive to study the modulus square of the amplitudes rather than the MDRC and MDTC in order to appreciate the behavior of the amplitudes of the waves scattered in the evanescent region as well as the ones scattered in the propagating region. Furthermore, in order to illustrate, to our knowledge, a new effect which can be considered as a generalization of the Brewster scattering effect for light scattered from p-polarized to circularly-polarized light, we show in Figs. 12-16 $|\rho^{(1)}_{\alpha\beta}|^2$ in the $\mathbf{p}$-plane for different polar angles of incidence. We let $\beta \in \{p, s, \circ\}$ represent the polarization of the incident light, where $\circ$ indicates unpolarized light, and we let $\alpha \in \{p, s, \sigma^+, \sigma^-\}$ represent the polarization of the light scattered from the surface. The subscripts $\sigma^\pm$ denote respectively left and right circular polarization states and the corresponding reflection amplitudes are derived from the p and s polarization states by

$$\rho^{(1)}_{\sigma^\pm\beta} = \frac{1}{\sqrt{2}}\left[\rho^{(1)}_{p\beta} \pm i\rho^{(1)}_{s\beta}\right], \tag{49}$$

and similarly for the transmission amplitudes. We con-

sider here only the case for which the medium of incidence is the denser one, as the circularly-polarized Brewster scattering effect only takes place when the reflected zero order wave undergoes total internal reflection. Note, however, that the effect can be observed both in the reflected *and* the transmitted scattered light. In Sec. IV D we have seen that the Brewster scattering effect exhibits a sudden transition when the reflected zero order wave undergoes total internal reflection. We have seen that, when restricted to scattering in the plane of incidence, the direction of zero p-polarized reflected intensity goes towards the x_3-direction as the polar angle of incidence approaches the critical angle for total internal reflection. Then the zero direction suddenly disappears from the propagating region as the polar angle of incidence goes beyond the critical angle for total internal reflection. This sudden transition was argued to be attributed to a transition of the dipolar response of the media, going from an oscillating behavior to a rotating behavior due to the phase shift between the incident excitation and the reflected zero order wave. We are now studying this transition in the full **p**-plane with particular attention on the scattered *circularly polarized* light, as it was shown in Sec. IV E that the radiation emitted by a rotating dipole in free space exhibits characteristic signatures in the emitted circularly-polarized light out of the plane of incidence.

First, for polar angles of incidence smaller than the critical angle, $\theta_0 < \theta_c$, we have seen that both $\rho^{(1)}_{p\beta}$ and $\rho^{(1)}_{s\beta}$ are real for scattering angles smaller than the Yoneda threshold. In that case the right-hand side in Eq. (49) vanishes if and only if both $\rho^{(1)}_{p\beta}$ and $\rho^{(1)}_{s\beta}$ are zero simultaneously. For an incident p-polarized wave, $\beta = p$, this occurs only where the curve of zero $p \to p$ scattering (cf. previous subsection) intersects with the plane of incidence in which $p \to s$ scattering is identically zero. This is illustrated for normal incidence, $\theta_0 = 0°$, in Figs. 12(a) and (d) showing $|\rho^{(1)}_{pp}|^2$ and $|\rho^{(1)}_{sp}|^2$ in the **p**-plane, where we recognize the curves of zero scattering for the p- and s-polarized light discussed in previous sections. It is also illustrated in Figs. 12(g) and (j) showing $|\rho^{(1)}_{\sigma^\pm p}|^2$ where two directions of zero $p \to \sigma^\pm$ scattering are present at $\mathbf{p} = \pm p_c\,\hat{\mathbf{e}}_1$, although they are hard to spot on this figure. The effect is clearer for oblique incidence, as in Figs. 13(g) and (j), for which $\theta_0 = 35°$. Figures 13(g) and (j) show a clear unique direction of zero intensity in $p \to \sigma^\pm$ scattering in the plane of incidence.

As the angle of incidence reaches the critical angle of incidence, $\theta_0 = \theta_c = 41.81°$, the direction of zero intensity in $p \to \sigma^\pm$ scattering reaches the x_3-direction, as illustrated in Figs. 14(g) and (j). Note that the x_3-direction also implies zero $p \to p$ scattering intensity as already explained earlier, and that the distribution of $|\rho^{(1)}_{pp}|^2$ and $|\rho^{(1)}_{\sigma^\pm p}|^2$ are cylindrical symmetric as shown in Fig. 14(a), (g) and (j). The cylindrical symmetry can be understood based on the radiation of an oscillating dipole aligned with the x_3-axis. Indeed, we have seen in Section IV E that the p-polarized radiation from such a dipole is cylindrically symmetric with zero radiation at the poles of the unit sphere. The radiation from such a dipole is also purely p-polarized, which has two consequences: (i) the s-polarized scattered light vanishes identically for *all* **p** [Fig. 14(d)]; (ii) the radiation can be decomposed into σ^+ and σ^- components of *equal* intensity, as can be observed in Figs. 14(g) and (j). Even though we have now based our interpretation on the radiation of an oscillating dipole in free space for the sake of simplicity, it is straightforward to verify these assertions based on the expressions of the amplitudes given in Eq. (30). For example, it is clear that for $\theta_0 = \theta_c$, the total zero order field $\mathbf{E}^{(0)}_{1,p}(\mathbf{p}_0)$ is along $\hat{\mathbf{e}}_3$ and the dot product in Eq. (30c) vanishes for all **p**.

For $\theta_0 > \theta_c$, it is convenient to expand the right-hand side in Eq. (49). By inserting Eq. (30) into Eq. (49), the reduced first order reflection amplitude, $\hat{\rho}^{(1)}_{\sigma^\pm p}$, for $\sigma^\pm$-polarized light scattered from incident p-polarized light is then given by

$$\hat{\rho}^{(1)}_{\sigma^\pm p}(\mathbf{p}\,|\,\mathbf{p}_0) = \frac{1}{\sqrt{2}}\left[\gamma(\mathbf{p})\,\hat{\mathbf{e}}^+_{p,2}(\mathbf{p}) \pm i\,\hat{\mathbf{e}}_s(\mathbf{p})\right]\cdot\mathbf{E}^{(0)}_{1,p}(\mathbf{p}_0)\,. \tag{50}$$

Here we have used the short-hand notation $\gamma(\mathbf{p}) = (\hat{\mathbf{e}}^+_{p,2}(\mathbf{p})\cdot\hat{\mathbf{e}}^+_{p,1}(\mathbf{p}))^{-1}$. For $\theta_0 > \theta_c$, the total zero order field amplitude $\mathbf{E}^{(0)}_{1,p}(\mathbf{p}_0)$ is complex. Therefore neither $\rho^{(1)}_{pp}$ nor $\rho^{(1)}_{sp}$ can be zero for propagating waves. We have seen in Section IV D that a zero intensity $p \to p$ scattering point can be found in the evanescent region since $\hat{\mathbf{e}}^+_{p,2}(\mathbf{p})$ becomes complex. However, a zero point in $p \to \sigma^\pm$ scattering may be found in the propagating region. Indeed, the fact that the square bracket in Eq. (50) is complex even for purely real values of $\hat{\mathbf{e}}^+_{p,2}(\mathbf{p})$ and $\hat{\mathbf{e}}_s(\mathbf{p})$ may compensate for the fact that $\mathbf{E}^{(0)}_{1,p}(\mathbf{p}_0)$ is complex and make the dot product in Eq. (50) vanish. Note the similarity with the right-hand side in Eq. (44) for the case of the radiation emitted by a rotating dipole, with the important difference that the p polarization vector is that of the Snell-conjugate wave. Since $\mathbf{E}^{(0)}_{1,p}(\mathbf{p}_0)$ represents a state of polarization of the media in which the dipole rotates in the plane of incidence (cf. discussion in Section IV D), we expect to find a zero in the $\sigma^\pm$ scattering intensity on each side ($\phi_r = \pm\pi/2$) of the plane of incidence. This is indeed what we observe in Figs. 15(a) and (d) in the $|\rho^{(1)}_{\sigma^\pm p}|^2$ distribution of $p \to \sigma^\pm$ scattering.

Finally, let us comment on $s \to \sigma^\pm$ scattering. In Figs. 12-16 it can be observed that the distribution for $|\rho^{(1)}_{\sigma^\pm s}|^2$ stays identical, up to an overall factor, as the angle of incidence varies. This can be understood from the dipole picture. For s-polarized incident light, the incident and zero order waves are s-polarized, so the dipoles oscillate along the x_2-direction independently of the angle of incidence. For scattering in the plane of incidence the first order waves are purely s-polarized and the two

$\sigma^{\pm}$ components have equal intensity. For scattering at $\phi_r = \pm\pi/2$, the first order waves are purely p-polarized and the two $\sigma^{\pm}$ components have again have equal intensity. We obtain the largest contrast between σ^{+} and σ^{-} for ϕ_r being a multiple of 45° since then the p- and s-polarized components are of similar amplitudes.

V. CONCLUSION

Based on a perturbative solution of the reduced Rayleigh equations to first order in the surface profile function, we have achieved a detailed mathematical and physical analysis of the scattering of polarized light by a weakly rough interface between two dielectric media. The first order amplitudes are factorized as a product of a scalar component, mainly representing the relative phases of the different scattering paths, and a polarization component. The polarization component can be interpreted as the signature of the polarization state of the dipoles in the media induced by the incident and zero order fields.

We have seen that the Yoneda phenomenon can be explained simply based on a scalar wave, single scattering picture as an intensity enhancement induced by the evanescence of the component of a scattered couple mode existing in the lesser dense medium, while all the energy allocated to the couple mode is radiated away by the component existing in the denser medium. This mechanism clearly answers previous questions put forward in the literature: we conclude that the phenomenon results from a so-called single scattering mechanism, and is not associated with surface (eigen) modes. In particular, the Yoneda phenomenon is nothing else but the continuous analogue of a Rayleigh anomaly for periodic dielectric grating, in the sense that the diffuse light here plays the role of probing what the efficiency of a diffracted order would be if it were tracked as the period of the grating would vary. This claim is easily verified with straightforward numerical calculation and the exact same perturbation analysis we have exposed here but adapted to gratings.

By factorizing the scalar behavior from that specific to a polarized wave, we have identified the geometrical criterion for the Brewster scattering phenomenon for p-polarized excitation, and more generally, for predicting the zeros of scattered intensity and amplitude for any polarization state. Simply put, these zeros are not different from those found for the radiation from a tilted oscillating dipole in free space, when the polarization of the emitted radiation is adequately measured in a fixed frame of reference. To be more accurate one may say that the physical essence is that of oscillating dipoles, but one must include the fact that arrays of dipoles yield conjugate waves as was described by e.g. Ewald and Doyle [26, 29]. The directions of zero scattering (also for evanescent waves) can then be easily interpreted geometrically in terms of Snell-conjugate waves. Moreover, we have discovered an interesting phenomenon of circularly-polarized Brewster scattering in the reflected and transmitted light scattered out of the plane of incidence when the light is incident in the dense medium and the zero order wave undergoes total internal reflection. The physical mechanism responsible for this effect was explained based on the emission of dipoles rotating in the plane of incidence (and by Snell-conjugate waves), which are induced by the fact that the reflected and transmitted zero order waves are out of phase with the incident wave.

In the present work, particular attention is given to the average phase of the scattered waves compared to previously published works on the Yoneda and Brewster scattering phenomena. We have seen that the Brewster scattering phenomenon is associated with a phase jump, while the region of polar scattering angles beyond the Yoneda threshold is associated with a gradually changing phase. These considerations on the phase of the scattered waves can be of particular interest for testing the theory against experiment, e.g. the phase behavior could be tested by the use of interferometry techniques. A simple way to measure the phase behavior associated with the Yoneda and the Brewster scattering effects is to study the scattering of light by a thin dielectric film deposited on a dielectric substrate, as was recently suggested and observed numerically in Ref. 30. For such a system, Selényi rings, which are interference rings in the intensity of the diffusely scattered light, are expected to exhibit: (i) a reversal of angular positions of the maxima and minima of intensity of the rings for p-polarized light as the Brewster scattering angle is surpassed; (ii) a gradual shift of the angular positions of the rings with respect to those predicted by the simple path difference argument for light scattered at angles beyond the Yoneda threshold due to the additional gradual phase change associated with the Yoneda phenomenon. In addition, a scattering experiment such as the one achieved in Ref. 16, but where the outgoing circularly-polarized light is measured instead of the linearly polarized light, would be of particular interest to verify the existence of a circularly-polarized Brewster scattering phenomenon out of the plane of incidence as it would strengthen the rotating dipole interpretation from which it originates.

Finally, we emphasize that the results presented in this work are approximate and are expected to be valid only for weakly rough surfaces. Additional experimental and theoretical investigations are therefore welcome to assess the range of validity of the presented hypotheses.

ACKNOWLEDGMENTS

This research was supported in part by The Research Council of Norway Contract No. 216699. The research of I.S. was supported in part by the French National Research Agency (ANR-15-CHIN-0003). This research was supported in part by NTNU and the Norwegian metacenter for High Performance Computing (NOTUR) by

the allocation of computer time.

Appendix A: Perturbative solution

This appendix is devoted to the derivation of the method known as small amplitude perturbation theory (SAPT) for obtaining approximate solutions of the reduced Rayleigh equations. The basic principle of the method is to expand the kernel factor $\mathcal{J}_{l,m}^{b,a}$ in a series of Fourier transforms of the power of the surface profile function ζ and to expand the unknown reflection and transmission amplitudes in a similar series and matching terms of the same order. The expansions can be expressed as follows

$$\begin{aligned}\mathcal{J}_{l,m}^{b,a}\left(\mathbf{p}\,|\,\mathbf{q}\right) &= \left[b\alpha_l\left(\mathbf{p}\right) - a\alpha_m\left(\mathbf{q}\right)\right]^{-1} \int \exp[-i(\mathbf{p}-\mathbf{q})\cdot\mathbf{x}_\parallel]\, \exp[-i(b\alpha_l\left(\mathbf{p}\right) - a\alpha_m\left(\mathbf{q}\right))\,\zeta(\mathbf{x}_\parallel)]\,\mathrm{d}^2x_\parallel \\ &= \sum_{n=0}^{\infty} \frac{(-i)^n}{n!}\left[b\alpha_l\left(\mathbf{p}\right) - a\alpha_m\left(\mathbf{q}\right)\right]^{n-1}\hat{\zeta}^{(n)}(\mathbf{p}-\mathbf{q}) \qquad \text{(A1a)}\end{aligned}$$

$$\mathbf{R}\left(\mathbf{q}\,|\,\mathbf{p}_0\right) = \sum_{j=0}^{\infty}\frac{(-i)^j}{j!}\,\mathbf{R}^{(j)}\left(\mathbf{q}\,|\,\mathbf{p}_0\right) \qquad \text{(A1b)}$$

$$\mathbf{T}\left(\mathbf{q}\,|\,\mathbf{p}_0\right) = \sum_{j=0}^{\infty}\frac{(-i)^j}{j!}\,\mathbf{T}^{(j)}\left(\mathbf{q}\,|\,\mathbf{p}_0\right)\,. \qquad \text{(A1c)}$$

In equation Eq. (A1a), we have defined the Fourier transform of the n^{th} power of ζ, which we will refer to as the n^{th} *Fourier moment of the surface profile*, as

$$\hat{\zeta}^{(n)}(\mathbf{q}) = \int \zeta^n(\mathbf{x}_\parallel)\,\exp[-i\,\mathbf{q}\cdot\mathbf{x}_\parallel]\,\mathrm{d}^2x_\parallel\,. \qquad \text{(A2)}$$

We are now ready to proceed with the perturbative method.

Reflection: We start by inserting Eqs. (A1a,A1b) into the reduced Rayleigh equation Eq. (17) in the case of reflection (see Eq. (18)). We obtain

$$\begin{aligned}&\sum_{n=0}^{\infty}\sum_{j=0}^{\infty}\frac{(-i)^{n+j}}{n!\,j!}\int\left[\alpha_2\left(\mathbf{p}\right) - \alpha_1\left(\mathbf{q}\right)\right]^{n-1}\hat{\zeta}^{(n)}(\mathbf{p}-\mathbf{q})\,\mathbf{M}_{2,1}^{+,+}\left(\mathbf{p}\,|\,\mathbf{q}\right)\,\mathbf{R}^{(j)}\left(\mathbf{q}\,|\,\mathbf{p}_0\right)\,\frac{\mathrm{d}^2q}{(2\pi)^2} \\ &= -\sum_{m=0}^{\infty}\frac{(-i)^m}{m!}\left[\alpha_2\left(\mathbf{p}\right) + \alpha_1(\mathbf{p}_0)\right]^{m-1}\hat{\zeta}^{(m)}(\mathbf{p}-\mathbf{p}_0)\,\mathbf{M}_{2,1}^{+,-}\left(\mathbf{p}\,|\,\mathbf{p}_0\right)\,. \qquad \text{(A3)}\end{aligned}$$

A summation over all $(n,j)\in\mathbb{N}^2$ is equivalent to a summation over subsets $\mathcal{S}_m = \{(n,j)\in\mathbb{N}^2\,|\,n+j=m\}$ of pairs of constant sum $m=n+j$, i.e. that we have $\sum_{n,j=0}^{\infty} \equiv \sum_{m=0}^{\infty}\sum_{(n,j)\in\mathcal{S}_m}$, therefore the previous equation can be recast as

$$\begin{aligned}&\sum_{m=0}^{\infty}\frac{(-i)^m}{m!}\sum_{n=0}^{m}\binom{m}{n}\int\left[\alpha_2\left(\mathbf{p}\right) - \alpha_1\left(\mathbf{q}\right)\right]^{n-1}\hat{\zeta}^{(n)}(\mathbf{p}-\mathbf{q})\,\mathbf{M}_{2,1}^{+,+}\left(\mathbf{p}\,|\,\mathbf{q}\right)\,\mathbf{R}^{(m-n)}\left(\mathbf{q}\,|\,\mathbf{p}_0\right)\,\frac{\mathrm{d}^2q}{(2\pi)^2} \\ &\qquad = -\sum_{m=0}^{\infty}\frac{(-i)^m}{m!}\left[\alpha_2\left(\mathbf{p}\right) + \alpha_1(\mathbf{p}_0)\right]^{m-1}\hat{\zeta}^{(m)}(\mathbf{p}-\mathbf{p}_0)\,\mathbf{M}_{2,1}^{+,-}\left(\mathbf{p}\,|\,\mathbf{p}_0\right)\,. \qquad \text{(A4)}\end{aligned}$$

Note that here we have used that $\frac{1}{n!\,(m-n)!} = \frac{1}{m!}\binom{m}{n}$ by definition of the binomial coefficients. The perturbation procedure consists in matching orders in both side of the equation. The order zero only consists of one term $n=m=0$ and gives

$$\begin{aligned}&\int\left[\alpha_2\left(\mathbf{p}\right) - \alpha_1\left(\mathbf{q}\right)\right]^{-1}\hat{\zeta}^{(0)}(\mathbf{p}-\mathbf{q})\,\mathbf{M}_{2,1}^{+,+}\left(\mathbf{p}\,|\,\mathbf{q}\right)\,\mathbf{R}^{(0)}\left(\mathbf{q}\,|\,\mathbf{p}_0\right)\,\frac{\mathrm{d}^2q}{(2\pi)^2} \\ &= -\left[\alpha_2\left(\mathbf{p}\right) + \alpha_1(\mathbf{p}_0)\right]^{-1}\hat{\zeta}^{(0)}(\mathbf{p}-\mathbf{p}_0)\,\mathbf{M}_{2,1}^{+,-}\left(\mathbf{p}\,|\,\mathbf{p}_0\right)\,. \qquad \text{(A5)}\end{aligned}$$

By using that $\hat{\zeta}^{(0)}(\mathbf{p}-\mathbf{q}) = (2\pi)^2\,\delta(\mathbf{p}-\mathbf{q})$, we finally obtain the zero order reflection amplitude

$$\mathbf{R}^{(0)}\left(\mathbf{p}\,|\,\mathbf{p}_0\right) = (2\pi)^2\,\delta(\mathbf{p}-\mathbf{p}_0)\,\frac{\alpha_1(\mathbf{p}_0)-\alpha_2(\mathbf{p}_0)}{\alpha_2(\mathbf{p}_0)+\alpha_1(\mathbf{p}_0)}\,\left[\mathbf{M}_{2,1}^{+,+}\left(\mathbf{p}_0\,|\,\mathbf{p}_0\right)\right]^{-1}\,\mathbf{M}_{2,1}^{+,-}\left(\mathbf{p}_0\,|\,\mathbf{p}_0\right) = (2\pi)^2\,\delta(\mathbf{p}-\mathbf{p}_0)\,\boldsymbol{\rho}^{(0)}(\mathbf{p}_0) \quad \text{(A6)}$$

We have just obtained that the zero order of the reflection amplitude corresponds exactly to the reflection amplitude for a planar surface and it is straightforward to show that $\boldsymbol{\rho}^{(0)}(\mathbf{p}_0)$ is a diagonal matrix containing the Fresnel amplitudes. This was to be expected in the sense that the zero order of the surface profile corresponds to its averaged plane. For orders $m \geq 1$, we have

$$\begin{aligned}\sum_{n=0}^{m}\binom{m}{n}\int\left[\alpha_2\left(\mathbf{p}\right)-\alpha_1\left(\mathbf{q}\right)\right]^{n-1}\hat{\zeta}^{(n)}(\mathbf{p}-\mathbf{q})\;\mathbf{M}_{2,1}^{+,+}\left(\mathbf{p}\,|\,\mathbf{q}\right)\,\mathbf{R}^{(m-n)}\left(\mathbf{q}\,|\,\mathbf{p}_0\right)\,\frac{\mathrm{d}^2q}{(2\pi)^2}\\ = -\left[\alpha_2\left(\mathbf{p}\right)+\alpha_1(\mathbf{p}_0)\right]^{m-1}\hat{\zeta}^{(m)}(\mathbf{p}-\mathbf{p}_0)\;\mathbf{M}_{2,1}^{+,-}\left(\mathbf{p}\,|\,\mathbf{p}_0\right), \end{aligned} \quad \text{(A7)}$$

which by isolating the term of interest, $n=0$ gives $\mathbf{R}^{(m)}$ as a function of $\mathbf{R}^{(m-1)}\cdots\mathbf{R}^{(0)}$, in other words we have a recursive relation for determining all orders,

$$\begin{aligned}\mathbf{R}^{(m)}\left(\mathbf{p}\,|\,\mathbf{p}_0\right) =&\left[\alpha_1\left(\mathbf{p}\right)-\alpha_2\left(\mathbf{p}\right)\right]\left[\mathbf{M}_{2,1}^{+,+}\left(\mathbf{p}\,|\,\mathbf{p}\right)\right]^{-1}\,\left[\left(\alpha_2\left(\mathbf{p}\right)+\alpha_1(\mathbf{p}_0)\right)^{m-1}\hat{\zeta}^{(m)}(\mathbf{p}-\mathbf{p}_0)\;\mathbf{M}_{2,1}^{+,-}\left(\mathbf{p}\,|\,\mathbf{p}_0\right)\right.\\ &\left.+\sum_{n=1}^{m}\binom{m}{n}\int\left[\alpha_2\left(\mathbf{p}\right)-\alpha_1\left(\mathbf{q}\right)\right]^{n-1}\hat{\zeta}^{(n)}(\mathbf{p}-\mathbf{q})\;\mathbf{M}_{2,1}^{+,+}\left(\mathbf{p}\,|\,\mathbf{q}\right)\,\mathbf{R}^{(m-n)}\left(\mathbf{q}\,|\,\mathbf{p}_0\right)\,\frac{\mathrm{d}^2q}{(2\pi)^2}\right]. \end{aligned} \quad \text{(A8)}$$

In general, the evaluation of high orders would require the evaluation of as many integrals as the order and can become costly. For the first order, only one such integral is to be evaluated and is straightforward thanks to the fact that $\mathbf{R}^{(0)}(\mathbf{q}\,|\,\mathbf{p}_0) \propto \delta(\mathbf{q}-\mathbf{p}_0)$. Applying the above equation for $m=1$ gives

$$\begin{aligned}\mathbf{R}^{(1)}\left(\mathbf{p}\,|\,\mathbf{p}_0\right) &= \left[\alpha_1\left(\mathbf{p}\right)-\alpha_2\left(\mathbf{p}\right)\right]\left[\mathbf{M}_{2,1}^{+,+}\left(\mathbf{p}\,|\,\mathbf{p}\right)\right]^{-1}\,\left[\hat{\zeta}^{(1)}(\mathbf{p}-\mathbf{p}_0)\;\mathbf{M}_{2,1}^{+,-}\left(\mathbf{p}\,|\,\mathbf{p}_0\right)\right.\\ &\quad\left.+\int\hat{\zeta}^{(1)}(\mathbf{p}-\mathbf{q})\;\mathbf{M}_{2,1}^{+,+}\left(\mathbf{p}\,|\,\mathbf{q}\right)\,\mathbf{R}^{(0)}\left(\mathbf{q}\,|\,\mathbf{p}_0\right)\,\frac{\mathrm{d}^2q}{(2\pi)^2}\right]\\ &= \left[\alpha_1\left(\mathbf{p}\right)-\alpha_2\left(\mathbf{p}\right)\right]\hat{\zeta}^{(1)}(\mathbf{p}-\mathbf{p}_0)\;\left[\mathbf{M}_{2,1}^{+,+}\left(\mathbf{p}\,|\,\mathbf{p}\right)\right]^{-1}\,\left[\mathbf{M}_{2,1}^{+,-}\left(\mathbf{p}\,|\,\mathbf{p}_0\right)+\mathbf{M}_{2,1}^{+,+}\left(\mathbf{p}\,|\,\mathbf{p}_0\right)\,\boldsymbol{\rho}^{(0)}(\mathbf{p}_0)\right]\\ &= \left[\alpha_1\left(\mathbf{p}\right)-\alpha_2\left(\mathbf{p}\right)\right]\hat{\zeta}^{(1)}(\mathbf{p}-\mathbf{p}_0)\,\hat{\boldsymbol{\rho}}^{(1)}\left(\mathbf{p}\,|\,\mathbf{p}_0\right) = \hat{\zeta}^{(1)}(\mathbf{p}-\mathbf{p}_0)\,\boldsymbol{\rho}^{(1)}\left(\mathbf{p}\,|\,\mathbf{p}_0\right). \end{aligned} \quad \text{(A9)}$$

In Eq. (A9), we define the amplitude $\hat{\boldsymbol{\rho}}^{(1)}\left(\mathbf{p}\,|\,\mathbf{p}_0\right)$ and $\boldsymbol{\rho}^{(1)}\left(\mathbf{p}\,|\,\mathbf{p}_0\right) = \left(\alpha_1\left(\mathbf{p}\right)-\alpha_2\left(\mathbf{p}\right)\right)\hat{\boldsymbol{\rho}}^{(1)}\left(\mathbf{p}\,|\,\mathbf{p}_0\right)$. The reason for these two alternative expressions is that the first one gives a factorization which is more easily interpreted from a physical point of view while the latter factorization aims at separating what depends on the realization of the surface profile, which is just $\hat{\zeta}$ here, and the amplitude factor $\boldsymbol{\rho}^{(1)}\left(\mathbf{p}\,|\,\mathbf{p}_0\right)$ which remains independent of the specific realization of the surface profile (see Section III).

Transmission: Repeating the reasoning for the transmission amplitudes, we start by inserting Eqs. (A1a,A1c) into Eq. (17) for transmission (see Eq. (18)) and get

$$\begin{aligned}\sum_{n=0}^{\infty}\sum_{j=0}^{\infty}\frac{(-i)^{n+j}}{n!\,j!}\int\left[-\alpha_1\left(\mathbf{p}\right)+\alpha_2\left(\mathbf{q}\right)\right]^{n-1}\hat{\zeta}^{(n)}(\mathbf{p}-\mathbf{q})\;\mathbf{M}_{1,2}^{-,-}\left(\mathbf{p}\,|\,\mathbf{q}\right)\,\mathbf{T}^{(j)}\left(\mathbf{q}\,|\,\mathbf{p}_0\right)\,\frac{\mathrm{d}^2q}{(2\pi)^2}\\ = \frac{2\,\sqrt{\epsilon_1\epsilon_2}\,\alpha_1(\mathbf{p}_0)}{\epsilon_2-\epsilon_1}\,(2\pi)^2\,\delta(\mathbf{p}-\mathbf{p}_0)\,\mathbf{I}_2\,. \end{aligned} \quad \text{(A10)}$$

By using the same re-summation argument as for reflection, the previous equation thus becomes

$$\begin{aligned}\sum_{m=0}^{\infty}\sum_{n=0}^{m}\frac{(-i)^{m}}{m!}\binom{m}{n}\int\left[-\alpha_1\left(\mathbf{p}\right)+\alpha_2\left(\mathbf{q}\right)\right]^{n-1}\hat{\zeta}^{(n)}(\mathbf{p}-\mathbf{q})\;\mathbf{M}_{1,2}^{-,-}\left(\mathbf{p}\,|\,\mathbf{q}\right)\,\mathbf{T}^{(m-n)}\left(\mathbf{q}\,|\,\mathbf{p}_0\right)\,\frac{\mathrm{d}^2q}{(2\pi)^2}\\ = \frac{2\,\sqrt{\epsilon_1\epsilon_2}\,\alpha_1(\mathbf{p}_0)}{\epsilon_2-\epsilon_1}\,(2\pi)^2\,\delta(\mathbf{p}-\mathbf{p}_0)\,\mathbf{I}_2\,. \end{aligned} \quad \text{(A11)}$$

Next we match the zero order to the right hand side and the other orders to zero. The zero order only consists of one term $n = m = 0$ and gives

$$\mathbf{T}^{(0)}\left(\mathbf{p}\,|\,\mathbf{p}_0\right) = \frac{2\,\sqrt{\epsilon_1\epsilon_2}\alpha_1(\mathbf{p}_0)}{\epsilon_2-\epsilon_1}\,(2\pi)^2\,\delta(\mathbf{p}-\mathbf{p}_0)\,\left[\alpha_2(\mathbf{p}_0)-\alpha_1(\mathbf{p}_0)\right]\,\left[\mathbf{M}^{-;-}_{1,2}\left(\mathbf{p}_0\,|\,\mathbf{p}_0\right)\right]^{-1} \tag{A12}$$

$$= (2\pi)^2\,\delta(\mathbf{p}-\mathbf{p}_0)\,\boldsymbol{\tau}^{(0)}(\mathbf{p}_0) \tag{A13}$$

Here we have used that $\hat{\zeta}^{(0)}(\mathbf{p}-\mathbf{q}) = (2\pi)^2\,\delta(\mathbf{p}-\mathbf{q})$. As observed for the reflection amplitudes, we have just obtained that the zero order of the transmission amplitudes corresponds exactly to the transmission amplitudes for a planar surface, i.e. that $\boldsymbol{\tau}^{(0)}(\mathbf{p}_0)$ is a diagonal matrix containing the Fresnel transmission amplitudes. For orders $m \geq 1$, we have

$$\sum_{n=0}^{m}\binom{m}{n}\,\int\left[\alpha_2\left(\mathbf{q}\right)-\alpha_1\left(\mathbf{p}\right)\right]^{n-1}\,\hat{\zeta}^{(n)}(\mathbf{p}-\mathbf{q})\;\mathbf{M}^{-;-}_{1,2}\left(\mathbf{p}\,|\,\mathbf{q}\right)\;\mathbf{T}^{(m-n)}\left(\mathbf{q}\,|\,\mathbf{p}_0\right)\;\frac{\mathrm{d}^2q}{(2\pi)^2} = \mathbf{0}\,, \tag{A14}$$

which by isolating the term of interest, $n = 0$ gives $\mathbf{T}^{(m)}$ as a function of $\mathbf{T}^{(m-1)}\cdots\mathbf{T}^{(0)}$, in other words we have a recursive relation for determining all orders,

$$\begin{aligned}\mathbf{T}^{(m)}\left(\mathbf{p}\,|\,\mathbf{p}_0\right) =& \left[\alpha_1\left(\mathbf{p}\right)-\alpha_2\left(\mathbf{p}\right)\right]\,\left[\mathbf{M}^{-;-}_{1,2}\left(\mathbf{p}\,|\,\mathbf{p}\right)\right]^{-1}\\ &\sum_{n=1}^{m}\binom{m}{n}\,\int\left[\alpha_2\left(\mathbf{q}\right)-\alpha_1\left(\mathbf{p}\right)\right]^{n-1}\,\hat{\zeta}^{(n)}(\mathbf{p}-\mathbf{q})\;\mathbf{M}^{-;-}_{1,2}\left(\mathbf{p}\,|\,\mathbf{q}\right)\;\mathbf{T}^{(m-n)}\left(\mathbf{q}\,|\,\mathbf{p}_0\right)\;\frac{\mathrm{d}^2q}{(2\pi)^2}\,.\end{aligned} \tag{A15}$$

Applying the above equation for $m = 1$ and using that $\mathbf{T}^{(0)}\left(\mathbf{q}\,|\,\mathbf{p}_0\right) \propto \delta(\mathbf{q}-\mathbf{p}_0)$ gives

$$\begin{aligned}\mathbf{T}^{(1)}\left(\mathbf{p}\,|\,\mathbf{p}_0\right) =& \left[\alpha_1\left(\mathbf{p}\right)-\alpha_2\left(\mathbf{p}\right)\right]\hat{\zeta}^{(1)}(\mathbf{p}-\mathbf{p}_0)\;\left[\mathbf{M}^{-;-}_{1,2}\left(\mathbf{p}\,|\,\mathbf{p}\right)\right]^{-1}\;\mathbf{M}^{-;-}_{1,2}\left(\mathbf{p}\,|\,\mathbf{p}_0\right)\;\boldsymbol{\tau}^{(0)}(\mathbf{p}_0)\\ =& \left[\alpha_1\left(\mathbf{p}\right)-\alpha_2\left(\mathbf{p}\right)\right]\hat{\zeta}^{(1)}(\mathbf{p}-\mathbf{p}_0)\;\hat{\boldsymbol{\tau}}^{(1)}\left(\mathbf{p}\,|\,\mathbf{p}_0\right) = \hat{\zeta}^{(1)}(\mathbf{p}-\mathbf{p}_0)\;\boldsymbol{\tau}^{(1)}\left(\mathbf{p}\,|\,\mathbf{p}_0\right)\,.\end{aligned} \tag{A16}$$

Appendix B: Differential reflection coefficient

Assuming we have obtained the reflection amplitudes $R_{\alpha\beta}(\mathbf{p}\,|\,\mathbf{p}_0)$ either by using the perturbative approach or by the purely numerical simulation, we can now proceed to express the differential reflection coefficient (DRC) defined as the time-averaged flux radiated around a given scattering direction (θ_r, ϕ) per unit solid angle and per unit incident flux and denoted $\partial R/\partial\Omega_r(\mathbf{p}\,|\,\mathbf{p}_0)$. Let a virtual hemisphere of radius $r \gg c/\omega$ lie on the plane $x_3 = 0$ on top of the scattering system. The support of this hemisphere is a disk of area $S = \pi r^2$. We consider the scattering from a *truncated* version of the scattering system in which the surface profiles are set to be flat outside the disk support. Consequently, the field amplitudes we will manipulate are not strictly speaking those of the full system of interest but will converge to them as $r \to \infty$. We will nevertheless keep the same notations as that from the full system introduced in Section III for simplicity. The time-averaged flux incident on this disk is given by

$$\begin{aligned}P_{\mathrm{inc}/S} &= -\mathrm{Re}\frac{c}{8\pi}\int_S\left[\mathbf{E}_0^*(\mathbf{p}_0)\times\left(\frac{c}{\omega}\;\mathbf{k}_1^-(\mathbf{p}_0)\times\mathbf{E}_0(\mathbf{p}_0)\right)\right]\cdot\hat{\mathbf{e}}_3\;\exp\left[-i(\mathbf{k}_1^{-*}(\mathbf{p}_0)-\mathbf{k}_1^-(\mathbf{p}_0))\cdot\mathbf{x}\right]\mathrm{d}^2x_\parallel\\ &= -\frac{c^2}{8\pi\omega}\,\mathrm{Re}\int_S\left[|\,\mathbf{E}_0(\mathbf{p}_0)|^2\;\mathbf{k}_1^-(\mathbf{p}_0)-\left(\mathbf{E}_0^*(\mathbf{p}_0)\cdot\mathbf{k}_1^-(\mathbf{p}_0)\right)\cdot\mathbf{E}_0(\mathbf{p}_0)\right]\cdot\hat{\mathbf{e}}_3\mathrm{d}^2x_\parallel\\ &= S\,\frac{c^2}{8\pi\omega}\,\alpha_1(\mathbf{p}_0)\,|\,\mathbf{E}_0(\mathbf{p}_0)|^2\\ &= S\,\frac{c^2}{8\pi\omega}\,\alpha_1(\mathbf{p}_0)\;\left[\left|\mathcal{E}_{0,p}\right|^2+\left|\mathcal{E}_{0,s}\right|^2\right].\end{aligned} \tag{B1}$$

Here, the * denotes the complex conjugate, and incident field amplitude $\mathbf{E}_0(\mathbf{p}_0) = \mathcal{E}_{0,p}\;\hat{\mathbf{e}}_p^-(\mathbf{p}_0)+\mathcal{E}_{0,s}\;\hat{\mathbf{e}}_s(\mathbf{p}_0)$ as defined in Eq. (13), the vector identity $\mathbf{a}\times(\mathbf{b}\times\mathbf{c}) = (\mathbf{a}\cdot\mathbf{c})\mathbf{b}-(\mathbf{a}\cdot\mathbf{b})\mathbf{c}$ and the orthogonality between the field and the wave vector $\mathbf{E}_0^*(\mathbf{p}_0)\cdot\mathbf{k}_1^-(\mathbf{p}_0) = 0$ have been used. Note that the flux incident on the disk is proportional to the disk area. Let us now consider the outgoing flux crossing an elementary surface $\mathrm{d}\sigma = r^2\sin\theta_r\mathrm{d}\theta_r\mathrm{d}\phi = r^2\mathrm{d}\Omega_r$ around a point $\mathbf{r} = r\,(\sin\theta_r\cos\phi\,\hat{\mathbf{e}}_1+\sin\theta_r\sin\phi\,\hat{\mathbf{e}}_2+\cos\theta_r\,\hat{\mathbf{e}}_3) = r\,\hat{\mathbf{n}}$. The flux crossing this elementary surface is given by

$$P_{\mathrm{d}\sigma} = \frac{c}{8\pi}\,\mathrm{Re}\left[\mathbf{E}_1^{+*}(\mathbf{r})\times\mathbf{H}_1^+(\mathbf{r})\right]\cdot\hat{\mathbf{n}}\,\mathrm{d}\sigma. \tag{B2}$$

We then use the well-known asymptotic expansion of the field in the far-field given by (see Refs. 44 and 45)

$$\mathbf{E}_1^+(\mathbf{r}) \sim -i\,\epsilon_1^{1/2}\frac{\omega}{2\pi\,c}\cos\theta_r\,\frac{\exp(i\epsilon_1^{1/2}\frac{\omega}{c}r)}{r}\;\mathbf{E}_1^+(\mathbf{p}) \tag{B3a}$$

$$\mathbf{H}_1^+(\mathbf{r}) \sim -i\,\epsilon_1\frac{\omega}{2\pi\,c}\cos\theta_r\,\frac{\exp(i\epsilon_1^{1/2}\frac{\omega}{c}r)}{r}\,\hat{\mathbf{n}}\times\mathbf{E}_1^+(\mathbf{p}) \tag{B3b}$$

where $\mathbf{p}=\sqrt{\epsilon_1}\frac{\omega}{c}(\sin\theta_r\cos\phi\,\hat{\mathbf{e}}_1+\sin\theta_r\sin\phi\,\hat{\mathbf{e}}_2)$. This asymptotic approximation will become more and more accurate as we let $r\to\infty$. Plugging Eq. (B3) into Eq. (B2) we obtain

$$P_{\mathrm{d}\sigma}=\epsilon_1^{3/2}\left(\frac{\omega}{2\pi\,c}\right)^2\cos^2\theta_r\,\frac{c}{8\pi}\,|\,\mathbf{E}_1^+(\mathbf{p})|^2\,\mathrm{d}\Omega_r=\epsilon_1^{3/2}\left(\frac{\omega}{2\pi\,c}\right)^2\cos^2\theta_r\,\frac{c}{8\pi}\,\left(|\,\mathcal{E}_{1,p}^+(\mathbf{p})|^2+|\,\mathcal{E}_{1,s}^+(\mathbf{p})|^2\right)\,\mathrm{d}\Omega_r. \tag{B4}$$

The total differential reflection coefficient is then given by

$$\frac{\partial R}{\partial\Omega_r}(\mathbf{p}\,|\,\mathbf{p}_0)=\lim_{r\to\infty}\frac{P_{\mathrm{d}\sigma}}{P_{\mathrm{inc}/S}\,\mathrm{d}\Omega_r}=\lim_{r\to\infty}\frac{\epsilon_1}{S}\left(\frac{\omega}{2\pi\,c}\right)^2\frac{\cos^2\theta_r}{\cos\theta_0}\,\frac{|\,\mathcal{E}_{1,p}^+(\mathbf{p})|^2+|\,\mathcal{E}_{1,s}^+(\mathbf{p})|^2}{|\,\mathcal{E}_{0,p}\,|^2+|\,\mathcal{E}_{0,s}\,|^2}. \tag{B5}$$

From the total differential reflection coefficient given by Eq. (B5), we deduce the differential reflection coefficient when an incident plane wave of polarization β, with lateral wave vector $\mathbf{p}_0$ is reflected into a plane wave of polarization α with lateral wave vector $\mathbf{p}$ given as

$$\frac{\partial R_{\alpha\beta}}{\partial\Omega_r}(\mathbf{p}\,|\,\mathbf{p}_0)=\lim_{r\to\infty}\frac{\epsilon_1}{S}\left(\frac{\omega}{2\pi\,c}\right)^2\frac{\cos^2\theta_r}{\cos\theta_0}\,|R_{\alpha\beta}(\mathbf{p}\,|\,\mathbf{p}_0)|^2=\lim_{r\to\infty}\frac{\partial R_{\alpha\beta}^{(S)}}{\partial\Omega_r}(\mathbf{p}\,|\,\mathbf{p}_0). \tag{B6}$$

As we are interested in averaging the optical response over realizations of the surface profiles, we consider the following ensemble average

$$\left\langle\frac{\partial R_{\alpha\beta}^{(S)}}{\partial\Omega_r}(\mathbf{p}\,|\,\mathbf{p}_0)\right\rangle=\frac{\epsilon_1}{S}\left(\frac{\omega}{2\pi\,c}\right)^2\frac{\cos^2\theta_r}{\cos\theta_0}\,\left\langle|R_{\alpha\beta}(\mathbf{p}\,|\,\mathbf{p}_0)|^2\right\rangle. \tag{B7}$$

A similar derivation for the differential transmitted coefficient yields

$$\left\langle\frac{\partial T_{\alpha\beta}^{(S)}}{\partial\Omega_t}(\mathbf{p}\,|\,\mathbf{p}_0)\right\rangle=\frac{\epsilon_2^{3/2}}{\epsilon_1^{1/2}S}\left(\frac{\omega}{2\pi\,c}\right)^2\frac{\cos^2\theta_t}{\cos\theta_0}\,\left\langle|T_{\alpha\beta}(\mathbf{p}\,|\,\mathbf{p}_0)|^2\right\rangle. \tag{B8}$$

By decomposing the reflection amplitudes as the sum of the mean and fluctuation (deviation from the mean)

$$R_{\alpha\beta}(\mathbf{p}\,|\,\mathbf{p}_0)=\langle R_{\alpha\beta}(\mathbf{p}\,|\,\mathbf{p}_0)\rangle+\left[R_{\alpha\beta}(\mathbf{p}\,|\,\mathbf{p}_0)-\langle R_{\alpha\beta}(\mathbf{p}\,|\,\mathbf{p}_0)\rangle\right]\,, \tag{B9}$$

we can decompose the MDRC as the sum of a coherent term and an incoherent term

$$\left\langle\frac{\partial R_{\alpha\beta}^{(S)}}{\partial\Omega_r}(\mathbf{p}\,|\,\mathbf{p}_0)\right\rangle=\left\langle\frac{\partial R_{\alpha\beta}^{(S)}}{\partial\Omega_r}(\mathbf{p}\,|\,\mathbf{p}_0)\right\rangle_{\mathrm{coh}}+\left\langle\frac{\partial R_{\alpha\beta}^{(S)}}{\partial\Omega_r}(\mathbf{p}\,|\,\mathbf{p}_0)\right\rangle_{\mathrm{incoh}}\,, \tag{B10}$$

where

$$\left\langle\frac{\partial R_{\alpha\beta}^{(S)}}{\partial\Omega_r}(\mathbf{p}\,|\,\mathbf{p}_0)\right\rangle_{\mathrm{coh}}=\frac{\epsilon_1}{S}\left(\frac{\omega}{2\pi\,c}\right)^2\frac{\cos^2\theta_r}{\cos\theta_0}\,|\langle R_{\alpha\beta}(\mathbf{p}\,|\,\mathbf{p}_0)\rangle|^2 \tag{B11a}$$

$$\left\langle\frac{\partial R_{\alpha\beta}^{(S)}}{\partial\Omega_r}(\mathbf{p}\,|\,\mathbf{p}_0)\right\rangle_{\mathrm{incoh}}=\frac{\epsilon_1}{S}\left(\frac{\omega}{2\pi\,c}\right)^2\frac{\cos^2\theta_r}{\cos\theta_0}\,\left[\left\langle|R_{\alpha\beta}(\mathbf{p}\,|\,\mathbf{p}_0)|^2\right\rangle-|\langle R_{\alpha\beta}(\mathbf{p}\,|\,\mathbf{p}_0)\rangle|^2\right]. \tag{B11b}$$

If we now use the expression found in A for the reflection amplitudes to first order in the product of surface profiles,

$$\mathbf{R}\,(\mathbf{p}\,|\,\mathbf{p}_0)\approx\mathbf{R}^{(0)}\,(\mathbf{p}\,|\,\mathbf{p}_0)-i\,\mathbf{R}^{(1)}\,(\mathbf{p}\,|\,\mathbf{p}_0)\,, \tag{B12}$$

where $\mathbf{R}^{(0)}\,(\mathbf{p}\,|\,\mathbf{p}_0)$ is the response from the corresponding system with planar interface, Eq. (A6), and $\mathbf{R}^{(1)}\,(\mathbf{p}\,|\,\mathbf{p}_0)$ is given in Eq. (A9), we obtain that the factor in the square bracket in Eq. (B11b) reads

$$\left\langle|R_{\alpha\beta}(\mathbf{p}\,|\,\mathbf{p}_0)|^2\right\rangle-|\langle R_{\alpha\beta}(\mathbf{p}\,|\,\mathbf{p}_0)\rangle|^2=\left\langle\left|R_{\alpha\beta}^{(1)}(\mathbf{p}\,|\,\mathbf{p}_0)\right|^2\right\rangle=\left\langle|\hat{\zeta}_S(\mathbf{p}-\mathbf{p}_0)|^2\right\rangle\,|\rho_{\alpha\beta}^{(1)}\,(\mathbf{p}\,|\,\mathbf{p}_0)\,|^2. \tag{B13}$$

Note here that we are still dealing with a scattering system whose surface profiles are flat outside the disk of radius r, hence the subscript S. For the statistical properties attributed to the surface profiles in Sec. II, we have

$$\begin{aligned}\left\langle \hat{\zeta}_S(\mathbf{q})\hat{\zeta}_S^*(\mathbf{q})\right\rangle &= \left\langle \int_S\int_S \zeta(\mathbf{x})\zeta(\mathbf{x}')\exp\left[i\,\mathbf{q}\cdot(\mathbf{x}-\mathbf{x}')\right]\,\mathrm{d}^2x\,\mathrm{d}^2x'\right\rangle \\ &= \int_S\int_S \langle\zeta(\mathbf{x})\zeta(\mathbf{x}')\rangle\,\exp\left[i\,\mathbf{q}\cdot(\mathbf{x}-\mathbf{x}')\right]\,\mathrm{d}^2x\,\mathrm{d}^2x' \\ &= \int_S\int_S \sigma^2\,W(\mathbf{x}-\mathbf{x}')\,\exp\left[i\,\mathbf{q}\cdot(\mathbf{x}-\mathbf{x}')\right]\,\mathrm{d}^2x\,\mathrm{d}^2x'. \end{aligned} \tag{B14}$$

Here we have used the definition of the Fourier transform, and the fact that ensemble average commutes with the integration of the surfaces and the definition of the correlation function. Via the change of variable $\mathbf{u}=\mathbf{x}-\mathbf{x}'$ we obtain

$$\left\langle \hat{\zeta}_S(\mathbf{q})\hat{\zeta}_S^*(\mathbf{q})\right\rangle = S\,\sigma^2\,\int_S W(\mathbf{u})\,\exp(i\,\mathbf{q}\cdot\mathbf{u})\,\mathrm{d}^2u = S\,\sigma^2\,g_S(\mathbf{q}). \tag{B15}$$

Thus

$$\left\langle |R_{\alpha\beta}(\mathbf{p}\,|\,\mathbf{p}_0)|^2\right\rangle - \left|\langle R_{\alpha\beta}(\mathbf{p}\,|\,\mathbf{p}_0)\rangle\right|^2 = S\,\sigma^2\,g_S(\mathbf{p}-\mathbf{p}_0)\,\left|\rho^{(1)}_{\alpha\beta}\left(\mathbf{p}\,|\,\mathbf{p}_0\right)\right|^2. \tag{B16}$$

Finally, by plugging the above equation into Eq. (B11b), the surface area S cancels and letting $r\to\infty$, $g_S\to g$ (where we remind the reader that g is the power spectrum of the surface profiles) and we finally obtain the expression for the incoherent component of the MDRC for the entire (infinite) system under the first order approximation of the reflected amplitudes in product of the surface profiles

$$\left\langle \frac{\partial R_{\alpha\beta}}{\partial\Omega_r}(\mathbf{p}\,|\,\mathbf{p}_0)\right\rangle_{\text{incoh}} = \epsilon_1\left(\frac{\omega}{2\pi c}\right)^2\,\frac{\cos^2\theta_r}{\cos\theta_0}\,g(\mathbf{p}-\mathbf{p}_0)\,\sigma^2\,\left|\rho^{(1)}_{\alpha\beta}\left(\mathbf{p}\,|\,\mathbf{p}_0\right)\right|^2. \tag{B17}$$

Similarly, for the transmitted light we obtain

$$\left\langle \frac{\partial T_{\alpha\beta}}{\partial\Omega_t}(\mathbf{p}\,|\,\mathbf{p}_0)\right\rangle_{\text{incoh}} = \frac{\epsilon_2^{3/2}}{\epsilon_1^{1/2}}\left(\frac{\omega}{2\pi c}\right)^2\,\frac{\cos^2\theta_t}{\cos\theta_0}\,g(\mathbf{p}-\mathbf{p}_0)\,\sigma^2\,\left|\tau^{(1)}_{\alpha\beta}\left(\mathbf{p}\,|\,\mathbf{p}_0\right)\right|^2. \tag{B18}$$

[1] Ø. S. Hetland, A. A. Maradudin, T. Nordam, and I. Simonsen, Phys. Rev. A **93**, 053819 (2016).

[2] Ø. S. Hetland, A. A. Maradudin, T. Nordam, P. A. Letnes, and I. Simonsen, Phys. Rev. A **95**, 043808 (2017).

[3] Y. Yoneda, Phys. Rev. **131**, 2010 (1963).

[4] G. H. Vineyard, Physical Review B **26**, 4146 (1982).

[5] S. K. Sinha, E. B. Sirota, S. Garoff, and H. B. Stanley, Phys. Rev. B **38**, 2297 (1988).

[6] E. E. Gorodnichev, S. L. Dudarev, D. B. Rogozkin, and M. I. Ryazanov, Sov. Phys. JETP Lett. **48**, 147 (1988).

[7] T. A. Leskova and A. A. Maradudin, Waves in Random Media **7**, 395 (1997).

[8] G. Renaud, R. Lazzari, and F. Leroy, Surf. Sci. Rep. **64**, 255 (2009).

[9] H. Dosch, Phys. Rev. B **35**, 2137 (1987).

[10] S. Stepanov, in *Exploration of Subsurface Phenomena by Particle Scattering*, edited by N. Lam, C. Melendres, and S. Sinha (International Advanced Studies Institute Press, North East, Maryland, 2000) pp. 119–137.

[11] A. Kitahara, K. Inoue, H. Kikkawa, K. Matsushita, and I. Takahashi, *X-ray Reflectivity study on polymeric surfaces near glass transition temperature*, Photon Factory Activity Report No. 20, Part B (unpublished) (2002) p. 83.

[12] J.-C. Gasse, D. Lützenkirchen-Hecht, R. Wagner, and R. Frahm, J. Phys.: Conf. Ser. **712**, 012028 (2016).

[13] T. Kawanishi, H. Ogura, and Z. L. Wang, Wave. Random Media **7**, 351 (1997).

[14] In an earlier numerical investigation of light scattering from one-dimensional dielectric rough surfaces, Nieto-Vesperinas and Sánchez-Gil [46] observed "sidelobes" in the angular intensity distributions. They did, however, not associate this observation with the Yoneda phenomenon.

[15] T. Tamir, in *Electromagnetic Surface Modes*, edited by A. D. Boardman (John Wiley & Sons, New York, 1982) Chap. 13.

[16] A. K. González-Alcalde, J.-P. Banon, Ø. S. Hetland, A. A. Maradudin, E. R. Méndez, T. Nordam, and I. Simonsen, Opt. Express **24**, 25995 (2016).

[17] D. Brewster, Philos. Trans. R. Soc. London **105**, 125

(1815).
[18] A. Lakhtakia, Opt. News **15**, 14 (1989).
[19] J. D. Jackson, *Classical Electrodynamics*, 3rd ed. (John Wiley & Sons, New York, 1999).
[20] E. Hecht, *Optics* (Addison-Wesley, 2002).
[21] A. Sommerfeld, J. Opt. Soc. Am. **7**, 501 (1923).
[22] J.-J. Greffet and A. Sentenac, in *Wave Propag. Scatt. Varied Media II*, Vol. 1558, edited by V. K. Varadan (1991) pp. 288–294.
[23] A. Sentenac and J.-J. Greffet, J. Opt. Soc. Am. A **15**, 528 (1998).
[24] O. Calvo-Perez, A. Sentenac, and J. J. Greffet, Radio Sci. **34**, 311 (1999).
[25] J. Lekner, *Theory of Reflection of Electromagnetic and Particle Waves*, Vol. 3 (Springer Science & Business Media, 1987).
[26] W. T. Doyle, Am. J. Phys. **53**, 463 (1985).
[27] J. Sein, Opt. Commun. **2**, 170 (1970).
[28] D. Pattanayak and E. Wolf, Opt. Commun. **6**, 217 (1972).
[29] P. P. Ewald, Annalen der Physik **354**, 1 (1916).
[30] J.-P. Banon, Ø.S. Hetland, and I. Simonsen, Annals of Physics **389**, 352 (2018).
[31] A. Soubret, G. Berginc, and C. Bourrely, Phys. Rev. B **63**, 245411 (2001).
[32] G. Brown, V. Celli, M. Haller, and A. Marvin, Surf. Sci. **136**, 381 (1984).
[33] A. Soubret, G. Berginc, and C. Bourrely, J. Opt. Soc. Am. A **18**, 2778 (2001).
[34] A. A. Maradudin and E. R. Méndez, Appl. Opt. **32**, 3335 (1993).
[35] A. Maradudin, A. R. McGurn, and E. R. Méndez, J. Opt. Soc. Am. A **12**, 2500 (1995).
[36] A. R. McGurn and A. A. Maradudin, Waves in Random Media **6**, 251 (1996), http://dx.doi.org/10.1088/0959-7174/6/3/006.
[37] I. Simonsen, Eur. Phys. J.-Spec. Top. **181**, 1 (2010).
[38] Assuming of course $\epsilon_1 \neq \epsilon_2$, otherwise the problem is trivial.
[39] U. Fano, J. Opt. Soc. Am. **31**, 213 (1941).
[40] The dot product here must be taken as the Hermitian inner product for complex vectors $\mathbf{a} \cdot \mathbf{b} = \sum_j a_j^* b_j$.
[41] Here limited to one medium, but in general both media sharing the interface could be dielectrics.
[42] W. T. Doyle, Am. J. Phys. **48**, 643 (1980).
[43] One may extend the construction to all vectors on the circle defined as the intersection of the unit sphere and the plane $\mathbf{E}^{(0)}_{p,1}(\mathbf{p}_0)^\perp$, but it would result in constructing twice the same set of wave vectors of zero scattering.
[44] G. S. Agarwal, Phys. Rev. B **15**, 2371 (1977).
[45] K. Miyamoto and E. Wolf, J. Opt. Soc. Am. **52**, 615 (1962).
[46] M. Nieto-Vesperinas and J. A. Sánchez-Gil, J. Opt. Soc. Am. A **9**, 424 (1992).

“
We are, you and I, at least one of the ways the universe knows itself.

— Carl Sagan